Thesis submitted for the degree of Doctor of Philosophy,
to the University of Oxford

Cenozoic Deformation in a Plate-Boundary Zone, Marlborough, New Zealand

Sara Vickery

University College
and
Department of Earth Sciences

Trinity Term

1994



Short Abstract

Thesis submitted for the degree of Doctor of Philosophy,
Trinity Term 1994

Cenozoic Deformation in a Plate-Boundary Zone, Marlborough, New Zealand

Sara Vickery

University College
and
Department of Earth Sciences
University of Oxford

The Marlborough Fault System is a zone of dextral transpression in continental crust at the southern end of the Hikurangi subduction system between the obliquely convergent Australian and Pacific plates. Detailed mapping of an area of deformed Tertiary cover sequence on the downthrown side of the Kekerengu Fault (the Kekerengu-Washdyke study area) has revealed two phases of deformation, D_e and D_l.

In the study area D_e consists of nine kilometre scale thrust faults cutting sediments derived from extra- and intra-basinal uplift. The timing of this episode is constrained by the age of the first clastic deposits and by a previously unidentified unconformity in this area of Late Miocene age. A clear sequence of D_l events is recognized deforming all earlier structures including Pliocene aged sediments. Although elsewhere in Marlborough a regional post-Pliocene *ca.* 20^o clockwise block rotation has been previously identified, in the Kekerengu-Washdyke study area one site suggested no post-Pliocene rotation and another a large *ca.* 100^o clockwise rotation. This lack of D_l rotation was unexplained and the large rotation attributed to localized Early Miocene deformation. Palaeomagnetic work carried out in this study has identified six more sites which contain this large rotation (average *ca.* 118 ± 11^o). The rotation therefore appears to be a regional event, likely to be a result of the location of Marlborough in the hinge zone at the southern end of the Hikurangi Margin. One site from dykes in basement rocks does not record this large rotation, indicating that the rotation occurred in upper layers detached from unrotating rock below by an unknown structure (such as a thrust fault), or that the rotation did not occur in this area. The large rotation is believed to have been achieved by pinning of the D_e thrusts to the south of the Marlborough region. The data suggests that the D_e thrusts in Marlborough were initially NW-trending and seaward, not landward-directed as was previously supposed. Palaeomagnetic work has also added to the evidence for a lack of D_l regional rotation on the downthrown side of the Kekerengu Fault. A previously unidentified second phase of D_l folding and 'bending' within the study area appears to have accommodated the regional rotation and suggests that the Kekerengu Fault acted as the eastern boundary of the D_l rotating block.

Long Abstract

Cenozoic Deformation in a Plate-Boundary Zone, Marlborough, New Zealand

Sara Vickery

University College
and
Department of Earth Sciences
University of Oxford

The instantaneous relative plate motion vector for the Australian-Pacific plate pair (Smith 1981; DeMets 1990) indicates that the New Zealand plate boundary zone accommodates oblique convergence between the two plates. Overlying the subducted Pacific slab in the North Island this convergence is accommodated by slip on the subduction thrust offshore and by strain partitioning into an accretionary complex fold and thrust belt along the east coast and dextral strike-slip further inland. To the south the plate boundary zone passes though continental crust of the South Island with motion transferred to the transform Alpine Fault via a zone of dextral transpression known as the Marlborough Fault System.

Plate reconstructions indicate that the plate tectonic setting has changed through time with the clockwise rotation of the plate margin from NW to NE-trending, and of the relative plate motion vector from *ca.* SW to W-directed (eg:- Walcott 1984c). These changes suggest that the New Zealand plate boundary zone should contain early compressional structures followed by structures to accommodate oblique convergence.

The following geological features mark the onset of subduction of the Pacific plate beneath New Zealand in the Early Miocene *Waitakian* stage (*ca.* 24 Ma): andesitic volcanism, an abrupt change in sedimentation rate and character, and the start of a period of intense deformation. Kilometre-scale thrust faults with associated flysch, debris flow and olistrome deposits are described from the east coast of the North Island as far south as the northern end of the South Island. The direction of thrusting varies from north to south along the length of the plate boundary zone from landward to seaward to landward. The upper timing of this thrusting is constrained by unconformably overlying Middle Miocene aged sediments. The structures and sediments from this earlier phase of deformation and the overlying sediments are tilted and cut by a later post-Pliocene phase of deformation which continues to the present day. The variations in structural style of

this later phase are linked with variations in the rotational strain determined from palaeomagnetic analysis to reveal rotational 'domains'. In the last *ca.* 4 Ma during the later phase of deformation, *ca.* 20^{o} of clockwise rotation is recorded by extension of the Central Volcanic Zone in the far north and by rigid body rotations in sediments from the east coast and as far south as the Marlborough Fault System at the southern limit of the seismically active subducted Pacific slab. This rotation refects the changing motion of the subducting slab in the last *ca.* 4 Ma (Walcott 1978)

Within this study sedimentological and structural mapping, dating by foraminifera identification and palaeomagnetic analysis were used to describe the accommodation and evolution of strain within the Marlborough Fault System since the onset of subduction in the Early Miocene. A previously poorly understood complexly deformed area of Tertiary cover sediment (the Kekerengu-Washdyke subregion) on the downthrown side of one of the main Marlborough faults, the Kekerengu Fault, is unravelled in terms of its sedimentary and structural evolution. Two phases of deformation are recognized within this subregion, D_e and D_l. D_e consists of nine exposed kilometre-scale thrust faults repeating clastic sediments derived from extra and intra basinal uplift. The level of thrust detachment and synsedimentary nature of this thrusting is identified (chapter 2). Dating of the sedimentary units by foraminifera identification (chapter 3) revealed a Late Miocene unconformity separating thrust-derived debris flow deposits from overlying flysch sediments which are not cut by these thrusts. This unconformity provides an upper limit (*Kapitean*) to the age of D_e thrusting in this area.

A later phase of deformation, D_l, deforms the whole sedimentary pile including Pliocene aged rocks (chapter 4). A clear sequence of deformational events is identified (chapter 5), from oldest to youngest: (1) kilometre-scale folding about a NNE-trenfing fold axis with associated thrust and back thrust structures; (2) a second phase of kilometre-scale folding about a NW-trending fold axis; (3) oversteepening of one of the fold limbs and 'bending' of the two halves of the study area accommodated by displacement on a kilometre scale sinistral strike-slip fault; and (4) dextral (and minor sinistral) strike-slip and reverse faulting.

The NNE-trending folding (1) is consistent with compression associated with dextral shear between the Kekerengu and Hope Faults. The strike-slip and reverse faulting (4) is also consistent with this shear. However, the second phase of folding (2) and 'bending' of the two halves (3), cannot be explained by progressive shear within the dextral shear zone because of their orientation; another explanation is sought.

Previous palaeomagnetic work in Marlborough has revealed a post 3.9 ± 0.8 Ma regional *ca.* 20^{o} clockwise block rotation in sites from the Northern Marlborough Domain (that part of Marlborough overlying seismically active subducted Pacific plate with a steep Beniof Zone extension). In comparison, in the younger rocks within the Kekerengu-Washdyke study area, two previous sites indicated zero rotation in *ca.* 3 Ma rocks, and *ca.* 100^{o} of clockwise rotation in *ca.* 18 Ma rocks. This lack of the regional

rotation recorded elsewhere in northern Marlborough was previously unexplained and the large rotation interpreted as a localized Early Miocene event.

Palaeomagnetic sites analysed in this study (chapters 6 and 7) both confirm the lack of post-Pliocene D_1 rotation in the Kekerengu-Washdyke study area (ruling out progressive shear within the zone), and identify three more sites within the study area and three elsewhere in Marlborough which record a similarly large rotation (*ca.* 118 ± 11^{o}). The results suggest that the large clockwise rotation is in fact a regional event (rather than a localized Early Miocene event) which affected the whole Marlborough region between *ca.* 18 and 8 Ma, and also that the original orientation of D_e thrusting in this region was NW-trending and seaward, not landward-directed as was previously supposed. A site taken from dykes in the basement showed only the younger *ca.* 20^{o} regional rotation, indicating the presence of some kind of detachment surface separating rotating upper crust from unrotating crust below, or that the rotation did not extend to this area. The close association between the timing of this rotation and D_e thrusting leads to the suggestion that if a detachment surface is present, that this structure is likely to be a large scale thrust fault. The original orientation of D_e thrusts is perpendicular to the relative plate motion vector for the Early Miocene (Smith 1981). It is suggested that the rotation was due to pinning of the thrust pile to the south of the Marlborough region, (possibly against a structural high), and that its cause is related to the location of Marlborough in the hinge area at the southern end of the rotating Hikurangi Margin.

The lack of D_1 regional rotation on the downthrown side of the Kekerengu Fault is explained by the discovery of the second phase of folding (2) and 'bending' between the two halves of this area (3). The orientation of compression associated with (2) and (3) is as would be expected from compression behind the area due to rotation of the Northern Marlborough Domain 'block'. This indicates that the Kekerengu Fault has acted as the eastern boundary of the D_1 regional rotating block, explaining the more complex deformation of this area in comparison to deformation elsewhere in Marlborough where the rotational component of strain is accommodated by large scale block rotation.

Acknowledgements

I would like to thank Dr. S. Lamb for introducing the problems to be addressed within this thesis and for all his assisstance throughout the last three years and particularly with the writing-up process. Thanks too to Dr. E. McClelland, Dr. S. Allerton, Dr. R. Thomas and Brian Daniels for all their time and advice with problems arising during the processing of palaeomagnetic data; to Dr. S. Marshall of Southampton for help with vitrinite reflectance analysis; and to Prof. J. Dewey for supervision and ideas early on in the project.

I especially want to thank Simon and Rosa Chaffey of Kekerengu, New Zealand. The many months of field work involved in this project were greatly enhanced by their absolute kindness and generosity in giving me a room in their gorgeous home, in providing me with such wonderful distractions, and for accepting me as one of the family. Also to their sons Sandy and Daniel, and to all the locals of Kekerengu who were so friendly and accommodating to the 'English Rock Doctor on her beloved red motorbike'. I have many many fond memories of all my time in New Zealand which will always be a very special place to me.

Thanks too to Dick and Gen Walcott, Angela Jayko and Rodney Grapes for so kindly putting me up in their homes during my stay in Wellington.

During the last three and a half years my time in Oxford and Wellington would not have been so enjoyable without all my friends, collegues and house-mates: to Dan Bishop, Fizz and Jeff in Wellington; and to the Oxford bunch, especially to Malcs, Jules (what a voice!), both Petes, Halcyon, Niels, Sanjeev, John Burton, Simon Allerton, Jo and Andy Kirker, Mike Searle and Andy Jephcoat.

A "HUGE" thanks to my fiancee Richard Thomas for all your love and support throughout the last two years which kept me going through the tough times. Also for your help with lab work and for being such a patient pack-horse and driller on my third field season.

Finally to my family: to Dad, Mum, Julia and Emma, and to my dearest Grandparents, for all your letters and calls, and for being there for me.

The funding for this project including fieldwork expenses was provided by a three year postgraduate N.E.R.C. research grant. Field assistant expenses in my final year were provided by the Burdette Cootes Fund.

CONTENTS

Abstract..... i
Extended Abstract..... ii
Acknowledgements..... v
Contents..... vi
Figure List..... xii
Tables List..... xviii

1. Introduction..... 1

1.1 General Tectonic Setting 1
1.2 Short-Term Deformation 1
1.3 Long-Term Deformation 3
1.3.1 Finite rotation poles 3
1.3.2 The onshore geology of continental New Zealand 3
1.3.2.1 The Raukumara domain 5
1.3.2.2 The Wairoa domain 5
1.3.2.3 The Wairarapa domain 5
1.3.2.4 The Marlborough domain 5
1.3.2.5 The Nelson domain 7
1.4 Summary 8
1.5 Aims of Thesis 8

2. Stratigraphy..... 10

2.1 Overview of the General Stratigraphy 10
2.2 Descriptions of the Lithologies 12
2.2.1 The Limestone Sequence 12
2.2.2 The Lower Siltstone Sequence 14
2.2.3 The Conglomeratic Sequence 16
2.2.4 The Upper Siltstone Sequence 23
2.3 Linking the Observed Lithological Units with their New Zealand Nomenclature Equivalents 24
2.4 Corrolations of Stratigraphy Between Subregions of Marlborough and Northern Canterbury 26

Appendix to Chapter 2: Vitrinite Reflectance of Coals within the Conglomeratic Sequence

3. Micropalaeontology.....

3.1 Introduction
3.2 Criteria used for Sample Collection
3.3 Extraction and Identification of Foraminifera
3.4 The Results
3.5 Conclusions

Appendix to Chapter 3: Foraminifera Identification
Part A Foraminifera lists
Part B Key species lists and SEM photographs

4. Structural Data.....

4.1 Introduction
4.2 Structural Data from the Benmore Subregion
4.2.1 Introduction
4.2.1.1 The Waima River Locality
4.2.1.1 The Isolation Creek Locality
4.2.2 Conclusions
4.3 Presentation of Structural Data from the Kekerengu-Washdyke Subregion
4.3.1 Introduction
4.3.2 Faulting
4.3.2.1 Large-scale faulting
4.3.2.1a Post-tilt dextral strike-slip faults
4.3.2.1b Post-tilt strike-slip along tilted lithological boundaries
4.3.2.1c Other post-tilt faults
4.3.2.1d Syn and post-tilt reverse faults
4.3.2.1e Pre-tilt faults
4.3.2.2 Mesoscopic Faulting
4.3.3 Folding
4.3.4 Cleavages
4.3.4.1 Bedding parallel cleavages

4.3.4.2 Axial planar cleavages 83
4.3.5 Cross Sections 84

5. Structural Interpretation 85
5.1 Introduction 85
5.2 The Nature and Timing of D_e in the Kekerengu-Washdyke Study Area 85
5.2.1 The nature of D_e thrusting 85
5.2.2 The timing of D_e thrusting 85
5.2.3 Conclusion
5.3 The Nature, Timing and Evolution of D_l Structures in the Kekerengu-Washdyke Study Area 88
5.3.1 Evidence for D_l Structures 88
5.3.1.1 Evidence for D_l faulted contacts 88
5.3.1.2 Evidence for D_l folding 89
5.3.2 Reconstructing the sequence of D_l events 90
5.3.2.1 Changes in fold axes across the study area 90
5.3.2.2 Refolding of fold axes 91
5.3.2.3 Conclusion 92
5.3.2.4 The overall sequence of events during D_l 92
5.3.2.5 Controlling structures
5.3.4 Mesofaulting 96
5.4 Comparison of the Sedimentation and Structural Histories of the Kekerengu-Washdyke Study Area with Other Subregions of Marlborough 96
5.4.1 A Summary of the Stratigraphy of Other Subregions 96
5.4.2 Comparison of Structures from Other Subregions (the identification of D_e and D_l) 97
5.4.2.1 The Benmore subregion
5.4.2.2 The Cape Campbell-Ward subregion 97
5.4.2.3 The Lower Awatere Valley subregion 97
5.4.3 Summary 98

6. Palaeomagnetism and Tectonic Rotations 99

6.1 Introduction
6.1.1 Introduction to Tectonic Rotations 99
6.1.2 Palaeomagnetism and the Measurement of Tectonic Rotations 102
6.1.2.1 The origin of magnetization in rocks 102
6.1.2.2 Demagnetization 105

6.1.2.3 Data plotting and the interpretation of component directions from demagnetization data 106
6.1.2.4 Tectonic corrections 107
6.1.2.5 Stability tests 108
6.2 The Collection of Palaeomagnetic Data 110
6.2.1 Criteria for Drilling Locations 110
6.2.2 Sampling Equipment and Technique 111
6.2.3 Laboratory Equipment 112
6.3 The Presentation of Palaeomagnetic Sites Collected During this Study 113
6.3.1 The Awatere Dykes 113
6.3.1.a Geological setting, litholgy and age 113
6.3.1.b Demagnetization data for the Awatere Dykes 116
6.3.1.c Assessment of the magnetic carriers 117
6.3.1.d Timing of the magnetization 119
6.3.2 Woodside Creek Limestone 120
6.3.2.a Geological setting, lithology and age 120
6.3.2.b Demagnetization data for the Woodside Creek sites 122
6.3.2.c Assessment of the magnetic carriers 122
6.3.2.d Timing of the magnetization 123
6.3.3 The Ward-Cape Campbell Limestone Ridge 123
6.3.3.a Geological setting, lithology and age 123
6.3.3.b Demagnetization 124
6.3.3.c Remanence carriers 125
6.3.3.d Timing of the magnetization 125
6.3.4 Heavers Creek Site (HC3) 126
6.3.4.a Geological setting, lithology and age 126
6.3.4 b Demagnetization 127
6.3.4.c Remanence carriers 127
6.3.4.d Timing of the magnetization 128
6.3.5 Heavers Creek Sites (HC1 and HC2) 128
6.3.5.a Geological setting, lithology and age 128
6.3.5.b Demagnetization 129
6.3.5.c Remanence carriers 129
6.3.5.d Timing of the magnetization 130
6.3.6 Valhalla Creek Sites (VC1 and VC2 130
6.3.6.a Geological setting, lithology and age 130
6.3.6.b Demagnetization 131
6.3.6.c Remanence carriers 132
6.3.6.d Timing of the magnetization 132

6.3.7 Woodbank Stream Site (WB1/2/3) 132
6.3.7.a Geological setting, lithology and age 132
6.3.7.b Demagnetization 133
6.3.7.c Remanence carriers 14
6.3.7.d Timing of the magnetization 134
6.3.8 Washdyke Stream Sites (WD1 and WD2) 134
6.3.8.a Geological setting, lithology and age 134
6.3.8.b Demagnetization 136
6.3.8.c Identification of the remanence carriers 136
6.3.8.d Timing of the magnetization 137
6.3.9 Washdyke Stream Site (WD3) 138
6.3.9.a Geological setting, lithology and age 138
6.3.9.b Demagnetization 138
6.3.9.c Remanence carriers 138
6.3.10 Silver Springs Site (SS1&2) 139
6.3.10.a Geological setting, lithology and age 139
6.3.10.b Demagnetization 140
6.3.10.c Remanence carriers 140
6.3.10.d Timing of the magnetization 140
6.4 Summary of the Remanence Carriers for all Sites 141
6.5 The Stratigraphic Thickness of Each Site 141

7. Palaeomagnetic Data Interpretation 151

7.1 Introduction 151
7.2 Tectonic Correction of Mean Site Vectors 152
7.2.1 Tectonic correction of sites outside the Kekerengu-Washdyke study area 152
7.2.2 Tectonic correction of sites from within the Kekerengu-Washdyke study area 154
7.3 Checking the Declination and Inclination of the Tectonically Corrected Mean Site Vectors 155
7.3.1 The Awatere Dykes 155
7.3.2 The Woodside Creek sites 158
7.3.3 The Boo Boo Stream site 160
7.3.4 HC3 161
7.3.5 HC1 161
7.3.6 HC2 161

7.3.7 VC2 161
7.3.8 WB 163
7.3.9 WD1-WD2 163
7.3.10 SS1&2 163
7.3.11 Summary 163
7.4 Fold Tests 163
7.4.1 Sites from this study 163
7.4.2 Sites from this study and from previous sites in Marlborough 164
7.5 Tectonic Rotations in Marlborough 165
7.5.1 The spatial and temporal distribution of rotational strain in Marlborough 165
7.5.2 The nature, timing and bounding structures of tectonic rotations in Marlborough 166
7.5.3 Implications for the orientation of D_e structures 168
7.5.4 D_1 structures and tectonic rotation in the Cape Campbell-Ward subregion 168
7.5.5 Overall implications for complex deformation in the Kekerengu-Washdyke study area 169

8. Conclusions 170
8.1 Introduction 170
8.2 Conclusions from this Study 172
8.2.1 The Sedimentary Evidence 172
8.2.2 The Structural Evidence 172
8.2.3 The Palaeomagnetic Evidence 174
8.3 The Incorporation of these Results into the Evolving New Zealand Plate-Boundary Zone 175
8.4 Summary 177
8.5 Suggestions for Future Work 178

References 179

FIGURE LIST

Chapter 1

Fig. 1.1: (a) Tectonic setting of the Hikurangi Margin with (b) cross section showing how strain accommodating the oblique convergence is partitioned into areas of strike-slip and compression.

Fig. 1.2: (a) Generalized maps of shear strain rates and velocities for New Zealand.
(b) Relative position of the Australian and Pacific plates at 20, 10 and 0 Ma.

Fig. 1.3: Map of New Zealand showing the main structural features and rotation domains.

Fig. 1.4: Simplified geological map of the Marlborough region.

Fig. 1.5: Simplified geological map of the Marlborough region showing the location of all previous palaeomagnetic sites.

Fig. 1.6: Mechanical model for the Marlborough domains.

Fig. 1.7: Simple mechanical models to explain the second order rotation between the Awatere and Clarence Faults.

Fig. 1.8: Reduced copies of the Kekerengu and Washdyke map sheets.

Chapter 2

Fig. 2.1: Simplified log of the Upper Cretaceous to Pliocene stratigraphy of Marlborough.

Fig. 2.2: Sketch map of limestone exposures within the Kekerengu-Washdyke study area.

Fig. 2.3: Stratigraphic logs of limestone lithologies within the Kekerengu-Washdyke study area.

Fig. 2.4: Sketch map of Lower Siltstone exposures within the Kekerengu-Washdyke study area.

Fig. 2.5: (a) Deformed limestone pebbles in the Lower Siltstone Sequence.
(b) Slump folds in turbiditic beds of the Conglomeratic Sequence.

Fig. 2.6: Sketch map of conglomerate exposures within the Kekerengu-Washdyke study area. Also showing location positions and simplified stratigraphic logs of sequences including conglomerate.

Fig. 2.7: (a) Photograph of Type 2 conglomerate
(b) Photograph of Type 6 conglomerate
(c) Photograph of limestone boulder within Type 4 conglomerate

Fig. 2.8: Stratigraphic log of the Washdyke Gorge Sequence.

Fig. 2.9: Sketch map of Upper Siltstone exposures within the Kekerengu-Washdyke study area.

Fig. 2.10: Summary of the age span of each of the lithological sequences from the Kekerengu-Washdyke study area (using New Zealand nomenclature).

Fig. 2.11: Summary of the Tertiary stratigraphies of each of the Marlborough subregions.

Fig. 2.12: Summary of uplift and subsidence in each of the Marlborough subregions.

Fig. 2.13: (a) Photograph of coal fragment within Type 2 conglomerate.
(b) Sketch map showing the location of the five coal samples collected for vitrinite reflectance analysis.

Chapter 3

Fig. 3.1: Paleocene and Neogene time scales for New Zealand.

Fig. 3.2: The age span of each dated sample from the Kekerengu-Washdyke study area.

Chapter 4

Fig. 4.1: (a) The division of Marlborough into subregions with enlargement of the Benmore subregion showing Waima River and Isolation Creek localities.
(b) The extent of lithological units at the Waima River locality.

Fig. 4.2: (a) Photograph of the Waima River shear zone (unit 1).
(b) Photograph of thrust fault from the Waima River locality.

Fig. 4.3: Stereoplots of fault planes, slickenside surfaces and lineations from the Waima River locality.

Fig. 4.4: Stereoplots of fold data from the Waima River locality.

Fig. 4.5: Structural elements from the Isolation Creek locality.

Fig. 4.6: Line drawing of the Isolation Creek locality.

Fig. 4.7: Sketch map of the Kekerengu-Washdyke study area with labelling (1 to 30) of the large-scale faults.

Fig. 4.8: Topographic contours from the Kekerengu-Washdyke study area with the position of the Kekerengu and Heavers Creek Faults.

Fig. 4.9: Sketch map showing features relating to the Kekerengu and Heavers Creek Faults.

Fig. 4.10: Sketch maps showing features relating to Faults 10, 11, 15, 30a and 30b.

Fig. 4.11: Sketch map showing features relating to Faults 16, 17, 18, 19, 20 and 23.

Fig. 4.12: Sketch maps showing features relating to Faults 1, 2, 3 and 4.

Fig. 4.13: Photograph of deformed smectitc mudstone from Fault 8.

Fig. 4.14: Line drawing of Fault 17 shear zone.

Fig. 4.15: (a) Sketch map showing features relating to Fault 19.
(b) Stereographic projections of restored beds at Fault 19.

Fig. 4.16: Sketch maps showing features relating to Faults 16, 20, 21, 22, 23, 25 and 26.

Fig. 4.17: Sketch map of the Kekerengu-Washdyke study area showing the position of subareas from which mesoscopic faults are described.

Fig. 4.18: Stereographic projections of mesoscopic faulting in subareas 1, 2, 4 and 5.

Fig. 4.19: Line drawing of left-lateral shear zone in Waitakian Marl along the Chaffey Fault.

Fig. 4.20: Stereographic projections of mesoscopic faulting in subareas 4 and 6.

Fig. 4.21: Plan view showing the sinistral strike-slip component of reverse faults in Amuri Limestone at Fault 17.

Fig. 4.22: Line drawing of thrust fault cutting Amuri Limestone beds at Waipapa bay.

Fig. 4.23: Sketch map of the Kekerengu-Washdyke study area showing fold data from each of the fold subareas.

Fig. 4.24: Photograph of crenulations folding an earlier bedding parallel fissility in the hinge of the Razor Fold.

Fig. 4.25: Sketch map showing features relating to the autochthonous limestone extending from the southern part of the Washdyke map sheet to Waipapa Bay.

Fig. 4.26: (a) Scaled line drawing of box folding in Amuri Limestone at Waipapa Bay.
(b) Stereographic projection showing the principal stress directions determined from box folding at Waipapa Bay.

Fig. 4.27: (a) Photograph of anastomosing marl seams in limestone from the Kekerengu-Washdyke study area
(b) Line drawing of pre-lithificational compaction and extension seen in thin section in Waitakian Marl from the Kekerengu-Washdyke study area.

Fig. 4.28: (a) Photograph of high angle to bedding cleavage in Amuri Limestone at Waipapa Bay.
(b) Stereographic projections showing fold data from box folds in Amuri Limestone at Waipapa Bay.

Fig. 4.29: (a) Photograph of fracture cleavage in turbiditic beds of the Kekerengu-Washdyke study area.
(b) Location and vergence from bedding of all examples of fracture cleavage found within the Kekerengu-Washdyke study area.

Chapter 5

Fig. 5.1: Stratigraphic columns of the pre-D_1 sedimentary sequence in the Kekerengu-Washdyke study area.

Fig. 5.2: Cartoon sketches of D_e thrust positions and nature of synsedimentary thrusting.

Fig. 5.3: Block diagram showing formation of the Razor Fold Syncline.

Fig. 5.4: Sketch map of area between the Kekerengu and Hope Faults showing D_1 structures relating to text.

Fig. 5.5: Stereographic projection of fold axes from the Kekerengu-Washdyke study area showing refolding about a NW-trending fold axis.

Fig. 5.6: Sketch of a plasticine model of the final fold form after subjection to two phases of folding.

Fig. 5.7: Sequence of sketches showing the evolution of D_1 structures affecting the area between the Hope and Kekerengu Faults.

Fig. 5.8: (a) Line drawing of episode (3) of D_1 in the Kekerengu-Washdyke study area.
(b) 'Bending' between the two map sheets with displacement along Fault 15.

Fig. 5.9: Geological map and cross-section of the Benmore subregion showing D_e thrusts cutting up-section.

Fig. 5.10: Sketch of the Benmore subregion to show the three-dimensional geometry of the D_e thrust stack prior to D_1 tilting.

Fig. 5.11: Three-dimensional diagram of D_1 deformation in the Benmore and Kekerengu-Washdyke subregions.

Fig. 5.12: Schematic block diagram of synsedimentary D_e thrusting in the Marlborough region.

Fig. 5.13: Stereographic projections of fabrics from Fault 19 showing pre-tilt D_e thrust transport direction.

Fig. 5.14: Expected orientations of mesoscopic fault types within an ENE-trending dextral shear zone.

Fig. 5.15: Cartoon cross-section showing Miocene uplift and subsidence in the Marlborough region.

Chapter 6

Fig. 6.1: Stereographic plots of poles to Awatere Dyke margins pre- and post-tectonic correction.

Fig. 6.2:Geological map of the Middle Awatere Valley.

Fig. 6.3: Thermal demagnetization and mean high temperature component of site GS1.

Fig. 6.4: Thermal demagnetization and great circle analysis of site WS1.

Fig. 6.5: Alternating field demagnetization and great circle analysis of site GS1.

Fig. 6.6: Alternating field demagnetization and great circle analysis of site WS1.

Fig. 6.7: Geological map of the Flags Creek Thrust Duplex and location of sites WC1 and WC2.

Fig. 6.8: Thermal demagnetization and mean high temperature component of site WC1.

Fig. 6.9 Thermal demagnetization and mean high temperature component of site WC2.

Fig. 6.10 Geological map of the Ward-Cape Campbell subregion with location of palaeomagnetic sites.

Fig. 6.11: Thermal demagnetization and mean high temperature component of site BB1&2.

Fig. 6.12: Bulk susceptibility and IRM graphs for sites GS1, WS1, WC2 and BB1&2.

Fig. 6.13: Photomicrographs of sampled lithologies at sites (a) WC1, (b) WB1 and (c) WD1.

Fig. 6.14: Sketch map of the Kekerengu-Washdyke study area showing location of all palaeomagnetic sites.

Fig. 6.15: Thermal demagnetization, mean high temperature component, bulk suseptibility and IRM graphs for site HC3.

Fig. 6.16: Thermal demagnetization, great circle analysis and bulk susceptibility for site HC1.

Fig. 6.17: Thermal demagnetization, great circle analysis and bulk susceptibility for site HC2.

Fig. 6.18: Thermal demagnetization and great circle analysis for site VC2.

Fig. 6.19: Thermal demagnetization and great circle analysis for site WB.

Fig. 6.20: Thermal demagnetization and mean high temperature components for sites WD1 and WD2.

Fig. 6.21: Alternating field demagnetization and mean high temperature component for site WD1.

Fig. 6.22: Bulk susceptibility and IRM graphs for sites VC1, VC2, WB, WD1 and WD2.

Fig. 6.23: Thermal demagnetization, mean high temperature component and bulk susceptibility for site WD3.

Fig. 6.24: Thermal demagnetization, great circle analysis, bulk susceptibility and IRM graphs for site SS1&2.

Chapter 7

Fig. 7.1: Graphs of observed palaeolatitude against age and expected palaeolatitude.

Fig. 7.2: (a) Stereographic projections of all Marlborough palaeomagnetic sites pre and post tectonic correction.
(b) Stereographic projections of all Marlborough palaeomagnetic sites post tectonic correction showing division into three groups.

Fig. 7.3: Stratigraphic columns showing the position of declination anomalies within separate sedimentary sequences of Marlborough.

Fig. 7.4: Geological map of Marlborough showing the position and mean site declination with declination error for all palaeomagnetic sites in Marlborough.

Fig. 7.5: Geological maps of Marlborough showing the spatial extent of each tectonic rotation within the two identified separate time intervals.

Fig. 7.6: D_1 structural map of NE Marlborough showing the continuation of dextral shear from the 'termination point' of the Clarence Fault.

Fig. 7.7: Cartoon sketch diagrams showing D_{12} buckling and D_{13} 'bending' in the Kekerengu-Washdyke subregion, due to the clockwise rotation of the rest of northern Marlborough.

Chapter 8

Fig. 8.1: Instantaneous pole positions for the Australian-Pacific plate pair at 20 Ma, 5 Ma and the present-day.

Fig. 8.2: Schematic block diagram showing the general sedimentary environment of the Marlborough region during D_e.

Fig. 8.3: Series of plate reconstructions showing the palaeogeographical and structural evolution of the New Zealand plate boundary zone, with the additional conclusions of this study.

TABLES

Chapter 2

Table 2.1: Characteristics of each location within the conglomeratic sequence.

Table 2.2: Results of vitrinite reflectance analysis.

Table 2.3: General corrolation between vitrinite reflectance, burial depth and temperature.

Chapter 4

Table 4.1: The Fault numbers within each large scale fault type found in the Kekerengu-Washdyke study area.

Table 4.2: Summary of mesoscopic fault trends within the Kekerengu-Washdyke study area.

Chapter 5

Table 5.1: A summary of the sequence of structural events affecting the Kekerengu-Washdyke study area.

Table 5.2: The orientation of D_e foliations and lineations after removal of D_1 tilt and plunge.

Chapter 6

Table 6.1: Summary of ferromagnetic mineral characteristics.

Table 6.2: Chemical analysis of Awatere Dykes.

Table 6.3: Ages from Grapes et al (1992) corresponding to cores from the Gladstone Stream and Winterton River sites.

Table 6.4: Nitrogen treatment data for sites GS1 and WS1.

Table 6.5: Summary of the remanence carriers from all sites

Table 6.6: Thickness of sediment and corresponding age span sampled at all sites.

Chapter 7

Table 7.1: Tectonic correction of sites WC1 and WC2.

Table 7.2: Tectonic correction of sites GS1 and WS1.

Table 7.3 (a) and (b): Summary of the palaeomagnetic site data including tectonic corrections and declination anomalies for all sites collected in this study.

Table 7.4: The declination and inclination errors and the spread in palaeolatitude of all sites collected in this study.

Table 7.5: Virtual and finite poles used in the calculation of the expected declination and inclination of the Awatere Dykes.

Table 7.6: The expected and obserbed declination and inclination for the Awatere Dykes.

Table 7.7: Virtual and finite poles used in the calculation of the expected declination and inclination of the Woodside Creek Limestone.

Table 7.8: The expected and obserbed declination and inclination for the Woodside Creek Limestone.

Table 7.9: Results of the McElhinney (1964) Fold Test for all palaeomagnetic sites in Marlborough.

CHAPTER 1

CHAPTER 1: INTRODUCTION

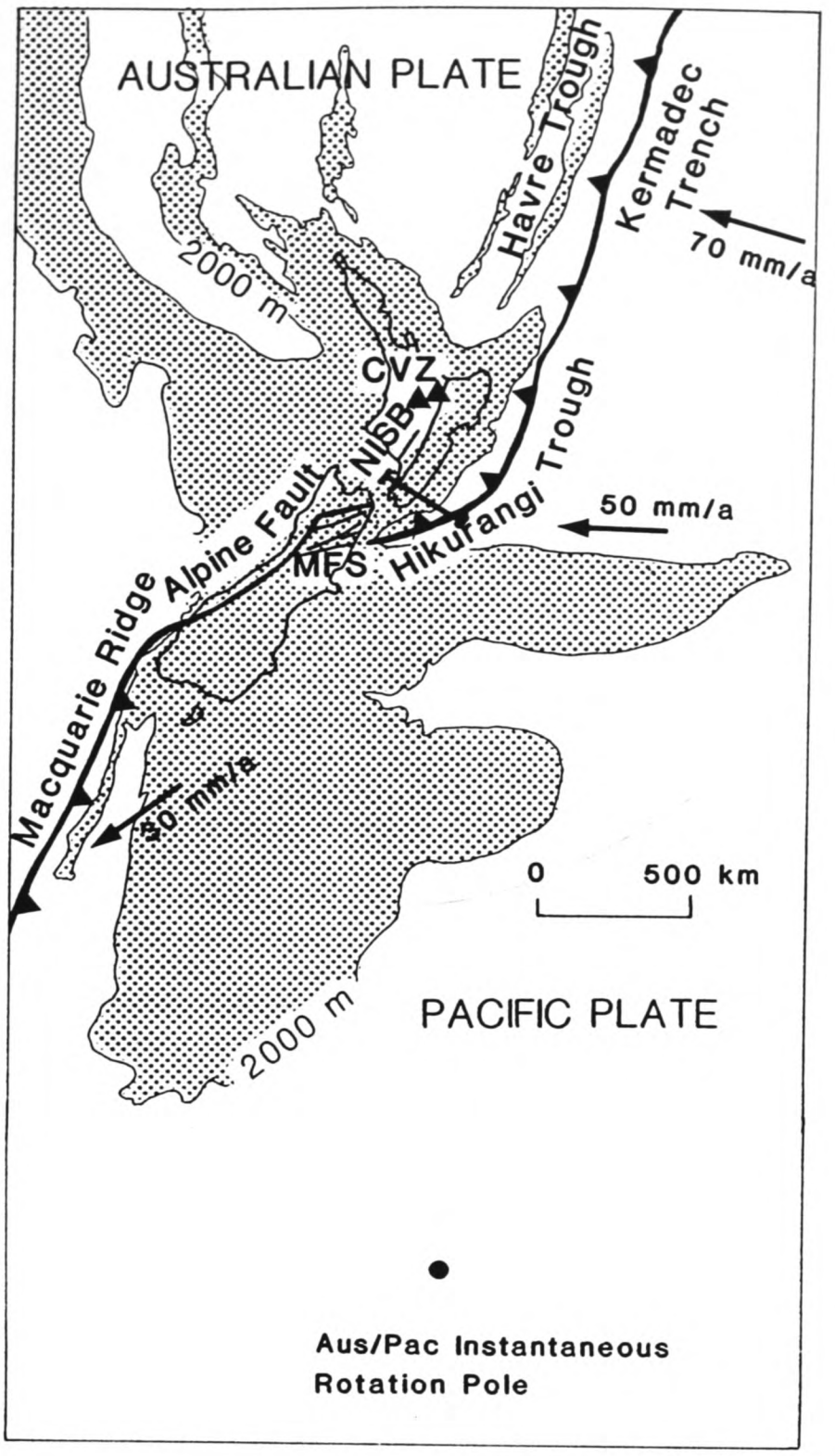
1.1 General Tectonic Setting

The region of New Zealand continental crust (defined by the 2000 m isobath, see fig. 1.1) lies astride the Australian-Pacific plate boundary in the southwest Pacific (Le Pichon 1968). The plate boundary through New Zealand changes significantly along its length. To the north the Pacific plate is subducted westward beneath Australian plate in the Tonga-Kermadec subduction zone, which continues offshore along the east coast of New Zealand's North Island where it is known as the Hikurangi Margin. Back arc extension in the Harvre Trough behind the volcanic arc (Weissel et al 1977; Malahoff et al 1982) extends into the northern part of the North Island. The region of onshore extension is known as the Central Volcanic Zone (Ballance 1988). Subduction along the plate boundary becomes markedly less important in the northern part of the South Island where a transform fault zone known as the Marlborough Fault System (Lensen 1962) separates continental rocks on both sides. It comprises five major faults (the Wairau, Awatere, Clarence, Kekerengu and Hope Faults, Lensen 1962) linking the subduction zone to a major intracontinental dextral transform fault, the Alpine Fault (Wellman 1952, 1964; Carman 1968). There is a change in the general trend of the Marlborough Faults to the south from *ca.* 055^{o} to *ca.* 070^{o} which was thought to coincide with the end of the seismically active subducting Pacific slab (Walcott 1979; Ansel and Adams 1986). However, improved seismograph coverage (Anderson et al 1993) has shown that the Benioff zone has similar dip in transects perpendicular to the margin to both sides of this dividing line, although at depths of below *ca.* 100 km the NE section has a steeply dipping extension to depths of *ca.* 250 km, whereas the SW section appears to terminate abruptly. Further south and offshore, motion along the Alpine Fault is transferred to the Macquarie Ridge subduction complex (McKenzie and Morgan 1969; Hayes et al. 1972) and ultimately to the Antarctica-Australian-Pacific triple junction (Falconer 1972).

1.2 Short-Term Deformation

The instantaneous plate motion for the Australian-Pacific plate pair has been computed by Chase (1978), Minster and Jordan (1978) and DeMets (1990). The most up-to-date of these, DeMets (1990), uses sea floor spreading rates (determined over the last 3 Ma), transform fault trends and earthquake slip vectors to determine a new global model (NUVEL-1) describing the geologically current motion between twelve

(a)



(b)

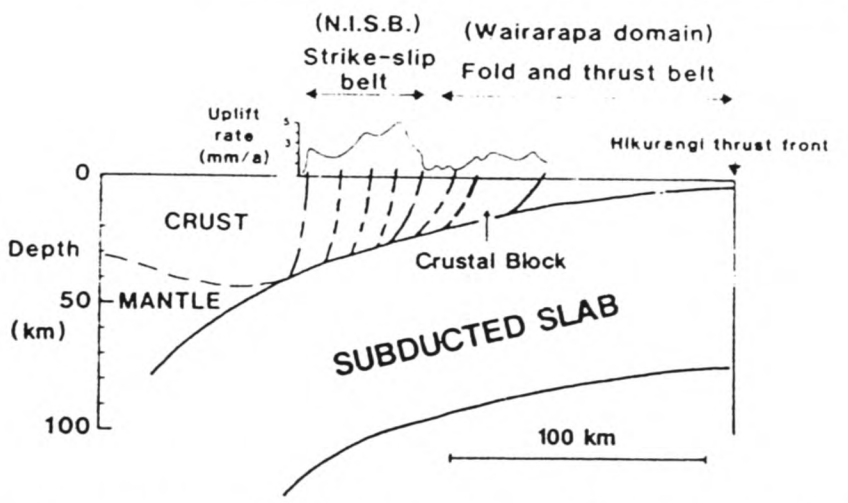


Fig. 1.1: (a) Map showing the tectonic setting of the Hikurangi Margin at the southern end of the Tonga-Kermadec subduction zone. The 2000 m isobath is taken to define the limits of continental and oceanic lithosphere (areas of continental crust are stippled). The main structural features of the plate boundary zone are shown, including: The Central Volcanic Zone (CVZ); The North Island Shear Belt (NISB); and the Marlborough Fault System (MFS). Also shown is the Australian-Pacific instantaneous pole of relative plate motion (DeMets 1990) and some velocities for the Pacific Plate relative to the Australian Plate. (b) Vertical cross-section through the plate boundary zone at the southern end of the North Island (line of section shown in (a)). This shows division into a fold and thrust belt accommodating motion perpendicular to the plate boundary zone, and a strike-slip belt (NISB) which is accommodating the parallel component. After Lamb (1988).

assumed-rigid plates. The results of this work in terms of the predicted convergence rate and direction of convergence for the Australian-Pacific plate boundary are as follows. To the north of New Zealand along the Tonga-Kermadec Trench (35°S/181°E) the predicted convergence rate is 53±1 mmy^{-1} and the direction of motion is at 88±1°. At the northern end of the South Island (41.5°S/172°E) the predicted rate is 42±1 mmy^{-1} directed at N75±2°E. Further south along the Alpine Fault (43.5°S/170°E) the predicted rate is 39 mmy^{-1} directed at N71°E.

All these features along with the general tectonic setting of New Zealand are summarized in fig. 1.1.

Geodetic Studies

Further insight into the short-term deformation of New Zealand comes from geodetic studies. Triangulation networks were first set-up in New Zealand in the late 1800's, and many more since. By measuring the changes in the angles between network stations within the past *ca.* 100 years, shear strain rates and instantaneous velocities throughout the deforming zone can be computed (Frank 1966; Bibby 1981; Haines 1982; Walcott 1978a, 1978b, 1984, 1987). Fig. 1.2a summarizes the pure and simple shear components of this instantaneous strain. These figures clearly pick out the dominant kinematic features in a wide area defined as the axial tectonic belt (Walcott 1978). Extension in the north (negative pure shear strain) produces a southeast directed velocity component of the Australian plate with respect to a fixed Pacific plate. This extension is manifest as normal faulting in the Central Volcanic Zone, the onland extension of back arc spreading in the Havre Trough. To the east, dextral strike-slip (positive simple shear) is indicated. Dextral strike-slip faulting is observed down the length of the North Island (the North Island Shear Belt). Local extension along the east coast of the North Island has been interpreted as a result of underplating causing thickening of the Australian crust and inducing surface extension (Walcott 1987). Further south, in the north of the South Island the strain rates indicate a significant component of shortening perpendicular to the plate boundary zone. The inferred instantaneous velocity at the subduction zone here is close to zero. Walcott (1978b) proposed a model of locked subduction in this part of the plate boundary zone which is in marked contrast to the large southeast directed instantaneous velocity in the north of the Hikurangi Margin. Walcott (1989) suggested that this difference is causing a clockwise rotation of the Australian plate margin with respect to the Pacific plate at *ca.* 7° /Ma.

Bibby (1981) integrated short-term strain rates to calculate the instantaneous velocity of the Australian relative to the Pacific plate in the northern part of the South Island. His results suggested a convergence rate of 54±9 mmy^{-1} directed at 84±10°. These values are more-or-less consistent with those of DeMets (1990). This supports

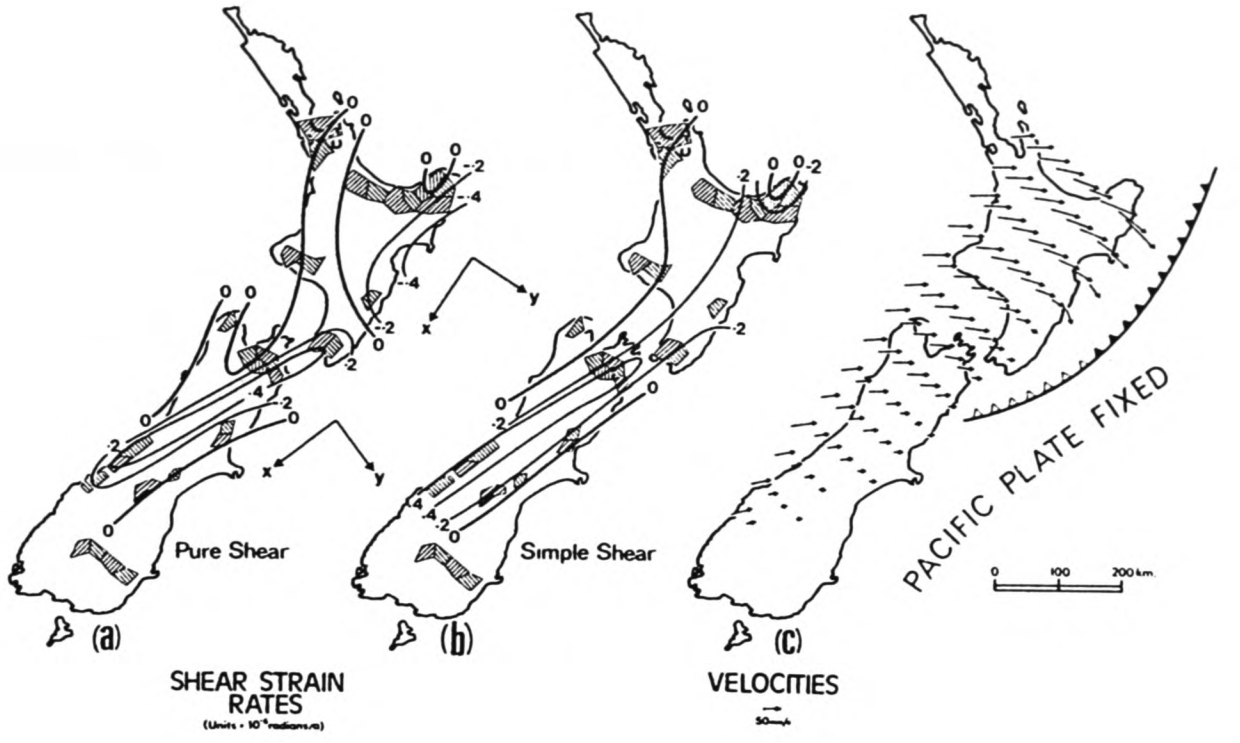


Fig. 1.2a: Generalized maps of (a) and (b) the shear strain rates from repeated geodetic data, and (c) the velocities determined from the shear strain rates by integration holding the Pacific plate fixed. Diagram from Walcott (1978, 1989).

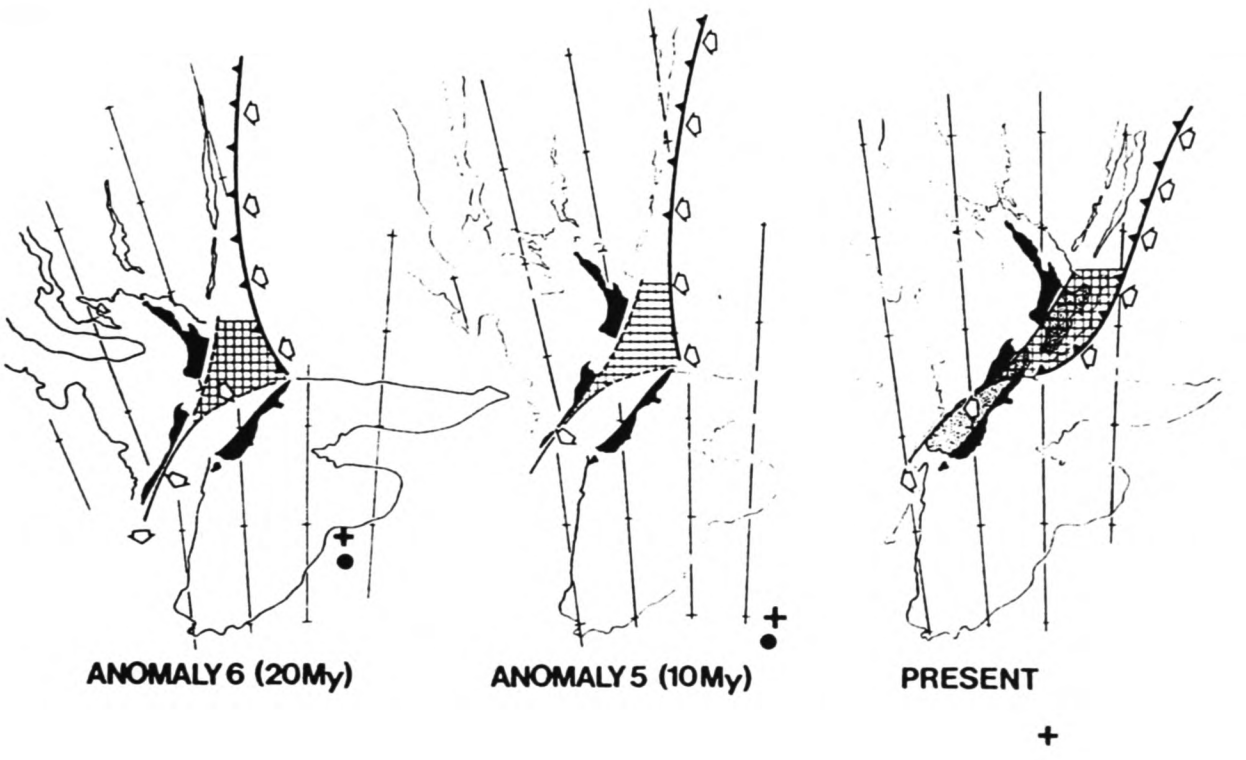


Fig. 1.2b: The relative position of the Australian and Pacific plates marked by the present day latitude and longtitude grid with present day coastlines and 2000 m isobaths. The gridded area in the plate boundary zone is the Hikurangi Margin. The Pacific plate is held fixed. These reconstructions show that the Australian plate has rotated *ca.* 20^{o} clockwise with respect to the Australian plate since anomaly 6 time. Diagram from Walcott (1978, 1989).

the locked subduction zone model for this region, with all the relative plate motion taking place on-shore in the vicinity of the triangulation networks.

1.3 Long-Term Deformation

As well as the short-term and instantaneous relative motions of the Australian-Pacific plate pair, the long-term tectonic history of this plate boundary zone can also be determined. There are two ways of observing this evolution: (1) by studying sea floor magnetic anomalies and transform faults to produce finite poles of rotation which describe the changing relative motion of the plate pair; or (2) by studying the onshore geology.

1.3.1 Finite Rotation Poles

Finite rotation poles have been calculated for New Zealand (Christoffel and Falconer 1972; Molnar et al. 1975; Weissel et al. 1976; Stock and Molnar 1987) for magnetic anomalies 13 to 5 (from Late Eocene to Late Miocene times). Sea floor magnetic anomalies suggest that the plate boundary through New Zealand formed in the Late Eocene (Stock and Molnar 1987). In contrast, Kamp (1987) using limestone sedimentological changes, places the plate boundary formation at the Oligocene-Miocene boundary. This discrepancy may be a result of motions between East and West Antarctica which have not been taken into account in most models of relative plate motion (Kamp 1987). These motions have yet to be resolved. Walcott (1978) observed a noticeable change in the direction of relative plate motion before and after anomaly 6 time. This change occurs at *ca.* 24 Ma, the beginning of the Miocene epoch, and naturally has a very important effect on the style of deformation within the plate boundary zone (see (2)).

Reconstructions of the New Zealand plate boundary zone based on sea floor spreading data back to *ca.* 18 Ma were made by Walcott (1989), see fig. 1.2b. These clearly show a clockwise rotation of the whole Hikurangi Margin with respect to the Pacific plate. This is in agreement with the short-term velocity data in fig. 1.2a.

1.3.2 The Onshore Geology of Continental New Zealand

The onshore geology of continental New Zealand holds the evidence for the geological events within the plate boundary zone. Detailed sedimentological and structural mapping, including the accurate dating of lithological units, can help to elucidate these events. In addition, the technique of palaeomagnetism can be used to observe the rotational component of strain, which is very difficult to detect by mapping alone.

Prior to and during initiation of the plate boundary zone, passive margin limestone facies of *M. Haumurian* to *Waitakian* age (Morris 1987) were deposited over New Zealand. This limestone Group is known as the Amuri Limestone and unconformably overlies deformed basement material of Triassic to Upper Cretaceous age (Suggate et al 1978). By the early Miocene (*ca.* 24 Ma) this mostly pelagic limestone is interbedded with marls and known as the Waitakian Marl (Suggate et al 1978; Kirker 1989). Overlying these marls is an up to *ca.* 2 km thick sequence of massive and turbiditic siltstones and debris flow conglomerates, deposited throughout the Early and Middle Miocene (Lewis et al. 1980; Osborne 1980; Charnier and Ferriere 1992). Clasts are both extra- and intra-basinally derived. Breccias and melanges associated with large-scale thrust sheets of intra-basinal Tertiary cover sediment are also described from within this period (Pettinga 1982; Van der Lingen 1982; Lamb and Bibby 1989; Charnier and Ferriere 1992). These beds are overlain by Pliocene siltstones.

The change from biogenic to clastic sedimentation throughout the plate boundary zone coincides with the change in plate configuration revealed by the long term finite rotation poles (*ca.* 24 Ma in the northern South Island and *ca.* 18 Ma in the North Island). These sediments are therefore ascribed to tectonic activity associated with the onset of subduction of the Pacific slab in the Early Miocene (Sporli 1980; Pettinga 1982; Van der Lingen 1982; Lamb and Bibby 1989; Rait et al. 1991).

The deformation of the sediments themselves within the axial tectonic belt also records the accommodation of strain produced during the convergence of the Australian and Pacific plates. Miocene thrust faults are identified (Lamb and Bibby 1989; Charnier and Ferriere 1992) as well as Post-Pliocene folding and strike-slip faulting (Lensen 1962; Sporli 1980). The main structural features are summarized in fig. 1.1.

Extensive normal faulting and volcanism are found in the onland extension of the Harvre Trough. This volcanism began at 21-22 Ma (Ballance 1988). Along the length of the North Island, strain appears to be partitioned into thrusting and folding along the east coast, uplifting the Coastal ranges, and dextral transcurrent faulting (along the North Island Shear Belt) further inland in the North Island Axial Ranges (Sporli 1980). At the northern end of the South Island, basement and Tertiary cover are folded and cut by movements on the dextral transcurrent faults of the Marlborough Fault System (Lensen 1962). Further south motion is transferred to the dextral transcurrent Alpine Fault causing uplift of the Southern Alps and *ca.* 460 km of dextral displacement (Wellman 1964; Carman 1968).

Palaeomagnetic work within the plate boundary zone has provided evidence of the rotational component of strain. This data together with observations of structural deformation within the axial tectonic belt led to the division of New Zealand into seven domains each consisting of single or clusters of crustal blocks which have similar

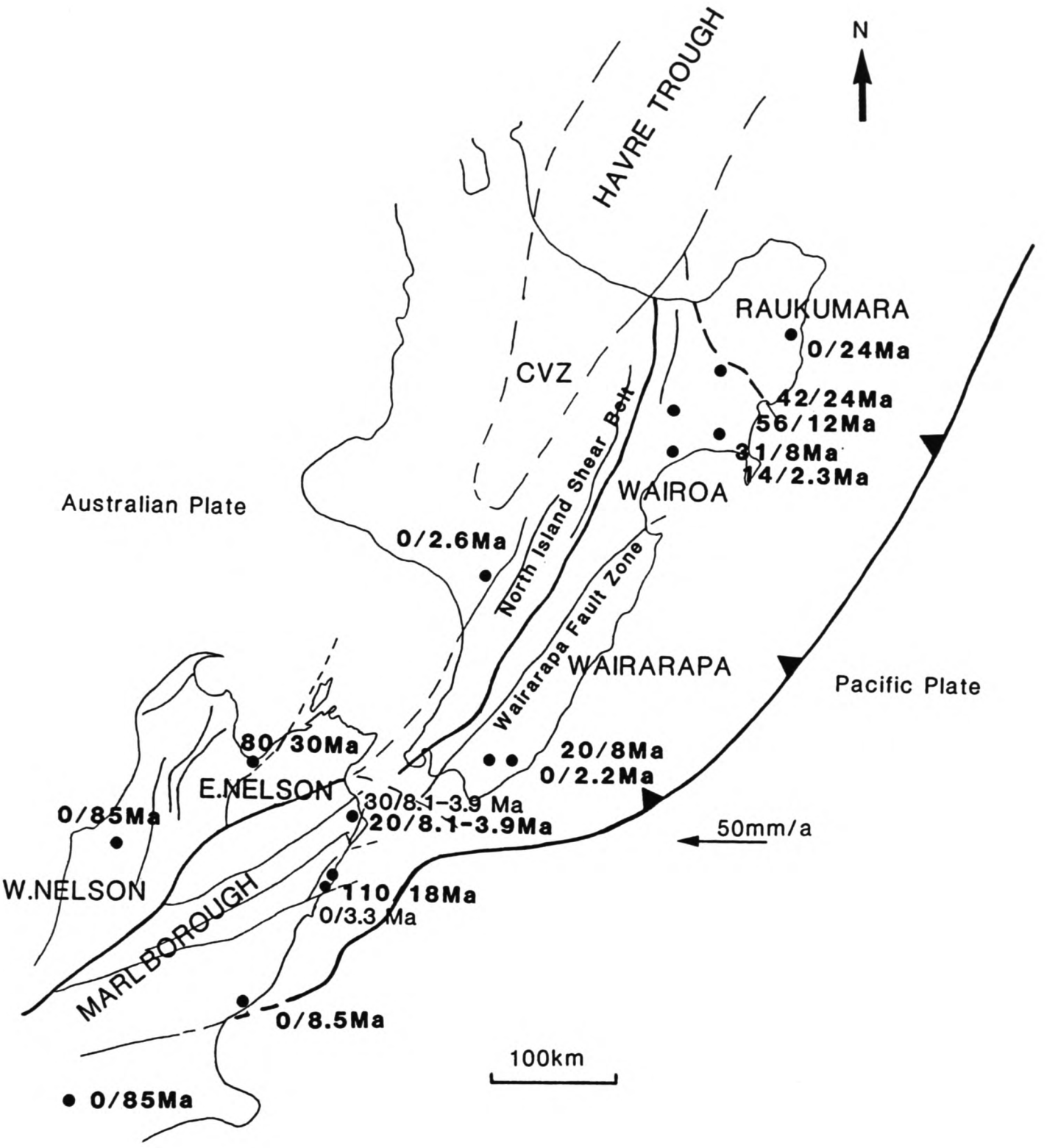


Fig. 1.3: Map of the northern part of the New Zealand plate boundary zone showing the major structural features and rotation domains (refer to section 1.3.2). The velocity vector for the Pacific relative to the Australian plate is shown, as are palaeomagnetic sample localities (black dots) and approximate clockwise rotations about vertical axes in each domain. All rotations are relative to the Australian plate except for those in the Marlborough domains which are with respect to the Pacific plate. This figure is based on a diagram in Lamb (1988). Palaeomagnetic sample data references are listed in the appropriate domain descriptions of section 1.3.2.

rotation histories (Lamb 1988). The boundaries to the domains are marked by narrow zones of deformation which are poorly constrained and which have generally not been palaeomagnetically sampled. The location and palaeomagnetic data from each of these domains is summarized in fig. 1.3. Brief descriptions of each domain follow, including a more detailed description of the Marlborough domain.

1.3.2.1 The Raukumara Domain

This domain is deformed by a complex arrangement of Neogene normal faults. These are believed to be a result of gravitational body forces in the cover rocks and not to horizontal deformation in the basement (Lamb 1988) due to the evidence for internal rigidity in this region (Yoshikawa et al 1980; Walcott 1984a). Palaeomagnetic work has revealed no rotation of this domain in the last *ca.* 20 Ma (Walcott and Mumme 1982; Mumme et al 1989). This domain has only translated during the opening of the Harvre Trough.

1.3.2.2 The Wairoa Domain

This domain consists of a broad NNE-trending syncline. Palaeomagnetic sites from this domain indicate *ca.* 20^{o} of clockwise rotation in the last *ca.* 4 Ma (Walcott and Mumme 1982; Mumme and Walcott 1985; Wright and Walcott 1986).

1.3.2.3 The Wairarapa Domain

This domain consists of a post-Pliocene NE to NNE-trending fold and thrust belt. It is bound to the west by the Wairarapa Fault of the North Island Shear Belt (NISB). Deformation in this region is partitioned (see inset, fig. 1.1) into dextral strike-slip on the NISB strike-slip faults and pure compression to the east in the Wairarapa Domain (Lamb and Vella 1987; Lamb 1988). Palaeomagnetic data reveals no rotation in the last 2.2 Ma, and 20 ± 8^{o} of clockwise rotation in the last 8 Ma (Walcott et al 1981). The regions to the northwest of the Wairarapa domain (Seward et al 1986) have also undergone negligible rotation relative to the Australian plate in the last *ca.* 2.6 Ma. Lamb (1988) proposed that the Australian plate at the back of the crustal wedge forming the Wairarapa domain has acted as a strong barrier inhibiting large rotations in the domain.

1.3.2.4 The Marlborough Domain

This domain straddles the southern limit of the seismically active subducted Pacific plate (Ansell and Adams 1986). Across this boundary from NE to SW is a change in the trend of the Marlborough faults of 055^{o} to 070^{o}. The northeastern part of this domain underlain by the subducted slab is known as the Northern Marlborough domain whilst the southern part not underlain by the subducted slab is known as the

Southern Marlborough domain (Lamb 1988). All tilting in this domain has occurred since the Pliocene. The post-Pliocene deformation is in fact rather complex (eg:- Lensen 1962; Lamb 1988; Lamb and Bibby 1989; Kirker 1989)

Palaeomagnetic data reveals *ca.* 20^{o} of clockwise rotation and zero rotation in 8.1 to 3.9 Ma cover rocks (Walcott et al 1981; Roberts 1992) and *ca.* 110^{o} of clockwise rotation in 18 Ma rocks (Walcott and Mumme 1985).

A more detailed discussion of the structure and rotational strain within this domain is given below since it is the Marlborough region with which this thesis is mostly concerned.

Summary of Structure in Marlborough

Fig. 1.4 shows a simplified geological map of the Marlborough region. Post-Pliocene uplift of pre-Tertiary basement and Tertiary cover sediments exposes these sediments between the Marlborough faults. The main structural features are as follows: formation of an anticlinal structure between the Clarence and Kekerengu Faults which folds earlier thrust faults (Prebble 1976; Waters 1988); NNE-trending thrust faulting and folding in northeast Marlborough (Lensen 1962; Price 1974); complex folding and faulting affecting thrust-repeated Tertiary cover sediments on the downthrown side of the Kekerengu Fault (Lamb and Bibby 1989); and large scale NE-trending thrust faulting between the Kekerengu and Hope Faults (Van Dissen and Yeats 1991). All these structures affect Pliocene aged rocks and therefore are of post-Pliocene age. Thrust faults between the Awatere and Clarence Faults (Melhuish 1988) were active in the Late Miocene and some of these faults are believed to have been re-activated in the post-Pliocene (Roberts 1992).

Summary of Tectonic Rotation in Marlborough

All previously determined tectonic rotation data from sites within the Marlborough region are listed in table 1.1 and their positions shown in fig. 1.5.

Lack of any macroscopic textural evidence of shearing on an outcrop scale suggests that penetrative shear is unlikely to be responsible for rotation in Marlborough. In addition the similarity in amounts and sense of rotation suggests that the region is and has rotated as rigid blocks (Roberts 1990). Prior to the results of Roberts (1990, 1992), Lamb (1988, 1989) modelled the deformation of Marlborough with a simple mechanical model in which Marlborough is divided into northern and southern domains. The northern domain is treated as a series of large rigid blocks linked to the southern domain by a trellis system (fig. 1.6a). In the model dextral displacement on the Marlborough faults and sinistral displacement on north trending sinistral antithetic faults in the southern domain leads to a clockwise rotation of small crustal blocks in the trellis system and pivoting of the large rigid blocks. The hinge zone between the two

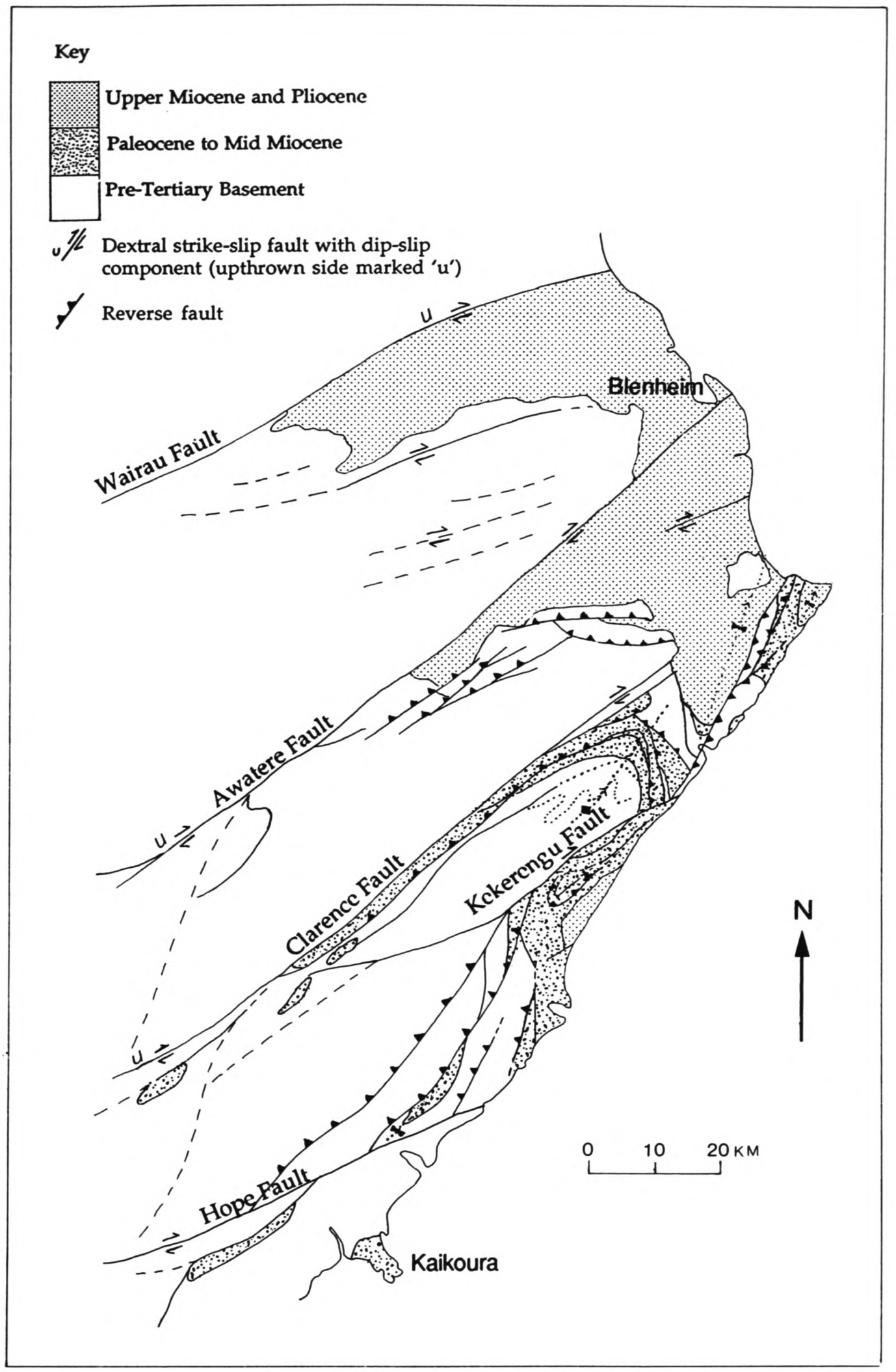


Fig. 1.4: Simplified geological map of the Marlborough region showing the position of different sediment age groups and the main structural features.

Location	D (°)	I (°)	α_{95} (°)	N	$\Delta \pm \delta$	Age (Ma)	Refs
1.Waihopai Valley	199.6	60.6	2.4	42	20.4±4	8±1	1
2.White Bluffs	204.2	67.0	3.6	29	24±7	3.9±0.8	1
3.Sea View	233.5	58.7	3.1	33	44±5	3.9±0.8	1
4.Richmond Brook	211.6	61.8	3.9	25	32±7	4.2±0.6	1
5.Blind River	212.6	59.5	2.0	132	33±3	4.8±0.2	2
6.Upton Brook	201.3	59.0	1.8	132	21±3	4.8±0.2	1
7.Boundary Stream	196.6	63.3	7.4	14	17±13	8±1	1
8.Cape Campbell	024.4	-60.5	5.4	12	24±9	8±1	3
9.Needles Creek	215.4	59.8	3.5	31	35±6	5.4±0.6	1
10.Deadman Stream	279.3	59.1	6.4	46	99±10	18±1	4
11.Camp Stream	174.8	59.3	2.8	52	-5±4	3.3±0.3	1
12.Swamp Stream	183.7	61.8	4.6	29	4±8	4.2±0.6	1

Table 1.1: Summary of palaeomagnetically determined tectonic rotation data for sites in Marlborough. References: (1) Roberts (1990; 1991); (2) Revised data of Turner et al (1989) by Roberts (1990); (3) Walcott et al (1981); (4) Mumme and Walcott (1984). The location of each of these sites is shown in fig. 1.5.

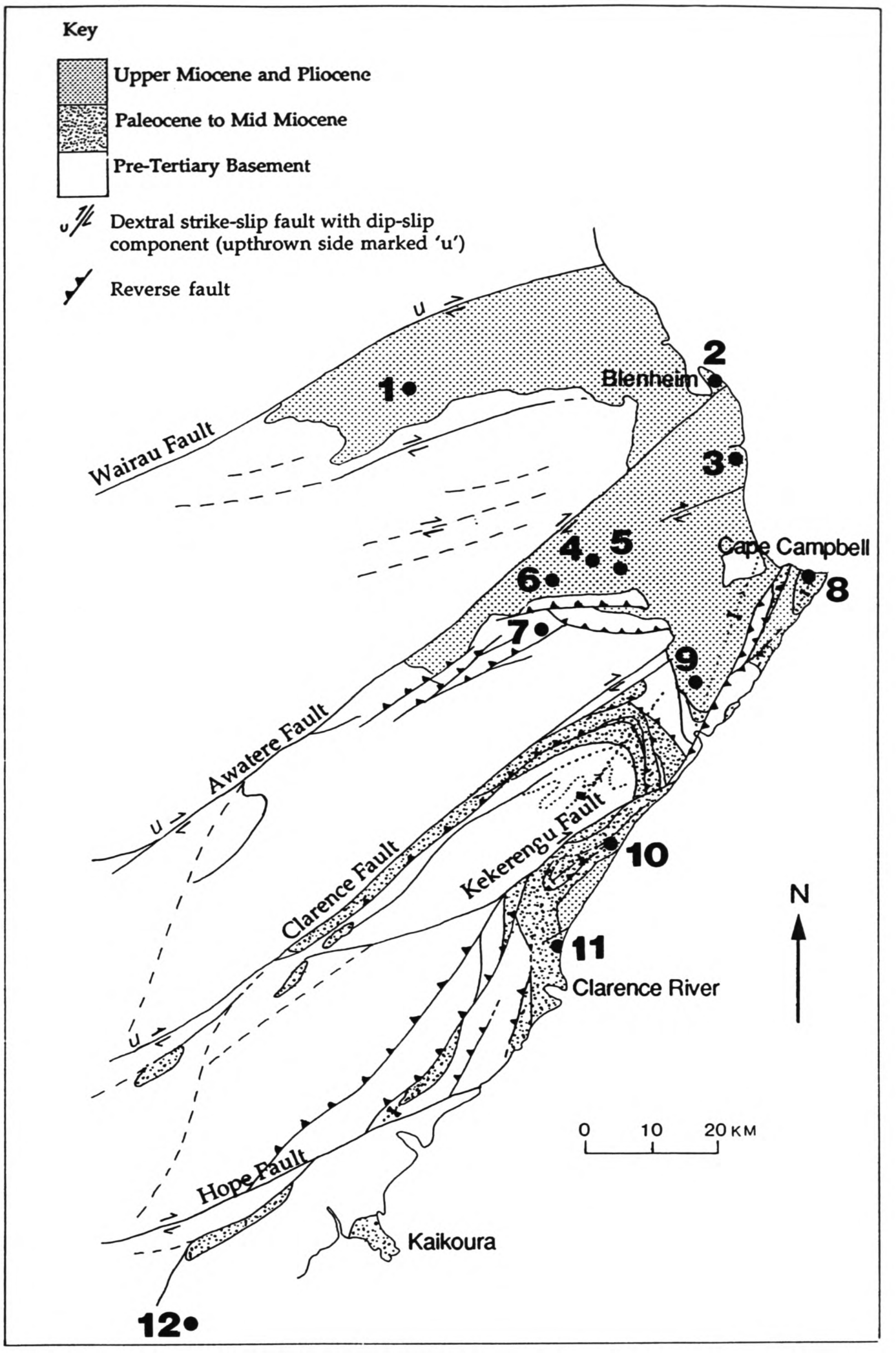


Fig. 1.5: Gelogical map of the Marlborough region showing the location of all existing palaeomagnetic sites. Location numbers correspond to data and references in table 1.1.

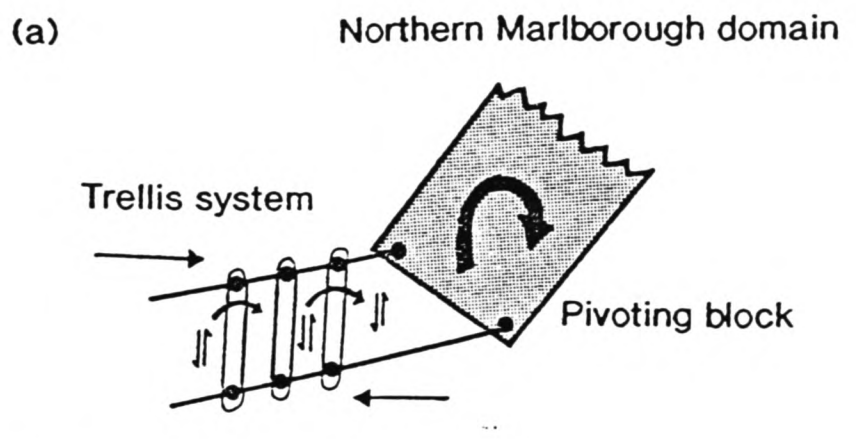


Fig. 1.6: Simple mechanical model for the Marlborough domains, after Lamb (1988). (a) Rigid block rotation of northern Marlborough domain and rotation on trellis system in southern Marlborough domain. (b) Illustration of possible progression of fault geometries in Marlborough during the Neogene. The main faults in the northern domain may have rotated from predominantly thrust (1) to predominantly strike-slip (3) while strike-slip displacement has predominated throughout in southern Marlborough.

domains coincides with the southwestern limit of seismicity associated with the subducted Pacific plate. In fact, fault trends in the southern domain are within 10° of the relative plate motion vector and strike-slip faulting is dominant (fig. 1.6b). Also, north-trending lineaments have been observed between the major faults. In contrast, in the northern domain the major faults are at a higher angle to the plate motion vector and thus accommodate thrust as well as strike-slip. Assuming this model is correct, the faults of the northern domain would have been at an even higher angle and therefore accommodated less strike-slip prior to rotating into their present position (fig. 1.6b).

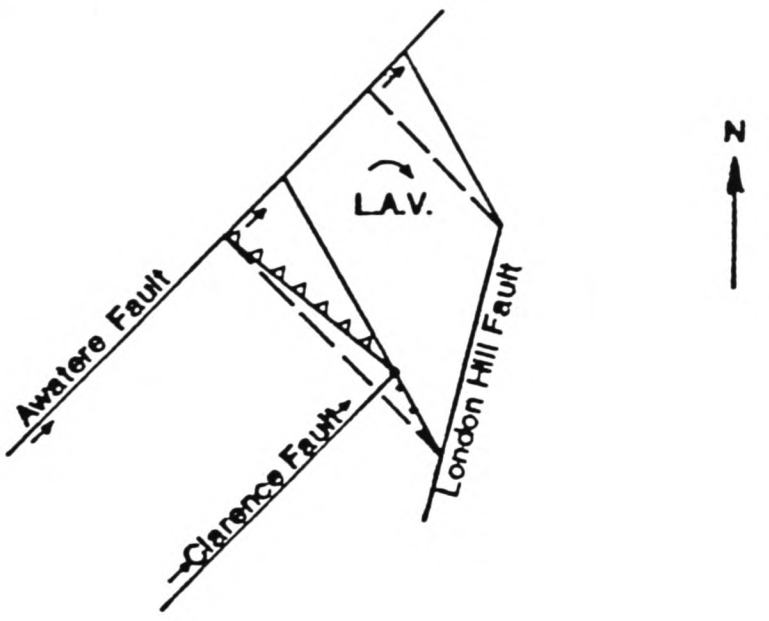
The tectonic rotation data (table 1.1) reveal a clockwise rotation of *ca.* 20° with a slightly higher clockwise rotation (extra *ca.* 15°) in the Lower Awatere Valley. Roberts (1990, 1992) suggested that the *ca.* 20° rotation can be explained by treating the northern Marlborough domain as a rigid block (as envisaged in the trellis model). He also suggested a second order differential clockwise rotation as a result of a velocity gradient set-up across the Lower Awatere Valley due to the termination of the Clarence Fault and continued displacement along the Awatere Fault to explain the differential rotation (see also Lamb and Bibby 1989). The two proposed models to explain this differential rotation are shown in fig. 1.7. Since pervasive shear has already been discounted, the rigid block model is preferred.

Unfortunately the palaeomagnetic sites from the area bound to the west by the Kekerengu Fault are less well understood. The Camp Steam site indicates no rotation in the last *ca.* 3 Ma, in contrast to the expected 20° clockwise rotation of the whole northern domain envisaged by the Trellis Model (Lamb 1988, 1989). The Deadman Stream site indicates 99° of clockwise rotation at some time since *ca.* 18 Ma. Since the younger sediments record no rotation, this large clockwise rotation is interpreted as a result of localized Early Miocene deformation.

1.3.2.5 The Nelson Domain

This domain is north of the Wairau Fault and is divided into two subdomains. In the eastern domain the sediments record a poorly constrained *ca.* 80° of clockwise rotation in the last *ca.* 30 Ma (Mumme and Walcott 1985). In contrast, in the western domain (where there has been a large amount of Neogene WNW-NW shortening with a substantial amount in the Plio-Pleistocene), less than 10° of clockwise rotation is recorded in the last *ca.* 40 Ma (Mumme and Walcott 1985). The large rotation in eastern Nelson is either a local effect or occurred prior to the Plio-Pleistocene.

(a). Simple shear across the Lower Awatere Valley.



(b). Rigid block rotation of the Lower Awatere Valley

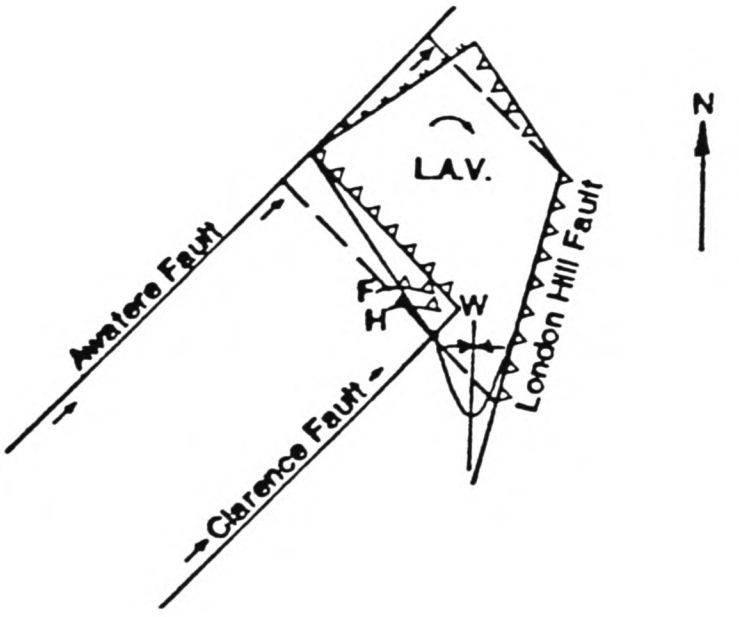


Fig. 1.7: Plan views of simple mechanical models to explain the second order rotations between the Awatere and Clarence Faults (from Roberts 1990). (a) Simple shear across the Lower Awatere Valley gives rise to differential rotations. (b) The Lower Awatere Valley rotates as a rigid block.

1.4 Summary

Structural evidence shows large variations in structural style within the plate boundary zone. The main features are as follows: extension in the Central Volcanic Zone; the partitioning of strain into compression normal to the zone along the east coast of the North Island and dextral strike-slip along large scale faults of the NISB further inland; and both uplift and dextral strike-slip faulting are recorded in the north South Island.

Subduction in the north imposes a SE-directed instantaneous velocity onto the Australian plate. Since subduction appears to be locked in the south, the Hikurangi Margin is rotating clockwise with respect to the Pacific Plate. Plate reconstructions suggest *ca.* 20^{o} of clockwise rotation of the boundary since *ca.* 20 Ma. This regional rotation has been detected by palaeomagnetic sampling in the Wairoa, Wairarapa and North Marlborough domains. Exceptions are found in several parts of the zone. In the Wairarapa domain 2.2 Ma sediments show no rotation. This is possibly due to the presence of the Australian plate at the back of the deforming crustal wedge acting as an inhibitor to rotation (Lamb 1988). No rotation was also recorded in ca. 3 Ma and 110^{o} of clockwise rotation in 18 Ma sediments on the downthrown side of the Kekerengu Fault in the North Marlborough domain. No explanations exist for these anomalous results. No rotations have been found in the South Marlborough domain. The trellis model of Lamb and Bibby (1988; 1989) explains the variations in rotational strain in the two domains by treating the Northern domain as large rigid crustal blocks linked to the South domain by a trellis system. The recent results of Roberts (1992) added a differential rotation caused by local structural variations to the northern Marlborough domain in this model.

1.5 Aims of Thesis

It is evident from sea floor spreading data and from geodetic studies that most of the relative plate motion within the Marlborough Fault System is accommodated by deformation of the continental crust, rather than by slip on the subduction thrust.

Uplifted pre-Tertiary basement and cover sediments are well exposed in Marlborough (see fig. 1.4). Fault slip data, structural, sedimentological, dating and palaeomagnetic studies are all available for this region. All this information can be used to understand the long term sedimentary and tectonic history of Marlborough.

The main aim of this thesis was to obtain a better understanding of the Tertiary to present-day evolution and accommodation of strain in the Marlborough region,

expanding and adding to the results of previous workers (Lamb and Bibby 1989; Osborne 1980; Prebble 1976; Mumme and Walcott 1985; Roberts 1992; Walcott and Mumme 1985; and Waters 1988). The information obtained could then be compared with deformation in other parts of the plate boundary zone resulting in a more complete idea of the evolution of this zone since its formation in the Early Miocene. It was hoped to provide a better understanding of the rotational component of strain affecting Marlborough throughout the Tertiary. By linking rotational data with structural information obtained from mapping, it might be possible to observe how the rotational strain is and was achieved and accommodated.

In particular it was hoped to unravel the complex deformation of the Tertiary cover sediments exposed on the downthrown side of the Kekerengu Fault and to explain the anomalous large clockwise rotation recorded in 18 Ma sediments (Mumme and Walcott 1985) and the lack of regional rotation recorded in Pliocene sediments here as oppose to those elsewhere in Marlborough (Walcott et al 1981; Roberts 1992).

This overall aim was achieved in several ways:

(1) Detailed mapping (chapters 2 and 4) of the area of exposed Tertiary cover sediments on the downthrown side of the Kekerengu Fault in eastern Marlborough (the Kekerengu-Washdyke subregion, fig. 4.1): Also, only some of the lithological units within this area had been previously dated (Lewis and Laird 1978; Osborne 1980; Prebble 1976; Scott 1979). It was hoped to obtain more dates to help constrain the timing of past tectonic activity producing the sediments and that of faulting in the area, and also to identify any unconformities which could help to constrain the timing of deformation events (chapter 3).

(2) The collection of sites for palaeomagnetic analysis (chapter 5). It was hoped to collect as many sites as possible from all over the Marlborough region to add to the existing sites of Mumme and Walcott (1985); Roberts (1992); and Walcott et al (1981). It was the intention to sample sites not only spatially distributed over the whole Marlborough region, but also to sample sites of different ages in order to place timing constraint on rotations should these exist.

(3) Re-look at structures in other subregions of Marlborough where Tertiary cover sediments are exposed in order to compare the different subregions in terms of their stratigraphic (chapter 2) and structural (chapters 4 and 6) differences.

Reduced copies of the two 1:15 000 map sheets of the Kekerengu-Washdyke study area are included at the end of this chapter for easy reference. The 1:50 000 sheets themselves can be found within the envelope inside the back cover of this thesis.

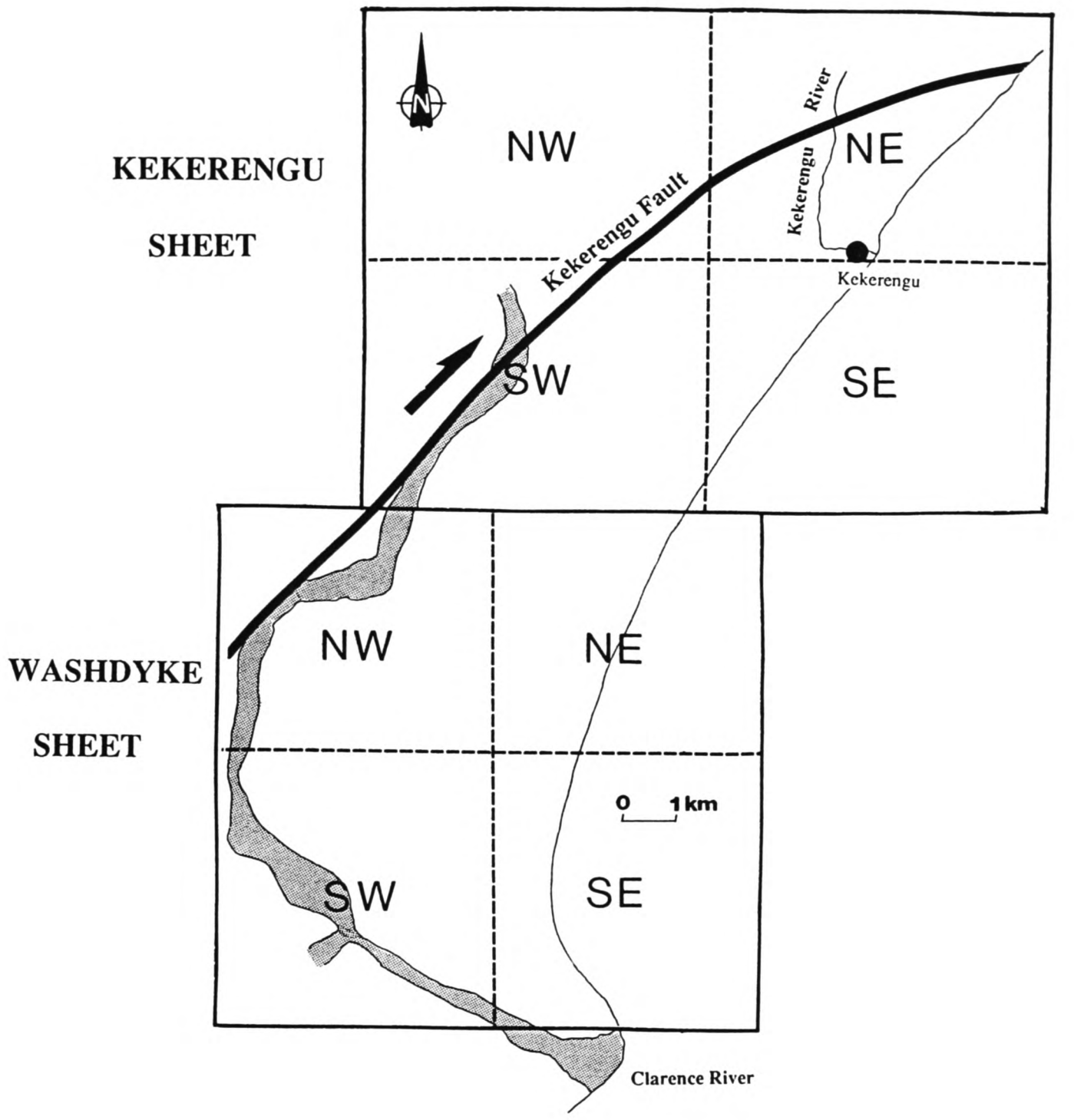
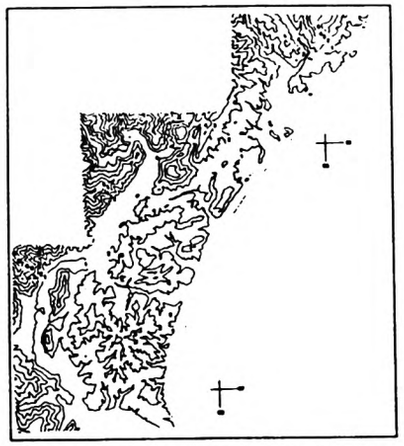


Fig. 1.8: Map showing the position of the Kekerengu and Washdyke map sheets. Quadrants defined by dashed lines represent the approximate geographical areas within each map which are mentioned in the text throughout this thesis. Reduced A3 size copies of the two map sheets are included here for easy reference.

Kekerengu Sheet



Hundred metre contours covering the Kekerengu and Washdyke maps

LITHOLOGICAL UNITS

Wb-WN	Pp	Whanganui Siltstone
Sc-Sw	Hl	Heavers Creek Formation
Pl-Bl	Gc	Great Marlborough Conglomerate
Pe-Ls	Ws	Waima Siltstone
Lw-Pg	Wm	Waitakian Marl
Mh-Lw	Am	Amuri Limestone
Pre-Mh	Z	Torlesse, Rakaumara + Mata Series

SYMBOLS

- Contact to <10m
- Contact to >10m
- Assumed Contact
- Thrust: Dθ
- Thrust: D|
- Strike Slip Fault (dextral)
- Syncline, Trace + Plunge
- Anticline, Trace + Plunge
- Bedding Strike + Dip
- Overturned Bedding Strike + Dip
- Cleavage
- Youngingg Direction

KEKERENGU

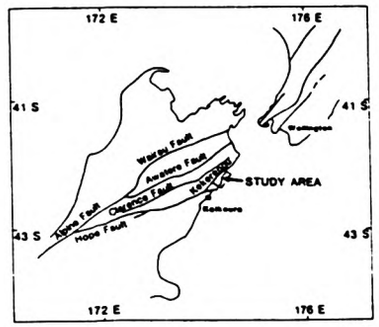
Kekerengu Fault
Heavers Creek Fault
Chalkley Fault
LADY RANGE
Glencoe Stream
Deadman Stream
Kekerengu River
Valhalla Stream
Boundary Stream

Tirohanga
Willawa
Matawa
Napoleon
Glencoe
Warewa
Blue Slip
Winterholme
Homai
Valhalla
Ellerton
Telhoa
Misty Hill
Mole Hill
Deadman Hill

A
A'
B
B'

SCALE 1:15 000

0 0.5 1.0 km



WASHDYKE

Washdyke Sheet

SCALE 1:15 000

0 0.5 1.0 km

CHAPTER 2

CHAPTER 2: STRATIGRAPHY

This chapter describes the stratigraphy and sedimentology of the main stratigraphic units in the study area. Formal New Zealand nomenclature is not used in order to avoid confusion with previous work in this area. However, an attempt is made to correlate the local stratigraphy in the study area with the more regional stratigraphy in this part of the plate boundary zone established by other workers (eg: Browne and Field 1985; Osborne 1980; Prebble 1976; Roberts and Wilson 1992).

Dating of the stratigraphy in the study area using foraminifera biostratigraphy is discussed in chapter 3 (refer to fig. 3.2). All foraminifera identified in this study are marine species. Thus the Upper Cretaceous and Tertiary sequences in the study were all deposited in a marine environment.

2.1 Overview of the General Stratigraphy

The general stratigraphic sequence in the study area has been briefly described in chapter 1. The oldest rocks exposed in Marlborough are Triassic to Mid Cretaceous, flysch deposits from a group known as the Torlesse Supergroup (Howell 1981). Torlesse group greywacke and argillite in Marlborough is conformably overlain by non-Torlesse sediments (Lensen 1962). The late Cretaceous stratigraphy is dominated by shallow marine clastic sediments topped by anoxic, sulphide rich siltstone and sandstone. These beds eventually give way to the calcareous Amuri Group by the end of the Cretaceous. This transition is conformable in Marlborough, although elsewhere in the South Island there is an unconformity (Warren 1978).

The Amuri Limestone Formation was the name introduced by Hutton (1874) for an argillaceous limestone found throughout North Canterbury and Marlborough. Lensen (1962) and Armstrong (1972) worked on descriptions of the formation. Hall (1964) and Prebble (1976) suggested a division of this group in Marlborough into seven members (three pelagic limestone units, a greensand, two bentonitic members and a flint member). The lowest member, called the Mead Hill Flint, contains the Cretaceous-Tertiary boundary (Strong 1977). The formation as a whole varies in thickness markedly and is known to be diachronous, its base progressively younger to the south (Browne and Field 1985). No formal stratigraphic definition of this formation exists, although a recent study by Morris (1987) provides a comprehensive, updated stratigraphy of the Amuri Limestone Group in Marlborough. The longest age range for the group is *M.Haumurian* to *U.Runangan* (Morris 1987). Conformably overlying the main group is a deposit of Waitakian (*ca.* 23 Ma) age known as the Waitakian Marl (Suggate et al 1978). This consists of interbedded blue marls and micritic limestones

and marks the increasingly argillaceous nature of limestone sedimentation in the Lower Miocene.

Early Miocene clastic siltstones and conglomerates overlie the Waitakian Marl. The Waima Siltstone Formation (Hall 1964) is a moderately indurated, calcareous, silty mudstone which is most extensive in coastal Marlborough (Hall 1964, Prebble 1976, 1980, Raey 1980). It was dated as *Otatian* to *Altonian* by Prebble (1976). Miocene age, poorly sorted conglomerates with megaclasts in Marlborough are mapped as the Great Marlborough Conglomerate (Thomson 1913), although no formal description or type locality exists. The deposit was first described by McKay (1886). The most documented section of this deposit is along Deadman Stream *ca.* 5 km south of Kekerengu. Thomson (1913) divided the succession here into two Great Marlborough Conglomerate units separated by fossiliferous, pebbly sandstones, called the Deadman Creek beds. King (1937) named the overlying mass of sandstones and conglomerates the Ericaburn Beds. The overall deposit was dated as *Altonian* to *Lillburnian* by Prebble (1976).

The Great Marlborough Conglomerate is overlain by M. Miocene siltstones, including the Heavers Creek siltstone (*Altonian* to *Waiauan*, Waters (1988); *Lillburnian* to *Waiauan*, Kirker (1989)). These M.Miocene deposits are rarely preserved in Marlborough. The sequence is topped by Upper Miocene to Pliocene siltstones and minor conglomerates (known as the Awatere Group in the Lower Awatere Valley (Roberts and Wilson 1992)), and ultimately by Quaternary to Recent beach deposits and river terrace sequences.

The general succession from Upper Cretaceous material to Pliocene siltstones is summarized in fig. 2.1.

The deposits themselves reflect a change from a passive to an active margin with the introduction of large volumes of terriginous material supplied to the Tertiary sedimentary basin. This change occurred at the beginning of the Miocene (*ca.* 24 Ma). The sediments themselves suggest tectonic uplift of a proximal continental landmass at this time, with both onland erosion by large rivers and transportation of material over large distances, and also erosion and resedimentation within the basin of deposition itself. These features, which have also been recognized along the east coast of the North Island of New Zealand (c.f. Charnier and Ferriere 1961; Pettinga 1982), coincide with the time of the change in direction of the relative plate motion between the Australian and Pacific plates (refer to 1.3). The clastic sediments are believed to mark the onset of subduction of the Pacific plate along the New Zealand plate boundary zone at *ca.* 24 Ma.

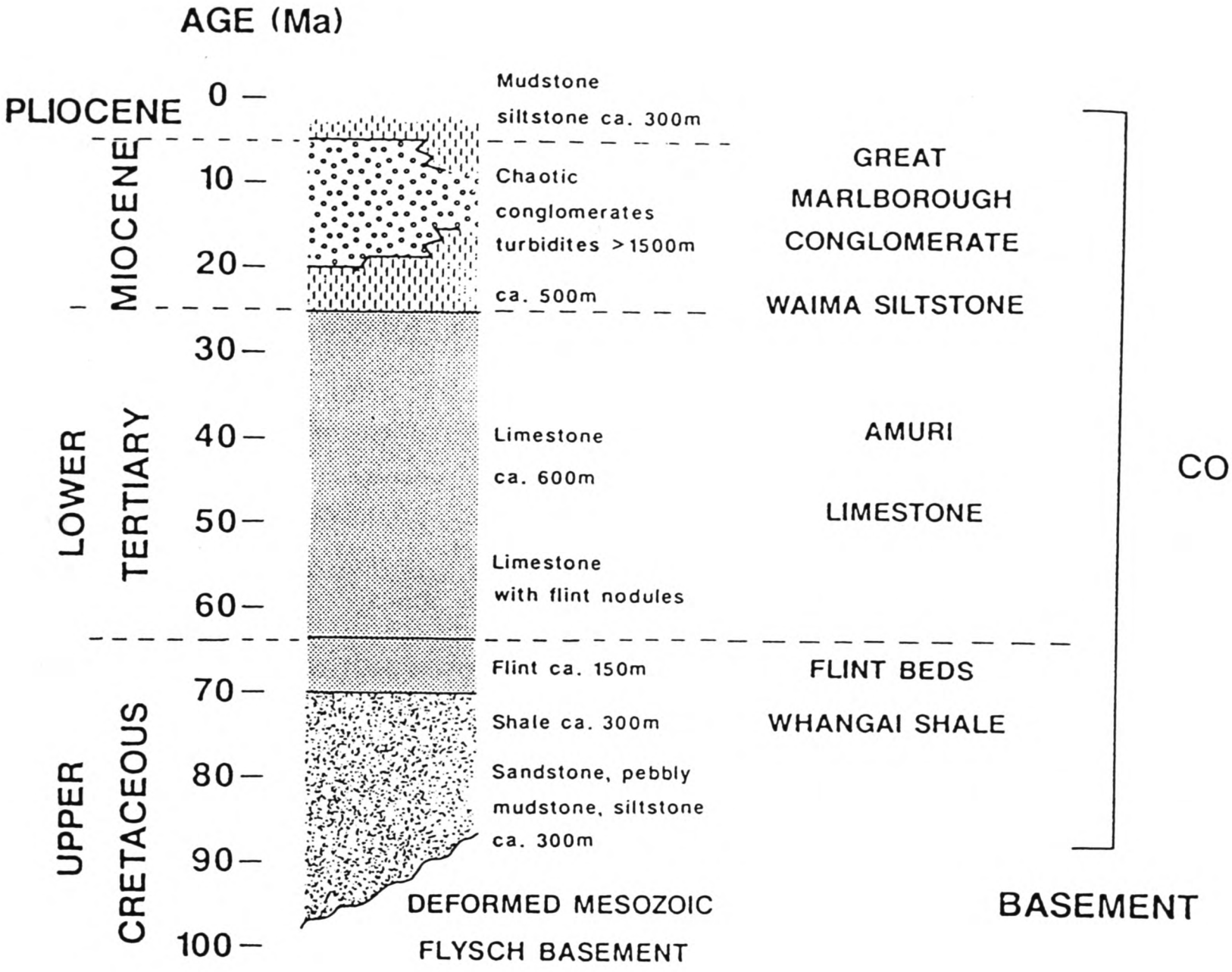


Fig. 2.1: Generalized stratigraphic column for the Marlborough region (from Roberts (1990)).

2.2 Descriptions of the Lithologies

The sequences in the study area which conformably overly the Torlesse basement rocks can be informally divided into four parts: (1) a basal limestone sequence; (2) a lower siltstone sequence; (3) a conglomerate sequence; and (4) an upper siltstone sequence. The stratigraphy and sedimentology of these main subdivisions are described in the following sections.

2.2.1 The Limestone Sequence

Description

Limestone exposures in the field area (labelled Am (Amuri Limestone Group) and Wm (Waitakian Marl) on main field maps) are shown in fig 2.2. Here, limestone which forms part of unfaulted successions resting on older siltstones and sandstones are distinguished from fault-bound isolated limestone exposures. The unfaulted successions vary in thickness from *ca.* 1.2 km in the western part of the Washdyke map sheet, to *ca.* 0.5 km for the limestone succession at Waipapa Bay. In comparison, isolated exposures average *ca.* 0.3 km in thickness. Internal lithological variations are common. Younging directions in all limestone sequences were identified mainly by the presence of trace fossils. For instance, traces from the zoophycus association of Seilacher (1967, 1978) were often found within marly horizons in the upper limestone units. These were produced by sediment feeders living in outer shelf environments. The upward closure of these fossils is a good indicator of way-up. Also found within the Amuri Limestone lithology were traces produced by suspension feeders and from the Cruziana association (Seilacher 1967). Such fossils are common in shallow shelf environments and can also be used to indicate way up by the curvature of displaced material within the traces.

Conformable Limestone

Within the study area conformable limestone is found on the downthrow side of the Kekerengu Fault in both the Kekerengu and Washdyke areas, and also on the upthrow side of the Kekerengu Fault as a part of the Benmore Anticline which is truncated by the Kekerengu Fault. (See column 2 of fig 2.3). Siliceous, white limestone with nodular to elongate cherts bedded on a scale of tens of centimetres, overlies (with no angular discordance) sulphur rich siltstones and shales in all these locations. The limestone is an indurated, micritic limestone containing coccolith, diatoms and globigerina tests (observed in thin section). At the base of the sequence are coalescing chert nodules. These cherts decrease in abundance upward over 126 m until the limestone includes no, or rare, chert material. The limestone stratigraphically above the occurrence of flint nodules is bedded on a centimetre scale. This thick sequence is

KEY

Allochthonous Limestone (types 1 and 2)

Autochthonous Limestone

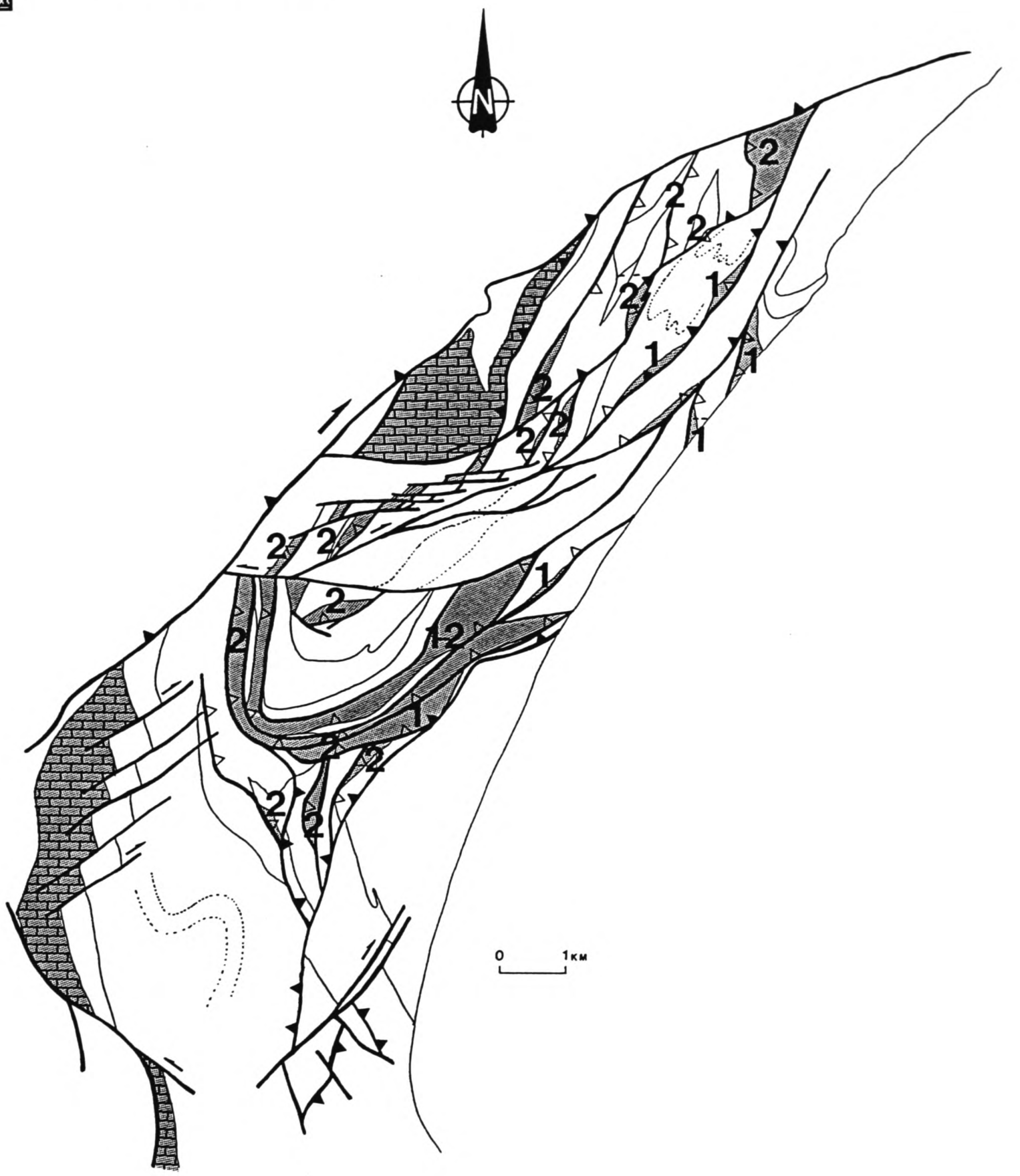


Fig. 2.2: Map of the Kekerengu-Washdyke study area showing limestone exposures. Distinction is made between unfaulted successions resting conformably on older siltstones and sandstones and fault-bound isolated limestone exposures. The allochthonous exposures can themselves be divided into two types: interbedded blue marl and limestone sequences (Type 1); and a sequence of limestone lithologies (Type 2). For descriptions of these lithologies refer to section 2.2.1.

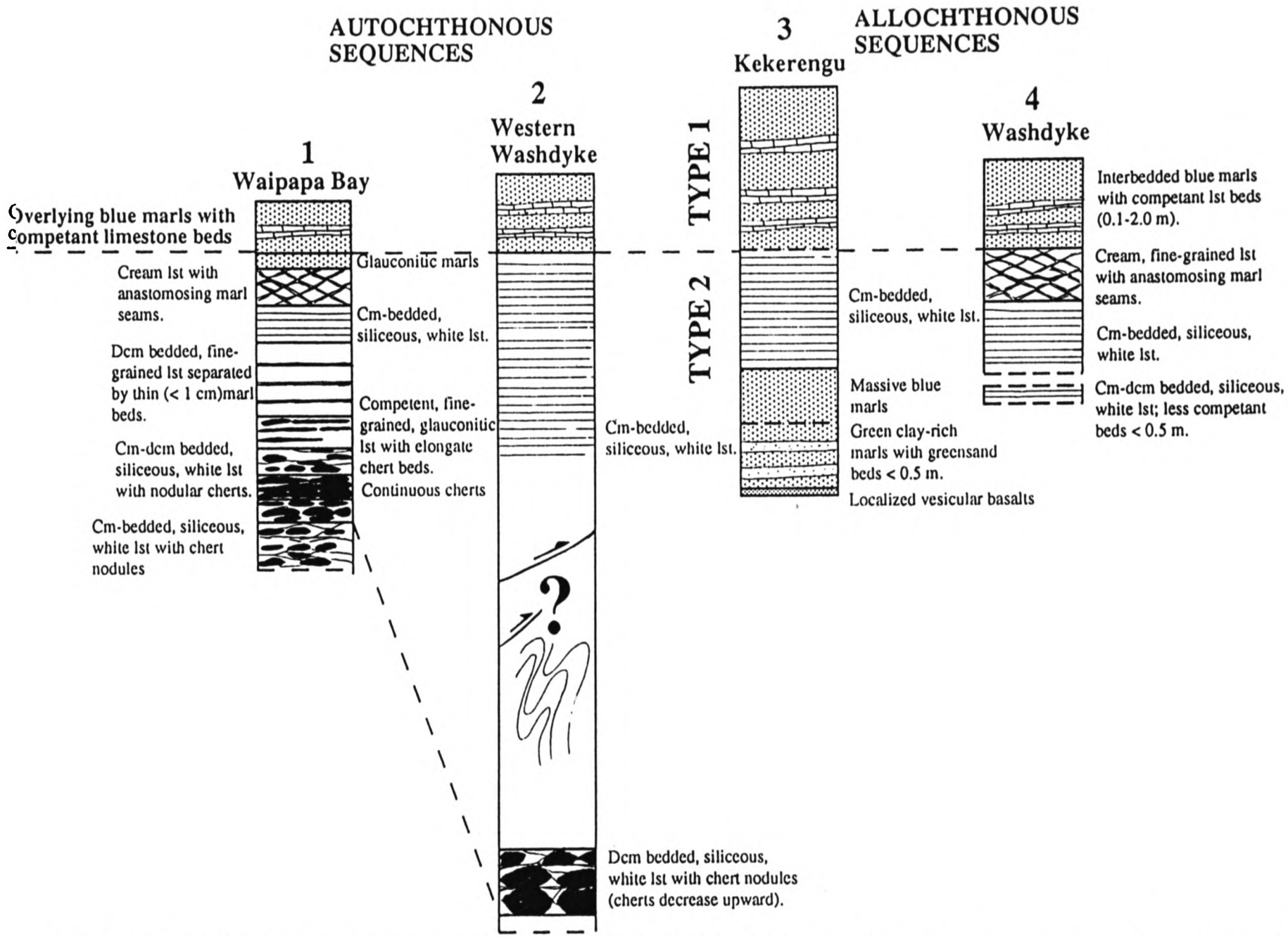


Fig. 2.3: Stratigraphic columns of autochthonous and allochthonous limestone successions from the study area. Autochthonous sequences are from Waipapa Bay (column 1) and from the western part of the Washdyke map sheet (column2). Allochthonous sequences are taken from limestone exposures of the Kekerengu map sheet (column 3) and the Washdyke map sheet (column 4). The latter are divided by lithology into Types 1 and 2. Refer to section 2.2.1 for descriptions of these lithologies. (Abbreviations: lst (limestone), Dcm-bedded (bedded on a scale of tens of centimetres), Cm-bedded (bedded on a centimetre scale))

topped by interbedded blue marls and limestone which pass up into the continuous, massive blue siltstone sequence of the overlying formation. The overlying formation has been dated as *Otaian* to *Lillburnian* (see chapter 3), placing an upper age limit on this limestone succession.

At Waipapa Bay a limestone sequence overlies conformable older, non-calcareous lithologies. This sequence is summarized in column 1 of fig. 2.3, where it can be directly compared with the sequence described from the Kekerengu and Washdyke areas (see column 2 of fig. 2.3). The thicknesses of chert beds at the base of both sequences are similar. At Waipapa Bay, the chert beds pass up into glauconitic limestones and limestones interbedded with thin marl seams, topped finally by interbedded blue marls and micritic limestones. The sequence between the upper marl-limestone beds and the lower chert horizons is of the order of 550 m, much thinner than the 1.2 km section further north (column 2 of fig. 2.3). This difference may either reflect a primary sedimentary thickness change, perhaps as a consequence of differences in the source proximity for the two sequences or is a peculiarity of the basin shape; or alternately a result of structural repetition.

Fault-bound Limestone

A number of structurally bound or allochthonous, thin limestone sequences were found in the Kekerengu area (map view dimensions average a maximum of *ca.* 2 km in length by *ca.* 0.3 km in thickness). These are of two types: (Type 1) isolated interbedded blue marl and limestone sequences; or (Type 2) a sequence of limestone lithologies. The latter sequence has localised, dark grey, vesicular basalts at its base, which are overlain by light green-grey, poorly indurated, micritic, clay-rich marls with greensand beds (< 0.5 m) and moderately indurated blue marls. At the top of this sequence is siliceous, white, micritic limestone bedded on a centimetre scale. Exposures of this kind are found in the limestone unit exposed at the termination of the Heavers Creek Fault (Fault 5, see chapter 4) and in the southern limestone unit outcropping along this same fault in the Kekerengu area. The Type 1 allochthonous limestone sequence appears to be younger than Type 2. This is because the marl of Type 1 appears to be at the top of the general limestone sequence. No limestones have been documented from above the overlying siltstone formation. The succession is summarized in column 3 of fig 2.3, though parts of the sequence may be missing due to the allochthonous nature of these deposits.

A number of structurally bound limestone units and sequences were also found in the Washdyke area folded around the main Razor Fold and in the area to the south of this fold. Four lithologies were observed, three of which are in direct succession. The oldest of these three was a centimetre-bedded, indurated, siliceous, white, micritic limestone. An identical lithology was observed in the Type 2 limestone succession of

the Kekerengu area. Beds up to 0.5 m thick of volcanic glass breccia were found near the contact of this lithology with the overlying lithology. The overlying lithology is a pale grey (weathered cream), indurated, micritic limestone with anastomosing marl seams defining bedding (fig. 4.24a). This in turn is overlain by interbedded blue marls and micritic limestones, the same Type 1 lithology as observed in the Kekerengu area. The only other lithology found structurally isolated in this area is an indurated, white, siliceous, micritic limestone bedded on a centimetre to tens of centimetres scale and with less competent beds < 0.5 m thick. This and the anastomosing limestone lithology have no equivalents in the Kekerengu area.

It is assumed that this wholly isolated lithology is in fact older than the sequence of three lithologies since these are topped by the interbedded marl-limestone unit believed to represent the uppermost limestone deposit before deposition of the overlying siltstone formation. The exact position of this last unit is unknown (see 2.3). The sequence is summarized in column 4 of fig 2.3. This and the anastomosing lithology are therefore included in the Type 2 division. Types 1 and 2 are distinguished in fig. 2.2.

Environment of deposition and timing

The presence of planktonic foraminifera and nannofossils in the lower siliceous limestones indicated a outer-shelf to bathyal environment of deposition (3.1). The introduction of terriginous clay-rich muds and glauconitic sands into the basin of deposition indicates uplift in the source area. The presence of Cruziana association trace fossils (Seilacher 1967) in the upper part are indicative of a shelf environment. Therefore definite upward shallowing is displayed within this limestone sequence. The overlying interbedded marls and micritic limestones contain planktonic foraminifera and Zoophycus association trace fossils. Both suggest an outer shelf environment.

The age of this sequence has been determined by Morris (1987), ranging from the *M.Haumurian* to the *Waitakian.*

2.2.2 The Lower Siltstone Sequence

Description

A massive siltstone sequence overlies with no angular discordance the upper part of the autochthonous limestone sequences (interbedded blue marl and limestone). The exposures of this unit are summarized in fig. 2.4. The gradual sedimentary progression from limestone to siltstone was observed at the top of all the base conformable limestone sequences. This was observed either directly or by sharp falls in topographic elevation as the lithology changes from harder limestone to less resistant siltstone. The progression was also observed on the top side of thrust blocks of the interbedded limestone. Sharply overlying this siltstone formation are clast supported

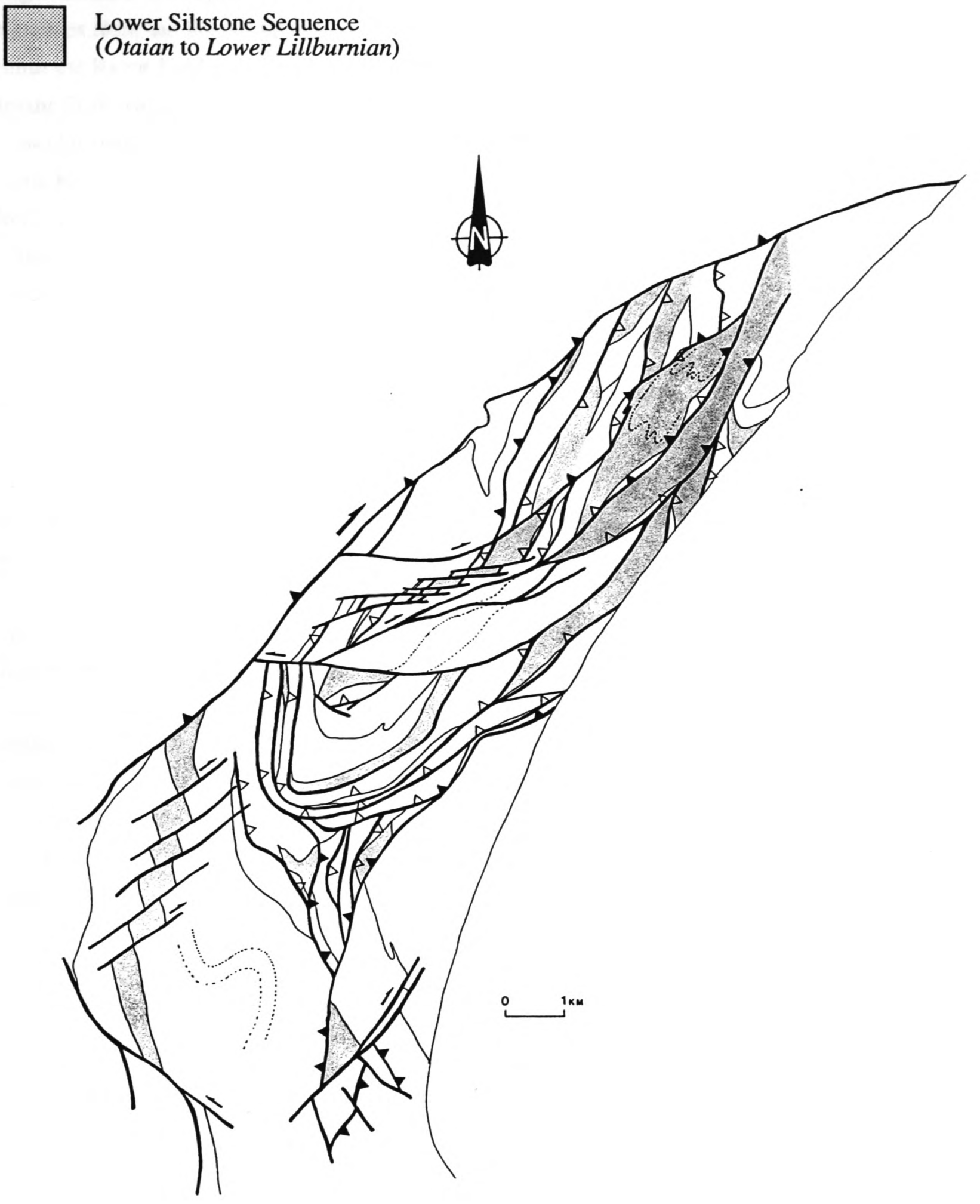


Fig. 2.4: Map of the Kekerengu-Washdyke study area with shaded areas marking exposure of the Lower Siltstone Sequence (refer to section 2.2.2).

conglomerates. This upper contact of the Lower Siltstone sequence within conformable sequences from the limestone beds below, was directly observed in Deadman stream, within the Razor Fold and in the western part of the Washdyke map sheet. In Deadman Stream fresh, stream smoothed exposures of the siltstone reveal the presence of sigmoidal shaped, deformed limestone pebbles (see fig. 2.5a). These indicated the plastic behaviour of these pebbles during sedimentary deformation. Gravity sliding is a likely cause of this deformation. Around the Razor Fold fine, laminations on a millimetre scale were visible in fresh, water smoothed exposures of this lithology. In the same locality cross beds were observed in sandier horizons. There are many dates available for this lower siltstone unit in these three locations, indicating an overall age of *Otaian* to *Middle Altonian* (see chapter 3, dated samples R17, R20, 114a, LL, 349b, 350a and O7).

Additional siltstone exposures were observed directly below conglomerate units but with faulted lower contacts obscuring their true relationship to underlying beds. Their position below conglomerates was taken as being indicative of their belonging to the same lower siltstone lithology. They may also represent siltstones between conglomerate units. Even so, siltstones interbedded with conglomerates were grouped together with this lower siltstone unit. The siltstone deposits include interbedded siltstone and sandstone beds from the northern Kekerengu area. The only dates available from such siltstone exposures was *Otaian* to *Clifdenian* (chapter 3, dated sample 231). It was then also possible to incorporate other massive to bedded siltstone units whose upper and lower contacts were not exposed, but whose ages fall within the same overall combined age range (*Otatian* to *Clifdenian*). For example, the area of massive to interbedded siltstone and sandstones between the Heavers Creek and Chaffey Faults. The sandstone beds were up to 10 m in thickness. Narrower sandstone beds commonly possess an upper rippled surfaces and planar laminations. Flecks of organic material are also common. Coarse sandstone beds and even a 2.5 m thick conglomerate lenses were found within this sequence.

The thickness of this siltstone unit in the western part of the Washdyke map sheet where the lower and upper contacts are exposed, is *ca.* 730 m. Its thickness elsewhere is indeterminable due to the faulting of one or other, or both, of the lower or upper contacts, and to internal folding.

Interbedded massive siltstone and sandstone beds and fine silt to coarse silt laminations are typical of flysch type deposits produced by turbidite flows.

Environment of deposition and timing

Whereas the Waitakian Marl deposit reflected the introduction of terriginous, clastic material into the marine basin, this change to purely clastic turbidite deposits of the lower siltstone sequence reflects an increased supply of material (possibly as a



Fig. 2.5a: Sigmoidal shaped deformed limestone pebbles from the Lower Siltstone Sequence of Deadman Stream. Refer to section 2.2.1.



Fig. 2.5b: Slump folding in the central turbiditic portion (conglomerate Type 5) of the Conglomeratic Sequence of Deadman Stream. Refer to section 2.2.3.

Fig. 2.5: Examples of sedimentary deformation in the Lower Siltstone and turbiditic portions of the Conglomeratic Sequence along Deadman Stream (southern part of the Kekerengu map sheet).

result of increased uplift) from the continental source area at around the beginning of the *Otaian* period. The foraminifera collected and identified from beds ascribed to this lower siltstone lithology are of both benthic and planktonic forms. This mix of foraminifera types indicated an outer shelf to upper slope environment (3.1). The unit is known to range up to *Clifdenian-Lillburnian* times (chapter 3).

2.2.3 The Conglomeratic Sequence

Description

Conglomeratic sequences are common throughout the study area. Fig. 2.6 summarizes the extent of these exposures. In the western part of the Washdyke map sheet and in the succession in the centre of the Razor Fold in the northern part of this sheet, this unit is conformable above the lower siltstone unit. The particular conglomerate lithological type varies quite considerably between locations. These variations are summarized with exact percentages in table 2.1 (location numbers correspond to the map of fig. 2.6). In table 2.1 the clast proportions listed are estimates (siltstone clasts make-up for unaccounted for clast percentages) and no distinction is made here between limestone clast lithologies. The clast or matrix supported description in the table refers to the conglomeratic portion of the particular location. The broad lithological types evident from these tables are summarized below.

Summary of lithological types

Severn broad lithological types have been recognized in this study (see fig. 2.7 for examples of these conglomerate types). In these descriptions a prominent clast component implies that this component forms more than *ca.* 30% of the clasts.

Type 1. Poorly sorted and clast to matrix-supported conglomerates with a prominent component of immature limestone clasts.

Type 2. Poorly sorted and clast to matrix-supported conglomerates with a prominent component of mature Torlesse clasts. Boulders of up to several metres in diameter are common in this group. An example of this lithological type is shown in fig.2.7a.

Type 3. Poorly sorted and clast to matrix supported conglomerates with approximately equal proportions of limestone and Torlesse clasts.

Type 4. Interbedded (on a scale of centimetres to metres) conglomerate, sandstone and siltstone with a prominent component of limestone clasts.

Type 5. Interbedded (on a scale of centimetres to metres) conglomerate, sandstone and siltstone with a prominent component of Torlesse clasts.

Type 6. Poor to moderately well sorted limestone breccia or conglomerate with a prominent component of angular limestone clasts. An example of this lithological type is shown in fig. 2.7b.

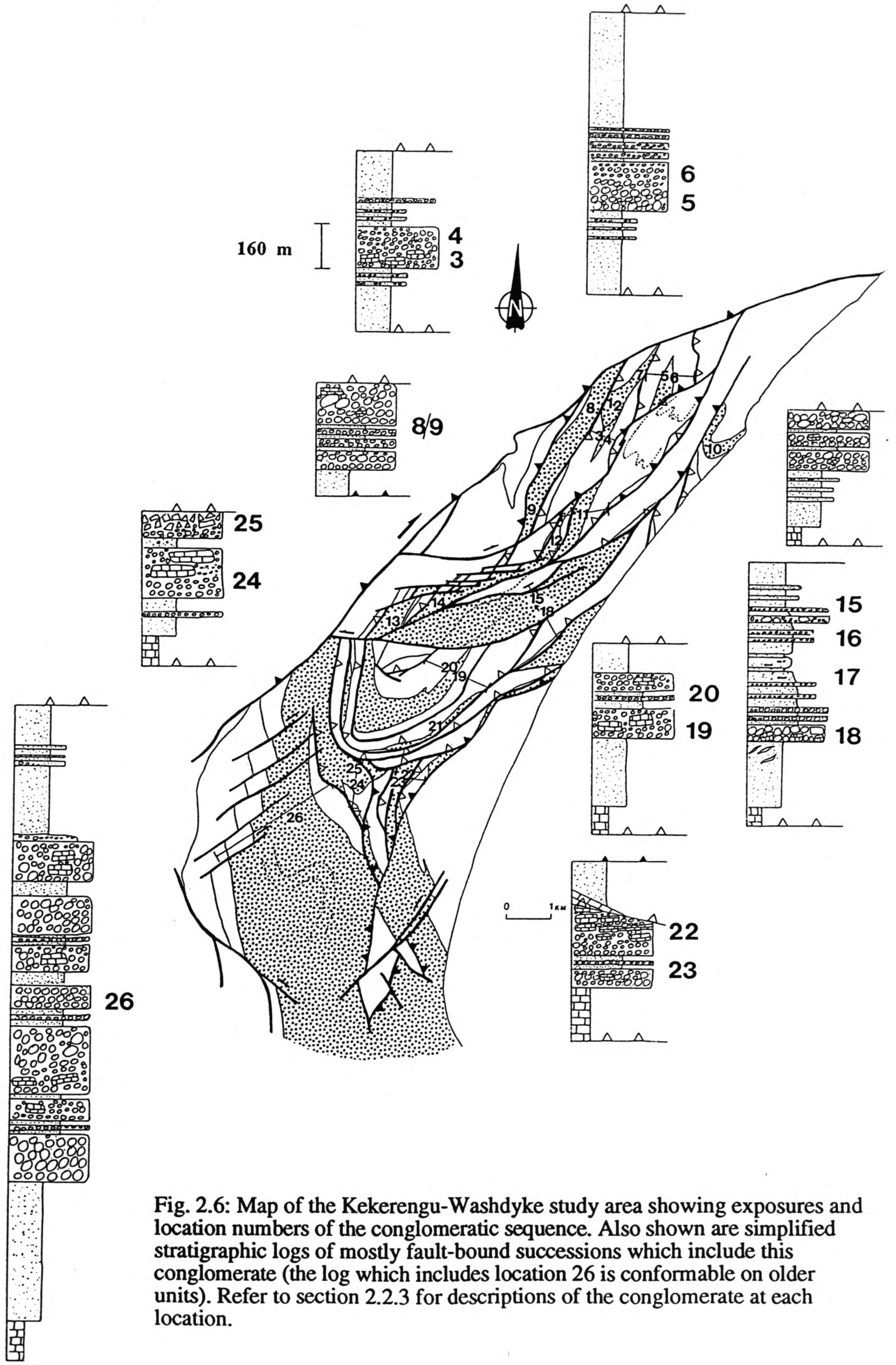


Fig. 2.6: Map of the Kekerengu-Washdyke study area showing exposures and location numbers of the conglomeratic sequence. Also shown are simplified stratigraphic logs of mostly fault-bound successions which include this conglomerate (the log which includes location 26 is conformable on older units). Refer to section 2.2.3 for descriptions of the conglomerate at each location.

Location	Lithotype	Sorting (cm)	Support	%Lst clasts	%G/W clasts	Boulders
1	conglomerate	poor: 7-12;7	clast	50-70: A-SR	30: R	limestone
2	turbiditic siltsts	poor: <10; 2/3	matrix	50-70: A-SR	30: R	limestone
3	conglomerate	mod: 0.5-3; <1	clast	<10: SR	80: R	limestone
4	turb siltsts-congl	good: <0.5	clast	<10: SR	80: R	none
5	conglomerate	poor: <8	clast	70: A	R	none
6	turb siltsts-congl	good: <2; 0.5	clast	25: R	R	none
7	conglomerate	poor: <1	clast	5: SR	90: R	limestone
8	conglomerate	poor: 1-15; 2/3	clast	<5: SR	80: R	;limestone
9	conglomerate	poor: 0.5-17; 2.5	clast	<10: SR	80: R	limestone*
10	conglomerate	poor: 0.1-15; 1.5	clast	40: A-SR	50: R	limestone
11	conglomerate	poor: 0.1-10; 1.5	clast	20: SR	80: R	lst, g/w, siltstone
12	turbiditic siltsts	good				none
13	conglomerate	poor: 0.1-25; 10	clast	<10: A-SR	80: R	g/w, siltstone
14	conglomerate	mod: 0.1-2; 1.5	clast	<2: R	90: R	rare limestone
15	turb siltsts-congl	good: <1.5	clast	45: A	50: R	none
16	conglomerate	poor: 0.2-20; 2	clast	5: SR	90: R	none
17	turb siltsts-congl	poor: 0.1-10; 4/5	clast	20-60: A	40-80: R	limestone
18	conglomerate	poor: 0.5-15; 6	clast	15: SR	80: R	lst, g/w, siltstone
19	conglomerate	poor: 0.5-20; 1.5	clast	50: SR	50: R	lst, g/w, siltstone
20	turbiditic siltsts	good		50: SR	50: R	none
21	conglomerate	poor: 0.2-40; 1.5	clast	<10: A-SR	90: R	none
22	limestone breccia	poor: 0.5-15; 4	clast	90: A	<10: R	limestone**, g/w
23	conglomerate	poor: 0.2-5; 1	clast	<10: SR	90: R	limestone
24	congl-siltstones	poor: 0.2-3; 0.5	matrix	<10: SR	90: R	limestone
25	congl + siltstones	poor: 0.2-10; 1	clast-matrix	50-85: A	<5: R	limestone
26	conglomerates	poor: 0.5-30; 3	clast	<5: A-SR	90: R	limestone

Table 2.1: Table showing sedimentary characteristics of the conglomeratic sequence from locations throughout the Kekerengu-Washdyke study area. Location numbers refer to fig. 2.7. The sorting of constituent clasts is described by values defining the maximum and minimum clast diameters, followed by the average clast diameter which forms at least 50% of all clasts. (Abbreviations: A(angular), SR (subrounded), R (rounded), Lst (limestone), G/W (Torlesse), siltsts (siltstones), congl (conglomerate), turb (turbiditic), mod (moderate)). *: In eastern half of conglomerate body. **: Limestone rafts.

Type 7. Massive and well-sorted siltstone with well-sorted, coarse sandstone horizons.

Rare coal nodules up to *ca*. 15 cm in diameter were observed within most conglomeratic units (fig. 2.13a).

Description of the lithological types in terms of depositional processes

It is possible to interpret the above lithological groups in terms of the relevant sedimentological process responsible for their formation, and in terms of the general basin setting. Catastrophic submarine debris flows may carry slabs weighing up to 2300 million kg (Marjanac 1985) and only require a small amount of interstitial matrix (*ca*. 5%) to allow flow on gentle slopes. The deposits of such high concentration flows are commonly poorly sorted, matrix supported and often lack distinct internal layering, although they may have a crude stratification (eg:- Thornton 1984). They are also generally poorly graded, either normal or reverse (eg:- Naylor 1980) and with a poorly developed clast fabric (eg:- Hiscott and James 1985). In contrast, deceleration of lower concentration turbidity flows generally produce massive structureless to planar laminated and rippled sandstones and siltstones (eg:- Bouma 1962; Harms and Fahnestock 1965; Walker 1965). High concentration turbidity flows tend to carry gravel and coarse sands. These flows produce a deposit with an inverse graded basal division, overlain by normally graded gravel and pebbly sand or stratified gravel and sand (Walker 1975). Alignment of grains is common within these deposits (Hiscott and Middleton 1979).

Conglomeratic Types 1, 2, 3 and 6 are marine (refer to chapter 3), poorly sorted, poorly graded, clast to matrix supported deposits with only crude stratification. These are therefore most likely to have been produced by debris flows. Types 4, 5 and 7 are normally graded well-sorted deposits and therefore are most likely to have been deposited by fairly high concentration turbidity flows.

The presence of large coal fragments suggests a nearby land source. Coal samples were collected throughout the sedimentary pile for vitrinite bireflectance analysis (see Appendix to chapter 2 and fig. 2.13). In hand-specimen some samples clearly retain their woody fabric with growth rings visible. These coals represent tree debris incorporated into the debris-flow deposit. Other coal samples displayed a fibrous plant texture when viewed under a microscope.

Overall the deposits probably reflect a substantial increase in the volume of material being supplied to the basin of deposition. Rounded Torlesse clasts indicate transportation over long distances from an actively eroding source area, possibly by large rivers and additional beach erosion. In comparison, less mature limestone and siltstone clasts are derived from within the Tertiary basin of deposition. Thus, erosion

not only appears to have occurred during distally on the continental landmass, but also within the basin of recently deposited shelf sediments.

The following descriptions discuss each conglomerate location (refer to fig. 2.6 and table 2.1) in terms of debris flows and turbidites. Where the lithological types are identical these locations are described together.

Locations 1 and 2.

Coarse, Type 1 conglomerates overlie (with sharp, erosive base) Type 7 turbidites. These conglomerates represent one or more debris flow deposits and young eastward into turbiditic siltstones of similar composition, suggesting a waning supply of coarse material. The thickness of this conglomerate body varies from *ca.* 240 m in the north to *ca.* 460 m, 0.8 km laterally to the south. This lateral thickness variation is interpreted as a result of channelling so that the thicker portions were deposited in the main axis of the debris flow channel. The shape of the conglomerate deposit with a thick central section with narrowing margins is of a channel-fill form. Large channel fills are typical of debris flow deposits as they tend to seek out bathymetric lows cut by other processes (Pickering et al 1989). These channel-fill deposits are approximately 3.5 km wide in outcrop and 0.5 km thick at its thickest part.

Locations 3 and 4.

Coarse debris flow conglomerates are found here, but unlike locations 1 and 2, these are rich in Torlesse clasts and therefore belong to the Type 2 division. These young eastward into turbiditic siltstones and conglomerates of identical composition (Type 4). The pattern of waning supply seems to be the same as that described above. This Torlesse-rich debris flow material must have either had a different sediment supply point source to those at localities 1 and 2 which appear to be in the same channel, or represent a lull in intra-basinal erosion, assuming that there is no later structural separation in this area.

This conglomerate unit is *ca.* 160 m thick. The overlying siltstones have an upper faulted contact, giving a minimum thickness of *ca.* 200 m.

Locations 5 and 6.

Type 1 debris flow conglomerates overlie turbiditic siltstone and coarse sandstone beds. The conglomerates young into finer turbiditic siltstone and sandstones with reversed limestone/greywacke proportions (Type 5). This change seems to signify the waning supply of not only coarse but also of immature, intrabasinal limestone material. The shape of this conglomerate body is suggestive of another channel fill deposit. Type 7 beds are the lateral equivalent of this conglomerate to the north.

The conglomerate has a very approximate minimum thickness of *ca.* 220 m, however both the lower and upper contacts of the overlying siltstones are not well constrained.

Location 7.

A massive Type 2 debris flow conglomerate with rare limestone boulders is found here. The unit youngs into Type 7 material and finally into massive siltstone, representing an identical cut-off in sediment supply observed in all the above cases.

The conglomerate body has a minimum thickness of *ca.* 200 m.

Locations 8 and 9.

Both locations are lithologically similar and come from laterally equivalent horizons of the same conglomerate body, defined as Type 2. Location 8 occupies a position structurally below locations 3 and 4, which are also of the same conglomerate type. The two are separated by a tilted thrust, upthrown side to the east. Removal of this thrusting in any orientation would place these two Torlesse-rich debris flows into a similar stratigraphic position. The deposit appears to represent a wide channel fill containing an indeterminable number of debris flow deposits.

In the north the unit is at least *ca.* 440 m thick (the upper contact is faulted).

Location 10.

Here, a fine-grained debris flow conglomerate of the Type 3 conglomerate division is conformable on lower siltstones. This has a minimum thickness of *ca.* 550 m.

Locations 11 and 12.

Here, a coarse, clast-supported Type 2 conglomerate (debris flow) appears to enclose a limestone block (dimensions in map view of 975 x 125 m). Turbiditic siltstones overlie this conglomerate. The limestone unit has clay-rich mudstone at its base including greensand beds, overlain by blue marl beds. There is very poor control on the thickness of both the conglomerate and overlying siltstones here. This limestone unit could be mistaken for a large slide block. However, as discussed in chapter 4 (section 4.3.2.1e) this limestone in fact represents material tectonically emplaced, caught up along one of the early thrust planes affecting this cover sequence.

Location 13.

A coarse, clast to matrix supported Type 2 conglomerate, separated from sediments to the west by a thrust fault is found here. This debris flow deposit has a minimum thickness of *ca.* 500 m.

Location 14.

A fine, clast-supported, Type 2 conglomerate with a faulted western contact is found at locality 14. Again there is poor control on the thickness of this unit. This conglomerate is infact conformable above conglomerate locations 11 and 12.

Locations 15 to 18.

Conglomeratic sequences at locations 15 to 18 young to the west forming a continuous sequence from location 18 upwards to location 15. The oldest (location 18) is a coarse, matrix supported, Type 2 debris flow conglomerate and with an unusually large (compared to other locations) proportion of boulder-sized material of all lithologies. This massive, debris flow deposit youngs upward with decreasing conglomerate bed thicknesses and clast size and increasing spacing between conglomerate beds. At location 17 the conglomerates are interbedded with turbiditic siltstones (Type 5 conglomerate). Slump folding recording sedimentary deformation was observed in this location (fig 2.5b). Clast proportions vary. These are overlain by a return to Torlesse rich Type 2 conglomerate beds (location 16) and ultimately to interbedded Type 5 debris flow conglomerates and turbidites (location 15). The whole sequence is overlain by massive siltstones which are turbiditic close to the contact.

The total thickness of these conglomerates is *ca.* 740 m.

Lewis, Laird and Powell (1980) interpreted this sequence as debris flow deposits filling wide channels cut into siltstone.

Locations 19 and 20.

Coarse, Type 3 debris flow conglomerates overlie massive siltstones and young into Group 7 turbiditic siltstone beds (with similar grain proportions in coarse sandstone beds). The sequence ultimately youngs into massive siltstone beds at the centre of the Razor Fold.

The conglomerate is *ca.* 390 m thick on the eastern limb of this fold. It thickens in the nose region, although folding and possibly faulting obscure the true thickness in this area.

Location 21.

A tectonic sliver of Type 2 debris flow conglomerate outcrops here. The minimum thickness of this conglomerate is *ca.* 140 m. It is the lateral equivalent of conglomerate Type 2 at location 13.

Locations 22 and 23.

This sequence is rather distinctive and is summarized in the log of fig. 2.8. At location 22 a large, mappable limestone block (dimensions in map view are 1.3 km x 210 m) is underlain by Type 6 limestone-rich conglomerate with scattered greywacke clasts (this unit is *ca.* 60 m thick). This inturn overlies a Type 2 conglomerate, representing an older debris flow deposit of mature, extra-basinal material (location 23). This unit has a minimum thickness of *ca.* 210 m. The limestone breccia has the highest percentage of angular limestone seen anywhere (*ca.* 90%) and presumably has formed from material shed from uplifted limestone within the basin of deposition. Its association immediately below the large limestone block suggests the shedding of material either from an advancing, intrabasinal thrust, or debris along the base of a limestone olistrome.

Locations 24 and 25.

The conglomerate here consists of Type 4 matrix-supported, limestone-rich conglomerates, pebbly siltstones and massive siltstones. Large limestone boulders are present throughout (up to 30 x 2 m in outcrop), but are particularly concentrated near the top of the sequence (fig. 2.7c). Intercalated on a large scale with this conglomerate are massive siltstone beds. The whole conglomerate sequence represents an indeterminable number of debris flow deposits separated by quieter periods. The limestone clast percentage decreases to the south (within older debris flow deposits), presumably indicating progressive intra-basinal uplift up sequence. To the north, limestone breccia (Type 6) is exposed (fig. 2.7b). This is directly beneath the outer Razor Fold thrust contact (Fault 16) and is a similar lithology to the breccia of location 22. Folding and faulting of this unit obscures its true thickness.

Location 26.

The whole southern part of the Washdyke map sheet is dominated by this thick, matrix supported, Type 2 debris flow conglomerate. Its basal contact lies conformably above massive lower siltstones of the western Washdyke. The upper contact is conformably below massive siltstone beds (east of Green Hill which is marked on the Washdyke map sheet). In the far east the upper contact of this thick conglomerate deposit is against massive to turbiditic siltstones. Its great thickness compared to other conglomerate exposures suggests the stacking of many individual debris flow deposits. However, folding of this unit obscures its true sedimentary thickness. Around the western side of the Razor Fold the unit thins to the north with a maximum thickness of *ca.* 1,750 m.

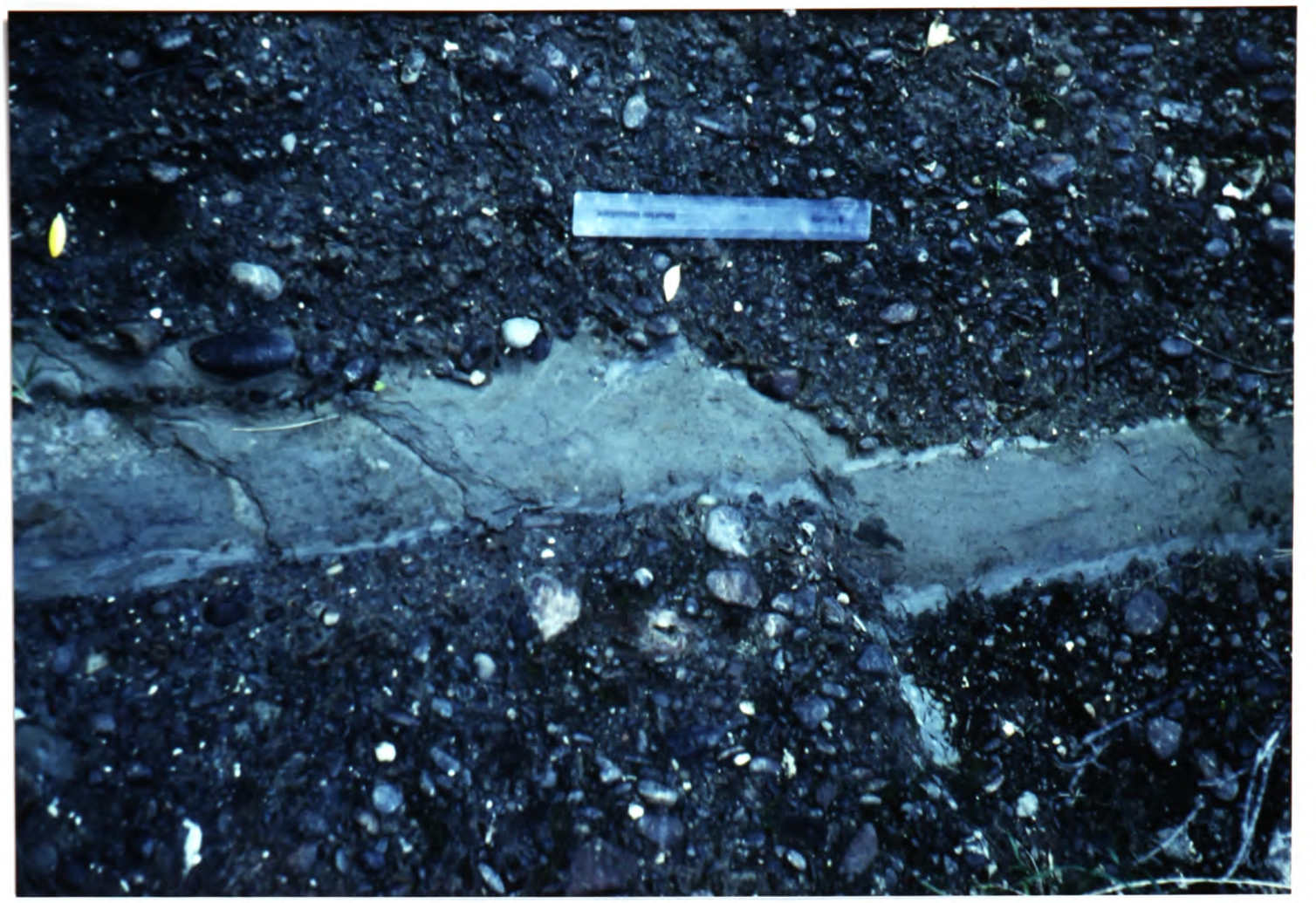


Fig. 2.7a: Type 2 conglomerate from location 26.

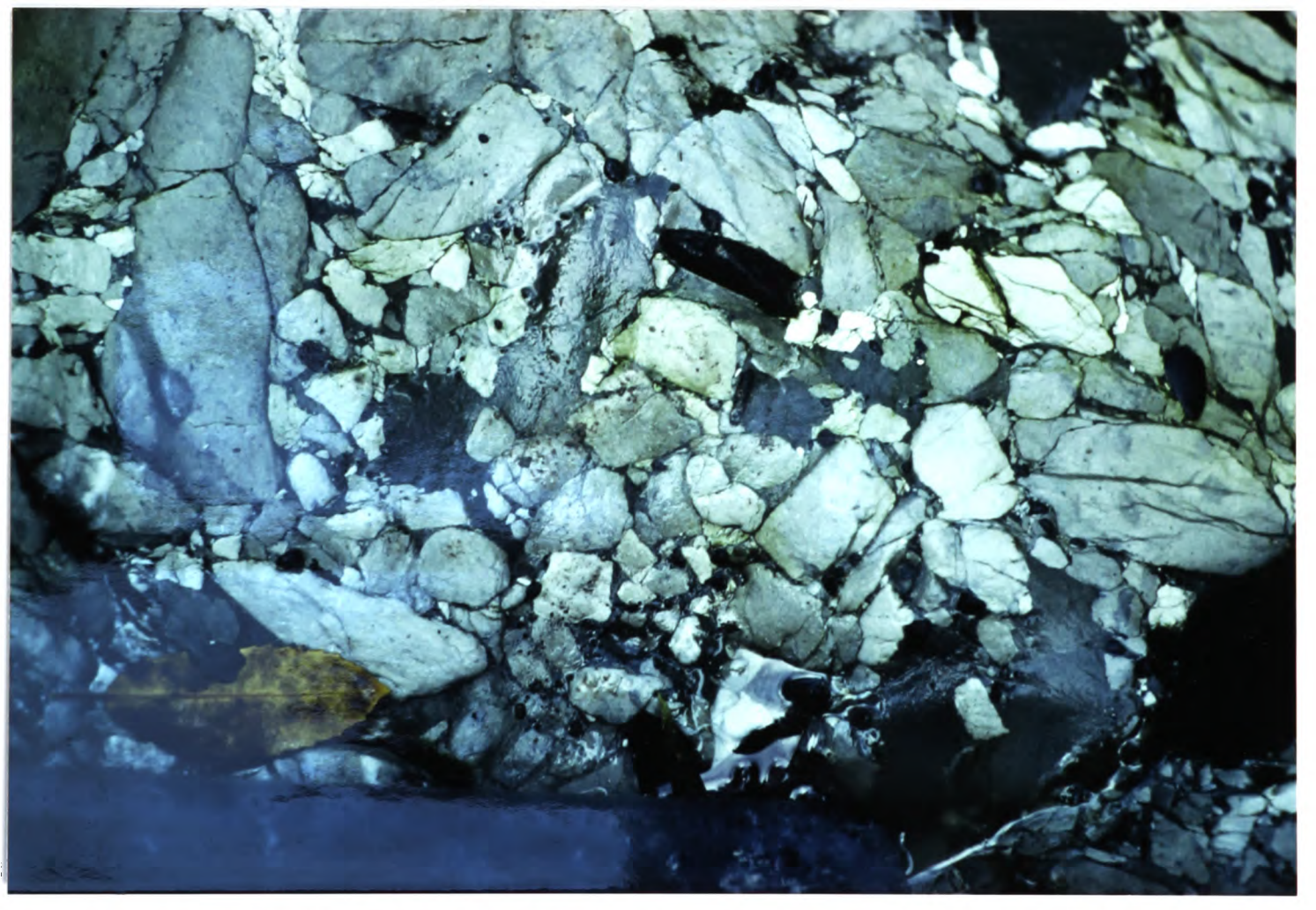


Fig. 2.7b: Type 6 conglomerate from location 25.

Fig. 2.7: Examples of the conglomeratic sequence from the Kekerengu-Washdyke study area. Refer to section 2.2.3 for Type descriptions and to fig. 2.6 for location positions.



Fig. 2.7c: Limestone boulder within Type 4 conglomerate from location 24 of the Kekerengu-Washdyke study area. Refer to section 2.2.3 for Type description and to fig. 2.6 for the location position.

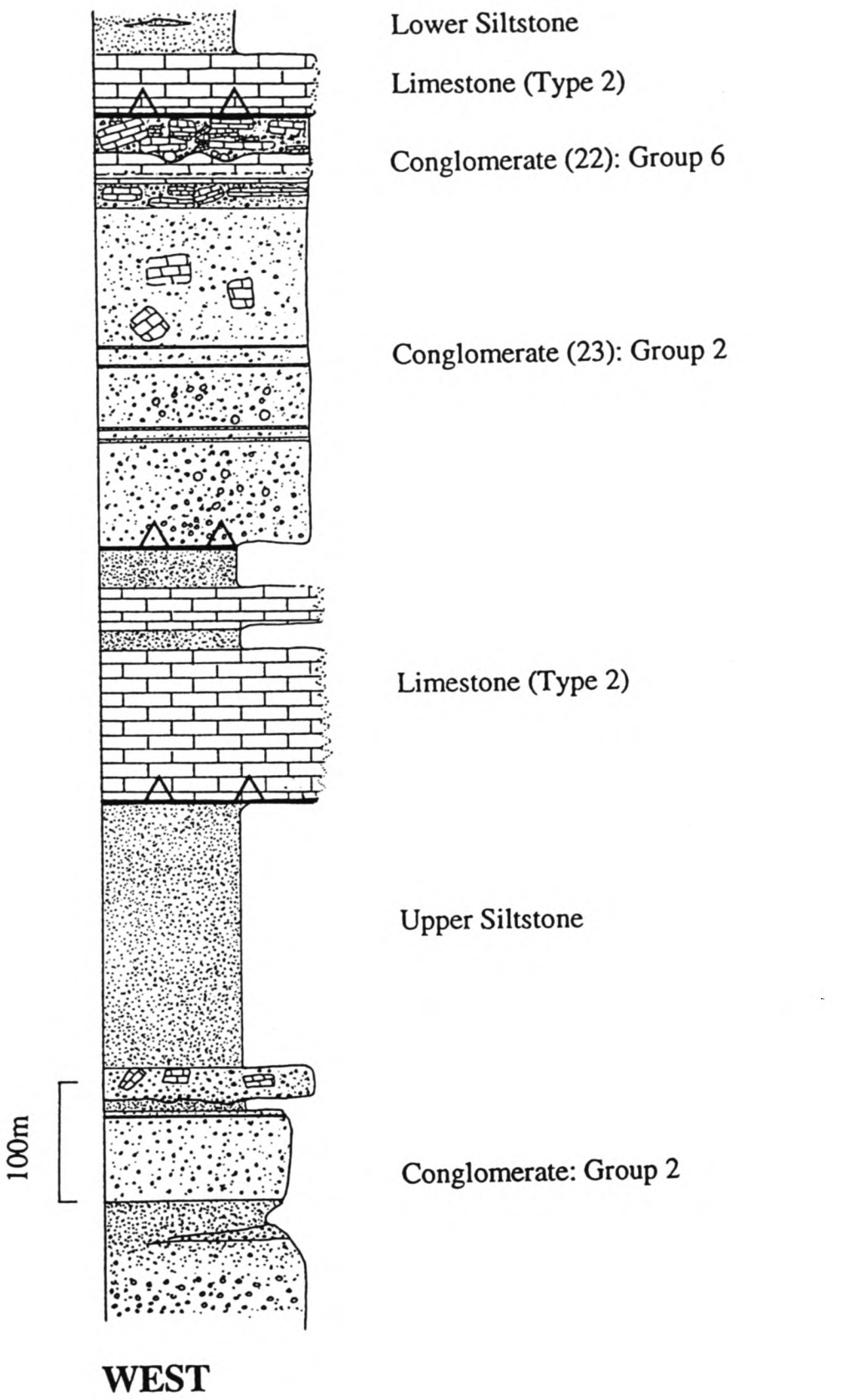


Fig. 2.8: Stratigraphic column of the Washdyke Gorge succession. Refer to section 2.2.3 for conglomerate location and lithological group numbering.

Previous work on the environment of deposition of the conglomerate unit

Marine resedimentated deposits can form in a number of environments from the outer shelf-upper slope, to bathyal regions. Bodies of sediment deposited at the base of the continental slope and spreading onto the bathyal plain are known as submarine fans. These fans comprise various morphological features including canyons, distributary channels, interlobe areas and levees. Much literature has been produced describing and putting forward models for the development of these fans (eg:- Mutti and Ricci Lucchi 1972; Walker 1978; Garrison et al 1982). Alternately, thick sequences of clastic sediments may be deposited in the outer shelf-upper slope environment without being redeposited downslope in the submarine fan, as would be sediments deposited on the continental slope itself. The nature of the sediments themselves can be used as evidence to the likely environment of deposition. Work of this kind was done by Lewis et al. (1980) for the Deadman Stream succession. This work is now summarized.

Lewis et al. (1980) described broad, relatively shallow, erosional channels cutting into mud and filled with thick accumulations of sediment. Turbidites and debris flows were believed to be responsible for the deposition of these sediments. Submarine fan channels are unlikely to exist long enough to accumulate thick sequences which suggested that the sediments were not from a submarine fan (Lewis et al 1980). The microfossils indicated an upper bathyal to outer neritic environment, as did the presence of symmetrical ripples and ripple cross bedding. Also noted was a deficiency of mud. Submarine fan deposits are typically mud-rich as a result of all the resedimented slope material. No rhythmic or cyclical patterns were observed, a common phenomena of submarine fans due to channel switching and aggradation (eg:- Mutti and Ricci-Lucchi 1978). Lastly, palaeocurrent data indicated a uniform flow direction during the accumulation of superimposed debris flow deposits. In comparison, distributary flow routes of submarine fans tend to meander and radiate from the main submarine canyon (Lewis et al 1980).

All the evidence pointed towards feeder channels shoreward of a submarine canyon and within the outer-shelf to uppermost slope environment.

Environment of deposition and timing

Turbidites and debris flow deposits dominate the sedimentary sequence from the Lower Miocene (*Otaian*) to Late Miocene times. The youngest dated conglomerate is the pebbly siltstone immediately overlying the conglomerate of location 26 in the eastern part of the Washdyke map sheet. This gave an age of *basal Tongaporutuan.* Thick debris flows fill submarine channels up to *ca.* 1 km in thickness. These channels cut into older, massive to turbiditic siltstones (flysch deposits). The clasts were derived from both extra basinal (rounded Torlesse) and intra basinal (angular limestone and siltstones) environments. From this it was apparent that uplift occurred of the distal

continental landmass and of the continental shelf itself. Variations exist in the percentage of limestone clasts (from *ca.* 2 to 90%) and in the size (from coarse sand grains to metre scale boulders) and angularity (from angular to rounded) of these clasts. These clast variations are likely to reflect variations in proximity to this intrabasinal uplift and in the timing of intrabasinal uplift events. Clues to the nature of this uplift came from the presence of limestone breccia beneath large thrust sheets (see section 4.3, Faults 16 and 26). This evidence indicated syn-sedimentary thrusting. Therefore thrusting is a likely cause of at least the intrabasinal uplift. A full discussion of this thrusting is given in chapter 6.

The foraminifera from samples covering the whole sequence revealed a mixture of benthic and planktonic forms suggesting deposition in an outershelf to upper slope environment. Within this area wide channels filled with progressive debris flows and turbidites, cutting into flysch deposited when uplift of the continental landmass began in the Lower Miocene.

2.2.4 The Upper Siltstone Sequence

Description

Massive siltstone was observed directly overlying conglomerate deposits in both the western and eastern parts of the Washdyke map sheet and in several localities from the Kekerengu map sheet. The extent of these units is summarized in fig. 2.9. In the western part of the Washdyke map sheet beds adjacent to this basal contact were dated as *Upper Lillburnian* to *Upper Waiauan* (chapter 3, dated sample 157). The siltstone here is predominantly massive with a poorly developed fissility. A few coarse sandstone beds were observed at the contact and an area with interbedded sandstones in the central section of this particular exposure. The upper contact of the siltstone here is faulted, causing the unit to structurally thin to the north. The minimum thickness is *ca.* 700 m at its widest part, though this is complicated by folding, thinning to zero. The same progression to overlying siltstone beds was observed in the centre of the Razor Fold.

In the eastern part of the Washdyke map sheet massive siltstone and siltstone with regularly interbedded coarser siltstone and fine sandstone horizons were also observed directly overlying debris flow conglomerates. However in this instance a pebbly siltstone lithology separating coarse conglomerates from the siltstone unit was dated as *Lower Tongaporutuan* (chapter 3, dated sample 53). The beds immediately above here were dated as *Waipipian* to *Nukumaruan*. The locations of these dated samples are marked on the Washdyke map sheet. The *Lower Tongaporutuan* age suggests that conglomerate deposition may have continued through to this time. There is then a *ca.* 5 Ma gap between this sample and the *Waipipian* to *Nukumaruan* siltstones. An unconformity or period of non-deposition is indicated. The siltstone in

KEY

Upper Siltstones (*Waipipian* to *Nukumaruan*)

Upper Siltstones (*Lillburnian* to *Waiauan*)

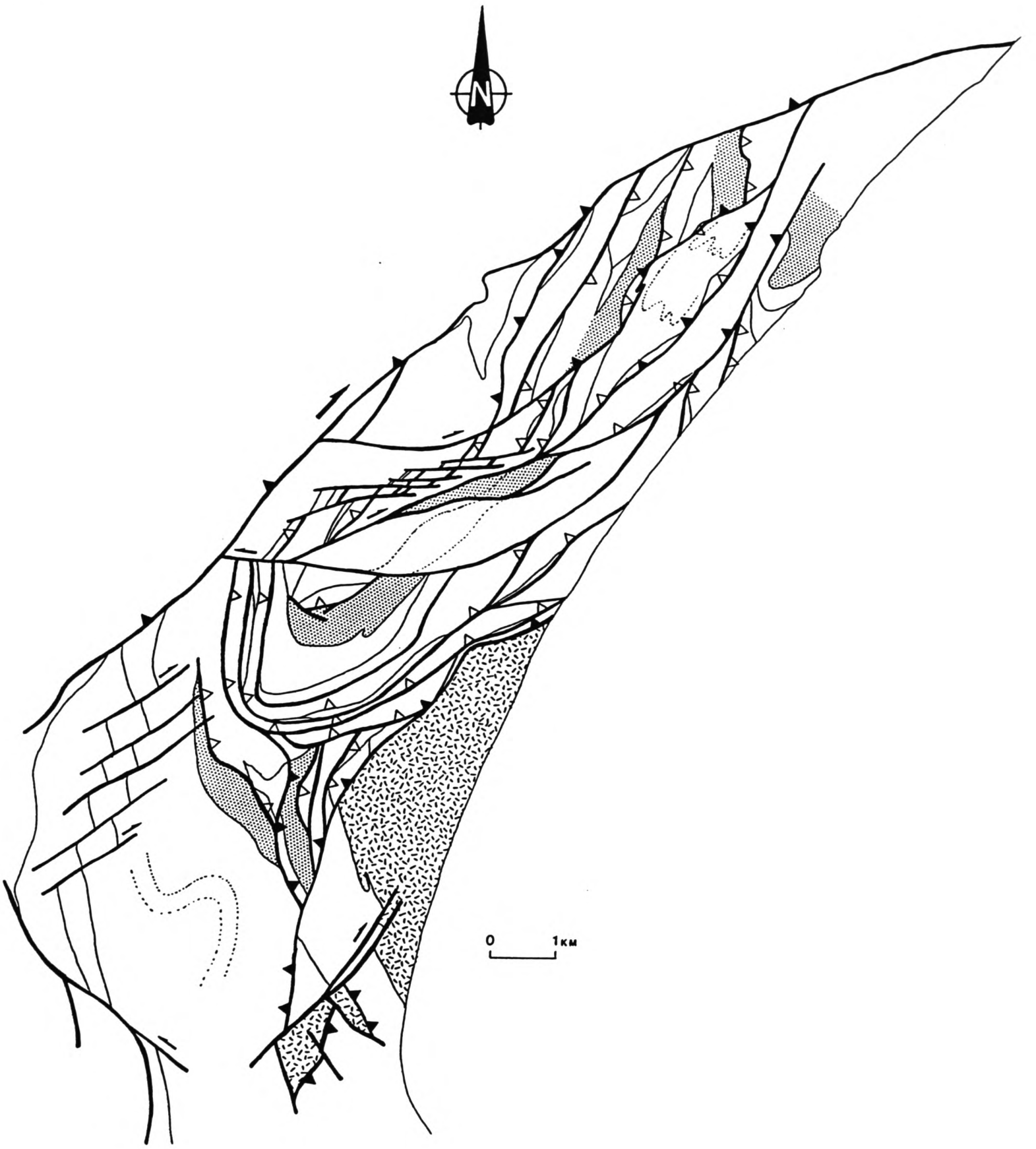


Fig. 2.9: Map of the Kekerengu-Washdyke study area showing exposures of the Upper Siltstone Sequence. Distinction is made between older *Lillburnian* to *Waiauan* siltstones conformably overlying conglomerate deposits, and the younger *Waipipian* to *Nukumaruan* siltstones found unconformably overlying conglomerates in the eastern part of the Washdyke map sheet (refer to section 2.2.4).

this eastern section is thus attributed to a separate, younger siltstone formation than the *Lillburnian* to *Waiauan* siltstone previously mentioned. Thus two upper siltstone units are present, distinguishable from each other on the grounds of age. Although not obviously distinguishable on lithological grounds, additional criteria for this division was revealed by palaeomagnetic samples collected from these siltstones (chapter 5). The data reveals a difference in the magnetic character of the two units. The older of the two units (sites WB2&3 and WD3) contain multi-domain magnetites, whereas the younger (sites WD1 and WD2) contain single-domain magnetites (refer to table 5.3).

This unconformity is a very important constraint on the timing of deformation within the study area. The two siltstone units are in fact separated by a large-scale reverse fault (Fault 21, chapter 4). This fault brings together conglomerate conformably overlain by siltstones of the older Upper Siltstone unit to the east, against conglomerate unconformably overlain by siltstones of the younger Upper Siltstone unit to the west. This suggests differential uplift and erosion of separate parts of the Tertiary sedimentary basin prior to *Waipipian* times. This point is elaborated upon in chapter 6.

The two Upper Siltstone types are distinguished in fig. 2.9. Similar aged siltstone to the younger upper siltstone unit is exposed in Camp stream, although here the lower contact is faulted. The lithology of this siltstone in Camp Stream is identical to that previously mentioned, with the additional observation of broken bivalvic material in coarse sandstone beds. Overall the deposit consists of flysch, massive to turbiditic siltstones.

Environment of deposition and timing

Foraminifera collected from these siltstone beds are of benthic and planktonic forms, indicating an outer shelf to upper continental slope environment (3.1). The bivalve material indicates derivation on the continental shelf. The earlier siltstone of this unit reflects a return to flysch deposition and therefore a decrease in the supply of coarse material. The younger siltstone reflects the continued supply of mostly fine grained material in the Pliocene period.

2.3 Linking the observed lithological units with their New Zealand nomenclature equivalents

The limestone lithologies described from the field area are in an identical stratigraphic position to the Amuri Limestone group (see 2.1) and are thus placed under this heading. How the different limestone lithologies are related to the exact member divisions (summarized by Morris (1987)) for this group is more problematical. Morris (1988) does not refer to any sequences within the field area and so comparisons are being made between different areas of the limestone basin.

It is not possible to relate the lower chert and limestone unit to the Lower or Upper Chert Members of Morris (1987) since the former is described as non-calcareous and both pass upward into muddy limestone. This in sharp contrast to the pure, siliceous, white limestone enclosing and lying above the field area cherts. It is therefore assumed that these beds are a part of the Flaxborne Limestone, described by Strong (at Needles Point) as a light grey-cream indurated limestone bedded on a scale of tends of centimetres with common chert nodules conformable above Woolshed Formation siltstone and sandstones. Whether this name includes the overlying siliceous, chert free limestone is not clear from the descriptions.

Limestone lithologies from the structurally isolated sequence of Kekerengu can also be linked to their likely equivalents. The volcanics and greensand lithologies at the base of this sequence are identical in lithology to the Fells Greensand and Grass seed Volcanics of Morris (1987). Their position below green, clay-rich marl beds also fits with this nomenclature correlation since the units are described as being within the Upper Marl Member of Morris (1987). However, the overlying blue marls in the field area do not fit into the Upper Marl Member description and indeed the combined thickness of the green marls and blue marls is in excess of three times the stated stratigraphic thickness of Morris (1987) for the Upper Marl Member. The transition from blue marls to cm bedded, siliceous, white limestone is similar to the transition from the Lower marl to Middle Limestone Members. If this is true, there must be a fault separating the blue and green marl lithologies, placing older above younger lithologies. The clay-rich marls described from the area were also described by Charnier and Ferriere (1991) as Eocene smectitic mudstones. The inclusion of greensand beds within this unit was also described in this paper.

No obvious equivalents to the structurally isolated Washdyke limestones or to the limestone sequences from this area were found within the descriptions of Morris (1988).

The age range (*Otaian* to *Clifdenian*), lithology and stratigraphic position of the Lower Siltstone links this unit with the Waima Siltstone Formation (*Otatian* to *Altonian*) of Hall (1964). Although the age range of the latter is slightly longer, the upper extension of this range was an upper limit and the unit may not actually continue to this time. The conglomerate age range (*Altonian* to *Lillburnian*, to *?basal Tongaporutuan*), lithology and stratigraphic position all relate this unit to the Great Marlborough Conglomerate (*Altonian* to *Lillburnian*). The lower of the two overlying siltstone deposits (*Clifdenian* to *Waiauan*) is attributed on the same grounds to the Heavers Creek Formation (*Altonian* to *Waiauan*). The upper overlying siltstone unit (*Opoitian* to *Nukumaruan*) is here named the Whanganui Siltstone due to its age. (There is no official New Zealand nomenclature for this siltstone).

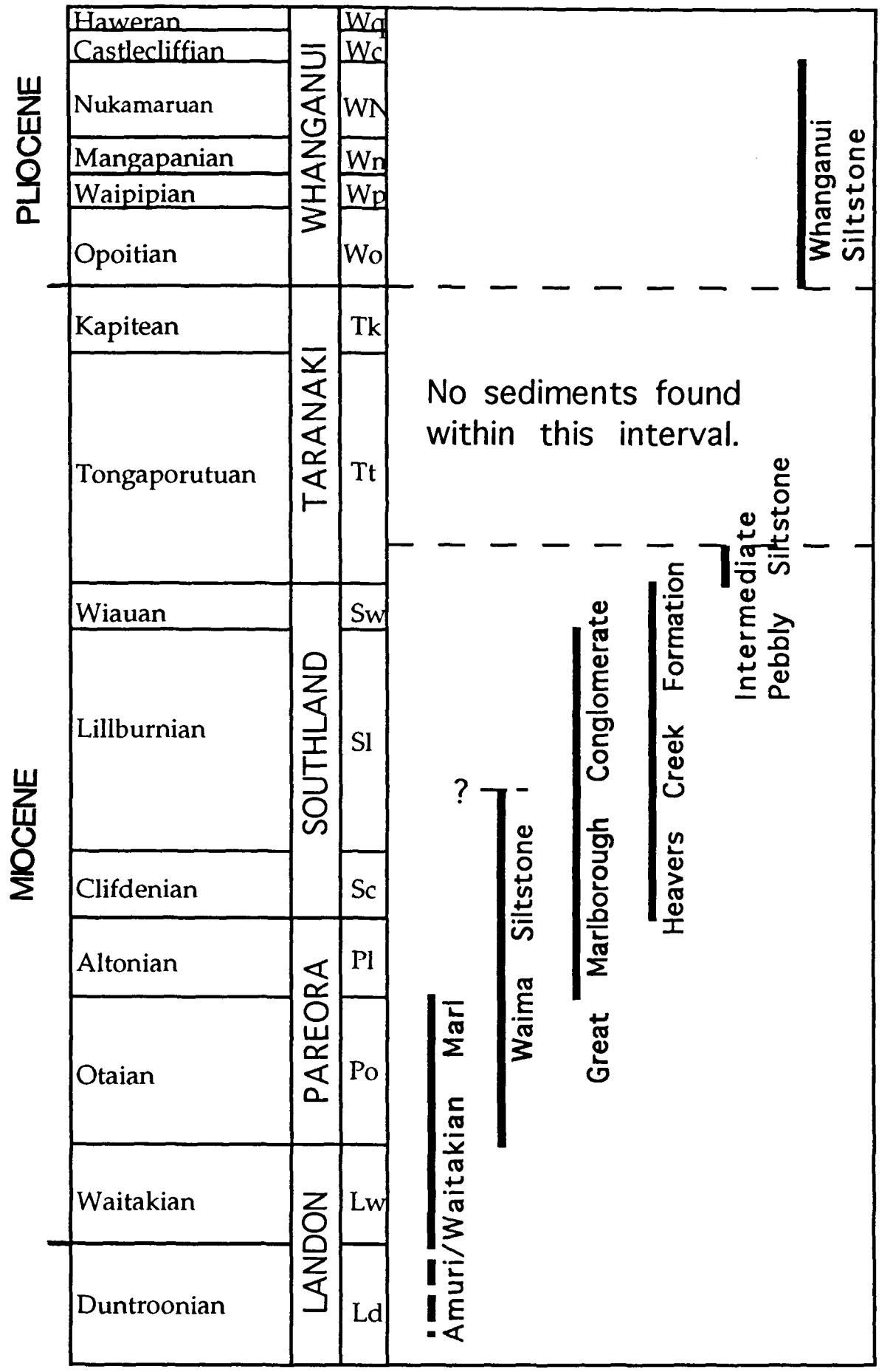


Fig. 2.10: Neogene time scale showing the age range (deduced in chapter 3) of each of the main lithological sequences described in section 2.2. The lower four sequences are labelled using New Zealand nomenclature (which does not exist for the upper two sequences).

Fig. 2.10 summarizes the age range (as deduced in chapter 3) of each of the main lithological sequences. These are labelled using the New Zealand nomenclature.

2.4 Corrolations of Stratigraphy Between Subregions of Marlborough and Northern Canterbury.

This section begins (2.4.1) by summarizing the Upper Cretaceous to Tertiary stratigraphy of the subregions within Marlborough and Northern Canterbury. This is followed by section 2.4.2 which summarizes the stratigraphic differences between these areas. The structural separations of the regions and the bearing of these on the stratigraphic differences are then discussed. Finally, section 2.4.3 discusses the timing and spatial distribution of all the unconformities present within the stratigraphic sequences of all the subregions, remarking on the implications of these with respect to the progression of deformation over the whole Marlborough and Northern Canterbury region throughout the Tertiary period.

2.4.1 The General Stratigraphy of Marlborough subregions and North Canterbury.

2.4.1a The Lower Awatere Valley

A simplified geological map of this sub-region is shown in fig. 6.2, (Roberts and Wilson 1992). The Lower Awatere Valley sediments consist mostly of marine basal conglomerates, pebbly sandstones, mudstones and siltstones, all lying with angular unconformity on Torlesse Supergroup rocks and with large topographic changes of the basement across the basin (Roberts and Wilson 1992). The sediments themselves change laterally due to proximity to source and depth of deposition. These sediments are known as the Awatere Group (King 1934) and are divided into three series on stratigraphic and palaeontological evidence: the Medway (*Tongaporutuan*), Upton (*Tongaporutuan* to *Kapitean*) and Starborough (*Upper Tongaporutuan* to *Mangapanian*) Series. Roberts and Wilson (1992) give a revision of the nomenclature associated with this Group.

2.4.1b Cape Campbell-Ward

A simplified geological map of this subregion is shown in fig. 6.10. Within this subregion are two markedly different stratigraphic sequences to the east and west of the London Hills Fault. The stratigraphy of these areas is summarized by Waters (1987). To the west of the fault basement flysch is overlain with angular unconformity by the

Hungry Hill Basalt and Paton Sandstone units (with Ngaianui Breccia at the base of the Paton Sandstone). These in turn are overlain by 550 m of Whangai Shale which is unconformably overlain by 2 to 300 m of Waima Siltstone (*Waitakian* to *Otaian*) and Tirohanga Sandstone (*Otaian* to *Altonian*). Another unconformity separates these siltstones and sandstones from 1 km of sandstones, mudstones and fossiliferous grits of the Upton Formation. Slightly further west Upton Formation sediments rest unconformably on basement (the Waima Siltstone is missing here). The Upton Formation is overlain by 500 m of Starborough Formation mudstones to fossiliferous sandy siltstones (*Waipipian*). Amuri Limestone is notably absent representing *ca.* 30 Ma of erosion; the Whaingaroan erosion interval, Morris (1987). Also absent is the Great Marlborough Conglomerate.

In contrast, to the east of the London Hills Fault Whangai Shale passes into flints and Amuri Limestone sediments. Near Needles Rock the Amuri Limestone is up to 1 km thick. Unconformably above this limestone are Upper Miocene Taranaki and Whanganui Series lithologies, both thinner than their equivalents west of the dividing fault, a feature attributed by to source proximity (Waters 1988).

2.4.1c The Benmore Subregion

This subregion preserves a sequence from Upper Cretaceous basement flysch in the core of the Benmore Anticline to Great Marlborough Conglomerate (with Hungry Hill and Burnt Creek Formations, Paton sandstone, Whangai Shale, Amuri Limestone, Woodside Formation siltstones and Cookson Volcanics, Waima Siltstone, and Tirohanga Sandstone between the two). Dating of these units was summarized by Prebble (1976) and Waters (1987). No known unconformities exist within the sedimentary pile and thicknesses are obscured by structural repetition.

2.4.1d Northern Canterbury

Early Miocene Waima Formation siltstones and local coarse mass flow deposits disconfomably overlie Amuri Limestone or conformably overlie Cookson Volcanics or Eyre Group rocks. Overlying the Early Miocene deposits are *Otaian* to *Tongaporutuan* Mount Brown Formation sediments. These constitute mass flow sandstones and siltstones, limestones and mass flow conglomerates with sandstone and siltstone beds at the top. The dominance of M.Miocene mass flow deposits correlates this formation with the Great Marlborough Conglomerate of Marlborough (*Altonian* to *basal Tongaporutuan*), although the base is slightly older. Differences in nomenclature make direct comparisons difficult. The Mount Brown Formation may incorporate the equivalents of the Marlborough Tirohanga Sandstone (*Otaian* to *Altonian*) and Upton Formation (*Waiauan* to *Kapitean*). The Mount Brown Formation is overlain by siltstones and local debris flows of the Greta Formation (*Clifdenian* to *Mangapanian*).

Finally, Kowai Formation (*Kapitean* to *Nukumaruan*) sandstone conglomerates and mudstones were deposited. *Opoitian* aged sediments are described on the Hurunui map sheet (Gregg 1964) as marine siltstones, sandstones and conglomerate bands with local large blocks of Tertiary and older rocks, mostly unconformable on older rocks.

The stratigraphies of all the Marlborough sub-regions, excluding the Kekerengu-Washdyke region which has been summarized in fig. 2.10, are summarized in fig. 2.11. The North Canterbury region is not included as this region shows significant local stratigraphic variations.

2.4.2 The Stratigraphic Differences and Structural Separation of each Sub-region

The Benmore and Kekerengu-Washdyke subregions both have similar Upper Cretaceous to Tertiary stratigraphies (see figs. 2.10 and 2.11). The former is preserved between the Clarence and Kekerengu Faults and the latter on the downthrow side of the Kekerengu Fault. It is thus assumed that these two regions were once receiving sediments from an identical source region. They were possibly both within the same continuous basin prior to displacement and uplift associated with movements on the Kekerengu and Clarence Faults.

The Campbell-Ward sub-region currently in the same northeastern corner of Marlborough as the Benmore and Kekerengu-Washdyke sub-regions, consists of very different stratigraphic sequences to them. West of the London Hills Fault is a total lack of limestone and M.Miocene debris flow material. This region was subjected to uplift during limestone deposition in the other sub-regions and subject to uplift or somehow cut off from the source of sedimentary supply during debris flow deposition in the other sub-regions. The region east of the London Hills Fault was not uplifting during limestone deposition, but was subject to the same uplift or cut in sediment supply as the region to the west of the London Hills Fault. To the east the L.Miocene which is exposed to the west, is absent, signifying greater uplift or an earlier cut in sediment supply compared to the region to the west.

The Ward region west of the London Hills Fault is separated from the Benmore region by the Flags Creek Thrust (Waters 1987), a large scale thrust fault which juxtaposes greywacke basement against the younger Tertiary cover material. The actual displacement on this thrust is unknown and its exact nature disputable (chapter 4). However, due to the very different stratigraphies of these two sub-regions it is seems likely that the two regions were originally separated by a large distance and subjected to different sedimentary histories prior to their juxtaposition possibly by movements along the Flags Creek Thrust.

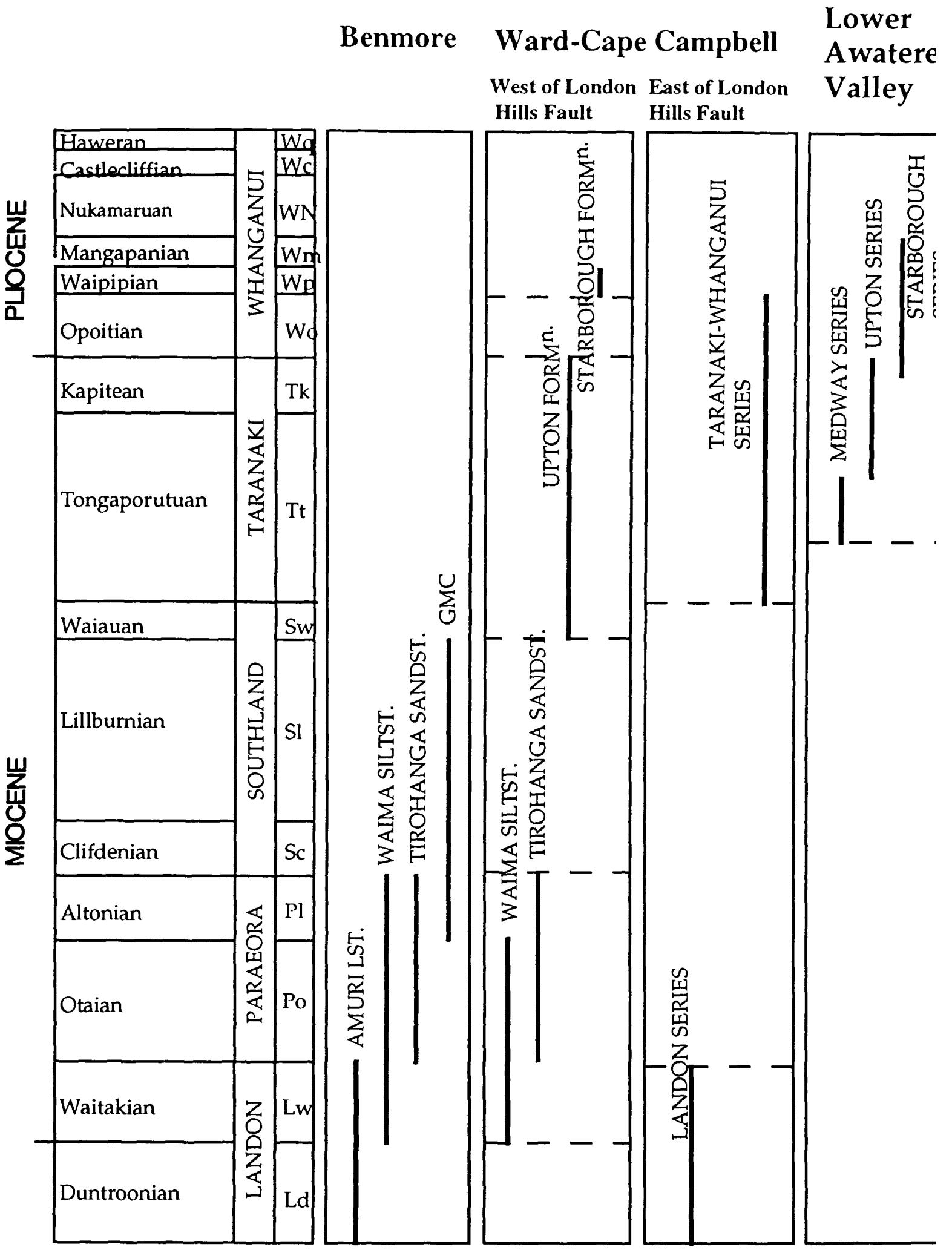


Fig. 2.11: Columns summarizing the stratigraphies of the Benmore, Ward-Cape Campbell and Lower Awatere Valley subregions of Marlborough against the New Zealand Neogene time scale. Dashed lines bound periods within which no sediments are found. Data from Prebble (1976); Waters (1988); and Roberts and Wilson (1992).

The two regions either side of the London Hills Fault must have themselves been separated by distance and subjected to different tectonic histories for one to receive limestone whilst the other did not. Both sides also show the same absence of M.Miocene material in sharp contrast to the Benmore and Kekerengu-Washdyke sub-regions which were receiving sediments during these times. These two regions are separated by the Flags Creek Thrust and it is therefore possible that it was this structure which later juxtaposed the two separate tectonic areas. The fault may itself have been responsible for the difference in tectonic style if it had been active at that time.

The London Hills Fault is mapped as a thrust fault (Prebble 1976)). If the displacement on this fault were large then it is easy to explain the juxtaposition of two so different settings. The larger unconformity east of the fault in the Miocene may also be a result of displacement along this fault, the eastern side representing the thrust hanging wall. If the unconformity is indeed directly related to this fault, then this suggests that the London Hills Fault has been active at least since the Miocene. Alternately the thrust may be younger and the changes to either side be a result of unpreserved structures or to source proximity.

The Lower Awatere Valley region of northeast Marlborough between the Awatere and Clarence Faults again has a very different tectonic history. Only U.Miocene sediments resting unconformably on basement are preserved. If this area received Lower and Middle Miocene sediments these were eroded prior to deposition of the U.Miocene sediments. Timing of displacement on the Clarence Fault is problematical. If the fault were present as a reverse fault during the Miocene (Browne 1992) then it may be directly responsible for the uplift in the Lower Awatere Valley prior to deposition in this area in the *middle Tongaporutuan*. Alternately it may be younger and an unobserved structure be responsible for the differences. In any case a very large amount of uplift occurred in the Lower Awatere Valley region whilst the Benmore and Kekerengu-Washdyke regions were receiving sediment. The Clarence Fault may be responsible for juxtaposing the different areas, or may have been an active separating structure which resulted in their different tectonic histories.

The Northern Canterbury region lies to the south of the Hope fault. Here a sequence similar to that of the Benmore and Kekerengu-Washdyke sub-regions is preserved. There are some differences between the two areas which are mainly concerned with the timing of unconformities (these are discussed in 2.4.3). The regions are fundamentally similar in terms of stratigraphy and it is therefore suggested that these sub-regions were within the same large catchment basin throughout the Miocene.

2.4.3 Unconformities and the Progression of Deformational Events

This section covers only Miocene and Pliocene unconformities since it is primarily this period which this study is attempting to describe and explain.

Fig. 2.12 summarizes the ranges of maximum uplift and subsidence in each sub-region below the current erosion level. It is clear from this that current uplift is greatest in the Benmore subregion. A glance at this figure shows the apparent existence of two (Middle and Upper Miocene) episodes of uplift. There are two approaches to the timing of these events depending on whether one considers uplift to have occurred progressively (1), or at a fixed point in time (2).

(1) Considering the older episode first: this effects subregions to each side of the London Hills Fault and also the Lower Awatere Valley. During this period of uplift the other regions were receiving sediment (mostly coarse debris flow deposits). It seems reasonable to conclude that the uplift of the subregions currently to the north and east (the Ward-Cape Campbell and Lower Awatere Valley subregions) was supplying the material deposited in the regions to the south and west (the Benmore, Kekerengu-washdyke and Northern Canterbury subregions). The unconformity to the west of the London Hills Fault, not apparent to the east of it, has already been interpreted as a possible result of uplift of the hanging-wall of this fault.

A further period of subsidence of the uplifted areas occurred initially west of the London Hills Fault, then to the east of it, and finally in the Lower Awatere Valley. The subsidence spread progressively westward at the beginning of the Late Miocene.

A second, younger episode of uplift effects Northern Canterbury and the Kekerengu-Washdyke subregion approximately simultaneously. This uplift began at the same time as subsidence of the Cape-Campbell and Lower Awatere Valley subregions. Throughout this uplift episode the Cape Campbell-Ward and Lower Awatere Valley subregions were receiving sediment. There appears to have been a reversal with uplift affecting areas previously receiving sediment and *vice versa*. What was separating these two areas? An even younger *Opoitian* aged unconformity is observed west of the London Hills Fault. This may represent the spread of this younger episode of uplift into this subregion. Alternately it may represent a separate unrelated uplift event due to local structures.

(2) Rather than uplift occurring in some areas whilst subsidence continued in others, uplift may have occurred in some areas late-on in the corresponding subsidence interval, immediately prior to deposition of the overlying sediments. In this case the oldest uplift event would have occurred immediately prior to the Upper Miocene, whereas the younger uplift event would have occurred immediately prior to the Early Pliocene.

The youngest Tertiary sediments affected by the current erosion level are of *Nukumaruan* age. These sediments are tilted and therefore tilting occurred post-*Nukumaruan*. Exposures of young Quaternary material are also tilted (Lensen 1962) which indicates the continued uplift and deformation of the Marlborough region to the present day.

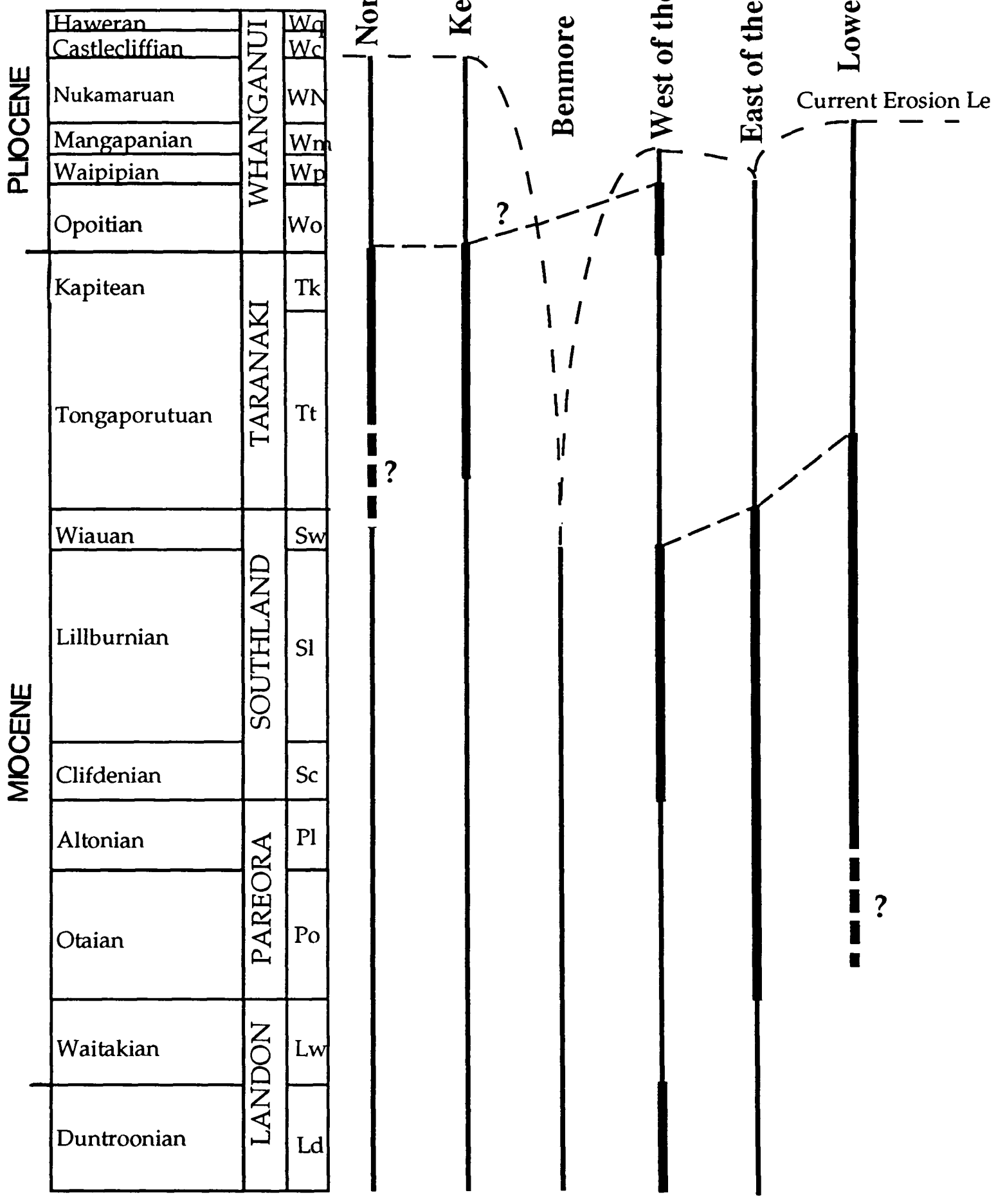


Fig. 2.12: Figure summarizing the maximum ranges of uplift (shown as thick lines) and subsidence (shown as thin lines) in each of the Marlborough subregions and in Northern Canterbury against the New Zealand Neogene time scale. The data is base on exposed stratigraphic sequences within each of these areas (see fig. 2.11). For ar explanation of this diagram refer to section 2.4.3.

Introduction

Rare coals of up to *ca.* 15 cm in diameter were found within the conglomeratic sequence (see fig. 2.13a). In hand specimen the coals are dull black and friable, to shiny black with a conchoidal fracture. Growth rings (indicating that these coals are tree debris) are visible in some of the more friable varieties.

The level of organic metamorphism (rank) of coal is known to be a function of burial temperature and time held at that temperature (Hilt's Law). Corrolations have been made between the reflectance value of vitrinite and the Rank of the sample from which that vitrinite is taken (Castano and Sparks 1974). Vitrinite is an organic constituent of coal, one of the coal macerals of Stopes (1935). The vitrinite maceral includes telinite (woody structures preserved) and collinite (structureless matrix, cement and cavity infilling). Vitrinite is typically a pale grey colour in transmitted light (crossed polars) and does not fluoresce under reflected light.

Five coal samples were collected from the conglomeratic sequence within the Kekerengu-Washdyke study area. The location of these samples is shown in fig. 2.13b. The method, results and interpretation of this work are described below.

Method

The analysis was carried out at the Department of Geology at the University of Southampton with Dr. J. Marshall. Random fragments from each sample were mounted in small plastic blocks which were then polished and covered in a layer of silicone oil. The mean random vitrinite bireflectance in oil (R_O) was measured at 546 nm with a Zeiss UMSP 50 microscope fitted with a 40X oil immersion objective and with a measuring spot diameter of 2.5 mm. For each sample R_O was calculated from *ca.* 50 individual reflectance measurements. Data acquisition and processing were performed by an IBM PC using the program 'SLAP' (S. Hillier).

Results

Transmitted light microscopy of the prepared samples revealed either woody plant material with good preservation of original cell structure (telinite), solid organic material (collinite), or sediment interbedded with narrow coal bands showing internal plant



Fig. 2.13a: Coal fragment from within the conglomeratic sequence from the northern part of the Washdyke map sheet (sample number 137b).

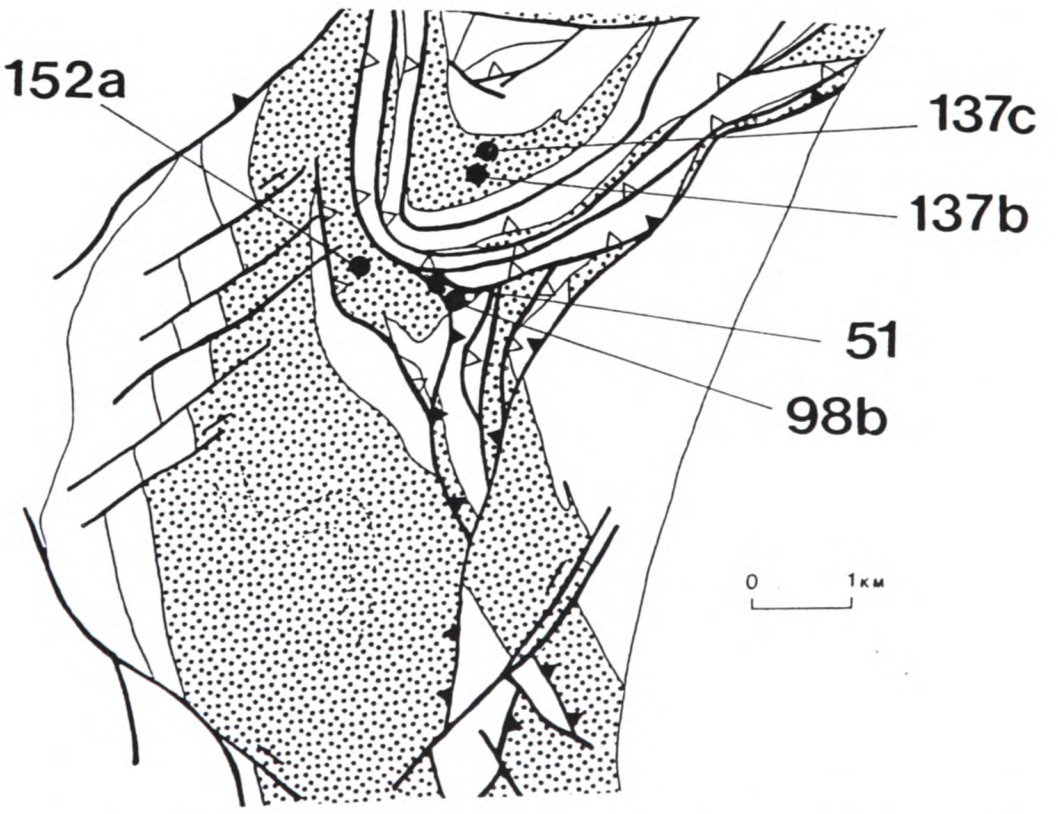


Fig. 2.13b: Sketch map of the Washdyke map sheet study area showing the location of the five coal samples collected for vitrinite reflectance analysis. All samples were found within the conglomeratic sequence.

structure (telinite). Areas of vitrinite were identified by their light-grey colouration under crossed polars.

Under reflected light all vitrinite areas showed a bluish colour, none of this material in any of the samples fluoresced, as is a characteristic of vitrinite. In contrast the groundmass of the preserved cell structure flouresced brown. These brown areas also had a slightly lower reflectance value compared to the blue vitrinite areas.

The mean reflectance values recorded under reflected light for each sample are shown below in table 2.2.

Sample number	**Mean Vitrinite Reflectance (R_O)**	**Standard Deviation**	**Number of Measurements**
51	0.301*	0.071	48
98b	0.195	0.021	50
137b	0.174	0.017	42
137c	0.384*	0.042	50
152a	0.220	0.014	50

Table 2.2: Results from vitrinite reflectance analyses (*: values exceeding the minimum for vitrinite formation).

Interpretation

The good preservation of cell structure in all samples is a clear indicator of the low rank of these coals. The brown fluorescent material between vitrinite is likely to be liptinite. Of all five samples, only two (SV51 and SV137c) have mean reflectance values above the minimum required for the formation of vitrinite (0.3%). This indicates extremely low rank in all cases.

The conversion of R_O to temperature and burial depth is not a straight forward one. The relationships vary depending on coal mineralogy, the geothermal gradient and the time held at certain temperatures. However, a general corrolation does exist as shown in table 2.3. All the samples from this study fall within the brown coal and lignite rank field, with temperatures well below 60^{O}C and suggesting burial depths of less than 1 km.

Conclusion

All the coal samples collected from the Kekerengu-Washdyke study area indicate that the conglomeratic sequence which contains them has not been subjected to burial to

depths of more than *ca.* 1 km, nor to temperatures of more than *ca.* 60 ^{o}C. Since their formation these sediments have remained at a high crustal level.

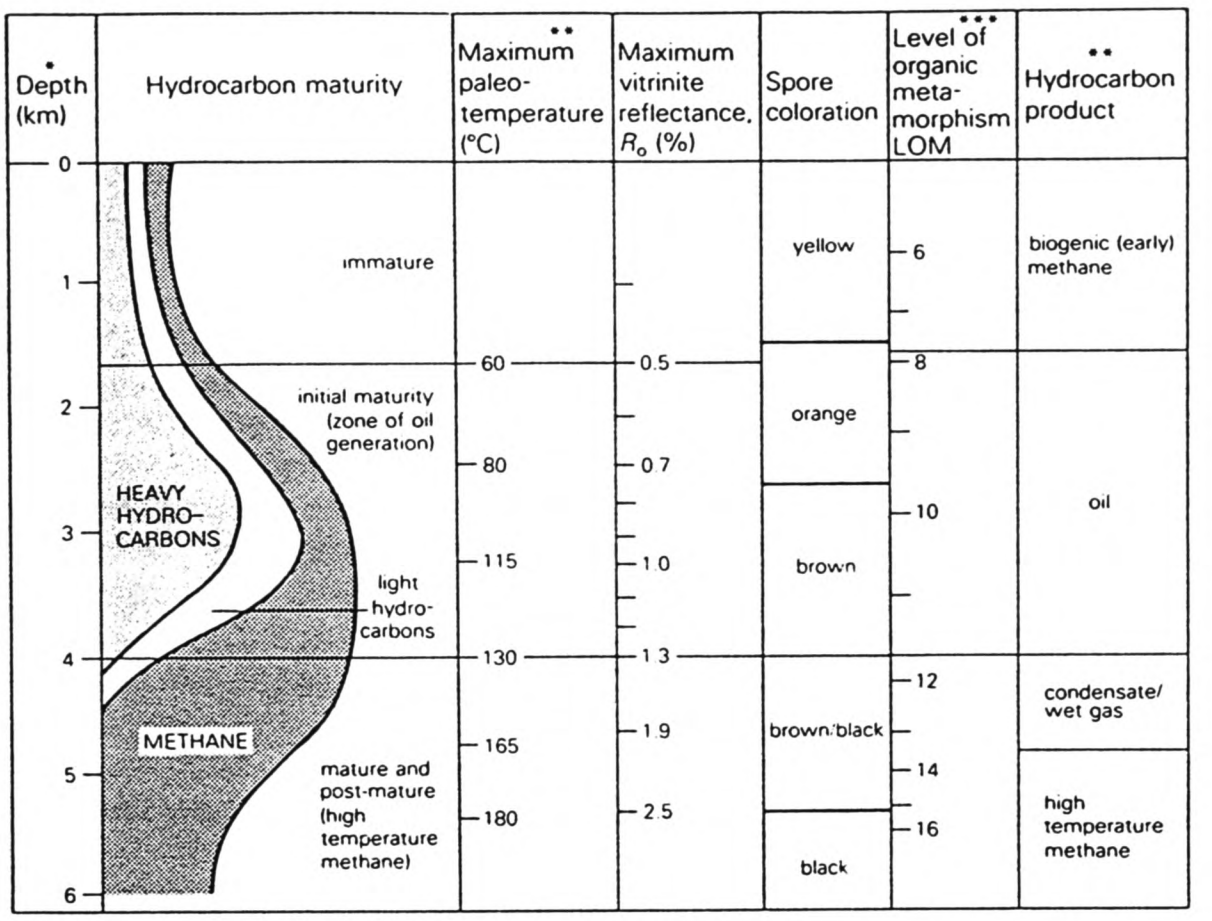


Table 2.3: General corrolation of organic maturation indices (from North 1985). The analysed samples have mean vitrinite reflectance values of between 0.174 and 0.384% and therefore have not been to depths of more than 1 km or to temperatures above *ca.* 60°C.

CHAPTER 3

CHAPTER 3: MICROPALAEONTOLOGY

3.1 Introduction

The New Zealand Cretaceous and Cenozoic are divided into regional stages. These are biostratigraphic units characterized by taxa with restricted ages. One or more key species (Finlay and Marwick 1940, 1947) define the stage boundaries. The basic framework for New Zealand biostratigraphy worked out by Finlay and Marwick followed on from the earlier work of Thompson (1916) and Allan (1933). The wide distribution and rapid dispersal of planktonic microfossils has made this group of free-floating protozoa ideal for the biostratigraphic division of oceanic facies. On death the empty tests are deposited on the ocean floor to form biogenic deposits (Vincent and Berger 1981) or are incorporated in clastic deposits. Restricted ages for benthic foraminifera and calcareous nannofossils are also known (Edwards 1971).

When the microfossil biostratigraphy is combined with dated palaeomagnetic reversal records (assuming spread rates and using radiometric dating) a reasonably reliable time-scale can be produced for the biostratigraphy. Suitable strata can therefore be dated by the extraction and identification of their microfossil content. The Palaeocene and Neogene time scales for New Zealand are shown in fig. 3.1. These are adaptions from Berggren et al (1985) and taken from Hornibrook et al (1989). The stage and series names displayed in this figure are referred to throughout this thesis. For clarity all New Zealand stage names are written in italics.

New Zealand calcareous Cenozoic rocks, including mudstone, greensand, sandstone and soft limestone lithologies, are usually fossiliferous. Also, New Zealand Cretaceous rocks often contain siliceous microfauna (Hornibrook et al 1989).

The foraminifera content can also be used to give an idea as to the particular palaeoenvironment of a sample. Unfortunately, although direct correlations between palaeodepth and foraminifera assemblage have been attempted (eg: Kafescioglu 1975; Murray 1976; Marks 1979) many other environmental factors, such as temperature, salinity, substrate character, sedimentation rate and turbulence influence the foraminifera assemblage (Hornibrook et al 1989). Simple diversity and abundance of foraminifera species are not sufficient to make accurate environment deductions. It is however possible to make suggestions as to the most likely environment using approximate proportions of planktonic and benthic species, and the general level of diversity.

Diverse assemblages with large proportions of planktonic species (in excess of *ca.* 70%) and minor benthic forms, are likely to indicate deposition on the lower slope

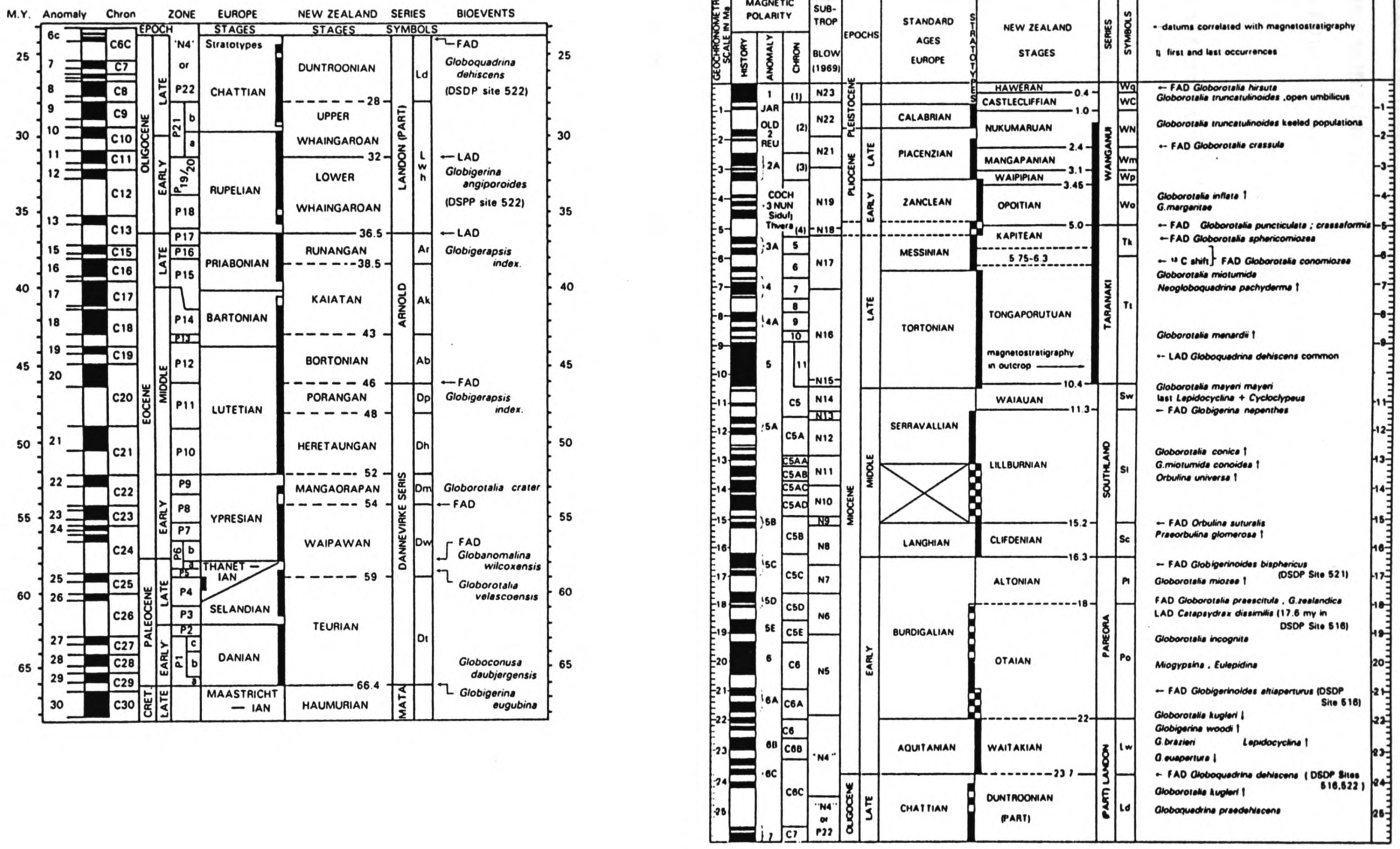


Fig. 3.1: Paleocene and Neogene time scales for New Zealand. (Taken from Hornibrook et al 1989, adapted from Blow 1983 and Berggren et al 1985).

to abyssal plain. Roughly equal proportions might suggest the outer shelf, whereas a dominance of diverse benthic species and rare planktonics would suggest the inner shelf to upper slope (Hayes 1981). The foraminifera may also have been reworked from one environment down-slope to another.

3.2 Criteria used for sample collection

One of the aims of this thesis was to add to and therefore create a more extensive dating of the Tertiary cover sequence within the study area. The study area consists of biogenic to argillaceous limestones and clastic sediments (chapter 2). As mentioned in 3.1, many of these lithologies are known to be rich in micro and nannofossils and have in fact been previously successfully dated by Lensen (1962); Lewis and Laird (1978), Osborne (1980), Prebble (1976); and Scott (1979).

It was not, however, the intention of this project to obtain a full documentation of the whole Tertiary sequence, rather to look in particular at those Miocene and Pliocene sedimentary rocks which provide information about the Tertiary sedimentary and structural history. Only siltstone and muddy siltstone samples were collected for dating. These lithologies have been shown by previous workers in this area to have been deposited throughout the Miocene to Pliocene period. These particular lithologies are often richly fossiliferous and also relatively simple to break down for microfossil extraction. Both planktonic and benthic foraminifera were sought, being well documented and thus more easily identifiable. Nannofossils are harder to extract and identify and give little additional information where microfossils data is also available.

Samples were collected from all siltstone units, mostly adjacent to faults or at sedimentary contacts. Only unweathered and undeformed material was taken in order to obtain well preserved foraminifera.

3.3 Extraction and Identification of Foraminifera

Preparation of samples was done in the Geology Departments at Victoria University of Wellington and Oxford. Samples were crushed by hand to pebble size and immersed in kerosene for several minutes. The kerosene was then poured off and the samples covered in boiling water with a little detergent and left to soak over night. This procedure breaks down the sample which is then sieved to remove the finer clay fraction and finally dried-out in a moderate heat oven. Prepared samples were observed under a reflected light microscope and the foraminifera extracted using a fine paintbrush dipped in water. Foraminifera from each sample were stored in individual

slide cases. Finally the foraminifera were identified by the author with reference to Hornibrook et al. (1989). At all stages of the extraction procedure all equipment was kept thoroughly clean to prevent any cross contamination.

Foraminifera from all samples were coated with a thin layer of gold and observed under a scanning electron microscope (SEM). This aided and confirmed identification by greater magnification of specimens (up to 120000x). SEM photographs were taken of the foraminifera.

3.4 The Results

A number of samples contained no or insufficiently well preserved foraminifera. Of the successful samples foraminifera tests formed between 1 and 30% of the sample after removal of the clay portion. Broken and unbroken tests were observed, but only unbroken varieties were used for identification. The diversity of species varied between samples, ranging from 1 to 9 separate species in a sample. Those samples with higher diversity also contained a higher percentage of foraminifera. In terms of the palaeoenvironment, only the occurrence of planktonic and or benthic species was used to comment on the possible environment for that sample (see 2.2).

All identified foraminifera and deduced sample ages are listed in Part A of the appendix to this chapter in order of sample number for samples from the Kekerengu and then from the Washdyke map sheets. Key foraminifera used for the age determination of each sample are starred and listed separately in Part B of this appendix with their corresponding age range (taken from Hornibrook et al 1989). SEM photographs of twelve of the key foraminifera are presented in fig. 3.3 and fig. 3.4.

All age results have been added to the Kekerengu and Washdyke map sheets (within dashed circles to distinguish from previously deduced ages which are within solid circles), and to fig 3.2 (as thicker lines, again to distinguish from previous ages which are shown as thin lines). Fig 2.10 summarizes the new and old data in terms of the age ranges of the five Tertiary lithological sequences as described in chapter 2.

3.5 Conclusions

All the listed foraminifera were well preserved and confidently identified. All species are marine. The age range of samples analysed in this way varied between restricted to long time intervals depending on the particular foraminifera species present in each sample. The samples provide a more accurate coverage for the dating of the individual units as existed prior to this study. These ages can then be used in assessing

the timing of deformation within the study area (see chapter 6). Of particular importance was the discovery of a pebbly siltstone of *basal Tongaporutuan* age overlying Type 2 conglomerate (chapter 2, location 26) in the eastern part of the Washdyke map sheet (dated sample 53). This sample increases by *ca*. 1.5 Ma the previous determination of the age range of this conglomerate (*Altonian* to *Lillburnian*, Prebble (1976)). It also defines more accurately the unconformity separating this unit from overlying Pliocene siltstones. This unconformity is believed to be an important constraint in the timing of an episode of thrust faulting in the Upper Miocene (chapter 6).

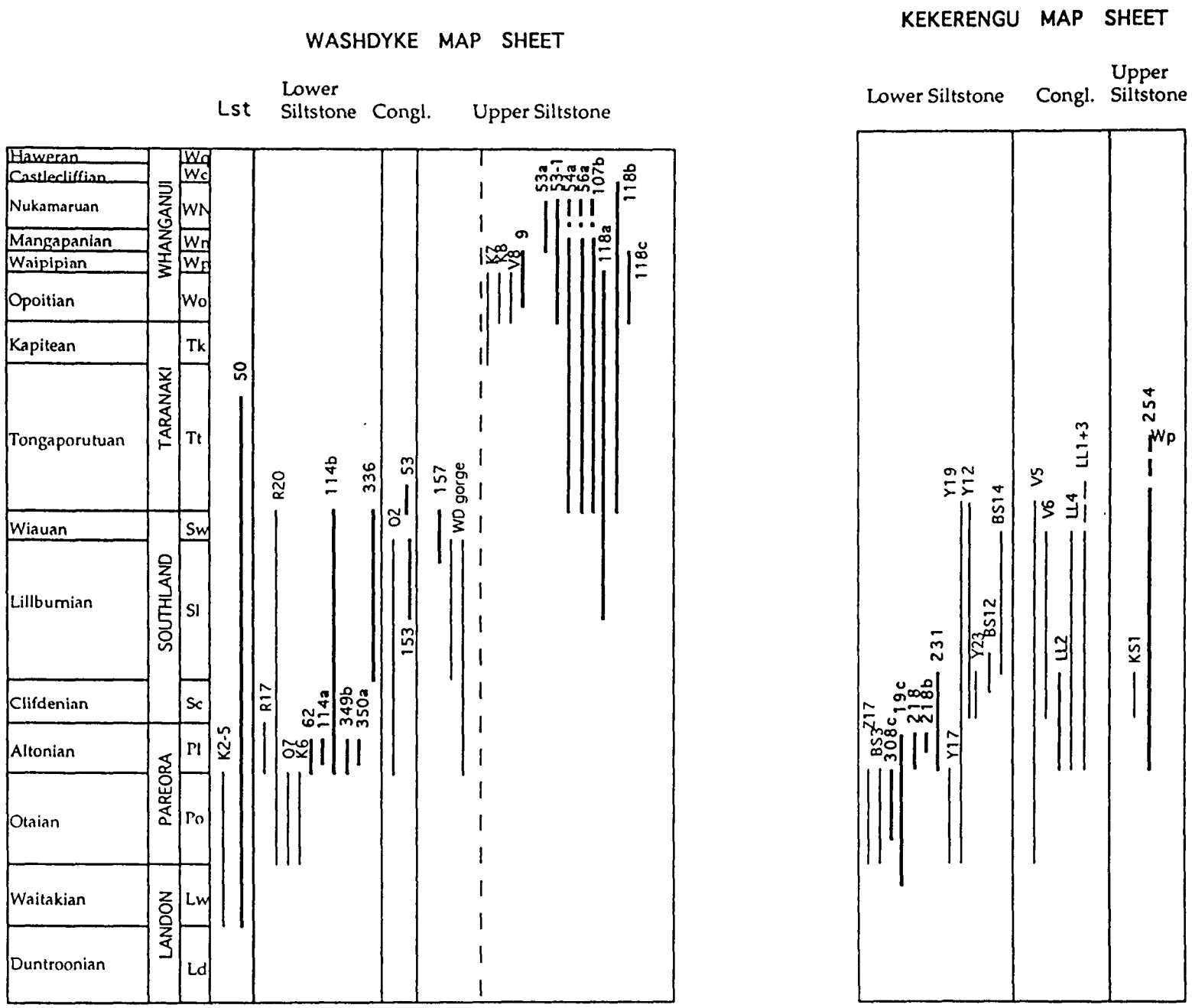


Fig. 3.2: The age range of each sample from the Kekerengu and Washdyke map sheets is shown against the New Zealand Neogene time scale. Thick lines represent samples analysed in this study, whereas thin lines represent previously dated samples from the two areas (Lensen 1962; Lewis and Laird 1978; Osborne 1980; Prebble 1976; and Scott 1979). Note that the Upper Siltstone is divided by age into two parts in the Washdyke area. Refer to Appendix 1 for foraminifera lists and key species used in the determination of these age ranges.

APPENDIX to Chapter 3: Foraminifera Identification

This appendix is divided into two parts: Part A lists the species of foraminifera identified within each sample collected for dating within the Kekerengu and Washdyke map sheets; Part B lists the key foraminifera species used to obtain the age range of each sample, including SEM photographs of twelve example key foraminifera.

PART A (foraminifera lists)

The foraminifera are listed for each sample in order of sample location number from all sites within the Kekerengu map sheet (Section 1) and the Washdyke map sheet (Section 2). The species within each sample used to determine the age of each sample (key species) are starred and then listed in Part B. The age range of each sample is given in abbreviated form (refer to fig. 3.1) at the end of each sample foraminifera list (R: Recent).

Section 1: Kekerengu Map Sheet Samples

19c

Anomalinoides sp.
Globigerina woodi
Globigerina woodi connecta *
Globoquadrina dehiscens
Plectofrondicularia sp.
Stilostomella sp.
U.Lw-M.Pl

218

Anomalinoides vitrinodus *
Globigerina woodi connecta *
Lenticulina mamilligera
Siphotextularia bolivina
Uvigerina ongleyi
L&M.Pl

218b

Globigerinoides trilobus *

Globigerina woodi
Globigerina woodi connecta *
M.Pl

231
Cibicides molestus
Globigerina woodi
Ruakituria mahoenuica
Uvigerina miozea *
Uvigerina ruatoria *
Pl-Sc

235
*Globigerina woodi gr.**
Lw-M.WN

254
Globigerinoides conglobatus *
Globigerinoides trilobus *
M.Pl-Wp

308c
Bulimina senta
Cibicides molestus
Globorotalia incognita *
Lenticulina loculosa
Uvigerina miozea
Uvigerina ongleyi
Uvigerina picki *
M&U.Po

Section 2: Washdyke Map Sheet Samples

9
Angiporides sphericus
Bolivinita quadrilatera
Bulumina aculeata
Globigerina woodi gr.

Globigerinoides trilobus
Globorotalia crassaconica *
Globorotalia inflata *
Oridosaris tenera
Stilostomella sp.
M.Wo-Wp

10
Bolivinita quadrilatera *
Oridosaris tenera
Quinqueloculina triangularis
L.Tt-R

27
Cibicides robertsonianus hopkinsina mioindex
Fissurina orbinyana
Globigerina bulloides
Globigerinoides conglobatus
Globoquadrina dehiscens *
Globigerina woodi *
Plectofrondicularia advena
M.Lw-M.Tt

32a
Globigerina bulloides
Glogigerina woodi
Globigerina sp.
Glogigerinoides conglobatus
Globigerina woodi connecta *
Gyroidina neosoldario
U.Lw-M.Pl

45a
Cibicides perforatus
Plectofrondicularia sp.
Globoquadrina dehiscens *
Stilostomella sp.
Spatangoid
Lw-Tt

49a

Globigerina woodi *

Lagena sp.

Uvigerina sp.

M.Lw-M.WN

49c

Globorotalia scitula *

Stilostomella sp.

Sphaeroidinella disjuncta *

Sl-Sw

50

Globigerina sp.

Globoquadrina dehiscens *

Radiolaria

Lw-M.Tt

53

Bolivinita quadrilatera *

Globigerina sp.

Nodosaria substrigata

Oridosaris tenera

Proxifrons sp.

Quinqueloculina triangularis

Siphotextularia ihunga *

Spatangoid

Basal Tt

53-1

Amphicryna hirsuta

Cibicides ?mediocras

Globigerina sp.

Haeuslerella pliozenica *

Lenticulina calcar *

Wo-WN

53a

Globigerina bulloides

Globigerinoides trilobus

Globorotalia puncticuloides *

Wm-M.WN

54a

Bolivinita quadrilatera *

Nodosaria substrigata

Spatangoid

Quinqueloculina triangularis

L.Tt-R

56a

Bolivinita quadrilatera *

Cibicides molestus *

Oridosaris tenera

L.Tt-Wp

56b

Bolivinita quadrilatera *

Lenticulina sp.

Miliolid

Spatangoids

Stilostomella lepidulus

L.Tt-R

58b

Buxella sp.

Globigerina falconensis *

Globorotalia (turboratalia) continuosa

Pl-Okehuan (Pleistocene)

62

Globigerina woodi connecta *

Globoquadrina dehiscens

Globorotatia zealandica *

lagena sp.

L&M.Pl

107a

Globigerina woodi *

Quinqueloculina triangularis

M.Lw-M.WN

107b

Bolivinita quadrilatera *

Quinqueloculina sp.

Spatangoids

L.Tt-R

114a

Cibicides molestus

Desidulina subglobosa

Globigerina woodi

Globigerina woodi connecta *

Globigerinoides ?trilobus *

Siphotextularia bolivinina

Stilostomella verneuilii

M.Pl

114b

Anomalinoides sphericus

Stilostomella sp.

Uvigerina ruatoria *

Pl-Sw

118a

Haeuslerella morgani *

Neouvigerina eketahuna

Plectofrondicularia sp.

Stilostomella antipoda

M.Sl-Wo

118b

Bolivinita quadrilatera

?Bulimina truncanella

Cibicides mediocras

Globorotalia falconensis
Notoratalia taranakia *
Plectofrondicularia pellucida *
Stilostomella lepidula
Tt-WN

118c
Bolivinita quadrilatera
Bulimina striata
Globigerina bulloides
Globorotalia punticulata *
Notoratalia taranakia
Uvigerina peregrina
Wo-Wp

153
Cibicides sp.
Plectofrondicularia parri *
Plectofrondicularia phona/parri *
Stilostomella sp.
Uvigerina sp.
M.Sl

157
Globigerina sp.
Globoquadrina dehiscens
Globorotalia turbotalia mayeri *
U.Sl-U.Sw

336
Globorotalia conica *
Lenticulina ?calcar
Stilostomella sp.
Sl-Sw

349b
Bulimina pupola
Globigerina woodi connecta *
Globoquadrina dehiscens

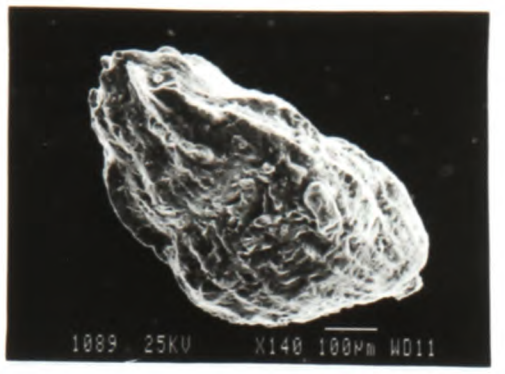
Globorotalia zealandica *
Gyroidinoides zealandicus
L&M.Pl

350a
Cibicides sp.
Globigerina woodi connecta *
Globigerinoides trilobus *
Lagena sp.
Sphaeroidinellopsis disjuncta
Radiolaria
M.Pl

PART B: (key species list)

Foraminifera are listed in alphabetical order with age ranges taken from Hornibrook et al (1989). Series names are kept in full whereas stage names are in their abbreviated form (refer to fig. 3.1). SEM photographs of twelve of the key foraminifera are shown in fig. 3.3 and fig. 3.4.

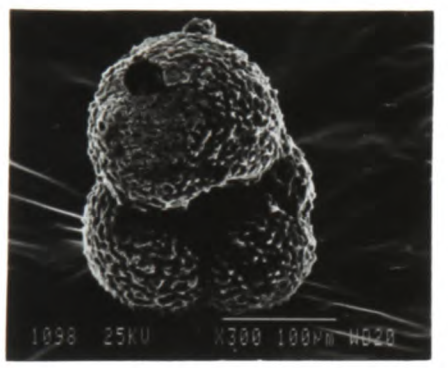
Anomalinoides vitrinodus	Pl-Wo
Bolivinita quadrilatera	L.Tt-R
Cibicides molestus	Bt-Wp
Globigerina falconensis	Pl-Okehuan (Pleistocene)
Globigerina woodi connecta	U.Lw-M.Pl
Globigerina woodi gr.	Lw-M.WN
Globigerina woodi	M.Lw-M.WN
Globigerinoides conglobatus	Lw-Wp
Globigerinoides trilobus	M.Pl-WN
Globoquadrina dehiscens	Lw-Tt
Globorotalia conica	Sl-Sw
Globorotalia crassaconica	Wo-Wp
Globorotalia incognita	U.Po-L.Pl
Globorotalia inflata	U.Wo-R
Globorotalia punticulata	Wo-Wp
Globorotalia punticuloides	Wm-M.WN
Globorotalia scitula	Sw-R
Globorotalia turbotalia mayeri	U.Sl-U.Sw
Globorotalia zealandica	Pl-Sc
Haeuslerella morgani	U.Southland-Taranaki-Wo
Haeuslerella pliozenica	U.Tt?-Tk-WN
Lenticulina calcar	Southland-L/M.Whanganui
Notorotalia taranakia	Tt-WN
Plectofrondicularia parri	U.Pareora-M.Southland
Plectofrondicularia parri-phona	U.Southland
Plectofrondicularia pellucida	Tt-WN
Rectuvigerina ruatoria	Pl-Sw
Siphotextularia ihunga	Lw-Sw
Uvigerina miozea	Po?-Pl-Sc
Uvigerina picki	Lw-Po



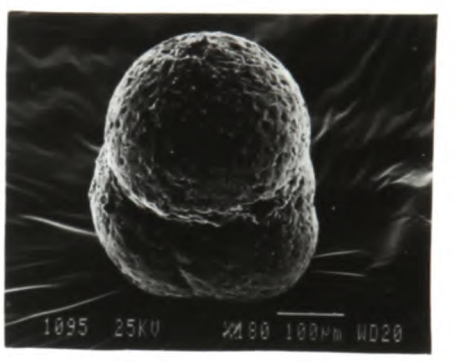
a



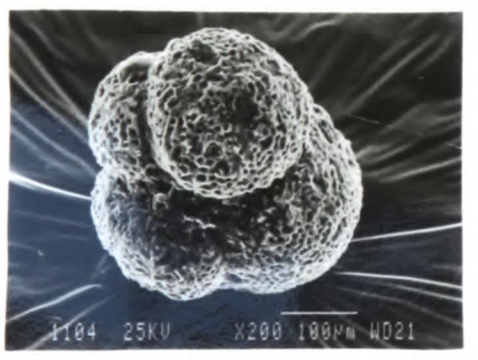
b



c



d



e

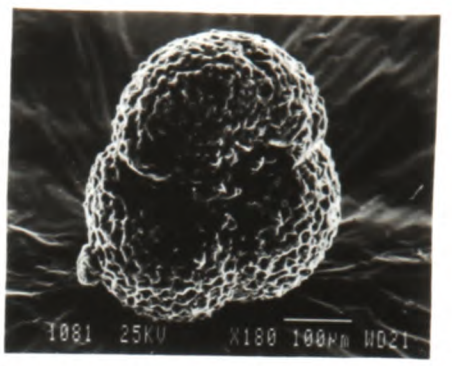


f

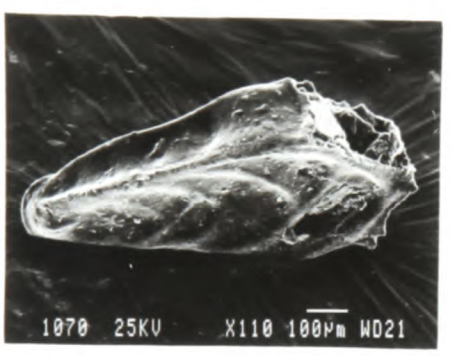
Fig. 3.3: SEM photographs of key foraminifera species from the Kekerengu map sheet. The sample number from which each of the foraminifera shown is taken is given in brackets alongside the species name. (a) *Uvigerina miozea* (231); (b) *Rectuvigerina ruatoria* (231); (c) *Globigerina woodi gr.* (235); (d) *Globigerinoides trilobus* (254); (e) *Globorotalia incognita* (308c); (f) *Uvigerina picki* (308c).



a



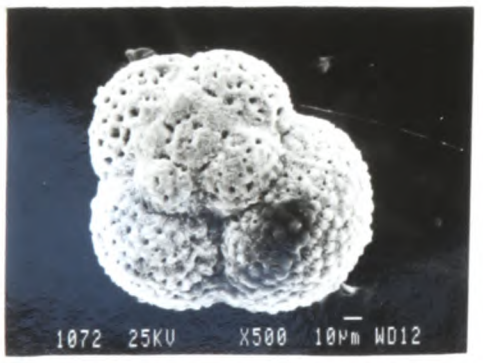
b



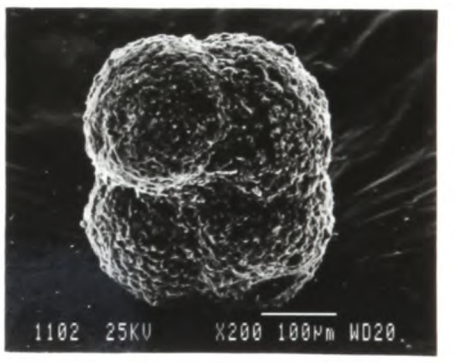
c



d



e



f

Fig. 3.4: SEM photographs of key foraminifera species from the Washdyke map sheet. The sample number from which each of the foraminifera shown is taken is given in brackets alongside the species name. (a) *Globoquadrina dehiscens* (27); (b) *Globigerina woodi* (27); (c) *Bolivinita quadrilatera* (53); (d) *Siphotextularia ihunga* (53); (e) *Globorotalia punticuloides* (53a); (f) *Globorotalia conica* (336).

CHAPTER 4

CHAPTER 4: STRUCTURAL DATA

4.1 Introduction

The study area can be divided into subregions based on the main outcrop regions of exposed Cretaceous-Tertiary rocks (see fig 4.1a). In detail the stratigraphy and general structure in these regions varies. However, a general sequence can be recognized within each subregion which is notably consistent, consisting of early thrusts which are folded and cut by later thrust, folds and strike-slip faults. These structures are found on all scales from kilometre scale folds and faults to millimetre scale faults and cleavages. The general chronological order of structural elements was used to label these elements. Two separate phases (D_e and D_l) can be readily defined. The earliest phase (D_e) resulted in thrusts T1, and folds F1, which sometimes have an associated axial-planar cleavage S1. The later phase (D_l) contains two fold and two fault events. F2 folds (some with an axial-planar cleavage) with associated syn-tilt faults T2, are folded by F3 folds. All these features are then cut by T3 late reverse, dextral and sinistral strike-slip faults.

In the following sections particularly well exposed examples of the structural elements are described for each subregion. Not all the structural elements were observed in all the subregions as will become apparent when each subregion is discussed.

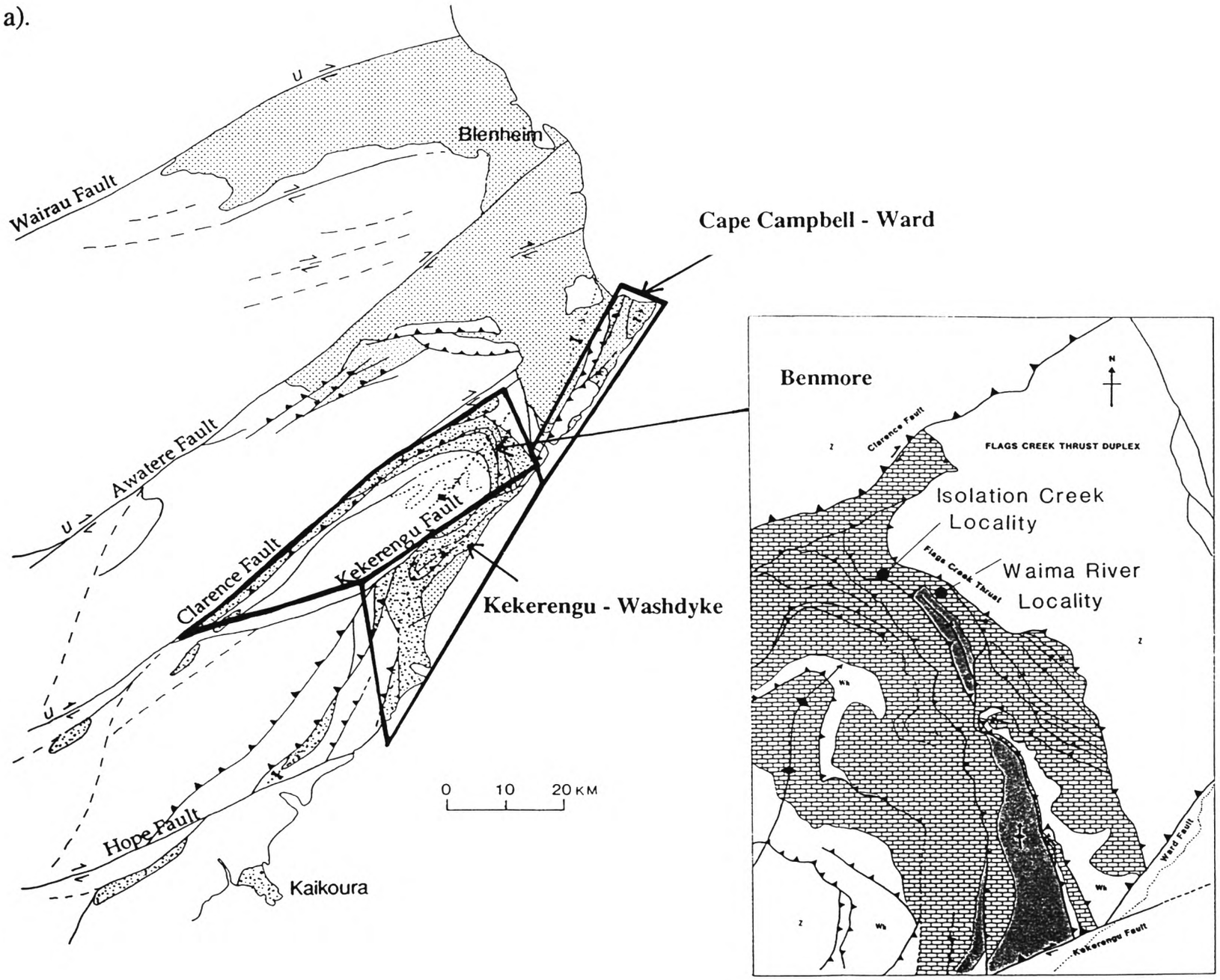
4.2 Structural Data from the Benmore Subregion

4.2.1 Introduction

This subregion is situated between the Clarence and Kekerengu Faults in northeastern Marlborough. The area consists of a folded set of faults within the Cretaceous-Tertiary sequences which was first described by Prebble (1976) and which is known as the Flags Creek Thrust Duplex (Waters 1988). Prebble (1976) and Waters (1988) both mapped the oldest, most northerly contact juxtaposing Amuri Limestone against greywacke basement as a thrust fault referred to as the Flags Creek Thrust by Waters (1988). The folded Cretaceous-Tertiary sequences are truncated by the bounding faults to the west and east.

Two main locations were studied within this area. These localities best illustrate the structural features of the Benmore subregion. The first locality, called the Waima River locality (grid ref: (P29) 95962425), transects the Flags Creek Thrust. This contact is generally poorly exposed and in places coincides with the Waima River. However, at

a).



b). The Waima River Locality

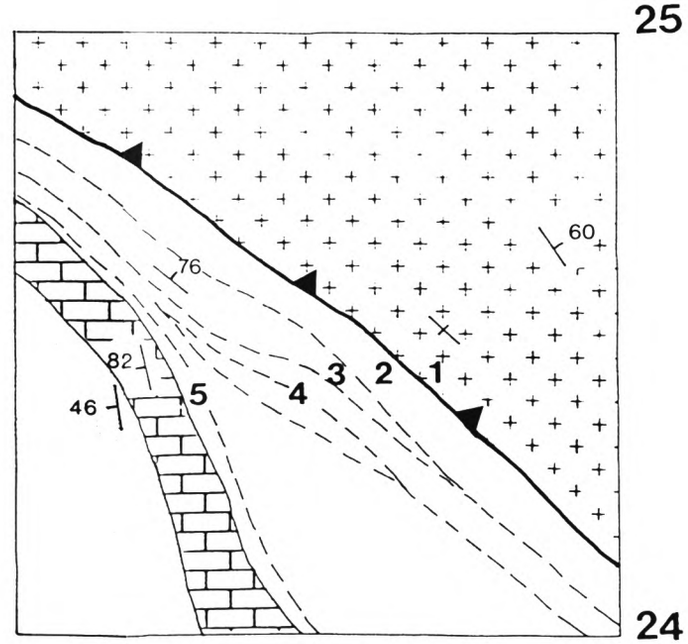


Fig. 4.1: a). Diagram showing the division of Marlborough into subregions of Tertiary exposure. An enlargement of the Benmore subregion is included to show the exact positions of the two described localities from within this area (see 4.2.1). b). The extent of lithological divisions (bound by dashed lines) at the Waima River locality of the Benmore subregion. For descriptions of these units refer to section 4.2.1.1.

the studied locality the Waima River cuts across this contact which is well exposed in the cliff sections. Here, the true nature of the Flags Creek Thrust could be studied. The second locality (grid ref: (P29) 923248) was found within Amuri Limestone structurally lower in the duplex. This locality consists of a large, well exposed outcrop of limestone clearly displaying several structural fabrics.

Fig 4.1a shows the location of these localities within the overall structure of this area.

4.2.1.1 The Waima River Location

Description

The Flags Creek Thrust was described by Browne (1992) as a SE-trending and NE dipping shear zone, less than 100m wide, of *cataclased* Torlesse Supergroup, Woolshed Shale, Amuri Limestone, Cookson Volcanics and Waima Siltstone Formations. The use of the term 'cataclased' by Browne is confusing as this implies crushed and fractured rock which has been ground to s powder (Teall 1887). In fact, fragments up to several metres across occur within the zone and overall the unit cannot be said to be cataclased. The summary map of fig. 4.1a shows how the Flags Creek Thrust cuts across thrusts and folds of the duplex on its southwest side.

At this locality the lithological divisions from north to south across this section of the contact zone are summarized below (fig. 4.1b). The zone can be divided into five units.

(1) The northern margin of the contact is made up of interbedded sandstone and siltstone of the Torlesse Supergroup including occasional < 1 m thick volcanic beds and sedimentary breccias. Close to the contact on both the northern and southern sides of the Waima River, a number of normal mesoscopic faults were found displacing these Torlesse sediments (fig 4.3).

(2) The second unit consists of a blue-grey siltstone with subrounded, altered, mafic volcanic clasts (3-27 cm length) similar to the Cookson Volcanics (c.f. Gregg 1965; Challis 1978; Raey 1980). Most of these clasts (*ca.* 90%) are either contained within or attached at some point to, siliceous white limestone 'blocks'. These limestone blocks vary in dimension between clasts enclosed by siltstone to elongate beds (minimum length 2 m) whose ends are not exposed within the extent of the outcrop. The larger limestone blocks possess a well developed, stylolitic cleavage. Greensand beds less than 0.6 m thick were observed with an underside of incompetent greensand, angular greensand fragments and incompetent, soft, white limestone material which flows around the fragments parallel to the base of the greensand bed. An example of this unit is shown in fig 4.2a.

(3) There is an abrupt transition over a few tens of centimetres from this mixed unit to a parallel and alternating sequence of glauconitic sandstones and siliceous



Fig 4.2a: Photograph of the first unit of the shear zone separating Torlesse Supergroup above from Amuri Limestone beds below at the Waima River locality of the Benmore region. Present are clasts of Amuri Limestone enclosing 'blocks' of Cookson Volcanics and Torlesse sandstones all within a silty Upper Cretaceous matrix (Whanganui Shale, Browne (1992)). A ruler is included for scale.



Fig 4.2b: Photograph of thrust fault within the second unit of the Waima River locality shear zone. A pencil is included for scale. The orientation of this fault is shown in fig 4.4a.

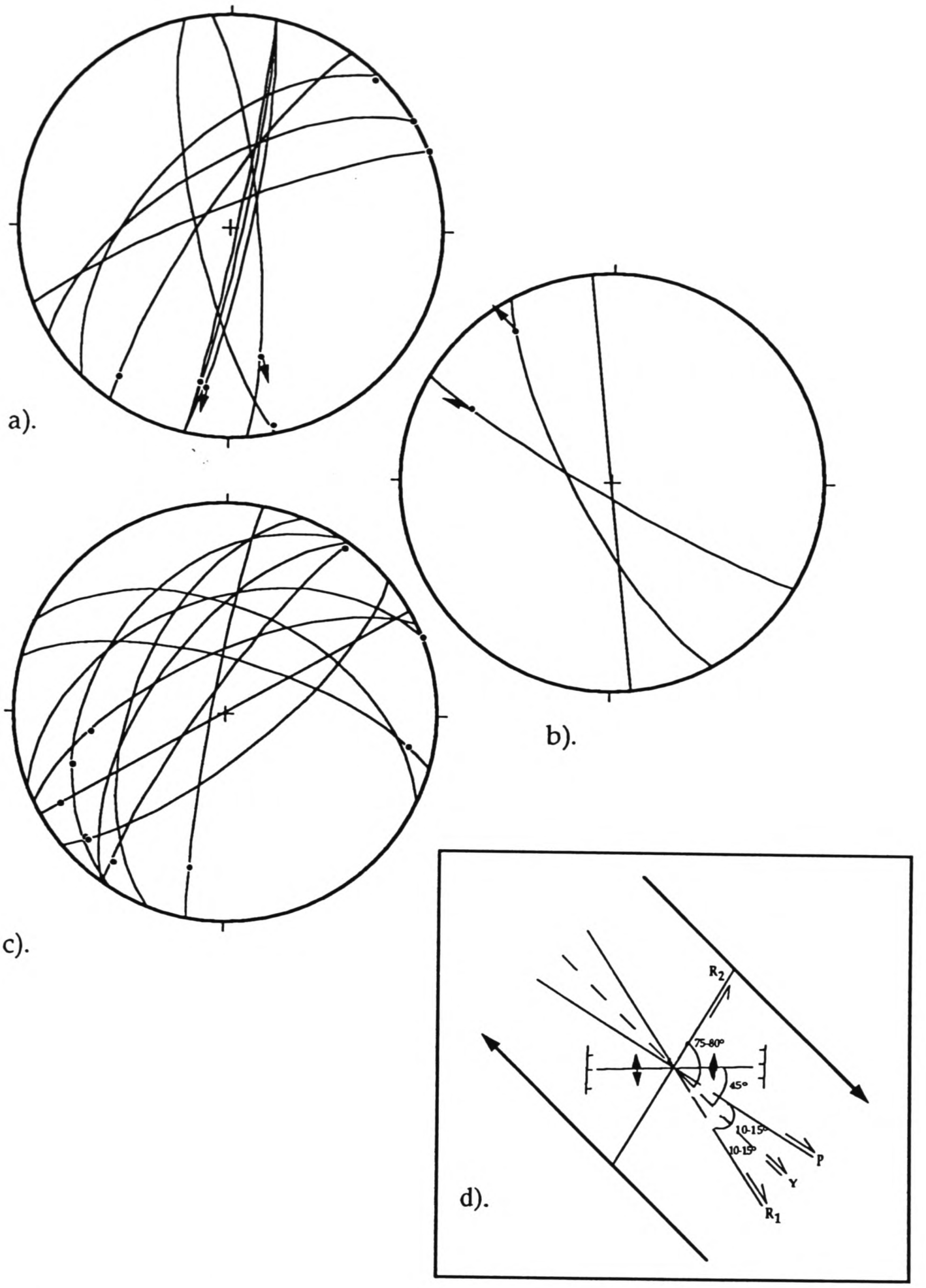
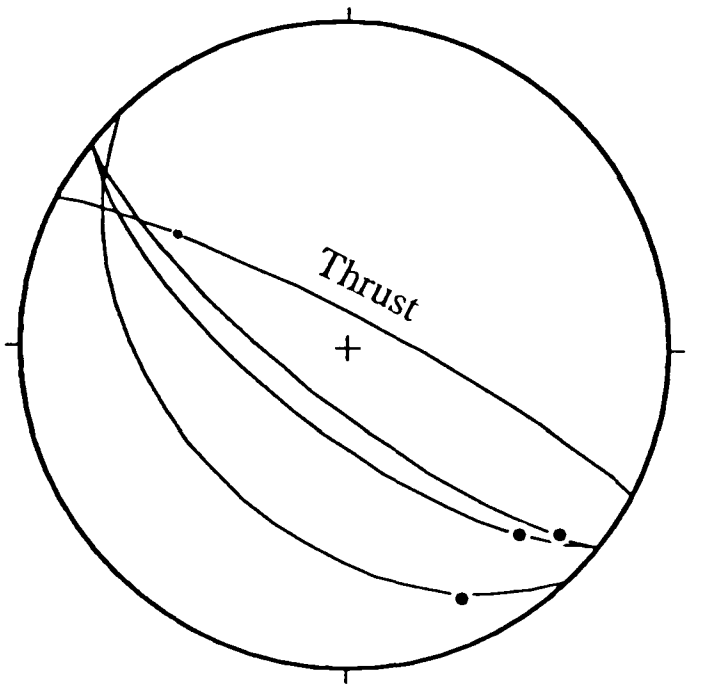
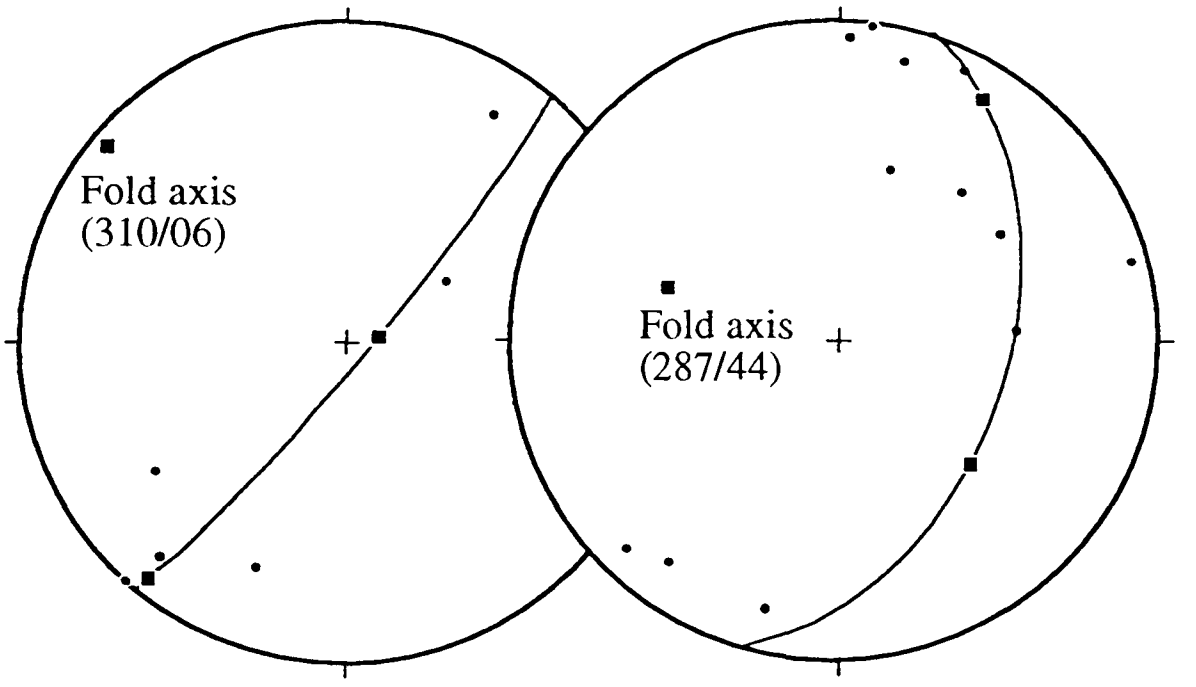


Fig 4.3: Fault planes and slickenside surfaces from the Waima River location of the Benmore subregion as described in section 4.2.1.1. All fault planes are shown as great circles on equal area lower hemisphere stereographic projections. Lineations on fault planes (small dots) and arrows to indicate the sence of slip of the fault hanging wall are plotted where these were available. Faults are from: (a).Torlesse sediments north of the shear zone; (b). within the shear zone itself; and c). in Amuri Limestone beds immediately south of the shear zone. For comparison inset (d) shows the orientation of fractures and fold axes expected within a SE-trending dextral shear zone.



a).



b).

Fig 4.4: Equal area, lower hemisphere stereographic plots of fold data from the Waima River locality of the Benmore subregion. a). Fold axial planes from within the third lithological unit of the shear zone are represented by great circles with thick dots marking the fold axis associated with each. Also shown in this plot is the low-angle to bedding reverse fault with slip lineation observed within the same unit. b). small dots represent the poles to bedding from (left) Torlesse sediments north of the shear zone, and (right) from beds within the shear zone itself. The fold axis and is marked in each case.

limestone, bedded on a scale of 0.5-8.0 cm. This unit is folded on a m-scale and is also internally highly faulted. One such fold displays a clear axial planar cleavage and extension around the hinge area of the outer folded surface. The lower limb of this fold is truncated by a bedding parallel fault within this unit (fig 4.2b). The stylolitic cleavage within the thicker siliceous limestone beds is itself displaced by the mesoscopic faults.

(4) There is another abrupt transition into a fourth unit of siltstone. On the western margin of this siltstone unit is a 4 m wide zone similar in appearance to the second unit described above with a mixed lithology. The fourth unit is adjacent to a 53 m wide unit of mafic volcanics which are referred to as the Cookson Volcanics (c.f. Gregg 1965).

(5) West of these volcanics is another unit of siltstone and red and green mudstone areas, as well as metre scale pink limestone blocks. The stratigraphic top of this unit is a 12 m thick limestone breccia which passes up into internally undeformed marly limestone and then to a thick, continuous sequence of Waima Siltstone beds.

A moderately siliceous, glauconitic limestone from the first creek to the southeast of the Waima River locality (GR:(P29) 959240) is cut by numerous slickenside surfaces (fig. 4.3c). A number of top-to-the-southwest thrusts were also observed at this location although it was not possible to measure these because of the poor access. This locality is south of the sequence described above and structurally lower in the sedimentary pile.

Interpretation

The sequence described above constitutes the tectonic shear zone described and defined by Browne (1992). However, the evidence collected in this study suggests a complex history for this zone. The zone consists of brecciated and sheared material. Fracturing to produce the breccias at either end of the shear zone (sandstone adjacent to Torlesse and limestone adjacent to continuous Amuri Limestone) may be a either a result of fault fluids circulating within the brittle shear zone or an effect of local submarine volcanism within the sedimentary basin. An alternative explanation to a straight forward shear zone exists for this sequence; that it is a volcanic breccia deposit with limestone and greensand rafts, hydrothermally altered muds and large scale fracturing of limestone and sandstone deposits, all within the basin sediment (the siltstone). Although a thin section showed that the siltstone does not contain any evidence for volcanic shards, this does not rule out a volcanic origin for the sequence as a whole.

The large scale structure of this region, with older Torlesse basement overlying younger Amuri Limestone lithologies across this contact, provides clear evidence for the large dip-slip displacement which must have occurred along this contact. However,

it is possible that the zone itself represents local primary volcanic breccias within a sandstone-limestone basin. This zone was then reactivated as a fault causing possible further brecciation and disruption of the primary breccias.

Of particular importance is the observation that the limestone cleavage pre-dates inclusion into this deposit and therefore pre dates at least the earliest thrust of the Benmore thrust duplex. This places a very early and possibly pre-tectonic timing on the formation of this cleavage.

Evidence for early deformation (D_e)

Evidence was found at the Waima River locality for early bedding parallel faulting and folding. Within unit 3 the folds are tight, SE-verging folds with NW-trending axial planes and subhorizontal fold axes. The lower limb of one such fold is truncated against a reverse fault which has the same strike as the fold axial planes and is at a low angle (less than 10^{o}) to bedding in this area.

These folds are not easily related to folding of the Benmore Anticline since this has a northeasterly trending fold axis almost at right angles to those described here. In fact the fold axes and thrust are parallel to the pre-Benmore Anticline duplex thrusts. It therefore seems likely that these folds formed under the earlier fold and thrust duplex formation event. After correcting for the late tilting associated with the formation of the Benmore Anticline, the back-tilted nature of these thrusts and folds is apparent (thrust at 296/73 N).

Poles to bedding from units to either side of the contact were plotted (fig 4.4b). These reveal a fold axis of 310/06NW from greywacke beds and 287/44W from beds within the shear zone. This folding is on a metre scale. The average fold axis for beds within the shear zone is the same as for the individually measured fold axes from the third shear zone unit. In comparison, the beds north of the contact are folded by a fold axis with a trend rotated clockwise to that folding beds within the zone (see next section). The fold axes are at a low angle to the orientation of the pre-Benmore Anticline thrusts and are interpreted as due to this early deformation.

Evidence for late deformation (D_l)

Fig 4.3 shows plots of all fault surfaces collected at this location (lineations and arrows to indicate the sense of hanging wall, relative to footwall, slip are shown where available). Several steep, N to NE-striking normal faults with sinistral strike-slip components of motion, displace Torlesse sediments close to the contact on both sides of the river (4.3a). SE-trending dextral strike-slip faults were observed in the third unit of the tectonic shear zone sequence (4.3b). Also found were NE and ESE-trending faults with horizontal lineations in Amuri Limestone beds south of the contact (4.3c). If these faults were related to thrust slip along this SE-trending contact then one would expect

them to parallel the contact trend. This is only true for the faults within the shear zone itself. Alternately, if these faults had formed within a post-tilt, SE-trending strike-slip zone then the SE and ESE-trending groups could represent dextral shears, and the N to NE-trending faults sinistral conjugate shears both within a dextral shear zone parallel to the Flags Creek Thrust (fig. 4.3d). The normal dip-slip components on the NE-trending faults would be expected due to the close orientations of extensional and synthetic shear faults within a brittle simple shear zone.

The discovery of strike-slip faulting and clockwise rotation of fold axes in beds to the north of this tectonic shear zone relative to further south, indicate that this contact has accommodated at least some dextral shear displacement. The folding within the shear zone is parallel to all other pre-Benmore Folding folds and thrusts and therefore the zone itself is believed to indeed be a result of this early deformation. However, this work has shown that this contact has been reactivated as a NW-SE dextral strike-slip fault zone. This fault zone strikes at a high angle to both the Clarence and Kekerengu Faults. Reactivation of this structure as a part of the regional active dextral strike-slip deformation would be expected principally to be sinistral shear. Thus, the evidence for dextral strike-slip suggests a more complex pattern of deformation which may be related to the block rotations of Northern Marlborough. .

4.2.1.2 The Isolation Creek location

Small scale fabrics within the Amuri Limestone are well exposed in the nose of the Benmore Anticline in Isolation Creek. These fabrics are described here in detail because they provide insight into the structural development of the whole Benmore subregion. The outcrop is along the Waima River section between the Blue mountain homestead and Isolation Creek (grid ref: (P29) 923248), fig. 4.1a and fig. 4.6.

Fabrics

The fabrics are summarized in the block diagram in fig 4.5a along with their corresponding orientations. The principal features are as follows.

(1) Bedding planes (5-30 cm separation) with striations on the bedding planes indicating north-south trending bedding plane slip.

(2) A well developed cleavage is at a high angle but truncated by bedding. The cleavage planes display the effects of simple shear between the bedding planes. Striations found on these cleavage planes are subparallel to the striations on bedding planes, indicating slip in an identical direction.

(3) Extensional fissures were observed in three dominant orientations, all with N-S strike. The relative timing of each extensional set varies over the outcrop, suggesting overall synchronicity of development. This is in contrast to the consistent relationship which would result from extension due to progressive folding and rotation

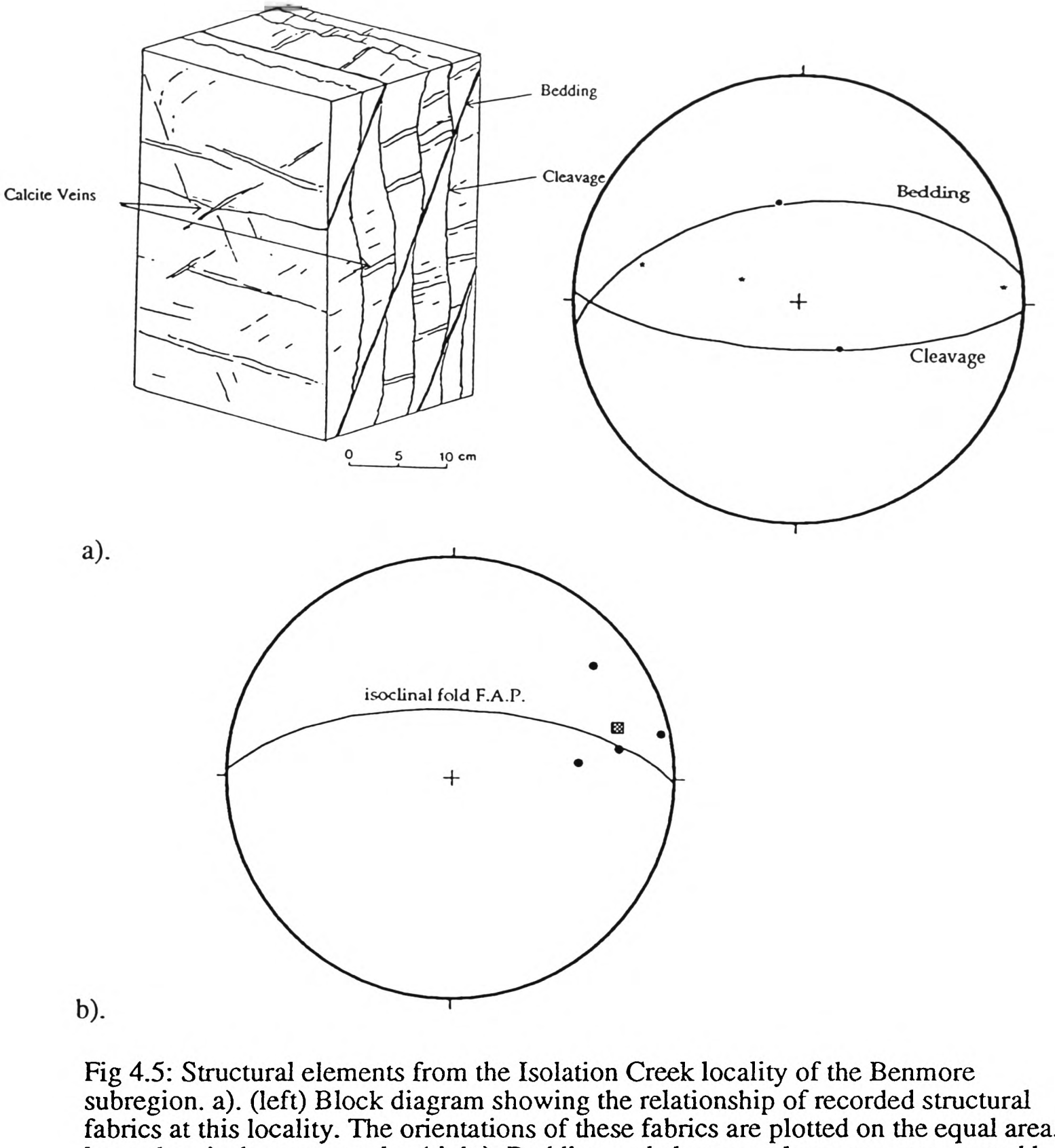


Fig 4.5: Structural elements from the Isolation Creek locality of the Benmore subregion. a). (left) Block diagram showing the relationship of recorded structural fabrics at this locality. The orientations of these fabrics are plotted on the equal area, lower hemisphere stereoplot (right). Bedding and cleavage planes are represented by great circles with small dots marking the lineations on these surfaces. Poles to extensional planes are marked by star symbols. These planes strike perpendiular to the bedding and cleavage planes. b). Stereoplot with a great circle representing the fold axial plane of the isoclinal fold within this locality. Thick dots mark fold axes calculated from bedding, axial planar cleavage and from direct field measurement. (Mean fold axis: 073/24).

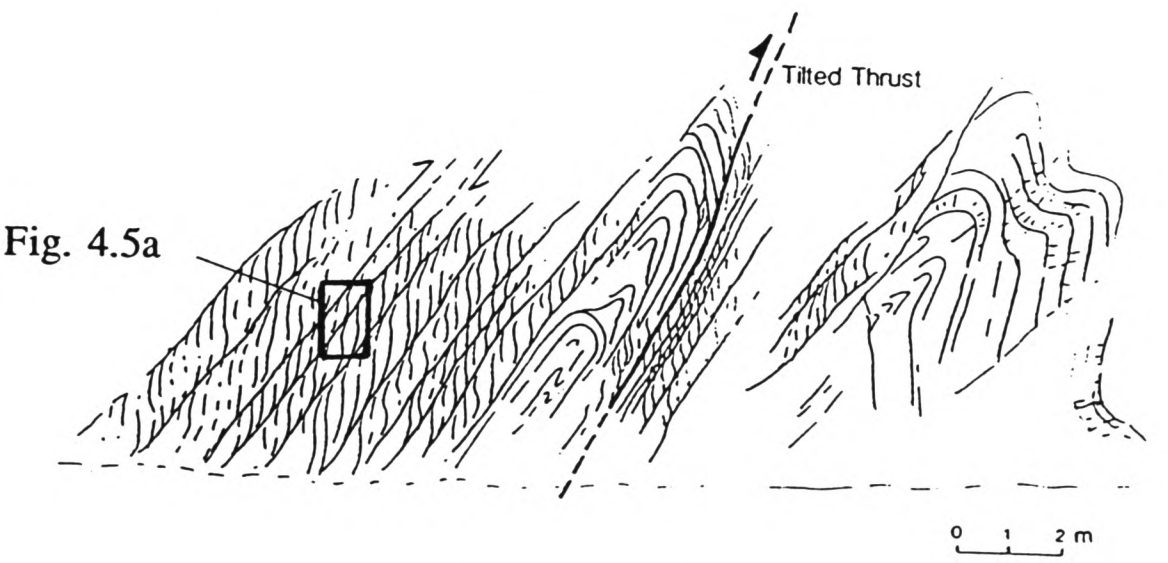


Fig. 4.6: Sketch of the Isolation Creek locality of the Benmore subregion showing the position of the tilted thrust. Also shown is the position of the block diagram of fig. 4.5a and the sence of bedding plane flexural slip indicated by the shearing of cleavage planes.

of the principal stress directions. Therefore the fissures were assumed to be due to accommodation during cleavage development. The shearing of cleavage along bedding planes is typical of flexural slip during folding.

Folding and faulting

Also within this outcrop was a tight, isoclinal fold with a fold axial plane subparallel to bedding (fig 4.5b and fig 4.6). The southern limb of this fold is cut by a truncation surface which ramps up-sequence, suggestive of a thrust fault. The bedding to cleavage vergence below this truncation surface is identical to that of the northern limb. Around the fold hinge fanning, axial planar cleavage was observed. Towards the southern end of the outcrop (the right-hand end of fig 4.6) are a number of southward verging folds with wavelengths of 2-10 m. These also clearly display axial planar cleavage. The fold axial plane and fold axis of the truncated fold and the fold axes (directly measured and calculated from the axial planar cleavages) of the latter folds are plotted in fig 4.5b. This plot illustrates the axial planar nature of this cleavage and suggests that the folding, cleavage development (and extensional fissures) and thrusting all formed under the same phase of compressional deformation.

It is not easy to relate the folding described above to the folding of the Benmore Anticline since the latter has a northeasterly fold axis (048/10 N) compared to the E-W trending folds in Isolation Creek. It seems more likely that these folds were subsequently tilted or refolded during the formation of the Benmore Anticline, tilting the beds in Isolation Creek *ca.* 10^{o} to the north. Removal of this late tilting rotates the mean fold axis in Isolation Creek to 072/15 and the thrust fold axial plane to 267/58 N.

4.2.2 Conclusions

Study of the Waima River locality revealed the reactivation of a primary volcanic breccia as an early D_e thrust zone. This thrust, together with D_e folds and reverse faults parallel to the kilometre scale thrusts of the Benmore region, were further tilted by the D_l Benmore Anticline. Also noted was a clockwise rotation in the trend of the D_e fold axes of beds to the north of this zone compared to the trend of the fold axes within it. This, combined with the discovery of late D_l dextral shear strike-slip faulting within and surrounding this zone, led to the conclusion that this primary breccia reactivated as a thrust fault was again reactivated as a dextral strike-slip fault zone.

The Isolation Creek location contains early D_e thrust and folded beds subsequently folded by the D_l Benmore Anticline. Axial-planar cleavage with extensional fissures to accommodate this compression are associated with this D_e folding. Clear evidence of bedding plane flexural slip was observed by the shearing of this cleavage.

4.3 Presentation of Structural Data from the Kekerengu-Washdyke Subregion

4.3.1 Introduction

This subregion is situated to the southeast of the Benmore subregion. It is bounded to the west by the Kekerengu Fault, which forms a major feature in the study area and will be described in more detail later on. The Pacific coastline forms the eastern boundary of this area. This subregion forms the main part of the study area described in this thesis and has been mapped in detail (see Kekerengu and Washdyke map sheets). All references to the Kekerengu area or the Washdyke area or to northern, southern, eastern or western parts of these areas, refer to the Kekerengu and Washdyke map sheets or to the appropriate segments of these map sheets.

In the following sections the major structural elements are described. The section is divided into three main parts which describe faults, folds and cleavages respectively. The description in each part is further subdivided, based on the scale of the feature. In each case, the youngest structures are described first. In addition, outcrops where the features are particularly well exposed are described in detail.

4.3.2 Faulting

This section deals with faulting and is divided into two main parts: kilometre scale faults which often form major lithological boundaries (4.3.2.1), and mesoscopic metre to centimetre scale faults (4.3.2.2).

4.3.2.1 Large Scale Faulting

Fig 4.7 shows the location of individual large scale faults within the Kekerengu-Washdyke field area. All the faults are numbered for ease of reference. Four main large scale fault-types were recognized. These types are listed below more-or-less in chronological order. However, the relative timing of the first three is not always easy to determine. Table 4.1 classifies the localities described in the text by fault type.

a). Post-tilt dextral strike-slip faults (T3). These faults clearly truncate both tilted beds, the youngest of which are of *Opoitian* to *Nukumaruan* age, and also all other faults over the region (see (c), (d), and (e) below). The faults in this group with the largest displacements are the Kekerengu (Fault 0) and the Heavers Creek (Fault 5) Faults. Both these faults are active today (see following descriptions, 4.3.2.1b). Also, in the Kekerengu area a post-tilt dextral strike-slip fault is found in the southern part of the Kekerengu map sheet, apparently connecting along strike with an early pre-tilt thrust surface in the northern part of the Kekerengu map sheet. The Heavers Creek fault also

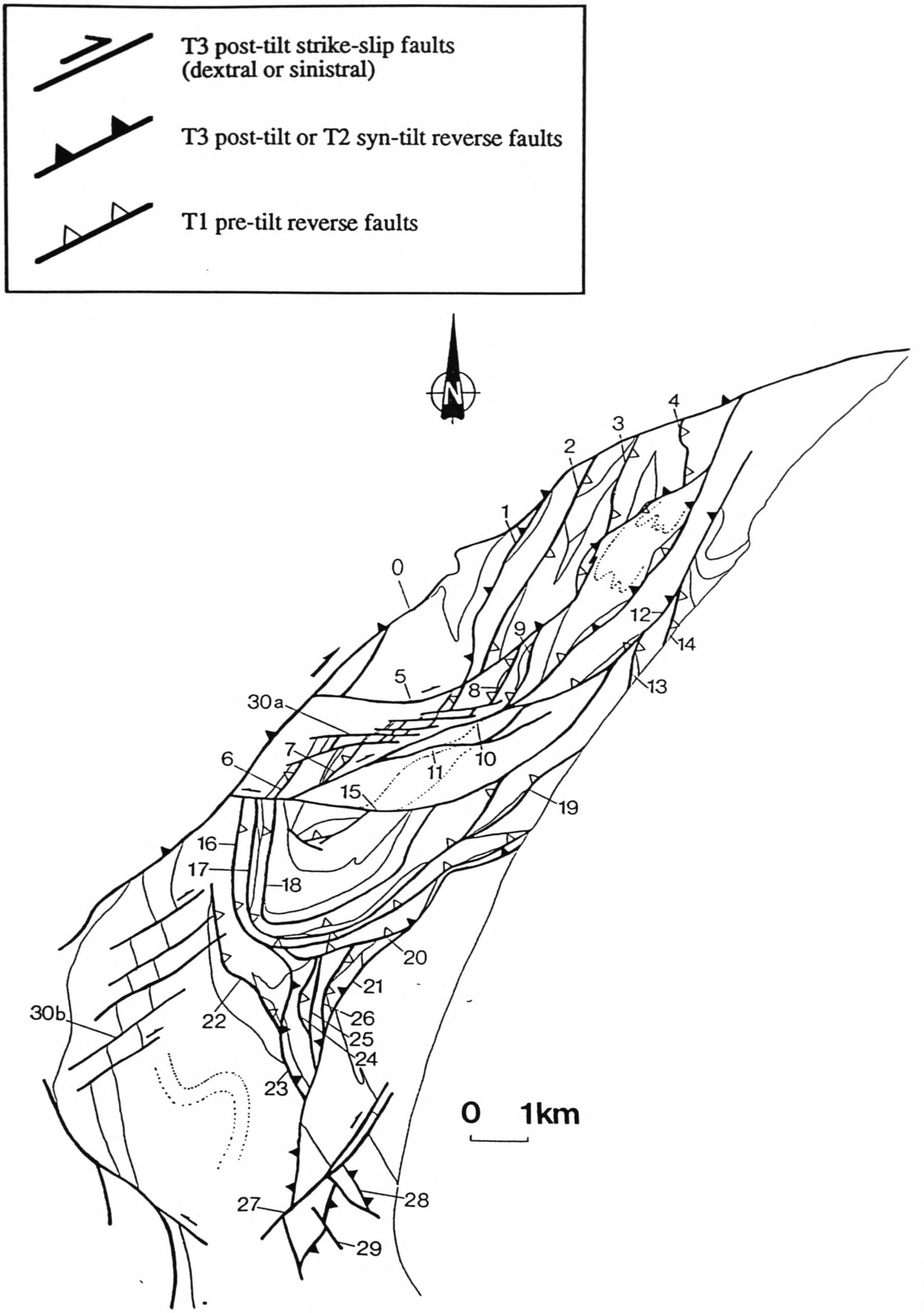


Fig 4.7: Geological map of the Kekerengu-Washdyke Marlborough subregion showing locality numbers corresponding to large-scale faults. All faults are marked by thick black lines as oppose to thin lines which represent lithological boundaries. See table 4.1 for a classification of these localities by fault-type.

FAULT TYPES	Fault contact numbers within each category
a). Post-tilt dextral strike -slip faults	0, 5, 10, 27, 30a, 30b
b). Late dextral shear along tilted lithological boundary	11, 15
c). Other	15*, 18
d).Post and syn-tilt reverse faults	1, 12, 21, 23
e). Pre-tilt thrust faults	2, 3, 4, 5**, 6, 7, 8, 9, 13, 14, 16, 17, 19, 20, 22, 24, 25, 26

Table 4.1: This table lists the fault contact numbers which come under each large-scale fault- type observed within the Kekerengu-Washdyke study area. *: Only applicable for the western extension of this fault. **: Only sections of this fault belong to this category. However, folding twice re-exposes this contact to the east and in these locations the contact is a pre-tilt thrust fault. For 'other' refer to 4.3.2.1c.

begins in the southern part of the Kekerengu map sheet before breaking into en-echelon sections linked by old thrust surfaces in the northern part of the Kekerengu map sheet.

b). Post-tilt dextral strike-slip along tilted lithological boundaries (T3). These are only observed in the southern part of the Kekerengu map sheet. No recordable displacement has occurred along these bedding planes but there is clear evidence for a large-scale sigmoidal shearing of bedding trace between these faults. These faults are not truncated by any other structures. The faults appear to link along strike with old pre-tilt thrust surfaces (see (d) below) in the northern part of the Kekerengu map sheet. The youngest rocks affected by these particular faults are Heavers Creek Formation in age. Since these faults are not offset by any other faults they are interpreted as late, post-Pliocene structures similar in age to (a). These faults are also immediately to the south of the Heavers Creek Fault, a late, post Pliocene dextral strike-slip fault. They therefore define a zone of dextral shear. Two examples of this type of fault were found, labelled Faults 11 and 15.

c). Other post-tilt faults (T3). There is evidence for late steepening of the western limb of the Razor Fold. For instance, there appears to have been tectonic thinning of and removal of younger beds on this limb and in the nose area of the fold. Strata on the western limb also appear to be sinistrally displaced. Dextral faults (a) immediately to the north truncate these displaced beds.

d). Syn and post-tilt reverse faults (T2). These faults are truncated by the post tilt dextral strike-slip faults (see (b) above) and truncate pre-tilt reverse faults (see e). below). Two such faults were observed on the Kekerengu map sheet (Faults 1 and 12) and two on the Washdyke map sheet (Faults 21 and 23). The youngest sediments affected by these faults are *Opoitian* to *Nukumaruan* aged.

e). Pre-tilt thrusts (T1). These were recognized over the whole region and are by far the commonest fault type. They are generally at a low angle to the bedding in the units to either side except in thrust ramp areas, and are cut by all previously described fault-types. Most are associated with limestone units either juxtaposing (1) upper limestone lithologies conformable with the overlying sedimentary sequence (Waitakian Marls); (2) or smectitic mudstone of Eocene age; or (3) large limestone thrust sheets with associated limestone breccia deposits signifying the syn-depositional, high level nature of these thrusts; and lastly (4), out-of-sequence limestone blocks along thrust faults. These thrusts were observed to affect the Miocene sedimentary sequences up to the siltstones of the Heavers Creek Formation (*Clifdenian* to *Waiauan*). See chapter 6 for a full discussion of these faults and an interpretation of the early basin evolution.

From the above it is apparent that there were two main phases of deformation; an early episode of pre-tilt thrusting (T1) affecting material up to ~*Waiauan* age (*ca.* 10.5 Ma), and a later episode of syn and post-tilt reverse and strike-slip faulting (T2 and

T3) which is active today affecting Pliocene and younger sediments. These phases are respectively labelled D_e and D_l. Note the broad similarity between these two phases and the two phases identified within the Benmore subregion. F3 folding within the Kekerengu-Washdyke subregion is not immediately apparent from the initial structural data. The early thrusts are distinguished on the Kekerengu and Washdyke field maps by open as opposed to filled triangles along the thrust surfaces. How these faults fit into the overall progression of deformation events in the region is discussed in Chapter 6 after all other structural data has been presented.

Examples of each of the above fault types are described below.

4.3.2.1a Post-tilt dextral strike-slip faults

Fault 0 The Kekerengu Fault

Description

This NE-trending fault is traceable over *ca.* 27 km. Its location is easily picked out by the transition from low ground consisting of Tertiary cover sediments, to higher ground consisting solely of uplifted Cretaceous greywacke (Lensen 1962). Fig. 4.8 shows the topographic variations across this fault. The fault cuts across tilted beds and pre-tilt thrust surfaces on its eastern side. Other late dextral strike-slip faults which transect and displace the footwall sediments merge with its trace. The sketch map of fig. 4.9 clearly shows dextral displacement of the conformable sequence (from pre to post-Amuri Limestone material) which has occurred along the Kekerengu Fault. The total dextral offset of this sequence is *ca.* 18 km.

Sediments to either side of this fault are most closely exposed around grid ref: (P30) 902122 where the fault is located to within *ca.* 10 m. A small gully in the hillside marks its surface expression.

Displacements of marker horizons to either side of the Kekerengu Fault were used by Lamb and Bibby (1989) to calculate average displacement rates along this fault. The Kekerengu fault offsets a series of river terraces adjacent to the Kekerengu River. These offsets suggest an average Holocene dextral strike-slip rate of *ca* 7 mm a^{-1} and a vertical slip rate of 0.15 mm a^{-1}. A dextral strike-slip offset of the 30 to 50 Ma Winterton Formation (Prebble 1976) also suggested an average dextral strike-slip rate over this period of between 5 and 10 mma^{-1}.

Interpretation

The Kekerengu Fault is a currently active dextral strike-slip fault with a dip-slip component uplifting older material on the faults western side. It is difficult to sort out the exact relation between tilting and displacement along this fault. If the faulting post dates tilting of the beds then the recorded offset of *ca.* 18 km is a reasonable value for

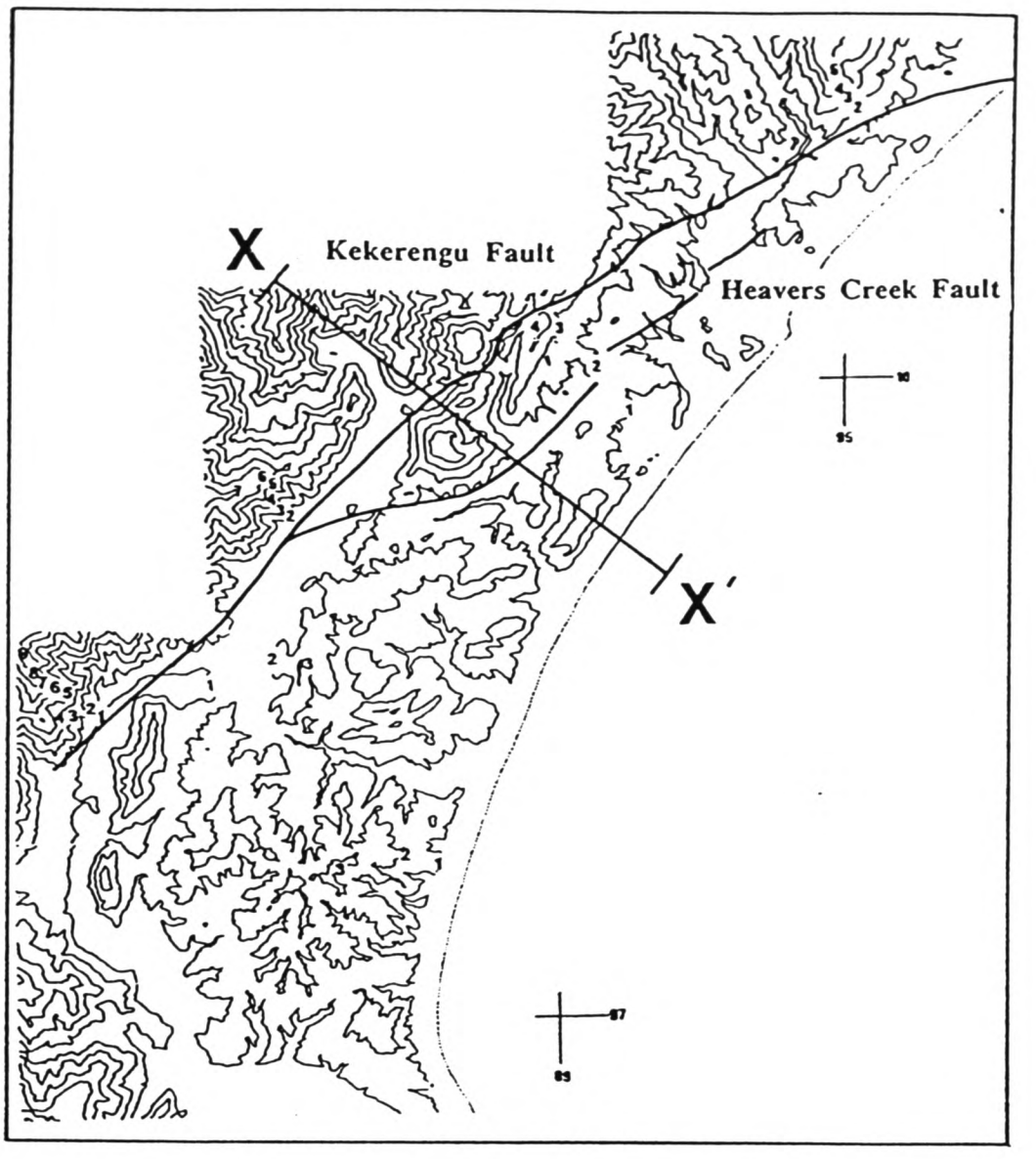


Fig. 4.8: Topographic contours and cross section of the Kekerengu-Washdyke study area. Surface traces of the Kekerengu and Heavers Creek Faults have been added to show how these faults are related to topographic changes. Contours are numbered in hundreds of metres. Refer to section 4.3.2.1a for descriptions of these faults.

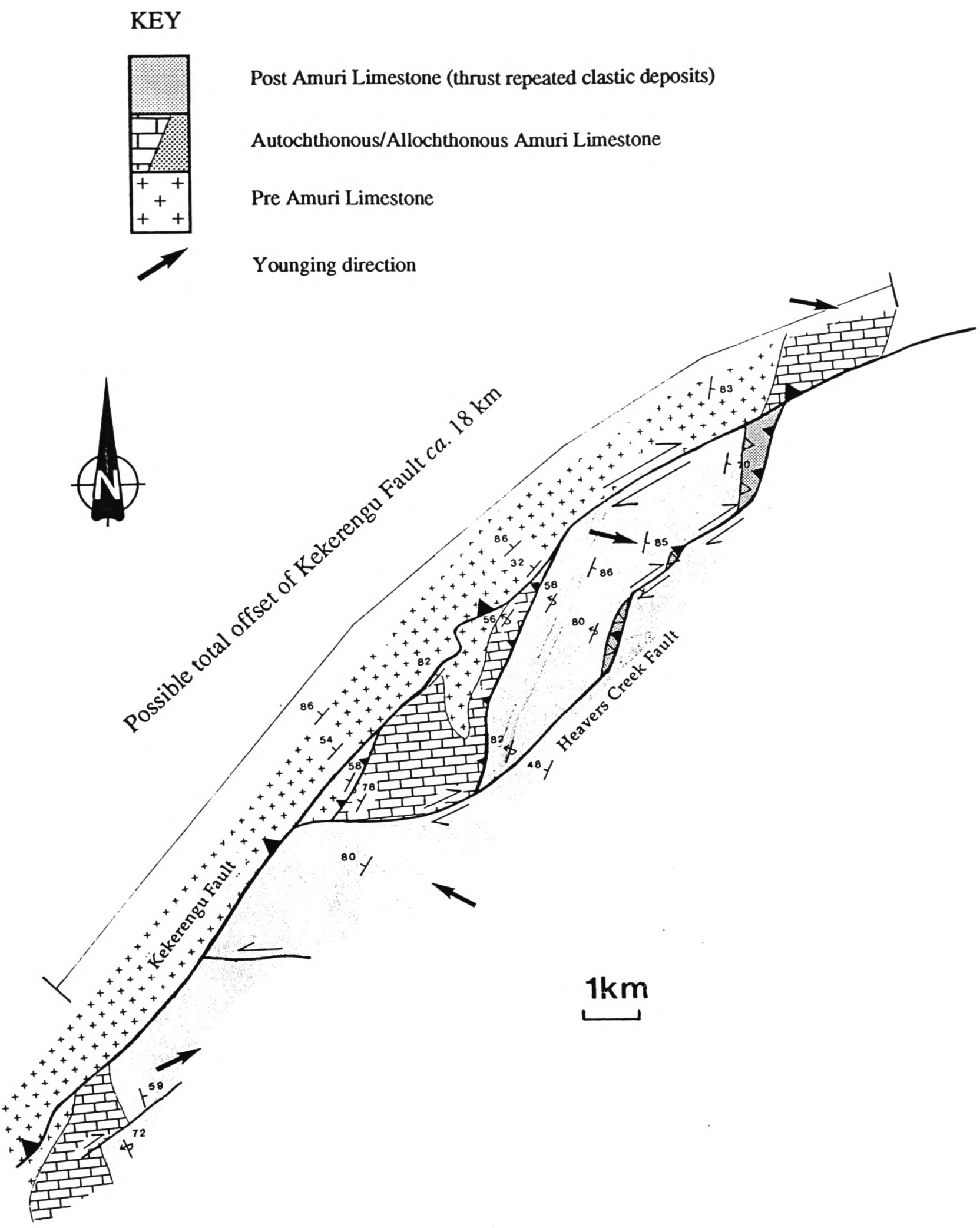


Fig. 4.9: Sketch map showing lithological units adjacent to the Kekerengu and Heavers Creek Faults. Offset of the conformable sequence boundaries from Torlesse to Miocene clastic deposits to either side of the Kekerengu Fault clearly shows the dextral sence of displacement along this fault (total offset *ca.* 18 km). See section 4.3.2.1a for descriptions of both faults. All symbols are the same as for the main study maps.

the total dextral displacement. However, if tilting and faulting occurred approximately simultaneously then it is hard to assess the true displacement value.

Fault 5 The Heavers Creek Fault

Description

This NE-trending fault (Lensen 1962) is traceable over *ca.* 10 km. The surface expression of this fault is also apparent from the topographic contrasts across it (see fig. 4.8).

This structure (see fig. 4.9) is mapped in this study as emerging from the Kekerengu Fault to the southwest of the Mole Hill and continuing ENE around the base of the Mole Hill truncating westward and eastward younging beds and bedding parallel structures to the south and north respectively. It then turns to trend NNE, juxtaposing eastward younging siltstone and debris flow deposits to the west against folded massive to turbiditic siltstones to the east. The siltstones to the west were believed to be from the Heavers Creek Formation, even though no accurate dates were obtained, due to their location above conglomerate beds. The siltstones to the east have been dated as *Otaian* to *Middle Altonian*, indicating that they are from the Waima Siltstone Formation. Along this northern section two limestone outcrops lie along the fault trace. The southern, larger outcrop contains a limestone sequence with the smectitic mudstone lithology at its base. The northern outcrop consists solely of this mudstone.

The fault contact is oblique to the strike of beds to either side in all areas except for the slivers of limestone which outcrop along the fault in northern Kekerengu. The bedding within and at the margins of these limestones were both at a low-angle to the bedding either side. The trace of this contact is not topographically controlled and it was thus interpreted as a subvertical structure.

It was not possible to estimate the total dextral displacement along this fault as no marker horizons are exposed to either side.

The displacement of a marker horizon was used by Lamb and Bibby (1989) to determine the average displacement rates along this fault. The fault offsets a surface underlain by the Parikawa Formation (Lenson 1962, Suggate et al 1978) deposited between 60 and 120 Ka. The average vertical displacement rate is *ca* 0.06 mma^{-1} and the average dextral strike-slip rate is *ca* 0.25 mm a^{-1}. The combined average strike-slip rate of the Kekerengu and Heavers Creek Faults is *ca* 7.5mm a^{-1}.

Interpretation

Recent Holocene offsets clearly indicate the post-tilt timing of this fault, at least in its later history. In the north segments of the fault trace are at a low angle to the bedding to either side. Limestone outcrops along these segments. The limestone is isolated from the units to either side. This, together with the juxtaposition of older

above younger sediments provided the evidence for these limestone segments representing pre-tilt thrust faults and ruled out an olistrome origin as proposed by Osborne (1980). The limestone sequence is identical in lithological type to that exposed above Fault 4 and included the same smectitic mudstone lithology as exposed along Faults 2 and 3.

As cross sections A-A' and B-B' show (fig. 4.30), the thrust surface outcropping along segments of this fault is folded and reappears twice at the surface further to the east. Here the thrust surface is called the Chaffey Fault for ease of reference even though it is the same fault. The age differences of the sediments to either side are the same. However it should be noted that the Chaffey Fault refers to late uplift associated with the folding of material in the northern Kekerengu, rather than to the thrust fault itself. Where this fault reappears at the surface the limestone is infact of a different lithology (Waitakian Marl). This limestone is conformable with the Waima Siltstone beds above the thrust fault. This feature is interpreted as a result of tectonic thinning of the out-of-sequence limestone and the cutting of this thrust at a lower level in this area.

The thrust segments are linked by fault trace segments whose trends cut across the general strike of bedding in this area. Further south the fault juxtaposes differently younging sequences and truncates bedding.

Sections of the Heavers Creek Fault were therefore concluded to be composed of reactivated earlier pre-tilt thrust surfaces which are now tilted and steep structures. Material west of the fault youngs to the east whereas material east of the fault youngs to the west. Although this westward younging was clear in the southern part of the Kekerengu map sheet, in the northern part of the Kekerengu map sheet folding complicates the initial younging direction. This area could not be distinguished from the westward younging, eastern limb of the Razor Fold in the northern Washdyke. Therefore sequences of opposing younging direction are juxtaposed along the Heavers Creek Fault. Since there is no obvious displacement of the Razor Fold it could only be concluded that the material on the western side of this fault was displaced dextrally from the eastward younging limb of the Razor Fold.

Overall it is concluded that this fault is a post-tilt, dextral strike-slip fault which reactivated tilted pre-tilt thrust horizons in the northern part of the Kekerengu map sheet. The fault trace segments between these reactivated surfaces define the en-echelon nature of this fault in the northern part of the Kekerengu map sheet. Reverse faulting within the limestone exposures between the fault segments (4.3.2.2, subarea 2) provides additional evidence for dextral strike-slip displacement along the Heavers Creek Fault since extensional structures would be expected if the fault were sinistral. This evidence is backed by the information obtained by Lamb and Bibby (1989) for young dextral strike-slip displacements along the Heavers Creek Fault.

Fault 10

Description

In the southern half of the Kekerengu map sheet westward-younging Heavers Creek Formation siltstones are juxtaposed against westward-younging conglomerate beds to the north and northwest along an ENE trending contact (fig. 4.10a). Bedding within the siltstone to the south of this contact is deformed into a right lateral, CS shear fabric. The sigmoidal shearing of beds rotated into parallelism with this contact and the placing of younger siltstones below older conglomerates indicated the existence of a fault.

Along strike (in the northern half of the Kekerengu map sheet) the contact changes to trend NNE where it is lost, appearing to link with the eastern surface exposure of the Chaffey Fault, an uplifted pre-tilt thrust horizon (see 4.3.2.1a). To the WSW it links with Fault 11.

Interpretation

When one considers the pre tilt sequence based on reconstructions of the area (chapter 6) it is evident that only right lateral slip on Fault 10 could have juxtaposed these two sequences. Overall the fault is interpreted as a post-tilt, dextral strike-slip fault (irrespective of whether the CS fabric is related to this motion or to earlier flexural slip). The fault terminates in the southern part of the Kekerengu map sheet where it appears to link with a pre-tilt thrust horizon. The linking of these different styles of deformation may be a result of the termination of dextral shear in the south and the continuation of dextral shear along the Kekerengu Fault to the north. This would create a region of compression between the two faults.

This contact has a post-tilt origin in the south, and a pre-tilt origin in the north and postdates *Lillburnian* times (dated samples BS12 and BS14).

Faults 30a and 30b

Description

Mapping in the southern part of the Kekerengu map sheet identified definite offsets in lithological boundaries bounded to the north by Fault 5 and to the south by Fault 10 (fig. 4.10b). These offsets are compatible with dextral faulting along five subvertical, dextral strike-slip faults (Faults 30a). For instance, the conformable sedimentary contact between lower Waima Siltstone and overlying conglomerate beds in the western Washdyke area showed significant offsets along strike between exposures (Faults 30b). The same offsets were indicated by the lower limestone to siltstone transition by changes in topographic relief. Although the evidence for the existence of dextral faulting here is strong, no actual exposures of these faults were

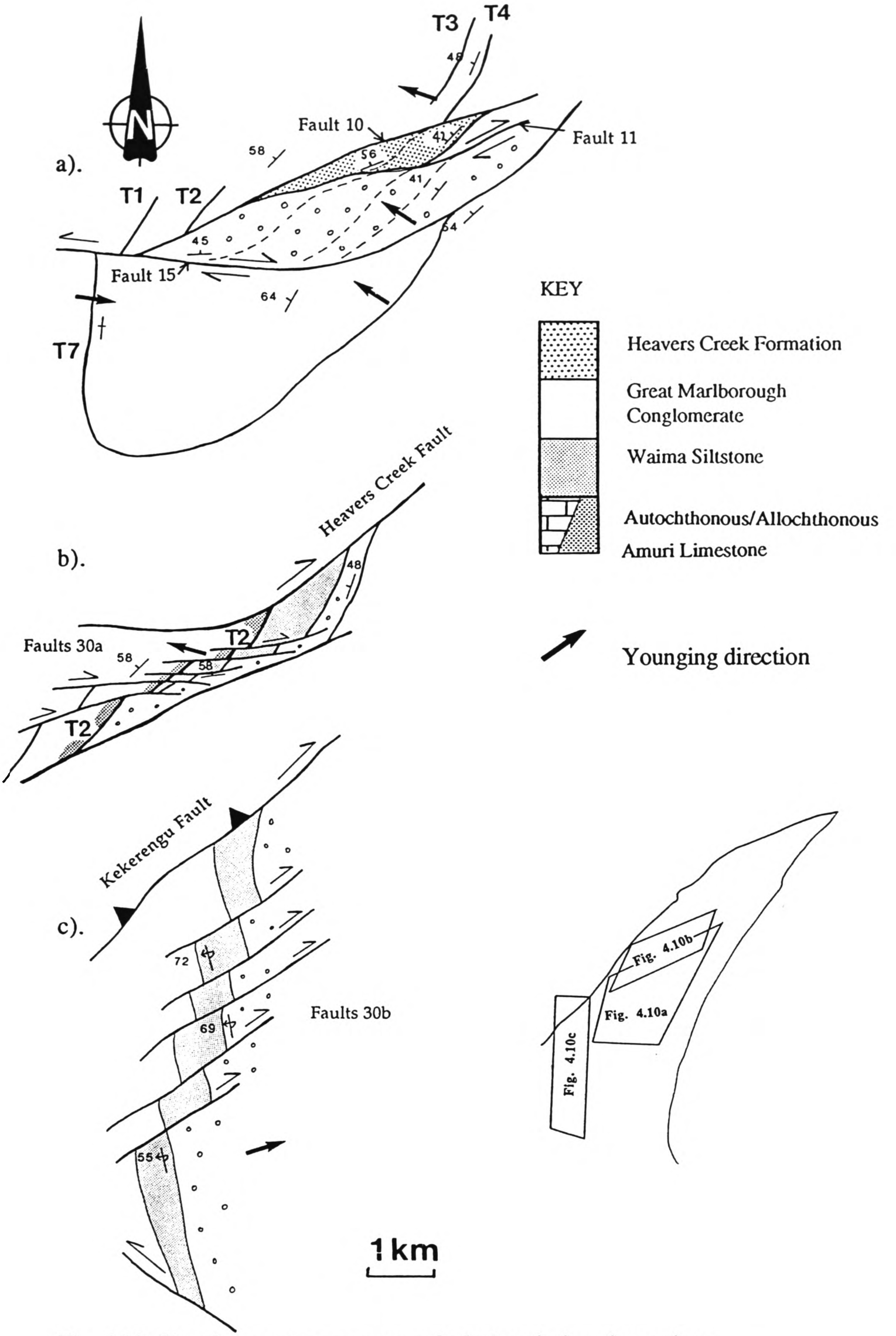


Fig. 4.10: Sketch maps to accompany fault descriptions in sections 4.3.2.1a and 4.3.2.1b. The inset shows the location of these maps within the Kekerengu-Washdyke study area. Dashed lines in (a) clearly display the dextral CS fabric defined by bedding trace within these lithological units. The bold numbering of faults in (a) and (b) refers to the relative order, numbered from top to bottom, of thrusts within the pre-tilt D_e thrust pile. Such numbering is used here to show the sence of offset on the described faults. All symbols are the same as for the main study maps.

found. Their straight traces implied a subvertical nature. These faults are shown in fig. 4.10c.

Interpretation

Faults 30a and 30b either represent steep pre-tilt normal faults or post tilt dextral strike-slip faults. Their orientation parallel with the Kekerengu Fault in this western part of the Washdyke map sheet indicated that these are more likely to be dextral strike-slip faults. The Kekerengu Fault is lost in the region immediately to the north of these faults and so it is suggested that these faults might relay dextral displacement to the Kekerengu Fault.

4.3.2.1b Post-tilt strike-slip along tilted lithological boundaries

Fault 11

Description

In southern part of the Kekerengu map sheet this contact trends ENE juxtaposing westward younging siltstones to the northwest against westward younging conglomerates to the south and southeast (fig. 4.10a). The siltstone unit has been assigned to the Heavers Creek Formation siltstone due to its position conformably above conglomerates. The beds immediately below and south of this contact display a clear sigmoidal shear fabric in plan view on map scale, so that the strike of the beds is rotated near the contact into parallelism with this contact. The straight trace of the contact suggests a subvertical fault. However, further NE in northern part of the Kekerengu map sheet, the contact is lost. It appears to link along strike with Fault 12.

Interpretation

Fault 11 is interpreted as a post tilt, dextral strike-slip fault which has made use of a former tilted lithological boundary between conglomerates and overlying massive siltstones which seems to have formed a line of weakness. The sigmoidal shear pattern is similar to s-c band structure. An s-c structure band structures developed inside shear zones where displacement and strain gradients are heterogeneous (Ramsay and Huber 1983).

Close to the termination of this fault in the southern part of the Kekerengu map sheet uplift has occurred along Fault 12. It is plausible that the linking of these two seemingly different structures could be interpreted as uplift associated with the termination of the dextral fault in the south with continued dextral shear along the Kekerengu fault further north creating a region of compression and uplift.

Fault 15

Description

This E-trending contact clearly follows a resistant ridge, seen easily on aerial photographs of the area. It separates folded Waima Siltstone Formation beds to the south from sheared conglomerates to the north (outcropping in the resistant ridge). All features of this contact are summarized in the sketch map of fig. 4.10a. The sheared beds to the north are rotated into parallelism with this contact as they near it. In the east the contact is mapped as a lithological boundary between Waima Formation siltstones and overlying conglomerates. However in the west the contact appears to truncate the folded beds to the south of it. The rotation of beds towards this contact, as well as the very different deformational styles to either side and the truncation of beds in one location, indicated at least some displacement along this tilted boundary.

Interpretation

The sigmoidal shear fabric clearly implies distributed dextral shear of the area bound to the south by this contact. This is assumed to be post-tilt shear due to the fact that this area is positioned immediately south of the Heavers Creek Fault, a post-tilt, dextral strike-slip fault (see 4.3.2.1a). Since the conglomerate in Deadman Stream is within a conformable sequence no recordable dextral displacement has occurred along this contact in the east. This is in marked contrast to the obvious truncation of southern beds to the west. Here the displacement appears to be left-lateral. The evidence seems to suggest opposing senses of displacement along this contact. The contact truncates a folded sequence of beds the youngest of which was dated as *Lillburnian* to *Waiauan* (dated sample 336). This displacement therefore occurred post this period. Another observation in this area provides a further clue to the nature of this fault. Fault 18 reflects an oversteepening of the western limb of the Razor Fold (see 4.3.2.1c). It is suggested that the sinistral displacement at the western end of Fault 15 could be a direct result of accommodation related to this oversteepening. This was subsequently followed by a phase of dextral shear and discrete faulting.

4.3.2.1c Other post-tilt faults

Fault 18

Description

This contact is folded around the Razor Fold syncline. It juxtaposes an upward facing limestone unit with an upward younging and overlying sequence of siltstones and conglomerates. The thick siltstone band above the contact on the eastern limb is truncated at the contact in the fold nose area so that on the western limb limestone is

directly juxtaposed with conglomerate beds at the contact. This siltstone band was dated by Osborne (1980) as *Otaian* (dated sample O7; Osborne (1980)). The limestone lithology is Waitakian Marl on both limbs except in the fold nose area, comprising the older greensand-volcanics-siliceous limestone lithology. The orientation of the contact is similar to that for Faults 16 and 17; a straight subvertical plane on the western limb and a slightly shallower (*ca.* 70^{o}) dip on the eastern limb. Bedding is generally parallel to the contact except close to the nose on the eastern limb.

All these features are summarized in fig. 4.11.

Interpretation

Across Fault 18 is a sequence from Waitakian Marl to *Otaian* siltstones. However, only the truncation of the siltstone band on the western limb and the change in limestone lithology around the fold nose suggest displacement along this contact. Elsewhere, the contact appears to be sedimentary. These phenomena can be explained by a late steepening of the western limb. It seems likely that the contact was not originally a faulted one (eg:- a thrust), but a sedimentary contact which has been subjected to late tectonic thinning by displacement along the western fold limb.

The parallelism of this contact on the western limb with Faults 16 and 17 on the same limb implies that these contacts (for which there is clear evidence for thrust fault origins), have also suffered this late rotation of the western limb.

It is suggested that the distribution of limestone lithologies and truncation of the siltstone band are a result of late steepening of this limb with discrete sinistral slip occurring immediately to the north along the western extension of Fault 15 in order to accommodate this limb rotation.

4.3.2.1d Syn and post-tilt reverse faults

Fault 1

Description

All features relating to this fault are summarized in the sketch map of fig. 4.12a. Eastward younging (Amuri) flints to siliceous, white, limestone beds are in contact with an eastward younging siltstone unit (maximum thickness 122 m) in the southern branch of Valhalla Creek, and with conglomerate beds (unknown younging) in the northern branch of Deadman Stream to the east of the Mole Hill. Both contacts are observed to within 10 m. The siltstone unit is not traceable between the two exposures. However, conglomerate beds conformably above (and east of) the siltstone can be linked laterally

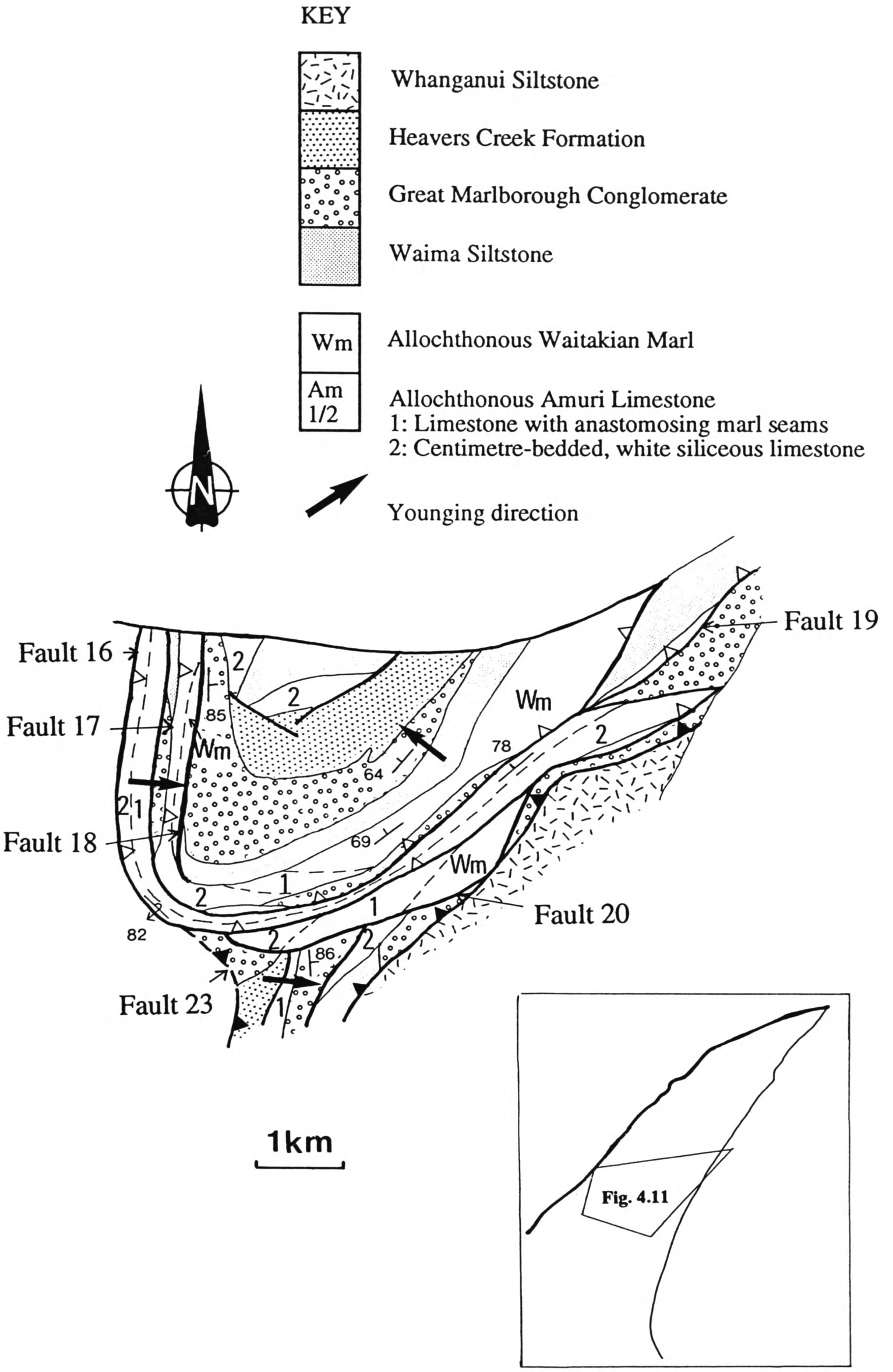


Fig. 4.11: Sketch map to accompany the descriptions of Faults 16, 17, 18, 19 and 20 in section 4.3.2.1e. The inset shows the position of this map within the Kekerengu-Washdyke study area.

with the conglomerate unit east of the contact in Deadman Stream. The siltstone is mapped as pinching out along the contact. All beds are overturned by up to 34°.

The contact trends NNW in the south to NNE in the north. Its straight trace indicates a steeply dipping structure. In Valhalla Creek, a dip of 70° west was measured. In the north, bedding in the siltstone unit is oblique to, and bedding in the conglomerate of similar strike and dip to the contact. In the south, bedding in the conglomerate is oblique to the contact and to bedding in the limestone. Both obliquely bedded units have strikes rotated anticlockwise of the contact.

The absence of upper limestone and Waima Siltstone lithologies, the pinching out of the siltstone, and the obliquity of beds east of the contact in the south, all indicated that discrete displacement has occurred along this contact.

Interpretation

The limestone and conglomerate units across Fault 1 young to the east. There is therefore no evidence for placing older material above younger along this contact. The fault is either a very low-angle pre-tilt, normal fault, or a steep, post-tilt, reverse fault. There is no evidence to determine which of these two options is the correct. The latter was preferred because the orientation of this structure is consistent with that for a reverse fault accommodating motion related to dextral shear along the Kekerengu Fault. Other mesoscopic reverse faults of this orientation were recorded in the sediments of the northern part of the Kekerengu map sheet (see 4.3.2.2).

The obliquity of bedding strike may be a feature related to Fault 2, or a result of dextral shear along this fault plane.

It has already been suggested that this is a post-tilt, reverse fault. The change in strike of the contact keeps the fault at a constant distance from the basal limestone contact, indicating that this fault is folded with the Torlesse and lower limestone in this area. It is truncated by the Kekerengu Fault to the north, and by the Heavers Creek Fault to the south thus pre-dating at least the last displacements on both of these structures. It is also of post-conglomerate age. No ages were available from the conglomerate beds here, but for the whole area, the conglomerate is known to span *Altonian* to basal *Tongaporutuan* (chapter 3). It is suggested that this is a post-tilt, reverse fault formed.

To summarize, subsequent to tilting and overturning of the sedimentary pile, this steep, reverse fault formed. Later folding of the beds to the west altered its trend, before being truncated to the north and south by displacements along the Kekerengu and Heavers Creek Faults respectively.

Fault 21

Description

All features relating to this contact are summarized in fig. 4.16. This contact is a large-scale structure separating eastward younging, tilted sediments and pre-tilt thrusts to the west against a tilted sequence from Waima Siltstone through conglomerates to Pliocene siltstones to the east. The contact is generally straight regardless of topography and is therefore a steeply dipping structure. Bedding in the units either side of the contact is oblique to it and is truncated by it. The contact itself is truncated by Fault 27 to the south.

The juxtaposition of older conglomerate and Waima Siltstone units against younger Pliocene siltstones and the truncation of bedding on either side indicated that the contact is a fault.

Interpretation

Fault 21 is of post *Opoitian* to *Nukumaruan* age and pre dates fault displacement along Fault 27. The juxtaposition of such different sequences suggests substantial reverse displacement along this fault, with an uplifted western side. An analysis of the structural evolution of the Washdyke map sheet suggests that this reverse fault is likely to be a syn-tilt structure (see Chapter 6).

Fault 23

Description

All features relating to this contact are summarized in fig. 4.16. The presence of this contact was marked by the existence of a fault zone between massive siltstone units (eastward younging Heavers Creek Formation siltstones to the east and northeast younging Waima Siltstones to the west). The zone is *ca.* 18.5 m wide and contains a 17 m thick conglomerate band with narrow borders of brecciated conglomerate fragments within a siltstone matrix. Zone margin parallel fault gouges up to 3 cm in thickness were also observed within the zone. The zone margins are vertical and at a low angle to bedding in the siltstones to either side. Without the brecciation this sequence might appear to be a sedimentary progression. However the brecciation suggested that at least some displacement had occurred along this zone. This along with the juxtaposition of different sequences and the observation of the similarity of the sequence to the east of this contact with the sequence below Fault 22 are suggestive of a fault repeated sequence.

Exposure in the area is poor and the contact untraceable to the north. It appears to merge with Fault 16. To the southeast the fault is truncated by Fault 21.

Interpretation

The juxtaposition of older with underlying younger material along a structure (Fault 23) at a low angle to the beds to either side suggests a dip-slip component of motion on this fault. It is interpreted as pre-tilt. The linking of this fault along strike to the south with Fault 21 and the opposing senses of dip-slip displacement on these two, led to the conclusion that this fault is a back-thrust related to thrust displacement along the syn-tilt reverse fault, Fault 21. The fault therefore also postdates *Opoitian* to *Nukumaruan* times. It was mapped as a late, post-Pliocene, syn-tilt, reverse fault.

4.3.2.1e Pre-tilt thrusts

Pre-tilt thrusts exhibit a variety of features. Differences mainly reflect variations in the material caught up along the thrust surfaces and the stratigraphic height at which the faults cut the sedimentary pile. The best examples of these are described below.

Fault 2

Description

This contact is exposed in the same stream sections as Fault 1, and also in the northern Valhalla branch. All features relating to this fault are summarized in fig. 4.12b. In the far south, conglomerate beds striking obliquely to this contact are separated from contact parallel eastward younging siltstones of the Waima Siltstone Formation (dated as *Altonian* to *Clifdenian*, this study, dated sample 231). No dates are available for the conglomerate unit. However, the general stratigraphic sequence from Waima Siltstone to conglomerates, and finally to overlying siltstones suggests that the conglomerate is in fact younger than the Waima Siltstone siltstones. Smectitic mudstone probably of Eocene age (c.f. Charnier and Ferriere (1991)) from the Amuri Limestone group was observed between the two lithologies. This mudstone can be traced along the contact thinning to the north and is ultimately lost in the northern Valhalla branch. In the north, the eastward younging conglomerate and siltstone beds parallel the contact. The presence of out-of-sequence mudstone, the placing of older Waima Siltstone above presumably younger conglomerates, the thinning of the mudstone, and the obliqueness of conglomerate beds in the south, implied that this contact is a fault.

Interpretation

The parallelism of beds across the contact in the north, in contrast to the obliquity of conglomerate beds below the fault further south, suggests a possible pre-tilt thrust. Younging evidence suggests that older smectitc mudstone is on the upthrown side of the thrust and that the conglomerate beds are below the thrust and folded into a footwall syncline. The smectitic mudstone unit is not conformable with the lithologies

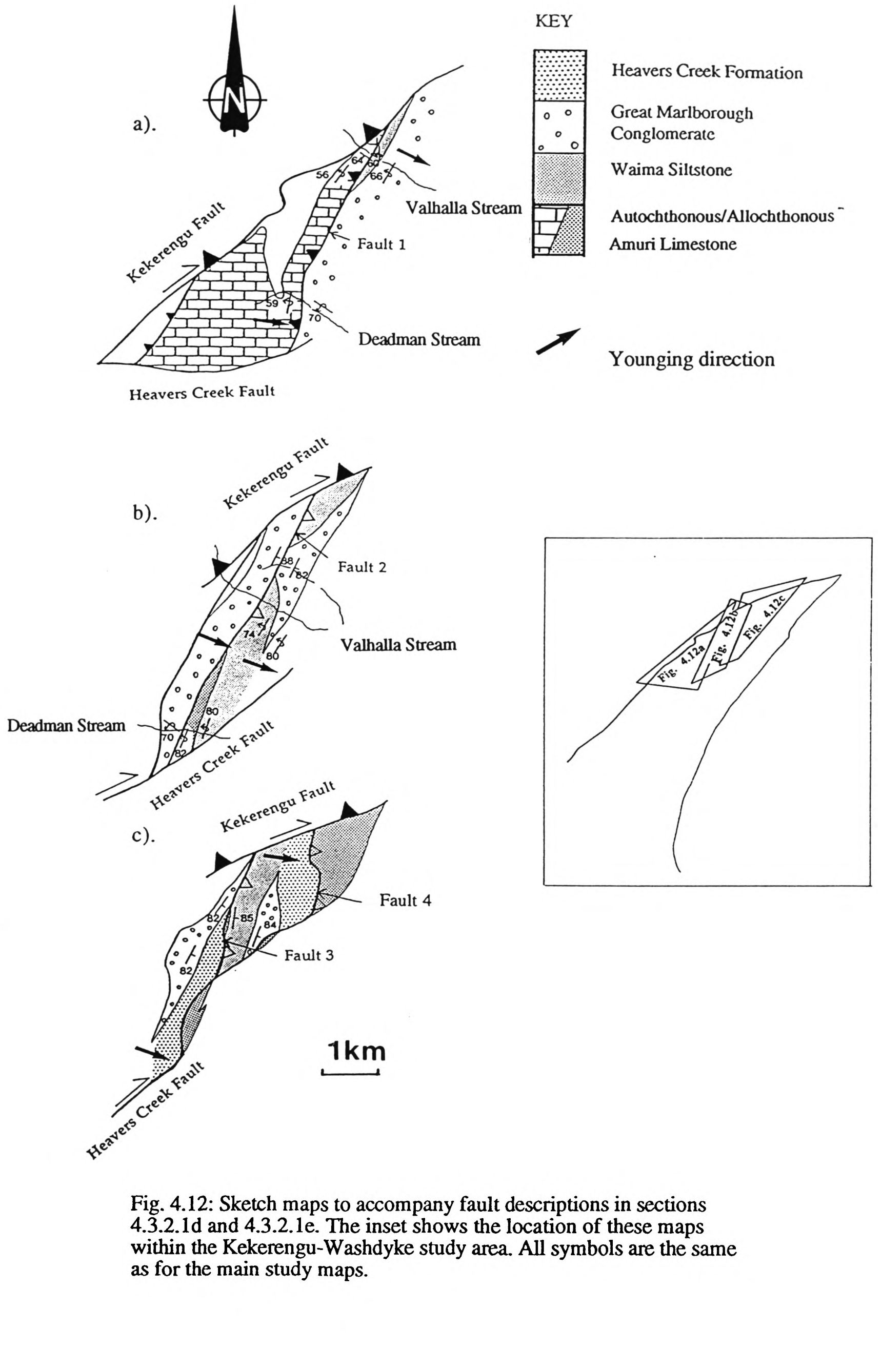


Fig. 4.12: Sketch maps to accompany fault descriptions in sections 4.3.2.1d and 4.3.2.1e. The inset shows the location of these maps within the Kekerengu-Washdyke study area. All symbols are the same as for the main study maps.

juxtaposed by this fault, and is probably a piece of the thrust decollement horizon or some other horizon through which the thrust passes, caught up along this fault.

Fault 3

Description

This particular contact is marked by the presence of a narrow limestone exposure (*ca.* 0.38 x 0.03 km in map view) between steeply dipping, eastward younging, massive siltstone units. All features relating to this fault are summarized in fig. 4.12c. The exact margins of the limestone are poorly constrained, but they appear to be at a low-angle to bedding in the surrounding siltstones. The limestone outcrops approximately along strike of a conglomerate bed within massive siltstones exposed in the northern Valhalla Creek branch. The internal limestone bedding dips as steeply as the beds to either side. However, there is a slight change in strike of the units to either side of this limestone suggesting faulted contacts. Dating of the siltstones to the west of this contact gave a poorly constrained age range of *Middle Altonian* to *Waipipian* (dated sample 254) and no dates are available for the beds to the east. However, the stratigraphic position of the beds to the west above conglomerates indicated that they are most likely to be Heavers Creek Formation. Likewise, the position of the beds to the east below conglomerate beds indicates that they are most likely to be Waima Siltstone Formation. The available younging evidence suggests that older rocks are positioned above younger rocks across the Fault 3 contact. This, together with the obliquity of the beds on either side, indicates that the contact is a fault.

Interpretation

Fault 3 places older above younger sediments across a contact which is at a low angle to the beds to either side and therefore appears to be a thrust fault. The slight change of bedding strike to either side of Fault 3 shows an anticlockwise rotation of beds on the west compared to the east side. This may indicate some post-tilt dextral shear along the tilted contact, or that this is the hanging-wall anticline of the thrust.

Both the proximity to the Heavers Creek Fault and similar interpreted origin to segments of this fault (4.3.2.1a, Fault 5) suggests that segments of the Heavers Creek Fault and this structure are linked. The fault is mapped as a thrust splay fault off the Heavers Creek Fault pre-tilt thrust surface with possible late dextral shear.

Fault 4

Description

This contact juxtaposes eastward younging, massive to turbiditic siltstones, believed to be from the Heavers Creek Formation by their position above conglomerates, against eastward younging limestone lithologies of the Glencoe

Limestone unit (fig. 4.12c). At the base of this limestone is the Eocene smectitic mudstone. There is very poor exposure in this area, making the exact location and nature of this contact difficult to map. However, the available exposure suggests that the contact is steeply dipping with a trend approximately subparallel to bedding in the turbidites and debris flow deposits to the west. It may be folded with the limestone lithologies. The juxtaposition of older limestone above younger Heavers Creek Formation siltstone does suggest a reverse fault. However, in this case, since it is unsure what lies above the limestone, it is possible that the limestone may represent a large slide block placing uplifted older limestone into the siltstone basin of deposition along a bedding plane.

Interpretation

Fault 4 places older Amuri Limestone above younger Heavers Creek Formation sediments. The limestone material is identical to that along Fault 5 which places older Waima Siltstones above younger Heavers Creek formation sediments.

Fault 8

Description

This contact is marked by the presence of a thin sliver of highly deformed smectitic mudstone separating westward younging Waima Siltstone (dated sample 308c) from westward younging conglomerate beds. The presence of older siltstone above younger conglomerate beds indicates a fault between the two units, marked by the sliver of out-of-sequence limestone. A photograph of this smectitic mudstone is shown in fig. 4.13.

Interpretation

The following features suggest that Fault 8 is a pre-tilt thrust: (1) The presence of a thin sliver of Eocene smectitic mudstone along the fault; (2) the subparallel nature of the contact to bedding either side; (3) the juxtaposition of older Waima Siltstone against and structurally above younger conglomerates. The thin sliver of smectitic mudstone appears to have acted as a decollement along the thrust surface.

Movement on such a pre-tilt thrust must post-date the overthrust conglomerate beds. Unfortunately there are no accurate dates from these conglomerates, though they are also cut by both the Heavers Creek Fault (Fault 5) and by the E-trending dextral strike-slip faults in this area (Faults 30a) and thus also predate displacements along both of these structures.



Fig 4.13: Photograph of deformed smectitc mudstone from along one of the pre-tilt thrust faults (Fault 8). This material separates older Waima Siltstone above from younger Great Marlborough Conglomerate beds below. A pencil is included for scale.

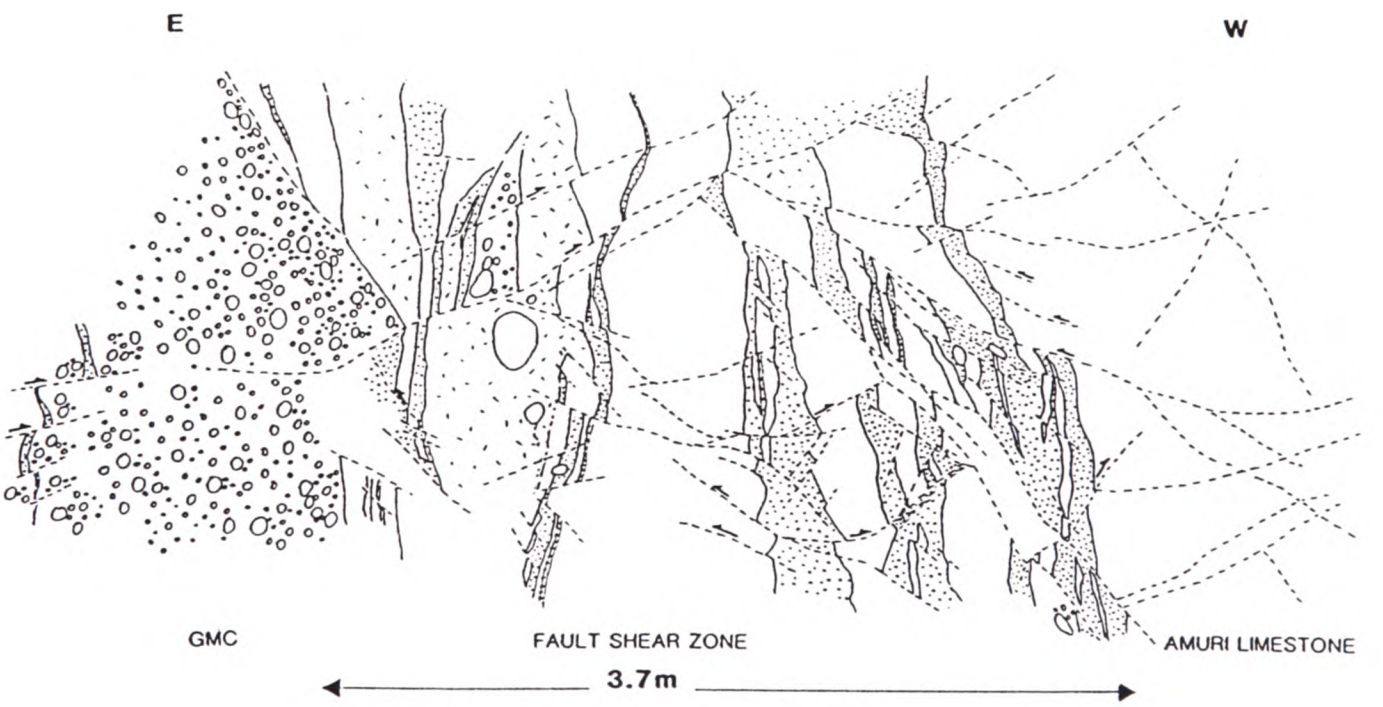


Fig 4.14: Sketch of a fault shear zone along another of the pre-tilt thrust faults (Fault 17). This thrust has placed older Amuri Limestone above younger Great Marlborough Conglomerate. The shear zone includes blocks and lenses of material from the two lithological units juxtaposed by this fault.

Fault 16

Description

This contact is folded around the steeply plunging Razor Fold Syncline in the northern part of the Washdyke map sheet (fig. 4.16). The position of this contact is well constrained by the topographic expression of limestone (high ridge) and by actual exposures. Its dip is not controlled by topographic changes and is thus steep to subvertical. There is one direct exposure of the contact in the fold nose region, and here the contact is marked by a narrow fault gouge (0.5 cm thick) oriented 000/65^{o}N. It juxtaposes Amuri Group Limestones above upward younging conglomerates (*Mid Lillburnian* (dated sample 153)) on the western limb and around the nose of the fold. On the eastern limb it juxtaposes limestone against obliquely striking Amuri Limestone to Waitakian Marl. Further around to the NE the limestone is juxtaposed against conglomerate again (with a narrow sliver of Waima Formation siltstone along the contact). There is no direct younging evidence from within the limestone unit. However the progression of limestone lithologies indicates upward younging.

The conglomerate lithology directly below the contact consists of a limestone breccia above less limestone rich thick debris flow deposits (refer to 2.2.3, locations 24 and 25).

Internal limestone bedding is subparallel to the contact. The bedding in the conglomerate is subparallel to the contact on both limbs.

The juxtaposition of limestone above upward younging conglomerate beds indicates a faulted contact with limestone on the upthrown side.

Interpretation

Fault 16 is both folded by the Razor Fold and is also at a very low-angle to bedding in the lithologies on either side. The sense of displacement suggested by the cross-cutting relationship with bedding seems to be consistent right round the fold, suggesting that this fault pre-dates folding and is not an accommodation feature such as flexural slip faulting, related to folding. The fault places older limestone above younger conglomerates, indicating a reverse fault. Unfolding the fault leaves a low-angle structure. For example, the dip of this contact in the nose area of the Razor Fold is 65^{o}N, while the fold itself plunges at *ca.* 70^{o} north, suggesting that the unfolded contact is nearly subhorizontal. The obliquity of limestone beds to this thrust on the western limb can be explained by a simple thrust hanging wall anticline. Along strike, on the eastern limb, conglomerate is not directly below this contact. Limestone directly below the contact is also oblique to the contact. This is interpreted as due to displacement along Fault 20.

The fault appears to be the base of a limestone thrust sheet which moved within the basin of deposition and is intricately associated with syndepositional debris flow

deposits. For instance, limestone-rich conglomerates and very coarse limestone breccias, such as those one might expect from an eroding limestone thrust sheet, occur below the fault (outcropping in the nose region of the Razor Syncline).

This thrust fault post-dates the conglomerate beds below it which have been dated as *Mid Lillburnian* (dated sample 153). It also pre-dates the folding of this area (the youngest folded sediments are *Lillburnian* to *Waiauan*). Therefore movement on this thrust is inferred to be pre-*basal Tongaporutuan*, the age of the youngest known conglomerate.

Fault 17

Description

This contact is folded by the Razor Fold syncline and is structurally above Fault 16 (fig. 4.11). The contact is marked by the presence of a 'sliver' (maximum thickness 150 m) of conglomerate and Waima Formation siltstone (dated sample 62; chapter 3) lithologies between upward younging limestone units. This sliver is exposed on both fold limbs, but not in the fold nose region. The limestone above this contact is a conformable sequence from Waitakian Marl through to Heavers Creek Formation siltstones. On the eastern and western limbs bedding in the limestone units either side of the contact is parallel to the contact and to bedding in the sliver. Nearer the nose of the fold however the limestone above the contact is oblique to the contact. On the western limb the contact has a straight trace and steeply dipping limestone beds suggesting a vertical structure in comparison to the *ca.* 70^{o} dip of the eastern limb.

The repetition of limestone lithologies and the presence of out-of-sequence units along this contact suggests that this contact is a fault.

Interpretation

Fault 17 is also restored to a low-angle structure if the Razor Fold is unfolded. This fault places older limestone over younger conglomerate and siltstone material and the limestone sequence is repeated across the fault, suggesting that this fault was originally a low-angle reverse fault.

The contact is well exposed at a number of localities. At two localities, conglomerate is juxtaposed directly with limestone with no intervening fault gouge or fault zone material. However, the contact in both exposures is steep and subparallel to the bedding to either side. Elsewhere a 3.7 m wide shear zone is found between Waitakian Marl and conglomerate (see fig. 4.14). The zone contains siltstone (of unknown age and weathered) alternating with limestone slices (from a few centimetres to 1 m in width) of the same lithological type to the limestone unit. These slices either pinch out along their length or are traceable throughout the outcrop. Scattered rounded clasts of Torlesse basement from the conglomerate unit are also present within the zone.

The limestone slices are parallel to the zone margins which are in turn parallel to bedding in the conglomerate and limestone units on either side. The limestone within the zone possesses a cleavage identical in nature to that of the limestone unit outside of the zone. This cleavage cannot be traced into the surrounding siltstone matrix. This suggests that it formed prior or at an early stage to formation of this shear zone. In other words, prior or at an early stage to motion along the thrust.

It is possible that the shear zone itself is disrupted thrust debris material similar to that observed beneath Fault 16.

The thrust clearly pre-dates tilting. It also either post-dates Heavers Creek Formation siltstones as these are included in the sedimentary package carried above this thrust, or is syn-sedimentary with respect to the Heavers Creek Formation if the Heavers Creek Formation were deposited in a 'moving' basin (Ori and Friend 1984). Lastly, assuming a piggy-back style of thrust formation (eg:- Boyer and Elliot 1982) then motion on this particular thrust presumably postdates that on the thrust below it (Fault 16).

Fault 19

Description

This contact is on the eastern limb of the Razor Syncline. All the following features are summarized in the sketch map of fig. 4.15. Conglomerate of unknown age is juxtaposed against limestone of Waitakian Marl lithology to the northwest. Conformably above this limestone are Waima Siltstone Formation beds (*Mid Altonian* (dated sample 350a, chapter 3) younging into conglomerates and ultimately to Heavers Creek Formation siltstones. The contact itself is directly exposed at one location along the farm track immediately north of Deadman Stream. Here a narrow fault gouge separates the two lithologies and a strong antithetic gouge fabric is developed in the conglomerate below the main contact gouge. The contact is of similar dip and strike to bedding in the limestone. Bedding in the conglomerate is less clear but appears to be at an angle to the contact and internal limestone beds. The juxtaposition of Waitakian Marl over conglomerate beds indicates a faulted contact, as is also suggested by the existence of a fault gouge.

Interpretation

Fault 19 is the along strike equivalent of Fault 17 (fig. 4.11). It is given two separate descriptions because of the along strike changes of this structure. This fault places a conformable sequence from Waitakian Marl at the base to Heavers Creek formation siltstones above massive, younger conglomerate (the oldest known age of which is *Altonian*, see Chapter 3) beds indicating a reverse fault contact, and is

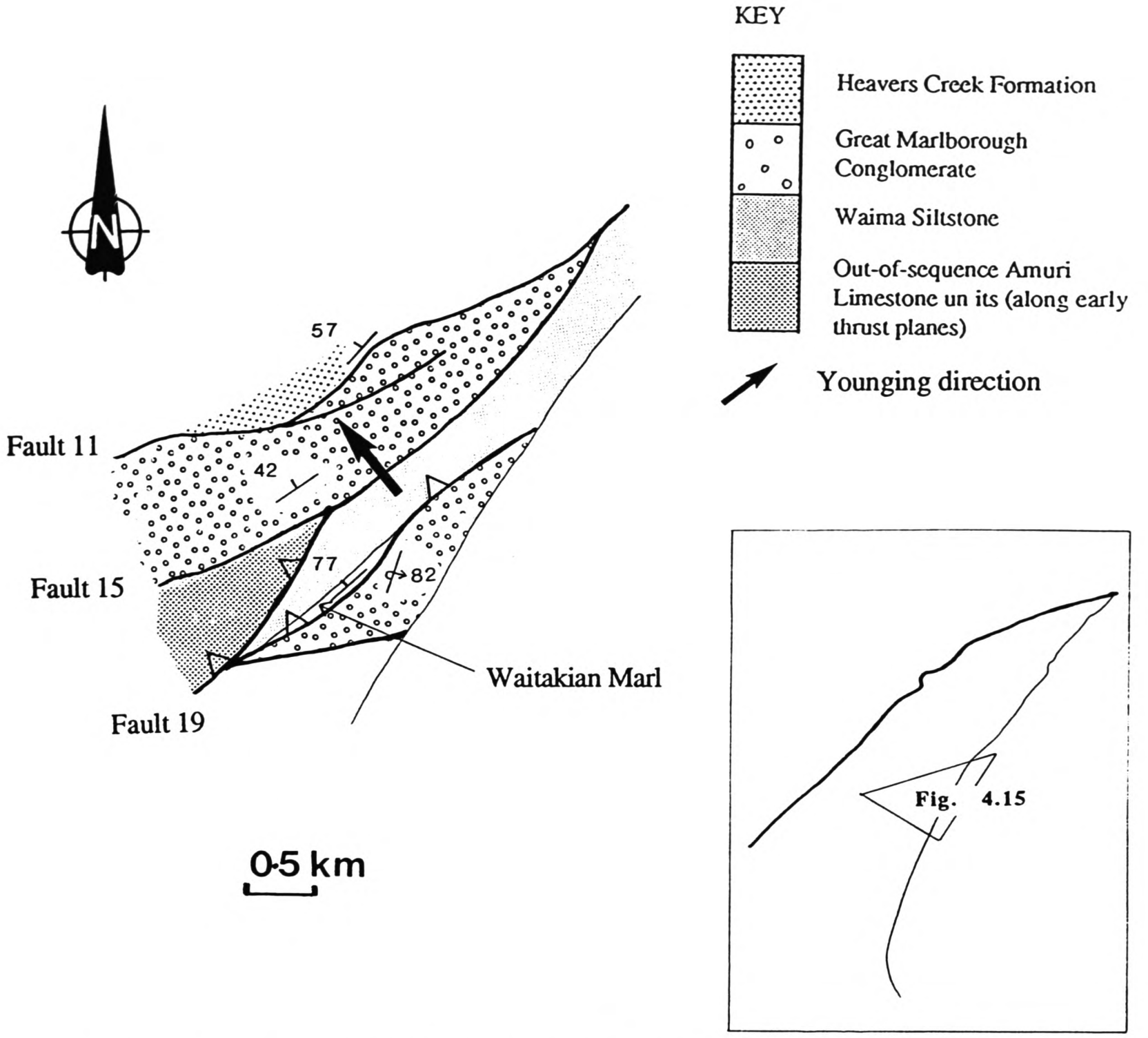


Fig. 4.15a: Sketch map showing features relating to Fault 19 with inset showing the location of this map within the Kekerengu-Washdyke study area.

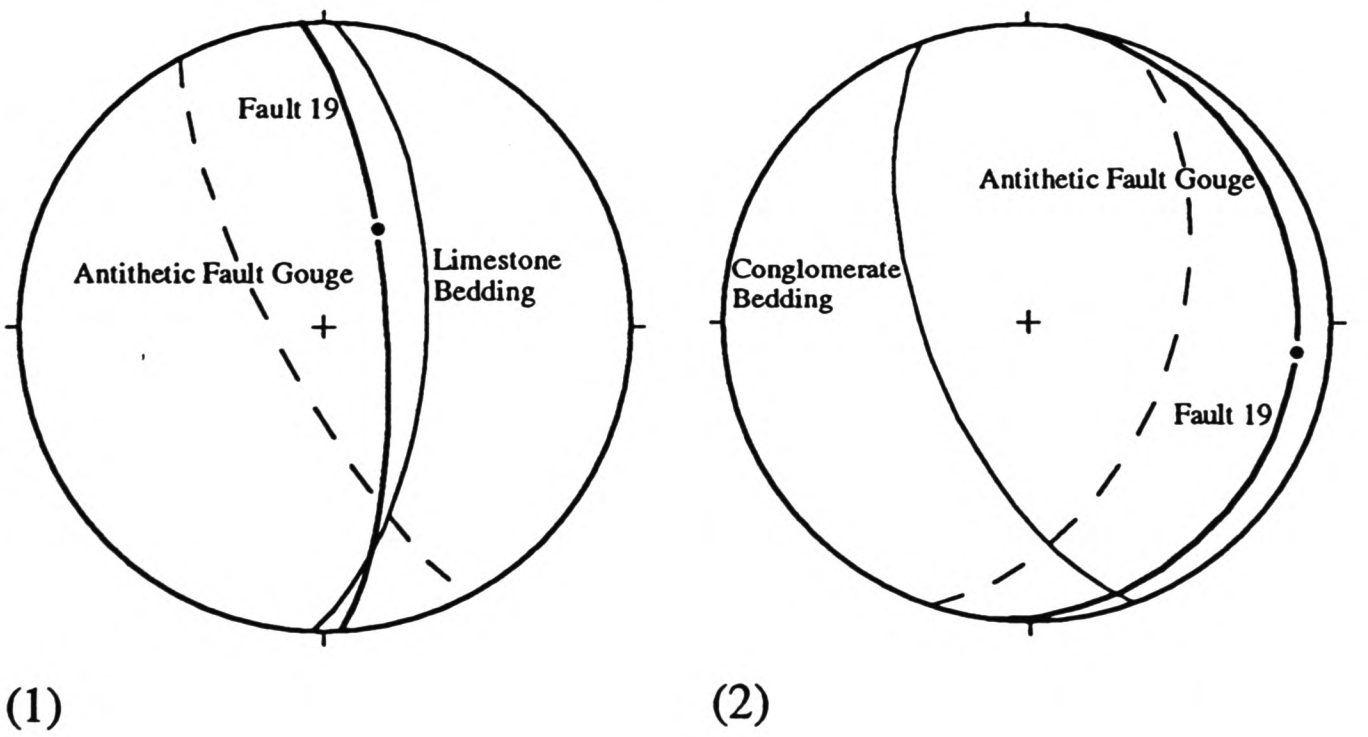


Fig. 4. 15b: Equal area lower hemisphere stereographic projections of the structural elements observed at Fault 19 along the Deadman Stream farm track. The pre-tilt orientations of these elements were found by first restoring the conglomerate beds (1) and then the limestone beds (2) back to the horizontal. This was done by unplunging and then untilting using the Razor Fold fold axis (320/67 NW). Refer to 4.3.1, Fault 19.

interpreted as a pre-tilt structure of post Heavers Creek Formation age (see description of Fault 17).

It is possible to observe a number of fabrics which appear to be associated with this fault. These were then corrected to their pre-fold orientations. The fold axis of the Razor Fold (320/67NW) was used to first plunge correct and then tilt correct the data. This was done by first restoring the conglomerate beds, then the limestone beds, back to the horizontal. In the former case, the pre-fold arrangement is as shown in fig. 4.15b (1); a steep reverse fault with limestone on its upthrown side. In contrast, fig. 4.15b (2) shows how restoring the limestone beds back to the horizontal resulted in an originally low-angle fault with the limestone beds apparently downthrown onto steeply dipping conglomerate beds. The former case is preferred as it is more likely that the hanging-wall rather than the foot-wall material should be steeply dipping. Overall this fault is assumed to be a steep reverse fault uplifting limestone against gently dipping younger conglomerate beds.

Fault 20

Description

This contact is exposed along a section of the eastern limb of the Razor Fold syncline (fig. 4.16). It juxtaposes obliquely bedded limestone lithologies above a sequence of highly oblique conglomerate, siltstone and limestone lithologies themselves separated by structural boundaries which are also truncated by this contact. The sequence to the south youngs to the east except west of Fault 23 where the beds young to the northeast. The truncation of bedding and differently younging sequences to either side of this contact is strong evidence for a fault.

The contact itself is directly exposed in two locations close to the fold nose. The first exposure (grid ref.: (P30) 845024) is of a subvertical 10 m wide brittle shear zone of deformed limestone blocks, siltstone and Torlesse clasts. At the second (grid ref.: (P30) 844024) conglomerate patches are found within intensely faulted limestone beds. Both localities represent brittle shear zones and add further evidence for the faulted nature of this contact.

Interpretation

Fault 20 is parallel to other pre-tilt thrusts such as Faults 16 and 17 and is folded around the Razor fold, placing older limestone above younger Miocene sediments (fig. 4. 16). Thus it is possible that this contact has a similar thrust origin to Faults 16 and 17. However, this fault also truncates at a high angle both bedding and pre-tilt faults further south. The changes in strike of beds to either side of the fault with respect to the trend of the fault itself suggest the origin of this fault. The obliquity of the limestone beds north of the fault can be explained by a hanging wall anticlinal structure associated

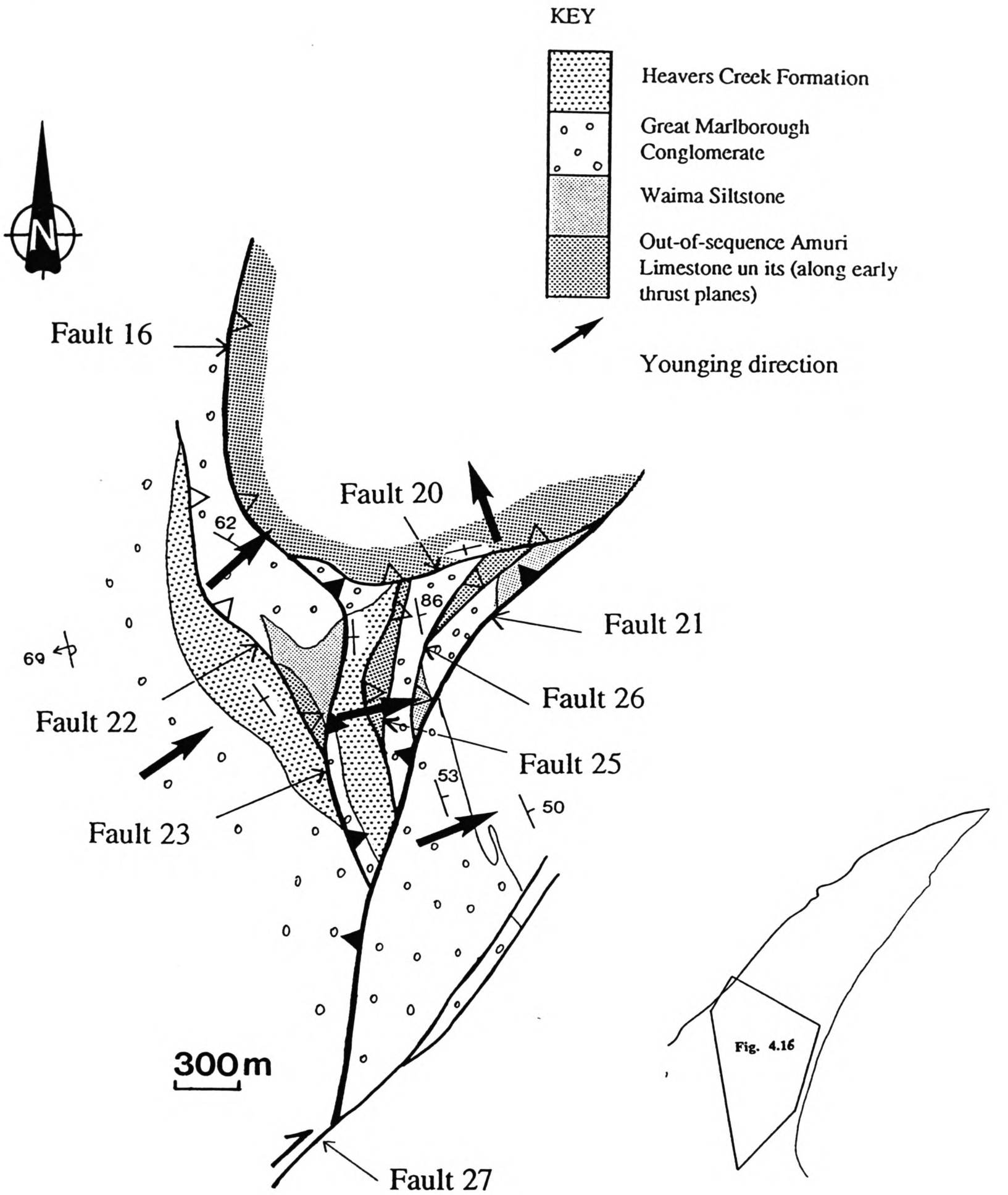


Fig. 4.16: Sketch map to accompany fault descriptions in sections 4.3.2.1d (Faults 21 and 23) and 4.3.2.1e (Faults 16, 20, 22, 25 and 26). All symbols are the same as for the main study maps.

with this fault. It is suggested that this is a thrust fault but that the truncation of late structures to the south signifies that at least some late displacement may have occurred along this thrust fault.

Fault 22

Description

This contact juxtaposes northeast younging massive Heavers Creek Formation siltstones against northeast younging conglomerate and Waima Siltstone beds to the north (fig. 4.16). There is a block of out-of-sequence Amuri Limestone along the southeast section of this contact. The contact is lost to the northwest (due to lack of exposure) and is truncated by Fault 21 to the southeast. The Heavers Creek Formation siltstones south of this contact thin to the northwest. The lack of topographic control on this structure implies that it is steep to subvertical.

Bedding in the siltstone and limestone to the south, and in the conglomerate beds to the north is at a low angle to the contact.

Dating of the lithologies to either side revealed older conglomerates (dated sample 153, chapter 3) above younger siltstones (dated sample 157, chapter 3). This evidence, together with the thinning of the siltstone and the presence of out-of-sequence limestone along this contact, indicates the presence of a reverse fault.

Interpretation

Fault 22 is at a low-angle to bedding either side, and juxtaposes older sedimentary rocks with structurally higher and younger units. These observations suggest a pre-tilt thrust origin for Fault 22. In addition, a limestone sliver (*ca.* 1.7 x 0.2 km in map view) occurs along the fault and is a feature typical of pre-tilt thrusts in the study area. This limestone sliver may originally have been a slide block which has slid into the basin of siltstone deposition, although there is no doubt that the contact has acted as a reverse dip-slip fault of post *Upper Lillburnian* to *Upper Waiauan* (dated sample 157, chapter 3) age. Fault 22 appears to be the structurally lowest pre-tilt thrust exposed in the area. Thus, if these all formed in a typical sequence of piggy-back thrusting, then this would also be the last D_e thrust to form prior to later D_l tilting (eg:- Boyer and Elliot 1982).

Fault 25

Description

This is the eastern boundary of the limestone unit bound to the west by Fault 24 where it is juxtaposed against eastward younging conglomerate beds (fig. 4.16). Although the limestone/conglomerate contact itself is not directly exposed, interbedded siltstone horizons within the limestone show clear evidence of shear, including thick

(ca. 0.5 to 3 cm) gouges and steep top-to-the-west faults oriented 329/78 E. These shear planes are subparallel to the contact and to the bedding in the juxtaposed conglomerate and limestone units. A significant amount of displacement appears to have occurred along this contact. The limestone block thins as it is traced to the south and the contact is truncated by Faults 20 and 21, and thus pre-dates them. The limestone is out of sequence separating older conglomerates above from younger Heavers Creek Formation siltstones below.

Interpretation

Fault 25 is parallel to bedding either side of it and juxtaposes older and overlying conglomerates with younger and underlying Heavers Creek Formation sediments. This suggests it is a reverse fault. The limestone lithology along this fault is identical to that along Fault 22 which is a pre-tilt thrust fault. Thus, Fault 25 is also interpreted as a pre-tilt thrust. Most of the shear along this contact appears to have occurred along the top margin of the limestone block. This top-to-the-west shear is probably either syn-tilt flexural slip imposed on the pre-tilt thrust fault (shear consistent with eastern limb of the anticline) or due to the actual pre-tilt thrust motion along this contact.

The lithologies separated by this fault are identical to those cut by Fault 22. It is believed that Faults 22 and 25 are in fact the same contact which has been subsequently displaced along Fault 23.

Fault 26

Description

In the Washdyke Gorge this contact separates eastward younging conglomerate beds to the west from a limestone block (*ca.* 1.2 x 0.2 km in map view). The limestone block thins at it is traced to the south, so that eventually *Otaian*-aged siltstones and conglomerates east of the limestone come into contact with the eastward younging conglomerate (fig. 4.16). Bedding in the limestone block is parallel to the contact. The contact is subvertical and trends NNE. Bedding in the conglomerates to the west and in the *Otaian* siltstones and conglomerates to the east of the block all have similar steep dips but are oblique to the contact (N to NNW strikes).

The contact itself is observed to within a few metres in the gorge. A summary log was made of the gorge sequence (see chapter 2, fig. 2.8). This log clearly shows the existence of a limestone rich breccia deposit beneath the limestone block and above a thick sequence of limestone poor conglomerates. The placing of older *Otaian* siltstones and out-of-sequence limestone above younger conglomerates suggests a dip-slip component of motion along this fault.

Interpretation

Limestone breccia is observed beneath a large limestone block along Fault 26. Below this breccia are basinal conglomerates. The placing of older limestone above younger conglomerates suggests a reverse fault, whilst the breccia could represent debris from the advancing fault. Thus the deposits suggest a syn-depositional reverse fault and therefore an early, pre-tilt fault emerging into the basin of deposition. This fault in fact occupies a similar structural position within the surrounding units as Fault 16. The low-angle of the bedding to either side of the contact indicates a probable thrust. Fault 26 is mapped as a splay thrust fault from Fault 16.

4.3.2.2 Mesoscopic faulting

Faults with displacements between 0.02 and 1.0 m are commonly observed cutting all formations in the Kekerengu-Washdyke area. Sometimes, striations on fault surfaces can be measured. These faults are of all kinds, with varying components of dip and strike-slip motion. When plotted on a stereogram the faults often show consistency in orientation. Fault data for mesoscopic faulting are presented for different areas (see fig. 4.17). Each sub-area is essentially defined by large scale bounding structures or by regions with similar lithologies. Uniform fault patterns are generally displayed within each area. Unfortunately very few fault striation data could be found for each fault set. The faults are described from these subareas from north to south down the length of the field area, and are presented in terms of their present orientations. It was not possible to distinguish any particular chronological order for this faulting. The relation between these structures and other structures in the Kekerengu-Washdyke area are discussed in chapter 6.

Subarea 1

Small scale faults within the Glencoe Limestone unit are plotted in fig 4.18a. The faults are E-trending normal and reverse, and N-trending strike-slip. In the turbiditic siltstones to the west of this limestone are NW-trending normal faults. The flint beds at the head of Valhalla Creek are cut by several E-trending normal faults. Further south, NNE to ENE-trending reverse faults were found. Within the limestone outcrops exposed along the Heavers Creek Fault NNE-trending reverse faults were observed along with a NNE-trending vertical fault with horizontal striations (see fig 4.18b). Both these fault types parallel the limestone margins.

Subarea 2

Between the Heavers Creek and Chaffey Faults numerous faults cut the massive to turbiditic siltstone beds. The faults appear to fall into two dominant types: (1) NW-

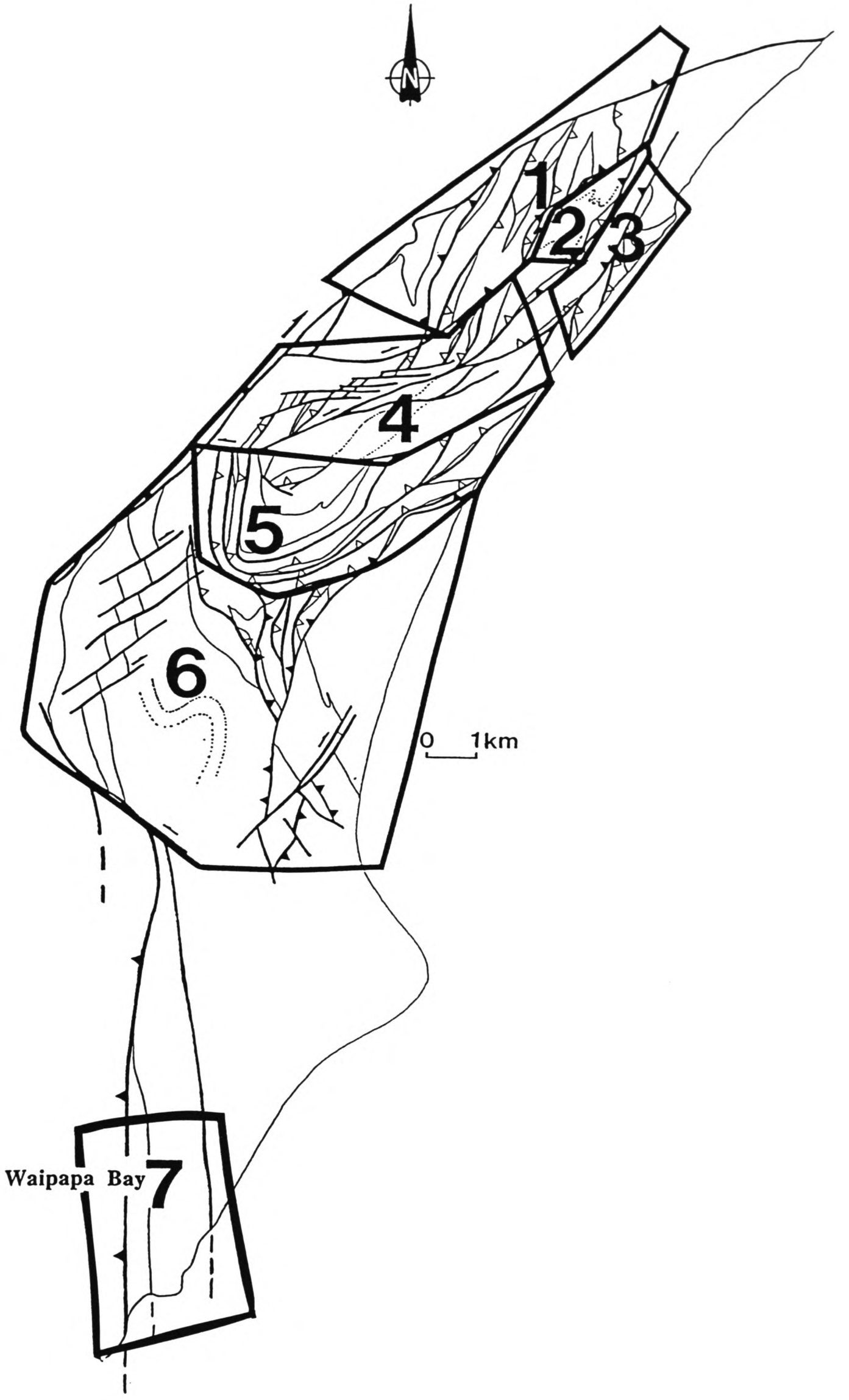


Fig. 4.17: Sketch map of the Kekerengu-Washdyke study area showing the position of mesoscopic fault subareas as described in 4.3.2.2.

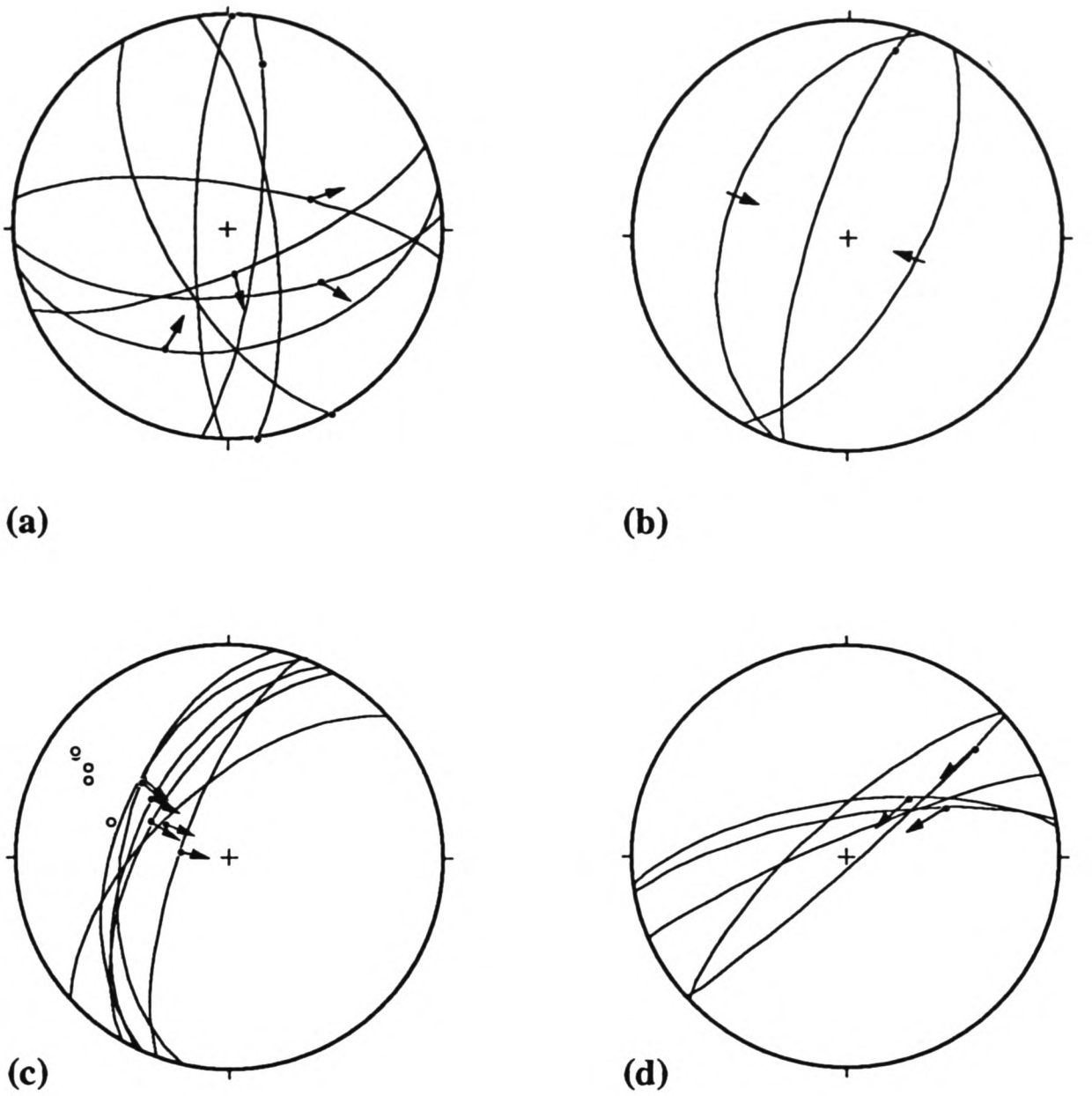


Fig. 4.18: Equal area, lower hemisphere stereographic projections of mesoscopic faults from the Kekerengu-Washdyke study area. Fault planes are represented by great circles. Dots mark lineations on fault planes and arrows the sense of hanging -wall slip where this data was available. Refer to text in section 4.3.2 and to fig. 4.16 for subarea locations. (a) Reverse, normal and strike-slip faulting within the Glencoe allochthonous limestone unit of subarea 1. (b) Reverse and strike-slip faulting in allochthonous limestone along the Heavers Creek Fault of subarea 1. (c) Reverse faulting in the northern Chaffey Fault limestone of subarea 2; also showing $\sigma 1$ orientations (open circles) calculated from single fault planes (mean $\sigma 1$: 299/26). (d) Sinistral faulting within the Heavers Creek Formation siltstone of subarea 4. (e) Reverse faulting across Fault 17 in subarea 5; also showing $\sigma 1$ orientations (open circles) calculated from single fault planes (mean $\sigma 1$: 302/17).

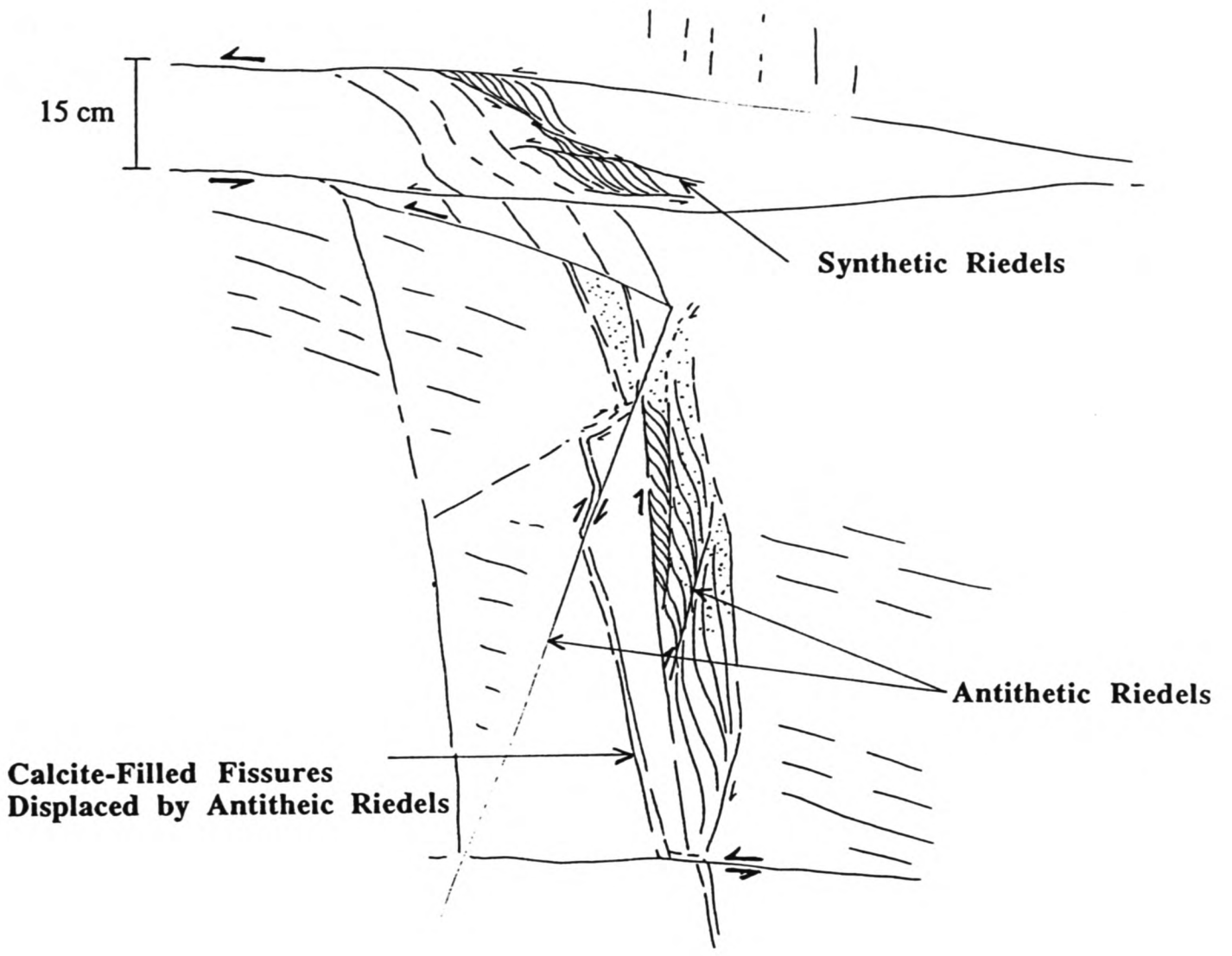


Fig. 4.19: Synthetic riedels, antithetic riedels and extensional fissures within a left-lateral shear zone exposed on a vertical surface. The shear zone cuts Waitakian Marl beds exposed in Valhalla Stream along the Chaffey Fault. For description refer to 4.3.2, subarea 2.

trending reverse and (2) N-trending reverse and normal faults. No striations were found on any of these fault planes.

The Valhalla Creek limestone exposure along the Chaffey Fault is cut by several NNE, pure dip-slip, reverse faults. See fig 4.18c. One such fault is traceable over a minimum distance of 10 m. Again these faults parallel the limestone margins. The large scale reverse fault has a 0.15 m wide upper displacement zone containing well developed synthetic reidels (fig. 4.19). Below this zone are further synthetic reidels and extensional fissures themselves displaced by antithetic and synthetic riedels. All faults appear to form part of a left lateral brittle shear zone. Horizontal striations were found on the subvertical synthetic faults. The maximum principal stress directions were deduced using the M-plane method (Marshak and Mitron 1988) on the reverse fault planes and are also shown in fig 4.18c (open circles). (Mean σ_1:298.7/26.3 *ca.* WNW).

Subarea 3

East of the Chaffey Fault both NNE-striking reverse faults and subvertical fault gouges, with horizontal striations, cut turbidite beds. To the east of the fault, further south, NE-striking reverse faults and vertical fault gouges were found. This change in orientation parallels the change in trend of the Chaffey Fault.

Fault data for the Homai Fold area are sparse. A few N-striking and low angle reverse and normal faults were found. The trend of these faults parallels the fold axis direction.

Close to Highway 1, at the mouth of Boundary Stream, NNE-striking vertical slickenslides cut the massive siltstone. Just to the west NNE-striking reverse faults cut the narrow limestone exposure.

Subarea 4

In the southern part of the Kekerengu map sheet, Heavers Creek Formation siltstone north of the main conglomerate body is cut by several steeply dipping, ENE-striking reverse faults with large sinistral strike-slip components (fig 4.18d). The limestone slice along Fault 9 contains NNE to NE-striking reverse faults with pure dip-slip to dip-slip and sinistral strike-slip components of motions. The area which is cut by large-scale E-trending dextral strike-slip faults (Faults 30a) is also affected by numerous faults which clearly group into three sets (fig. 4.20a). These are: (1) ENE-striking reverse faults with a dextral shear component; (2) NW-striking sinistral strike-slip faults (often associated with kinking); and (3) NNE-striking reverse dip-slip faults.

The main conglomerate body of the southern part of the Kekerengu map sheet is cut by many faults (fig 4.20b). For the lithology as a whole two dominant fault sets are visible: (1) a well defined set of NE-striking reverse faults, some with large components

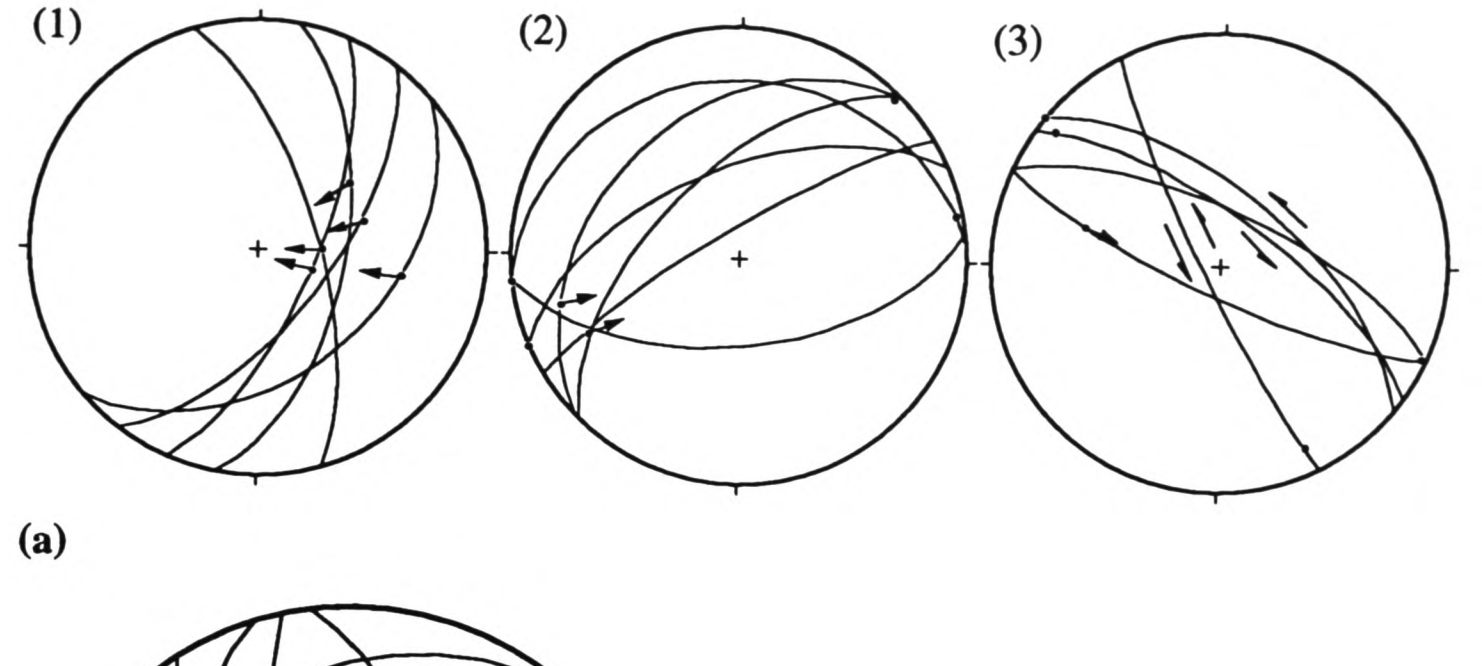


Fig 4.20: Equal area, lower hemisphere stereographic projections of mesoscopic faults from the Kekerengu-Washdyke study area. Fault planes are represented by great circles. Dots mark lineations on fault planes and arrows the sense of hanging wall slip where this data was available. Refer to text in section 4.3.2 and to fig. 4.16 for subarea locations. (a) Dip and strike-slip faulting within allochthonous limestone of subarea 4. (b) Reverse and normal faulting within the conglomerate of subarea 4. (c) Reverse, normal and strike-slip faulting in the autochthonous limestone of subarea 6.

of dextral motion; and (2) less well defined set of NW to N-striking normal and reverse faults, mostly with large sinistral components.

Subarea 5

The Razor Fold syncline is cut by numerous small scale faults. Very few striations were found on any of these fault planes. NNE to NE-striking reverse faults cut limestone on the western limb, whilst NE-striking reverse faults and NW-striking normal and reverse faults cut beds of the eastern limb. One location on the eastern limb displayed well preserved faults with striations which cut a tilted thrust contact (see fig. 4.14, section 4.3.2.1e, Fault 17). The orientations of the faults are shown in fig 4.18e. Displacements on these faults range from a few cms to 0.4 m. All faults are reverse with large strike-slip components. The faults are as follows: (1) NE-striking top-to-the-west reverse faults with a dextral shear component; (2) NE-striking top-to-the-southeast reverse faults with a sinistral shear component; and (3) NW-striking top-to-the-northeast reverse faults also with a sinistral shear component. The strike-slip components are visible on plan view surfaces within the limestone. In plan view, the faults are stepped and display clear strike-slip senses (fig. 4.21). No conjugate fault sets with lineations were found. The M-plane method (Marshak and Mitron 1988) was used to calculate the likely maximum principal stress directions for the tectonic regime in which these faults formed. The results of this are also plotted in fig 4.18e. All vectors lie along the WNW azimuth (mean σ_1 direction: 294.6/36.6). The similarity of all tested faults suggests that their development under the same compressional phase. One should also note the similarity of this σ_1 direction with that obtained in the northern part of the Kekerengu map sheet (refer to fig 4.18c).

The pattern of faulting affecting conglomerate beds on the eastern limb is very different. Here a few W and NNW-striking normal faults were recorded.

The siltstones exposed along the eastern reaches of Deadman Stream are cut by NNE-trending reverse faults with a sinistral strike-slip component. The limestone below these siltstones contains examples of pure dip-slip, ENE-trending reverse and normal faults.

Subarea 6

Faulting in the conglomerate beds of the Washdyke gorge falls into two sets: (1) N to NNE-striking reverse faults with a dextral shear component; and (2) NNW- to NW-striking sinistral strike-slip faults and normal faults with sinistral components of motion. Faults within the massive siltstones in this gorge group into NW and NE-striking sets, though no sense or lineations are available for this data.

Conglomerates and siltstones to the south and west of the gorge contain N to NNE-striking reverse faults with minor dextral shear components, identical to the faults

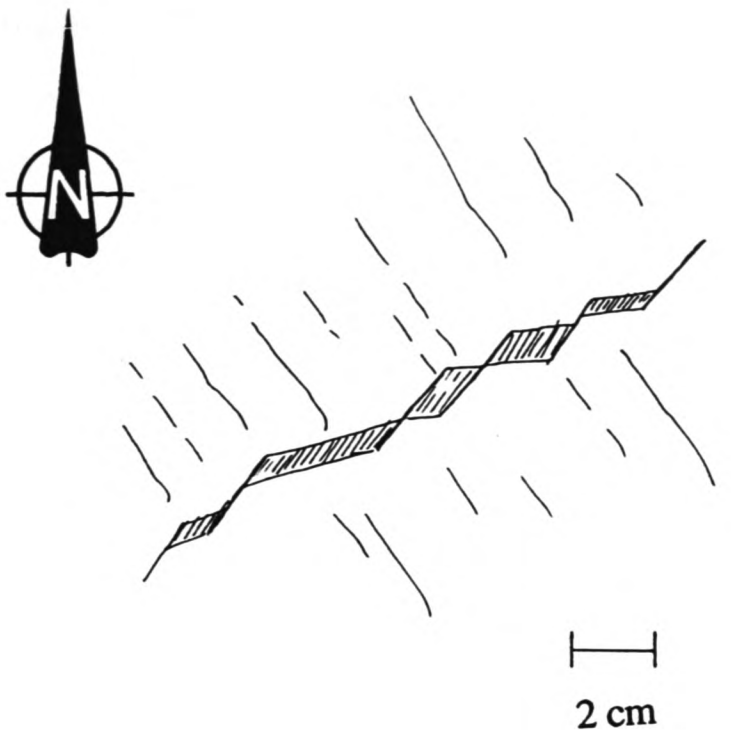


Fig. 4.21: Plan view of NE-striking reverse fault cutting Amuri Limestone beds adjacent to Fault 17. The fault is stepped displaying a clear sinistral strike-slip component. For description refer to 4.3.2, subarea 5.

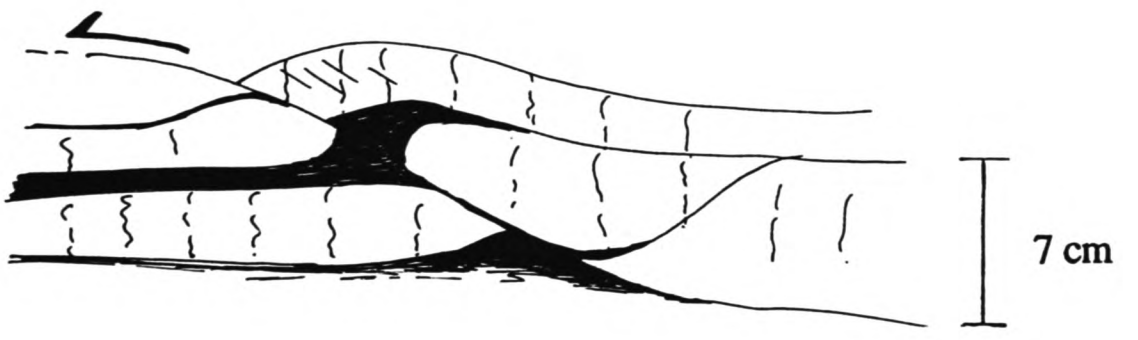


Fig. 4.22: Thrust fault cutting Amuri Limestone beds at Waipapa Bay. The fault offsets an earlier high angle to bedding cleavage. For description refer to 4.3.2, subarea 7.

of the gorge. Rare NW-striking faults were observed in the siltstones. Along the northern contact of the thick conglomerate unit which dominates the southern part of the Washdyke map sheet are NNW-striking, normal faults.

The lowest conformable siltstone in the southwestern part of the Washdyke map sheet contains several N-striking faults with dextral slip components.

The lower limestone of the western part of the Washdyke map sheet contains numerous N-striking normal and reverse faults with dextral slip components recorded on a few of these surfaces. W-striking normal faults were also found. Fig 4.20c.

Faulting in the thick conglomerate of the southern part of the Washdyke map sheet is substantial but cannot be divided into consistent fault sets. Only an approximately NW-striking set of normal and reverse faults, some with sinistral shear components, can be picked out.

Subarea 7

Faults cutting limestone lithologies in the Waipapa Bay region are consistently steep and trend N to NE. No striations were found. A typical example of such faulting is shown in fig. 4.22. The fault is at a low angle to the tilted beds which it displaces and has a well developed hanging wall anticline. The majority of cases displace east side to the north (insitu). The remaining cases show opposite senses of displacement suggesting back thrust or conjugate thrust structures. These faults were observed cutting the axial planar box fold cleavage described in section 4.3.4.

Summary of mesofaulting

This data is summarized in table 4.2. In the northern part of the Kekerengu map sheet and west of the Heavers Creek Fault (subarea 1), W to NW-trending normal faulting was observed. In the same area, NNE to ENE-trending reverse faults and subvertical NNE-trending faults with horizontal lineations were also observed.

In the area between the Heavers Creek and Chaffey Faults (subarea 2) and the conglomerate body of the southern part of the Kekerengu map sheet (subarea 4), dextral slip components were recognized on some of the NE to ENE-trending reverse faults and sinistral slip components on some of the NW-trending normal faults. However, also in subarea 4 are NNE and ENE-trending reverse faults with sinistral slip components.

In the Washdyke map sheet (subareas 5 and 6) identical N to NE-trending reverse faults with dextral slip components and W to NW-trending normal faults with sinistral components were observed.

Overall two main types of faulting were observed within the main Kekerengu-Washdyke study area: N to ENE-trending reverse faults with dextral slip components and W to NW-trending normal faults with sinistral slip components. The only exceptions to this were the two cases cited above from subarea 4, where sinistral shear

FAULT SUB-AREA	NORMAL			REVERSE			STRIKE-SLIP			
	Pure	+Sinist	+Dex	Pure	+Sinist	+Dex	Sinist	Dextral	Sence	Unknown
1	W-NW^{r}			NNE-E^{r}					N-NNE^{r}	
2	N*	NW^{r}		N-ENE* NW*		NE-ENE*			NNE^{r}	
3	N^{r}			N-NE^{r}					NNE-NE^{r}	
4		NW-N*		NNE-NE*	NNE-ENE^{r} NW-N^{r}	NE-ENE*	NW*			
5	NW-NNW^{r} ENE-E^{r}	W-NW^{r}		NNE-ENE^{r}	NNE-NE^{r} NW^{r}	N-NE*				
6	NW-NNW*	W-NW^{r}	N*			N-NE*	NW-NNW*			
7				N-NE*						

Table 4.2: A quantitiative summary of the trends of mesoscopic faults within subareas of the Kekerengu-Washdyke study area. These faults are described in 4.3.2.2 and the location of the subareas shown in fig.4.17. *: numerous (*ca.* in excess of 6) faults found with this trend; ^{r}: only rare (*ca.* fewer than 6) faults found with this trend.

is associated with reverse faults. The thrust faults from Waipapa Bay (subarea 7) are peculiar to this southern extension of the Tertiary cover sediments and were not observed in the Kekerengu-Washdyke area itself.

The explanation for all the observed faults and their distribution is discussed in chapter 6.

4.3.3 Folding

Stratigraphic units and some structural elements are folded: both outcrop scale folds with wavelengths of less than a few metres, and larger scale folds with wavelengths of up to a km in length are common. The latter are defined by the distribution of poles to bedding within the various subareas. Interpretations of these structures are discussed in chapter 6.

Fig 4.23 shows all collected fold axes data in the mapped area; outcrop scale fold axes are plotted directly, whereas larger scale fold axes are determined from stereographic plots of poles to bedding. The separate fold plots are labelled by the subarea within which they occur. These subareas are clearly labelled in fig. 4.23.

Subarea A

A close, metre scale fold was found in turbidite beds west of the Heavers Creek Fault. The fold has a slight eastward vergence.

Subarea B

The plotting of poles to bedding within the Glencoe Limestone unit, which is bound to the north and south respectively by the Kekerengu and Heavers Creek Faults, suggests folding about a rather poorly defined and steeply plunging fold axis (214/76 W). The distribution of limestone lithologies within the unit also suggests folding about a similar axis. In addition, two examples of mesoscopic folding with identical fold axes to the large scale folding were found within the limestone unit. Though there is no direct younging evidence, the limestone sequence indicate a general eastward younging direction.

Subarea C

Between the Heavers Creek and Chaffey (eastern surface exposure of the Heavers Creek Fault) Faults the distribution of bedding in the siltstones shows clear evidence for folding. The folds are close to tight with wavelengths from 150 m to 1.85 km. The few cases of younging evidence along these stream sections agree with the general fold pattern suggested by the bedding distribution. All the beds are right way up except in the southern Valhalla branch where the beds are overturned against the

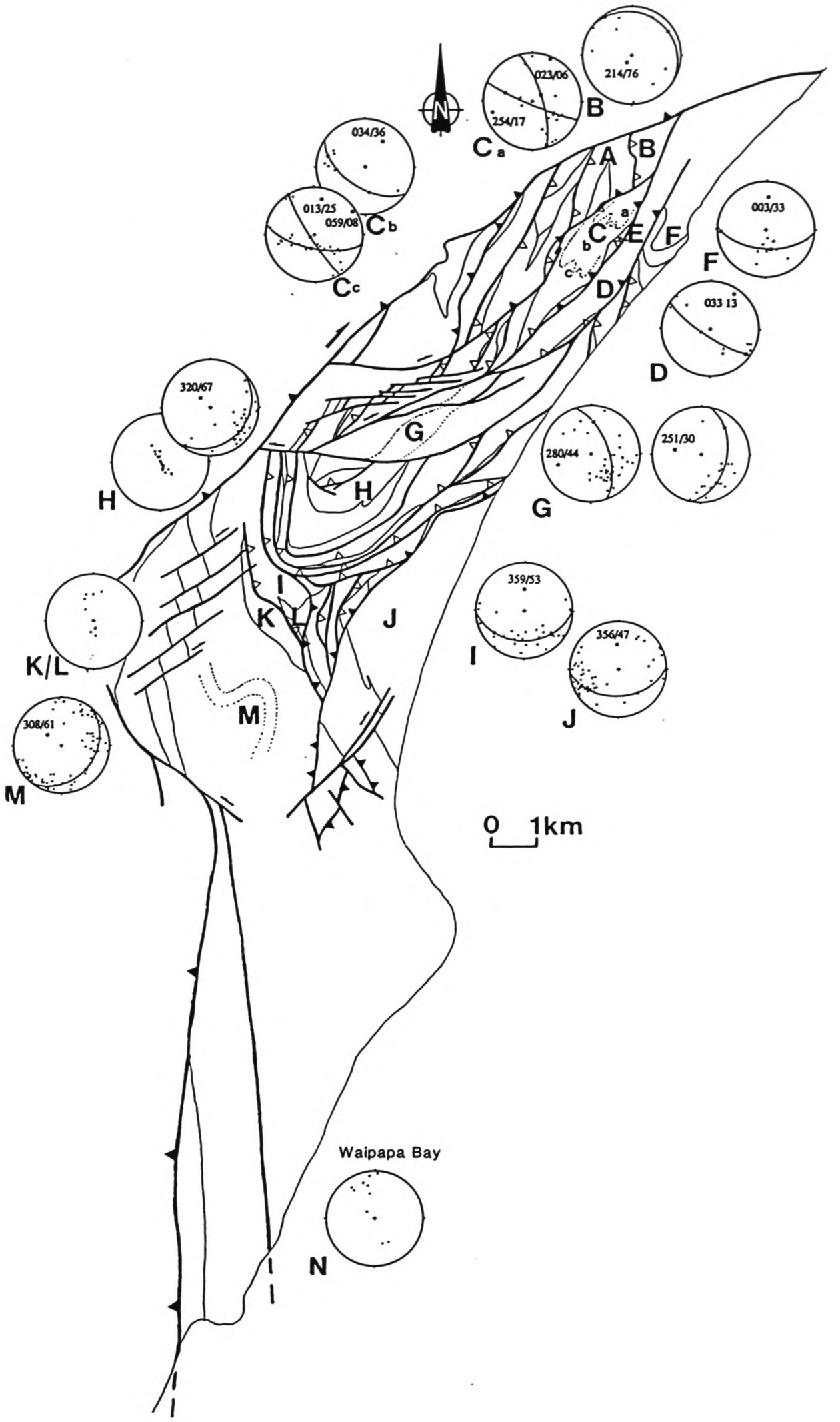


Fig. 4.23: Map of the Kekerengu-Washdyke study area showing equal area lower hemisphere stereographic projections of all fold data. Projections within each defined subarea (labelled A to N) are of two sorts: (1) plots of poles to bedding used to deduce the fold axis; and (2) the plotting of fold axes where these could be directly measured in the field. Refer to 4.3.3 for descriptions of this data.

Heavers Creek Fault. Poles to the seemingly continuous beds were plotted in three ESE-trending traverses labelled separately as Ca, Cb and Cc from north to south. The first traverse is along Heavers Creek (Ca) , whilst the second and third are along the Valhalla Creek north and south branches (Cb) and (Cc) respectively. Traverses (Ca) and (Cc) are perpendicular to the general bedding strike and are 1.3 km apart. The stereoplots for these two traverses both clearly show the existence of two distinct fold axes. Those beds furthest from the Heavers Creek Fault have NNE-trending fold axes (023/06 N and 013/25 N). In comparison, those beds nearer to the Heavers Creek Fault define more ENE-trending fold axes (254/17 W and 059/08 E). Poles to bedding along the north Valhalla branch give a fold axis of 034/36N.

Subarea D

Poles to bedding from massive siltstone between the Chaffey Fault to the west and the reverse fault (Fault 12) in the northern part of the Kekerengu map sheet suggest folding about a fold axis of 033/13 NE.

Subarea E

The northern limestone outcrop along the Chaffey Fault is folded into an anticline with a wavelength of *ca.* 200 m. Such folding was clearly observed within the outcrop itself. The fold axis (222/23 S) is defined by the distribution of poles to bedding on a stereographic plot.

Subarea F

This fold was clearly picked out by the trace of beds east of Fault 12. Upward younging and southward closure of the sequence from Waitakian Marl to Heavers Creek Formation sediments indicates a northward plunging syncline. It is a close fold with a wavelength of *ca.* 1.2 km. The poles to bedding define a fold axis (003/33 N) in rough agreement with that suggested by the trace of the beds, although the data is sparse and this fold axis is not accurately determined.

Subarea G

Poles to bedding from the conglomerate body bounded by Faults 11 and 15 suggest the existence of folding within this unit (fold axis 280/44 W). The beds themselves dip at 30-60^{o} and young to the west. The actual bedding distribution defines a clear s-c band structure, so that beds appear rotated into parallel with the bounding faults.

Poles to bedding from the conglomerate and siltstone beds to the north of this folded conglomerate body define a great circle with a fold axis of 251/30 W, similar to that of the folded conglomerate body further south.

Subarea H

This fold dominates the northern half of the Washdyke map sheet. Lithologies younging inward relative to the outer folded surface (Fault 16) and the closure of bedding to the south indicates a northward plunging syncline. Beds on the eastern limb dip steeply towards the fold axial plane at *ca.* 60-70^{o}, whereas those on the western limb are mostly vertical. The fold axis trends *ca.* 026^{o}. A plot of the poles to bedding from the fold's central siltstone/conglomerate/siltstone sequence suggests a fold axis of 320/67 NW. In the hinge region there is a well developed crenulation (with wavelengths of 7-120 cm) of a bedding parallel cleavage within limestone (fig. 4.24). These folds have an associated axial planar cleavage. The fold axes of these crenulations trend NNW and plunge steeply at 60-70^{o}. They are subparallel to the fold axis of the large scale fold structure. This large scale fold structure is referred to as the Razor Fold.

Subarea I

Poles to bedding were plotted from the conglomerate beds south of the most southerly clearly folded lithological unit of the Razor Fold. These beds young and dip to the north and west. The poles define a general great circle with a north plunging and trending fold axis (359/53 N).

Subarea J

Pliocene siltstones in the eastern part of the Washdyke map sheet have moderate to steep eastward dips and generally young eastwards. A stereographic plot of the poles to these beds define a great circle with a fold axis similar to that of the conglomerate beds south of the Razor Fold (subarea I).

Subarea K

Crenulations with wavelengths of 7-20 cm and N-trending axes, fold a weakly developed fissility within the massive siltstone unit south of Fault 22. Folds of identical trend were found within the limestone unit directly north of this contact (*subarea L*). Both show a similar range of plunge variation from approximately 5^{o} north to 40^{o} south.

Subarea M

Poles to bedding were plotted from the thick conglomerate body which dominates the southern half of the Washdyke map. The plot of these poles suggests folding about a fold axis 308/61NW. The beds young to the NE and ENE and are commonly overturned by up to 50^{o}. The trace of the beds also suggests folding (with a



Fig. 4.24: Crenulation folding of an earlier bedding parallel fissility within Type 2 allochthonous limestone in the hinge region of fold subarea H. Refer to section 4.3.3 and to fig. 4.21 for subarea location. A pen is included for scale.

fold axial trace trending approximately NNE). This folding is notably similar in scale and orientation to the large scale Razor Fold syncline.

Subarea N

Several cases of folding were observed in the limestone unit which extends along strike from Waipapa Bay in the south to the southern part of the Washdyke map sheet (fig. 4.25). Symmetrical, close to tight folds with wavelengths of 0.65-4.0 m were found (see fig. 4.25). No axial planar cleavages were recognized, probably because they are masked by the dense jointing in this limestone. A similarity was noted between these fold axes in terms of their scale and variation in fold axis plunge, with those within subareas K and L.

One of the limestone lithologies at Waipapa Bay is deformed into symmetrical, conjugate kink folds (box folds) rather than into the cylindrical folds just described. A sketch diagram of this folding is shown in fig 4.26a. The box folds have a maximum hinge to hinge separation of approximately 3 m. The particular lithology consists of regularly spaced hard limestone beds separated by thin marly horizons and thus as a whole has a strong anisotropy, making kink band formation possible. Such folding only forms at confining pressures of < 3 kbars (Ramsay and Huber 1983). The kink bands also have a well developed axial planar cleavage (see fig. 4.28a). Similar kinking was observed in the northernmost extension of this limestone, in a similarly anisotropic lithology. For symmetric, conjugate kinks to form the principal stress directions are most likely to be parallel and perpendicular to the general trend of the planar surfaces unlike for single kinks which generally form when the directions are oblique. With these assumptions the principal stress directions were calculated using the axial surfaces from one of the box folds. The results are shown in fig. 4.26b (σ_1: 200/28).

If one assumes no change in the length of lines along a folded surface perpendicular to the fold axis, then by measuring the length of any folded surface and comparing this to its original length, it is possible to estimate the strain in this direction involved in the kink formation. To allow perfect compatibility of the kink geometry, angles A and B must be approximately equal and *ca.* 60° (Ramsay and Huber 1983). Field measurements indicate that this is a good approximation. The following simple calculations were used to deduce the strain, where L_o is the original length of PP' and L_f is the final length of PP' (see fig. 4.23a):

$$\text{Strain} = \frac{L_o - L_f}{L_o} = 1 - \frac{L_f}{L_o} = 1 - \frac{0.6}{2(1.6) + 2.5 + 2(0.3 / \text{Sin}60)} = 0.475$$

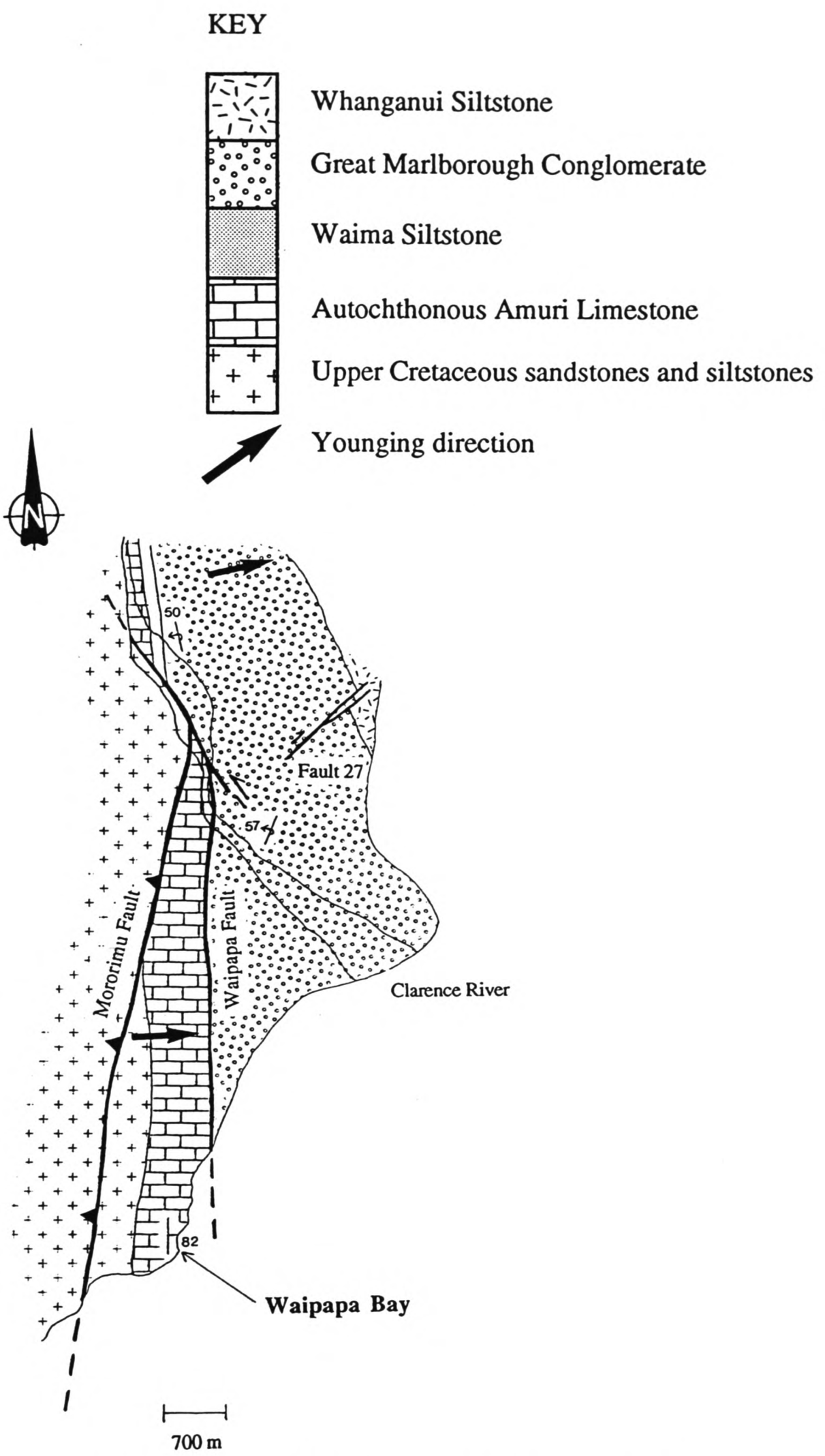


Fig. 4.25: Sketch map of the main features relating to the autocthonous Amuri Limestone extending from the southern part of the Washdyke map sheet to Waipapa Bay. Mesoscopic folding within this limestone is described in 4.3.3, subarea N.

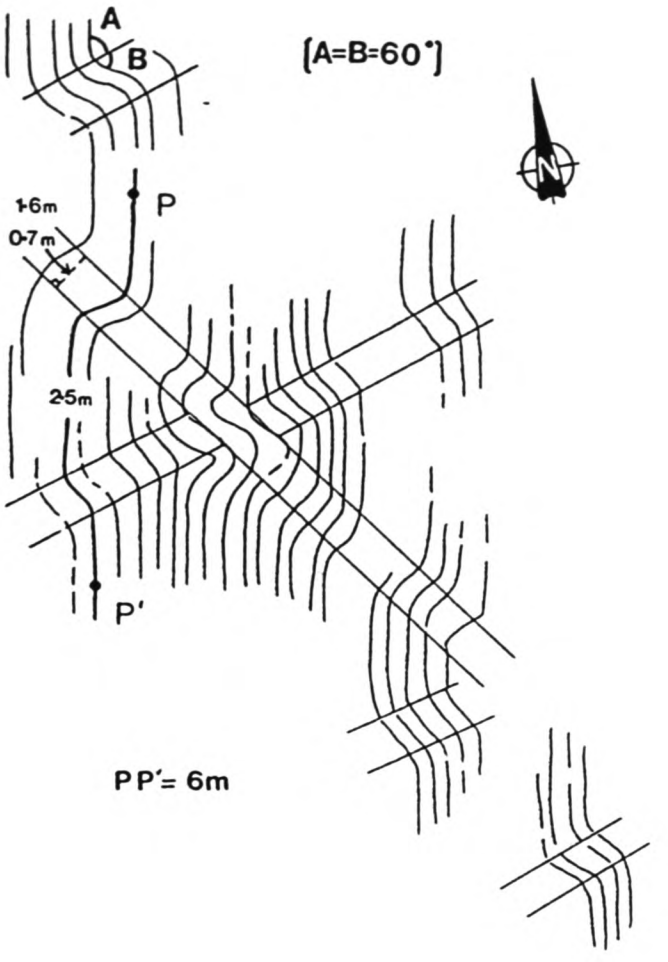


Fig. 4.26a: Field sketch of box folding in Amuri Limestone beds at Waipapa Bay. The strain involved in this deformation can be estimated by comparing the length of line PP' before and after folding (see section 4.3.3; subarea N).

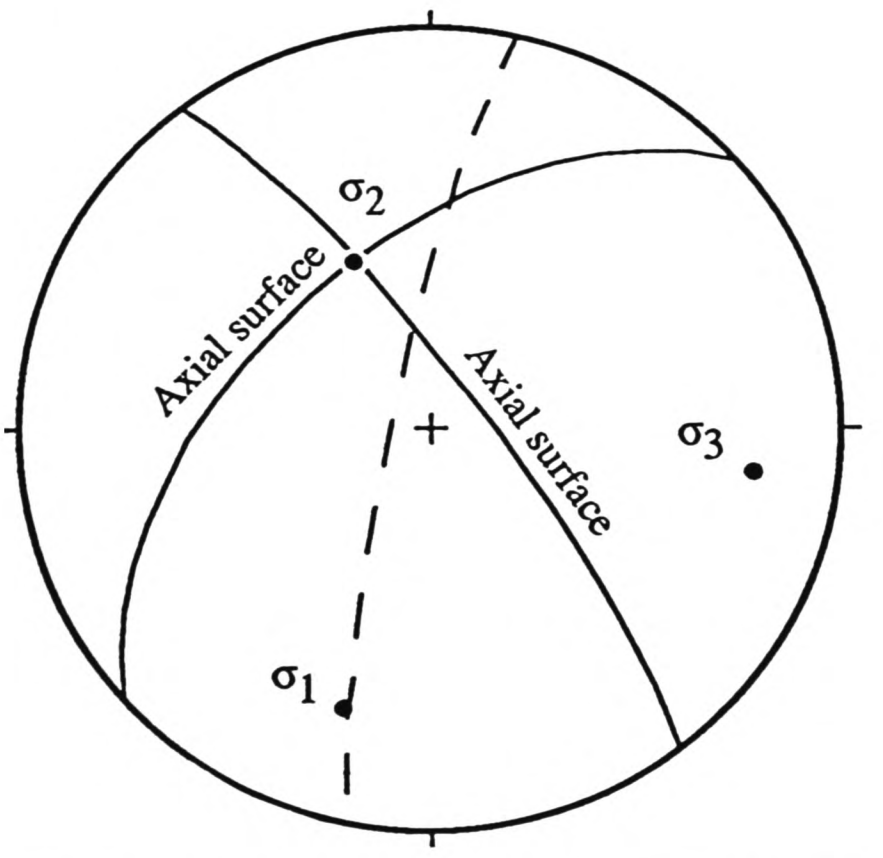


Fig. 4.26b: Stereographic plot used to deduce the principal strain directions involved in the formation of box folds at Waipapa Bay (fig. 4.23a). Axial surfaces are plotted as great circles and the principal stress directions as points. The orientation of unfolded bedding in the limestone is shown as a dashed great circle. The principal stress directions are as follows: σ_1: 200/28; σ_2: 335/53; and σ_3: 98/22.

Summary of folding

Folds with wavelengths of a few centimetres to a few kilometres affect the Cretaceous to Tertiary cover sequence throughout the study area. However, the nature of folding varies markedly along the length of the study area. These variations are summarized below. From these descriptions alone there is no evidence for fold phases. That more than one phase of folding does in fact exist will become apparent in the discussion of the folding of the whole Kekerengu-Washdyke study area (chapter 6).

(1) Folding in the northern part of the Kekerengu map sheet (subareas A to F) is characterized by N to NE-trending folds plunging to the north and northeast at 6^{o}-36^{o}. These fold the Cretaceous to Tertiary cover sequences. Two exceptions were noted: (1) siltstone beds close to the Heavers Creek Fault are folded about a gently plunging fold axis trending WSW (subarea C, traverse (a)); and (2) the Glencoe Limestone unit of subarea B is folded about a steeply plunging (at 76^{o}) fold axis (subarea B).

(2) In the southern part of the Kekerengu map sheet (subarea G) the folding has a very different attitude. Here WSW-trending fold axes plunge at 30^{o} to 44^{o}. These folds define a sigmoidal shear fabric (asymptotic towards the dextral strike-slip bounding faults) in this area.

(3) The northern part of the Washdyke map sheet is dominated by the kilometre scale steeply plunging Razor Fold (subarea H). This fold has a NW-trending fold axis which plunges at *ca.* 70^{o} to the NW. Crenulations in the fold hinge area fold an earlier foliation, and suggest significant compression in this area. These crenulations have the same orientation as the large-scale fold. South of the Razor Fold the beds are folded by N-trending fold axes which plunge at *ca.* 50^{o} to the north (subareas I, J, K and L). It is not clear whether the same orientation of folding also affects the tilted Pliocene siltstone (subarea J).

(4) In the southern Washdyke area (subarea M) folding similar in style to that of the Razor Fold is clearly defined by both the stratigraphy and distribution of poles to bedding.

(5) Further south still, box folding with subhorizontal fold plunge was observed in a particularly anisotropic limestone lithology at Waipapa Bay (subarea N).

(6) Finally, although not independently described in this study, a southward plunging syncline has previously been documented from Camp Stream in the southern Washdyke (Roberts 1990).

These observations are further discussed in chapter 6 together with all other structural information analysed in this study.

4.3.4 Cleavages

Cleavages within this region can be divided into three distinct types: (1) a bedding parallel cleavage or fissility developed in limestone lithologies; (2) an axial planar cleavage associated with F2 meso-folding in limestone lithologies; and (3) a fracture cleavage relating to large-scale F2 folding and affecting turbidite beds.

4.3.4.1 Bedding parallel cleavages

There is a well developed, anastomosing cleavage (fig. 4.27a) in both limestone blocks which are a part of a coarse debris flow deposit and also in those which form thrust sheets of the northern part of the Washdyke map sheet. This cleavage is generally subparallel to bedding. Also, there is commonly stylolitization along bedding-parallel seams in the lower, siliceous limestone lithologies. In all other lithologies bedding is defined by a planar fissility. Lamb and Bibby (1989) thought that these bedding-parallel foliations were of tectonic origin and post-lithification. However, evidence collected in this study suggests that they are an early diagenetic, compactional feature and not related to tectonic deformation.

The anastomosing bedding parallel fissility shows no obvious direct relation to the thrusts in the Washdyke area (fig. 4.11). In fact, it is often found adjacent to other lithologies which contain no obvious cleavage, and seems to be no more than finely laminated but anastomosing marl interbeds.

A sample of limestone with this fabric, exposed at Waipapa Bay, was thin-sectioned. Although in hand specimen this limestone appeared to have a strong cleavage, in thin section the fabric appeared as symmetrically disposed muddy flasers. These seams are interpreted as a sedimentary fabric which has been accentuated by pre-lithification compaction.

A number of thin-sections were cut and examined from other limestone lithologies. For instance, a silty, foliated horizon from within the lower chert beds is a moderately immature clay-siltstone with a well-preserved sedimentary fabric, defined by changes in the silt content. All original sedimentary features are well-preserved, though replacive dolomite rhombs are common. In other limestone samples, fine bedding parallel clay seams are common. These do not truncate foraminifera grains and are thus likely to be sedimentary in origin.

In another limestone lithotype, cavities filled with dark, oxide rich micritic material are perpendicular to thin, bedding parallel clay-residue seams. These perpendicular features are enclosed by fissures filled with fibrous calcite and are offset by microstep faulting. Such faulting is a common phenomena of readjustments during early diagenesis (Park and Schot 1968). The intricate association of the extensional fissures and the microfaults implies that the extension is also an early diagenetic feature. The nature of the dark micritic areas suggested trace burrows. Extension is



Fig. 4.27a: Anastomosing marl seams within Type 2 allochthonous limestone from the northern part of the Washdyke map sheet (section 4.3.4.3). A pen is included for scale.

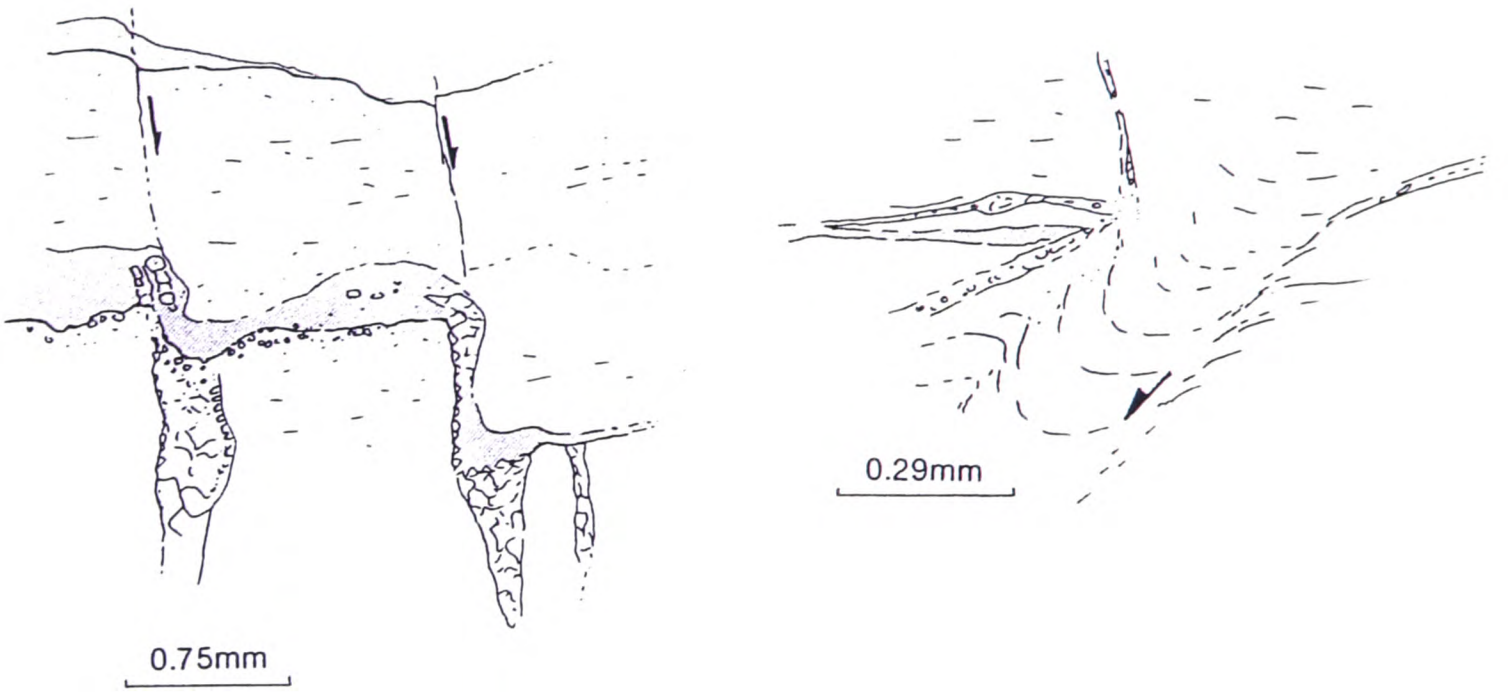


Fig. 4.27b: Pre-lithification normal faulting, bedding-perpendicular extension and bedding-parallel clay seams (shaded areas) in muddy biomicrite. The sample is from Type 1 allochthonous limestone in the northern part of the Kekerengu map sheet (section 4.3.4.1).

perpendicular to the clay residue seams and is interpreted as due to the same deformational event. Thus, there is only evidence for compactional features.

A section was taken from a limestone horizon within Waitakian Marl beds at the mouth of Valhalla Creek. A sketch of this section is shown in fig 4.27b. Microfaulting similar to that already mentioned is observed. This faulting is clearly early diagenetic and there is no evidence for any tectonic deformation.

4.3.4.2 Axial planar cleavages

Non-bedding parallel cleavages were also found. One such cleavage has already been mentioned; a cleavage at a high angle to bedding within the box fold lithology of Waipapa Bay (fig. 4.28a). It was at first uncertain whether this cleavage pre-dated and was subsequently folded by the box folds, or whether it represented an axial planar cleavage associated with the same compressional stresses which produced the box folds. Poles to the cleavage planes around one fold give an identical fold axis to that defined by the poles to fold axial planes from the same location (fig 4.28b). This suggests that the two were probably formed under the same deformational phase and that the cleavage is in all respects an axial planar cleavage. A similar high angle cleavage was observed in the Waitakian Marl beds at the mouth of Deadman Stream.

Axial planar cleavages are also associated with the crenulations in the Razor Fold nose area.

Fracture cleavage

Several examples of fracture cleavage (a non-penetrative axial planar cleavage) were found throughout the region. An example of this is shown in fig. 4.29a. If cleavage is a direct result of strain development during the fold forming process, the overall geometric relationships between orientation and intensity of cleavage are systematically related to the fold form (Ramsay and Huber 1983). The relationship between cleavage and lithological layering in an outcrop can be a useful guide to where that outcrop is within the overall major fold structure. On a normal limb the cleavage is at a higher angle of dip in comparison to the layering, whereas on an overturned limb it is at a lower angle of dip in comparison to the layering. At the fold hinge the cleavage and layering are approximately perpendicular, parallel to the axial surface of the fold. The acute angle between bedding and cleavage on the fold limbs varies not only with position within the major fold, but as a result of cleavage refraction through lithological layers of differing competency (Ramsay and Huber 1983).

The location, bedding, and angle in degrees of the acute angle between bedding and cleavage at each location is summarized in fig 4.29b. All the lithologies possessing the fracture cleavage are turbiditic siltstone and sandstones, making it possible to comment on the corresponding angular relationships of these sites.

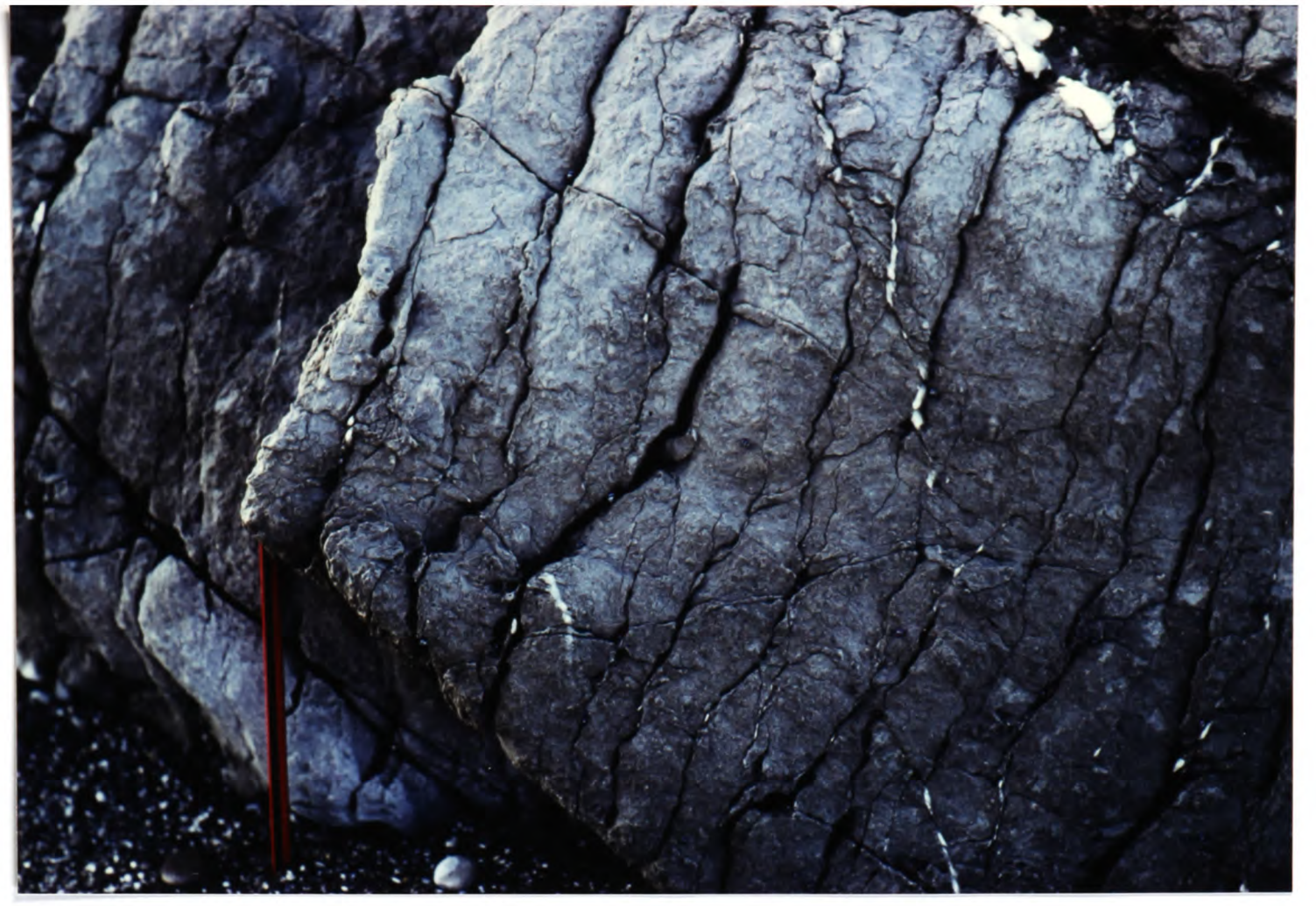


Fig. 4.28a: Well-developed, non-penetrative cleavage at a high-angle to bedding in Amuri Limesone at Waipapa Bay. The cleavage in this picture is intersecting a bedding plane. A pencil is included for scale.

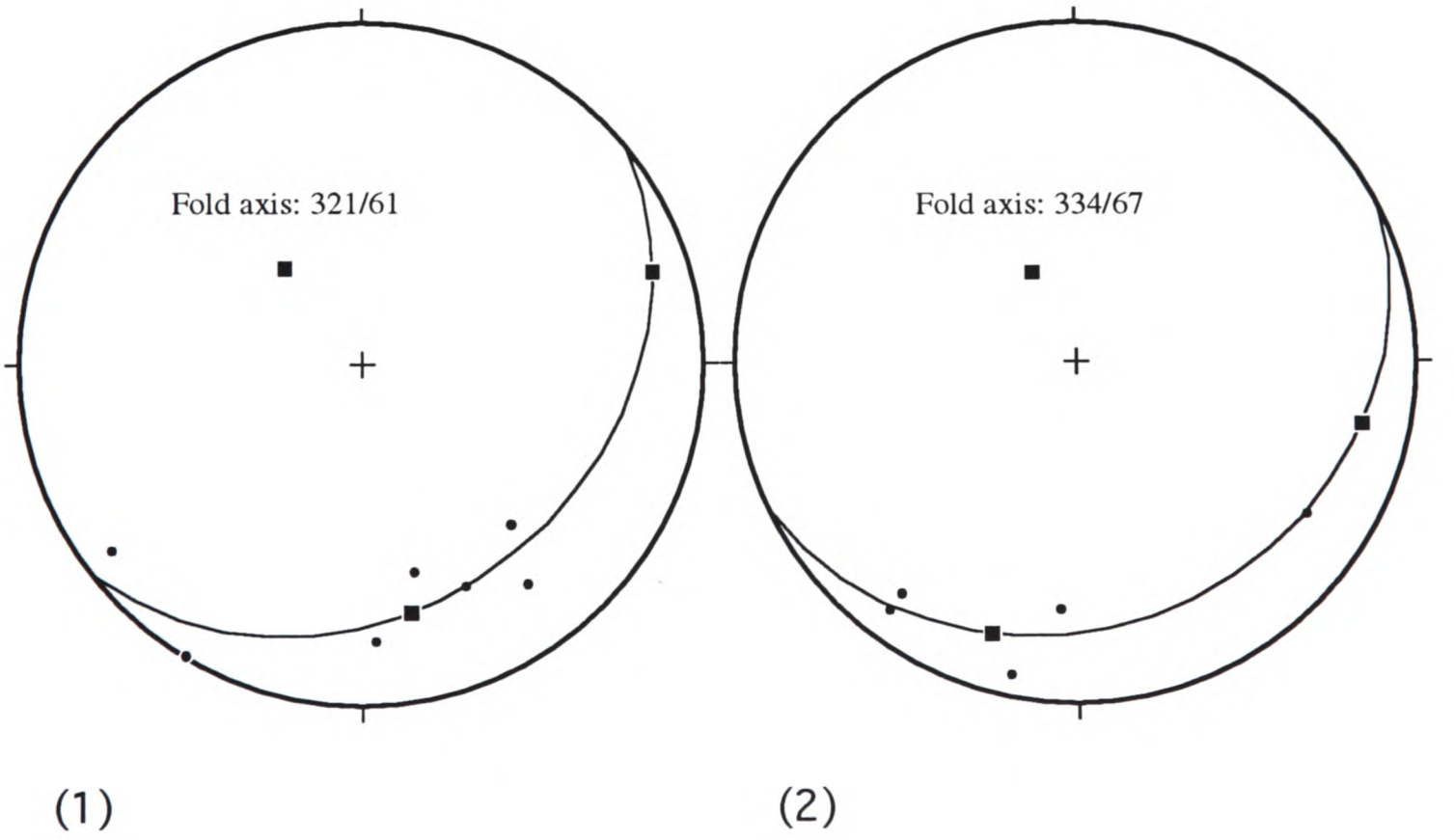


Fig. 4.28b: Equal-area, lower hemisphere stereographic projection showing fold axes determined from (1) poles to fold axial planes, and (2) poles to cleavage planes within an area deformed into box folds.



Fig. 4.29a: Non-penetrative cleavage (fracture cleavage) cutting turbidite beds from the conglomeratic sequence in the southern part of the Kekerengu map sheet (refer to section 4.3.4.3). A hammer is included for scale.

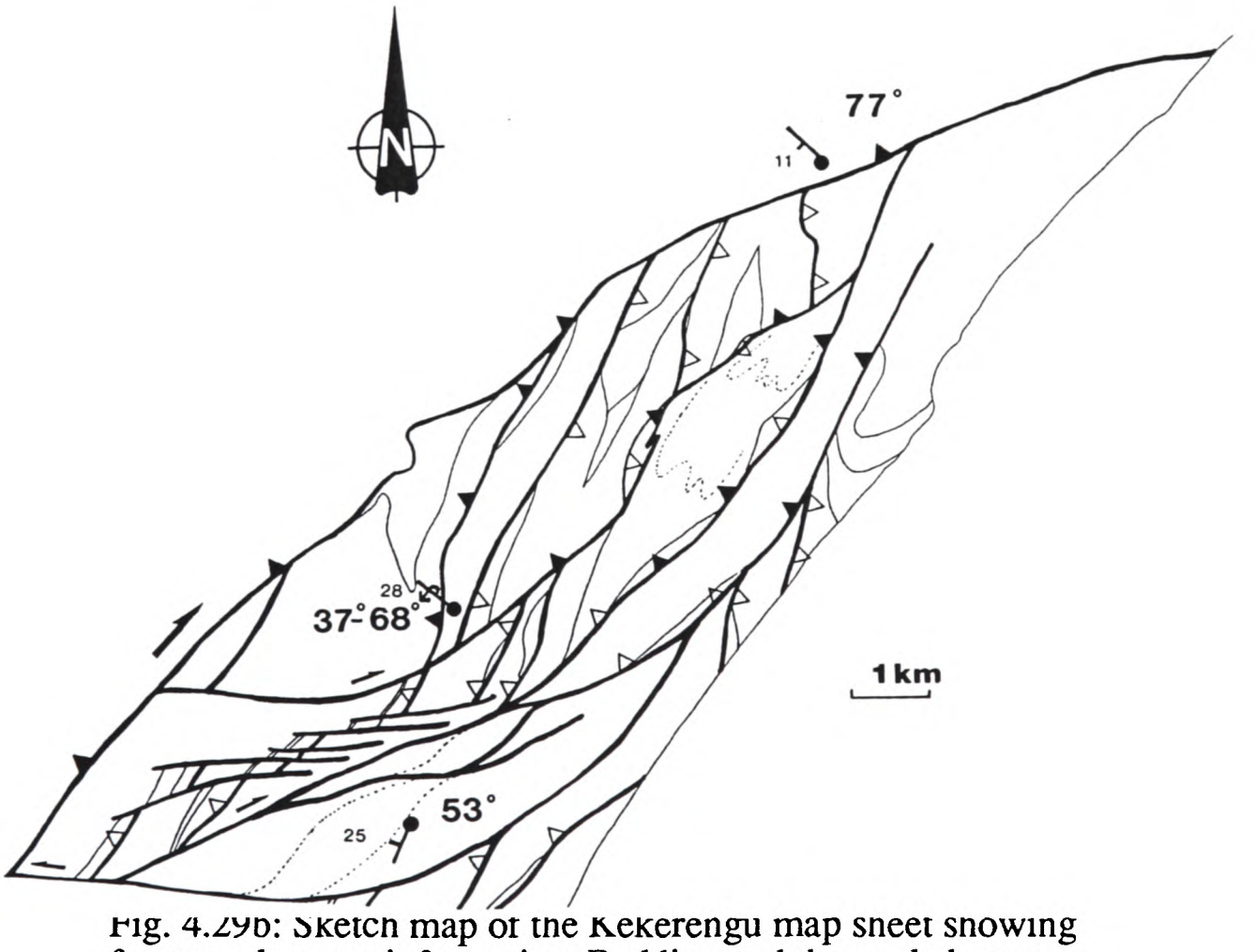


Fig. 4.29b: Sketch map of the Kekerengu map sheet showing fracture cleavage information. Bedding and the angle between bedding and cleavage planes is shown for each of the three locations where fracture cleavage is found (section 4.3.4.3).

The first site is in the north and is the only example of this cleavage found on the upthrown side of the Kekerengu Fault. Here, the acute angle between subhorizontal turbidite beds and the fracture cleavage planes are at a relatively high angle (77^{o}). This angle, being close to perpendicular, suggests that this site is in the hinge area of the hanging wall anticline associated with uplift along the Kekerengu Fault.

West of the Mole Hill, overturned turbidite beds of the Great Marlborough Conglomerate dip gently to the southwest. The cleavage is at 37-68^{o} to the bedding representing cleavage refraction through differently competent layers. The position of this site is on the eastern limb of the anticline associated with the Kekerengu Fault. The generally lower angle to bedding is taken as evidence for its location further down the fold limb compared to the last hinge area site, as is assumed from mapping.

Lastly, many cases of a similar cleavage were found within turbidite beds of the debris flow deposits west of Deadman Hill (example in fig. 4.29a). Their location on the eastern limb of synclinally folded, right-way-up beds agrees with this cleavage evidence. Minor offsets are visible along the cleavage planes.

In all cases the relationship of cleavage to bedding is as expected from the large-scale folding interpretations already made from mapping, thus backing up these interpretations. It is concluded that this cleavage is associated with the young D2 tilting of the Kekerengu-Washdyke region.

4.3.5 Cross Sections

Six cross sections were constructed for the Kekerengu-Washdyke study area. Extrapolations to depths of more than *ca.* 4 km are not made due to the subvertical dip of most strata. The sections are constructed from general mapping of lithological units (including dating of units by foraminifera identification, (chapter 3)), large scale fault descriptions (4.3.2.1) and fold axis data (4.3.3).

Five ENE-trending cross sections (approximately at right angles to the general strike of bedding) and their locations are shown in fig. 4.30. An additional NNE-trending cross section (approximately parallel to the general strike of bedding) shows the changes in fold axes along the length of the Kekerengu-Washdyke study area. This cross section and its location are shown in fig. 4.31.

Interpretation of the variation in structural style and deduction of the overall evolution of the study area is discussed in chapter 5.

KEY

Whanganui Siltstone
(*Opoitian - Nukumaruan*)

Heavers Creek Formation
(*Clifdenian - Waiauan*)

Great Marlborough Conglomerate
(*Altonian - Basal Tongaporutuan*)

Waima Siltstone
(*Otaian - ~M.Lillburnian*)

Autochthonous / Allochthonous Limestone (*M.Haumurian - Waitakian*)

Sandstones and siltstones
(Upper Cretaceous)

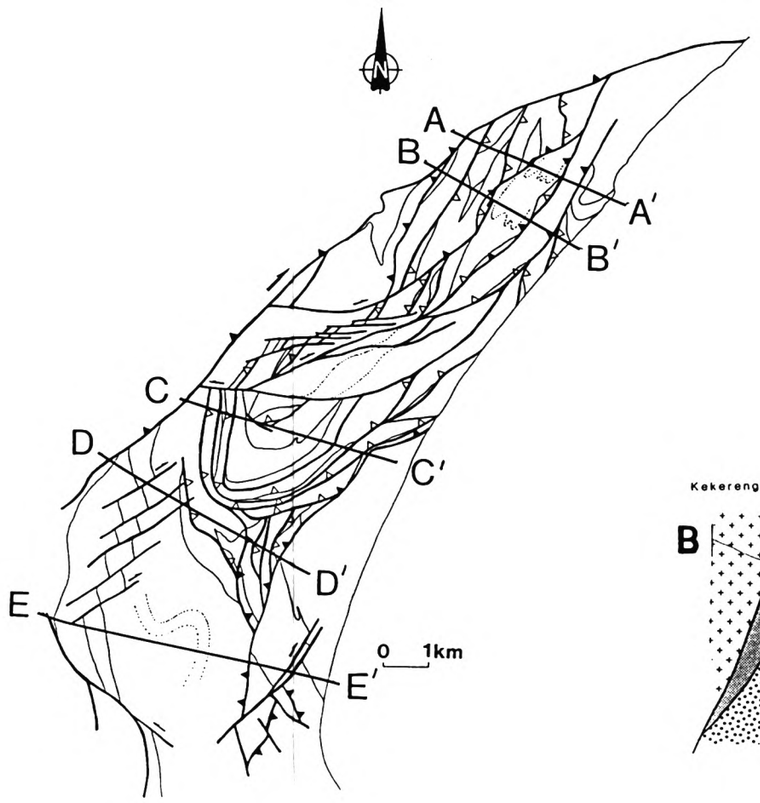
Younging direction

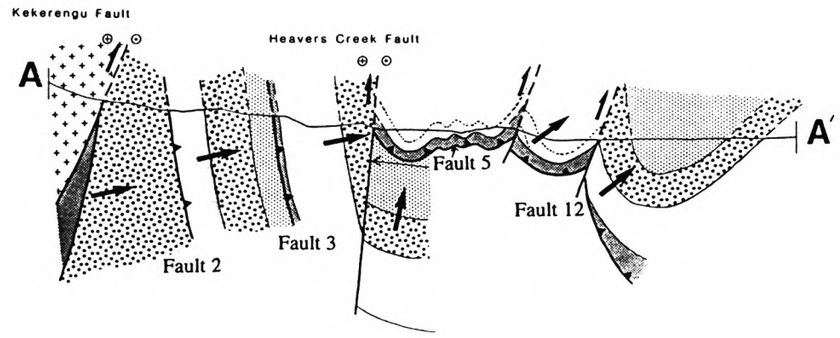
D_e reverse fault

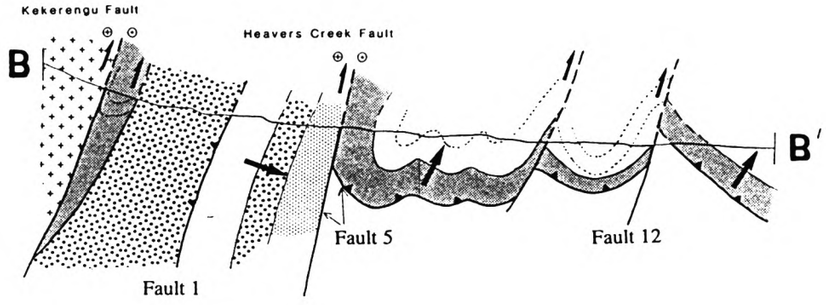
D_l reverse fault

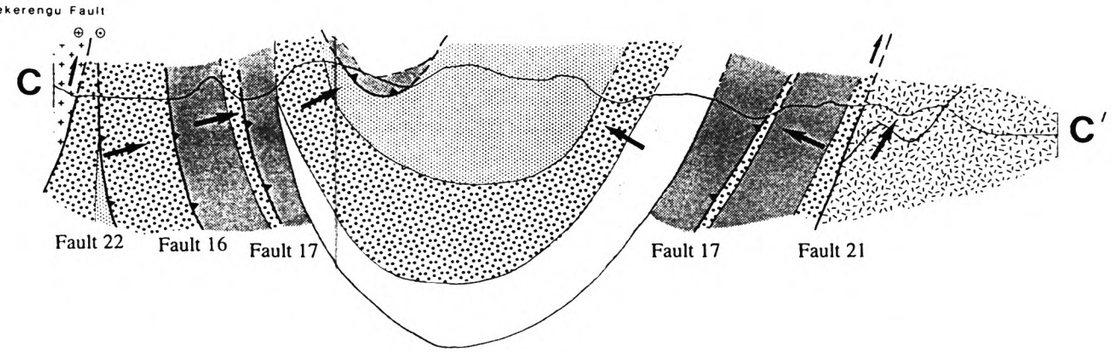
⊕ Motion into paper

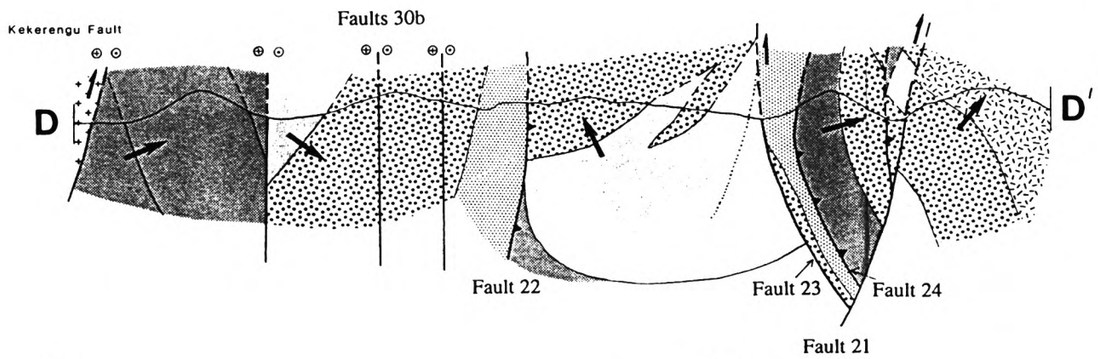
⊙ Motion out of paper











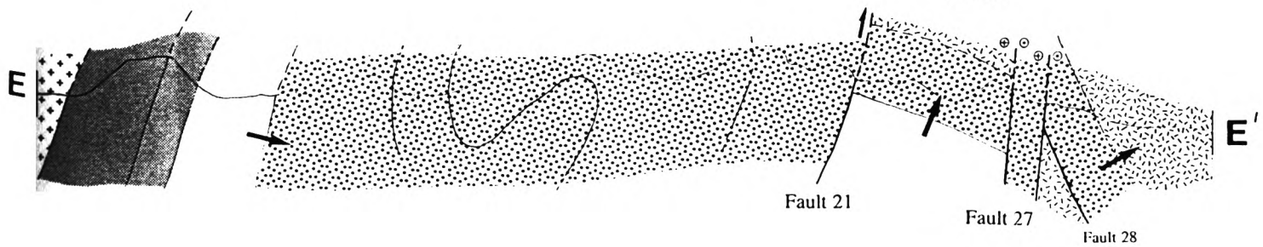


Fig. 4.30: Cross-sections showing assumed subsurface geology for five transects running approximately perpendicular to the Kekerengu Fault. Inset shows position of cross-sections on a sketch map of the Kekerengu-Washdyke study area. Scale *ca.* 1: 40 000.

KEY

Whanganui Siltstone
(*Opoitian - Nukumaruan*)

Heavers Creek Formation
(*Clifdenian - Waiauan*)

Great Marlborough Conglomerate
(*Altonian - Basal Tongaporutuan*)

Waima Siltstone
(*Otaian - ~M.Lillburnian*)

Autochthonous / Allochthonous
Limestone *(M.Haumurian - Waitakian)*

Sandstones and siltstones
(Upper Cretaceous)

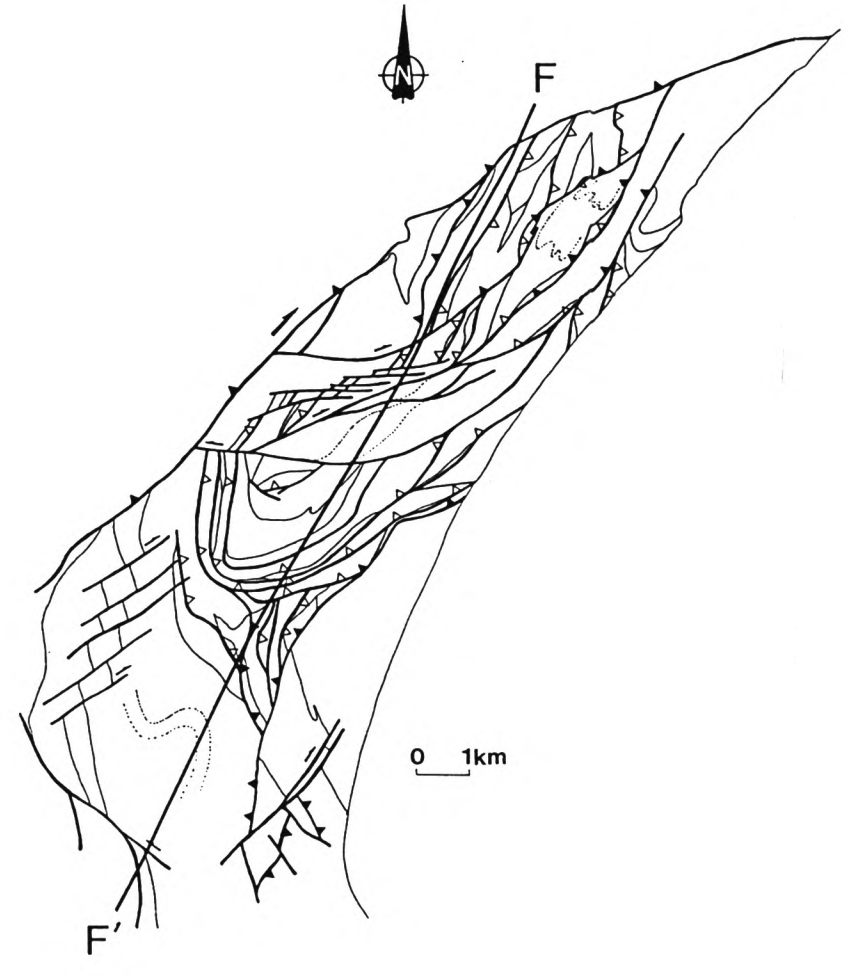
Younging direction

D_e reverse fault

D_I reverse fault

⊕ Motion into paper

⊙ Motion out of paper



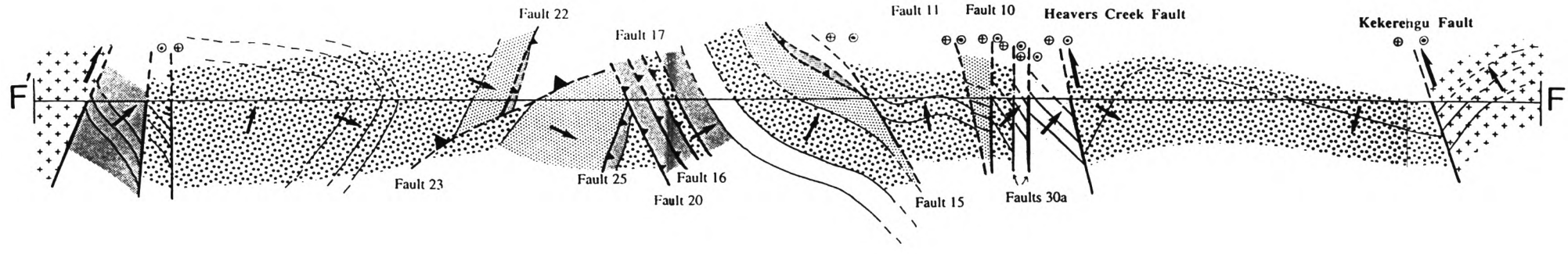


Fig. 4.31: Cross-section showing assumed subsurface geology for a transect running approximately parallel to the Kekerengu Fault. Inset shows position of cross-section on a sketch map of the Kekerengu-Washdyke study area. Scale *ca.* 1: 70 000.

CHAPTER 5

CHAPTER 5: STRUCTURAL SYNTHESIS AND INTERPRETATION

5.1 Introduction

Chapter 4 has presented all the structural data collected from the Benmore and Kekerengu-Washdyke subregions. In both subregions, two phases of deformation are recognized: D_e thrust faulting and folding; and D_l folding, reverse, sinistral and dextral strike-slip faulting. Since at least some of the D_e thrust faults appear to be syn-sedimentary in nature, any synthesis of this earlier phase must refer to descriptions of the associated sedimentation (chapter 2). The timing of each phase in the Kekerengu-Washdyke study area is constrained by the dating of both thrust-repeated and unconformably overlying sediments in the case of D_e, and by the age of sediments tilted and cut by D_l folds and faults. All dating information is listed in chapter 3.

This chapter uses all the above information from chapters 2, 3 and 4 to interpret and synthesize the exact nature, timing and evolution of each phase in the study area. The chapter is divided into three parts: sections 5.2 and 5.3 respectively cover phases D_e and D_l; section 5.4 summarizes the stratigraphic and structural variations between the subregions of Marlborough.

5.2 The Nature and Timing of D_e in the Kekerengu-Washdyke Study Area

5.2.1 The Nature of D_e Thrusting

Within the Kekerengu-Washdyke study area, a total of nine kilometre-scale thrust faults are found involving Amuri Limestone to Heavers Creek Formation Tertiary cover sediments. The thrust-repeated sedimentary pile and overlying Pliocene sediments are then tilted and cut by D_l structures.

Fig 5.1 summarizes the early thrusts observed within the Kekerengu-Washdyke study area in their respective positions prior to later, post-Pliocene deformation. Several different types of thrust are recognized in the study area.

The lithologies of the deformed sedimentary rocks themselves suggests both an abrupt change from biogenic to clastic sedimentation and an increase in sedimentation rate in Marlborough in the *Waitakian*. The clastic sediments consist of flysch and turbidite deposits passing upwards into massive debris flow conglomerates interbedded and

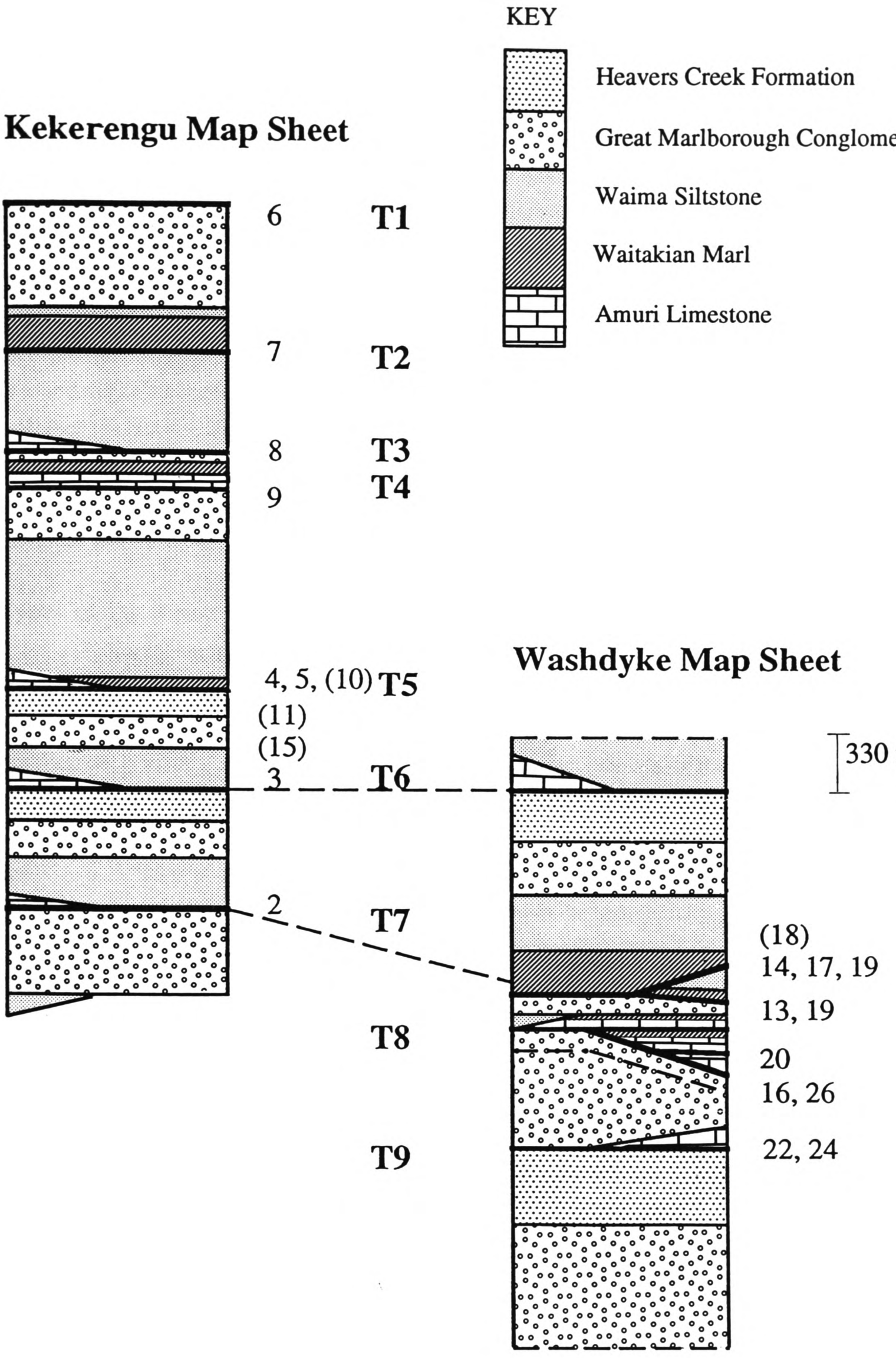


Fig. 5.1: Stratigraphic columns of the pre D_l sedimentary sequence in the Kekerengu-Washdyke study area showing the extent of D_e reverse faulting. The corresponding large scale fault numbers as described in 4.3.2.1 are shown along side each D_e fault. Numbers in brackets represent lithological boundaries used as D_l strike-slip surfaces. All D_e faults are marked by thick black lines and numbered from T1 to T9 from highest to lowest in the sedimentary pile. In comparison lithological boundaries are marked by thinner lines.

overlain by turbiditic siltstones. Clasts include rounded greywacke basement and intrabasinal angular to subrounded Amuri Limestone and siltstones. It is clear that uplift of a land source and the transport of clasts over long distances by rivers was occurring prior to deposition in the Tertiary basin, and that uplift was also occurring within the Tertiary basin itself. Limestone boulders up to several metres in length (cf. fig. 2.7c) are found throughout the conglomerate sequences. These, together with the angularity and large grain size of intrabasinally derived clasts, suggest proximal uplift prior to incorporation into debris flows. In one location within the study area, a limestone breccia is found directly beneath a kilometre-scale thrust transporting limestone on its hanging wall (see (3) below). This indicates that intrabasinal thrusting was occurring within the Tertiary basin. Thus, the close association of intrabasinal uplift, clastic sediments and thrust faulting indicates that basin sedimentation from the *Waitakian* is controlled by both marginal and intra-basinal thrust faulting.

Types of D_e thrust fault

(1) Eocene mudstone (cf. fig. 4.13) to Waitakian Marl sequences are observed along several of the thrust planes. These lithologies are relatively ductile in comparison to more competent limestones of the Amuri Group, making them suitable for thrust decollement horizons. All thrusts with these lithologies along their length are assumed to have initiated at a similar stratigraphic level and to be a result of the same phase of thrusting. This thrusting clearly involves sediments of up to Heavers Creek Formation age (fig. 5.1). Several other thrusts are observed cutting close to the base of the Waima Siltstone unit, at a slightly higher stratigraphic position in the sedimentary pile than the previously mentioned thrusts (fig. 5.1). These are assumed to be part of the same thrust phase.

(2) One of the thrusts (Fault 22; fig. 5.1, T9) has older, more competent Amuri Limestone occurring as allochthonous slivers along its length. The youngest sediments involved in this thrusting are also from the Heavers Creek Formation. The limestone slivers may either have been eroded from intrabasinal limestone thrust sheets and were subsequently overridden, or may represent decollement limestone as in (1).

(3) One of the large scale thrust faults (Fault 16; fig. 5.1, T8) has a kilometre-scale Amuri Limestone thrust sheet on its hanging wall with limestone breccia (cf. fig. 2.7b) deposited onto marine debris flow conglomerates directly beneath the fault. The breccia has a siltstone matrix, indicating that it was deposited in a marine environment, and contains no evidence of shear, suggesting a very high level of thrusting. This fact is backed-up by vitrinite reflectance analyses of coals presented in the Appendix to chapter 2 which suggest depths of less than *ca.* 1 km. This must be a synsedimentary fault uplifting older limestone above younger thrust-derived sediments, producing fault breccias at the base of the thrust which are subsequently overridden by the thrust sheet itself. An

overlying thrust fault (Fault 17) has transported material including Heavers Creek formation siltstones (fig. 5.2).

The exact nature and timing of all these thrusts is problematical because it is difficult to determine whether the thrusts formed after deposition of the youngest sediments involved in this thrusting (Heavers Creek Formation), or whether sediments continued to be deposited whilst thrusting continued (moving basins carried piggyback on active thrust faults, as described by Ori and Friend 1984). The latter is likely given the relatively short time span of *ca.* 7 Ma for D_e deformation if all this deformation was post Heavers Creek Formation (refer to 5.2.2.).

All the features discussed in this section are summarized in the cartoon sketches of fig. 5.2.

5.2.2 The Timing of D_e Thrusting

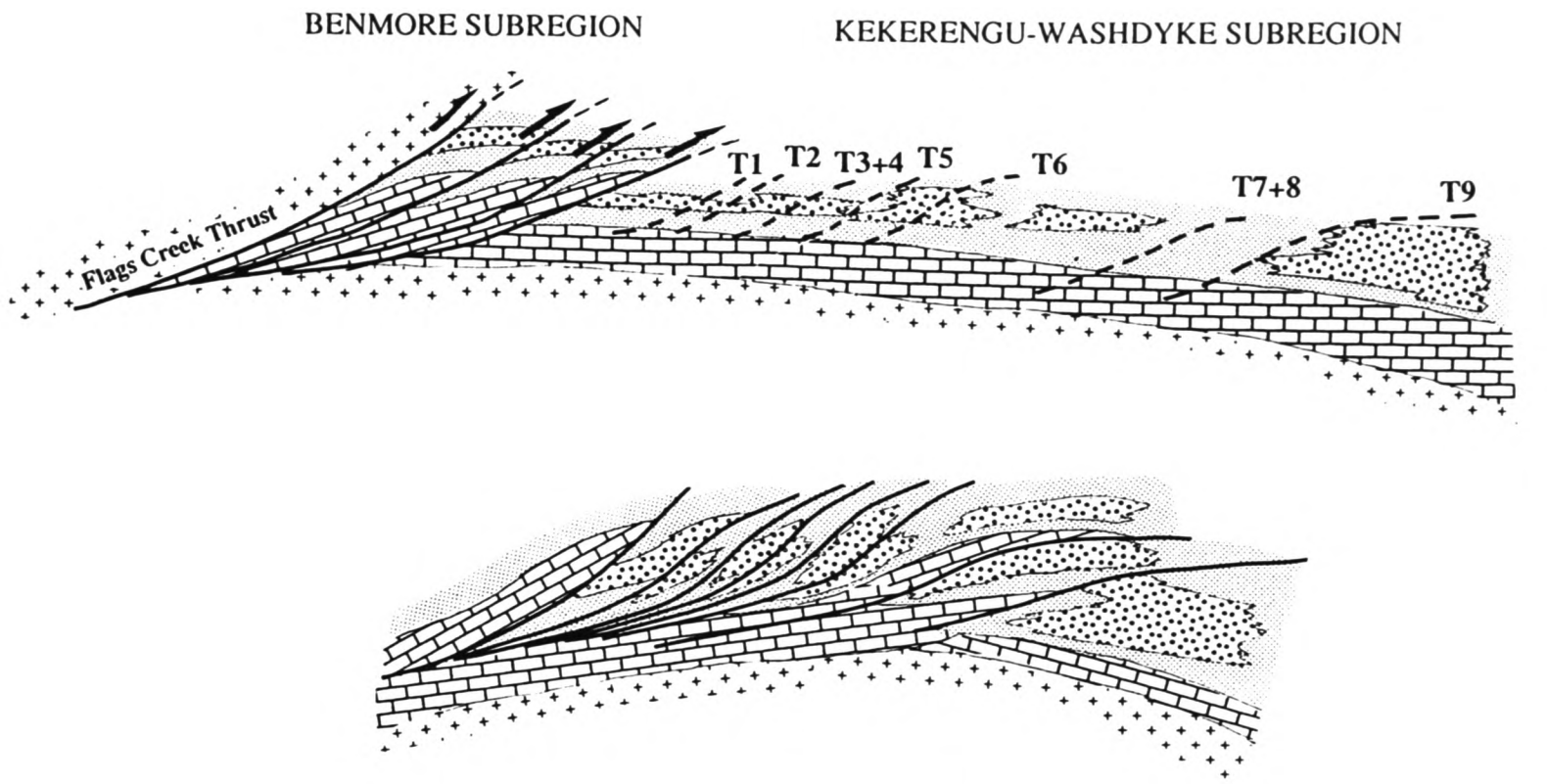
The thrust-derived sediments which are themselves cut by D_e thrusts mark the onset of D_e deformation, giving a *Waitakian* (*ca.* 24 Ma) age for the beginning of this phase. D_e thrusting does not appear to cut any of the younger Pliocene sediments in the study area, suggesting that thrusting had ceased by this time. More evidence for the upper age of this thrusting comes from dating the upper conglomerate to siltstone contact from the eastern part of the Washdyke map sheet (2.2.4). A *ca.* 5 Ma unconformable gap in stratigraphy separates *basal Tongaporutuan* pebbly siltstone (assigned to the Great Marlborough Conglomerate) from overlying Pliocene (*Waipipian* to *Nukumarian*) siltstones. This unconformity suggests an upper age limit for D_e thrusting in the study area, suggesting that D_e thrusting had ceased by *Waipipian* (*ca.* 3 Ma) times, but was active in the *Tongaporutuan* (*ca.* 10 Ma). This is an important observation because an unconformity east of the London Hills Fault in the Cape Campbell-Ward subregion (fig. 2.11) suggests that thrusting had ceased here by the *Tongaporutuan*. The unconformity identified in the Kekerengu-Washdyke study area suggests that although thrusting had ceased in the Cape Campbell-Ward subregion part of the basin, it continued elsewhere in the basin through to *Waipipian* time .

The overlying Pliocene siltstones reflect a return to flysch sedimentation after the cessation of this early thrusting episode (D_e).

5.2.3. Conclusion

A period of pre-Pliocene thrust faulting, beginning in the *Waitakian* and continuing through to the *Waipipian*, is recognized in the study area. Thrust-derived sediments are themselves subjected to intrabasinal uplift and erosion by thrust faults originating in Upper Amuri Limestone (and up to the base of the Waima Siltstone)

(a)



(b)

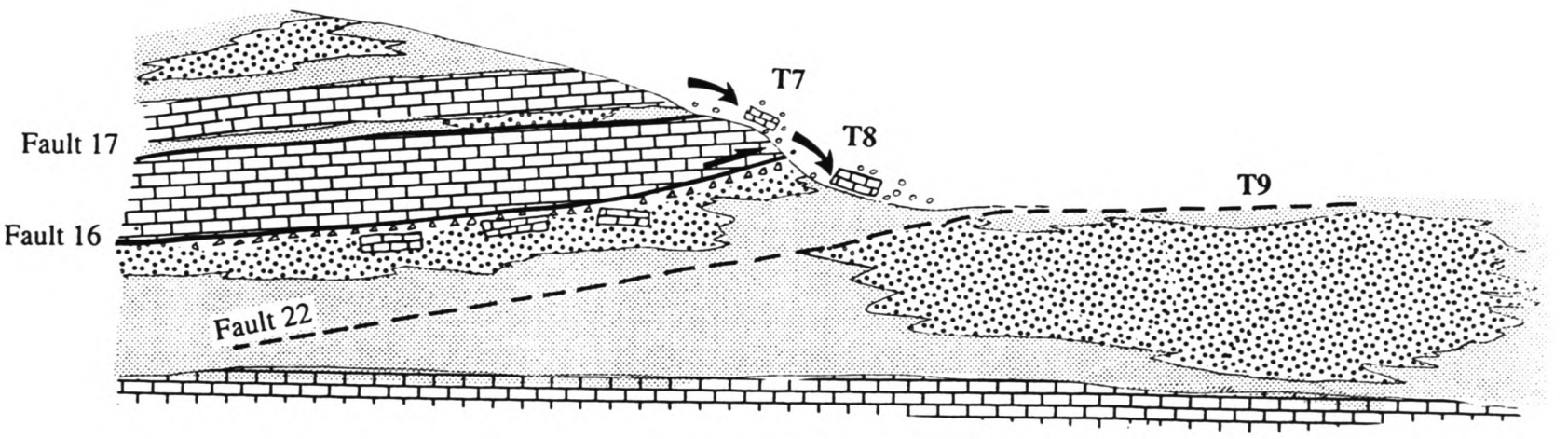


Fig. 5.2: Cartoon diagram (not to scale) of D_e thrusting in the Benmore and Kekerengu-Washdyke subregions. (a) D_e thrusting in both subregions with the positions of kilometre scale thrusts in the Kekerengu-Washdyke study area marked by dashed lines and labelled according to fig. 5.1. (b) T8 Amuri Limestone thrust sheet producing and overriding limestone fault breccia and earlier thrust-derived debris flow deposits. T7 (carried piggyback on T8) and the future position of T9 are also shown. D_e thrusting began in the *Waitakian* and continued through to the *Kapitean*. However, much of the thrusting observed within the study area is believed to have occurred in the Taranaki Series (*Tongaporutuan* to *Kapitean*). For descriptions and explanation refer to section 5.2.

horizons. In one case, the thrusts cut deeper into the Amuri Limestone producing large kilometre-scale thrust sheets of Amuri Limestone which override earlier thrust-derived debris-flow conglomerates, indicating the progressive nature of this thrusting. All these features have been summarized in fig. 5.2.

5.3 The Nature, Timing and Evolution of D_1 Structures in the Kekerengu-Washdyke Study Area

The thrust-repeated Tertiary cover sediments from the study area are tilted with beds dipping steeply to overturned. This tilting affects lithologies of up to Pliocene age and therefore at least some of this tilting occurred post-Pliocene. Tilting within the study area is controlled by several fold axes (4.3.3) and cut by numerous faults from large-scale mappable fault contacts (4.3.2.1) to mesoscopic faulting (4.3.2.2). The tilted beds have an associated fracture cleavage (4.3.4.3). The evidence for this younger phase of deformation is summarized below.

5.3.1 Evidence for D_1 Structures

5.3.1.1 Evidence for D_1 faulted contacts (refer to 4.3.2.1)

The Kekerengu-Washdyke Study Area

The Kekerengu and Heavers Creek Faults both displace Holocene terraces (Lamb and Bibby 1989) and are therefore active. Fault 1 is interpreted as a reverse fault linked to the Kekerengu fault and thus is also interpreted as a late and possibly active structure. Fault 12 is interpreted as a post-Pliocene fault due to its similar orientation and form to the Heavers Creek Fault. Faults 10 and 11 and the east-west trending strike-slip faults in the southern part of the Kekerengu map sheet (Faults 30a) cut pre-tilt thrust faults and lie within an area immediately to the south of the Heavers Creek Fault and it seems that this area is part of a zone of young dextral strike-slip faulting. Fault 15 appears to have acted as the southern bounding dextral shear fault in the southern part of the Kekerengu map sheet zone of dextral strike-slip.

In the Washdyke area, Fault 21 clearly cuts Pliocene siltstones. Linked to this fault is Fault 23 which may be a back-thrust associated with Fault 21. Therefore this too is probably a post-Pliocene fault. Faults 27 and 28 clearly cut Pliocene siltstones and are also post-Pliocene. Lastly, Faults 30b are interpreted as post-Pliocene because of their nature and position, relaying dextral strike-slip from the Kekerengu-Fault, which is transferred as folding between the Kekerengu and Hope Faults (see fig. 5.7, episode 4 and Washdyke map sheet).

5.3.1.2 Evidence for D_1 folding (refer to 4.3.3)

The Kekerengu-Washdyke Study Area

The Glencoe Limestone unit is folded by a steep fold axis. It is suggested that this folding may represent buckle folding of this tilted limestone succession due to compression associated with the vertical slip component on the Kekerengu Fault. Since tilting and displacement on the Kekerengu Fault are known to be young, post-Pliocene structures, so too then is this folding. The only other example of mesoscopic folding west of the Heavers Creek fault showed eastward vergence. This vergence is also consistent with the uplift and tilting associated with movement on the post-Pliocene Kekerengu Fault (see section 4.3.5, cross sections AA' and BB').

A clockwise rotation of the trend of the fold axes in the region between the Heavers Creek and Chaffey Faults (section 4.3.3, subarea C) can be seen in beds close to the Heavers Creek Fault. This rotation is interpreted as a result of dextral shear along the Heavers Creek Fault. If the folds are rotated by this fault, they must predate the last movements of this fault. The cross-sections AA' and BB' (section 4.3.5) clearly show how the folding of this siltstone is a result of its position in the centre of the regional syncline associated with uplift on the Kekerengu Fault. Since this uplift is post-Pliocene, so too is this folding. The cross-sections also show the Homai Fold in the eastern part of the Kekerengu map sheet as a syncline associated with uplift on the young reverse fault (Fault 12) and therefore related to post-Pliocene uplift.

In the southern part of the Kekerengu map sheet beds are folded, forming a type of large scale c-s fabric (section 4.3.3, subarea G) between the three post-Pliocene dextral shear faults of this area (refer to fig. 4.10a). It is assumed that these faults have a similar origin to the post-Pliocene Heavers Creek Fault to the north of them. The apparent c-s fabric substantiates this assumption.

By studying all the large scale faults and folded beds in the Washdyke area, it is possible to deduce the timing of tilting and faulting in this area. The Razor Fold syncline (section 4.3.3, subarea H) seems to be related to movement on a post-Pliocene reverse fault (Fault 21, fig. 5.3b). Whether this syncline formed as a result of the thrusting on Fault 21 or whether the thrusting on Fault 21 occurred late in the syncline formation is unclear.

The distribution of poles to bedding on a stereogram from beds to the south of the Razor Fold (section 4.3.3, subarea I) suggests folding about a N-plunging fold axis, but it is not possible to identify a single fold trace in the field. Thus, folding here may be on a small scale (tens to hundreds of metres). Pliocene siltstone beds in the eastern part of the Washdyke map sheet are folded (section 4.3.3, subarea J). These folds have similar fold axes to the small scale folds south of the Razor Fold, suggesting that these too are of post-Pliocene age. Cross-sections CC' and DD' (section 4.3.5) show how the folding of Pliocene beds appears to be related to uplift along Fault 21, the reverse fault which

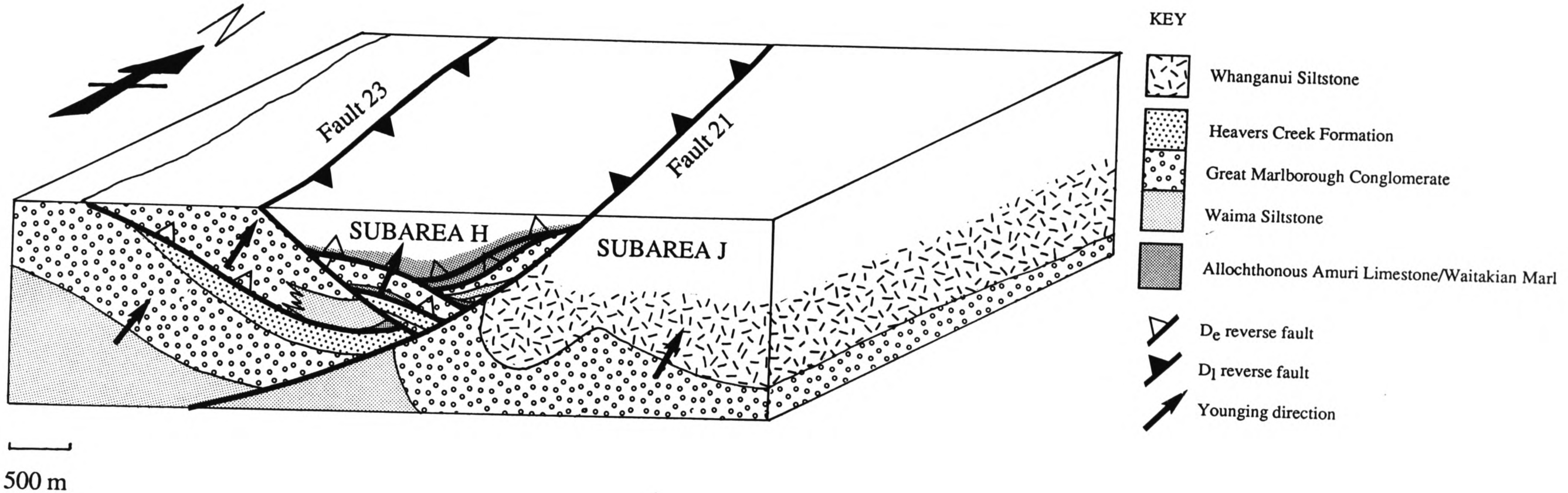


Fig. 5.3: Schematic block diagram showing formation of the Razor Fold Syncline as a pop-up structure between D_{I1} reverse faults, Fault 21 and Fault 23. Refolding of this earliest episode of folding and reverse faulting (D_{I2}) resulted in the tilting of this structure to the north. Refer to sections 5.3.1 and 5.3.2.

bounds this unit to the west (fig. 5.3b). The conglomerate in the southern part of the Washdyke map sheet is folded by the same fold axis as that producing the Razor Fold (section 4.3.3, subarea M). This similarity was again taken as indicative of the post-Pliocene timing of this folding.

Waipapa Bay

The timing of box folding in the Waipapa Bay limestone (4.3.3, fig. 4.26) could not be ascertained by simple field relations. In this case the only line of evidence comes from looking at the regional geology of this area (fig. 5.4). The box folds indicate an in situ shortening direction of 200/28. The Waipapa Bay limestone is a part of a fold related to reverse faulting along the Jordan Thrust (Van Dissen and Yeats 1991).This thrust takes up some of the late Pleistocene to Holocene slip on the Hope Fault further south. The Puhi-Puhi Syncline is affected by two phases of folding. McCone (1985) describes NNE trending fold axial planes with axial planar cleavage and later box folds (with E-W, steep axial planes) also with axial planar cleavage and perpendicular to the first fold axial planes. The compression indicated by the box folds at Waipapa Bay (s_1: NNE) is identical to this second phase of deformation in the Puhi-Puhi as described by McCone (1985). Since both are a part of the same folded structure it is assumed that this folding is caused by the same event. The box folding is therefore a very young, late Pleistocene to Holocene feature. The same two fold phase phenomenon has been documented at Kaikoura (Campbell, pers comm). Campbell recognizes two fold phases: the first with NE-trending and the second with NW-trending axial planes which intersect the first phase folds to produce a basin and dome interference pattern (second fold axis: 000/55).

5.3.2 Reconstructing the sequence of D_1 events

The identification of D_1 structures in the study area reveals that the thrust repeated cover sediments east of the dextral transpressive Kekerengu Fault are deformed by tilting and reverse and strike-slip faults. Also, variations in the structural style of D_1 are observed. Variations occur in the trend and plunge of fold axes, in fold scale and in the location of young dextral and reverse faulting.

In this section the general D_1 post-Pliocene structural evolution, based on field relationships of these structures, is discussed.

5.3.2.1 Changes in fold axes across the study area

Variations exist in the plunge and trend of fold axes (fig. 4.23). There are several possible explanations for this.

(1) The existence of a later fold phase which refolds an earlier fold phase, as has been observed south of the field area at Kaikoura, in the Puhi-Puhi Syncline and at Waipapa Bay (McCone 1985; Campbell; this study).

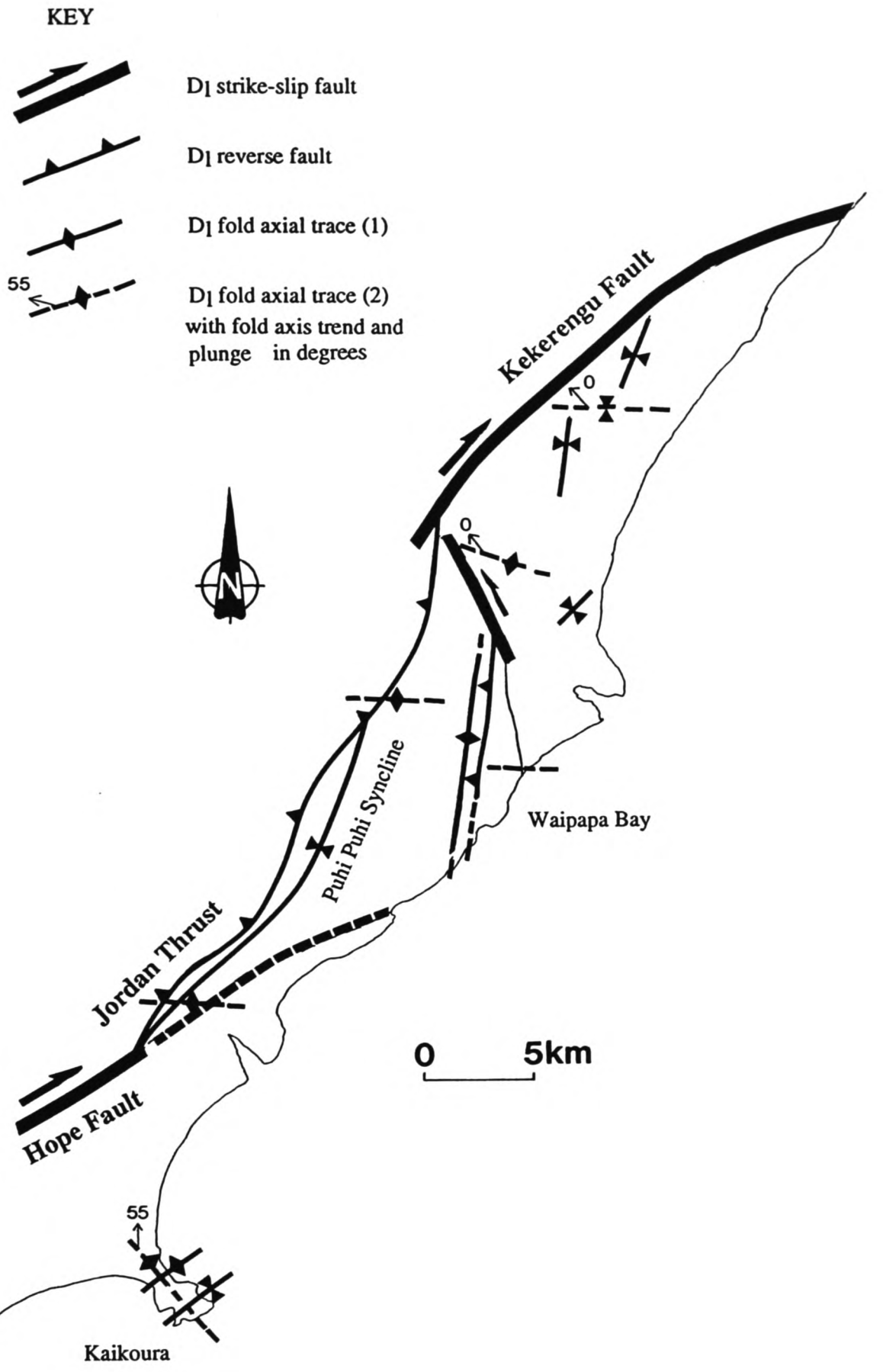


Fig. 5.4: Map of the area between the Kekerengu and Hope Faults showing D_1 faults and first and second phase D_1 fold axial traces. For description refer to section 5.3.1.

(2) Rotations associated with movement on young fault planes in the study area.

(3) The plunge variations may have arisen as the folds die out along strike. However this last cause could not explain the observed variations in fold axis trend.

(4) The pre D_1 thrust geometry might be responsible with changes in the trend and dip of thrusts caused by features such as lateral ramping. It is difficult to test this possibility within the study area due to the intensity of the overprinting D_1 deformation.

None of these possibilities can be ruled out completely and may contribute to the overall variations. However, the following evidence suggests that the first possibility is probably the main reason.

5.3.2.2 Refolding of fold axes

(1) The fold axes from the study area were plotted as lineations on an equal area lower hemisphere stereographic projection (fig. 5.5). Excluded are: (i) fold axes forming part of large-scale c-s type fabrics which are related to late dextral faulting; (ii) fold axes close to the Heavers Creek Fault which may have been affected by late dextral shear; and (iii) mesoscopic folds with highly variable fold axes. In the simplest case, if a set of early fold axes had been subjected to a second phase of folding, then the early fold axes might be expected to fall on a small circle, when plotted on a stereogram, about a pole which is the fold axis of the second phase folding. The fold axes do in fact plot on a small circle and therefore indicate a second phase of folding about a NW-trending fold axis of *ca.* 321/00.

At Waipapa Bay, box folds have an axial planar cleavage in the highly anisotropic limestone (see fig. 4.28a). N to NE-trending thrust faults are also found within the alternating competent-incompetent bedded lithologies which displace the cleavage. These two structures appear to represent accommodation under the same compressive stresses, accommodating along strike shortening. It is however impossible to tell from this information alone whether these structures formed pre- or post-tilting. The evidence for this comes from the gentle refolding of the Puhi-Puhi Syncline (manifest mainly as box folds (McCone 1985)). The shortening direction from this second phase of folding is the same as that obtained from the structures at Waipapa Bay, suggesting that the box folding and thrusts were infact imposed onto already tilted layers. The second fold axis deduced from fold axis data in the study area also gave a similar direction of compression. Therefore it is assumed that there are indeed two phases of folding affecting the study area and the area to the south of the study area as far south as Kaikoura. The first phase is assumed to have a NNE-trending fold axis with an approximate zero plunge (taken from the orientation of the Puhi-Puhi and Waipapa Bay regional trends, and also from the intersection of the small circle of rotated fold axes on a stereoplot with the horizontal, which trends *ca.* NNE).

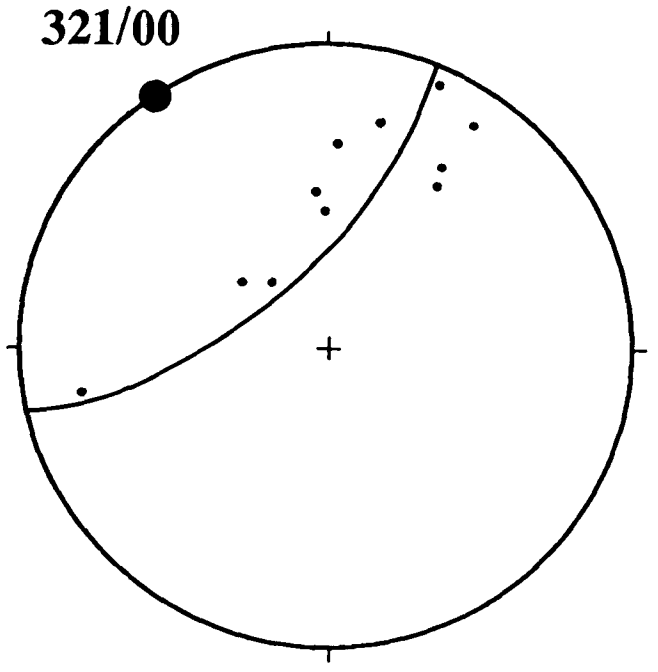


Fig. 5.5: Equal area lower hemisphere stereographic projection of fold axes from the Kekerengu-Washdyke study area. The data fall on a small circle about a NW-trending horizontal pole of rotation (321/00). This suggests refolding of an earlier fold phase about a secondary fold axis of *ca.* 321/00. For a description and interpretation of this data refer to section 5.3.2.2.

5.3.2.3 Conclusion

It is clear that refolding of an earlier NNE-trending folding in the area between the Hope and Kekerengu Faults about a NW-trending fold axis is indeed a plausible solution to explain the pattern of folding within the study area. In order to check this further, a simple plasticine model was made of the two phase deformation. The resulting shape is shown in fig 5.6. This model reproduces all the fold axis trend and plunge variations throughout the study area and explains a number of other observed phenomena. Foremost, was the realization that the resulting fold form would cause the pinching out or disappearance of certain units such as Fault 15 in map view down-plunge to the north (this plane could have easily acted as a late dextral shear fault plane, as was suggested in 4.3.2.1b). The model also gives the approximate position of the second phase fold axial traces. The sinistral offset of the Waipapa Bay limestone from the conformable limestone of the western part of the Washdyke map sheet lies along a second phase fold hinge line (there is a sharp change in the trend of bedding across this area). Thinning and the left lateral displacement of this limestone unit suggests the formation of a sinistral strike-slip fault in this hinge area with associated tectonic thinning of the limestone sequence.

5.3.2.4 The overall sequence of events during D_1

It is now possible to incorporate the above two phase fold model of D_1 deformation with the rest of the post-Pliocene structures from the study area to determine the overall sequence of events during D_1. The order of these events is summarized in table 5.1 along with the evidence used to deduce this order. Where it is impossible to obtain a relative timing between events these are put under the same number. Such structures may have developed synchronously. The sequence is shown graphically in fig. 5.7.

Two phases of folding are recognized which are themselves cut by all the other structural elements. The first phase of folding (referred to as D_{11}) is about a *ca.* NNE-trending fold axis and is associated with syn-tilt reverse faulting in the Washdyke map sheet (Faults 21 and 23). The second phase of folding (referred to as D_{12}) refolds the first phase. The earliest event postdating the second phase of folding appears to be over-steepening of the western limb of the Razor Fold and sinistral displacement along the western section of Fault 15 in the northern part of the Washdyke map sheet, and NE-trending dextral faulting in the western part of the Washdyke map sheet (referred to as D_{13}).

The next episode (referred to as D_{14}) constitutes dextral strike-slip faulting in the southern part of the Kekerengu map sheet (continuing into the northern part of the Kekerengu map sheet along segments of the Heavers Creek Fault). This faulting causes the rotation of bedding between fault planes and large amounts of actual discrete displacement on both limbs of the regional syncline. The relative timing of the individual dextral faults is not known although the Heavers Creek Fault offsets a 100 ka marine

Fold axis plunging at ca. 70° to the NW

(NORTHERN PART OF WASHDYKE MAP SHEET: Razor Fold)

Fold axis plunging gently to the south

(SOUTHERN PART OF WASHDYKE MAP SHEET: Camp Stream Syncline)

Fold axis plunging at *ca.* 30° to the north

(NORTHERN PART OF KEKERENGU MAP SHEET)

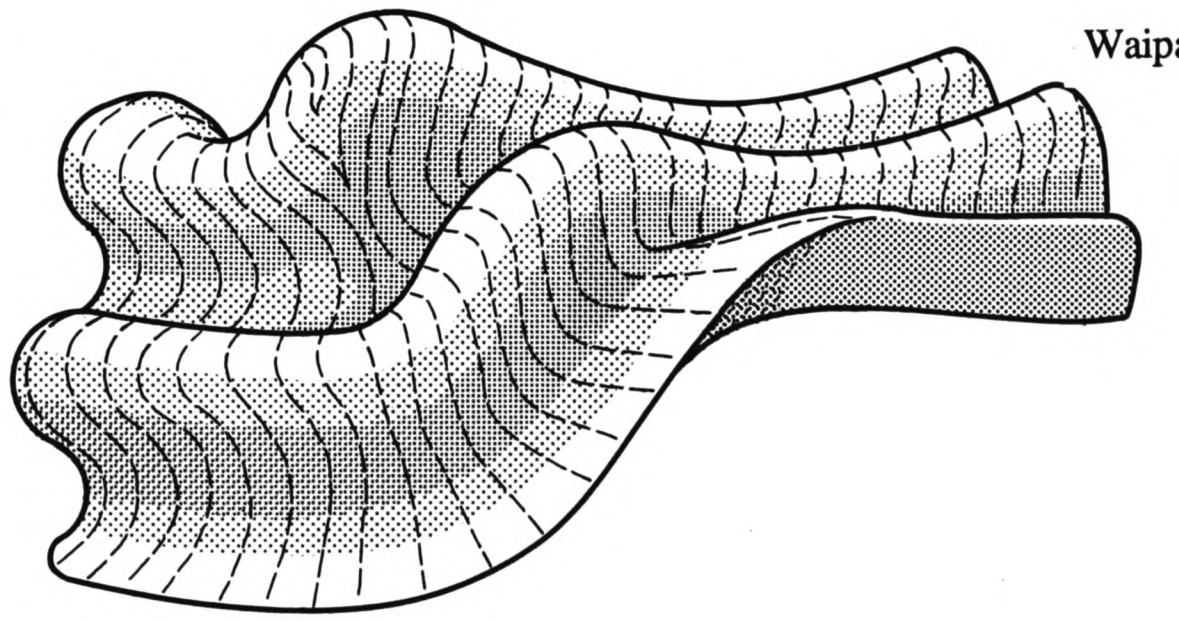
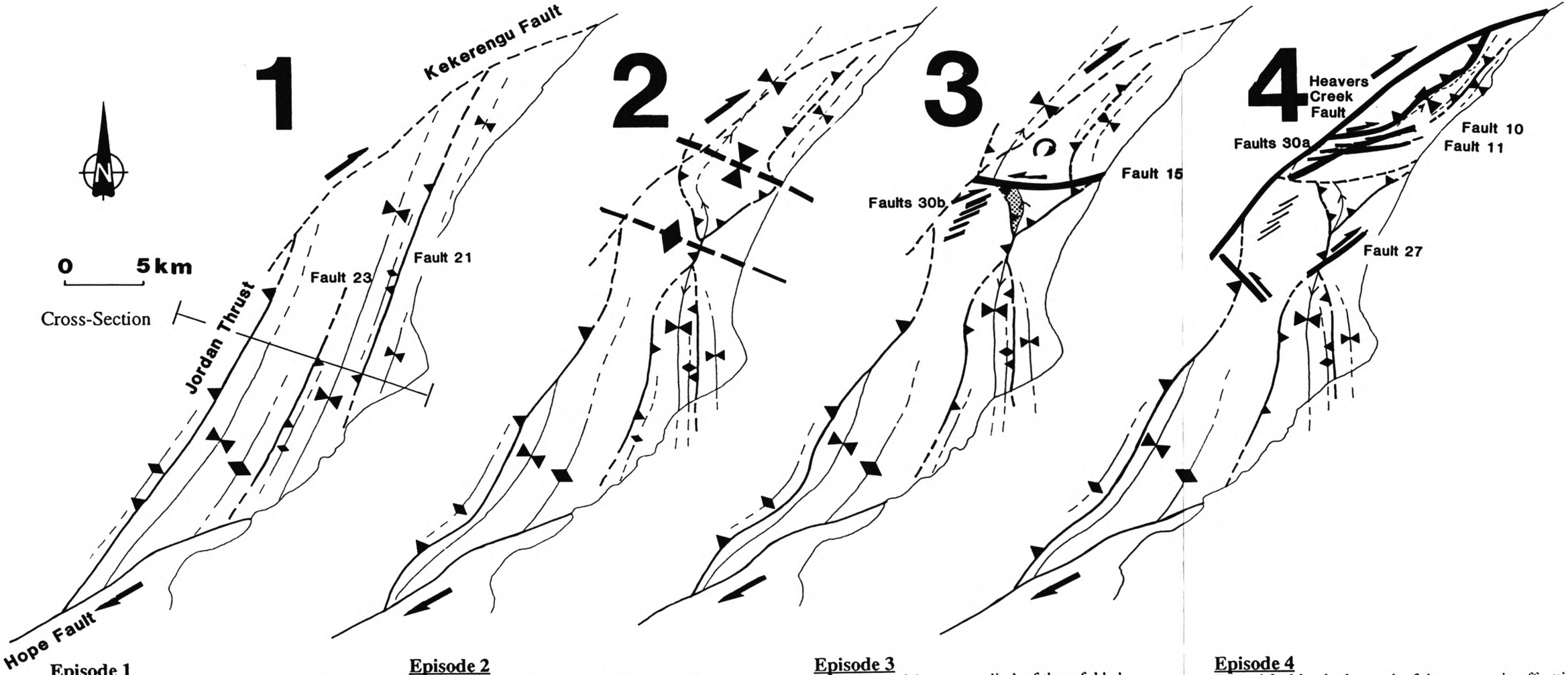


Fig. 5.6: Sketch of a plasticine model subjected to two phases of folding with NNE and NW-trending fold axes. The resulting fold form explains the variations in fold characteristics throughout the Kekerengu-Washdyke study area and as far south as the Hope Fault. For explanation refer to section 5.3.2.



Episode 1
NNE-trending seaward directed thrusts (and back-thrust) and folds with horizontal fold axes.

Episode 2
Refolding of NNE-trending fold axes and thrusts about a NW-trending horizontal fold axis, producing variations in the trend and plunge of Episode 1 structures.

Episode 3
Steepening of the western limb of the refolded syncline in the centre of the area (stippled). This is apparently synchronous with dextral faulting to the west (Faults 30b) and offset of the syncline axis by sinistral displacement along an E-trending fault plane (Fault 15). This sinistral faulting probably accommodates bending between the areas to either side of it, with a clockwise rotation of the area to the north.

Episode 4
Dextral faulting in the north of the area again offsetting the syncline axis with reverse faulting linking segments of the Heavers Creek Fault. The reverse fault and syncline in the NE may or may not be the offset refolded Episode 1 reverse fault and syncline. Compression associated with this phase produces folding between the two reverse faults in the north. Dextral and sinistral faulting in the south of the area is also recorded.

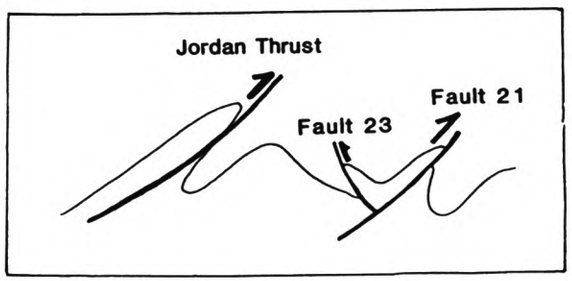


Fig. 5.3. A sequence of sketches of the area between the Kekerengu and Hope Faults showing the progressive evolution of D_1 faulting and folding within this area. D_1 is divided into four main structural episodes which are labelled from oldest (1) to youngest (4). New structures at each stage are identified by bold lines. All faults are labelled in the episode in which they appear (4.3.2.1). The inset shows a cartoon cross-section of Episode 1 folding and reverse faulting. Refer to section 5.3.2 for the reasoning behind these interpretations.

ELEMENTS OF DEFORMATION	EVIDENCE FOR TIMING
D_e (*Waitakian* to *Opoitian*)	
(I). Thrusting.	Does not cut Pliocene beds Folded and offset by all D_l post-Pliocene structures.
D_l (*Waipipian/Nukumaruan* to present)	
Kekerengu Fault active.	Dextral shear results in (I) folding.
(I). Folding with NNE-trending fold axial plane (with associated axial planar cleavage in Kekerengu). **Reverse, thrust and back thrust faulting.**	Fold and offset early thrusts, including Pliocene beds. Cut and folded by elements (II) to (V).
(II). Folding about a fold axis of 321/00.	Refolds first phase folding resulting in former fold axis trend and plunge variations throughout the study area. Cut by elements (III) to (V).
(III). Steepening of Razor Fold western limb with associated sinistral displacement and NE-trending dextral faulting in the western part of the Washdyke map sheet.	Dextral faulting (IV) is not affected by these events.
(IV). E-NE trending, dextral strike-slip fault zone in the southern part of the Kekerengu map sheet (Heavers Creek Fault continues into northern Kekerengu).	Uses steeply plunging bedding in hinge produced by second phase folding. (Heavers Creek fault offsets 100 Ka marine terrace; Lamb and Bibby 1989). Rotates refolded beds between Heavers Creek and Chaffey Faults.
NNE-trending, reverse faulting, northern Kekerengu.	Uplift of old (D_e) thrust surfaces in hinges of refolded (I) folds. Possibly associated with termination of dextral faults in the southern part of the Kekerengu map sheet.
NE-trending, dextral strike-slip faulting, southeast Washdyke.	Faults cut syn-tilt reverse fault and refolded beds.
NW-trending, sinistral strike-slip faulting, southern Washdyke.	Fault cuts refolded beds.
(V). Kekerengu Fault cuts surface.	Truncates all other elements. (Kekerengu Fault offsets 4 Ka river terrace; Lamb and Bibby 1989).

Table 5.1: Table summarizing the sequence of structural events affecting the Kekerengu-Washdyke study area along with the evidence used to deduce this progression. Refer to section 5.3.2.3.

terrace (Lamb and Bibby 1989). The timing of folding with wavelengths of up to *ca.* 1 km in subarea C (4.3.3.), between the Heavers Creek and Chaffey Faults, is hard to distinguish from the timing of this dextral strike-slip faulting, although at least some of the dextral strike-slip appears to post-date these folds since there appears to be a clockwise rotation about a vertical axis of the trend of the fold axes adjacent to the Heavers Creek Fault.

The Kekerengu Fault truncates all other structures indicating that the offset of the present erosion level by this fault is a very young (and possibly the most recent) event. The fault is known to offset a *ca.* 4 ka river terrace (Lamb and Bibby 1989).

5.3.2.5 Controlling Structures

The Kekerengu Fault may have been active throughout D_1 deformation in this area. Pleistocene strike-slip displacement along the Hope Fault terminates onshore with motion transferred to the NNE-trending Jordan Thrust (Van Dissen and Yeats 1991). It is suggested that all NNE-trending folding and reverse faulting associated with the first phase of D_1 deformation within the study area (D_{11}) is likewise due to the transfer of dextral strike-slip between the Hope and Kekerengu Faults (see fig. 5.7).

It is now necessary to explain the second phase of D_1 folding (D_{12}) in the study area (2). It is possible that progressive dextral shear rotated the orientation of the first phase fold axes so that their orientation with respect to the shear zone margins changed. Continued dextral shear could have then subjected the rotated fold axes to a component of compression along their length. Alternatively, the secondary folding may be a result of a more complex pattern of deformation in the region. Palaeomagnetic data (refer to sections 7.4 and 7.5) provides evidence to support this possibility, suggesting that D_{12} is a result of compression associated with accommodation of the regional clockwise rotation of northern Marlborough. This rotation is recorded all over northern Marlborough, except in the Kekerengu-Washdyke study area. It is suggested that the Kekerengu Fault has acted as the eastern boundary of the rotating region and that this rotation imposed a component of compression onto the Kekerengu-Washdyke area causing the second phase folding. folding.

An explanation is also sought for D_{13}. Oversteepening of the Razor Fold's western limb, sinistral offset along Fault 15, and dextral faulting in the western part of the Washdyke map sheet (Faults 30b) all appear to accommodate the same deformation event (fig. 5.8a). Faults 30b are of a similar orientation to the Kekerengu Fault immediately to the north of the most northern of these faults and at a distance approximately equal to the spacing between them. They appear to represent relay faults transferring displacement to the Kekerengu Fault. The oversteepening of the western limb is then a direct consequence of this relay faulting. The sinistral offset along Fault 15 may accommodate this oversteepening. Alternatively, it is possible that this sinistral offset

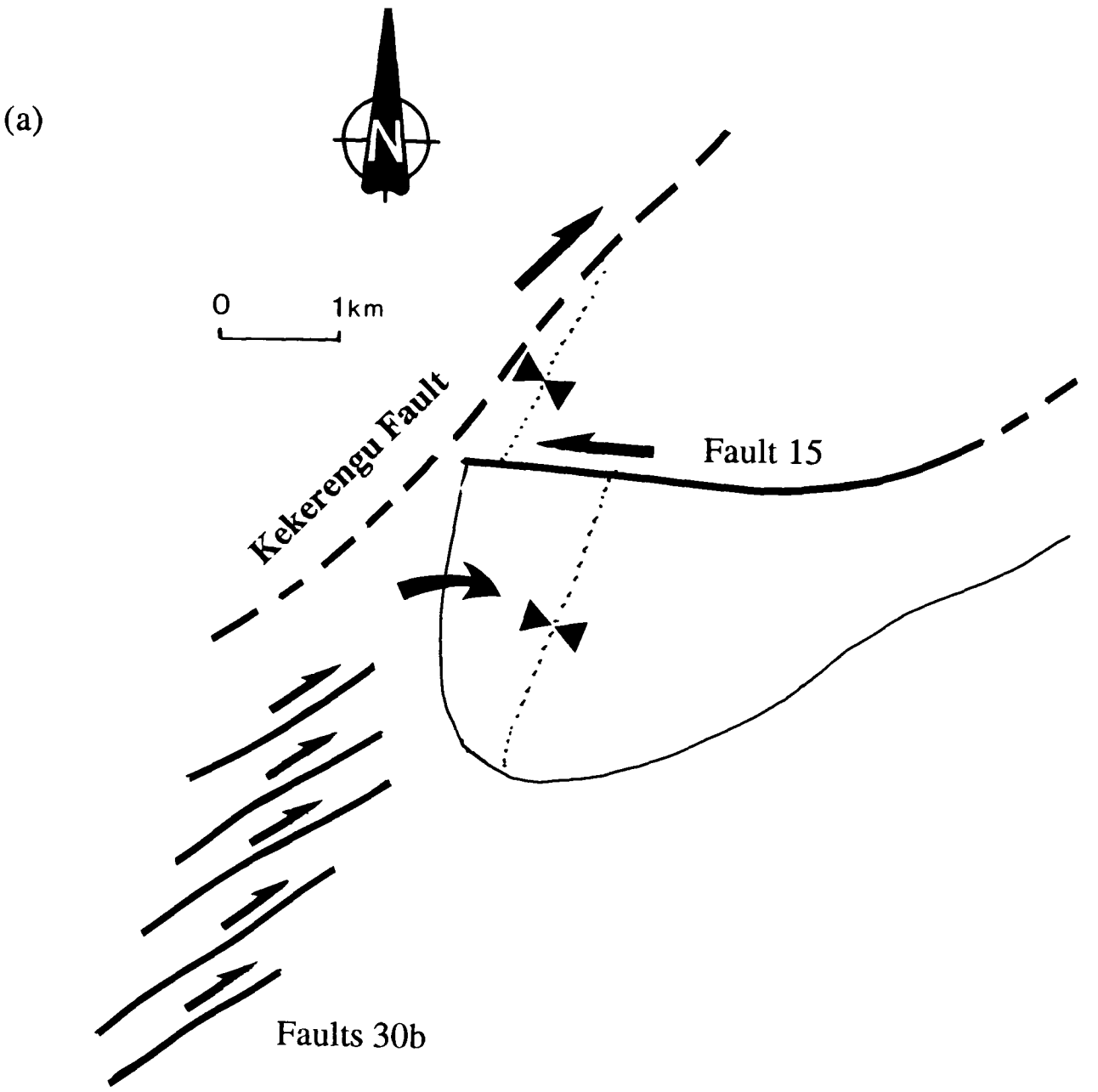


Fig. 5.8: (a) Sketch showing structures of D_1 episode 3 in the Kekerengu-Washdyke study area. (b) Possible explanation for sinistral strike-slip on Fault 15; bending between the Kekerengu and Washdyke map sheets. Although no conclusive palaeomagnetic evidence exists for the clockwise rotation of the Kekerengu map sheet, errors involved in the palaeomagnetic site data could easily hide such a rotation.

may be a hinge type structure accommodating the displacement between areas (the Kekerengu and Washdyke map sheets) that have rotated about a vertical axis by different amounts (i.e. a similar phenomena to that which could explain D_{J2} folding (fig. 5.8b)). It should be possible to decide between these two possibilities by palaeomagnetic analysis. Discrete sinistral faulting along the fault would produce no differential rotations between the two maps. In contrast, the second option involves the bending about a vertical axis of one of the areas. In this case, a differential rotation may be picked up by palaeomagnetic data in either the Kekerengu or Washdyke map sheets. Reference to 7.4 and 7.5 shows that there is no conclusive evidence for a post-Pliocene differential rotation between the two maps. However, errors on the declination data of sites from the study area could easily disguise a small *ca.* 5-10^{o} clockwise rotation. The bending model is preferred since there is evidence for compression in the Kekerengu-Washdyke study area associated with the regional rotation of the rest of northern Marlborough, and since such bending would be expected under such circumstances.

Fig. 5.7 illustrates the progressive evolution of D_J faulting and folding in the region between the Kekerengu and Hope Faults.

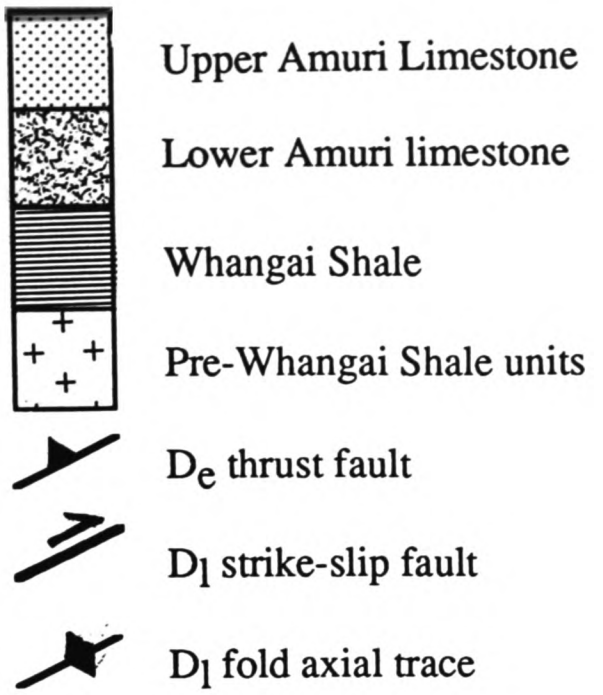
5.3.3 The Pre-D_J Transport Direction of D_e Thrust Faulting in the Benmore and Kekerengu-Washdyke Subregions

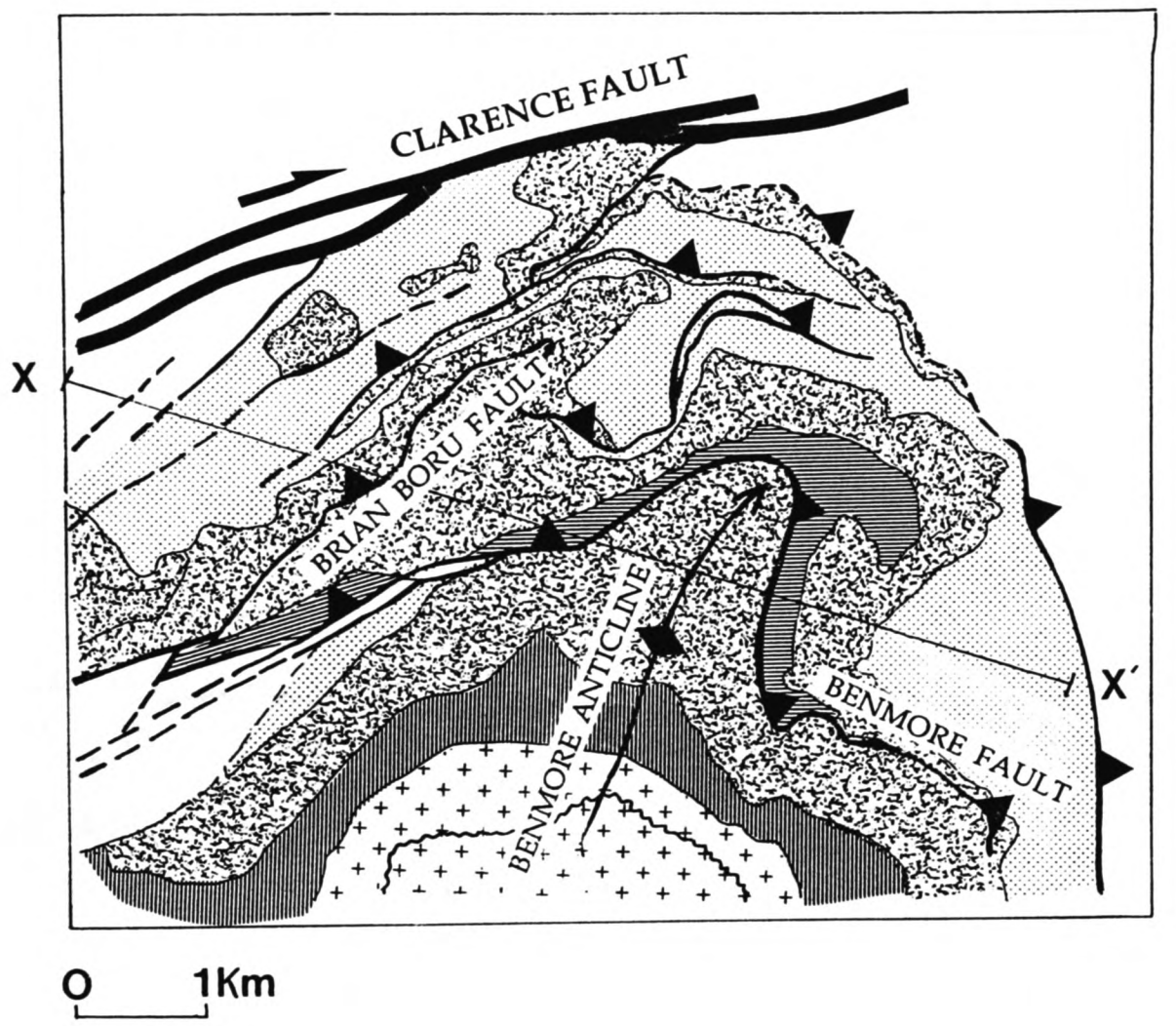
5.3.3.1 Introduction

There are several features available in the Marlborough region which can be used to assess the transport direction of D_e thrusting. These are as follows: (1) the direction of ramping up sequence of thrusts folded in the Benmore Anticline; (2) the overall sense of uplift suggested by the relative position of basement, Amuri Limestone and clastic cover sediments; (3) the direction of the local palaeoslope, inferred from palaeocurrent data, which may be a consequence of thrust motion; and (4) rare fabrics and lineations associated with D_e thrust faults in the Kekerengu-Washdyke subregion.

5.3.3.2 Results and Conclusions

(1) The Tirohanga and Deep Creek Faults of the Benmore subregion (Prebble 1976) both cut progressively younger strata to the SSE (fig. 5.9). Restoration of these strata to their pre-D_J orientation results in thrusts oriented 290/29 N and 238/21 N respectively. These thrust orientations themselves cannot be used to conclusively state transport direction as local variations in thrust morphology are to be expected. However, study of the whole folded thrust stack in this subregion reveals thrusts which ramp up-section around to the east. This regional cross-cutting relationship to bedding, after





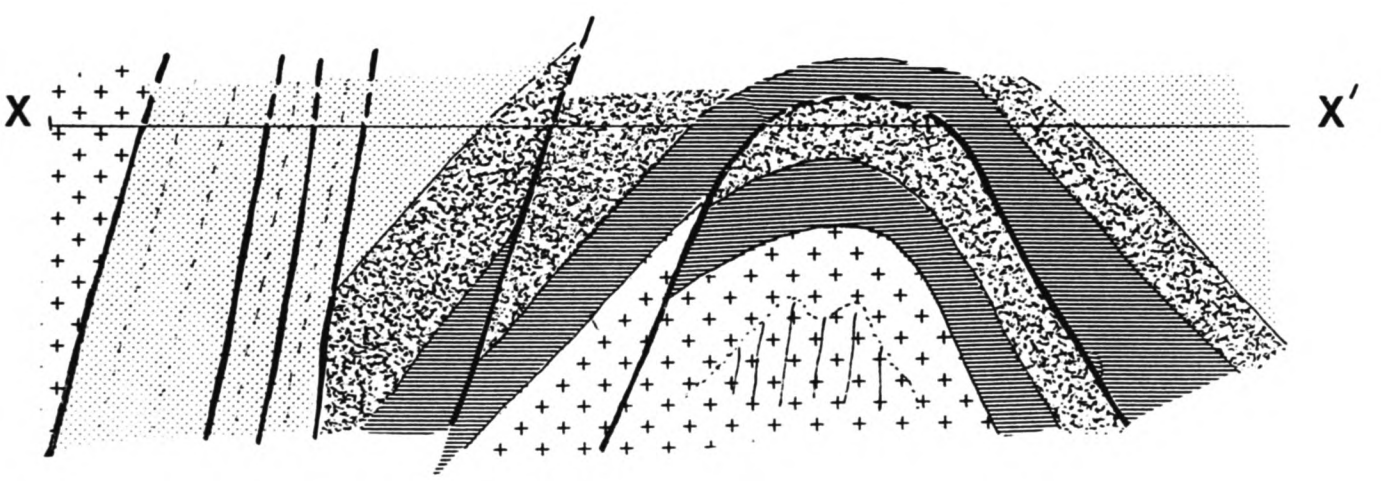


Fig. 5.9: Geological map and cross-section of the central part of the Benmore subregion (after Prebble 1976). D_e thrust faults are folded around the D_l Benmore Anticline which formed as a result of dextral shear between the Clarence and Kekerengu Faults. The Benmore and Brian Boru thrust faults can be seen cutting up-section around to the east.

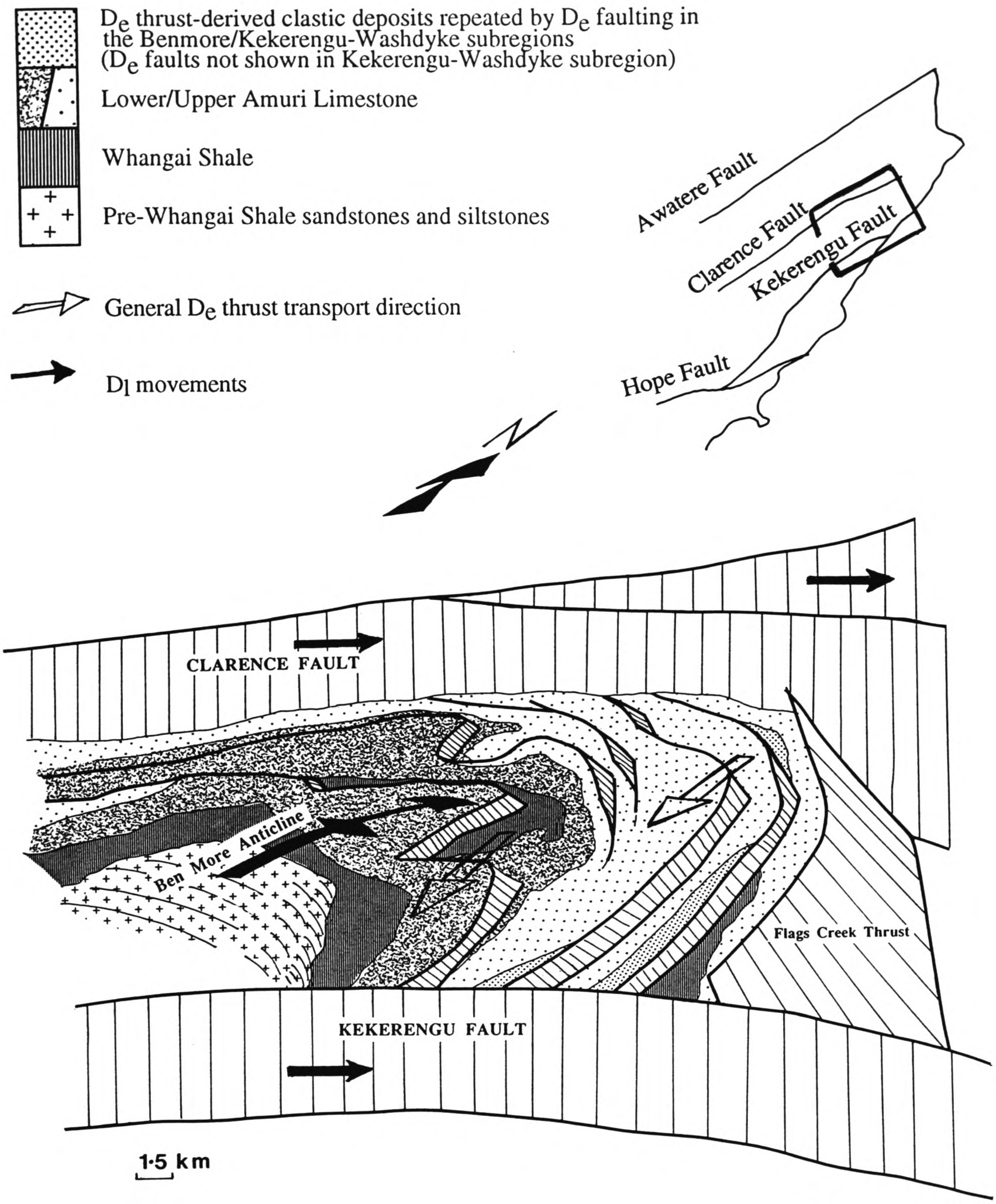


Fig. 5.10: Perspective three-dimensional block diagram of the Benmore subregion. D_e thrust faults are folded around the Benmore Anticline which formed as a result of dextral shear between the Clarence and Kekerengu Faults. D_e thrust faults can be clearly seen cutting up-section around to the east. This feature is due to thrust ramping and is used to suggest a *ca.* S D_e thrust transport direction after removal of D_l tilt, plunge and tectonic rotation.

KEY



D_e thrust-derived clastic deposits repeated by D_e faulting in the Benmore/Kekerengu-Washdyke subregions (D_e faults not shown in Kekerengu-Washdyke subregion)

Undifferentiated Amuri Limestone

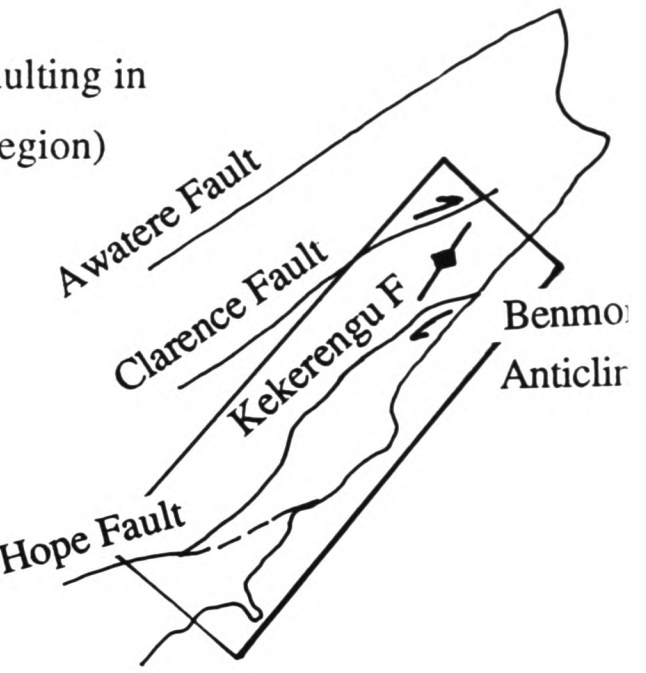
Lower/Upper Amuri Limestone

Pre-Amuri Limestone sandstones and siltstones

Younging direction

D_1 fold axial trace

D_1 fault movement



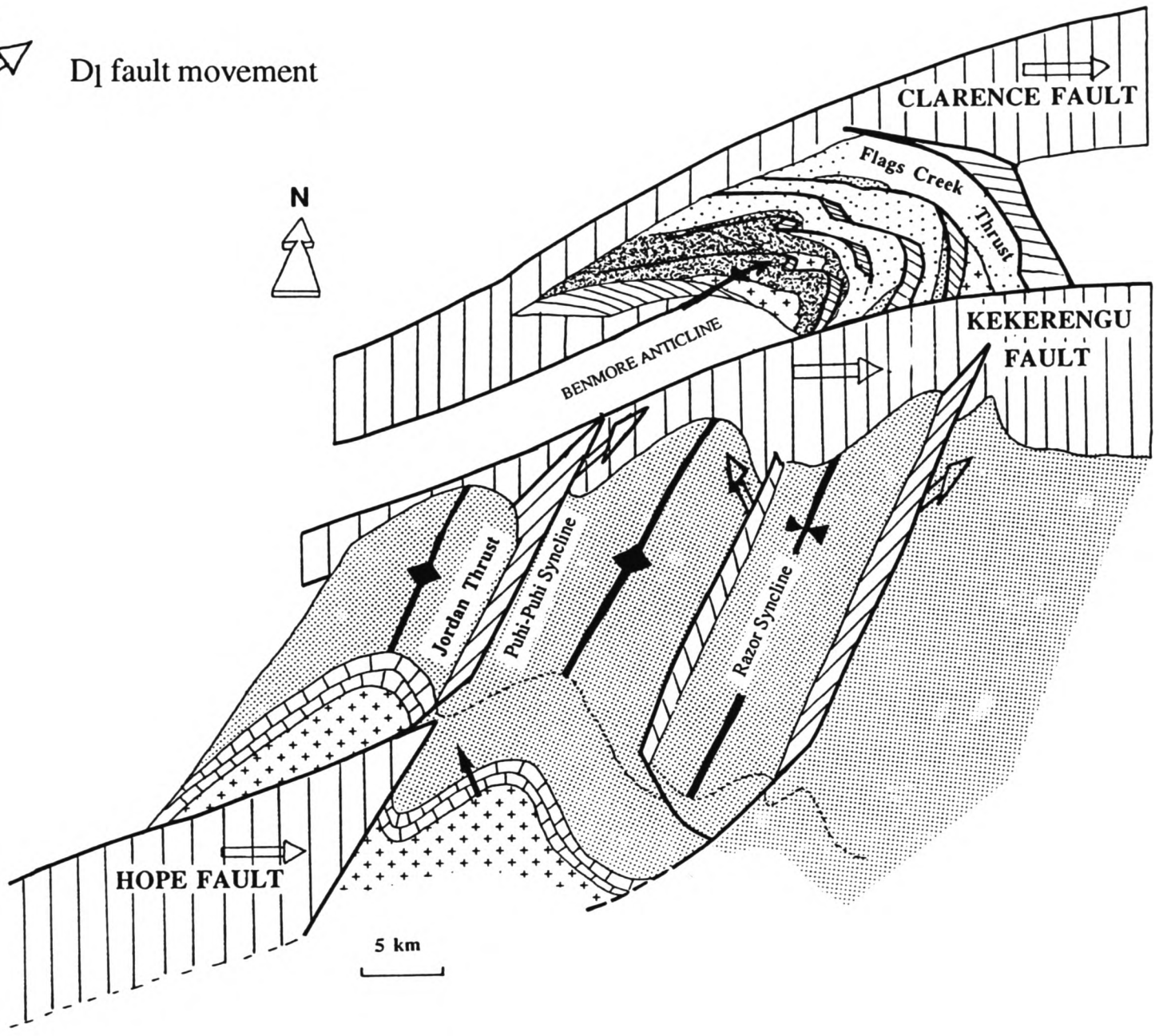


Fig. 5.11: (a) Three-dimensional diagram showing deformation between the Clarence, Kekerengu and Hope Faults after NNE-trending D_{11} folding in the Kekerengu-Washdyke subregion. This diagram aims to show the general relationship between the Kekerengu-Washdyke and Benmore subregions: since D_{12}, D_{13} and D_{14} obscure this relationship the diagram is shown at D_{11}. D_1 deformation in the Benmore subregion consists of the formation of the Benmore Anticline due to dextral shear between the Clarence and Kekerengu Faults. Since deformation in the Kekerengu-Washdyke subregion preceeds D_{13} and D_{14} which accommodate the regional rotation of the northern Marlborough domain of which this diagram is a part, all structures are drawn in their orientation prior to D_1 (*ca.* 20^o clockwise) rotation. In order to clearly observe the general structure of the Kekerengu-Washdyke subregion, D_e thrust faults are not shown (the stippled area represents D_e thrust derived and repeated clastic cover sediments). However, in the Benmore subregion D_e thrusts are shown cutting up-section as this three-dimensional geometry has been used to ascertain the D_e *ca.* S thrust transport direction (see section 5.3.3; fig. 5.9 and fig. 5.10).

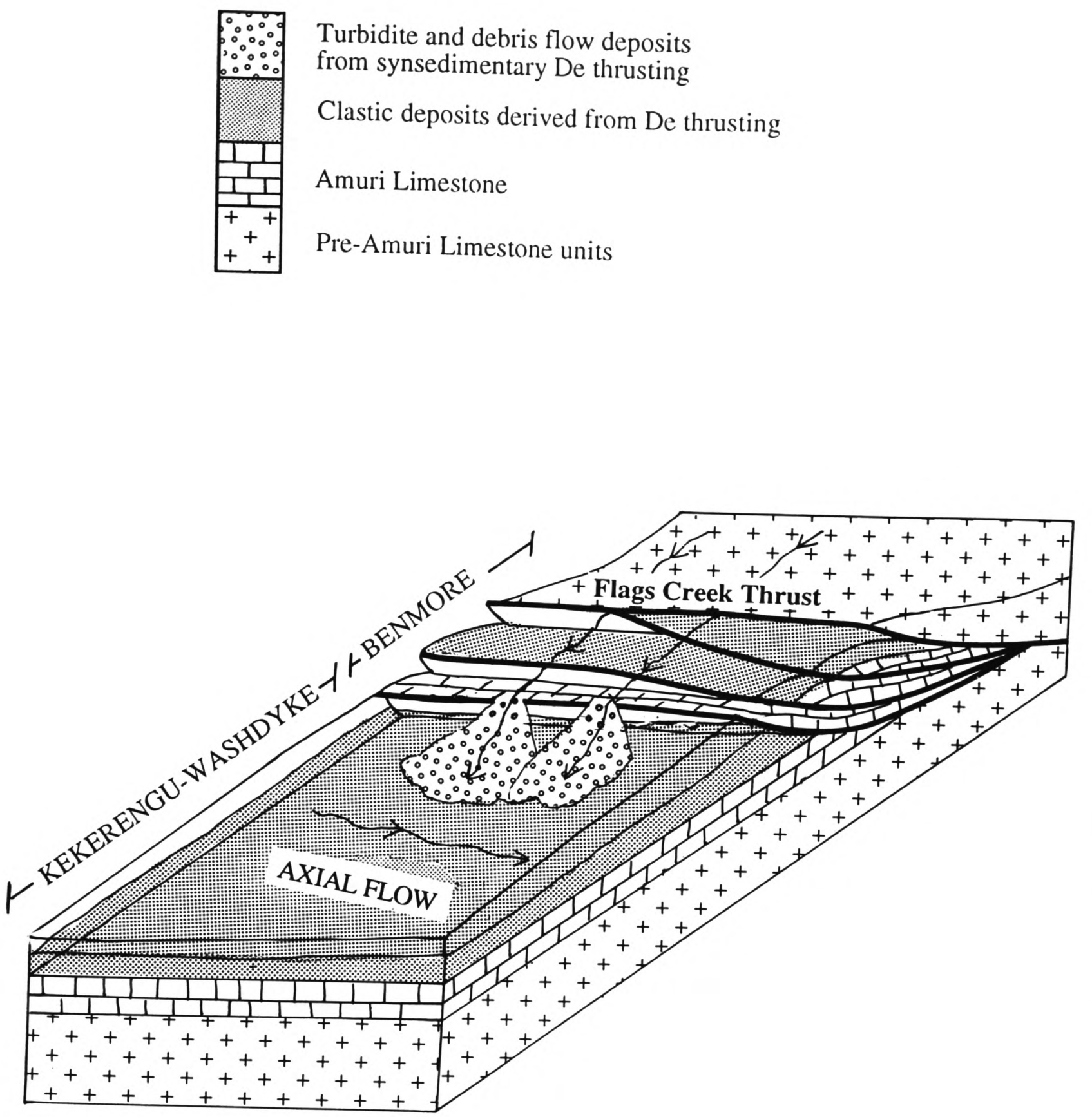
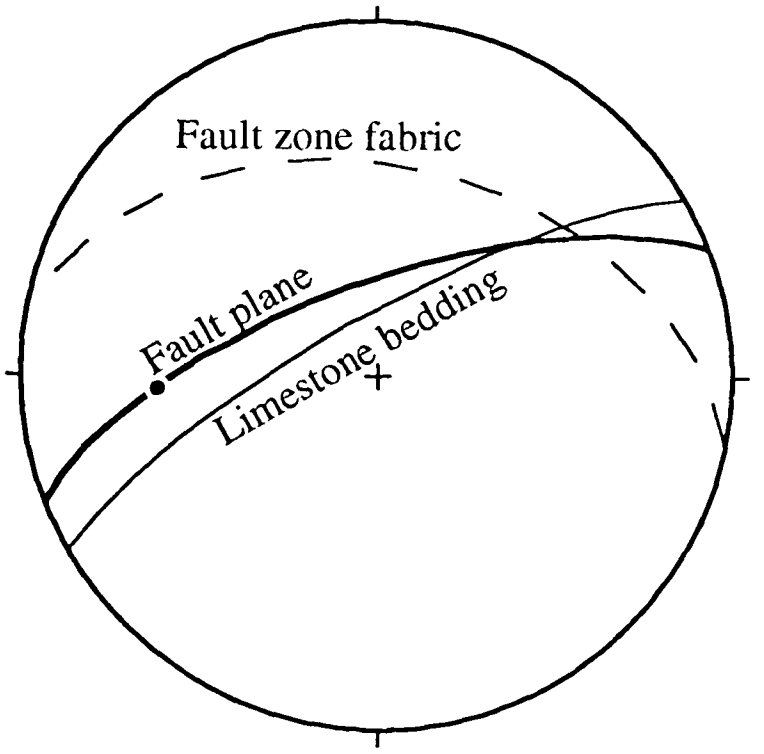
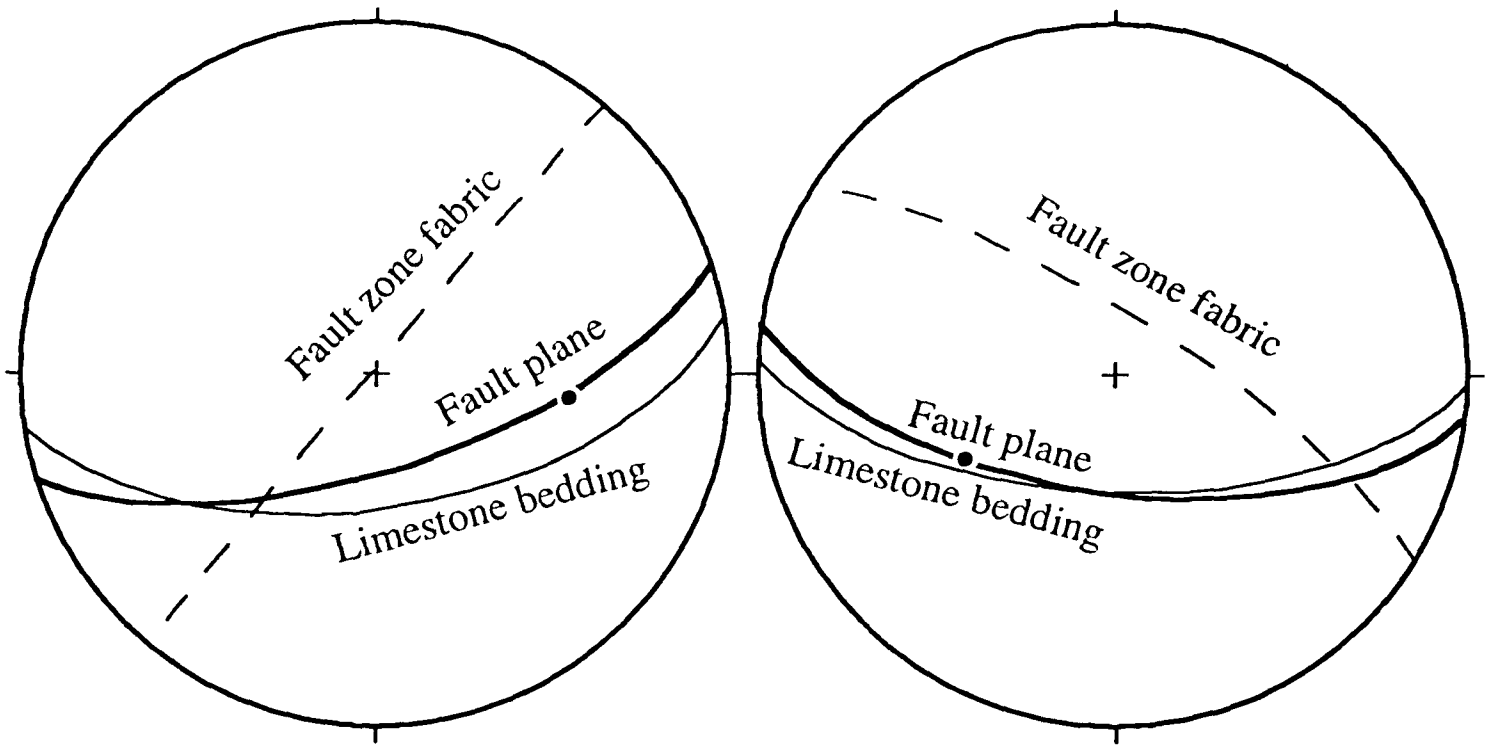


Fig. 5.12: Schematic block diagram showing Early Miocene S-directed synsedimentary thrusting in the Benmore subregion where earlier thrust-derived sediments are caught-up in later thrusting. Turbidite and debris flow deposits from D_e thrusting are deposited to the south of the uplifted areas (in the Kekerengu-Washdyke subregion) and contain evidence of axial sedimentary flow from the WNW.



(a) Uncorrected



(b) Tilt correction Plunge and tilt correction

Fig. 5.13: Equal area lower hemisphere stereographic projections of fabrics from Fault 19 at the mouth of Deadman Stream. Planes are plotted as great circles and lineations as points. (a) Fabrics in present, uncorrected orientations. (b) Fabrics in corrected orientations using: a simple tilt correction (001/82 E); and a plunge and tilt correction for two phase folding (fold axis: 320/67 NW). This data is used to ascertain the approximate transport direction of D_e thrust faulting. Refer to 5.3.3.

removal of tilt, indicates *ca.* S-directed thrust transport direction. These features are summarized in fig. 5.9 and fig. 5.10.

(2) Although the actual finite displacement on the Kekerengu Fault is unclear (due to the unknown extent of D_{J2} folding and amounts of uplift on the Clarence and Kekerengu Faults), after the removal of $D_{J4, 3, \text{ and } 2}$ deformation, and the D_J regional rotation which affects the Benmore subregion (chapter 6), the clastic thrust-derived sediments are to the S and SW of the uplifting areas at the time of D_e thrusting (fig. 5.10). This is in agreement with information obtained in (1).

(3) Study of the Great Marlborough Conglomerate and Ericaburn beds along Deadman Stream (Lewis et al 1980) have provided palaeocurrent and palaeoslope data using symmetrical ripple axes, parting lineations, grooves and channel axes, cross-bedding azimuths, and clast imbrication. All these indicate flow from the *ca.* WNW after correction for a 40^{o} NW tectonic tilt. This orientation is at a high angle to the general D_e thrust transport direction derived above, suggesting that the local palaeoslope created by these thrusts resulted in axial flow (fig. 5.12).

(4) At the mouth of Deadman Stream, a D_e reverse fault (Fault 19, chapter 4) places a conformable sequence with Waitakian Marl at the base, above younger conglomerates. A lineation on this fault plane, a fault shear zone fabric and bedding in the lithologies to either side, have been measured (fig. 5.13a). Restoration of all these elements to their pre-D_J orientation reveals an E-trending thrust fault, and lineation indicating slip in a *ca.* NE-direction (fig. 5.13b). This information is in general agreement with the information obtained from (1) and (2) but is opposite in direction, suggesting a possible back-thrust structure.

Palaeomagnetic data analysed in chapter 6 and interpreted in chapter 7 reveals that tectonic rotations about vertical axes have occurred in the Marlborough region affecting Tertiary cover and thrust-repeated sediments. Two rotations are observed: a regional *ca.* 118 ± 11^{o} clockwise rotation affecting sediments aged between *ca.* 18 and 8 Ma, and a regional *ca.* 20^{o} Plio-Pleistocene clockwise rotation affecting sediments of the Marlborough region apparently excluding those on the downthrown side of the Kekerengu Fault. If one assumes that the large rotation postdates the D_e thrusts from which orientation information has been obtained in this section, then in order to deduce the initial orientation of the transport direction of these thrusts, the data must be corrected for these rotations (only for the large rotation in the Kekerengu-Washdyke subregion). This procedure suggests that the D_e thrusts initially formed with a *ca.* NE-trending transport direction with axial flow of thrust-derived debris to the NW.

The results are in keeping with the approximate trend of the plate margin in the Marlborough region in the Early Miocene based on plate reconstructions (Walcott 1984, see fig. 8.3).

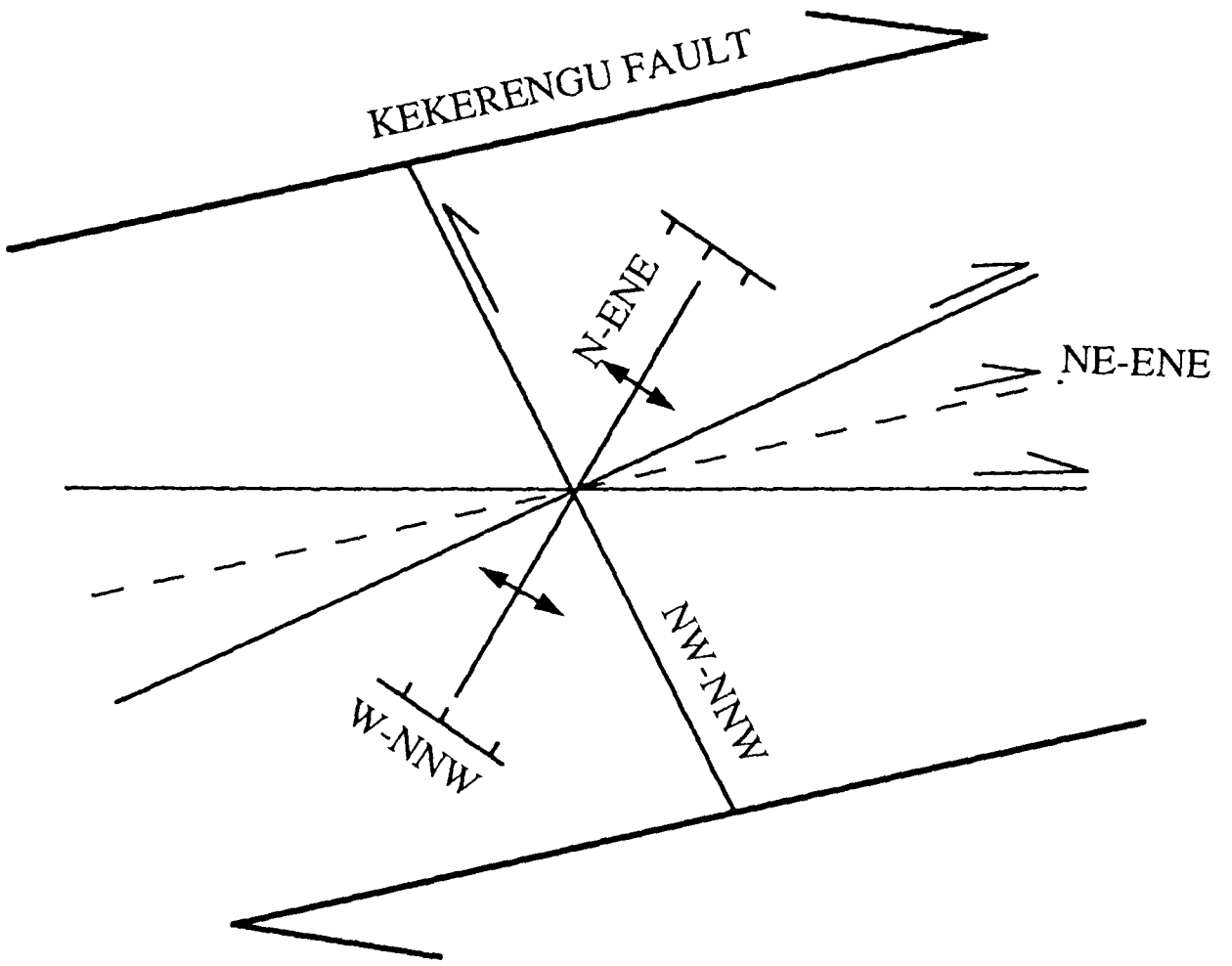


Fig. 5.14: Sketch showing the expected orientation of structures within an ENE-trending dextral shear zone. The orientations of mesoscopic faults of each type from the Kekerengu-Washdyke study area are marked alongside the corresponding structure. The majority of this data generally fits into the expected orientations of faults within this ENE-trending dextral shear zone. Refer to sections 5.3.4 and 4.3.2.2. (including table 4.2).

5.3.4 Mesofaulting

Due to the difficulty in allocating these faults to one or other of the deformation phases, only tentative conclusions can be drawn from this data. The faults (refer to 4.3.2.2 and to table 4.2) are of several dominant types: NNE to ENE-trending reverse faults with dextral strike-slip components and NW to N-trending sinistral faults or normal faults with a sinistral component. Exceptions exist, such as rare NW to N-trending reverse faults with a sinistral component.

Overall, this data is broadly consistent with faulting within a NE-trending dextral shear zone between the Kekerengu and Hope Faults (fig. 5.14).

5.4 Comparison of the Sedimentation and Structural Histories of the Kekerengu-Washdyke Study area with Other Subregions of Marlborough

5.4.1 A Summary of the Stratigraphy of Other Subregions

The stratigraphies of all of the Marlborough subregions have already been discussed and summarized in 2.4. Maps of these areas which show the general stratigraphy and structure can be found in fig 6.2 (Lower Awatere Valley), fig. 6.11 (Cape Campbell-Ward), and fig. 4.1a (Benmore). Figs 2.10 and 2.11 summarize the stratigraphy in each area.

Comparison of the stratigraphic columns reveals the similar stratigraphies within the Benmore, Kekerengu-Washdyke and Northern Canterbury subregions, in contrast to the stratigraphies within the Cape Campbell-Ward and Lower Awatere Valley areas. Two unconformities are recognized. The first (Early to Middle Miocene) affects subregions to the north and north-east (Cape Campbell-Ward and the Lower Awatere Valley) whilst sedimentation continues to the south and south-west (Benmore, Kekerengu-Washdyke and Northern Canterbury). The second (Upper Miocene to Early Pliocene) reverses this pattern with uplift/non-deposition in the south and south-west and subsidence in the north and north-east.

These periods of deposition and non-deposition can be tentatively linked to the deformation on structures which bound each subregion. The two unconformities are found in the areas either one side or the other of the Flags Creek Thrust and it is suggested that this structure might have been active at both these times.

5.4.2 Comparison of Structures from Other Subregions (the identification of D_e and D_l)

This section summarizes the structural information from the Benmore, Cape Campbell-Ward, and Lower Awatere Valley subregions and attempts to distinguish between D_e and D_l structures within these areas.

5.4.2.1 The Benmore Subregion

Bedding parallel reverse faulting and folding, with SE-vergence and associated axial-planar cleavage, are identified in this subregion (refer to section 4.2). All these elements parallel the main thrusts in the duplex which dominates this area (fig. 4.1a). These thrusts and earlier elements are all folded by the Benmore Anticline with its NE-trending fold axis. This folding is consistent with compression associated with dextral shear between the Clarence and Kekerengu Faults which bound this area to the northwest and southeast respectively (refer to fig. 5.11).

The earlier elements folded by the Benmore Anticline, are considered part of D_e. The timing of the D_e thrusts in the Benmore subregion is constrained by the Middle Miocene unconformity west of the London Hills Fault which indicates that deformation in the Benmore region had ceased by *Waiauan* (Waters 1988). However, in this study it is noted that although sedimentation returned to previously uplifted areas at this time, uplift was transferred to the Kekerengu-Washdyke and northern Canterbury subregions at this time. This uplift continued through to the *Kapitean*. Since it is not possible to separate D_e structures in the Kekerengu-Washdyke subregion into those belonging to the earlier uplift of northern areas and those which belong to the uplift of the southern areas, D_e is assumed to have continued through to the *Kapitean*.

5.4.2.2 The Cape Campbell-Ward Subregion

NNE-trending folding (the Cape Campbell and Ward Synclines) and reverse faulting (the London Hills Fault and back thrusts related to this fault) affect sequences up to Whanganui Series, and are therefore post-Pliocene structures, allocated to D_l. No clear evidence of D_e structures have been recognized in this area. The unconformity in this area suggests that it formed an uplifted block during the interval of D_e faulting and sedimentation in the areas to the south and south-west (Benmore, Cape Campbell-Ward and northern Canterbury).

5.4.2.3 The Lower Awatere Valley Subregion

Early Tongaporutuan to *late Middle Tongaporutuan* faulting has been described from the Lower Awatere Valley. These faults are known as the Medway Faults and appear to have moved synchronously with the onset of debris flow deposits of the Medway and overlying Formations in this area (Melhuish 1988). Activity on these faults

spread progressively to the north-west. The Late Miocene timing of these faults suggests that they are in effect part of D_e. However, it has been suggested by Roberts (1990) that some of these faults have in fact been reactivated as thrust faults during D_l in order to accommodate recent block rotation of the Lower Awatere Valley (refer to sections 7.4 and 7.5). Several Pliocene to Pleistocene D_l reverse and strike-slip faults have also been described (Lensen 1962; Melhuish 1988).

5.4.3 Summary

The Neogene evolution of Marlborough consists of two intervals of uplift and subsidence. Uplift of the Lower Awatere Valley and Cape Campbell-Ward subregions occurred in the Lower and Middle Miocene synchronously with sedimentation and intra-basinal thrusting in the Benmore, Kekerengu-Washdyke and Northern Canterbury subregions. This phase produced sediments and structures described as D_e. In the Upper Miocene, uplift occurred in the subregions formerly receiving sediment, synchronous with subsidence of the formerly uplifting subregions. It appears that in this interval some of the D_e faults in the Kekerengu-Washdyke area were still active. The main uplift during this second interval occurred in Northern Canterbury and the eastern part of the Washdyke map sheet with intrabasinal thrusting in the main part of the Kekerengu-Washdyke subregion and in the submerged Lower Awatere Valley. The Cape Campbell-Ward subregion was receiving sediment throughout this uplift. An interval of uplift west of the London Hills Fault in the *Opoitian* may represent the spread of this uplift into this subregion into Early Pliocene times.

Overall the D_e structures and sediments record a progressive spread of uplift from the north to the south with resubmergence of previously uplifted areas (fig. 5.15).

Pliocene sediments were deposited over the whole region and subsequently tilted and cut by D_l structures. The five main dextral faults of the Marlborough Fault System were active at this time and remain active to the present day (eg:- Lensen 1962).

The nature of D_l structures in the Kekerengu-Washdyke subregion has been summarized in section 5.2 and in fig. 5.7. The complexity of D_l folding, refolding and faulting in this subregion is in contrast to the relatively simple formation of the Benmore Anticline between the Clarence and Kekerengu Faults, the NNE-trending folding and thrusting in the Cape Campbell-Ward subregion, and the few reverse and strike-slip faults in the Lower Awatere Valley. This is considered to be a consequence of the complex accommodation of the regional tectonic rotation, observed in the rest of northern Marlborough, in the Kekerengu-Washdyke subregion of northern Marlborough (refer to section 7.5).

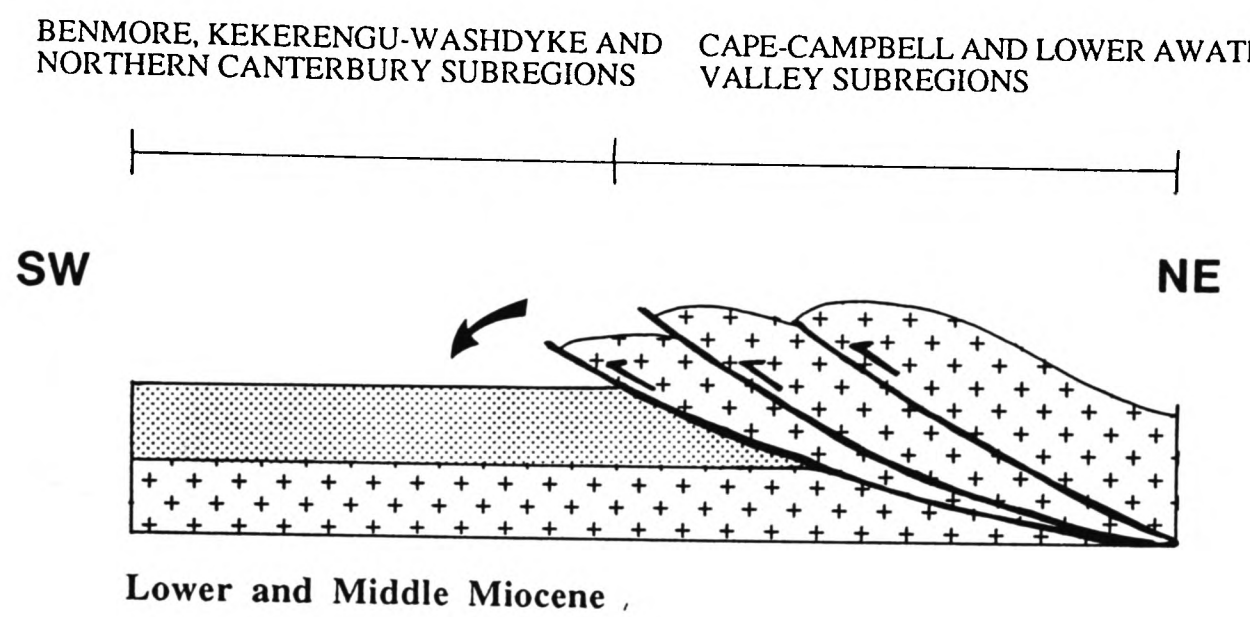


Fig. 5.15: NE-SW cartoon sketch cross-section showing the progression of Miocene D_e thrust related uplift and subsidence in the Marlborough region. Note that re-submergence of previously uplifted areas in the Upper Miocene is due to back-tilting associated with later D_e thrusting.

CHAPTER 6

CHAPTER 6: PALAEOMAGNETISM AND TECTONIC ROTATIONS

The chapter begins (6.1.1) by introducing the rotational component of strain in deforming continental lithosphere and describes the situations in which such rotations have been observed. The next section (6.1.2) gives an explanation of how palaeomagnetism is used to deduce tectonic rotations. Following this introductory section, section 6.2 covers sampling criteria, techniques and equipment used. The presentation of palaeomagnetic data collected in this study is presented in 6.3. Sections 6.4 and 6.5 respectively present a summary of site remanence carriers and site stratigraphic thicknesses. All interpretations and new models for the evolution of the New Zealand plate boundary zone arising from all this work are discussed in chapter 7 where they are linked with further tests of stability and with interpretations from the structural data (chapter 5).

6.1 Introduction

6.1.1 Introduction to Tectonic Rotations

The theory of Plate Tectonics states that the Earth's surface consists of large, rigid lithospheric plates which are in relative motion. The relative motion is accommodated by deformation at the plate boundaries. In the oceans, narrow bands of seismicity (< 10 km) define the plate boundaries, whereas for the continents deformation is distributed over horizontal distances far greater than the plate thickness extending to hundreds or thousands of kilometres (England and Jackson 1989). The effect of all the deformation in these wide zones is to accommodate the relative plate motion. However, plate tectonics cannot predict how the deformation is distributed in detail within the deforming zone. If the deformation is accommodated by many faults then at some large scale, much greater than the spacing of the faults, it is possible to describe the deformation as a continuum (McKenzie and Jackson 1983), though at smaller scales this is not true.

In a uniformly deforming zone, the instantaneous deformation within a continental plate boundary zone is summarized in the Velocity Gradient Tensor (**L**). This tensor incorporates all velocity components in all three orthogonal directions relative to the boundaries of the deforming zone. The tensor can be divided into a symmetric part (**S**), the strain rate tensor, and an asymmetric part (**A**), the rotational tensor. The rotational tensor corresponds to a rigid body rotation and implies that rotational strain is an integral part of the overall strain.

In-situ block rotations about near vertical axes have been recognized in many deforming continental zones using palaeomagnetic evidence. It is not possible to detect these rotations from structural analysis or seismology alone (McKenzie and Jackson 1983, 1986). Most of the recent advances in this field are summarized by Kissel and Laj (1989).

In some regions, such as California and New Zealand where there is a large component of plate motion parallel to the boundary of the deforming zone, a uniform sense of rotation is observed (Beck 1976, 1980; Kamerling and Luyendyk 1979; Walcott 1984). The sense is consistent with the sense of shear imposed by the relative motion of the plates (Walcott 1984; Nelson and Jones 1987).

Rotations have also been described from areas under oblique extension (McKenzie and Jackson 1983, 1986), in accretionary complexes where accreted crustal fragments from subduction or oblique subduction may rotate (Simpson and Cox 1977, accreted seamounts, Oregon), and from oroclinal bending where an initially straight orogenic belt is subsequently bent (McClelland and McCaig 1989; Coward and Potts 1983; Boyer and Elliot 1982).

There has been considerable discussion concerning the models of how to generate such rotations. Understandably the different settings in which these occur have a large effect on the particular model. One of the earliest proposals (Beck 1976) was of circular blocks rotating between two plates moving as strike-slip faults (the ball-bearing model). There is no evidence for such a mechanism. An alternative scheme (Freud 1970; Garfunkal 1974; Luyendyk et al 1980; Ron et al 1984) invokes the taking up of deformation on systems of strike-slip faults (slat models). Although much more realistic, in cases of oblique compression and extension, two systems of strike-slip faults with different strikes are required. These create problems of locking where the two fault sets intersect, and also the conservation of surface area in these models does not allow for the extension or compressional components of the stress.

Under oblique compression blocks defined by strike-slip faults may rotate by overlapping onto thrust faults as they move laterally, such as in foreland accretion.

The McKenzie and Jackson model (1983) described the movement of inclined faults to produce rotations. The blocks thus have horizontal as well as vertical vorticity. Movement on the faults involves only shear and conserves volume. This model can accommodate strike-slip and compression or extension without requiring the movement of material along strike of the zone. The relationship between the angle between the faults and the strike of the zone, and the angular velocity of the blocks, is constrained by the plate motions.

If we assume that the brittle crust behaves as fault-bound blocks which are floating on and following passively the ductile deformation in the deeper parts of the lithosphere, then we can assume that the large scale continuum description of the brittle

crust will be the same as that for the underlying ductile lithosphere. In this case, circular crustal blocks (in plan view) will rotate about a vertical axis at a rate which is equal to half the vertical vorticity (w) of the underlying fluid flow.

$$d\theta / dt = w / 2 \qquad (1)$$

However, the effect of interactions between blocks and the influence on the fluid below by the blocks have not yet been adequately considered.

Lamb (1987) modelled small floating crustal blocks as isolated rigid ellipsoidal floats. He derived an equation which relates the instantaneous rotation rate about a vertical axis to the aspect ratio, orientation within the zone and obliquity of convergence of the margin of the deforming zone. Note that the angular velocity changes as the blocks rotate.

$$d\phi / dt = -0.5(\partial u / \partial y)[((1-k^2) / (1+k^2)) \times (\cos 2\phi + \tan \theta \sin 2\phi) - 1] \qquad (2)$$

where $\partial u / \partial y$ is the vorticity vector (**w**) of the velocity field at a great distance from the ellipsoid, **k** is the horizontal aspect ratio of the crustal block (**b/a, a>b**), ϕ is the angle of the a axis relative to the zone margins, and θ is the angle between the relative motion vector and the zone margins.

Rotated crustal blocks have also been modelled in the laboratory (eg:- Cobbold et al 1989; sandbox experiments produced rotating fault blocks about vertical axes. All the rotations were associated with progressive displacement on the faults, especially wrench faults where localized block rotations were produced by, in particular, domino mechanisms).

To summarize, block rotations about vertical to inclined axes have been observed in many different tectonic situations. The models explaining these rotations vary according to the particular setting. Although the driving forces in the upper and lower lithosphere provide the necessity for rotational strain, the actual mechanism of rotation appears to be largely controlled by the pattern and type of crustal faulting. Complexities exist regarding components of compression or extension, compatibility, the size and shape of rotating blocks, values of rotation, interactions between fault blocks and pre-existing structures and their orientations. Even though it may be possible over a large scale to predict the vorticity from continuum assumptions, the actual surficial structures and their interactions with each other will influence the rotation rates and pattern of evolving deformation at the surface.

When attempting to document the strain within a continental plate boundary zone one should attempt to identify and observe the orientation of faults which may be controlling rotating blocks. In this way it should be possible to attempt to construct a model for the particular area. Only such observations can help to provide an insight into the problematical aspect of how rotational strain of this kind is achieved and how it fits into the overall accommodation of strain. The models themselves can only serve as guidelines in each case due to their oversimplification and relevance to certain structural styles.

6.1.2 Palaeomagnetism and the Measurement of Tectonic Rotations

This section explains how the magnetic properties of rocks can record a rigid body rotation about a subvertical axis. The explanation is divided into six parts.

In the first part (6.1.2.1) the origin of magnetization in rocks is discussed. The second part (section 6.1.2.2) describes how demagnetization is used to extract the vector components of magnetization within a rock sample. 6.1.2.3 discusses data presentation and the extraction of the component directions from demagnetization data. 6.1.2.4 covers the application of tectonic corrections, and finally stability tests including the identification of the remanence carriers are described in 6.1.2.5.

6.1.2.1 The origin of magnetization in rocks

An electron possesses a magnetic dipole moment as a result of its spin of its electrons about their axes. The electrons in atoms are ordered into orbitals; in filled orbitals the electrons with opposite spins pair-off to cancel out the net magnetization, however, in most atoms and ionized atoms un-paired electrons exist, leaving them with overall magnetic moments. In minerals the atomic species are usually present as ions and their extremely weak magnetic individual moments need to be aligned before the mineral can have a significant net magnetization. This alignment occurs due to a process known as exchange interaction, where the spins of nearby species align parallel or anti-parallel depending on the number of unpaired electrons that they have in their outer shells. The preferred orientation of the individual moments and net moments of ions within the crystal lattice will depend on crystallographic factors and is known as the easy axis. This is the source of crystalline anisotropy.

When a magnetic field is applied to a magnetic particle or grain (such as the Earth's magnetic field), the grain will minimize it's potential energy and thus attempt to acquire the closest possible alignment with the applied field. However, a grain will only change its magnetization if the activation energy for such change is overcome. The available energy will increase with temperature, and as a result the time for a grain to relax into a new alignment (t_0) will depend on the temperature and the grain size (grain

volume). The coercivity (Hc) of a magnetic grain is a measure of the field strength at which the activation energy is overcome. The spontaneous magnetization (Js) is the inherent magnetization of the grain produced by long range ordering of individual atomic moments by exchange interaction, and it is a decreasing function of temperature. Js goes to zero at the Curie Temperature (T_C). The following equation (Neel 1949) expresses the theoretical dependence of relaxation time ($\mathbf{t_o}$) on these variables for single-domain, non-interacting grains.

$$1/\ t_o = c.\ e^{-(v\ .\ Hc.\ Js\ /\ 2kT)} \qquad (3)$$

where **Js** is the spontaneous magnetization at temperature **T**, **v** is the grain volume, **Hc** the coercivity, **c** the frequency factor and **k** boltzman constant.

This relaxation time can be used to introduce the concept of blocking temperature. It is not only temperature which can influence magnetic change, but also the time for which a grain is held at that temperature. The blocking temperature is the temperature at which a grain will change its magnetization if it is maintained at that temperature for a set time. That hold time is the relaxation time required to 'unblock' the grain. As laboratory experiments often involve relatively short hold times, laboratory blocking temperatures need to be higher than natural ones to produce the same magnetic changes.

For a whole rock of any kind if the constituent magnetic grains have randomly oriented easy axes, the rock can acquire a net magnetic moment along the ambient magnetic field direction. This total magnetization is a vector conventionally defined directionally by inclination and declination and with a magnitude known as the intensity. Should crystallographic anisotropy not be the dominant anisotropy, but shape instead, then a non-random grain alignment may strongly influence the net magnetization. For example, flow fabrics in sedimentary and some volcanic rocks will result in a preferred orientation of the magnetic grains. Such rocks are thus not reliable for studies of palaeofield direction.

Randomly distributed ferromagnetic minerals are able to record the orientation of the ambient field at or near the time they were incorporated into a rock. In nature where the ambient field is the Earth's magnetic field, this direction is known as the primary natural remanent magnetization, the primary NRM. This net magnetization can be produced in a number of ways, each determined by the formation (and subsequent development) of the particular rock unit. Thermal remanent magnetism (TRM) is acquired in igneous (or metamorphic) rocks as their constituent magnetic minerals cool through their blocking temperatures. Chemical remanent magnetization (CRM) is acquired through precipitation of a magnetic mineral out of solution or alteration of one

mineral to another, such as the oxidation of magnetite to haematite. Detrital remanent magnetism (DRM) is acquired by sedimentary rocks as the grains attempt to align their moments with the external field by motion in water. Elongate grains with their magnetizations dominated by shape anisotropy are very important here because sedimentary flow can create non-random grain distributions and preferential alignment of grains. In a sedimentary environment it is the process of dewatering and consolidation which 'freezes-in' the magnetization. Some disorientation will occur during consolidation, but the statistical alignment remains good. Smaller, interstitial grains may align later and produce a partial DRM (pDRM) which may complicate interpretation should the external field change before total consolidation. This problem is decreased with increased deposition rate, decreased bioturbation, and decreased grain size. The inclination in sedimentary rocks is often lower than expected and this is thought to be due to elongate magnetic particles lying with their axes parallel to the depositional surface. The grain size effect is also important in sedimentary rocks. Larger grains are less free to rotate physically and are often multi-domain thus of lower magnetic intensity and more prone to viscous remanent magnetization (see following paragraph) as a result of their lower coercivity (Hc), equation (3). In addition sedimentary rocks made up of coarser grained material often have greater permeability which increases the likelihood of chemical reactions in ground waters, and pDRM formation.

Subsequent to acquisition of a rock's primary NRM, other secondary magnetizations may be acquired due to time alone or to time and temperature changes (metamorphism). The changes produced as a function of time alone are known as viscous remanent magnetization (VRM). Within a typical assemblage of remanence carriers the mineral grains have various relaxation times at a particular temperature. Those with short enough relaxation times will be remagnetized. This VRM is thus acquired isothermally. Temperature changes also affect the rock, and heating during low grade metamorphism may partially reset the magnetization. The primary NRM will only be fully reset if the Curie temperature of all the constituent magnetic grains is exceeded. Any secondary magnetizations will be parallel to the external field present when they were produced. In most cases only a proportion of the grains (for rocks not subjected to high grade metamorphism), change their magnetization, leaving higher (laboratory) blocking temperature remanence carriers with their original magnetizations. As a result any one rock may contain a multitude of magnetic components depending on its thermal history since formation. The magnetization directions are vectors and can be added and subtracted as such.

6.1.2.2 Demagnetization

The laboratory technique of demagnetization is used to uncover the component magnetic directions within a sample. Thermal and alternating-field demagnetization are used. The principles behind these techniques are described below.

Thermal demagnetization

As equation 3 showed, if T is increased, the relaxation time of magnetic minerals falls exponentially. Thus, if a sample is heated, the magnetic grains with certain relaxation times at the initial temperature will have shorter relaxation times at the elevated temperature. In thermal demagnetization, a batch of samples are heated to a temperature T, held at that temperature for 15-30 minutes, then cooled down in a zero magnetic field. Those grains with relaxation times within the hold time of the oven at the new elevated temperature will become superparamagnetic and loose their previous magnetization if there is no ambient field. On cooling the magnetization of these grains is therefore randomized and their net magnetization zeroed.

Grains with relaxation times higher than the hold time for the particular temperature will not demagnetize until the temperature is increased sufficiently that their relaxation time falls enough to cause demagnetization within the oven hold time, ie:- the temperature must be increased to demagnetize the higher blocking temperature grains. Thus the procedure is repeated, increasing temperature in, usually, 50^{o}C steps. This technique progressively randomizes the magnetization from lower to higher blocking temperature grains within the samples. The direction and intensity of the remaining net magnetization is measured after each step (using a cryogenic or spinner magnetometer). The procedure is continued until all the magnetization is randomized and the intensity has effectively fallen to zero.

Recording the progressive removal of the magnetization of higher blocking temperature grains will reveal the component vectors held by these grains. Thus it is possible to observe the component remanent magnetizations within a sample. The origin of the components must be checked as heating can introduce grain alteration (the destruction and creation of new magnetic minerals). To do this the bulk susceptibility is measured after each heating step to indicate when and if such alterations occur.

Alternating field demagnetization

This method of demagnetization uses a strong applied field to provide the activation energy to reset the grain magnetization. Samples are exposed to an alternating field of progressively increasing peak strength. The magnetization of grains with coercivities less than the applied field, follow the field. The field is then decreased, leaving these moments in random orientations but not affecting the original magnetization held by higher coercivity grains. The demagnetizing field is increased in

steps and the remaining remanence measured after each step until the magnetization ceases to decrease.

The problem with this method is that most alternating field instruments only demagnetize up to around 100 mT, therefore carriers with Hc more than that, such as most haematite grains, cannot be demagnetized this way. Magnetite is the only carrier with low enough Hc to respond to this technique, hence sediments are often not demagnetized this way. Although the procedure is somewhat restricted in its applicability, it does not cause the destruction or chemical alteration often associated with thermal demagnetization, and allows the total proportion of the initial intensity carried by magnetite phases to be assessed.

6.1.2.3 Data plotting and the interpretation of component directions from demagnetization data

The intensity of magnetization at each stage of demagnetization is plotted on a demagnetization curve, a plot of the varying intensity against the demagnetization temperature. The intensity is normalized to the initial intensity prior to demagnetization.

Displaying the actual directions of magnetization at each step requires graphical techniques which allow changes in three-dimensional vectors to be displayed on a two-dimensional page. Equal area projections (Wulf net projections) are one way of representing the vector data but only show directional information. The standard technique actually allows the presentation of both direction and intensity information on a single diagram by projecting the vector onto two orthogonal planes. These are known as Ziderveld plots (hereafter Z-plots). Each vector is decomposed into its declination (north and east) and inclination (up and down) components. At each step the separate vector end points are plotted using different symbols. In the Oxford laboratory filled points are used for the projection of each vector end point onto the horizontal plane and open points for projections onto the vertical plane. Removal of a single component will plot along straight lines as the intensity falls. Best-fit straight lines through the temperature points defining a single component can be computed. This was done using the IAPD package in the Oxford laboratory which uses a least-squares fitting program (eg:- Kirchvink 1980).

If more than one component is present in a sample and if the magnetic phases carrying each of these components have overlapping blocking temperature spectra (or coercivity spectra for alternating field demagnetization), then rather than separate straight line segments defining the separate components, the Z-plots display curvature where the components are being simultaneously removed. By taking the straight line segments above and below the overlap region it may be still possible to estimate each

component. Equal area stereoplots of the demagnetization between two components held by grains with overlapping coercivity spectra will fall on a great circle through the two component directions. Points on these curves track away from the low temperature or coercivity component and towards the high temperature or coercivity component. If the high temperature component is reached (a stable end point), then this can be read from the Z-plot above the overlap region. If this point is not reached then as long as the lower temperature components are sufficiently different, the higher temperature component can be computed using the technique of great circle analysis (first proposed by Hoffman and Day 1978). This technique takes the intersection point of two or more of the great circles from the cores from a single palaeomagnetic site. It is often difficult to be sure that a stable end point has infact been reached and so great circle analysis should be attempted to check that the true high temperature component is found.

6.1.2.4 Tectonic corrections

In certain cases (excluding many volcanic deposits or sediments deposited onto topographic slopes), it can be assumed that rocks were deposited more-or-less horizontally and that they acquired their primary magnetization along the Earth's field at or near their time of formation. Since formation, as well as possibly acquiring secondary magnetizations, any post-depositional deformation of the rock will reorientate any existing component remanent directions. The primary NRM within a sample is especially useful as this direction would originally have had a roughly NS magnetization aligned along the axial dipole field. The measured NRM can be compared with the polar wander path of the particular continental area from which the sample comes, taking into account the sample age. It is important to check the stability of the magnetization and its timing to confirm whether the magnetization is primary or not. In theory it should be possible to take an insitu primary remanence direction and correct it for all subsequent tectonic deformation which has affected it. This should reveal the primary NRM. However, the axial dipole is not fixed, it experiences secular variation. This variation of the Earth's magnetic field must be taken into account. A palaeomagnetic site is a unit of constant dip and strike from which at least six cores are taken which span a stratigraphic thickness large enough to average out the effects of secular variation (10 000 years is normally sufficient, Butler (1992)). The demagnetization plots from all the cores are viewed in insitu co-ordinates so that the remanence directions can be observed within a fixed framework. It is then possible to plot the primary component of magnetization from all site cores on a stereoplot and to compute the mean direction of these over the particular site. This mean direction is for the rock's present geographical and structural position and may bear no relation to the present earth field at the site.

As long as the deformation history of the site is thoroughly understood corrections can be applied to the mean NRM to restore it to its original pre-tilt inclination and declination. A thorough understanding of the deformation must comprise the order of deformation events. In cases where anything more than simple tilting has occurred, the relevant tilt and plunge must be known. The resulting vector can then be checked against the expected declination and inclination for the site's age, latitude and longitude. Tectonic rotations are picked up by declination anomalies for inclinations within error of the expected inclination. Such an inclination is evidence for the primary nature of this magnetization.

Reversals of the Earth's magnetic field are well documented through geological time as far back as the Ordovician. Thus for any one site cores may span any number of reversals and one commonly sees both reversed and normally magnetized cores. For normal cores the declination anomaly is measured from north, whereas for reversed cores it is measured from south.

6.1.2.5 Stability tests

It is important to be sure of the timing and stability of the NRM upon which one is basing an estimate of tectonic rotation.

Various field stability tests can be applied: fold tests (particularly relevant in this study), conglomerate and dyke contact tests, respectively provide information as to the timing of magnetization with respect to folding, conglomerate deposition and dyke intrusion. Only the dyke test can tell if the dyke remanence is primary or not. The others provide important constraints on the timing of the magnetization.

Mineralogical experiments to identify the remanence carriers are also necessary to help determine whether the components are held by stable or unstable phases and to check for evidence for alteration of magnetic phases which would place uncertainty on any assumptions of the primary nature of a component.

The identification of remanence carriers

Sharp increases in intensity during demagnetization are often associated with unstable, tectonically meaningless vector directions. Recognition of the magnetic minerals responsible for carrying the stable magnetization components can be achieved using several techniques.

The first of these is by simple microscopy. Ferromagnetic minerals are opaque and so reflected light microscopy is the more useful in identifying the actual carrier phases. A Scanning Electron Microscope (SEM) or microprobe with Energy Dispersive Spectrum (EDS) can be used to observe smaller grain sizes and detailed grain textures. The EDS allows a rough compositional analysis of grains. Recognition of the shape and

position of magnetic grains may provide evidence for whether these grains formed at the same time as the rock or at some later stage. However, magnetic grains are often below the limit of optical resolution or dispersed with a very low concentration in the rock. In this case magnetic experiments give more information as to the carrier types.

Ferromagnetic Minerals	**Curie Temperature (T_c)**	**Alternating Field Demagnetization**	**Isothermal Remanent Magnetization (IRM)**
(Ti) Magnetite	575°C	will demagnetize	Acquires IRM in $H \leq 300$ mT.
Haematite	680°C	cannot demagnetize	IRM gradually acquired in $H \leq 3$ T.
Pyrrhotite	320°C	cannot demagnetize	Acquires IRM in $H \leq 300$ mT.
Geothite	120°C	cannot demagnetize	IRM gradually acquired in $H \leq 3$T.

Table 6.1: Summary of ferromagnetic mineral characteristics used in the determination of remanence carriers within this study. Data from Butler (1992); O'Reilly (1984).

Study of the demagnetization data can alone provide quite a lot of information on possible carriers. The temperatures at which each component is totally removed provide clues as to possible carriers. The Curie Temperatures (T_C) of particular minerals vary depending on the exact compositions of the phases present. The maximum Curie Temperatures for the common magnetic grains are magnetites (*ca.* 575°C), haematites (*ca.* 680°C), pyrrhotites (*ca.* 320°C) and geothites (*ca.* 120°C). As previously mentioned in 6.1.2.2, alternating field demagnetization provides evidence for the presence of magnetites in a sample.

Isothermal Remanent Magnetization (IRM) acquisition can be used to identify remanence carriers. This technique uses the contrast in coercive force between titanomagnetites ($h_{C(max)}$ *ca.* 300 mT) and haematite and geothite (h_C *ca.* 1 T) to distinguish the phases. Samples are exposed to progressively increasing magnetizing fields. After each exposure the IRM is measured. This is repeated until saturation or until the peak field strength of the inducing equipment is reached. If only magnetites are present in a sample then a graph of the normalized IRM against the applied field strength will show rapid IRM acquisition up to *ca.* 300 mT whereafter saturation is achieved. If haematites or geothites are also present in the sample the graphs will

display rapid IRM acquisition followed by gradual acquisition of additional IRM in stronger magnetizing fields. If no magnetites are present IRM is gradually acquired throughout application of the increasing magnetizing fields.

All these features are summarized in table 6.1.

6.2 The collection of palaeomagnetic data

The summary geological map of the Marlborough region (fig. 1.4) and the two detailed 1:15 000 maps made during this study show the existence of oblique strike-slip faulting over much of the region. As apparent from the previous discussion, such faulting is likely to be associated with block rotations during the deformation of this section of the New Zealand plate boundary zone. One of the principal aims of this thesis was to collect as many palaeomagnetic sites as possible within the Marlborough region for deduction of tectonic rotations. It was hoped to both test and improve existing models for the evolution of the Marlborough region by using any new rotations alongside a thorough study of the structures. The overall aim was to provide a better insight into the exact nature of strain partitioning in this section of the plate boundary zone.

6.2.1 Criteria for drilling locations

Several criteria were used to identify possible sites. A number of successful sites (sites with stable magnetization) have been drilled in New Zealand prior to the time of this study. Many of these sites were drilled from fine-grained Miocene to Pliocene aged mudstone and siltstone flysch and turbidite deposits. The locations and results of all these sites are summarized in section 1.3.2. The Upper Cretaceous Mount Somers Volcanics of Canterbury have also produced a stable magnetization (Oliver et al 1979). In addition many unsuccessful sites have been drilled which were born in mind when considering which units to drill. Amuri Limestone Group lithologies (including the Waitakian Marl unit) have tended to show weak intensities (Morris 1987; Mumme and Walcott 1985) and were therefore not extensively sampled. However, within the Amuri Limestone Group at several localities in Marlborough is a pale-pink coloured limestone; the pink colour of this lithology suggests the presence of trace quantities of the ferromagnetic mineral haematite and so this limestone was drilled in the hope of finding a stable magnetization. Waima Siltstone exposures in Marlborough were described as being too fractured for drilling (Roberts 1990). The Great Marlborough Conglomerate deposit of Marlborough is both coarse-grained and its

deposition rate too poorly constrained to making it mostly unsuitable for palaeomagnetic analysis.

Outcrops suitable for drilling should, where possible, be of relatively fresh, unweathered material and so stream or newly cut road sections are preferred. Each site must have a clear and constant bedding which spans sufficient stratigraphic thickness (which will depend on the particular sedimentation rate) to average out the effects of secular variation. A good knowledge of the regional structure of which the site is a part is necessary in order to make the relevant tectonic corrections to the primary magnetization directions.

In the Kekerengu-Washdyke study area all criteria were used to identify as many drill site locations as possible. Sites were mainly drilled from Waima Siltstone units which were not in fact too fractured to sample. In the Benmore and Cape Campbell-Ward subregions Miocene to Pliocene aged sites have been extensively sampled (Roberts 1990; Walcott et al 1984; Mumme and Walcott 1985). Therefore in these subregions only the pink Amuri Limestone was sampled in order to assess the stability of this particular lithology. Cores were also taken from the previously unsampled Awatere Dykes in the Middle Awatere Valley.

6.2.2 Sampling equipment and technique.

Miocene to Pliocene siltstone and mudstone outcrops commonly display the effects of weathering. This leads to a drying out and fracturing (often conchoidal) of the outcrop surface. Such drying has been shown to produce a strong overprint viscous remanence (Roberts 1990). In order to avoid this effect oriented cores were sampled from unweathered, water-saturated outcrops close to stream level. The dried or fractured outer surface of each outcrop was cut back to remove any weathered material.

For the limestone sites only fresh, unweathered material was sampled. Occasionally a thin outer crust of weathered limestone exists. Joints are also relatively common in this limestone. Cores were only drilled in unweathered areas far from joint planes.

All cores were drilled with a diamond-tipped, brass drill barrel attached to a portable petrol-powered drill (borrowed from Victoria University of Wellington). The drill barrel had an internal diameter of 25 mm.

After drilling all cores were oriented using a magnetic compass. The Oxford convention was used for orienting in order to maintain consistency in the Oxford laboratory. For each core the azimuth relating to the direction of maximum plunge and the value of this plunge from the horizontal was recorded. Whilst still in position marks were made on each core along this direction. After this initial orienting the cores were carefully removed from their positions and marked along their length by a score on the underside of the core along the direction of maximum plunge. Arrows pointing down-

6.3 The Presentation of Palaeomagnetic Sites Collected During this Study

Section 6.3 presents the data from all palaeomagnetic sites analysed in this study. The section is subdivided on the basis of site locations. Within each subdivision the data from sites from the same lithological formation and from within the same structural 'block' is presented. The subdivisions are numbered from 6.3.1 to 6.3.10 beginning in chronological order for sites outside the main Kekerengu-Washdyke study area and then in an order from north to south for sites within the Kekerengu-Washdyke study area. Each subdivision is further divided into four parts. These are (a) geological setting which includes a general overview of the stratigraphy and structural of the area from which the sites are taken and the lithology and the age of the sites; (b) the demagnetization data; (c) remanence carrier identification; and (d) general timing of the magnetization for the sites within this subdivision. See Appendix to chapter 5 at the end of this chapter for lists of all core component directions used within this chapter.

Section 6.4 summarizes the remanence carriers from all the sites. This is followed by section 6.5 which discusses the stratigraphic thickness sampled by each site with reference to the averaging out of secular variation.

6.3.1 The Awatere Dykes (sites GS1 and WS1).

GS1: 173°34'/41°59' (GR: (O30) 570147).

WS1: 173°34'/41°59' (GR: (O30) 556140).

6.3.1a Geological setting, lithology and age

Summary of the stratigraphy and structure of the Middle Awatere Valley.

Fig 6.2 shows the structure of the Middle Awatere Valley and the position of sites drilled. (Information taken from Challis 1966 and Grapes et al 1992).

The Awatere and Clarence faults enclose a block of Pre-Cretaceous greywacke and Cretaceous sediments (Challis 1960, 1961 and Nicol 1977). Lower Cretaceous rocks are divided into three formations. The oldest of these is the Gladstone Formation (type section at Gladstone stream), a fining-upward sequence from coarse conglomerate at the base, through sandy grits and sandstone, to mudstone beds. In the east of the area the basal contact of this formation is a thrust fault. The Gladstone Formation is succeeded mostly conformably by the Winterton Formation. To the south-west of the Lookout area this rests unconformably on greywacke. The Winterton Formation is a fining-upward sequence of sediments which thickens rapidly to the north and which is derived from the south/south-west. Winterton

sediments are conformably overlain by the third formation, the Lookout Formation. This consists of thick subaerial basalt flows with interbedded subaerial tuffs and agglomerates, changing to subaqueous pillow lavas, tuffs, limestone and fossiliferous grits at the top of the formation. Dating of these grits gives them a *Ngaterian* age (Challis 1966). The top of the Winterton Formation at the base of these flows is dated as *Motuan.*

The eastern part of this Middle Awatere Valley area is dominated by a dyke swarm of more than five hundred dykes which intrude Cretaceous sediments. The dykes are of consistent orientation, striking at approximately 100^{o} though this strike changes to the north, swinging to 030^{o} in the Hodder River area. Challis reported that a couple of the dykes terminate upward into Upper Cretaceous Lookout volcanics (in Middlehurst Creek), indicating that the dykes were infact feeders to the basalt flow.

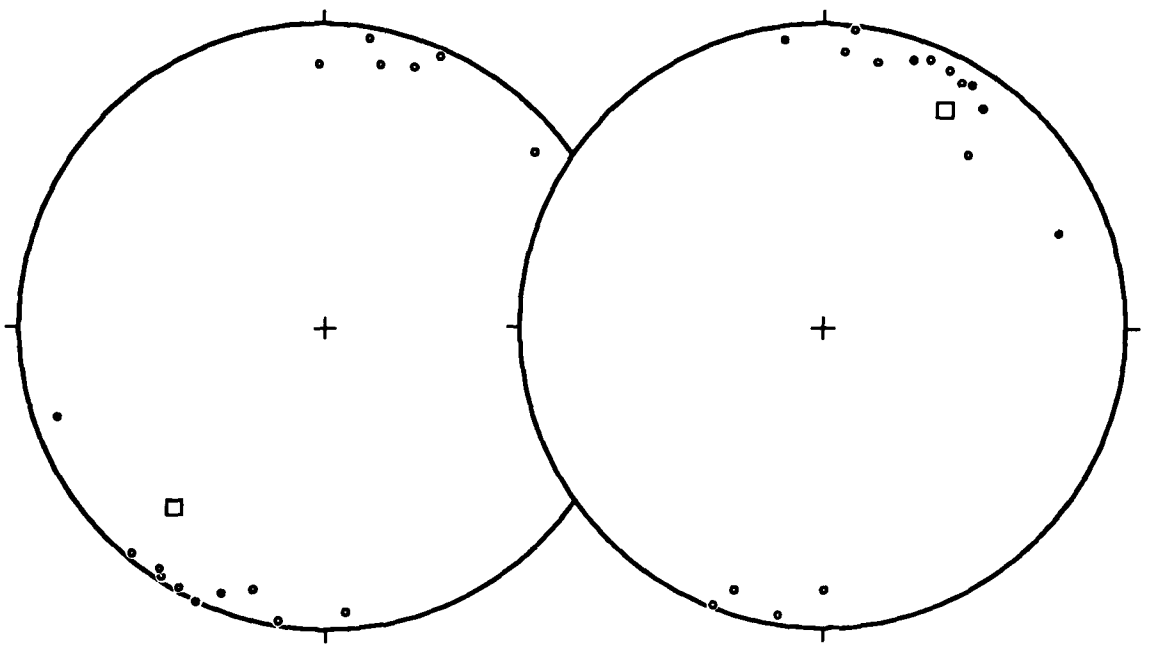
All three formations and the dykes are gently folded and displaced by a few faults. In the eastern part of this region the sequence is folded into a broad syncline and anticline, trending 040^{o} and plunging at $5\text{-}7^{o}$ to the southwest. The dykes are also folded, though their orientation at right angles to the fold axis obscures this fact. The folds are subsequently faulted by splays off the main Awatere Fault and by a number of normal faults (including several at right angles to the fold-axis orientation observed within the Lookout Volcanics). The Lookout Volcanics are folded into a shallow syncline trending 010^{o} and show rotation of this earlier folding by younger faulting adjacent to the Awatere Fault. The dykes themselves are not internally folded or faulted.

The drilling itself was done at two localities; Gladstone Stream (GS1) and the Winterton River (WS1), as shown in fig 6.2. The two sites are structurally separated by a low angle thrust fault which the dykes infact intrude and thus post-date. Gladstone Stream dykes intrude late Jurassic greywacke below, whereas the Winterton site dykes intrude Cretaceous Gladstone and Winterton Formation sediments on the hanging wall of this thrust.

The orientations of the drilled dykes show a roughly consistent ESE-trend. Their position at right angles to the fold axis and the very gentle plunge (7^{o}) of this fold axis means that tectonic correction hardly changes their orientation. Fig 6.1 shows poles to the dyke margins for pre and post-tectonic correction. The mean dyke margin before correction (310/67 NE) is slightly steepened and its strike rotated a few degrees anticlockwise after tectonic correction (119/71 SW).

The dyke lithologies

Samples from a number of the drilled dykes, as well as a number of other dykes from the same areas and from the Awatere River were collected by R.Grapes on the same trip. These he analyzed mineralogically and deduced K/Ar dates for all the samples (table 6.2). The results of these can be found in Grapes et al (1992). This work reveals that the dykes are all tephrite basanites mostly near to trachybasalt/basalt compositions. Challis (1966), Nicol (1977) and George (1988) extend the dyke compositions into the



(a). Pre-tectonic correction
Mean: 220/23

(b). Post-tectonic correction
Mean: 029/19

Fig 6.1: Equal area lower hemisphere stereographic projections of poles to dyke margins from the Gladstone Stream and Winterton River palaeomagnetic sites. Separate plots show a). poles prior to tectonic correction, and b). poles after tectonic correction. Open squares represent the mean vector in each case. These correspond respectively to mean dyke margins of 310/67 NE and 119/71 SW for cases (a) and (b).

Table 6.2: XRF, trace element analyses and K-Ar ages of basanitic dykes, Awatere Valley, Marlborough (after Grapes et al 1992).

Sample no.	32446	33067*	33068	33069*	32447*	32448*	32449*	32450*	33070	33071*	33072	33073*	33074*	32451*	32452	32453*	32454*	32455*	32456	32457*	32458	Age correlation†	
SiO_2	42.62	42.42	41.56	41.81	46.81	43.81	43.08	43.91	43.31	45.15	42.93	44.69	41.45	43.80	43.66	42.75	42.94	44.24	44.68	43.71	43.47	-.6332	.015
TiO_2	4.22	4.38	4.20	3.97	3.50	3.88	4.73	4.25	4.53	4.38	4.53	4.48	4.31	3.51	3.54	4.47	4.15	4.51	4.01	4.08	4.47	.0210	.943
Al_2O_3	13.78	13.46	12.00	14.83	15.35	15.50	14.50	15.53	14.00	14.12	12.81	13.75	11.39	16.31	13.60	14.56	14.19	14.32	13.19	13.89	14.06	-.4707	.089
Fe_2O_3	5.51	4.09	6.17	5.79	4.17	3.76	5.01	4.42	4.59	4.42	5.54	4.22	6.90	3.02	4.72	4.07	5.68	5.55	3.86	2.87	4.20	.4669	.092
FeO	7.48	8.83	7.38	6.09	6.41	8.28	8.93	8.41	8.69	8.42	8.52	8.37	6.31	7.43	6.64	8.15	6.93	7.73	8.33	9.17	9.19	-.3019	.294
MnO	0.28	0.18	0.23	0.24	0.19	0.18	0.22	0.18	0.19	0.24	0.26	0.25	0.18	0.20	0.15	0.20	0.19	0.19	0.19	0.18	0.20	-.1679	.566
MgO	6.18	5.60	7.24	5.51	4.16	4.89	5.22	4.24	6.06	5.44	5.75	5.17	8.03	4.00	7.52	4.80	5.62	4.89	7.02	6.39	5.04	.6070	.021
CaO	10.53	10.01	12.14	10.06	8.18	7.89	7.46	6.58	11.40	6.97	10.18	8.10	13.00	9.53	11.05	10.97	9.47	8.93	11.39	11.13	10.05	.5429	.045
Na_2O	3.19	3.21	2.11	2.72	3.47	3.53	4.28	4.47	3.04	3.81	3.11	3.69	1.93	2.68	2.10	2.92	3.01	3.34	2.91	2.55	3.10	-.5492	.042
K_2O	1.30	1.16	0.86	1.60	3.53	2.07	0.52	1.08	1.51	1.82	1.02	1.50	1.26	3.03	1.83	2.36	2.35	1.80	1.43	1.46	1.52	-.3316	.247
P_2O_5	0.82	0.92	0.63	1.09	1.27	0.96	0.81	1.04	0.99	0.87	0.72	0.92	0.81	1.11	0.57	1.23	0.89	0.80	0.78	0.86	0.75	-.4509	.106
F	0.16	0.20	0.18	0.19	0.20	0.18	0.23	0.24	0.23	0.19	0.21	0.18	0.16	0.20	0.10	0.20	0.17	0.12	0.17	0.18	0.18	-.4744	.087
Cl	0.01	0.01	0.01	0.01	0.03	0.01	0.01	0.02	0.02	0.01	0.01	0.02	0.02	0.02	0.01	0.03	0.02	0.02	0.01	0.01	0.01	-.4986	.070
S	0.12	0.10	0.12	0.08	0.11	0.14	0.13	0.16	0.11	0.20	0.14	0.15	0.09	0.12	0.09	0.09	0.15	0.14	0.08	0.11	0.15	-.4868	.078
CO_2	0.22	0.70	0.66	0.15	0.18	1.06	0.92	1.17	0.07	0.95	0.73	0.88	1.03	0.48	0.73	0.44	1.28	0.48	0.11	0.18	0.22	-.1042	.723
H_2O+	3.03	3.74	3.51	4.41	2.22	3.47	2.72	3.22	1.35	2.54	2.81	2.42	2.21	4.34	2.86	2.95	2.59	2.89	1.71	2.82	3.36	.3196	.265
H_2O-	1.07	1.07	0.89	1.57	0.42	0.63	1.73	1.06	0.19	0.55	0.77	1.01	1.33	0.42	0.91	0.30	0.44	0.52	0.45	0.80	0.32	.4770	.085
Total	100.52	100.08	99.89	100.12	100.20	100.24	100.50	99.98	100.28	100.08	100.04	99.80	100.41	100.20	100.08	100.49	100.07	100.47	100.32	100.39	100.29		
ppm																							
As	2	2	1	3	2	2	2	2	3	2	1	1	1	3	1	1	2	3	1	7	3	.2110	.469
Ba	411	298	460	379	786	846	227	817	449	1268	443	635	377	564	518	621	701	464	416	501	327	-.6193	.018
Ce	152	147	106	151	183	169	155	182	154	141	123	140	129	185	84	198	162	141	137	154	148	-.6168	.019
Cr	123	37	145	79	3	25	28	1	106	2	58	2	276	1	166	6	42	5	259	120	22	.6120	.020
Cu	80	48	51	76	12	41	57	6	86	21	59	9	91	14	50	18	47	28	75	70	34	.8066	.000
Ga	26	24	21	25	21	27	29	26	26	23	23	22	22	27	23	24	23	25	25	27	26	.0655	.824
La	59	62	45	70	84	72	56	74	62	53	46	59	57	83	36	83	66	56	57	60	56	-.3946	.163
Nb	77	79	54	89	103	101	79	100	77	75	64	79	66	110	45	107	87	75	72	81	71	-.5071	.064
Ni	90	48	92	78	5	37	49	3	73	20	68	13	133	6	83	12	53	34	109	72	37	.7959	.000
Pb	7	5	4	6	5	8	7	6	5	5	4	6	5	7	5	8	8	7	6	6	9	-.1549	.155
Rb	28	29	21	40	96	47	11	20	36	38	25	38	28	82	57	57	61	64	34	30	46	-.2306	.428
Sc	16	14	20	15	11	14	15	9	18	14	17	13	26	7	20	14	17	12	18	15	14	.5323	.050
Sr	835	454	181	732	1265	781	584	612	1071	666	165	223	724	1174	841	1123	799	591	955	1042	835	-.2681	.354
Th	6	7	5	8	9	10	7	6	5	7	7	8	8	10	6	10	7	6	7	7	8	-.1790	.540
U	2	1	1	3	3	3	1	3	3	2	1	2	2	3	1	3	3	1	1	1	2	-.3450	.227
V	300	334	384	261	243	270	343	259	334	310	386	316	351	191	291	276	306	321	289	273	325	.3514	.218
Y	39	37	32	39	52	41	38	46	40	40	34	40	35	47	32	46	40	42	36	38	39	-.6793	.008
Zn	119	130	101	106	113	111	120	131	117	128	115	122	102	115	86	117	114	105	105	125	121	-.4763	.085
Zr	370	337	289	399	486	447	377	450	372	385	323	387	364	486	237	480	403	374	365	394	356	-.6296	.016
D.I.‡	31.3	31.6	22.7	31.8	47.4	39.6	38.2	43.2	30.4	42.7	31.3	39.7	21.7	37.4	27.8	33.6	36	32.9	30.1	28.4	32.9		
Mg§	0.6	0.53	0.64	0.62	0.54	0.51	0.65	0.47	0.55	0.54	0.55	0.52	0.69	0.49	0.67	0.51	0.59	0.53	0.6	0.55	0.49		
K-Ar age	93.7±1.4	92.1±1.8	71.0±1.5	93.6±2.1	70.6±1.2	83.3±1.3	78.0±1.3	67.4±1.0	86.4±1.7	59.6±1.2	75.1±1.8	74.0±1.4	93.2±1.5	76.3±1.3	68.3±0.9	65.6±1.0	81.4±1.2	85.8±1.2	82.3±1.2	82.8±1.2	100.0±1.4		
	92.7±1.3		72.4±2.3	94.8±1.9	70.6±1.1			68.6±1.8	90.9±1.6	60.0±1.0	77.0±2.2					66.7±1.0		87.0±1.5					
K wt%	1.04	1.001	0.655	1.343	2.961	1.708	1.47	0.893	1.262	1.79	0.915	1.32	0.817	2.565	1.411	1.945	2.074	1.516	1.215	1.194	1.202		
40Ar(rad) nl/g	3.884	3.675	1.842	5.099	8.275	5.652	1.456	2.383	4.338	4.216	2.726	3.872	3.035	7.762	3.814	5.051	6.711	5.171	3.972	3.927	4.799		
	3.844		1.88	5.168	8.282			2.424	4.57	4.241	2.796					5.137		5.246					
% total	88	64	66	52	90	87	64	77	74	72	55	65	81	91	86	87	93	87	87	79	62		
	85		39	59	92			78	74	73	58					85		84					

* Fine grained, phenocryst-poor or phenocryst-absent dikes.
†Pearson correlation coefficients, Probability > |R| under Ho: ρ=0.
‡Differentiation Index (Normative Q+Or+Ab+Ne+Ks+Lc).
§Molecular MgO/(MgO + FeO).

K-Ar ages are of 200–400 μm size fractions of rock samples.
Decay constants 40K: $\lambda_\beta = 0.4962 \times 10^{-9}yr^{-1}$; $\lambda_\varepsilon = 0.581 \times 10^{-10}yr^{-1}$.
Isotopic abundance 40K/K = 0.01167% atomic.
Errors are two standard deviations.

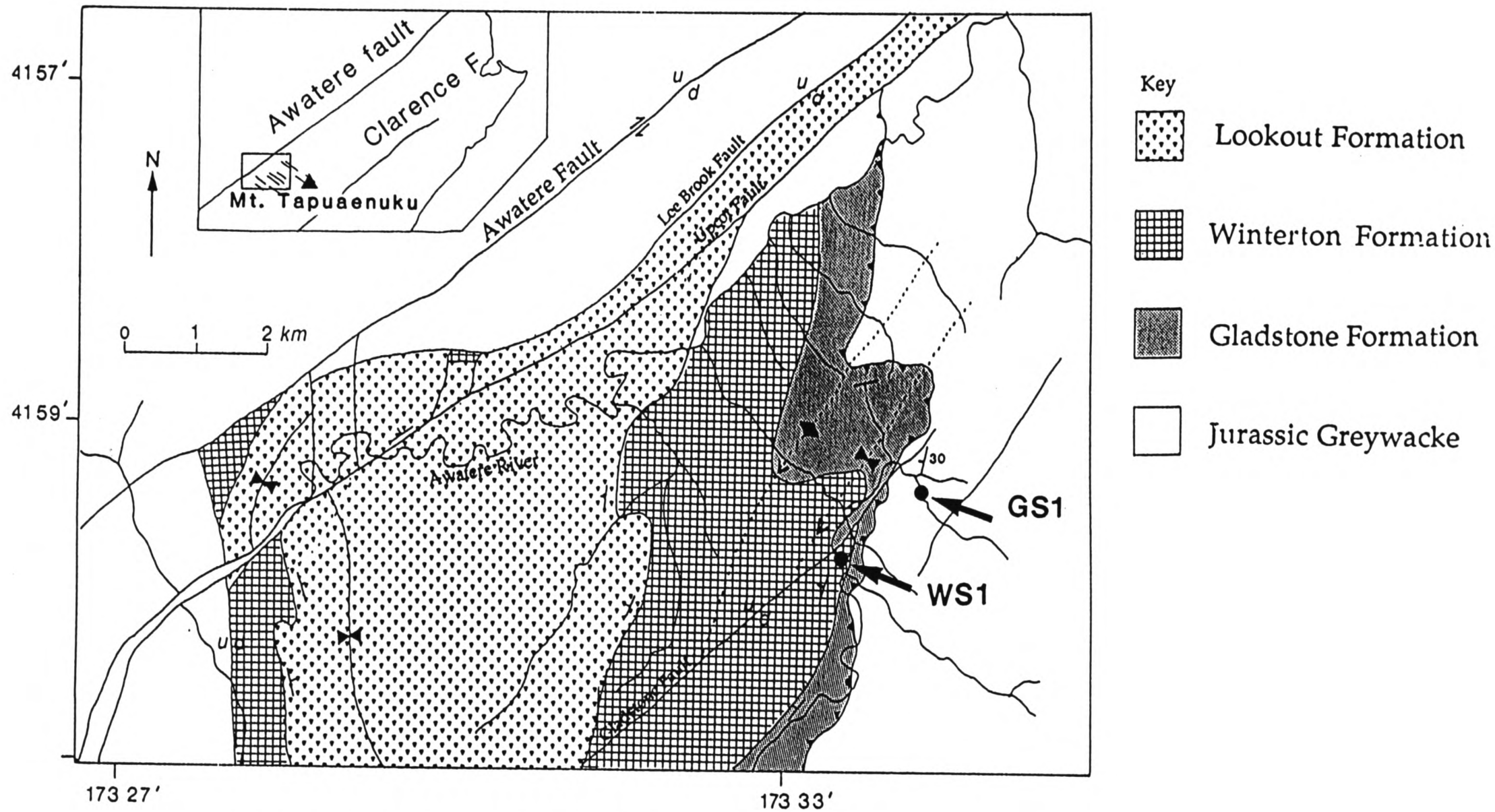


Fig 6.2: Geological map of the Middle Awatere Valley showing location of drilled dykes at sites GS1 and WS1 (after Grapes et al 1992).

trachyandesite field. The dykes have a clear alkaline affinity indicated by their high TiO2 (3.51-4.53 wt%), low Zr/Nb (3.7-5.5) and mineral assemblage; pl±Ksp, Ti-augite±olivine (altered to nontronite), Ti-hornblende, Ti-magnetite, ilmenite, apatite, titanite, calcite±zeolite, nontronite/saponite (mesostasis), and pyrite.

At the Gladstone Stream site fresh, water-smoothed, unweathered and unjointed dykes were sampled. The dykes were both single and multiple, with coarse-grained, phenocrystic (olivine and pyroxene) centres and medium grey, finer-grained margins lacking visible phenocrysts. Calcite ocelli are common in the finer-grained material. Ten separate dykes were drilled, six of which were dated and analyzed mineralogically by Grapes et al (1992).

At the Winterton River site six separate dykes were drilled; all cores are medium grey and fine-grained, with calcite ocelli. All the sampled dykes were also dated and analyzed mineralogically by Grapes et al (1992). The extent of weathering at this site was noted as being high in comparison to the Gladstone Stream location.

Dyke ages

K/Ar dating of the dykes (Grapes et al 1992) revealed ages spanning the period from 100±1.4 Ma to 59.8±1.1 Ma, (early late Cretaceous (*Cenomanian*) to mid Palaeocene (*Danian*)), with breaks between 60-65 Ma and 96-100 Ma. Grapes et al (1992) found no evidence for alteration and concluded the age span to be real. In comparison to other igneous rocks in Marlborough; the Lookout Volcanics of the Awatere Valley are Ngaterian (Challis 1966), the Gridiron Volcanics of the Clarence Valley cover 100-90 Ma (C.Adams-unpublished data) and the Tapuaenuku intrusives span 103-90 Ma (Baker 1990, Nicol 1977). The dykes of the Awatere Valley appear to span an additional 30 Ma. Younger still volcanics (the Mid Eocene Grasseed Volcanics and the early Oligocene Cookson Volcanics, Lenson 1963, Challis 1978 and Raey 1980) are found in the Clarence Valley and Coastal Marlborough.

Since a good percentage of the analyzed dykes (Grapes et al 1992) coincide with the drilled dykes at each site, the ages of most palaeomagnetically studied dykes are well constrained.

Table 6.3 below gives direct comparisons between the K/Ar ages of Grapes et al (1992) and the drilled cores. It is clear that the drilled cores span the entire 40 Ma interval of dyke intrusion.

Gladstone Stream		*Winterton River*	
Core	*Age(Ma)*	*Core*	*Age(Ma)*
A	76.3±1.3	A	70.6±1.2
B	66.0±1.0	B	83.3±1.3
D	81.4±1.2	C	78.0±1.3
F	85.8±1.2	D	74.0±1.4
G	82.3±1.2	E	59.6±1.2
J	100+1.4	F	67.4±1.0

Table 6.3: Ages obtained by K-Ar dating of sampled dykes (after Grapes et al 1992).

6.3.1b Demagnetization data for the Awatere Dykes

Gladstone Stream Site

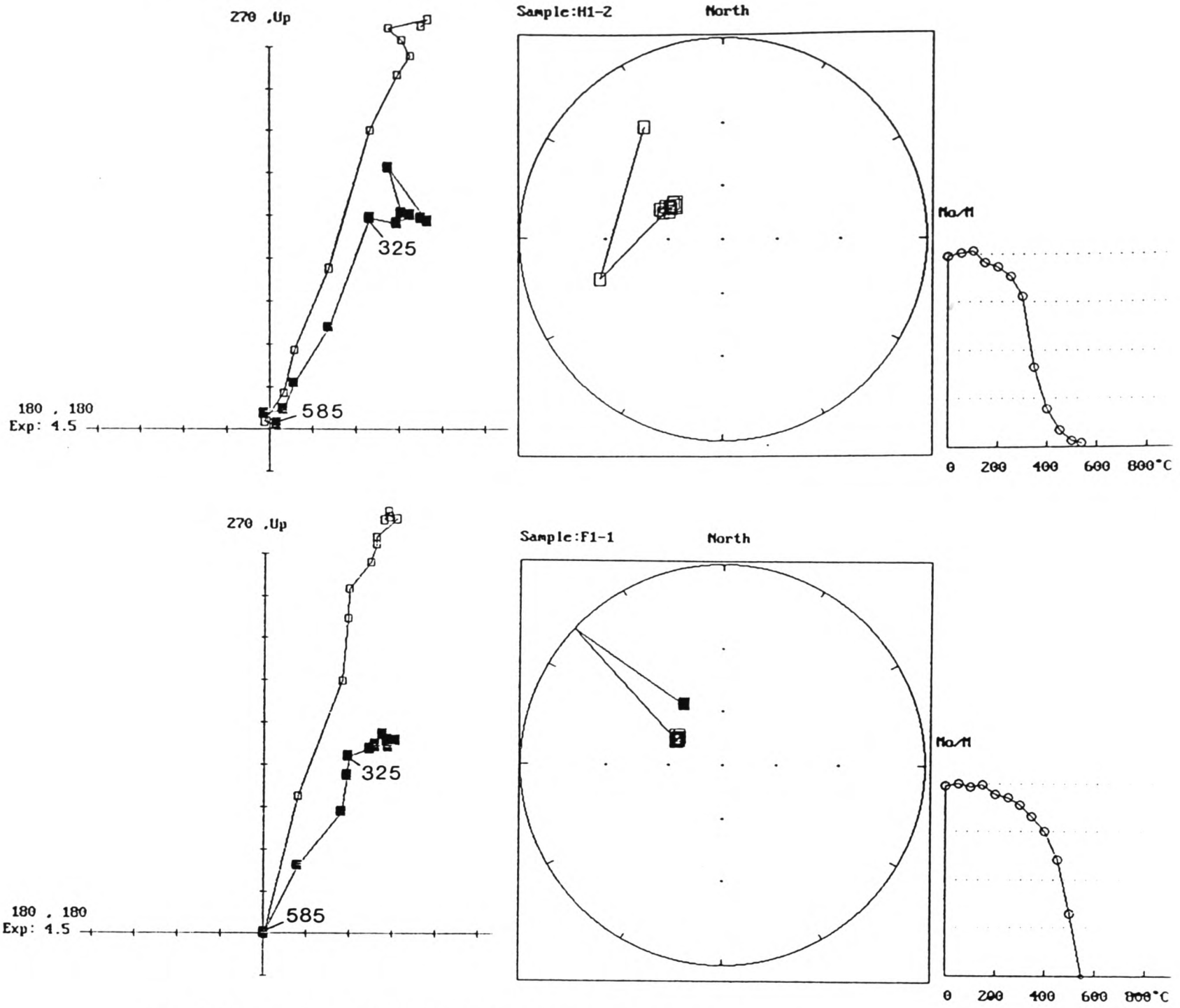
Z-plots showing the demagnetization of these cores are shown in fig 6.3a alongside corresponding graphs of intensity change and Wulf net projections of magnetization change with temperature. An unstable low temperature component was removed after heating to 270/325^{o}C and a stable high temperature component removed between 270/325 and 585^{o}C. The high temperature component trends to the origin. This component is clearly picked out on Wulf net projections of the demagnetization.

The high temperature components from each core were computed using IAPD and the resulting vectors plotted in fig 6.3b. The mean, primary magnetization for site GS1 is 313/-60^{o} (α95: 4.8).

Winterton River Site

Two representative Z-plots with corresponding intensity change for this site are shown in fig 6.4a. Removal of a low temperature, unstable magnetization was observed in three of the cores after heating to 100^{o}C. This is followed by a linear progression to the origin during removal of the high temperature component between 100 and 585^{o}C. The remaining cores again displayed two components of magnetization. However, although these samples give an apparently reliable stable end point, the plotting of the high temperature component gave considerable variability. The straight line, single component segments in these samples are separated by a curved segment. This is a common phenomena of overlapping blocking temperature spectra of the remanence carrier grains. This also explains the variability in the high temperature components. Wulf net projections of the demagnetization of these cores plot on great circles. Examples of each type of demagnetization are shown in fig 6.4a. It was attempted to obtain the high temperature component using great circle analysis on all samples displaying overlapping blocking

a). GS1 thermal demagnetization.



b). GS1 uncorrected high temperature components.

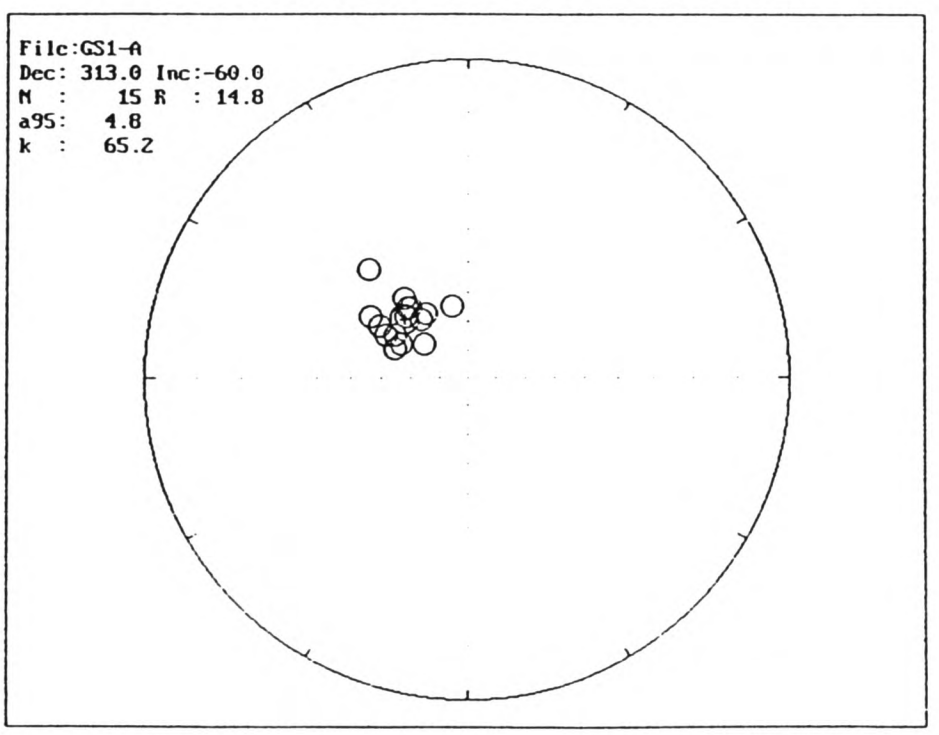
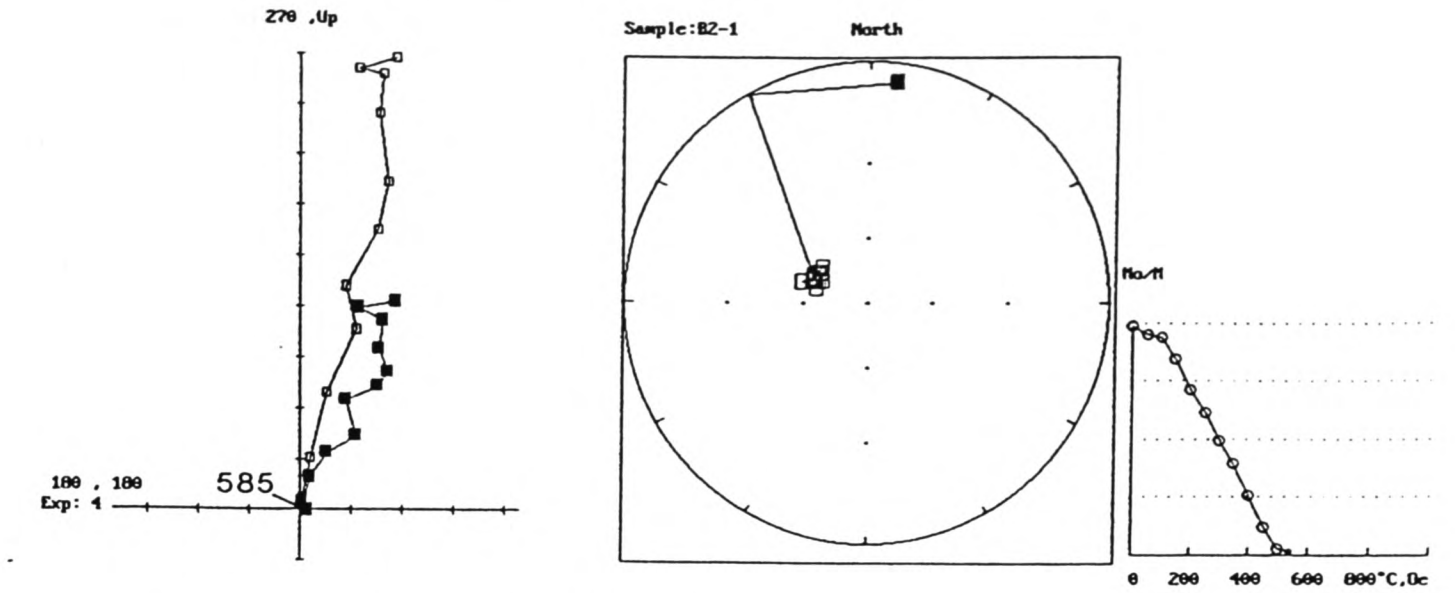
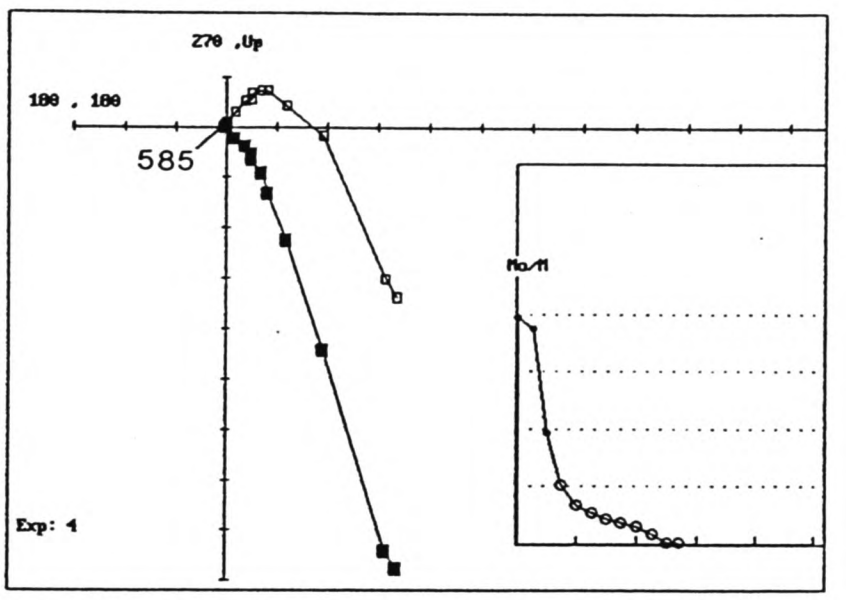


Fig 6.3: Data from Gladstone Stream (GS1). a). typical behaviour during thermal demagnetization of GS1 site cores. b). high temperature components from all GS1 site cores. All data is uncorrected.

a). WS1 thermal demagnetization.



(example of core reaching a stable end point)



(example of core reaching an apparent but spurious 'stable' end point)

b). great circles

c). calculation of the mean primary direction.

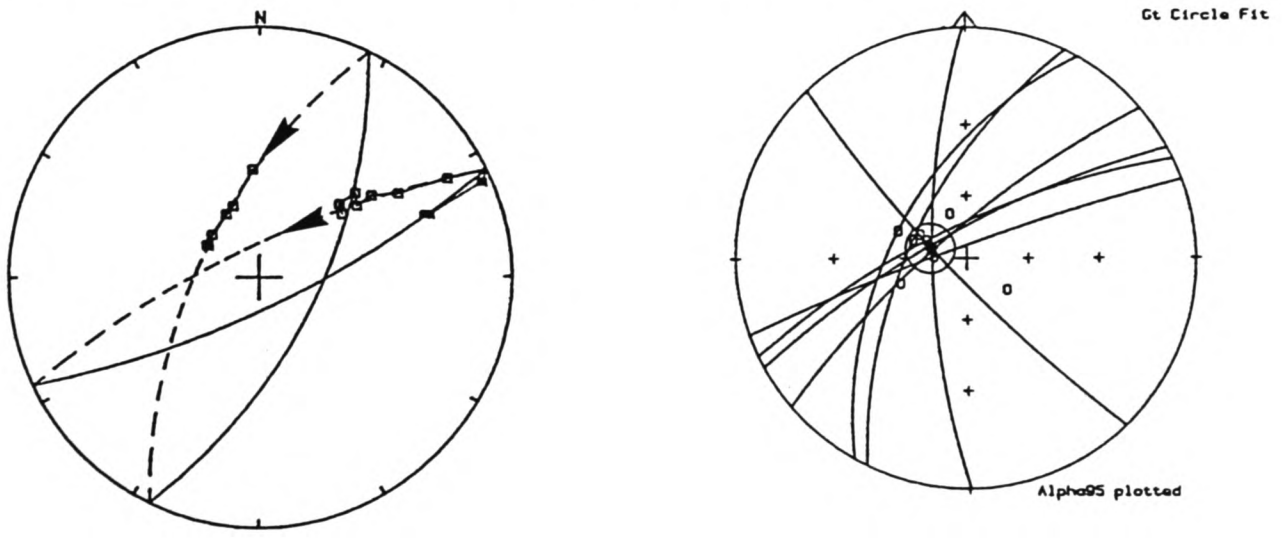


Fig 6.4: Data from the Winterton River (WS1). a). typical behaviour during thermal demagnetization of WS1 site cores. b). example of intersecting great circles used in the calculation of the primary component and c). calculation of the mean primary component from all thermally demagnetized cores. All data is uncorrected.

temperature spectra (figs 6.4b and 6.4c). The reason that great circle analysis succeeded in this case to recover the primary component from cores from a single site, was because the overprinted, secondary components varied from core to core and thus the vectors track from different directions. It is postulated that this variable secondary magnetization is a consequence of the random remagnetization of low coercivity grains during the collection and storage of these samples prior to analysis. Fig 6.4b shows two of the intersecting great circles used to calculate a primary magnetic vector. Fig 6.4c presents the calculation of the mean primary component using all the great circles and the three end point directions. The mean intersection point (the mean primary component) from these cores is 285.19/-75.06 (α_{95}: 11.83).

6.3.1c Assessment of the magnetic carriers

Grapes et al (1992) list the mineral assemblage of the dykes. The only listed ferromagnetic mineral is Titanomagnetite and therefore it is this mineral which must hold both the secondary and primary components. Total demagnetization was achieved after heating to 585^{o}. This is close to the maximum Curie Temperature of magnetite grains (575^{o}). The low temperature component was removed by 325^{o}C. This temperature is close to the temperature for disorder of pyrrhotites (*ca.* 310^{o}). However there is no evidence for the presence of this mineral and low blocking temperature magnetite grains could be responsible. The high initial intensities of all these samples indicated that single domain rather than lower coercivity multi domain magnetites are likely to be present.

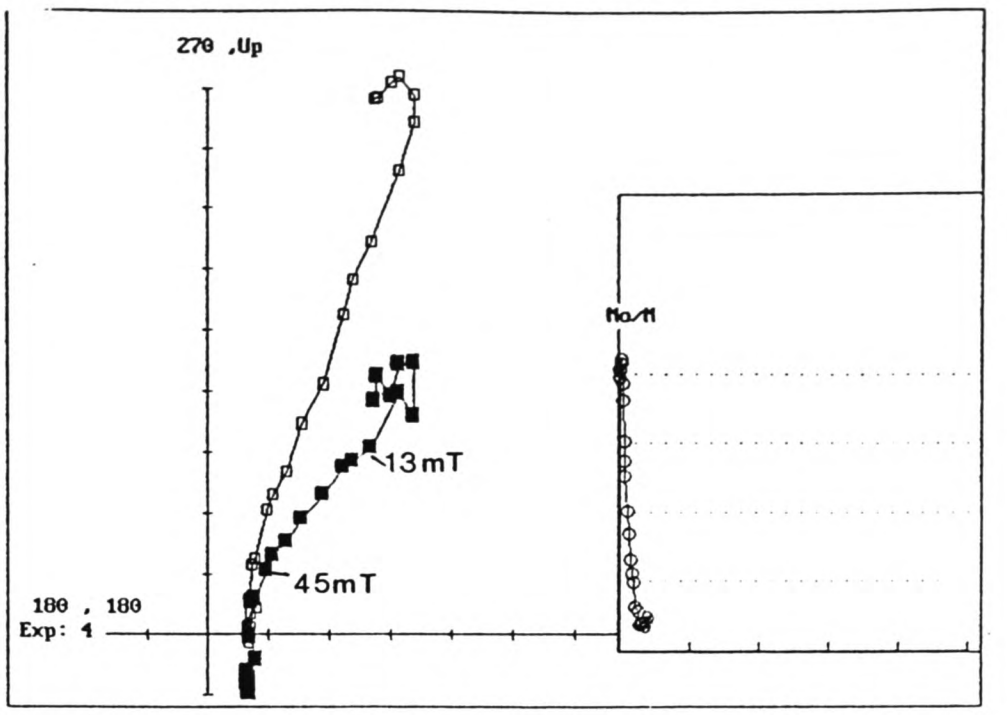
Alternating Field Demagnetization

Four cores from site GS1 and five from WS1 were demagnetized by this technique in order to confirm whether magnetite was the remanence carrier. Demagnetization Z-plots for the GS1 and WS1 sites are shown in figs 6.5 and 6.6 respectively.

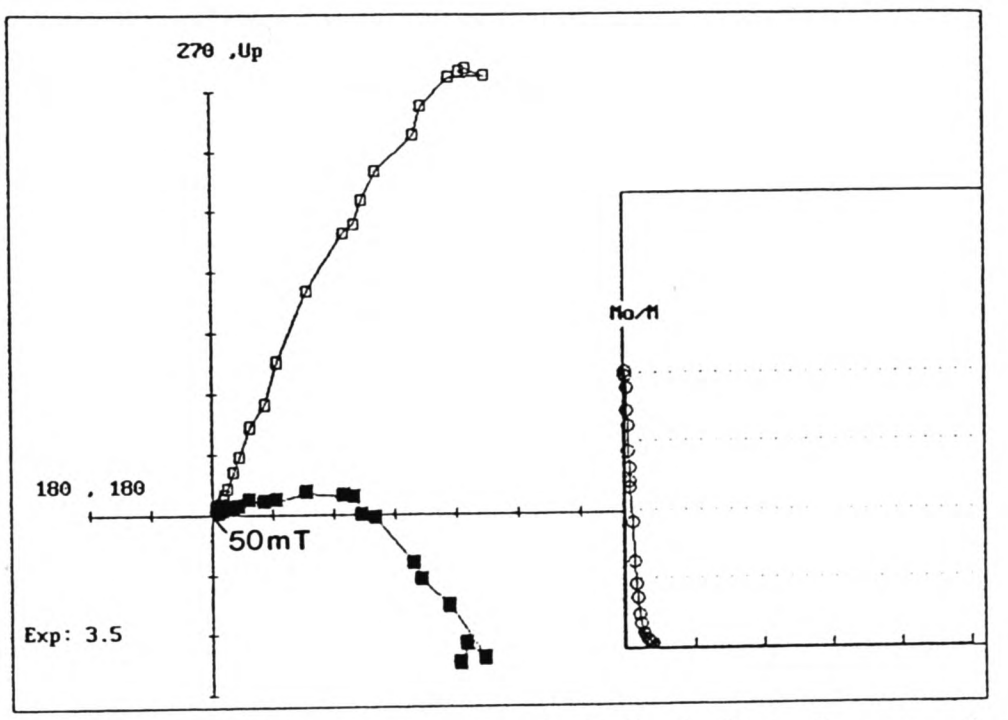
Gladstone Stream. All Z-plots display a low coercivity component removed after exposure to an alternating field of 13 mT and a high coercivity component removed between 13 and 50 mT. However the paths are not straight lines but are curved. In two of the four cores, the primary component is diverted from its path towards the origin after 45 mT. After this point these samples became unstable. This was most likely a result of the growth of a new magnetic phase.

Due to the curvature of all these plots the high coercivity components were calculated using great circle analysis, fig 6.5b and 6.5c. The mean high coercivity component from this technique is 317.84/-63.54 (α_{95}: 13.12). This error circle clearly overlaps that of the mean primary magnetization direction obtained by thermal demagnetization. The same component has therefore been removed by both techniques, indicating that the primary magnetization was indeed held by magnetite grains.

a). GS1 alternating field demagnetization.



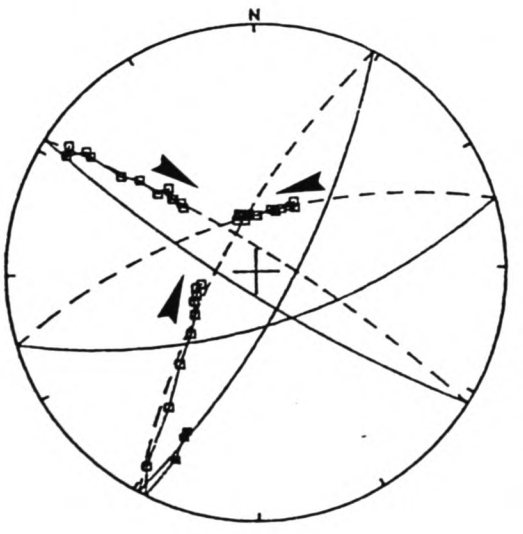
a1-2



c3-1

b). Great circles.

c). Calculation of mean primary direction.



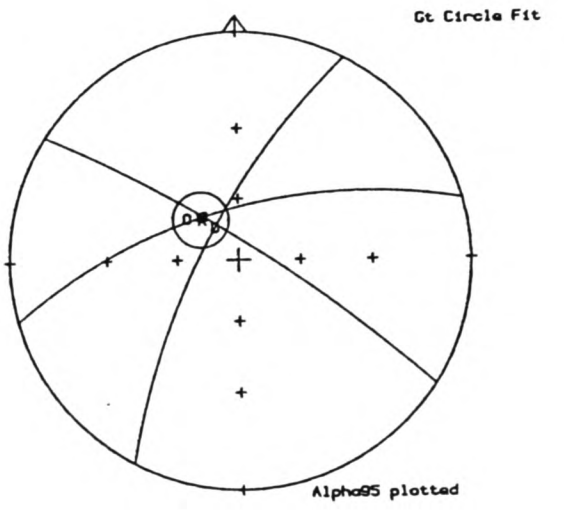


Fig 6.5: a). Typical behaviour during alternating field demagnetization of samples from the Gladstone Stream site (GS1). b). example of great circles used to calculate the high coercivity component, and c). the mean primary component from great circle analysis of all cores. All data is uncorrected.

Thermal demagnetization of cores from this site did not show overlapping blocking temperature spectra. The fact that cores demagnetized by alternating field displayed overlapping coercivity spectra must be a property of the particular magnetic phases present.

Winterton Stream. For this site it was possible to distinguish two components separated by curved segments identical to those obtained by thermal demagnetization. In all cases a low coercivity component was removed by exposure to an alternating field of 13 mT. All demagnetization paths appeared to reach a stable end point at the origin after exposure to an alternating field of 50 mT. However, due to the curvature of the plots the mean primary magnetization direction was calculated using great circle analysis (figs 6.6b and 6.6c). The mean primary magnetization direction from this data is 289.63/-69.56, a_{95}: 18.02). This overlaps with the mean primary component as obtained by thermal demagnetization, indicating that magnetite grains also hold the primary component at this site.

Nitrogen Treatment

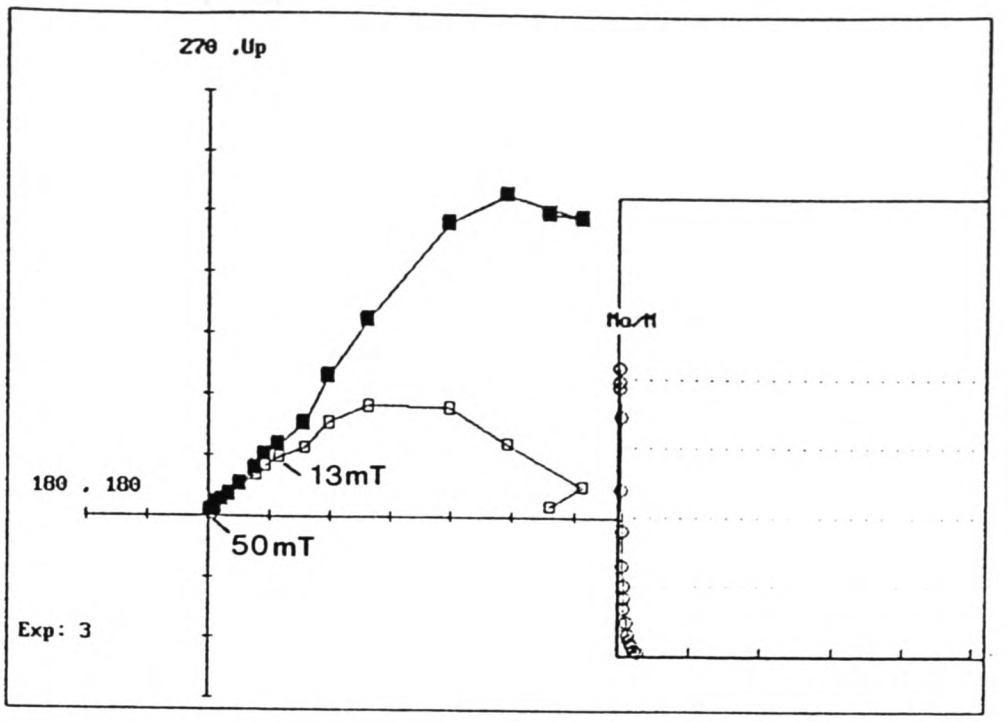
The same cores which were subjected to alternating field demagnetized were subsequently tested for percentage of single and multi-domain magnetites (eg: Merril 1970). This technique involves measuring the NRM intensity, then submerging the cores in liquid nitrogen to randomize all the multi-domain material. This was done in a m-metal box to ensure that the multi-domain material did not become magnetized on warming. The intensity was then measured again to record the intensity held by single domain grains. See table 6.4 for results. The percentage changes for all cores tested in this way were minimal (a few degrees only) which indicated that single-domain magnetites are the dominant magnetic phase.

Bulk Susceptibility

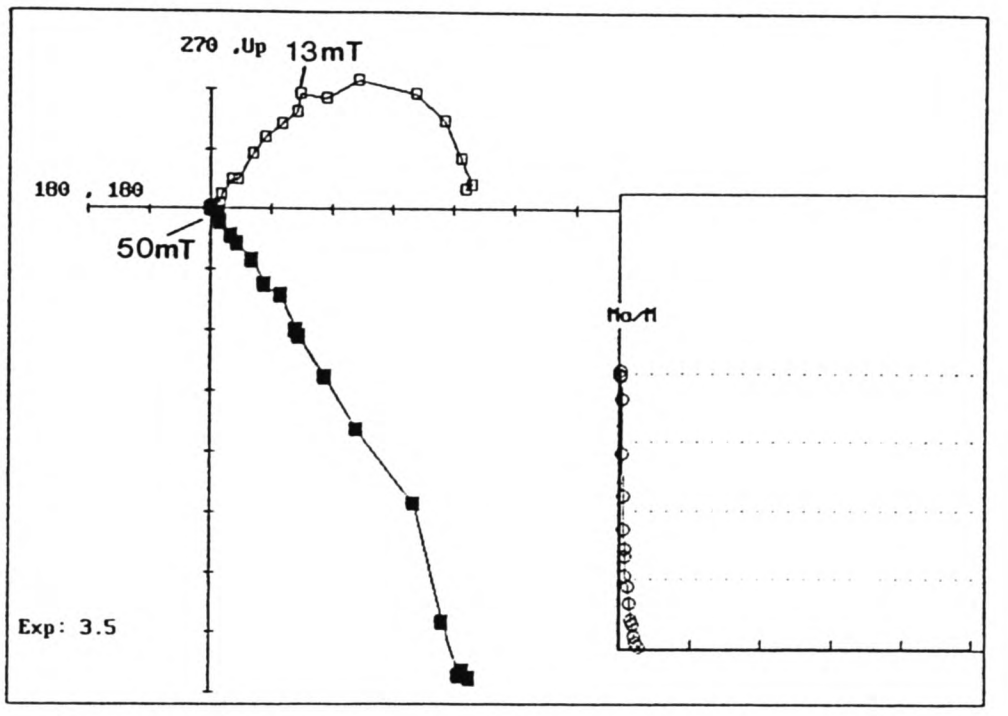
The bulk susceptibility of all thermally demagnetized cores was measured after each temperature step. A plot of normalized bulk susceptibility against temperature for three representative GS1 site cores is shown in fig 6.12a. Bulk susceptibility is seen to rise gradually after heating to 100^{o}C.

Fig 6.12b shows representative bulk susceptibility plots for WS1 site cores. All display a gradual increase to *ca.* 200^{o}C remaining constant to *ca.* 375^{o}C and then falling to 585^{o}C. The primary component was removed during the decreasing section of this graph.

a). WS1 alternating field demagnetization.



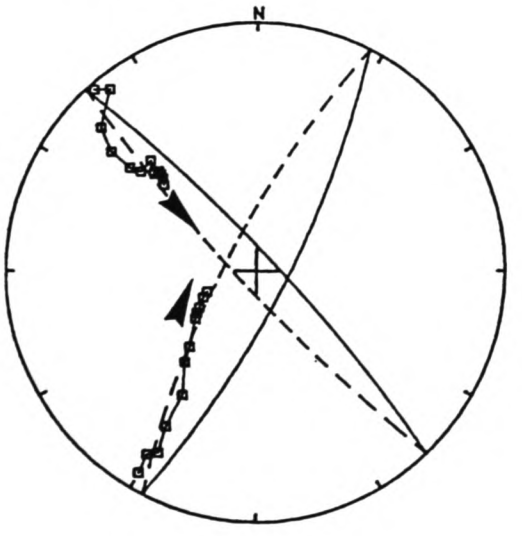
a1-2



c3-1

b). great circles.

c). calculation of the mean primary direction.



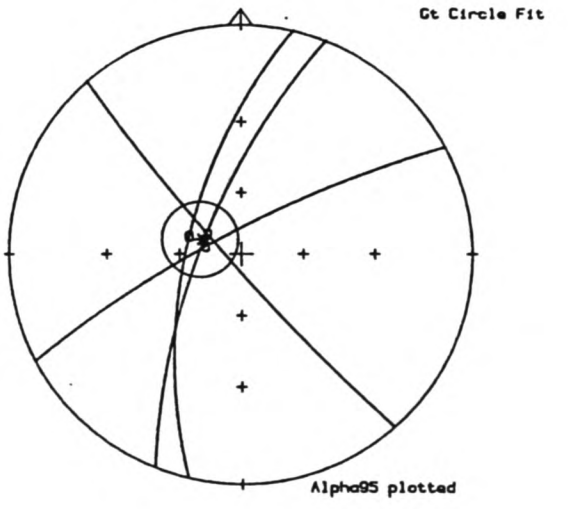


Fig 6.6: a). Typical behaviour during alternating field demagnetization of samples from the Winterton River site (WS1). b). example of intersecting great circles and c). calculation of the mean primary component from all cores demagnetized in this way. All data is uncorrected.

	Initial intensity	Intensity after treatment	% of initial intensity
GS1 cores			
a2-2	1615.907	1636.953	101
c3-2	0773.682	0787.525	102
e1-2	0777.189	0757.846	098
e2-2	0378.432	0403.027	106
g1-3	0808.298	0813.816	101
h2-2	0671.217	0628.410	094
j2-4	1243.519	1307.289	105
WS1 cores			
a1-3	0946.236	0850.528	090
b1-3	0019.576	0020.389	104
c1-3	1048.674	1021.220	097
c3-2	0727.558	0707.826	097
e1-4	0749.600	0571.743	076

Table 6.4: Nitrogen treatment data for sites GS1 and WS1.

Induced Remanent Magnetization

Three GS1 cores were treated in this way (fig. 6.12a). All these show identical graphs rising sharply and then levelling off after exposure to *ca.* 100 mT. The graphs all indicate the presence of magnetite, Ti-magnetite or pyrrhotites and the absence of haematite and geothite. The variations in the intensity reached at saturation point for each of the cores is a reflection of the differing amounts of Ti-magnetite or Ti-haematite present in each core.

Overall, single domain, titanomagnetite grains were the only identified remanence carriers.

6.3.1d Timing of the Magnetization

The mean directions from each site are identical within error with overlapping error circles. Since the same structural correction was used for both sites, this might imply either a regional, late, post-tilt magnetization, or an early pre-tilt magnetization. It is therefore important to determine the timing of magnetization to differentiate these two possibilities. Grapes et al (1992) found no evidence from either the field relations, changes in dyke chemistry, general geochemistry or petrography for evidence of weathering or later

hydrothermal activity. Thus it seems plausible that the magnetization was coeval with dyke crystallization between *ca.* 100 and 60 Ma (Grapes et al 1992).

A further attempt was made to determine the age of magnetization by sampling the country rock adjacent to a dyke. This constitutes a dyke test to ascertain the relative timing of the dyke magnetization with the magnetization in the wall-rock. Unfortunately the wall-rock is unsuitable for drilling and no full sequences of sediment at distances from any dyke could be collected. One core collected 2 cm from a dyke contact yielded an identical high temperature component direction to that of the dyke itself. This one would expect in baked wall-rock whose magnetization had been reset at the time of dyke intrusion. This alone provides no insight into the timing of magnetization which could have occurred at any time subsequent to dyke emplacement. A core from the chilled dyke margin gave an unusual high temperature component direction, as one might expect due to the fast cooling rate in this area of the dyke. The magnetic grains might record secular variation. This together with the lack of any evidence for alteration (Grapes et al 1992), suggests that the magnetization is indeed related to dyke intrusion. Furthermore, after tectonic correction the inclination for both sites restores to a value in keeping with the approximate age of these dykes (refer to section 7.2.1). This indicates that the magnetization was not only obtained pre-tilt, but that it is also likely to be related to the formation of these samples.

6.3.2 Woodside Creek Limestone (sites WC1 and WC2).

WC1: 174°04'/41°56' (GR: (P30) 990192).
WC2: 174°05'/41°56' (GR: (P30) 995184).

6.3.2a Geological Setting, lithology and age

Stratigraphy and structure of the area

These sites are located within a thrust pile subsequently folded into an anticlinal structure (the gently plunging Benmore Anticline which has a fold axis of 048/10) between the Clarence and Kekerengu Faults. The eastern limb of this anticline is truncated by the Kekerengu Fault and London Hills Fault. The western limb outcrops parallel to the Clarence Fault. The location and nature of this structure is shown in fig. 4.1. Detailed mapping of the area was first completed by Prebble (1976) and then later by Waters (1988) who labelled the area the Flags Creek Duplex. The stratigraphy of Late Cretaceous to Middle Miocene sediments has already been mentioned in section 2.4. Pre-fold thrusts duplicate Upper Cretaceous to Tertiary cover sediments, particularly Amuri Limestone lithologies. More information regarding the detailed pre-fold thrusts and fold related fabrics is described in section 4.2.1.

Fig 6.7 shows a map of the duplex taken from Waters (1988). This figure also shows the location of sites WC1 and WC2 within the structure. The sites are found close to

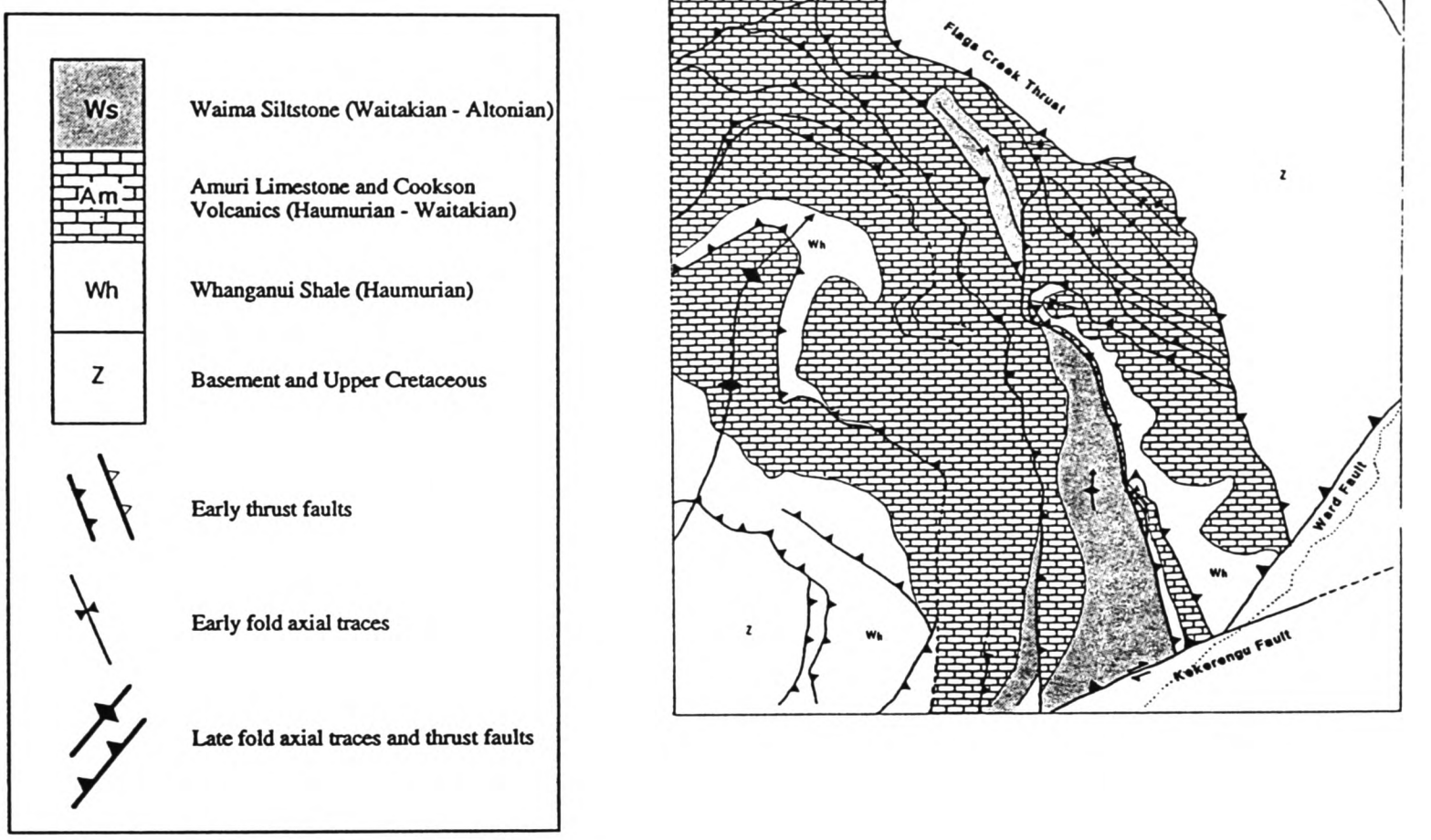


Fig 6.7: Geology of the Flags Creek Thrust Duplex and location of drilled sites along Woodside Creek (WC1 and WC2).

the NNW-trending Flags Creek Thrust in the eastern nose region of the Benmore Anticline. The unit youngs and dips at *ca.* 50^{o} to the NNE between NNW-trending thrust surfaces which dip steeply at *ca.* 70-80^{o} to the ENE.

Lithology of the limestone

Both sites are taken from a siliceous limestone which has an irregularly mottled pink-white colour. Fresh, unweathered rock from the steep sides of the river gorge was sampled. Sedimentary structures are not apparent except for scattered lenticular chert nodules (3-4 cm thick) which define bedding. Planar to slightly undulating spaced fracture surfaces (separation 0.5-2.0 m) parallel the cherts at site WC1. The same is true at WC2, although here the undulation of bedding parallel surfaces is more defined and the separation of these planes is closer at 0.15-0.5 m. Calcite filled fissures are commonly perpendicular to bedding.

The limestone in thin section (fig. 6.13a) appears as a foraminiferal biomicrite and sparite filled *globigerina* tests make up 40% of the rock. Angular silt grains and subangular glauconite grains constitute a further 1%. Rare tiny opaques were observed which tend to cluster. All these were enclosed within a dark micritic matrix. The foraminifera indicate a pelagic limestone. However, the presence of quartz and glauconite grains suggests that it was not far from the continental shelf.

The colour variation in this limestone can be seen both on an outcrop and thin-section scale. The pink colour indicates the presence of trace haematite in the rock. In thin-section this colour variation is seen to be a direct result of differing concentrations of dark micritic matrix in comparison to lighter areas dominated by *globigerina* tests. The pink colouration therefore seems to be concentrated within the micritic matrix. Attempts to identify oxide grains within the matrix were made using the microprobe, SEM and EDS. None of these techniques were successful due to the grain size of these grains being beyond the resolution of these machines. The opaque grains seen in thin section are Fe-rich, Ca-Si minerals.

Also apparent in thin section were thin (0.002 mm), dark, short seams which showed minor truncation of *globigerina* tests. (All techniques to identify oxides within these seams also failed). Their non-traceability, poorly defined nature and lack of oxides indicated tiny concentrations of clay material formed under early diagenetic, compactional stress.

All attempts to identify oxides (particularly haematite whose presence is indicated by the pink colouration of this limestone) by microscopic techniques failed because of the minute grain size of these grains. Magnetic experiments were more successful (see section 6.3.2c).

Age of the limestone

The pinkish limestone at site WC1 unit sits 45 m horizontally above the K/T boundary (Strong 1977). Using an average dip of 51^{o} N over this distance the sites are

approximately 35 m above the K/T. Assuming a maximum average sedimentation rate (see 5.5) of 2 cm/ka indicates that the sites are 1.75 Ma younger than the K/T, approximately 63 Ma (Paleocene). Alternatively if one assumes a minimum sedimentation rate of 0.3 cm/ka, the site is aged at approximately 54 Ma (Lower Eocene). The exact age is likely to fall somewhere between the two values (63-54 Ma). A sample collected from limestone on the north side of the Woodside Creek gorge by Warren (1976) gave an age of *Teurian* to *Waipawan*, which corresponds to *ca.* 66-54 Ma, overlapping with the estimated age range from sedimentation rates.

Site WC2 is from a similar stratigraphic position, although is less well constrained in position due to its more isolated location.

6.3.2b Demagnetization data for the Woodside Creek sites

Prior to demagnetization the cores had low initial intensities starting at *ca.* 0.5 mAm^{-1} for site WC1 and even weaker at *ca.* 0.17 mAm^{-1} for WC2. Representative Z-plots, demagnetization curves and Wulf net projections are shown in figs 6.8 and 6.9 for WC1 and WC2 respectively. For the WC1 cores demagnetization Z-plots clearly displayed two components with a linear, high temperature component removed between 220 and 640^{o}C to the origin. The components were less clearly picked out for the weaker WC2 site cores. However, linear sections of the plots were recognized directed towards the origin and which were removed at the same high temperature demagnetization steps as those for the high temperature component of WC1.

All the high temperature components were calculated using IAPD and are plotted in figs 6.8b and 6.9b for the WC1 and WC2 sites respectively. The mean primary component at site WC1 is 235/45 (α_{95}: 3.2) and at WC2 is 330/76 (α_{95}: 8.0).

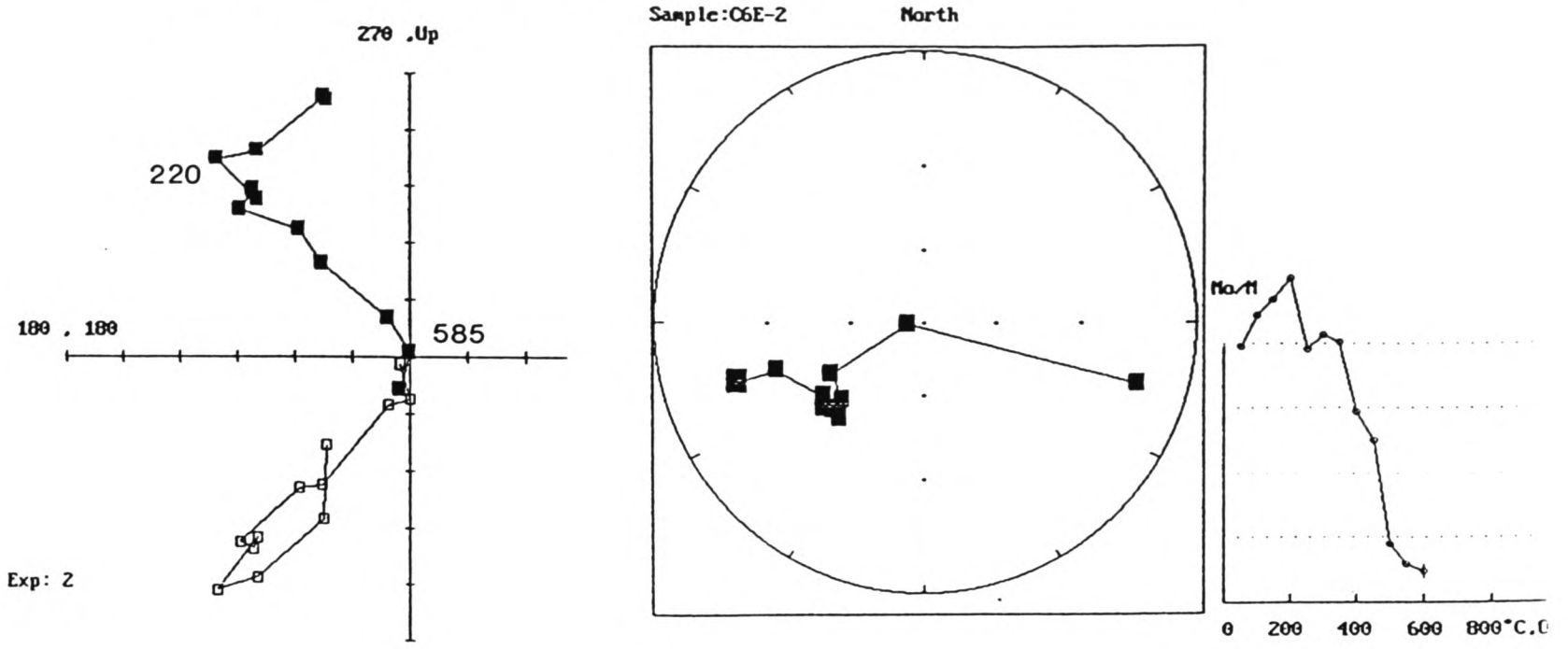
6.3.2c Assessment of the magnetic carriers

As stated in 6.3.2b, all attempts to identify ferromagnetic minerals by probe, EDS, SEM and reflected light were unsuccessful. The maximum temperature required to remove the magnetization in these cores was *ca.* 640^{o}C. This temperature is beyond that of the maximum temperature at which magnetite grains are known to unblock and close to the maximum unblocking temperature of haematite (575^{o}C). This suggests that haematite holds at least in part some of the high temperature component. The pink colouration of these cores also indicates the presence of haematite in trace amounts. Magnetite grains, if present, are likely to be multidomain due to the low initial intensities of these samples.

IRM

Fig 6.12c shows a typical plot of intensity against induced field strength in cores of this lithology. All cores treated in this way showed identical graphs of increasing intensity up to *ca.* 100 mT and levelling off between 100 and 200 mT, before rising continuously to

a). WC1 thermal demagnetization.



b). WC1 uncorrected high temperature components.

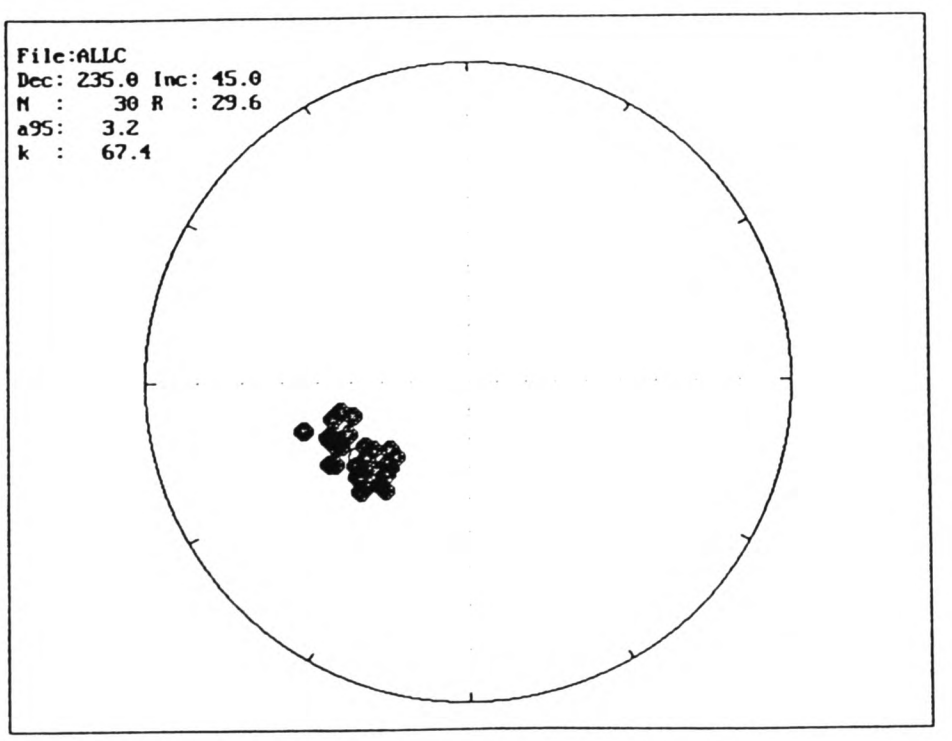
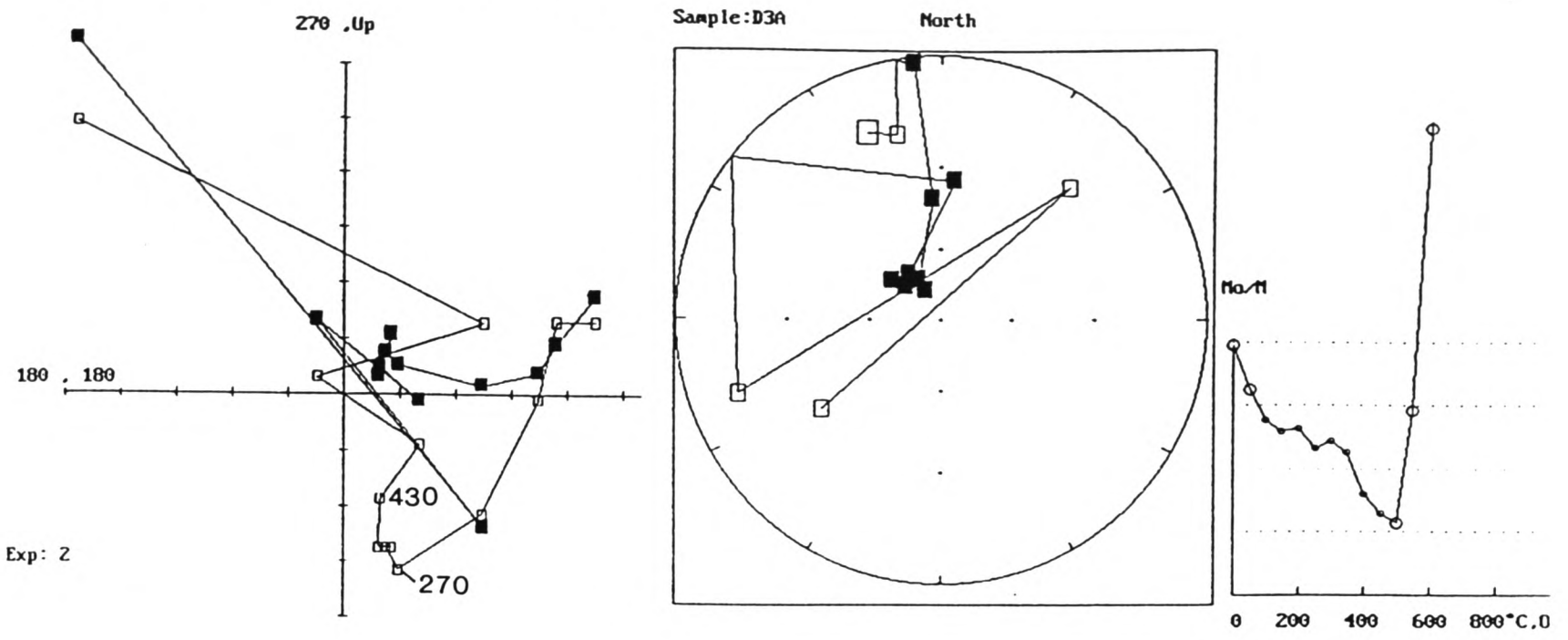
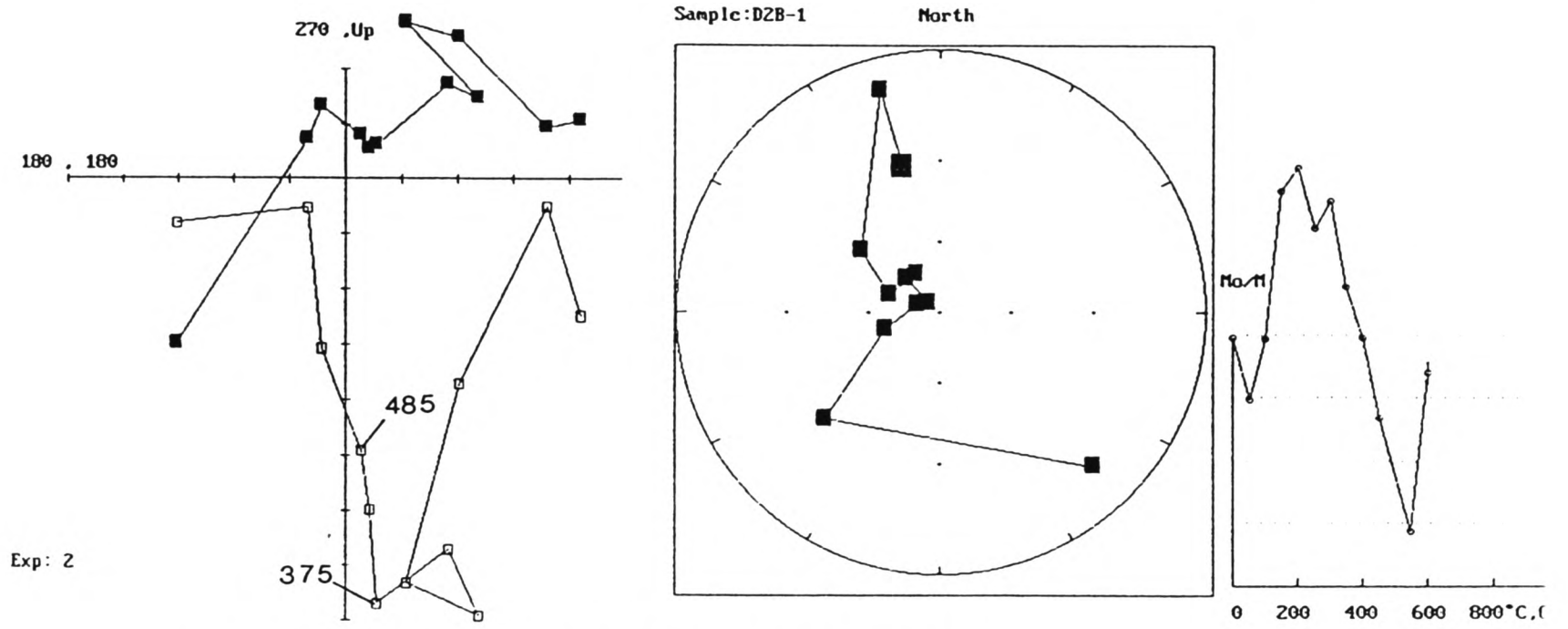


Fig 6.8: Data from Woodside Creek (WC1). a). typical behaviour during thermal demagnetization of WC1 site cores. b). high temperature components from all WC1 site cores. All data is uncorrected.

a). WC2 thermal demagnetization.





b). WC2 uncorrected high temperature components.

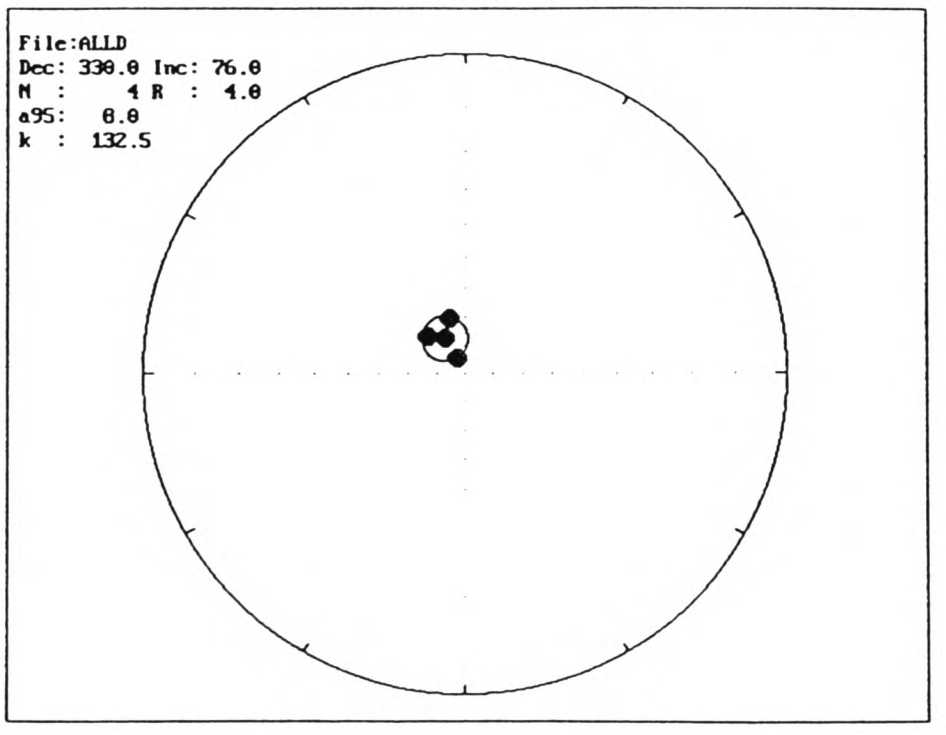


Fig 6.9: Data from Woodside Creek (WC2). a). typical behaviour during thermal demagnetization of WC2 site cores. b). high temperature components from all WC2 site cores. All data is uncorrected.

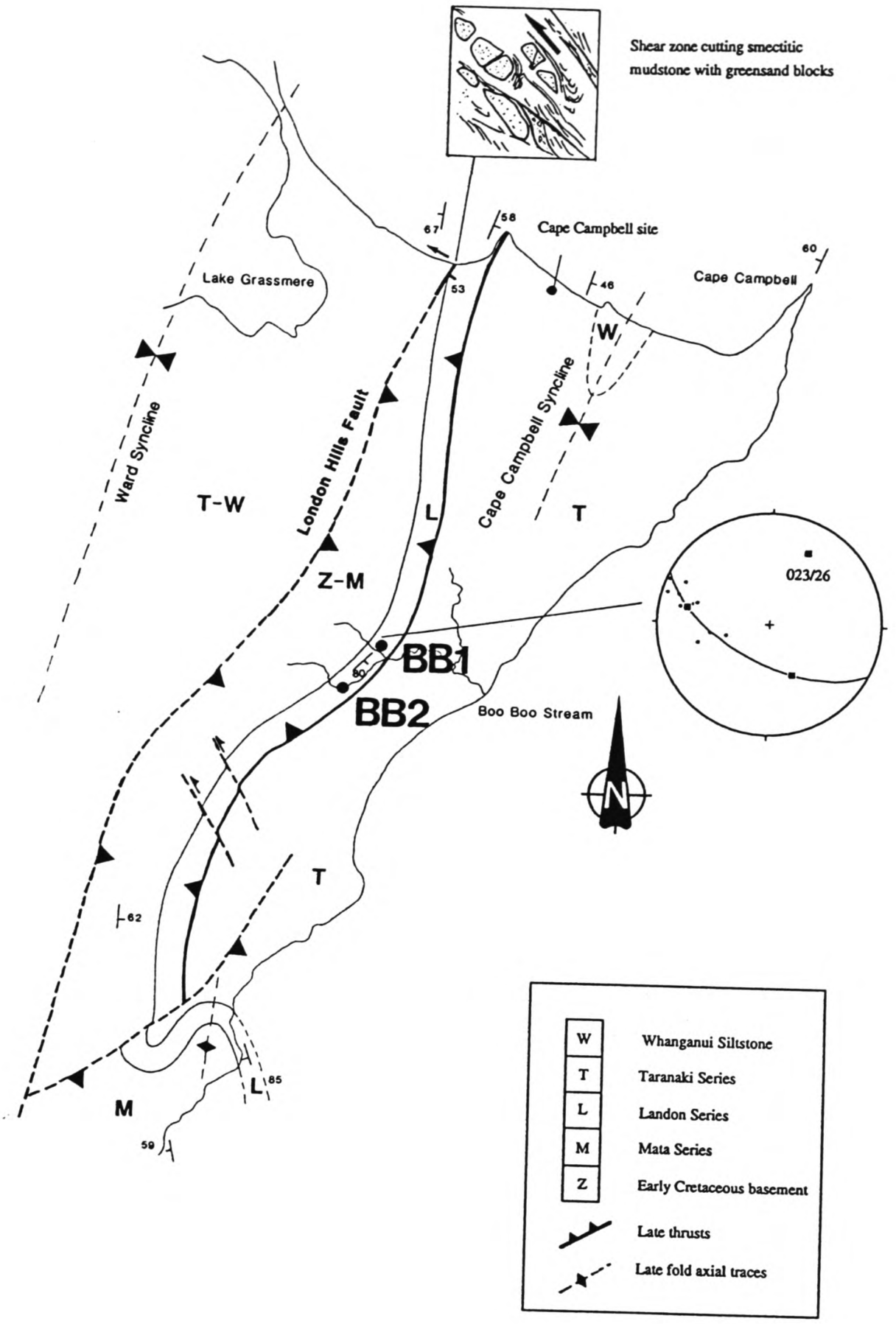


Fig 6.10: Geological map of the Ward - Cape Campbell subregion showing location of drilled sites (BB1&2, this study; Cape Campbell site, Walcott et al 1984).

magnetization. Typical Z-plots of the demagnetization of these cores are shown in fig 6.11a alongside their corresponding intensity change graphs and Wulf net projections. An unstable, low temperature magnetization removed by 220°C. A stable, high temperature component was then removed between 220 and 585°C. In most cases, this second component plots on a line to the origin. It is linear but not perfectly so, a refection of the weak initial intensity of these cores. Fig 6.112b shows a plot of all the high temperature components for both sites together calculated using IAPD. (Mean direction: 303/9, $\alpha 95$: 12.8). It should be noted that the individual data points in fig 6.11b come from beds with slightly different dip and strike. This explains the relatively high variability to the mean direction.

6.3.3c Remanence carriers

The maximum temperature required to remove all the primary magnetization component was 585°C. This is close to the maximum unblocking temperature of magnetite grains (575°C), suggesting that at least some of the magnetization is held by magnetite grains. The low initial intensities of these cores suggests that the magnetites are multidomainal. The faint pink colouration suggests trace quantities of haematite which may also be contributing to the magnetization though this is not apparent on the demagnetization plots.

Bulk susceptibility

Graphs of bulk susceptibility from two of these cores are shown in fig 6.12d. A sharp increase in bulk susceptibility after 500°C suggests alteration of the mineralogy at this temperature corresponding to an unstable magnetization.

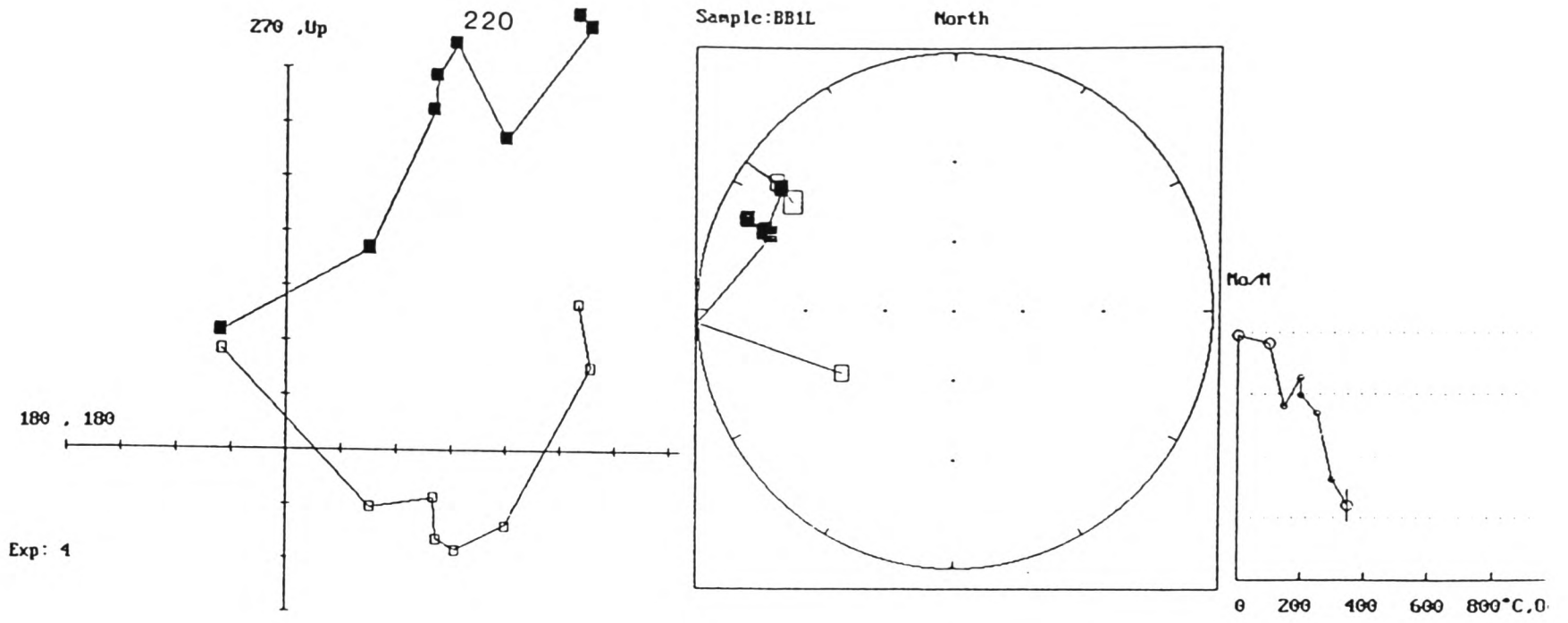
IRM

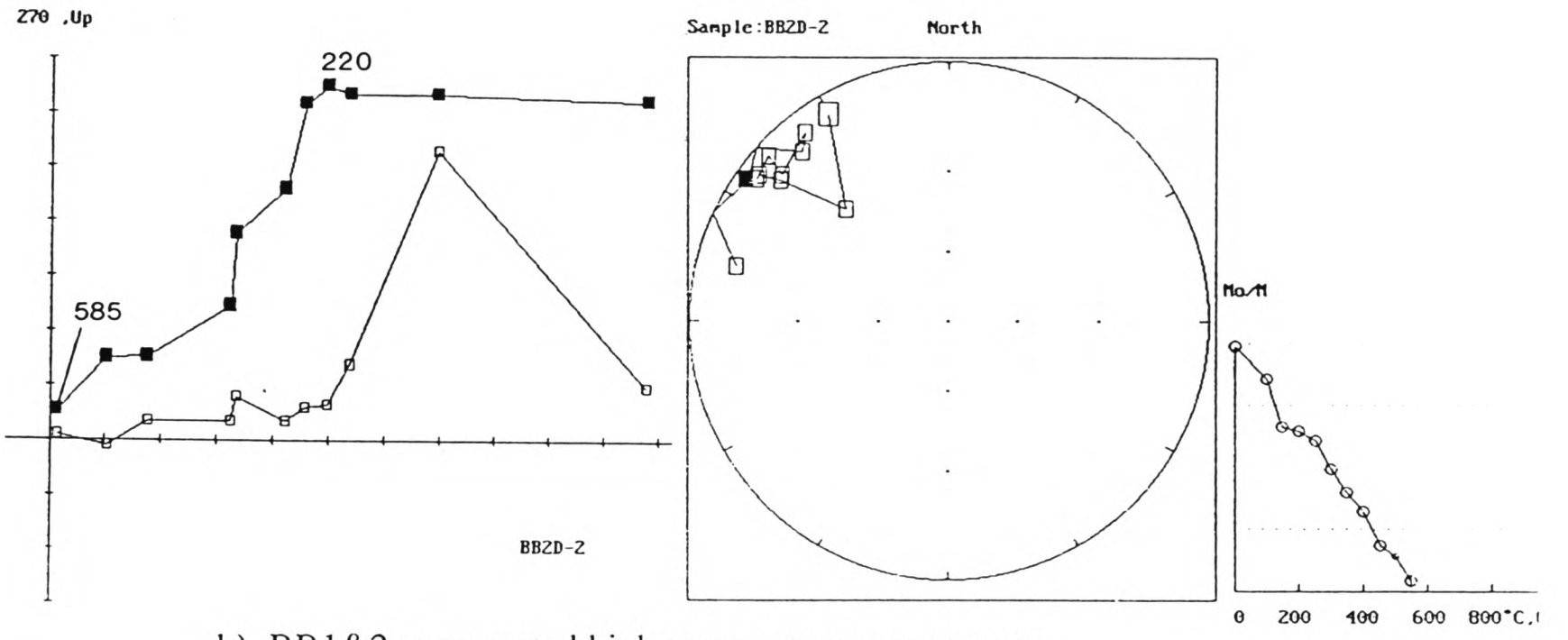
Fig 6.12d also shows a graph of intensity against induced magnetization for one of the Boo Boo stream site cores. This plot clearly indicated the presence of multi-domain magnetite, Ti-magnetite, or pyrrhotites by the levelling off after rapid increase in intensity up to *ca.* 100 mT. However, rather than remaining horizontal, the curve slopes very gently upward. This positive slope above *ca.* 100 mT indicated the additional presence of a mineral not saturated by 100 mT. This other mineral may be either geothite or haematite. Due to the very faint pink colouration of some of the cores from these sites haematite is likely to be the other mineral hinted at by this graph.

6.3.3d Timing of the magnetization

No evidence to suggest alteration was found in this lithology. Only fresh crystals were observed. After tectonic correction (section 7.2.1) the $\alpha 95$ value decreased and the inclination became a more acceptable value considering the age of this limestone. This

a). BB1&2 thermal demagnetization.





b). BB1&2 uncorrected high temperature components.

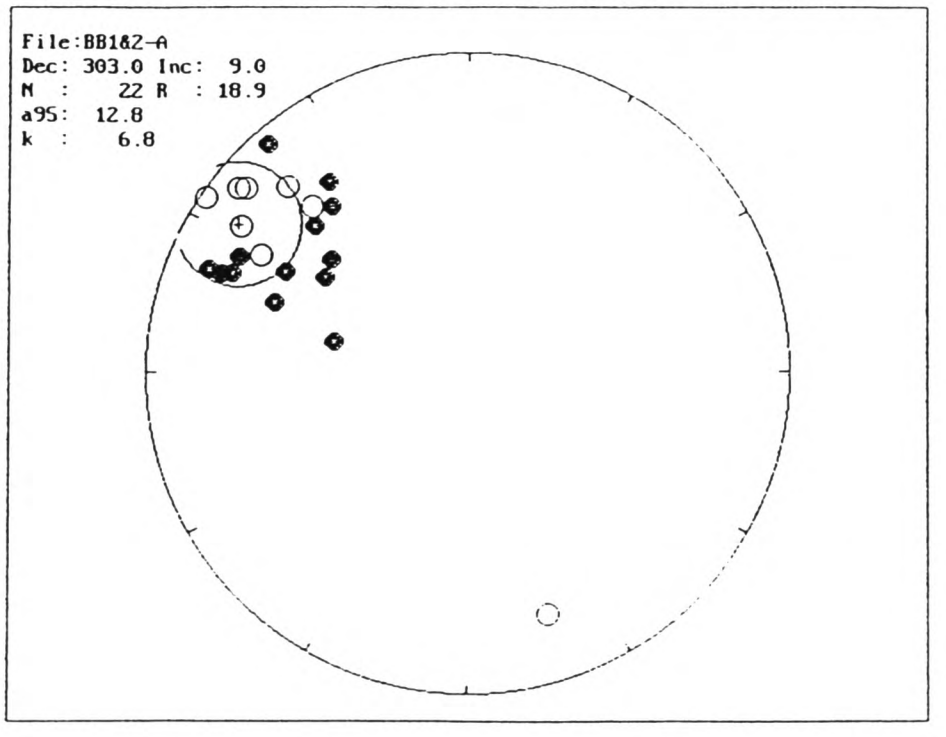
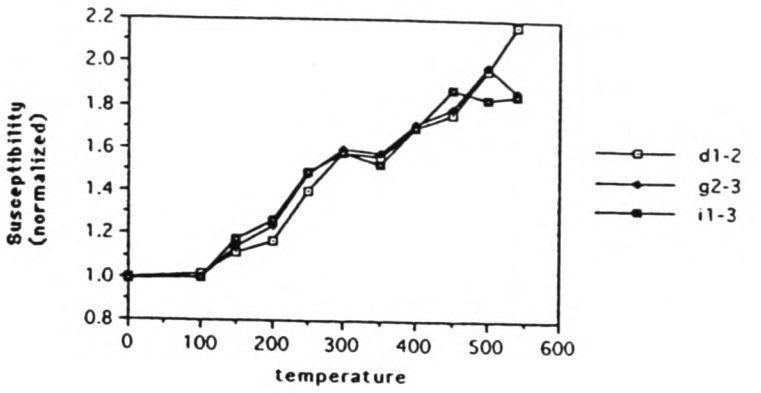
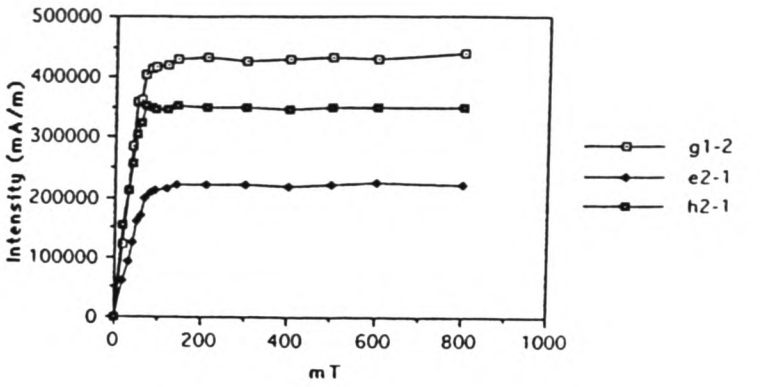


Fig 6.11: Data from Boo Boo Stream (BB1&2). a). typical behaviour during thermal demagnetization of BB1&2 site cores. b). high temperature components from all BB1&2 site cores. All data is uncorrected.

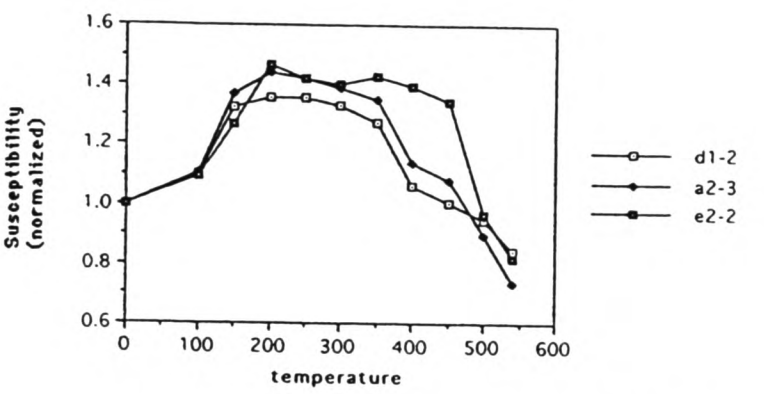
a). GS1 bulk susceptibility



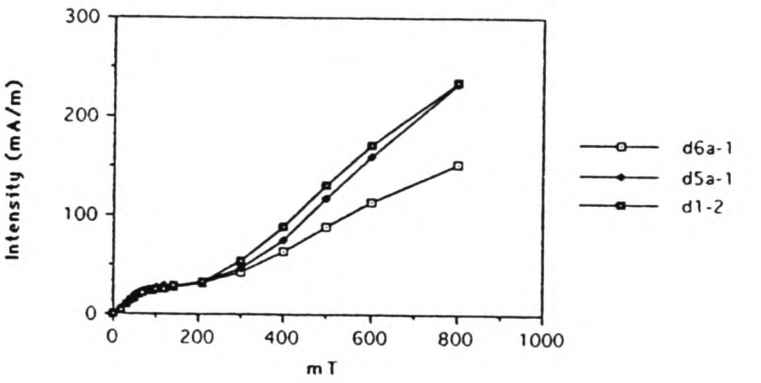
IRM



b). WS1 bulk suceptibility

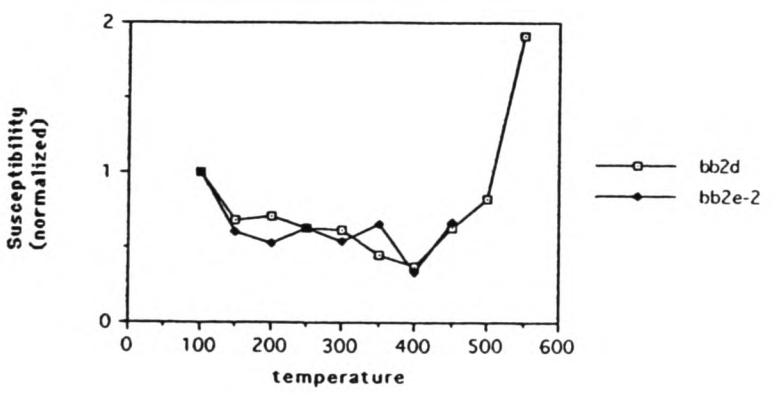


c). WC2 IRM



d). BB1&2 bulk suceptibility

IRM



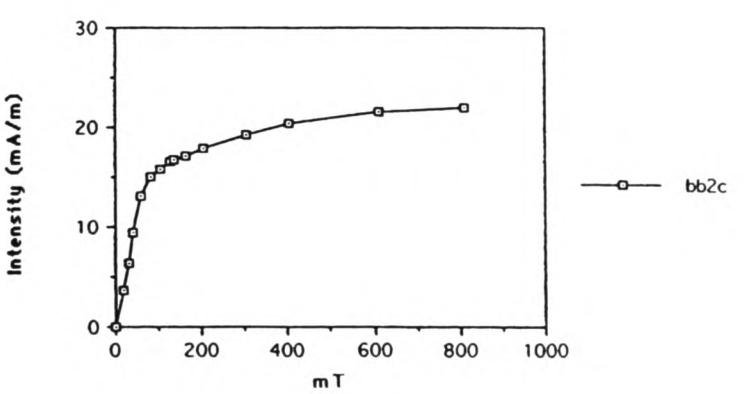


Fig 6.12: Bulk susceptibility and IRM graphs for sites a). GS1, b). WS1, c). WC2 and d). BB1&2.

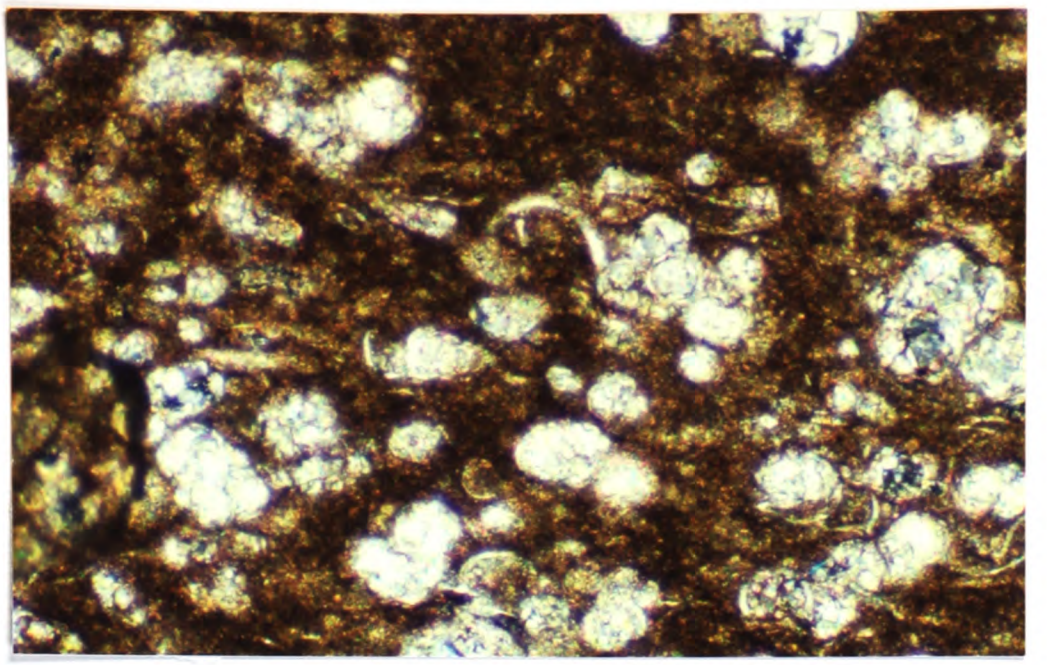


Fig. 6.13a: Photomicrograph of biomicritc pelagic limestone from the Amuri Limestone Group. Broken and un-broken globigerina tests are clearly visible. Sample taken from site WC1. Long axis of photograph: *ca.* 0.5 mm.

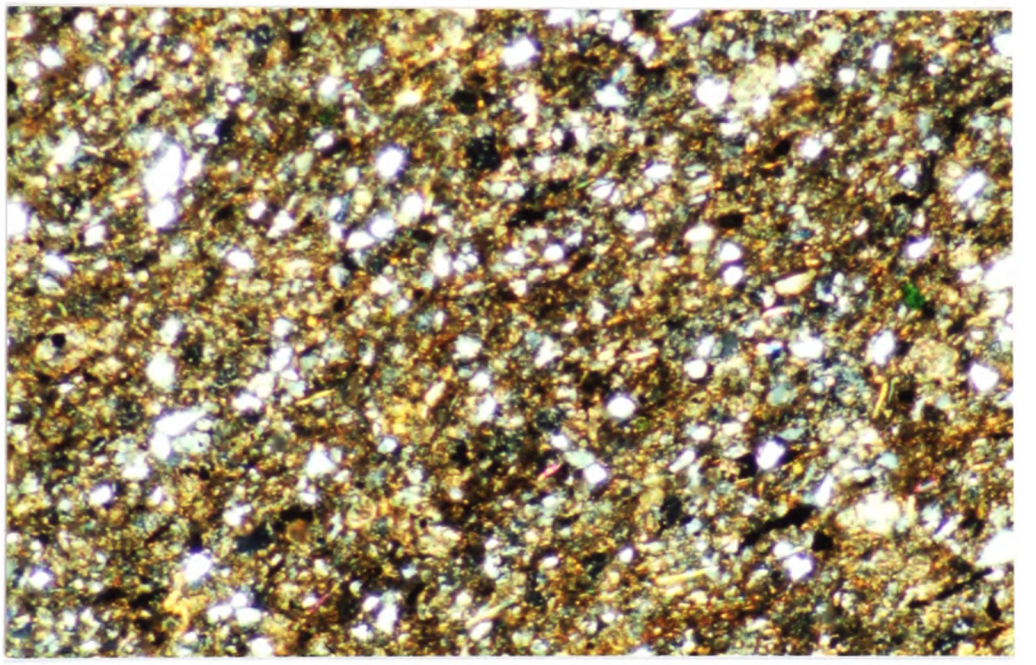


Fig. 6.13b: Photomicrograph of turbiditic siltstone from the Waima Siltstone Formation. Sample from site WB1. Long axis of photograph: *ca.* 1.5 mm.

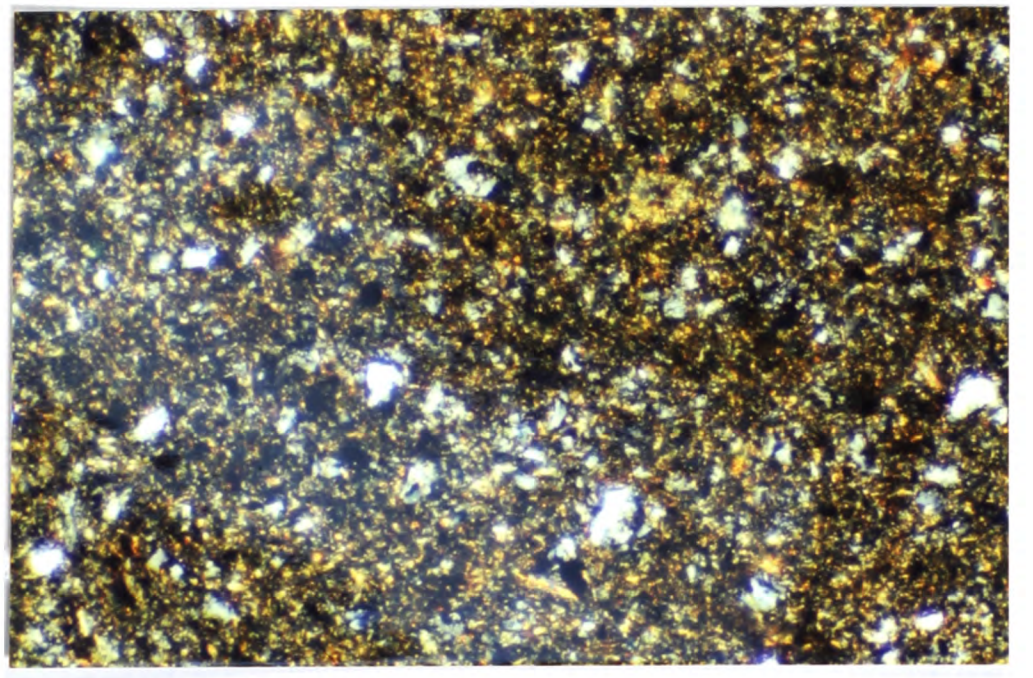


Fig. 6.13c: Photomicrograph of muddy siltstone from the Whanganui Siltstone Formation, site WD1. Long axis of photograph: *ca.* 1.5 mm.

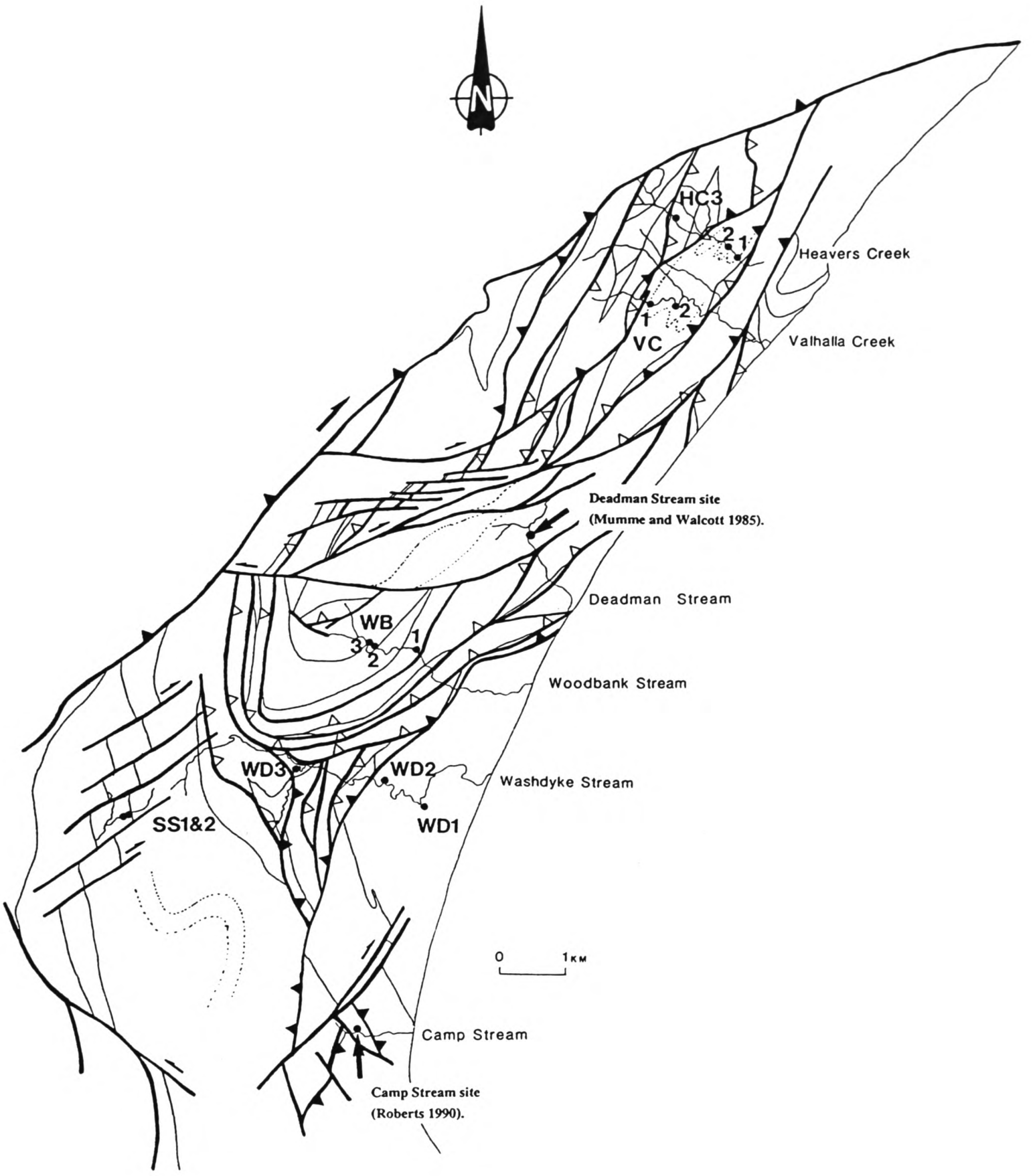


Fig 6.14: Geological map of the Kekerengu-Washdyke study area showing the location of palaeomagnetic sites drilled during this study. Also shown are the two previously sampled locations along Deadman Stream (Mumme and Walcott 1985) and Camp Stream (Roberts 1990).

indicated that the magnetization pre-dates tilting. The value of the tectonically corrected mean high temperature component inclination is within error of the expected inclination considering the age of this site. This indicates that the high temperature component is likely to have been acquired at the time of formation of these limestones.

The Kekerengu-Washdyke Study Area Sites

Thirteen sites were sampled over this region, all from siltstone lithologies of Waima Siltstone, Great Marlborough Conglomerate, Heavers Creek and Whanganui Siltstone Formations. The location of all these sites are plotted in fig. 6.14. The sites are presented from north to south by stream section.

6.3.4 Heavers Creek Site (HC3).

HC3: 173°59'/42°00' (GR: (P30) 911122).

6.3.4a Geological Setting, lithology and age

Structure

This site was drilled in siltstone beds west of the Heavers Creek fault along Heavers Creek. The beds here young and dip (at 60°) to the east. The site is 43.3 m above Fault 3, a D_e pre-tilt thrust horizon (Chapter 4). Although no fold data is available for this exact location, the regional structure of this area dictates position of HC3 on the western limb of the syncline which affects the whole northern Kekerengu region. Turbiditic silts of the same siltstone unit contains a mesoscopic, metre-scale fold with a fold axis of 032/30 NE (fold A). It was assumed that this is the relevant fold axis for the regional folding which tilted the beds of this site.

Lithology

Cores were drilled from an outcrop of blue-grey siltstone with interbedded coarser grained beds (< 4 cm thick with erosive bases, fining upward and rippled top surfaces). Only the fine-grained beds were drilled. A thin section of this material revealed *ca.* 10% angular to subangular, moderately sorted, silt-sized quartz grains together with minor micas, opaques, heavy minerals and glauconite grains within a muddy calcitic cement. The presence of glauconite grains and the general fine-grained nature of these siltstones indicates an outer shelf environment of turbidite type deposition close to an eroding landmass.

Age

Samples collected for dating in this study yielded no suitable foraminifera for dating. However the position of this siltstone below Great Marlborough Conglomerate beds

suggests that these siltstones probably belong to the Waima Siltstone Formation (*Otaian* to *Lillburnian*).

6.3.4b Demagnetization

All these cores were thermally demagnetized. The cores had relatively strong initial intensities (I_0), the maximum I_0 *ca.* 5.5 mA/m. A typical Z-plot of the demagnetization of these cores with corresponding intensity graphs and Wulf net projection is shown in fig 6.15a. The Z-plot shows the removal of two components. A low temperature component was removed between 0 and 100°C, and a high temperature component defining a straight line reaching a stable end point at the origin was removed between 100 and 450°C. Several of the cores displayed an unstable magnetization after heating up to 400°C with a corresponding intensity rise after this point. All the high temperature components from this site computed using IAPD are plotted in fig 6.15b. The vectors group well with a mean value of 118/-10 (α_{95}: 6.4).

6.3.4c Remanence carriers

The low temperature component removed after 100°C may be held by geothite grains due to the low blocking temperature of these grains. The maximum unblocking temperature of the high temperature component, 450°C, is higher than the maximum unblocking temperature for pyrrhotites and greigite and less than that of haematite. Magnetite grains are therefore likely to hold at least some of the high temperature component. These are probably multidomain grains due to the low initial intensities of these cores.

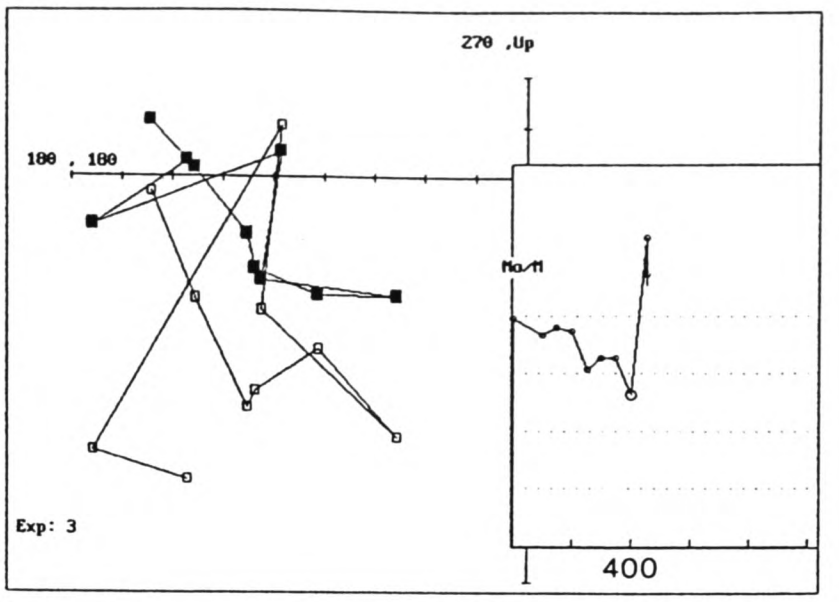
Bulk Susceptibility

Fig 6.15c shows a graph of bulk susceptibility change for three representative HC3 site cores. The bulk susceptibility remained constant throughout demagnetization until 400°C whereafter a sharp rise in bulk susceptibility was observed. Such a rise is in keeping with the increase in intensity and the unstable magnetizations observed in several of the cores during thermal demagnetization. The flat portion of these graphs indicated no growth or destruction of magnetic phases, or that the effects of these cancel out.

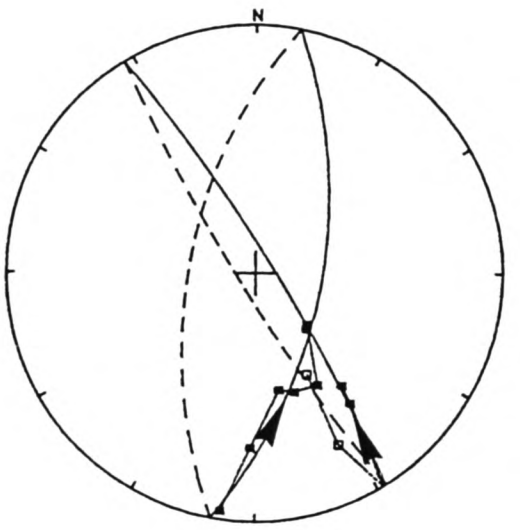
IRM

Fig 6.15d shows the variation in intensity of an HC3 site core during induced magnetization steps. The pattern of this graph with intensity rising rapidly and subsequently saturated after 140 mT was indicative of the presence of magnetites, Ti-magnetites, Ti-haematite or pyrrhotites. There is notable absence of geothite or haematite in this sample.

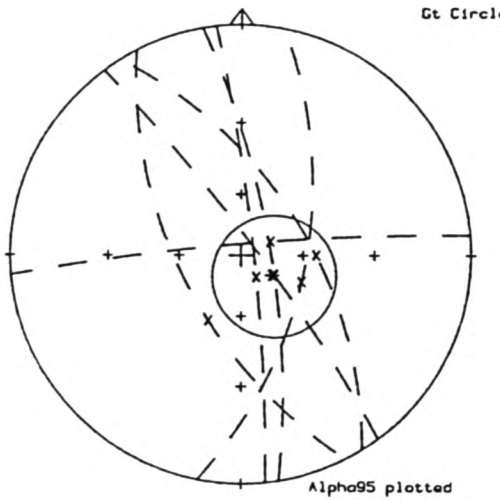
a). HC1 thermal demagnetization.



b). great circles



c). calculation of the mean primary direction.



d). HC1 bulk suceptibility.

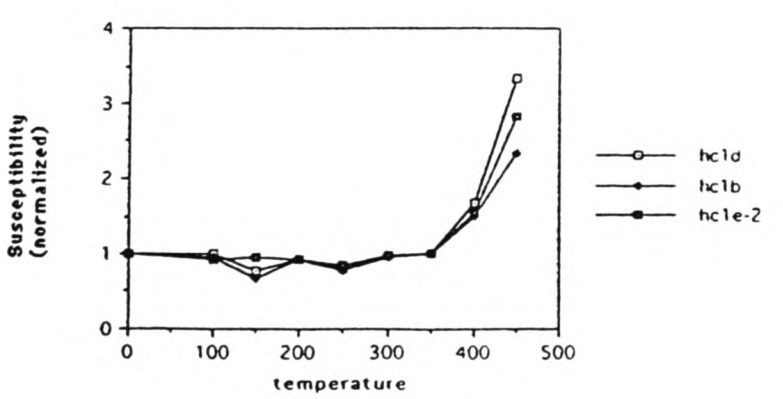


Fig 6.15: Data from Heavers Creek (site HC3). a). typical behaviour during thermal demagnetization. b). high temperature components from all HC3 site cores. c). typical bulk suceptibility for this site and d). IRM graphs for cores from sites HC1, HC2 and HC3. All data is uncorrected.

6.3.4.d Timing of the magnetization

After tectonic correction the mean inclination at this site restores to a value within error of the expected inclination considering the age of this siltstone (refer to section 7.3.4). This suggests a pre-tilt, primary magnetization.

6.3.5 Heavers Creek Sites (HC1 and HC2).

HC1: 174°00'/42°00' (GR: (P30) 923113).
HC2: 173°59'/42°00' (GR: (P30) 920116).

6.3.5a Geological Setting, lithology and age

Structure

Both sites were drilled from siltstone beds along Heavers Creek between the Heavers Creek and Chaffey Faults. Poles to bedding along this stream are plotted in fig 4.23, section 4.3.3, revealing the presence of two fold axes (023/06 N and 254/17 W). The bedding distribution is easily fitted to the fold stereoplot data, indicating the presence of four tightly folded synclines. Beds nearest to the Heavers Creek Fault are folded by the fold axis with a trend of clockwise azimuth to the trend of the fold axis affecting beds further to the east. Sites HC1 and HC2 were drilled from beds folded by the NNE-trending fold axis (023/06 N) and the WSW trending fold axis (254/17 W) respectively.

Site HC1 beds are located 27 m above the Chaffey Fault limestone. The beds dip at 33° and young to the west on an eastern syncline limb. Site HC2 beds were drilled further west along Heavers Creek. The beds are taken from the western limb of the third syncline along this stream and are slightly overturned, dipping at 86° to the west.

Younging evidence at both sites is well constrained by ripples in finely laminated sandier horizons.

To summarize, these siltstones represent material on the upthrow side of a D_e pre-tilt thrust along which limestone from the thrust decollment horizon, is caught up. Subsequently, the whole Kekerengu region was folded (D_l). This area is situated in the regional (D_l) synclinal hinge where smaller scale folding formed. In addition, reverse faulting associated with the termination of dextral strike-slip faults in southern Kekerengu, uplifted the limestone thrust horizon material. This interpretation also holds for sites VC1 and VC2.

Lithology

Both sites consist at outcrop of blue-grey siltstone interbedded with sandstone beds (4-6 cm thick with erosive bases, fining upward and rippled upper surfaces). Cores were only drilled from the fine-grained beds. Thin sections of this material revealed *ca.* 30% of

subangular, well sorted, silt-sized quartz grains with minor glauconite, opaques, micas and heavy minerals within a calcitic cement. Also observed were rare *globigerina* and *cibicides sp.* tests. The evidence indicates an outer shelf environment of turbidite type deposits close to an eroding landmass.

Age

Sites HC1 and HC2 are in the Waima Siltstone Formation. A sample collected during this study (dated sample 218b, chapter 3) gave an age of *Middle Altonian* for site HC1. It was not possible to date site HC2 because of a lack of well preserved foraminifera. However, it is at approximately the same stratigraphic position as site HC1 and therefore is assumed to have a similar age. This site was expected to be younger than the *Otaian* siltstones in Valhalla Creek because of the regional northward plunge of folding in this unit.

6.3.5b Demagnetization

All cores from these two sites were thermally demagnetized. The cores had weak initial intensities (HC1 $I_o$max: 0.14 mA/m, HC2 $I_o$max: 0.19 mA/m) which were reflected in the relatively unstable Z-plots. Figs 6.16a and 6.17a show examples of these plots with corresponding intensity graphs and Wulf net projections. It was possible to pick out straight line segments directed to the origin in the Z-plots for two of the cores from site HC2. This component was removed between 150 and 300^{o}C. These segments are directed towards the origin even though they do not reach it, indicating the presence of a second component. The growth of an unstable phase during thermal demagnetization appears to dominate the magnetization held by even higher blocking temperature grains. The demagnetization from the remaining three cores of this site plotted on great circles. Great circle analysis was done using these great circles and the two stable directions (fig 6.17b). In comparison, it was not possible to pick any primary linear components from the samples of site HC1. Reference to the stereoplots revealed that all the demagnetization paths fall on great circles and so great circle analysis was done on all the samples from this site (figs 6.16b and 6.16c). The mean of the primary components from each site are 122.57/71.38 (α_{95}: 29.22) and 147.16/20.94 (α_{95}: 17.29) for sites HC1 and HC2 respectively. The errors for both are high.

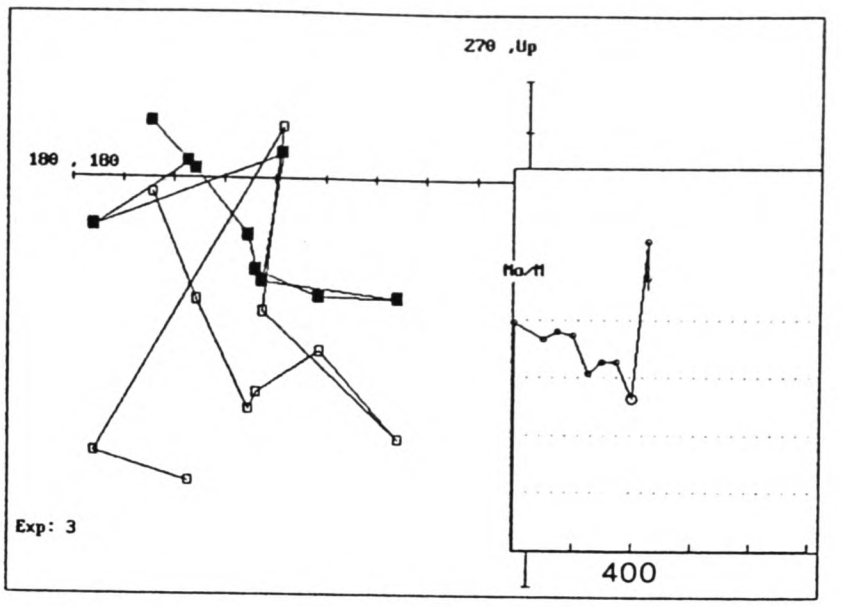
6.3.5c Remanence carriers

The low temperature component may be held by geothite (T_c: 170^{o}C) and the high temperature component by monoclinic pyrrhotite (T_c: 325^{o}C) or multi-domain magnetites due to the low initial intensities of these cores.

Bulk Susceptibility

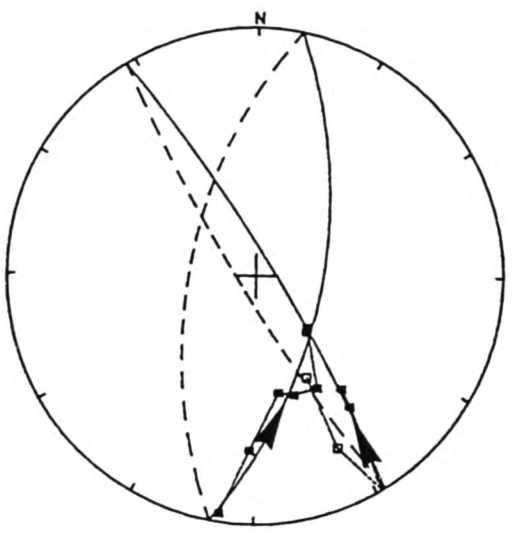
Figs 6.16d and 6.17c show graphs of the changes in bulk susceptibility during demagnetization for representative HC1 and HC2 site cores. The graphs consistently show

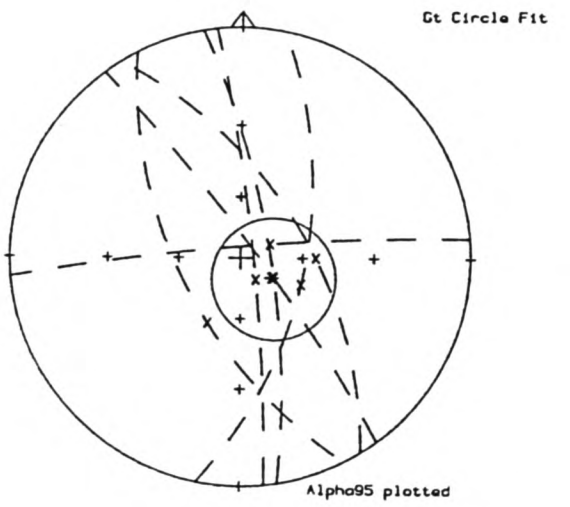
a). HC1 thermal demagnetization.



b). great circles

c). calculation of the mean primary direction.





d). HC1 bulk suceptibility.

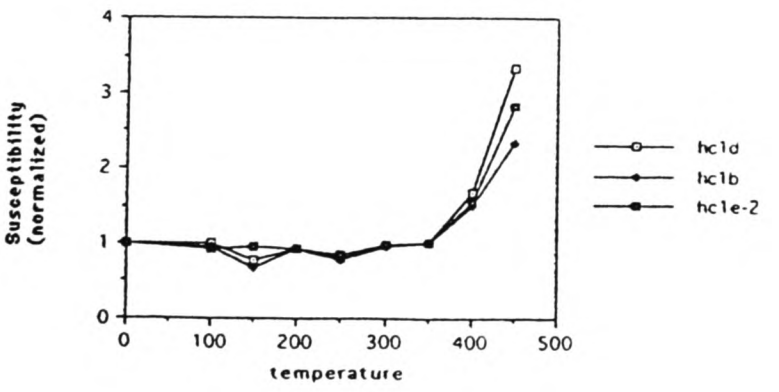
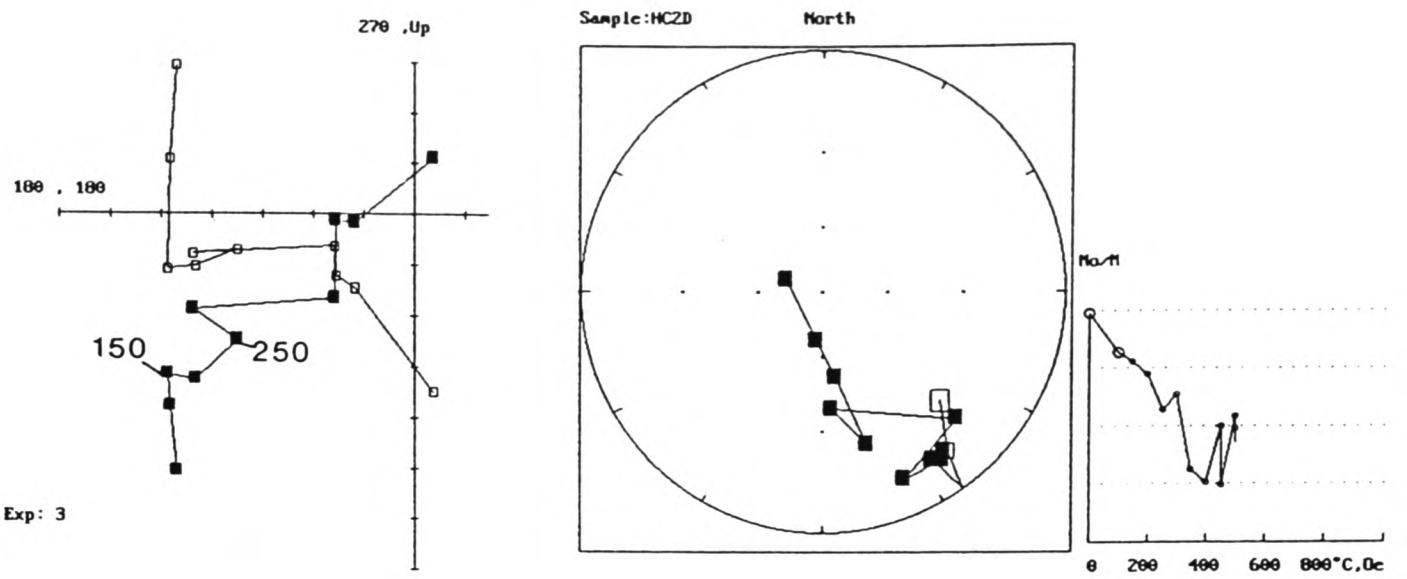
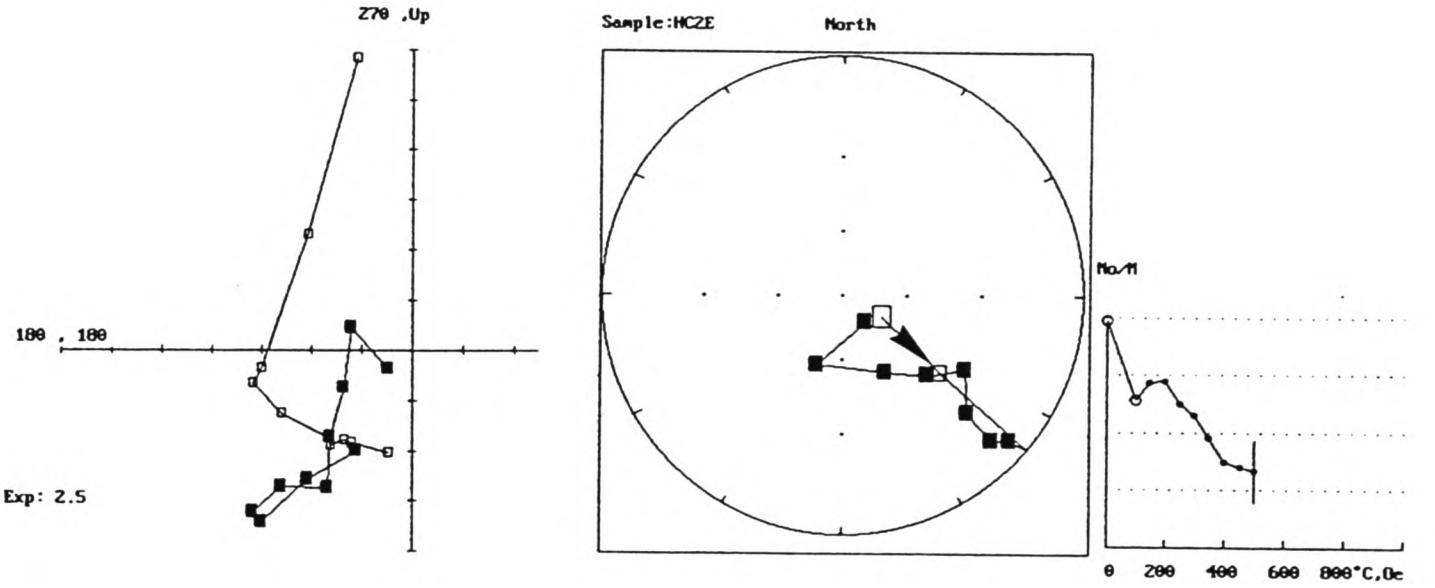


Fig 6.16: Data from Heavers Creek (site HC1). a). typical behaviour during thermal demagnetization. b). example of intersecting great circles, c). calculation of the mean primary component from all thermally demagnetized cores, and d). typical bulk suceptibility for this site. All data is uncorrected.

a). HC2 thermal demagnetization.

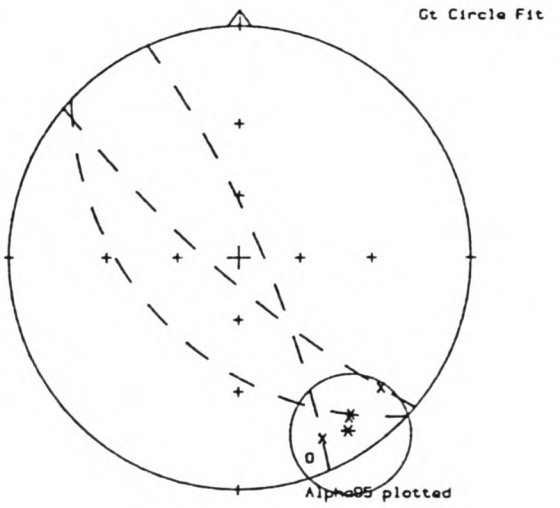


(Example of core reaching a stable end point)



(Example of core not reaching a stable end point)

b). Great circle analysis



c). Bulk suceptibility.

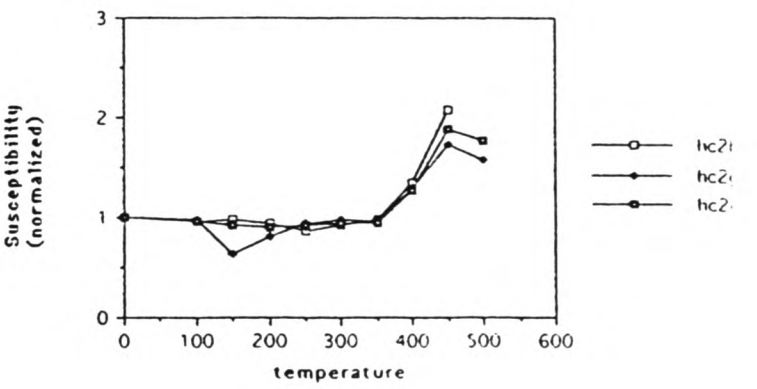


Fig 6.17: Data from Heavers Creek (site HC2). a). examples of behaviour during thermal demagnetization. b). calculation of the mean primary component from all thermally demagnetized cores and c). typical bulk suceptibility for this site. All data is uncorrected.

bulk susceptibility remaining constant up to 350°C whereafter sharp increases in bulk susceptibility were observed. These increases correspond to the unstable portions of the Z-plots discussed above. The rise is likely to be due to the growth of new magnetic phases at this point which would result in an unstable magnetization.

IRM

The intensity against induced field strength graph of fig 6.15d includes representative cores from both these sites as well from site HC3. The pattern of both was identical, rising steeply until 140 mT whereafter the curves flattened off to the horizontal. This technique indicated the presence of magnetites, Ti-magnetites, or pyrrhotites, and the absence of geothite or haematite.

6.3.5d Timing of the magnetization

Reference to sections 7.3.5 and 7.3.6 shows how the mean primary vector at site HC2 becomes within error of the inclination expected considering the age of this site after tectonic correction in comparison to before. This indicates not only the pre-fold timing of this magnetization but also that it was probably acquired at the time of formation of this unit. The large error obtained from site HC1 meant that interpretation of this mean component could produce no meaningful result.

6.3.6 Valhalla Creek Sites (VC1 and VC2).

VC1: 173°58'/42°00' (GR: (P30) 906106).

VC2: 173°59'/42°00' (GR: (P30) 912106).

6.3.6a Geological Setting, lithology and age

Structure

Sites VC1 and VC2 were drilled from siltstone beds along Valhalla Creek between the Heavers Creek and Chaffey Faults. For an overall interpretation of the structure of this area one should refer to section 6.3 5 (structure). Poles to bedding for the whole section (see section 4.3.3) again indicated the presence in space of two separate fold axes (013/25 N and 059/08 E). The beds nearer to the Heavers Creek Fault are folded by a fold axis with a plunge direction of clockwise trend compared to the trend of the fold axis plunge direction for beds further to the east. Two tightly folded synclines adjacent to each fault separated by two anticlines and an openly folded syncline were recognized by the bedding distribution in map view.

Site VC2 is situated on the western limb of the central open syncline. The beds here dip at 70° to the northeast and are right-way-up. The relevant fold axis for this site is 013/25

N. Site VC2 was drilled in siltstone closer to the Heavers Creek fault. The beds here are also on the western limb of a syncline (though a tightly folded one), but are overturned, dipping steeply (83^{o}) to the west and younging to the east. The fold axis associated with this site is 059/08 E.

Lithology

These sites were drilled from a blue-grey siltstone outcrop with interbedded coarser beds (< 0.3 m thick, with erosive bases, fining upward, and laminations defining ripple and load structures). Cores were only drilled from the fine-grained beds. Thin sections of this lithology revealed between 10 and 20% subrounded, moderately sorted, silt-sized quartz grains with minor opaques, micas and glauconite within a muddy, calcitic matrix. The opaques tend to be aligned in a consistent orientation, reflecting bedding. Several globigerina tests were also observed. The evidence suggests turbiditic type deposition in an outer shelf environment adjacent to an eroding landmass.

Age

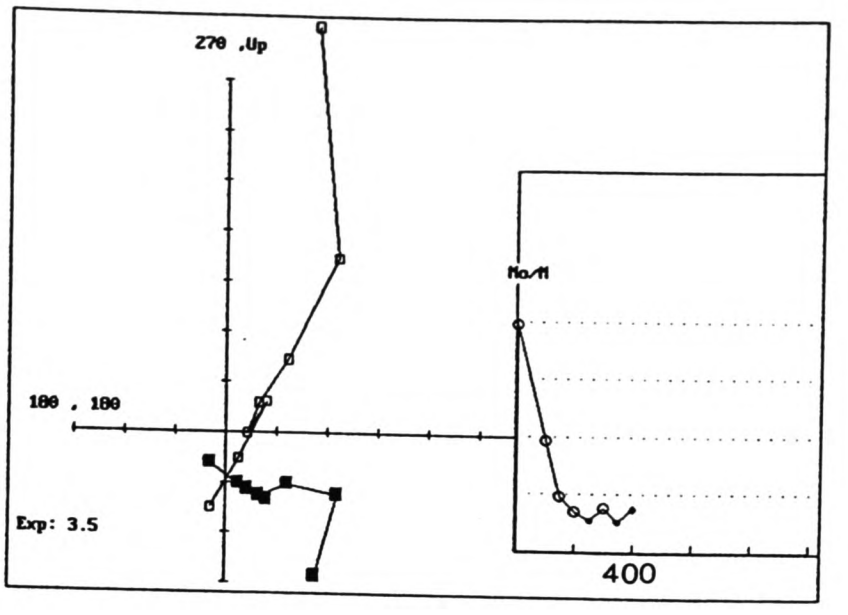
Samples were collected in this study from both these sites. Neither yielded sufficient suitable foraminifera for dating. Two samples (Y17 and Y19) collected by Osborne (1980) indicate an *Otaian* age for the siltstones along this stream closer to the Chaffey fault. Sites VC1 and VC2 are both at approximately the same stratigraphic position as Osborne's sample Y17. Therefore both sites were assumed to be of *Otaian* age, belonging to the Waima Siltstone formation.

6.3.6b Demagnetization

A representative thermal demagnetization Z-plot for site VC2 is shown in fig 6.18a. The I_{O}max's of these cores were weak, 0.2 mA/m and 0.65 mA/m for VC1 and VC2 site cores respectively. As with sites HC1 and HC2, the plots from these sites were again suggestive of unstable magnetizations over much of the temperature range. For site VC1 it was not possible to pick a straight line primary component from the data of any of the cores. Infact the data fall on great circles and so great circle analysis was attempted. Unfortunately the overprint magnetization directions of individual cores were the same, making it impossible to obtain a statistically meaningful intersection point corresponding to the primary magnetization. However, for site VC2 all the cores demagnetized along well-defined great circle paths (figs 6.18b and 6.18c). The overprint magnetization directions in this case were sufficiently different to enable an intersection point to be found with reasonable accuracy. Mean primary magnetization for site VC2: 237.9/44.56, α_{95}: 7.83.

6.3.6c Remanence carriers

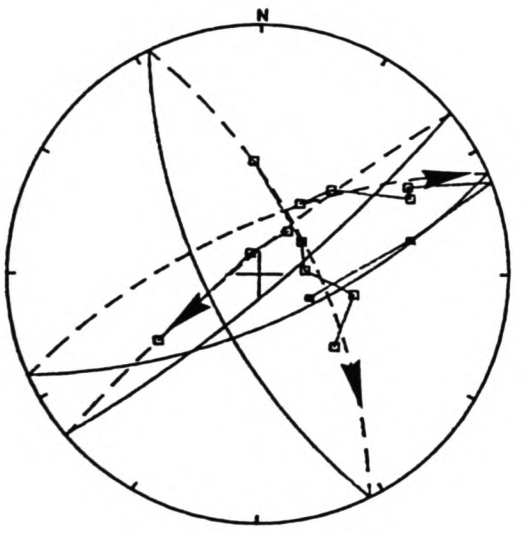
a). VC2 thermal demagnetization.



(cores do not reach stable end points)

b). great circles

c). calculation of the mean primary direction.



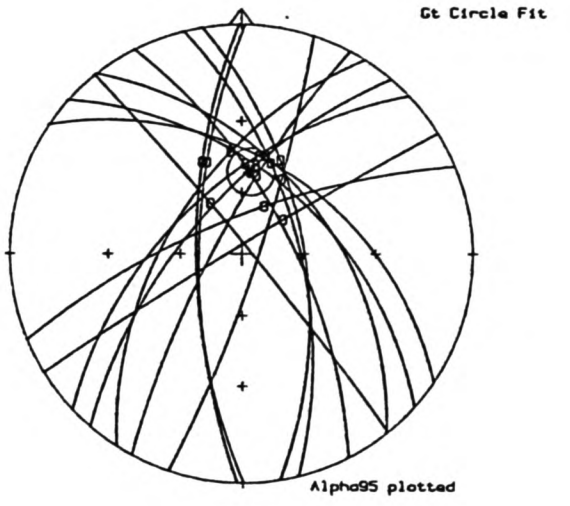


Fig 6.18: Data from Valhalla Creek (site VC2). a). example of typical behaviour during thermal demagnetization, b). example of intersecting great circles, and c). calculation of the mean primary component from all thermally demagnetized cores. All data is uncorrected.

The demagnetization behaviour suggests that the low temperature component may be held by geothite grains and the high temperature component by pyrrhotites or magnetite grains (probably multi-domain due to the low initial intensities of these cores).

Bulk Susceptibility

Figs 6.22a and 6.22b show the changes in bulk susceptibility for representative cores from each site. All the cores show constant susceptibility up to 350°C, whereafter bulk susceptibility rises. This rise corresponds to the unstable magnetization observed above this temperature on most of the demagnetization Z-plots. The rise in susceptibility suggests the growth of a new, unstable magnetic phase.

IRM

Fig. 6.22a also shows intensity against induced field strength for cores from each site. Both show intensity rise up to *ca.* 140 mT. After this point the graphs are horizontal. This indicated the presence of multi-domain magnetites, Ti-magnetites, or pyrrhotites, and the absence of geothite or haematite.

6.3.6d Timing

Reference to section 7.3.7 shows how the mean vector inclination from site VC2 became close to the expected inclination considering the age, latitude and longitude of this site after tectonic correction. However, in this case the error involved is large and the nature of this magnetization unclear.

6.3.7 Woodbank Stream Site (WB1, 2 and 3).

WB1: 173°56'/42°04' (GR: (P30) 866044).
WB2: 173°55'/42°04' (GR: (P30) 859046).
WB3: 173°55'/42°04' (GR: (P30) 857046).

6.3.7a Geological setting, lithology and age

Structure

This Woodbank Stream site was taken from siltstone lithologies within the Razor Fold syncline structure which dominates the geology of the northern Washdyke map. Three separate exposures with constant bedding were drilled along the stream. The Razor Fold folds a stack of early thrust repeated Tertiary sediments. The syncline has a steeply plunging fold axis of 320/67 NW (see section 4.3.3). All sites are situated on the eastern limb of this fold within the inner siltstone-conglomerate succession. The beds dip consistently at *ca.* 70° to the NW.

Lithology

WB1 site cores were drilled from a massive, blue-grey siltstone unit. Bedding at this location was defined by thin, mm-scale laminations. A thin section of this lithology (fig. 6.13b) revealed 20% of relatively well sorted, silt-sized quartz grains with minor micas, opaques and glauconite within a muddy, calcitic matrix. Also present and constituting *ca.* 5% of the rock were globigerina tests. At this scale the laminations could be identified by alternations between the above and clay-rich beds.

Sites WB2&3 were drilled from thick siltstone beds within a unit interbedded with conglomerate bands. Thin sections of the lithology revealed *ca.* 20% of subangular, relatively well sorted, coarse silt-sized quartz grains with minor micas and opaques within a muddy calcitic matrix. Narrow bands of fine sand-sized quartz grains were also observed.

The evidence from both sites indicates a middle to outer shelf environment adjacent to an eroding landmass. The change to bedded conglomerates observed at sites WB2&3 indicate a change in uplift of the source area to supply this much coarser, debris-flow material.

Age

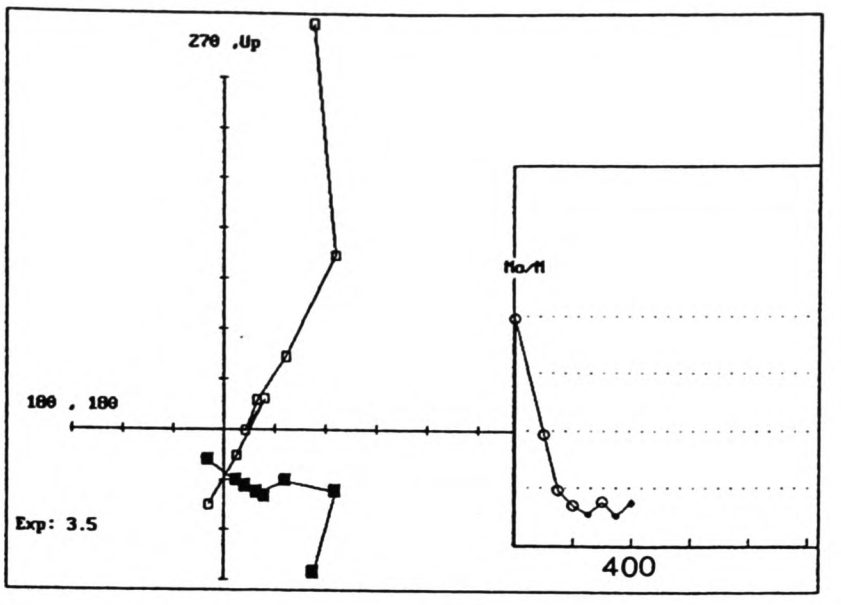
Siltstones from the same location as site WB1 were dated by Osborne (1980) as *Otaian* (sample O7). These silts thus belong to the Waima Siltstone Formation. Their position below Great Marlborough Conglomerate beds substantiates this age. Samples from site WB2&3 were unsuccessfully dated due to their rare and poorly preserved foraminifera. Their position above the GMC beds and lack of any evidence for structural separation both suggest that these siltstones belong to the Heavers Creek Formation. An approximate age of *Lillburnian* (the oldest Heavers Creek Formation silts known elsewhere) is given to these sites.

6.3.7b Demagnetization

Again the initial intensities of these cores were relatively weak (I_0max: 0.52 mA/m). A representative Z-plot of the demagnetization is shown in fig. 6.19a. It was not possible to identify straight line segments to the origin. However, stereographic projections revealed that sections of the demagnetization paths fall on great circles. Therefore great circle analysis was done on the data from all the cores. The results are shown in figs 6.19b and 6.19c. Magnetization above 250^{o}C is generally unstable with corresponding intensity rise.

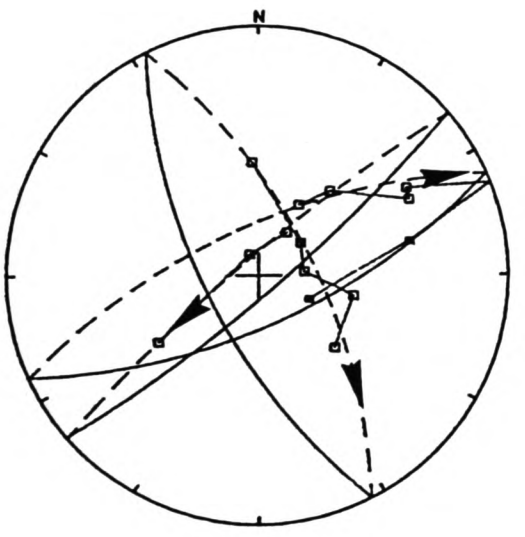
Great circle analysis for this site is shown in fig. 6.19c (mean intersection point: 7.08/-50.87, α_{95}: 10.47). This direction corresponds to the present day field direction for the Marlborough region. The great circle paths track away from this point as would be expected of a secondary component rather than of a higher temperature component. The great circle paths are infact widely distributed. This indicated two possibilities, that the high

a). WB thermal demagnetization.



(cores do not reach stable end points)

b). intersecting great circles



c). great circle analysis.

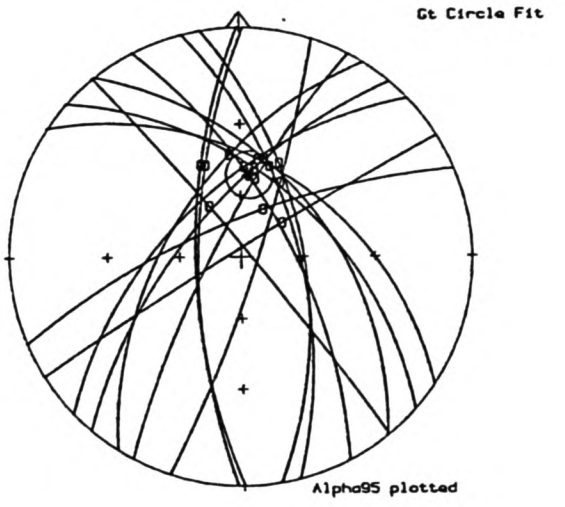


Fig 6.19: Data from Woodbank Stream (site WB1, 2, and 3). a). example of typical behaviour during thermal demagnetization, b). example of intersecting great circles, and c). great circle analysis attempting to identify the mean primary component from all thermally demagnetized cores. In this case the only intersection obtained is the present day field direction. All data is uncorrected.

temperature component is random, or that it is more-or-less antiparallel to the overprint direction. The fact that the recorded intersection point agrees so well with the present day field direction led to the assumption that the former is true, that the high temperature component is random. Therefore it was not possible to obtain the high temperature component direction from great circle analysis.

6.3.7c Remanence carriers

The very low temperature of these components suggest geothites, pyrrhotites or low blocking temperature magnetites (probably multidomain due to the low initial intensities of these cores) as the remanence carriers.

Bulk Susceptibility

Fig. 6.22c shows the changes in bulk susceptibility recorded for a few of the cores from the site. The graphs are consistently horizontal (constant susceptibility) up to 400°C whereafter there is a sharp rise. This rise corresponds at least in part to the unstable portion of the Z-plots.

IRM

Plots of intensity against induced field strength for cores from this site are also shown in fig. 6.22c. These all rise rapidly to *ca.* 140 mT whereafter the curves flatten to the horizontal, indicating the presence of magnetites, Ti-magnetites, or pyrrhotites, and the absence of geothite and haematite.

6.3.7d Timing of the magnetization

The mean magnetization corresponds to the present day field direction making this a recent magnetization and not a primary one associated with the formation of these siltstones. Refer also to section 7.3.8.

6.3.8 Washdyke Steam Sites (WD1 and WD2).

WD1: 173°56'/42°05' (GR: (P30) 866017).

WD2: 173°55'/42°05' (GR: (P30) 860022).

6.3.8a Geological setting, lithology and age

Structure

Massive to turbiditic siltstones are exposed along the east coast of the Washdyke map. In the south these siltstones are in sedimentary contact with and lie directly above older conglomerates. However, there is a marked age difference across this contact which suggests an unconformity (see section 2.2.4). The siltstone beds themselves strike NNW

and dip mostly at 50-86° to the east. Eastward younging evidence was found in the south close to the lower contact with the conglomerate.

Fig 4.23 shows a stereoplot of the poles to bedding within the siltstone unit. The plot suggested possible folding about a fold axis of 356/47 N. However, the only younging evidence is in the south and the bedding distributions do not clearly indicate folding. Dating within the unit is not precise enough to indicate whether younging is constantly to the east or not. The slight variations in dip and strike may be a result of small scale upright folding, unobserved faulting, or to another phenomena such as bedding parallel compression or extension.

Lithology

This unit mainly consists of massive blue-grey siltstone. Coarser beds (< 0.3 m) were observed in a few locations. Bedding is defined by organic flecks at site WD1 and by thin siltier beds at site WD2.

A thin section of the siltstone (fig. 6.13c) revealed a poorly sorted, silty mudstone. Angular quartz grains form *ca.* 5 to 10% of the rock and varied in width from coarse silt to mud-sized, though were dominantly of silt grade. Also observed in thin section were patches of dark, organic matter which aligned parallel to bedding (as seen in outcrop). Rare heavy minerals (sphene and rutile), micas and < 1% opaques made up the remainder. Probe and EDS analyses confirmed the presence of sphene and rutile and identified the opaque grains as Fe-rich feldspars and micas. Rare, scattered foraminifera were also observed. These foraminifera were extracted and identified for dating purposes (see following section). A mixture of benthics and planktic forms were found. The evidence suggests a middle to outer shelf environment of slow background to turbiditic deposition, close to an eroding landmass.

Age

Both sites are from the siltstone unit disconformably above Great Marlborough Conglomerate beds. The unit has an overall age range of *basal Tongaporutuan* to *Waipipian* (see section 2.2.4). Samples were taken from both sites and dated during this study. The presence of *globigerina crassaconica* and *globigerina inflata* at site WD1 (dated sample 9, chapter 3) tied down the age range of this site to *Middle Opoitian* to *Waipipian.* Foraminifera at site WD2 (dated sample 10, chapter 3) give a less confined age range of *Lower Tongaporutuan* to *Recent.* Since the exact structure is unknown it is hard to establish the relative age of the two sites. The siltstones are from the Upper Siltstone (Whanganui Siltstone) Formation.

6.3.8b Demagnetization

Cores were demagnetized by heating to 100°C and thereafter in 50°C steps until the intensity of magnetization had fallen to zero. The cores had reasonable initial intensities ranging from 36-1 mAm^{-1} but typically below 10 mAm^{-1}. Initial intensities for WD2 site cores were generally lower than WD1 site cores, reflecting a variation in sedimentary supply of magnetic grains between the two sites.

Examples of demagnetization plots for each site are shown in figs 6.20a and 6.20b with their corresponding intensity fall-off with temperature graphs and Wulf net projections. It was immediately clear that thermal demagnetization removes two distinct components. The first of these is a low temperature magnetization removed after heating to 100°C. All points above 100°C define a linear progression towards the origin signifying the removal of a high temperature component. This high temperature component was removed between 100 and 350°C. The high temperature components from each core are plotted in figs 6.20c and 6.20d. These components group tightly about mean orientations of 62/-32 ($\alpha 95$: 3.4) and 84/-31 ($\alpha 95$: 6.3) for sites WD1 and WD2 respectively. The low temperature components are not consistent and reflect a viscous remanent magnetization probably picked up during transportation and storage of the cores.

6.3.8c Identification of the remanence carriers

Probe, EDS and reflected light analysis

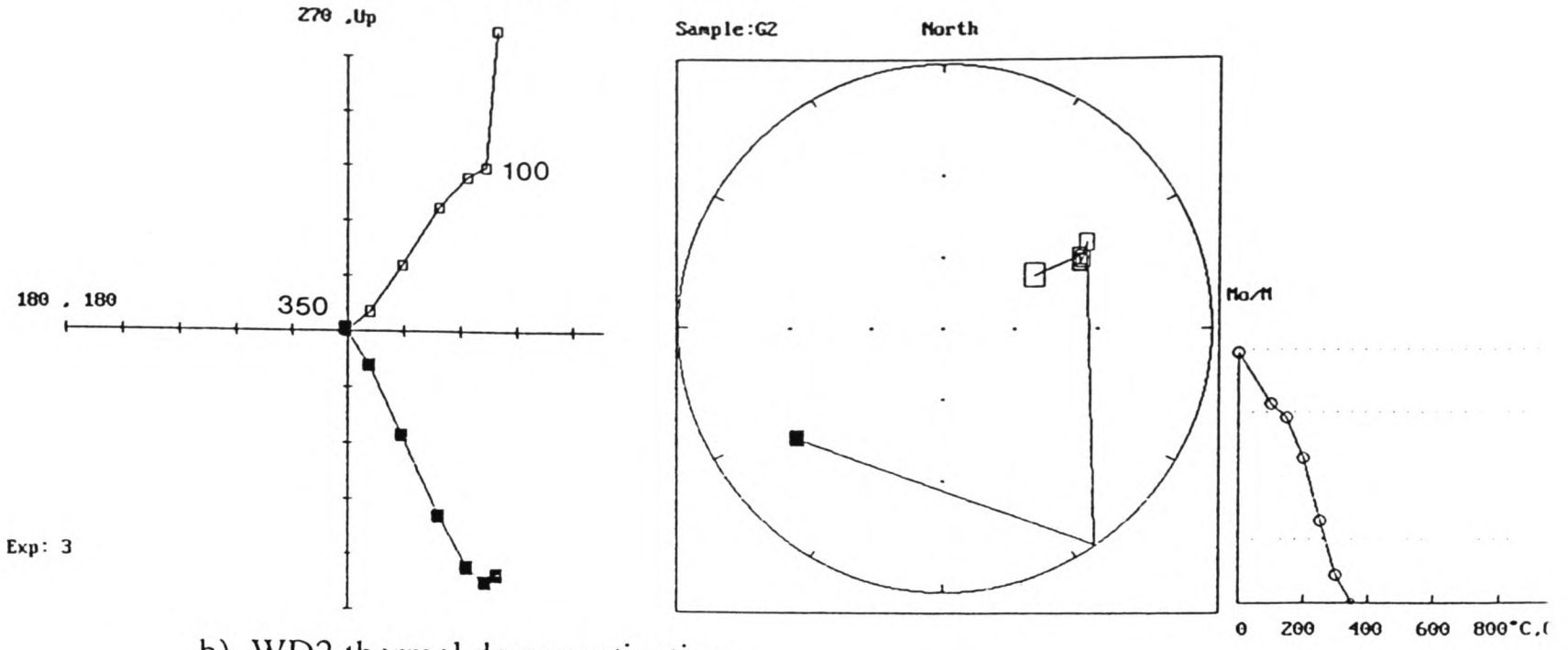
Probe analysis of the opaque grains observed in thin section revealed these to be non-metallic. Using EDS the opaques were identified as Fe-rich feldspars and micas. Under reflected light, rare (*ca.* 5 per slide) detrital grains with bright yellow reflectance were found. With knowledge of the position and form of these grains, EDS analysis was then able to show these grains to consist solely of Fe and S. The only ferromagnetic Fe sulphide mineral is pyrrhotite, although it is of course possible that these grains are non-magnetic sulphides. However pyrrhotite is in keeping with the demagnetization temperatures.

The removal temperatures of each component provide some insight into possible remanence carriers. All the magnetization is lost after heating to 350°C. This temperature suggests magnetites, titanomagnetites or pyrrhotites (magnetic disorder at 310°C). Geothite and low blocking temperature magnetites may hold the low temperature component. The stability of these cores and high initial intensities indicate that magnetites are likely to be single domain rather than multidomain.

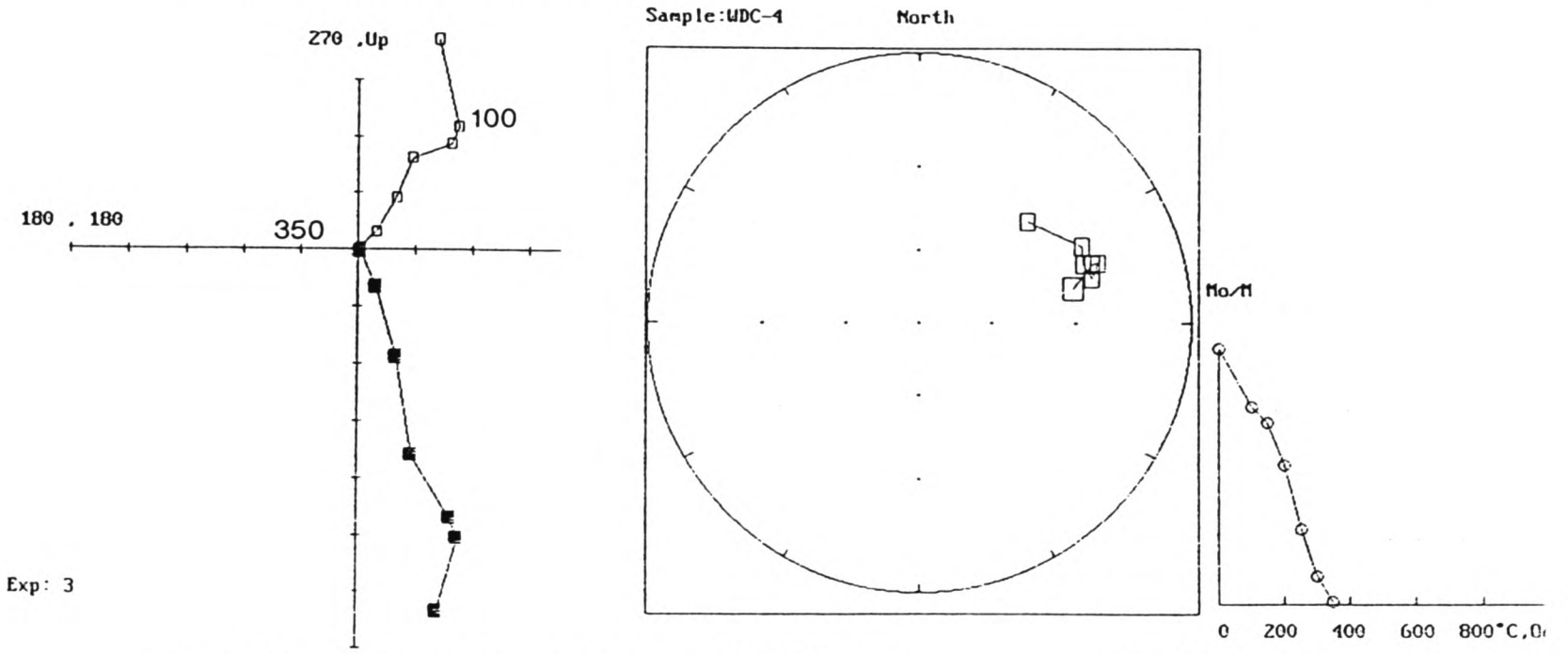
Bulk Susceptibility

Plots of bulk susceptibility against temperature for cores from both sites are identical apart from the higher bulk susceptibility values for site WD1 cores compared to site WD2 cores (as observed in the initial intensities from these sites). Figs 6.22d and 6.22e show

a). WD1 thermal demagnetization.



b). WD2 thermal demagnetization.



c). High temperature components of WD1 and d). WD2.

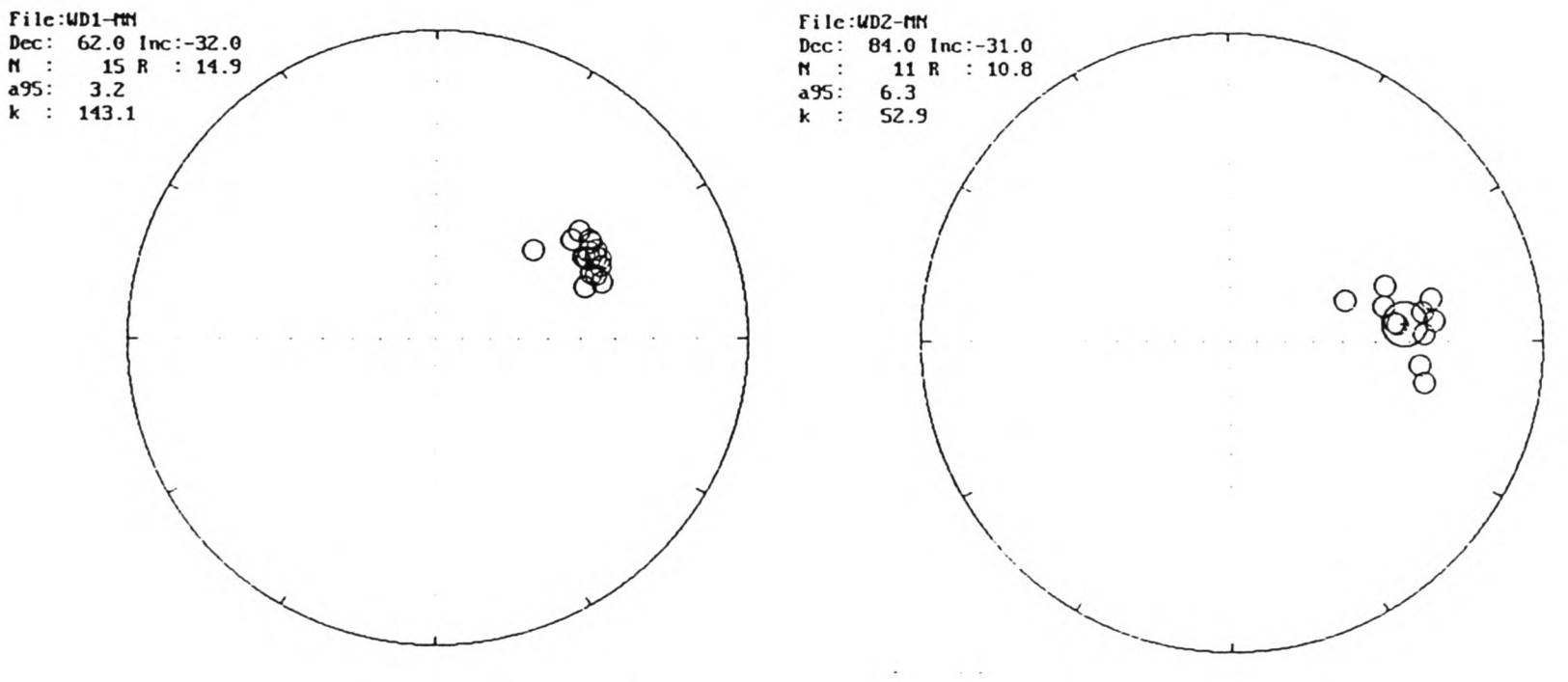


Fig 6.20: Data from the Washdyke Stream (sites WD1 and WD2). a). typical behaviour during thermal demagnetization of WD1 and b). WD2 cores. c). High temperature components from all WD1 and d). WD2 site cores. All data is uncorrected.

examples of these plots. The plots all show a linear decrease in bulk susceptibility from 0-300°C followed by a sharp increase at 350°C. Geothite is known to dewater to haematite at 350°C which might explain this sudden change.

IRM

Fig. 6.22e also shows the intensity change against induced field strength for three WD1 site cores. All show a rise in intensity up to *ca.* 140 mT whereafter saturation is reached. This saturation indicated the presence of magnetites, pyrrhotites, or Ti-magnetites and the absence of geothite or haematite. (Therefore dewatering of geothite is not occurring). There is, however, a slightly gentler gradient at low field strengths which for some magnetite phases can be indicative of single-domain magnetites. The higher intensities and more stable magnetization of cores from these sites as oppose to siltstone cores from other sites probably reflects the single-domain character of the magnetites in these rocks. Pyrrhotite may also be present.

Alternating field demagnetization

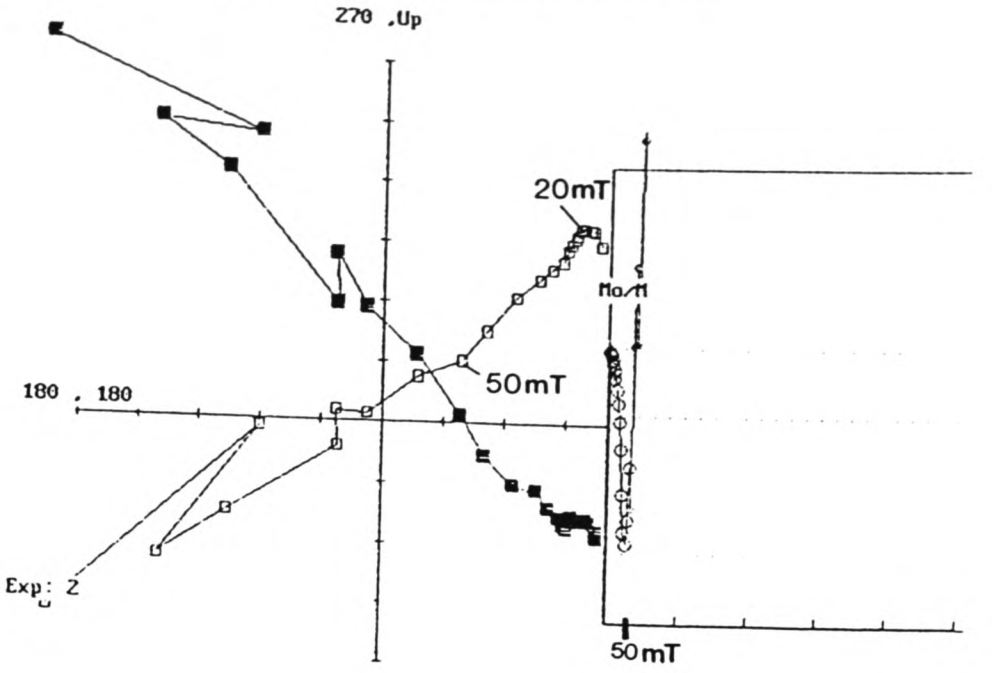
Several cores from site WD1 were demagnetized by application of an alternating field. See fig. 6.21a for example Z-plots of this demagnetization. Two linear components are visible, a low coercivity component removed after exposure to an alternating field of strength 5-20 mT and a second linear component removed between 5-20 and 50 mT with corresponding decreasing intensity. At field strengths above 50 mT systematic increases in intensity were observed associated with strange directions. This phenomena is attributed to the picking up of gyroremanent magnetization by single domain magnetite grains during static alternating field demagnetization (Stephenson 1993). Fig. 6.21b shows a plot of the high coercivity component obtained by this method of demagnetization. Comparison of this plot with that in fig. 6.20c shows that this component is identical within errors to the high temperature component removed by thermal demagnetization. With this evidence it was possible to conclude the presence of magnetite grains as carriers of the primary remanence.

6.3.8d Timing of the magnetization

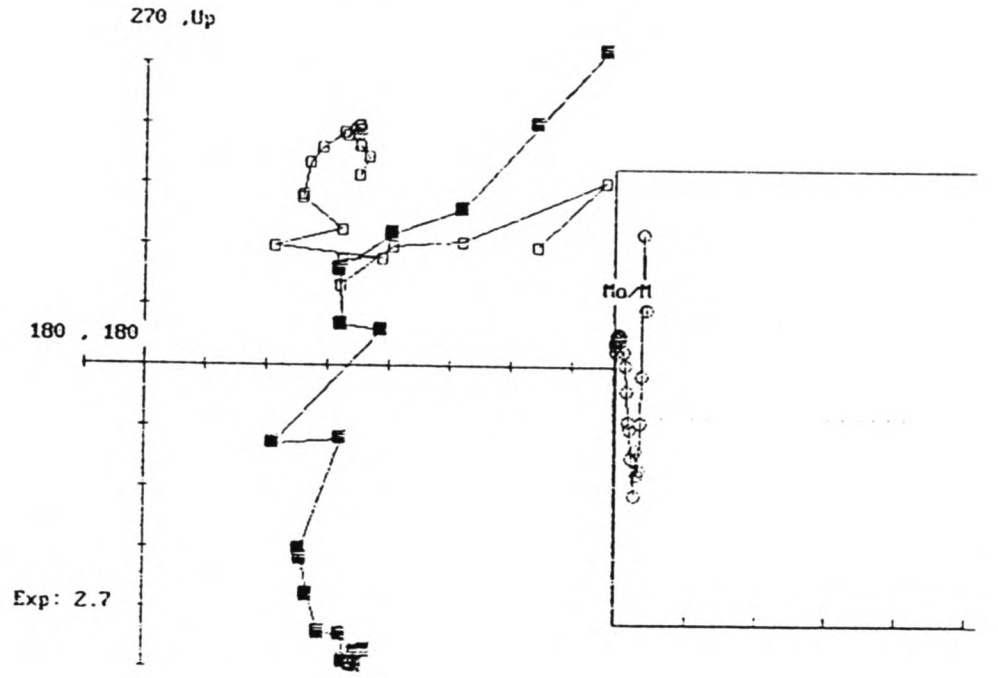
Reference to section 7.3.9 shows that after tectonic correction the mean inclination of the high temperature component at both sites becomes closer to the expected inclination for the age of these siltstones. Also after tectonic correction the declinations converge. The component appears to represent a pre-tilt primary magnetization.

6.3.9 Washdyke Stream Site (WD3).

a). WD1 alternating field demagnetization.



I1



K1

b). WD1 uncorrected high coercivity components.

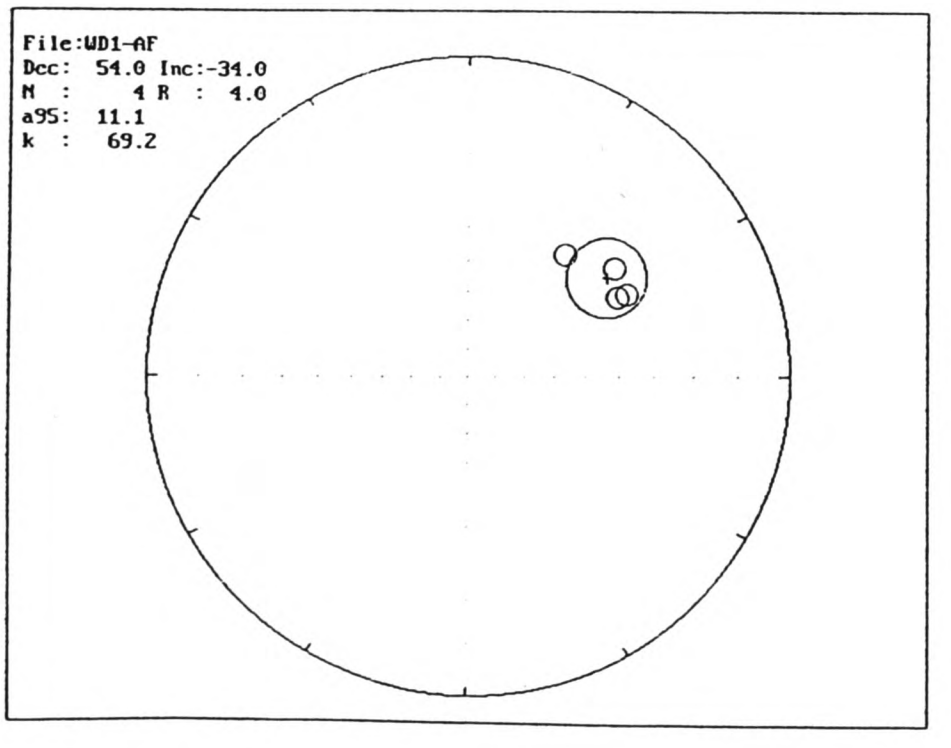
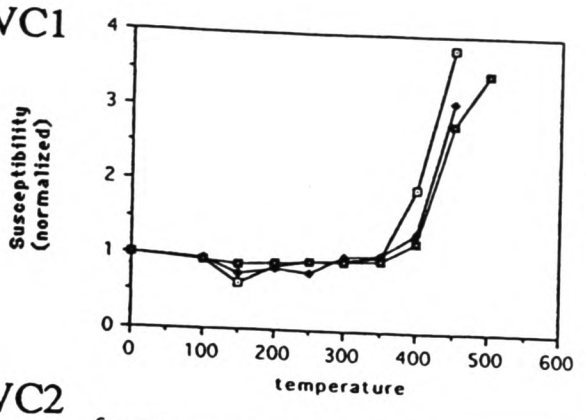


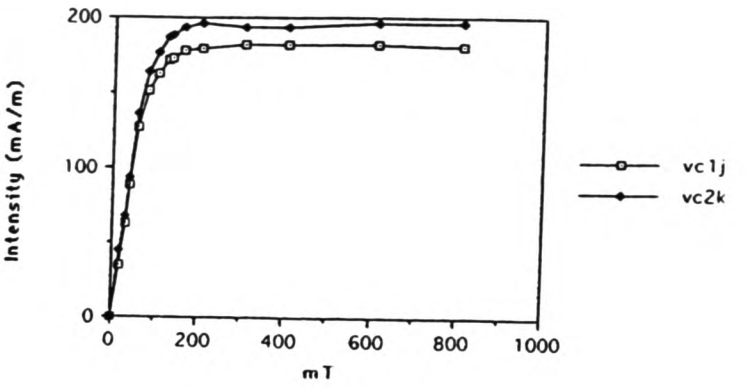
Fig 6.21: a). typical behaviour during alternating field demagnetization of samples from the Washdyke Stream site (WD1). b). high coercivity components from all WD1 cores.

Bulk Suceptibility

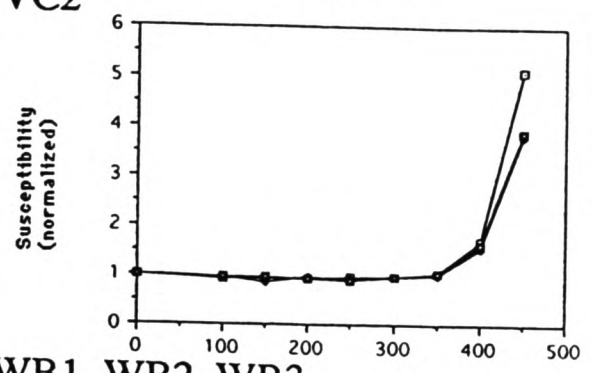
IRM

a). VC1

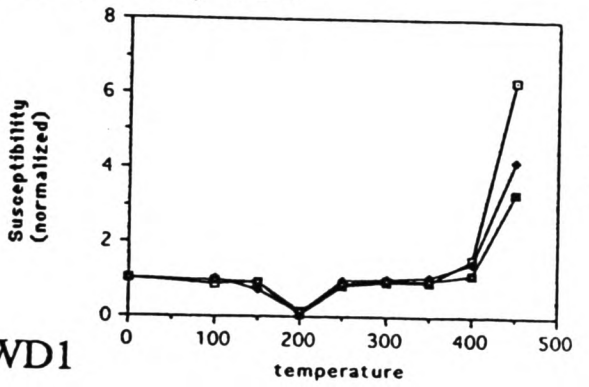


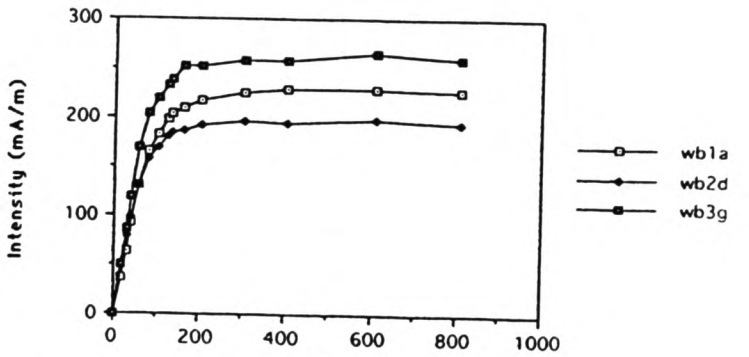


b). VC2

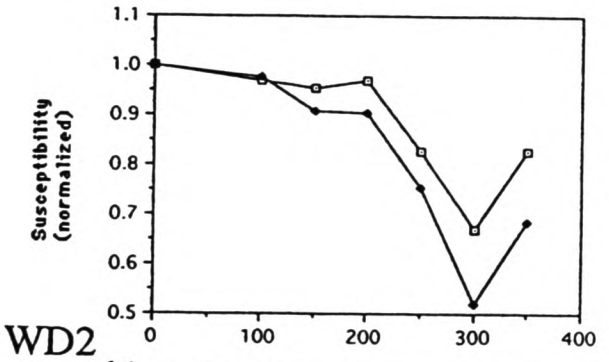


c). WB1, WB2, WB3

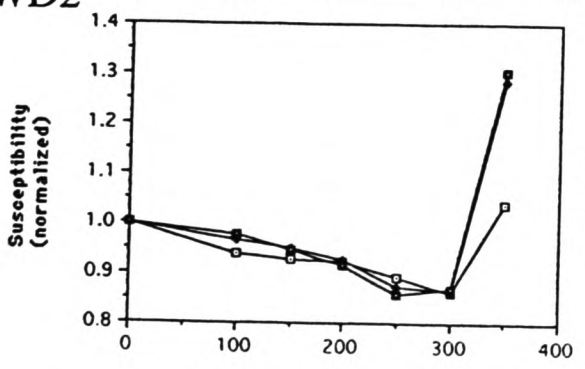




d). WD1



e). WD2



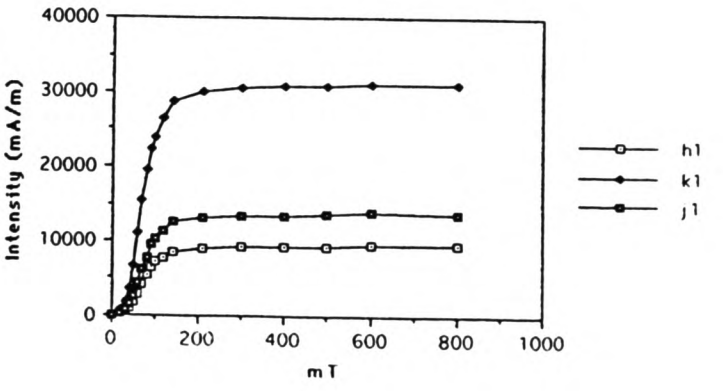


Fig 6.22: Bulk susceptibility and IRM graphs for sites a). VC1, b). VC2, c). WB1, WB2, WB3, d). WD1 and e). WD2.

WD3: 173°54'/42°05' (GR: (P30) 844024).

6.3.9a Geological Setting, lithology and age

Structure

This site was drilled in siltstones west of the Washdyke back thrust (Fault 23). Unfortunately the bedding data from this unit is sparse and no fold information could be deduced.

Lithology

Cores were drilled from a massive blue-grey siltstone unit with bedding defined by mm-scale laminations and flecks of organic material. A thin section of this lithology revealed *ca.* 20% of subangular, moderately well sorted, silt-sized quartz grains with minor micas, opaques, glauconite and heavy minerals. Also present and forming approximately 5% of the rock were *globigerina* tests and rare fragments of bivalve shell. The evidence indicates an outer shelf environment of slow deposition adjacent to an eroding land mass.

Age

Two samples from this siltstone unit were analyzed by Osborne (1980) giving a combined age of *Lillburnian* (Heavers Creek Formation siltstones) for the Washdyke Stream exposure of these siltstones. A sample collected during this study from the site itself was unsuccessfully dated due to the poor preservation of foraminifera in the sample. The *Lillburnian* age is arbitrarily assumed to include site WD3.

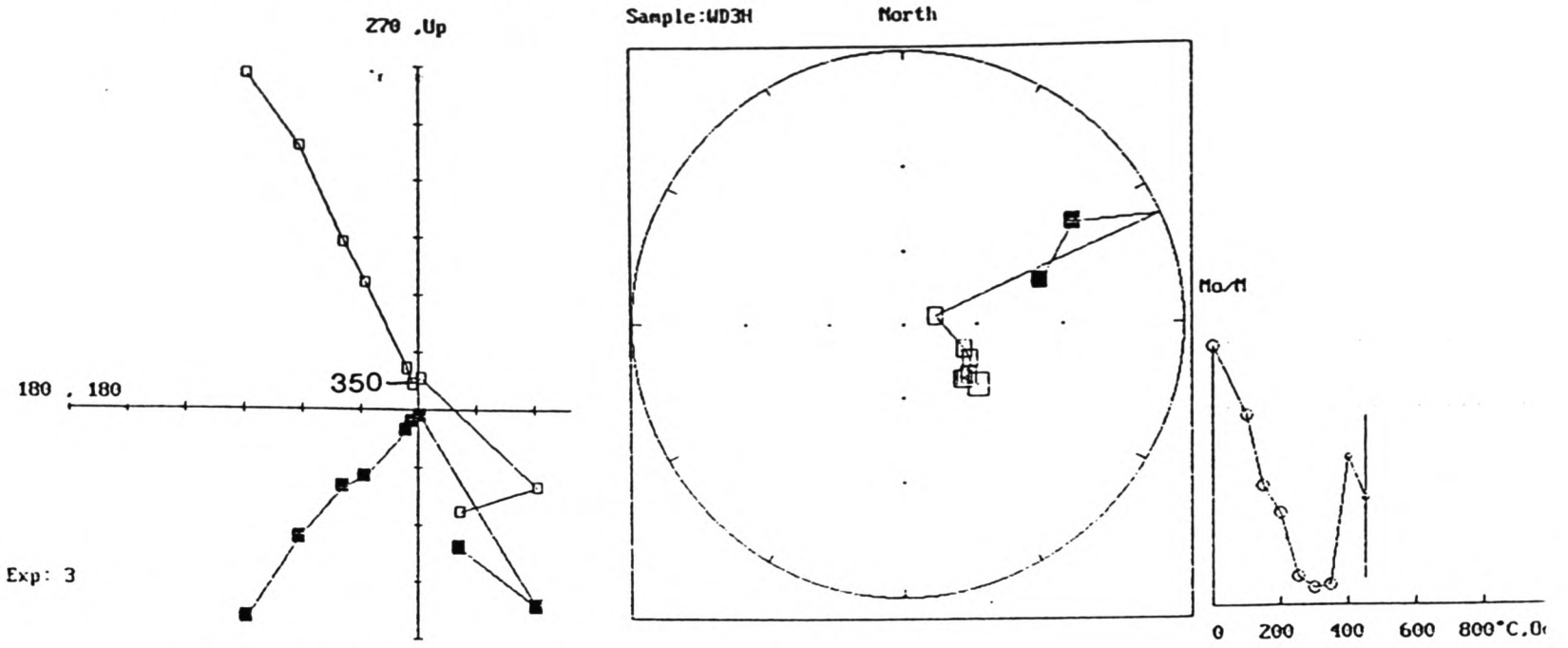
6.3.9b Demagnetization

Cores from this site had a maximum I_0 of 0.503 mA/m. An example Z-plots is shown in fig. 6.23a. All cores displayed a single component demagnetization to the origin removed between 0 and 350°C. Above this temperature the magnetization was unstable with corresponding intensity rise. The components (fig. 6.23b) did not group well (mean vector: 114/-69, α_{95}: 34.3). This scatter can only be interpreted as due to low viscosity grains having picked up viscous overprints. Due to this high scatter it was not felt possible to attempt to tectonically correct the data from this site.

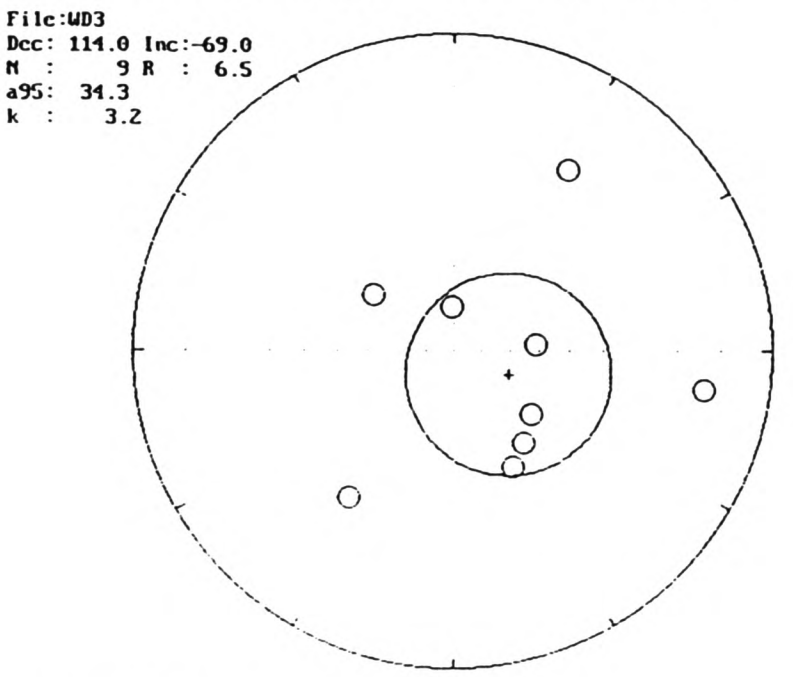
6.3.9c Remanence carriers

Geothite, low blocking temperature magnetites, (probably multidomain due to the low initial intensity of these cores) and pyrrhotites are all possible remanence carriers. Geothite dewatering at 350°C might explain the unstable intensity increase at this point.

a). WD3 thermal demagnetization.



b). WD3 high temperature components.



c). WD3 bulk suceptibility.

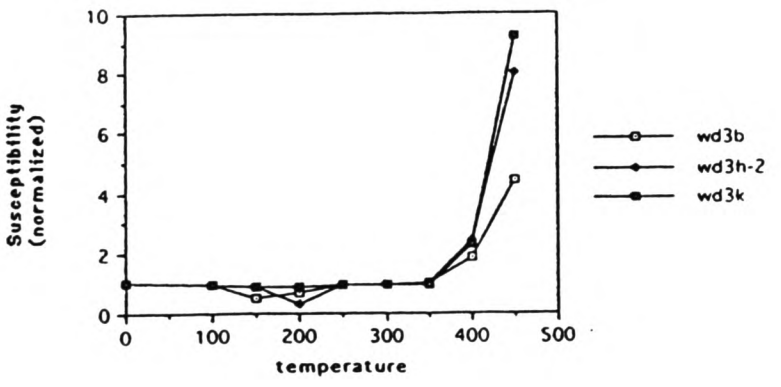


Fig 6.23: Data from the Washdyke Stream (site WD3). a). typical behaviour during thermal demagnetization. b). high temperature components from all WD3 site cores. c). typical bulk suceptibility for this site. All data is uncorrected.

Bulk susceptibility

An example of this is shown in fig. 6.23c. Susceptibility remains constant until 350°C whereafter it rises sharply corresponding to the increase in intensity and unstable magnetization observed at this point.

6.3.10 Silver Springs Site (SS1&2).

SS1&2: 173°52'/42°00' (GR: (P30) 814015).

6.3.10a Geological Setting, lithology and age

Structure

This site was drilled from siltstones exposed along the stream which terminates at the Silver Springs homestead in the western part of the Washdyke map sheet. The sequence of beds here from Upper Cretaceous through to Tertiary conglomerates has been interpreted as a conformable one (section 2.2). The sequence has been tilted and the eastward younging beds are presently slightly overturned, dipping at *ca.* 70° to the west. The tilted beds are cut by five dextral strike-slip faults (Faults 30b).

Bedding is clearly visible at site SS1. However the siltstones between this site and site SS2 are massive and no further bedding surfaces were identified. Beds much further to the west have the same dip and strike as at site SS1, which suggested that the beds inbetween (SS2) also have the same dip and strike. For this reason the two sites are put together as one site, site SS1&2.

No direct fold information is available for this site. However the beds are just west of the Razor fold and just north of the large-scale folding in the thick conglomerate body of the southern Washdyke. Both these folds have fold axes which plunge at *ca.* 60° to the NW. The strike of beds in the western part of the Washdyke map sheet is close to this fold axis direction. This together with the proximity of this site to these other folds for which data is available, suggested that the beds in question were tilted by folding about the same fold axis. These beds are closer to the Kekerengu Fault, therefore one would expect them to be the first to be overturned by compression from the west. The Razor Fold western limb would be affected later by this compression and therefore here the beds are only vertical and not yet overturned.

Lithology

Cores were drilled from a massive siltstone unit, Bedding was defined by flecks of organic material and confirmed by bedding in the conglomerate beds just above this location. A thin section of this lithology revealed *ca.* 45% of subangular, moderately well sorted, silt-sized quartz grains with minor glauconite, micas, opaques and heavy minerals within a

micritic matrix. Also observed were rare fragments of *globigerina* test. The evidence points to an outer shelf environment of relatively slow deposition, adjacent to an eroding landmass.

Ages

Two samples (samples R17 and R20, chapter 3) were analysed by Osborne (1980) from this lower siltstone lithology further to the north than site SS1&2. These gave an *Altonian* age. A sample taken from site SS1 (dated sample 114a, chapter 3) this study, gave an age of *Middle Altonian*. The siltstone is a part of the Waima Siltstone Formation.

6.3.10b Demagnetization

All cores from this site had weak initial intensities, $I_O$max: 0.19 mA/m. This is reflected in the example Z-plot of fig. 6.24a. It was not possible to recognize a primary, straight line component to the origin within any of these samples. Study of the stereoplots revealed that great circle analysis might enable the calculation of a primary component (figs 6.24b and 6.24c). This was successful and gave a mean direction of 118.4/53.93 (α95: 10.82). Above 350^{o}C unstable magnetization and an increase in intensity were observed.

6.3.10c Remanence carriers

The temperatures suggest geothite, low blocking temperature (probably multi-domain due to the low initial intensity of these cores) magnetites, Ti-magnetites or pyrrhotites. The intensity increase at 350^{o}C may be due to the dewatering of geothite at this temperature.

Bulk Susceptibility

Fig. 6.24c shows the changes in bulk susceptibility for several of the cores from this site. All show the same pattern of constant susceptibility up to 350^{o}C whereafter there is a sharp increase in susceptibility which corresponds to the intensity increase and unstable magnetization observed on the Z-plots. Mineral alteration of some kind is occurring at this point.

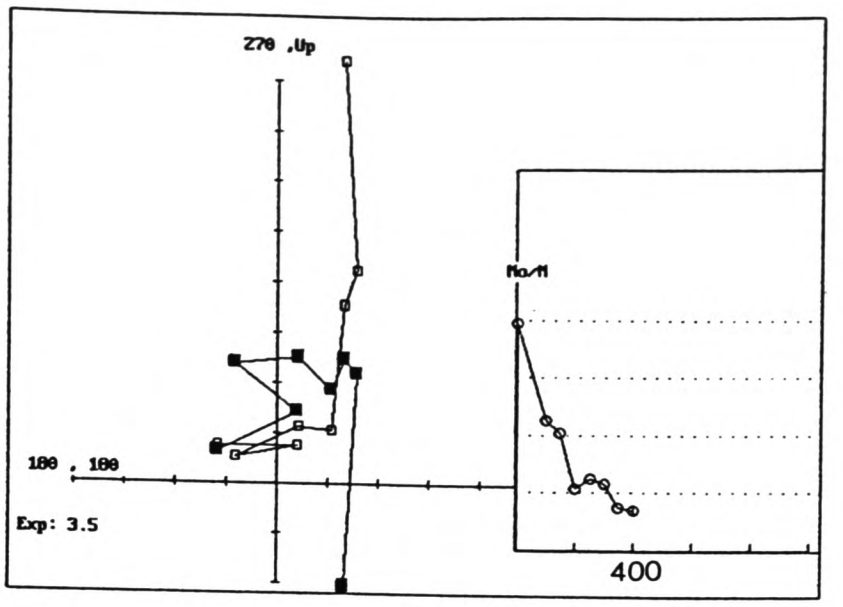
IRM

It is clear from fig. 6.24d that saturation is reached at *ca.* 140 mT signifying the presence of magnetites, Ti-magnetites, or pyrrhotites, and the absence of geothite or haematite (therefore the dewatering of geothite did not occur).

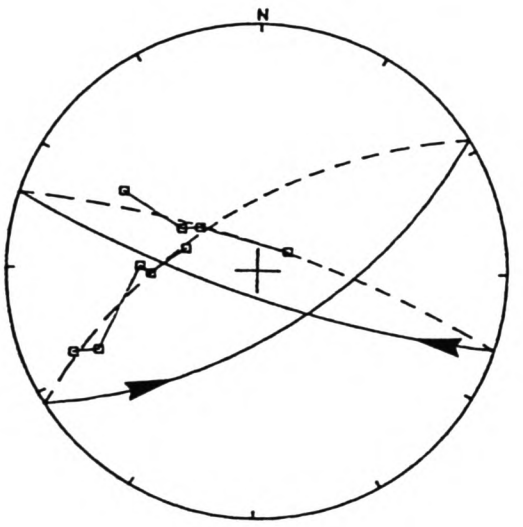
6.3.10.d Timing of the magnetization

After tectonic correction the mean inclination restores to a value closer to the expected inclination for the age of these siltstones, suggesting a pre-tilt, primary magnetization. This is discussed in more detail in section 7.3.10.

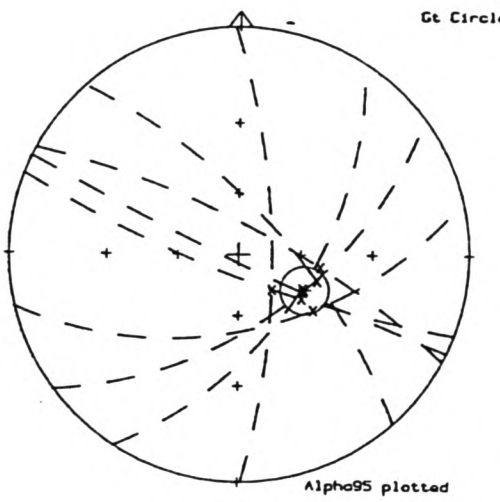
a). SS1&2 thermal demagnetization.



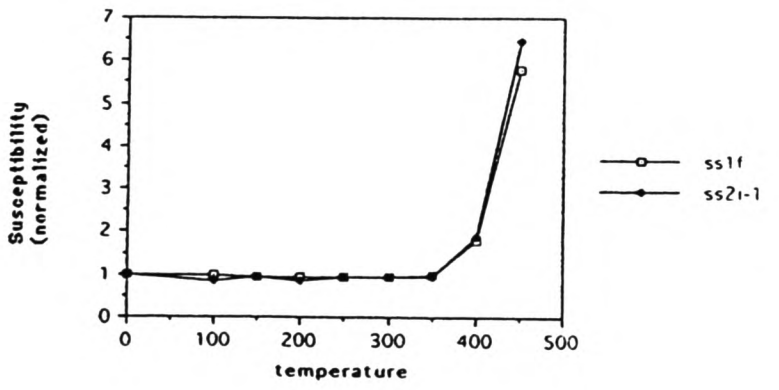
b). great circles



c). calculation of the mean primary direction.



d). SS1&2 bulk suceptibility



e). SS1&2 IRM data.

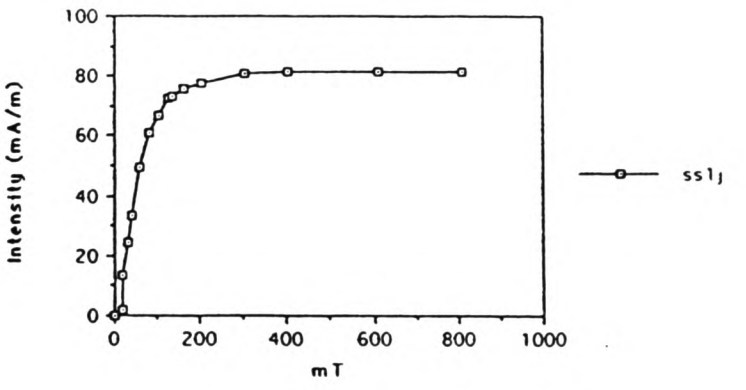


Fig 6.24: Data from Silver Springs (site SS1&2). a). typical behaviour during thermal demagnetization, b). example of intersecting great circles, and c). calculation of the mean primary component from all thermally demagnetized cores. d). Typical bulk suceptibility and e). IRM graphs for this site. All data is uncorrected.

6.4 Summary of the Remanence Carriers for all Sites

The table below (table 6.5) summarizes the remanence carriers deduced in the c). section of each palaeomagnetic site description. From the previous descriptions it became apparent that the majority of sites within the same lithological formation have identical remanence carriers, thus these are grouped under the relevant heading. The exception to this is that all Waima Siltstone and Heavers Creek Formation sites are mineralogically indistinguishable in terms of the magnetic grains which they contain. This is not a surprising result considering that the two units represent different stages of the same episode of uplift and erosion and that they are often labelled on the grounds of their position with respect to conglomerate horizons, rather than on a pure biostratigraphic basis.

	Sites	**I_o max - min (mAm^{-1})**	**Remanence carriers**
Basanitic dykes	GS1, WS1	2041.1 - 9.4	SD Ti-magnetite
Amuri Limestone	WC1, WC2, BB1&2	0.5 - 0.05	Haematite ± geothite, (Ti)magnetite
Waima Siltstone Formation	HC1, HC2, HC3, VC1, VC2, SS1&2 WB1	0.65 - 0.09	MD (Ti)magnetite ± pyrrhotite
Heavers Creek Formation	WB2&3, WD3	0.52 - 0.12	MD (Ti)magnetite ± pyrrhotite
Whanganui Siltstone	WD1, WD2	35.9 - 0.9	SD (Ti)magnetite ± pyrrhotite

Table 6.5: Summary of the remanence carriers from all palaeomagnetic sites.

6.5 The Stratigraphic Thicknesses of Each Site

It is important to average out the effects of secular variation by sampling over a wide enough stratigraphic thickness. In general approximately 10 000 years of sedimentation is required to average out these effects (Butler 1992). The stratigraphic thickness sampled at each site was recorded and used in conjunction with estimates of sedimentation rate to calculate the approximate time spanned by each site. Table 6.6 summarizes these results.

SITE	Thickness (m)	Approx. age span sampled (ka)
GS1	-	~40 000*
WS1	-	~40 000*
WC1	006.86	2287-343
WC2	002.10	0700-105
BB1&2	002.64	0880-132
HC3	005.80	0011.60
HC1	003.40	0006.80
HC2	004.50	0009.00
VC1	005.50	0011.00
VC2	004.90	0009.80
WB	720.00	1440.00
WD1	006.90	0013.80
WD2	006.90	0013.80
WD3	003.30	0006.60
SS1&2	052.50	0105.00

Table 6.6: Table summarizing the thickness of sediment sampled by each site and the corresponding age span deduced from estimates of sedimentation rate (see text 6.5). *: Age span after Grapes et al (1992).

The required thickness will of course also vary depending on the speed at which the magnetization was acquired. For particularly slow acquisition rates one would require still greater thicknesses of sediment to average out these effects.

In general the time span sampled by most sites is approximately 10 ka and above and it is assumed that secular variation is averaged in all cases.

The estimates of sedimentation rate are poorly constrained since very little data of this kind is available. Roberts (1992) used an average sedimentation rate of 500 mm ka^{-1} for his sites. This value was taken from magnetostratigraphic studies of silty mudstone strata in the Lower Awatere Valley (Kennett and Watkins 1974; Turner et al 1989; Roberts 1990). This data applies to Upper Miocene, *Tongaporutuan* to *Opoitian* aged sediments. Siltstone sites collected in this study are mostly of Lower and Middle Miocene, *Otaian* to *Lillburnian* age. Although the lithologies are similar the ages and particular tectonic settings are different and it may be unreliable to use the same value for all the siltstone sites except maybe for sites WD1 and WD2 which do fall into the same age range. However, this is the best available estimate.

Pelagic oozes are known to accumulate at rates of 3-60 mm Ka^{-1} (Berger 1974). Compaction will obviously affect these values when considering the lithified limestone thickness in terms of deposition rate. Turner (1975) gives an average sedimentation rate of 20 mm ka^{-1} for the Pendleside Limestone, a dark, fine-grained limestone alternating with marls. This was considered to be an approximate maximum rate. The massive, pelagic limestones in this study were assumed to have been deposited at a rate between 3 and 20 mm ka^{-1}. Table 6.6 below lists the thickness of sediment sampled by each site and the corresponding estimated age span of this thickness

APPENDIX to Chapter 6

Palaeomagnetic Demagnetization Data

This appendix lists all the palaeomagnetic demagnetization data described in Chapter 6. The appendix is divided into three parts. The first two parts (parts A and B) cover thermally demagnetized cores whilst the third (part C) covers cores demagnetized by the alternating field technique.

Part A presents the data from sites with non-overlapping blocking temperature or coercivity spectra. For these sites a least-squares fitting program was used to compute the high temperature components from each core. For each site the uncorrected in-situ declination and inclination from all cores (samples) and the corresponding bedding attitude is listed alongside each sample name.

Part B presents the data from sites with overlapping blocking temperature or coercivity spectra. For these sites great circle analysis was used to extract the components. For each site any set points (components found using a least-squares fitting program) used in the calculation of the mean magnetization direction are listed first. These are followed by the poles to the great circles from each sample whose demagnetization curve falls along a great circle through two component directions.

Part C presents alternating field demagnetization data. This data was used as evidence for the presence of magnetite grains as remanence carriers. For one of the three sites demagnetized in this way (site WD1) a least-squares fitting program was used to compute the components. For the other two sites (GS1 and WS1) great circle analysis was applicable.

PART A (thermal demagnetization, linefind data)

SITE: GS1

Sample	Uncorrected Dec	Inc	Bedding
B1-1	307	-71	193/30 W
B2-1	298	-58	193/30 W
C2-1	322	-55	193/30 W
C3-1	297	-64	193/30 W
D1-1	292	-63	193/30 W
D2-1	348	-64	193/30 W
E3	322	-64	193/30 W
F1-1	301	-61	193/30 W
F3-1	315	-60	193/30 W
G1-1	328	-63	193/30 W
G2-1	321	-59	193/30 W
H1-2	301	-55	193/30 W
I1-1	320	-58	193/30 W
J1-1	318	-41	193/30 W
J2-1	302	-51	193/30 W

SITE: WC1

Sample	Uncorrected Dec	Inc	Bedding
a2	233	43	292/47 N
a3-1	238	49	292/47 N
a5-1	229	41	292/47 N
a7-1	233	47	292/47 N
b1-1	226	47	292/47 N
b2-1	230	43	292/47 N
b4-1	243	42	292/47 N
b5-1	238	38	292/47 N
b6-2	217	44	292/47 N
c2a-1	245	41	292/47 N
c2a-2	239	37	292/47 N
c2b	253	34	292/47 N
c3b-2	248	42	292/47 N
c3c-4	247	46	292/47 N
c3e-2	257	46	292/47 N
c3b-3	247	40	292/47 N
c3a-2	255	43	292/47 N
c3d-2	248	40	292/47 N
c3f-2	254	49	292/47 N
c5a	229	54	292/47 N
c5f	220	44	292/47 N
c6d	221	48	292/47 N
c6i	222	50	292/47 N
c6b	224	41	292/47 N
c6e-2	224	39	292/47 N
c6g-3	221	44	292/47 N
c6j-2	234	50	292/47 N
c6a-2	229	43	292/47 N
c6f-2	223	54	292/47 N
c6h-2	224	51	292/47 N

SITE: WC2

Sample	Uncorrected Dec	Inc	Bedding
D2B-1	333	84	215/20 W
D3A	344	70	215/20 W
D3B	315	72	215/20 W
D4A	330	76	215/20 W

SITE: BB1&2

Sample	Uncorrected Dec	Inc	Bedding
BB1a	303	-10	016/84 E
BB1b-1	314	23	010/69 E
BB1c-2	324	17	013/60 E
BB1c-3	304	-1	013/60 E
BB1d	321	22	344/55 E

BB1f	297	13	015/56 E
BB1g-1	310	32	350/44 E
BB1g-2	304	34	350/44 E
BB1h	290	25	343/32 E
BB1j-2	283	44	343/32 E
BB1k	299	24	343/32 E
BB1l	292	11	343/32 E
BB1e	292	8	344/55 E
BB2a	162	-13	025/72 E
BB2c	316	-12	017/73 E
BB2d	319	3	017/73 E
BB2d-2	309	-5	017/73 E
BB2e	304	-1	017/73 E
BB2e-2	310	-6	017/73 E
BB2f-1	300	-17	017/73 E
BB2f-2	317	-19	017/73 E
BB2h	293	13	017/73 E

SITE: HC3

Sample	Uncorrected Dec	Inc	Bedding
HC3B	125	-12	024 60 E
HC3C	114	2	024 60 E
HC3D	123	-17	024 60 E
HC3G	125	-7	024 60 E
HC3H	112	-13	024 60 E
HC3H-2	114	-6	024 60 E
HC3I-2	115	-14	024 60 E

SITE: WD1

Sample	Uncorrected Dec	Inc	Bedding
A1	67	-33	011 66 E
B2	61	-29	011 66 E
C2	66	-30	011 66 E
D2	60	-31	011 66 E
E1-2	53	-30	011 66 E
E2-2	68	-32	011 66 E
F3	61	-33	011 66 E
G2	63	-30	011 66 E
M2	64	-29	011 66 E
N2	71	-31	011 66 E
O1	54	-33	011 66 E
P2	57	-29	011 66 E
Q1	48	-44	011 66 E
R2	71	-36	011 66 E
S3	58	-29	011 66 E

SITE: WD2

Sample	Uncorrected Dec	Inc	Bedding
WDA-1	70	-47	031/78 E
WDB-3	81	-26	031/78 E
WDC-2	70	-34	031/78 E
WDE-2	77	-36	031/78 E
WDF-1	84	-33	031/78 E
WDG-1	84	-23	031/78 E
WDH-3	78	-23	031/78 E
WDK-3	88	-26	031/78 E
WDM-1	102	-25	031/78 E
WDN-3	97	-27	031/78 E
WDO-2	83	-34	031/78 E

SITE: WD3

Sample	Uncorrected Dec	Inc	Bedding
WD3A	153	-45	025/80 W
WD3B	215	-31	025/80 W
WD3F	32	-22	025/80 W
WD3G	99	-13	025/80 W
WD3H	130	-55	025/80 W
WD3H-2	143	-50	025/80 W
WD3I	86	-61	025/80 W
WD3K	306	-56	025/80 W
WD3L	358	-74	025/80 W

PART B (thermal demagnetization, great circle analysis data)

SITE: WS1 **[Bedding: 193/30 W]**

Set-points

Sample	Uncorrected Dec	Inc
a1-1	340	-67
a3-1	249	-56
b1-1	128	-65
b2-1	297	-65

Great circles

Sample	Pole to great circle Dip dir$^{n.}$	Dip
a2-3	340	5
c1-1	297	32
c2-1	272	15
c3-3	335	17
d1-2	233	5
e1-2	340	5
e2-1	321	15
f1-1	331	14

SITE: HC1 **[Bedding: 005/33 W]**

Great circles

Sample	Pole to great circle Dip dir$^{n.}$	Dip
HC1a	232	9
HC1b	059	31
HC1d	264	7
HC1e-1	173	2
HC1e-2	260	15
HC1g	281	32
HC1h-2	234	16

SITE: HC2 **[Bedding: 069/86 W (overturned)]**

Set-points

Sample	Uncorrected Dec	Inc
HC2D	145	0
HC2B	160	-5

Great circles

Sample	Pole to great circle Dip dir$^{n.}$	Dip
HC2C	244	14
HC2E	43	7
HC2G	39	31

SITE: VC1 **[Bedding: 059/83 W (overturned)]**

Great circles

Sample	Pole to great circle Dip dir$^{n.}$	Dip
VC1B	314	54
VC1C	351	19
VC1G	331	19
VC1H	004	38
VC1I	338	34
VC1K	352	33
VC1L	326	15

SITE: VC2 **[Bedding: 319/70 N]**

Great circles

Sample	Pole to great circle Dip dir$^{n.}$	Dip
VC2a	133	38
VC2d	143	8
VC2e-1	332	4
VC2f	330	2
VC2h	345	4
VC2i	157	1
VC2j	299	34
VC2k	350	33
VC2l	338	17
VC2m	335	10
VC2n	340	8

SITE: WB **[Bedding: 255/70 N]**

Great circles

Sample	Pole to great circle Dip dir$^{n.}$	Dip
WB1F	266	21
WB1G-1	72	42
WB1H	34	41
WB1I-1	109	15
WB1J	71	24
WB1K	103	8
WB2B-1	44	5
WB2B-2	312	27
WB2C-1	317	35
WB2E-2	47	39
WB3B-3	297	12
WB3D	332	6
WB3E-1	48	44
WB3E-2	63	24
WB3G	267	21
WB3H-2	303	35
WB3H	323	5

SITE: SS1&2 **[Bedding: 180/76 W (overturned)]**

Great circles

Sample	Pole to great circle Dip dir$^{n.}$	Dip
SS1B	268	17
SS2B	310	30
SS2E	349	34
SS2G-2	326	29
SS2I-2	225	22
SS2J-1	18	12
SS2J-2	22	7
SS2K	209	17

PART C (alternating field demagnetization data)

SITE: WD1

Sample	Uncorrected Dec	Inc	Bedding
H1	62	-35	011/66 E
I1	38	-38	011/66 E
K1	62	-32	011/66 E
K2	53	-31	011/66 E

SITE: GS1 **[Bedding: 193/30 W]**

Set-points

Sample	Uncorrected Dec	Inc
e2-1	309	-58

Great circles

Sample	Pole to great circle Dip dir$^{n.}$	Dip
e1-1	33	10
h2-1	299	16
g1-2	343	25

SITE: WS1 **[Bedding: 193/30 W]**

Great circles

Sample	Pole to great circle Dip dir$^{n.}$	Dip
a1-2	229	7
c1-2	281	17
c2-2	294	17
c3-1	333	13

CHAPTER 7

CHAPTER 7: INTERPRETATION OF PALAEOMAGNETIC DATA

7.1 Introduction

If crustal blocks in a zone of deformation have rotated about a vertical axis, then the corrected primary remanent magnetization (after thermal or alternating field cleaning) for the blocks will have a declination divergent from coeval rocks in the adjacent undeformed boundary at the time of acquisition of the magnetization. The inclination of this magnetization must that expected for the latitude of the crustal block at the time of magnetization.

Plate reconstructions of the southwest Pacific during the Cenozoic based on seafloor spreading data (Walcott 1984b; Stock and Molnar 1987) and on the apparent polar wander paths of Embleton (1981) and Idnurm (1985), all show that the Australian plate has rotated *ca.* 20^{o} clockwise relative to the Pacific plate in the New Zealand region in the last 20 Ma (since Anomaly 6 time). During this time the Pacific plate has undergone negligible rotation relative to true north although there has been some latitudinal drift (Lawver et al 1992). Since the Marlborough region is contiguous with the Pacific plate, all rotations are quoted with respect to this plate. For rocks younger than 20 Ma, the amount of rotation will be equal to the mean palaeomagnetic declination minus the axial geocentric dipole declination (0^{o} for normal polarity and 180^{o} for reversed polarity) provided that the mean inclination is equal to that expected at the site palaeolatitude for a geocentric axial dipole field.

The tectonically corrected mean inclination can be converted to palaeolatitude using equation (1) below:

$$\text{Tan}\,(I) = 2\text{Tan}\,(\lambda) \qquad (1)$$

where I is the mean inclination and λ is the site palaeolatitude.

The inclinations and corresponding palaeolatitudes with errors are listed in table 7.4. The palaeolatitude can then be compared with the expected palaeolatitude considering the particular age of the site, using the plate tectonic reconstructions of Lawver et al (1992). As long as the observed inclination (or palaeolatitude) falls within error of the expected inclination (or palaeolatitude), and as long as confidence exists in the tectonic correction of the data, then any declination divergences may be interpreted as tectonic rotations about vertical axes.

For rocks older than 20 Ma, there has been substantial rotation of the Pacific plate relative to true north due to changes in longitude as well as latitude prior to this time. Because of this added complexity, it is not sufficient to simply take any declination anomalies from the north direction. In order to assess the expected declination and inclination for sites of a particular age in such cases, finite rotation and virtual geographic poles (VGP) were used to calculate the expected declination and inclination for each site at its present latitude and longitude. This technique involves selecting a VGP from a continent. The pole must be of the same age as the site under consideration. This VGP is then rotated back using the relevant finite rotation poles for motion between this continent and the New Zealand region, in order to determine the relevant VGP for the New Zealand region. The corresponding declination and inclination for a site of the age of this VGP can be calculated using the site's latitude and longitude. Once the effects of these latitude and longitudinal changes have been taken into account, any variations in declination (assuming inclinations are within error of the expected inclination) can be interpreted in terms of local tectonic rotations about a vertical axis.

7.2 Tectonic Correction of Mean Site Vectors

In order to interpret the palaeomagnetic data in terms of possible local tectonic rotations, the in-situ mean primary magnetization direction for each site must be restored to its respective orientations prior to tilting. This assumes that the magnetization was acquired pre-tilt. If this were not true the corrected inclination would predict a palaeolatitude widely different from that expected for the region.

Two separate tectonic corrections are applied to the high temperature or high coercivity component from each site (excluding site WB which was found to contain only a present-day field overprint). The first correction (correction 1) is a straight tilt correction (rotation about bedding strike). The second correction (correction 2) consists of a fold plunge and tilt correction for sites outside the Kekerengu-Washdyke study area, and of a two fold phase removal for sites within this area. The two phase fold correction is discussed in section 7.2.2.

7.2.1 Tectonic correction of sites outside the Kekerengu-Washdyke study area

The Awatere Dykes

Sediments in the Middle Awatere Valley area (fig. 6.2) are folded into a broad syncline with a slight southward plunge (FA: 220/07). This folding affects the whole sequence and therefore the primary magnetization directions of sites GS1 and WS1 have

been tilted into their present orientations. To check for local tectonic rotation about a vertical axis, the primary mean magnetization at each site must be corrected for plunge and tilt. The data used in this correction are shown below in table 7.1. These values can be compared with the uncorrected components (figs 6.3b and 6.4b).

	Bedding	Uncorrected mean magnetization	Plunge corrected mean magnetization	Plunge corrected bedding	Final tilt corrected mean magnetization	α_{95}
GS1	193/30 W	313/-60	324/-59	205/27.5	24/-75	4.8
WS1	197/30 W	285.2/-75.1	307.5/-73.8	209.1/27.9	107.8/-78	11.83

Table 7.1: Tectonic correction of sites GS1 and WS1.

The Woodside Creek Limestone

Sites WC1 and WC2 are a part of the Benmore Anticline (fold axis: 048/10 NE). Therefore plunge and tilt corrections are applied to the uncorrected mean magnetization direction at each site. The data used in this correction are shown below in table 7.2. These values can be compared with the uncorrected components (see also figs 6.8b and 6.9b.

	Bedding	Uncorrected mean magnetization	Plunge corrected mean magnetization	Plunge corrected bedding	Final tilt corrected mean magnetization	α_{95}
WC1	292/47 N	235/45	237/55	219.1/18.9	310/66	3.2
WC2	215/20 W	330/76	0.7/71.2	192.4/24.2	318/57	8.0

Table 7.2: Tectonic correction of sites WC1 and WC2.

The Boo Boo Stream Limestone

This site is within a limestone unit which is folded about a fold axis of 023/26 N (see fig. 6.10). Cores were drilled from many different bedding attitudes within each location. If one assumes that the primary magnetization was acquired pre-tilt, then the primary component from each core must be corrected for plunge and tilt using the correct bedding value for each core. The mean magnetization after these corrections has a value

of: 315/55, a95: 11.7. This should be compared with the same components prior to tectonic correction as shown in fig 6.11b.

7.2.2 Tectonic correction of sites from within the Kekerengu-Washdyke study area

The overall sequence of structures affecting the Kekerengu-Washdyke study area is described in 5.3.2.4. From this it is apparent that the sites have undergone early D_e thrusting and folding followed by a later D_l episode of tilting about a NNE-trending fold axis (D_{l1}), refolding about a NW-trending fold axis (D_{l2}), localized steepening of the major syncline western limb and 'bending' of the study area (D_{l3}), followed finally by young dextral strike-slip and reverse faulting (D_{l4}).

The first tectonic correction (Correction 1) involved a simple tilt correction taking into account the way-up of the beds. This however does not take into account the plunge of folding or the fact that the area has been interpreted as having been subjected to two phases of folding.

The second correction (Correction 2) takes into account fold plunge and the two phases of folding. All the sites have been subjected to two phases of folding with differing amounts of rotation under the second phase. To remove the second phase of folding, the amount and sense of rotation of the first phase fold axes must be known. With this information the site mean magnetization direction and the site bedding strike and dip can be corrected to their orientations prior to the second folding. The value of this rotation can be read from the small circle of fig. 5.5 if it is assumed that the first phase folds had zero plunge. The available data suggests that this is a reasonable assumption as the thrust stack due to earlier deformation (D_e) seems to have been more-or-less horizontal.

The second tectonic correction therefore involved reading from the stereographic projection the sense and amount of rotation by which the fold axis relevant to each site has rotated from the horizontal about the second fold phase fold axis (321/00). The mean direction and bedding were then rotated by this amount in the opposite sense about the second phase fold axis. It then only remained to make a tilt correction to the new magnetization direction using the new bedding strike and dip.

In addition to the Kekerengu-Washdyke area sites obtained in this study, magnetization directions obtained in previous studies (Deadman Stream and Camp Stream) have been recorrected using the correction described above.

This correction 2 procedure is sufficient in cases where the site has only been affected by the two phases of folding. One exception to this is site VC1 which was taken from beds subjected to a late rotation during displacement along the Heavers Creek Fault. Unfortunately it was not possible to obtain a stable primary component for this site and so this need not be considered. The only other sites with possible additional deformation

		Uncorrected	Correction 1		Correction 2							
SITE	LAT (^{0})	D/I (^{0})	D/I (^{0})	$\Delta\pm\delta$ (^{0})	-Plunge D/I (^{0})	-Tilt D/I (^{0})	Expected I (^{0})	α_{95} (^{0})	N	K	$\Delta\pm\delta$ (^{0})	Age (Ma)
GS1	41.98	313/-60	26/-75	24±15	324/-59	24/-75	72.2^r	4.8	15	65	22 ±15	83
WS1	41.98	285/-75	101/-75	99±42	307/-74	108/-78	72.2^r	12	12	15	106±63	83
WC1	41.93	235/45	308/66	136±6	237/55	310/66	55.5^r	3.2	30	67	138±6	55
WC2	41.93	330/76	316/57	144±11	0.7/71	318/57	55.5^r	8.0	4	133	146±11	55
BB	41.78	309/0	328/55	148±17	306/4	315/55	65.0^L	12^c	22	8	135±17	24

Table 7.3a: Palaeomagnetic data from sites outside the Kekerengu-Washdyke study area. Two tectonic corrections were made: correction 1, a simple tilt correction, and correction 2 where separate plunge and tilt corrections corresponding to the local structure were applied. Declination anomalies are given for both corrections. Positive anomalies indicate clockwise rotations (negative anomalies indicate anticlockwise rotations). Ages are approximate. ^{r}: expected inclination obtained by back rotation of virtual pole; ^{L}: expected inclination derived by taking the approximate age of each site and comparing this against the plate reconstructions of Lawver et al (1992); ^{c}: α_{95} after tectonic correction.

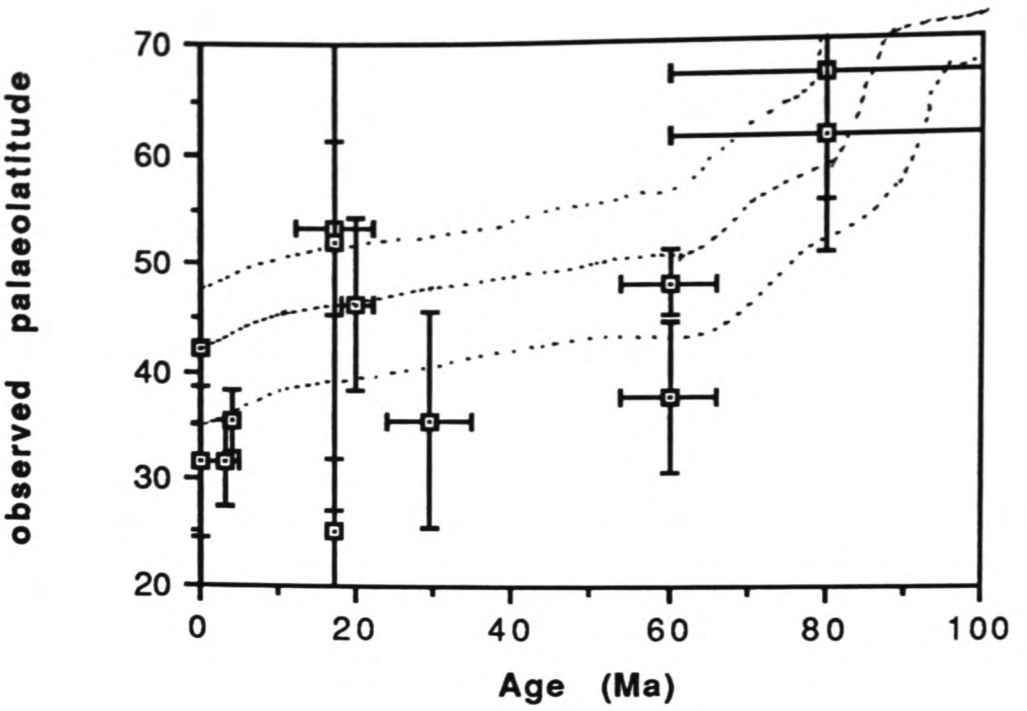
		Uncorrected	Correction 1		Correction 2							
SITE	LAT (^{0})	D/I (^{0})	D/I (^{0})	$\Delta\pm\delta$ (^{0})	-Plunge D/I (^{0})	-Tilt D/I (^{0})	Expected I (^{0})	α_{95} (^{0})	N	K	$\Delta\pm\delta$ (^{0})	Age (Ma)
HC3	42.00	118/-10	125/-70	125±15	129/-22	106/-70	65.00^L	6.4	7	90	106±15	Po-Sl
HC1	42.00	123/71*	247/71.6	67±0	106/68	249/72	65.00^L	29	7	6.9	69±X	M.Pl
HC2	42.00	147/21*	126/-70	126±59	144/23	121/-69	65.00^L	17	26	26	121±55	M.Pl
VC2	42.00	238/45*	43/64	-137±14	250/75	035/64	65.00^L	7.8	11	42	-145±15	Po
WB	42.07	7.1/-51*	PDF				61.02^P	10.5	16	15		
WD1	42.08	62/-32	349/-55	-11±5	167/-80	322/-55	61.03^P	3.4	15	143	-38±5	M.Wo-Wp
WD2	42.08	84/-31	356/-51	-4±8	155/-61	313/-51	61.03^P	6.3	11	53	-37±8	Wo-WN
SS	42.00	118/54*	122/-44	122±12	84/10	79/-44	65.00^L	11	8	37	79±12	M.Pl

Table 7.3b: Palaeomagnetic data from sites within the Kekerengu-Washdyke study area. Two tectonic corrections were made: correction 1, a simple tilt correction, and correction 2 where two phases of folding are separately removed (see section 7.2). Declination anomalies are given for each correction. Positive anomalies indicate clockwise and negative anomalies anticlockwise tectonic rotations. *: Mean calculated using great circle analysis; PDF: present day field, not tectonically corrected; X: declination error indeterminable due to steep inclination and large α_{95}; ^{L}: expected inclinations derived by taking the approximate age of each site and comparing this against the plate reconstructions of Lawver et al (1992); ^{P}: inclination derived using the present day site latitude and longtitude of these younger sites since no significant change in latitude is believed to have occurred since the formation of these sediments (Lawver et al 1992).

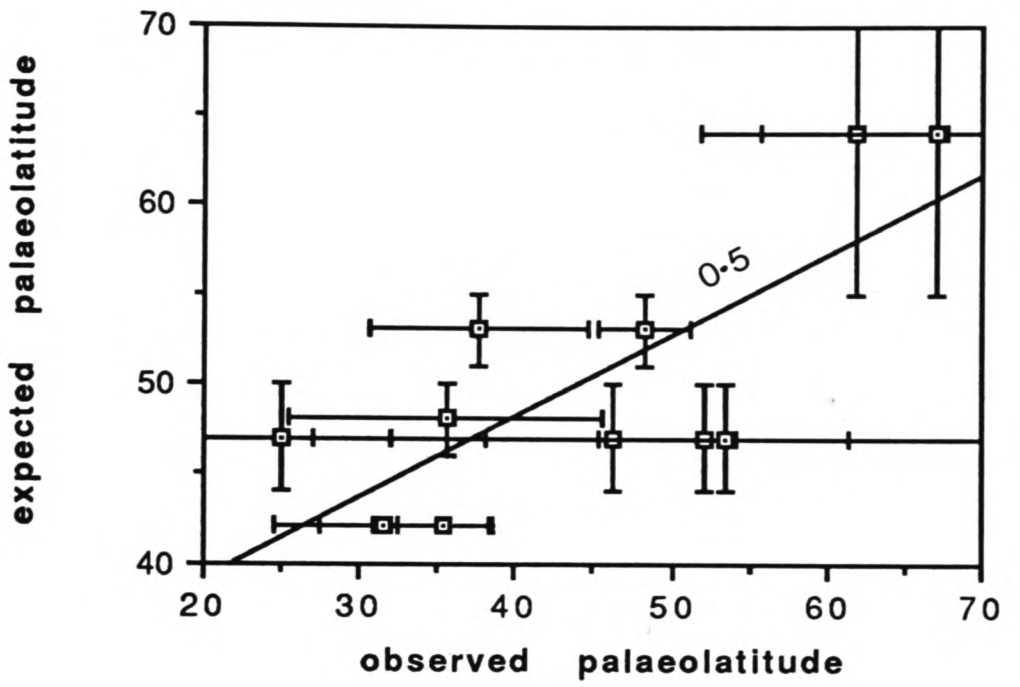
SITE	Declination Error D (^{0})	Inclination Error I (^{0})	PALAEOLATITUDE (^{0} S) Min.	Mean	Max.
GS1	14.90	03.79	55.76	61.81	68.38
WS1	42.22	09.48	47.68	61.81	79.06
WC1	06.31	02.56	45.01	48.32	51.85
WC2	11.25	06.08	31.62	37.59	44.56
BB1&2	17.00	09.60	26.89	35.53	46.48
HC3	14.84	04.99	47.01	53.95	61.80
HC1	00.00	29.00	24.69	56.36	69.48
HC2	58.74	17.00	33.57	53.95	84.02
VC2	14.25	06.16	38.49	45.71	54.19
WB	13.22	08.27	24.69	31.57	39.92
WD1	04.69	02.69	32.91	35.53	38.33
WD2	07.93	04.98	27.39	31.69	36.53
SS1&2	12.00	08.58	19.58	25.77	33.16

Table 7.4: Declination and inclination errors and range of palaeolatitude computed for each successfully demagnetized site. All results are based on correction 1 data: any minor differences in inclination after correction 1 and correction 2 are a result of the rounding up of values during the correction procedure. These results can be compared with the expected palaeolatitudes considering the age and position of each site. Refer to section 7.3 and to tables 7.3a and 7.3b.

(a)



(b)



(c)

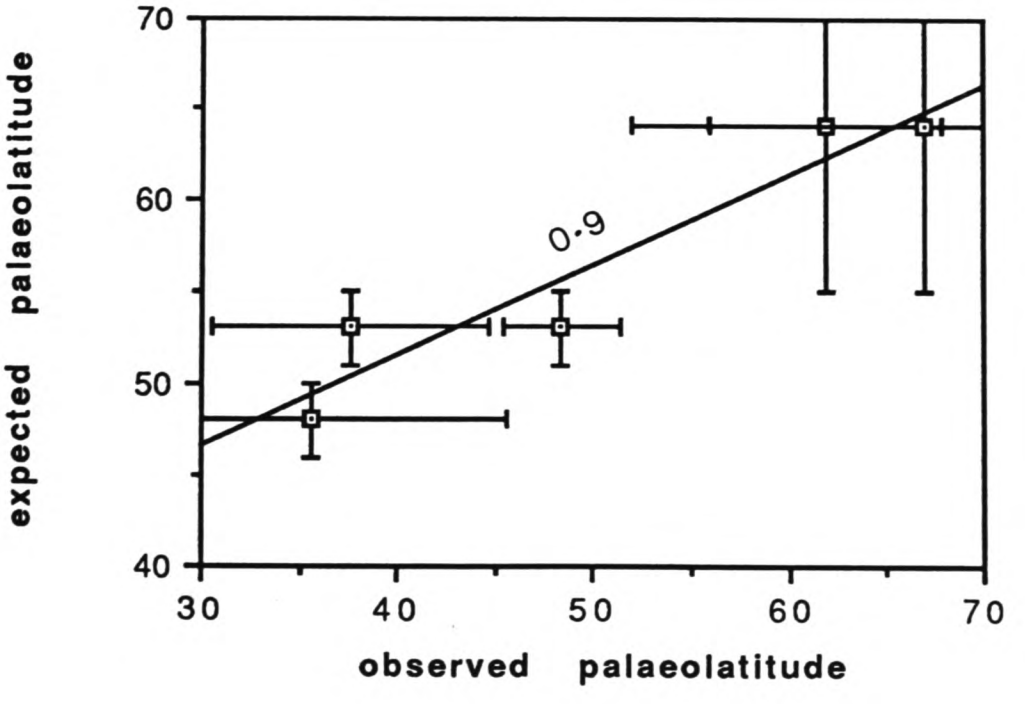


Fig. 7.1: Graphs comparing observed palaeolatitude for all successfully demagnetized palaeomagnetic sites against: (a) site age (in Ma); and against expected palaeolatitude for (b) all sites, and (c) sites aged over 20 Ma. A comparitive graph of expected palaeolatitude with age (after Lawver et al (1992)) has been added to graph (a).

were sites SS1&2. These were drilled from a unit displaced by NE-trending dextral strike-slip faults post-dating the two phases of folding. It is not clear if this faulting would have had an effect on reorientating the magnetization direction.

Tables 7.3a and 7.3b summarize the palaeomagnetic data and tectonic corrections for each site. Reference should also be made to table 7.4, which lists the declination and inclination and the observed palaeolatitude ranges for the tectonically corrected data of all the sites.

The following section (section 7.3) compares the tectonically corrected data against the expected inclinations considering the age and position of each site, and therefore deduces any local tectonic rotations (declination anomalies).

7.3 Checking the Declination and Inclination of the Tectonically Corrected Mean Site Vectors.

7.3.1 The Awatere Dykes

The following procedure was performed in order to check the corrected magnetization from site GS1 with the expected declination and inclination of coeval rocks of the south New Zealand with similar latitude and longitude. To perform this check the dyke age must be accurately known. As explained in section 6.3.1.a, this is believed to be between 60 and 100 Ma (Grapes et al 1992). It is possible to do a quick check of this age span using other New Zealand palaeomagnetic sites of these ages to see if the palaeolatitude of the dykes falls within error of the palaeolatitudes indicated by other sites. At either end of the spectrum, data is available for the 95 Ma Mount Somers Volcanics (Oliver et al 1979) and for the 54-66 Ma Amuri Limestone (Warren 1976; see also site WC1 in this study). The palaeomagnetic data for the dykes obtained during this study indicates a span in palaeolatitude of 55.76 to 68.38^{o} S (see table 7.4). The Mount Somers Volcanics give a palaeolatitude of *ca.* 80^{o} S (with an unquantifiable but large error). The Amuri Limestone gives a span in palaeolatitude of 45.01 to 51.85^{o} S. The errors of the Mount Somers Volcanics data are not known and so an overlap with this end-member cannot be ruled out. At the other end of the range, the palaeolatitude from the limestone site is of a marginally lower value than the lowest implied by the dykes. This limestone is in fact believed to be closer to 56-54 Ma, younger than the age of the youngest dyke (60 Ma). However, the values are so close as to suggest that the dykes could indeed range through to an age of *ca.* 60 Ma, as was concluded by Grapes et al. (1992).

The tectonically corrected palaeomagnetic data (both corrections) from GS1 gave a mean inclination of -75^{o}. This inclination corresponds to a mean paleolatitude of

61.87° S (table 7.4), a value expected for South New Zealand at *ca.* 80 Ma (reconstructions, Lawver et al 1992). Using the same reconstructions, the errors in paleolatitude are equivalent to an uncertainty in the age of ±10 Ma. Rifting is known to have begun in the Bounty Trough and Great South Basin at 90 Ma and continued through to *ca.* 80 Ma (Lawver et al 1992). The age inferred by the paleolatitude of the dyke data is therefore in keeping with these reconstructions.

Additional evidence to constrain the age of the dykes is the normal polarity of the dykes. The age of the dykes cannot be between 79-83 Ma because a major reversal occurred during this period (Harland et al 1982). Therefore, the Awatere dykes must have been intruded either between 70-79 Ma or 83-90 Ma. Since the main period of extension associated with the break-up of this part of Gondwana occurred between 80-90 Ma (Lawver et al 1992), the 83-90 Ma age range for the dykes is preferred. The mean paleolatitude would suggest that the age is nearer to 83 Ma. Therefore, although the errors in the inclination of the dyke magnetization suggest that the dykes could span a *ca.* 40 Ma age range, the mean magnetization and additional evidence of the polarity of the magnetization suggest an approximate age of *ca.* 83 Ma. This corrolates well with a phase of tectonic extension in this part of New Zealand, associated with the break-up of Gondwana.

The span in palaeolatitude implied from the WS1 site dykes is similar to that from site GS1, but with a slightly larger error. The dykes are of the same composition and come from a location close to site GS1. It was assumed that the two sites represent dykes intruded in the same extensional event and therefore of the same age.

It was then necessary to obtain an accurate expected declination and inclination with which to compare the tectonically corrected mean primary magnetization for the site latitude and longitude for undeformed South New Zealand rocks of the same age. This expected value was found by a series of back rotations of a known north VGP for Africa in the Cretaceous. This pole was chosen because it has an age close to that inferred for the dykes (ca. 83 Ma). The African VGP was then rotated back about the Africa/Antarctica finite rotation pole for 84 Ma. The resultant VGP was then rotated back about the South New Zealand/Antarctica (Marie Byrd Land) finite rotation pole for 84 Ma. The declination and inclination were then calculated from this final pole position for the latitude and longitude of the dykes. This value could then be compared with the declination and inclination of the tilt corrected data from this study. The data used is shown in table 7.5.

Virtual North Pole	Age (Ma)	Lat' (^{o}N)	Long' (^{o}E)	α_{95} (^{o})	Ref
S. Africa	81+4	68.3	248.6	3.4	1
Finite Rotn. Poles	**Age (Ma)**	**Lat' (^{o}S)**	**Long' (^{o}W)**	**Angle**	
Antarctica: Africa	84	-1.52	-40.03	17.23	2
S.NZ: Antarctica	84	65.10	-55.29	43.3	3

Table 7.5: Data used for comparison of remanent magnetization with expected declination and inclination for *ca.* 83 Ma dykes. 1: Wesselton site, Southern African Kimberlites, Hargraves (1989), 2: Scotese et al (1988), 3: Lawver and Scotese (1987).

The Results

Using the data in table 7.5 the Southern African palaeomagnetic pole for 83-92 Ma was rotated back to its position relative to South New Zealand at this time. The resulting pole position and the corresponding declination and inclination for the Awatere dyke site GS1, as well as the observed declination and inclination of magnetization for the Awatere dykes (after removal of fold plunge and tilt, this study), are listed in table 7.6 below.

Rotated north VGP	349.3/74.6
Expected Dec. and Incl. for site lat' and long'	01.9/-72.2 (α_{95}: 3.4)
Actual tectonically corrected Dec. and Incl.	24/-75 (α_{95}: 4.8)

Table 7.6: Results comparing the expected and actual remanent magnetizations for site GS1. The expected values are computed by the program VGP.

Conclusion

Tectonically corrected Awatere dyke magnetization suggests a palaeolatitude that is the same as the expected palaeolatitude based on the reconstructions of Lawver et al (1992) if the age of this site is *ca.* 84 Ma (refer to fig. 7.1). Table 7.6 shows the expected declination and inclination for undeformed 84 Ma rocks at the same latitude and longitude

as the dykes present location. Table 7.4 lists the separate declination and inclination errors for site GS1.

There is an anomaly of 22±15° in the declination data. This value excludes the uncertainty in the expected value (a95: 3.4) since it is not practical to separate the declination and inclination errors for this data as errors also exist in the finite rotation pole values. There appears to be evidence for a clockwise (the dykes are of normal polarity) rotation about a vertical axis which must have occurred since the acquisition of the primary magnetization in these dykes *ca.* 84 Ma ago. In the case of correction 1 (simple tilt correction) very little difference exists, indicating an extra clockwise rotation of 2°.

Assuming that site WS1 is of the same age as site GS1, it is possible to compare the component direction from this site with the expected declination and inclination from the rotated poles described above. The corrected inclination is within error of the expected inclination deduced from the series of back rotations. Comparison of the observed against the expected palaeolatitude from the reconstructions of Lawver et al (1992) also shows overlap (refer to fig. 7.1). The declination anomaly for this site is 106±63°. This large error is due to the steep inclination and high a95 of this site which make interpretation of this anomaly difficult.

7.3.2 The Woodside Creek Limestone sites

The age of these sites is known to be between 66 and 54 Ma (Warren 1976). Assuming maximum and minimum sedimentation rate for these rocks, an age range of 63 to 54 Ma is inferred (refer to section 6.3.2.a). A similar check of the declination and inclination to that applied to the Awatere Dyke data can be made. However, a more exact age is needed in order to choose a correct virtual pole and finite rotation pole with which to perform the procedure. Cores from both sites are reversed. Five periods of reversal are documented between 63 and 54 Ma. The palaeolatitude, with errors, of the corrected palaeomagnetic direction after plunge and tilt correction is shown in table 7.4. The variation in palaeolatitude corresponds to approximate ages of between 40 and 60 Ma (using the plate reconstructions of Lawver et al 1992), though the age of this limestone lies between 54 and 60 Ma. Three reversals are known from this range (Harland et al 1982). For site WC1 (spanning 7 m of sedimentary thickness), if one assumes a slow sedimentation rate of 3 mm/Ka, then *ca.* 2.3 Ma of reversal would be required to deposit this amount of sediment. Only the youngest reversal, occurring between 53.5 and 56 Ma (Early Eocene), spans a long enough time range. The faster rates would imply any of the three age ranges (20 mm/Ka over 0.3 Ma could deposit 7 m of sediment). However, the slower rate is considered to be the more likely because the pelagic and fine-grained limestone lithology suggests a slow sedimentation rate, closer to 3 mm/Ka. It is assumed that site WC2, which also contains reversed cores of identical lithology, is of a similar age.

The available data used to check the observed and expected declination and inclination of *ca.* 54 Ma limestone at the latitude and longitude of the Woodside Creek sites are listed below in table 7.7. For these sites, a south palaeomagnetic pole (calculated as an average of VGPs within the said age range) is chosen, rather than a single VGP, because this is the closest pole in terms of age found in the literature for which a relevant finite rotation pole also exists.

South Palaeomagnetic Pole	**Age (Ma)**	**Lat' (^{o}S)**	**Long' (^{o}E)**	**A95 (^{o})**	**Ref**
Antarctic Peninsula	54	70	017	8.2	1
Finite Rotation Pole	**Age (Ma)**	**Lat' (^{o}S)**	**Long' (^{o}W)**	**Angle**	
South N.Z: Antarctica (Marie Byrd-Land)	59.2	71.4	-59.57	38.28	2

Table 7.7: Data used for comparison of remanent magnetization with expected declination and inclination for 56-54 Ma limestone. 1: Watts et al 1984, 2: Scotese et al (1988).

The Results

The rotated south palaeomagnetic pole and corresponding expected declination and inclination for *ca.* 56-54 Ma rocks at the Woodside Creek sites are listed below in table 7.8. These can then be compared with the declination and inclination of the tilt corrected mean primary magnetization for the Woodside Creek sites.

Rotated palaeomagnetic pole	119.6/81.9
Expected Dec. and Incl. for site lat' and long'	351.9/-55.5
Actual Dec. and Incl.	310/66 (WC1)
	318/57 (WC2)

Table 7.6: Results comparing the expected and actual observed remanent magnetization directions for site WC1. The expected values are computed using the program VGP.

Conclusions

The inclinations of each site after tectonic correction are close to the expected inclination calculated by the back-rotation of the Antarctic Peninsula south palaeomagnetic pole. Any errors can be explained by: (i) the fact that a palaeomagnetic pole rather than a VGP is used; (ii) the finite rotation pole is slightly older than the assumed age of the limestone; and (iii) because the errors involved in both the determination of the age and in the expected declination and inclination are unknown.

Comparison of the range of palaeolatitudes from these sites with the expected palaeolatitude from the reconstructions of Lawver et al (1992) shows that site WC1 falls well within the error of the expected values, whereas site WC2 has a shallowed inclination but comes into the expected range. This suggests that the magnetizations are pre-tilt primary directions.

Since the inclinations are within error of coeval rocks in the adjacent undeformed boundary, correction 2 implies a clockwise rotation about a vertical axis of 138 ± 6^{o} and 146 ± 11^{o} for sites WC1 and WC2 respectively. Correction 1 suggests similar clockwise rotations (each 2^{o} lower than under correction 2).

7.3.3 Boo Boo Stream Site

The spread in possible palaeolatitude indicated by the palaeomagnetic data can be compared with the plate reconstructions of Lawver et al (1992). It is evident from this that the maximum palaeolatitude for this site (46.17^{o} S) is similar to that expected for the Oligocene age of this limestone (section 6.3.3.a), indicating an approximate age between 24 and 30 Ma. This age is close enough to the period in which rotation of the Pacific Plate has been negligible. Therefore, any declination anomaly at this site is taken from the north-direction.

The mean corrected inclination is slightly shallower than the expected inclination, based on the reconstructions of Lawver et al 1992, (see table 7.3a and fig. 7.1a). Such shallowing of inclination is a common phenomena of sedimentary rocks (Arason and Levi 1990a; Coe et al 1985). It can be produced by DRM acquisition in larger-grained sediments, by compaction (and therefore also by the rate of cementation), and by tectonic strain. If it is assumed that the shallowing of the Boo Boo Stream site is a sedimentary feature which has no effect on the declination, then the magnetization is a primary pre-tilt magnetization. The declination after tectonic correction 2 implies a large clockwise rotation of 135 ± 17^{o}. Correction 1 implies a similarly large rotation (but 13^{o} less).

7.3.4 HC3

Using the reconstructions of Lawver et al (1992), the tectonically corrected palaeolatitude is within error of the expected palaeolatitude considering the *ca.* 17 Ma age of this site. Therefore the results suggest a primary pre-tilt magnetization and a clockwise rotation of 125 ± 15^{o} and $106+15^{o}$ under corrections 1 and 2 respectively. This rotation must have occurred sometime since acquisition of the magnetization.

7.3.5 HC1

The tectonically corrected inclination overlaps with the expected inclination value considering the age and latitude and longitude of this site. In this case, the inclination before and after correction is similar, making it difficult to ascertain with any certainty the timing of this magnetization in relation to folding. The high α_{95} (29^{o}), coupled with the steep inclination, means that the declination error is extremely large and beyond the actual value of the declination anomaly recorded (67-69^{o} of clockwise rotation). Therefore, there is no actual evidence for or against a declination anomaly here since the acquisition of this magnetization, and the site cannot be used as evidence for or against tectonic rotation.

7.3.6 HC2

The large α_{95} value from the palaeomagnetic data at this site results in large declination and inclination errors. The corrected inclination falls within error of the expected inclination for rocks of the age and latitude and longitude of this site using the reconstructions of Lawver et al (1992), see fig 7.1. This suggests that the magnetization is both primary and pre-tilt.

Even considering the large errors involved in this case, a declination anomaly corresponding to a clockwise rotation about a vertical axis of 121 ± 55^{o} is indicated. Little can be based solely on this anomaly, but when considered together with the data from other more accurately constrained declination anomalies, the site backs-up this other evidence.

7.3.7 VC2

Although the formal error for this site was not particularly large (a_{95}: 7.8), the great circle analysis technique used to deduce the mean site declination and inclination consists of a large percentage of great circles of similar orientation. The mean direction is based quite heavily on one great circle which transects the others. The corrected inclination falls within error of the expected inclination considering the age and site latitude and longitude using the reconstructions of Lawver et al (1992), see fig. 7.1. The declination anomaly associated with the corrected magnetization suggests a large anticlockwise rotation about a vertical axis of 145 ± 15^{o}. This result is in marked contrast

to the clockwise rotations of the other sites from the same area (refer to HC3, HC2 and SS1&2). This result was discarded on the basis of it being based on unreliable great circle analysis data.

7.3.8 WB

The only magnetization component obtained from this site is a present day field overprint direction. The inclination of the mean component direction value is only 2^{o} outside of the expected range in palaeolatitude considering the present-day latitude and longitude of this site. The declination error indicates overlap of the mean declination with the present day axial dipole north- direction. This data suggests that no declination anomalies have occurred since acquisition of the present day field overprint in this area.

7.3.9 WD1-WD2

The corrected inclinations after tectonic correction for both these sites lie just outside the expected values using Lawver et al (1992), considering the present site latitudes and longitudes (site WD1 by *ca.* 3^{o} and site WD2 by *ca.* 5^{o}). This is clear on the graph of fig 7.1. The inclinations are shallower than expected.

If one considers these inclinations to be primary, pre-tilt components, then quite different declination anomalies are implied depending on the type of tectonic correction applied. Simple tilt corrections produce declination anomalies of -11 ± 4.7^{o} and -4 ± 8.0^{o} for sites WD1 and WD2 respectively. In comparison, correction 2 produces declination anomalies of -38 ± 4.7^{o} and -47 ± 8.0^{o} for sites WD1 and WD2 respectively. These two sites are the only sites which result in significantly different rotations depending on the particular tectonic correction applied. Which, if any, should be believed is hinted at by the palaeomagnetic data of Roberts (1990) from Camp Stream, immediately to the south of this area and within siltstones of identical age. This site was corrected for southward plunge and tilt and gave a declination anomaly of -5 ± 4^{o}. It is possible that the Washdyke Stream sites are in fact part of a unit refolded by the second phase of folding with a subhorizontal fold axis and therefore require only a simple tilt correction. This would make sense, considering the position of this area between a steeply northward plunging area (the Razor Fold) and a southward plunging area (Camp Stream). Thus, the fold vicinity of these sites may be nearly horizontal, rather than the same as that for the Razor Fold as assumed in correction 2. If one assumes then that correction 1 is the relevant tectonic correction to apply in this case, then site WD1 has rotated at least 6^{o} anticlockwise (-11 ± 4.7^{o}) whilst site WD2 shows essentially no declination anomaly (-4 ± 8.0^{o}).

7.3.10 SS1&2

The inclination of the mean magnetization direction after tectonic correction does not fall within error of the expected inclination considering the age and latitude and longitude of this site (fig. 7.1). The inclination is shallower than expected. If one assumes that this is a flattened primary magnetization, then corrections 1 and 2 respectively suggest clockwise rotations of 122 ± 12^{o} and 79 ± 12^{o} since acquisition of this magnetization.

7.3.11 Summary

Of the 15 drilled sites in this study, 14 were found to contain enough information to obtain a stable component (site WD3 is discarded). In only one of these cases (WB) was the mean, stable component interpreted as a present-day, overprint direction. A further three cases were discarded on the grounds of the large error involved (HC1) or the unreliability of the great circle analysis method of deducing the mean component for these sites (VC1 and VC2). For all the remaining sites, comparison of the corrected inclination tallies approximately with the expected inclinations for these sites considering their age and position. Several of the sites (WD1, WD2, SS1&2, BB and WC2) have a similar but slightly shallower inclination than expected. This is believed to be due to sedimentary factors which do not effect the interpretation of these magnetizations as primary.

Although the data discussed in the previous sections is suggestive of primary, pre-tilt magnetizations, further statistical tests are needed. Fold tests are used to obtain statistical comparisons of the uncorrected versus the corrected data in order to assess the timing of magnetization in relation to folding.

7.4 Fold Tests

The most straight forward and rigorous fold test is the McElhinney Fold Test (McElhinney, 1964). This test compares the direction dispersions before (k_1) and after (k_2) tectonic correction. It is important to compare like with like and so all directions within one data set must be of the same polarity. If this is not so, then the data should be inverted so that the reversed equivalents of these vectors are included.

7.4.1 Sites from this study

All the mean magnetization directions from this study (excluding the five discarded cases) were plotted together for cases of pre and post tectonic correction. The direction dispersions and the ratio of these values are listed in table 7.9 (row 1). The ratio exceeds that required for pre-fold magnetization at the 99% confidence limit which

suggests that the magnetization is in fact a pre-fold magnetization. Even so, there is considerable scatter of the mean directions after tectonic correction (a95: 16.6). With the knowledge that the inclinations are close to the expected inclinations for the sites, the results suggest rotations about vertical axes between 11 ± 4.7^{o} anticlockwise and 146 ± 11^{o} clockwise. The directions also appear to cluster into three groups: one group with a north-south declination; one with a *ca.* NNE-trending declination; and one with a declination trending *ca.* ESE-SE. The scatter in the third of these groups is as large as the difference between the other two. There is also significant scatter of the declinations within the second group. It is assumed that the scatter in inclination within each group corresponds to variations in the age of each site, with steeper inclinations in the older sites (refer to fig. 7.1).

It should be noted that the declination error for site WS1 is very large ($\pm63^{o}$) making it uncertain as to whether this site should be placed within the second or the third groups (it is arbitrarily placed within the third).

7.4.2 Sites from this study and from previous sites in Marlborough

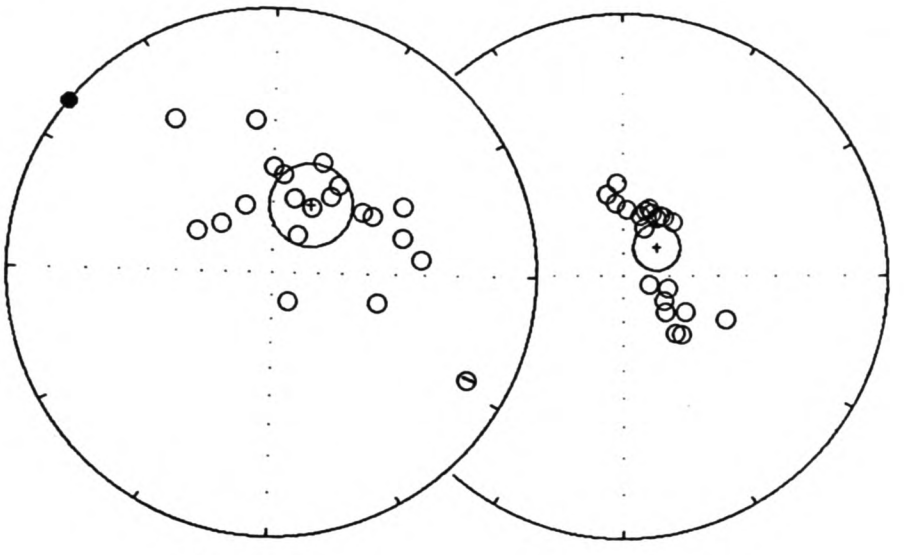
It was decided to investigate whether or not the three-fold grouping of the tectonically corrected magnetization directions is observable in the other palaeomagnetic sites of Marlborough (Roberts 1990, Mumme and Walcott 1985; Walcott et al 1984). All the data for the Marlborough region are plotted in both their pre- and post-tectonic correction orientations. These plots are shown in fig 7.2 and the dispersion values and ratio for the McElhinney Fold Test listed in table 7.9 (row 2). Again the dispersion ratio exceeds the required value for a pre-fold magnetization at the 99% confidence limit, suggesting that the magnetization is a pre-tilt magnetization.

The plots in fig. 7.2 show that the tectonically corrected data from all palaeomagnetic sites in Marlborough display the same three fold grouping of declination observed in the sites obtained only during this study. This, then appears to be a regional feature. These groups are shown in fig. 7.2 along with their corresponding mean tectonically corrected magnetization directions. Each group individually passes the McFadden Fold Test at the 99% confidence limit (table 7.9 (rows 3, 4 and 5)).

The explanation of these three seemingly distinct groups of different amounts of tectonic rotation is important to our understanding of the overall spatial and temporal partitioning of strain in the Marlborough region. Some sites have rotated up to *ca.* 130^{o} clockwise, whilst some only show clockwise rotations of the order of 20^{o} and others have not rotated at all. The question arises as to whether these different tectonic rotations can be linked to the particular ages of the sites which contain them, or whether structural boundaries of some kind are causing the distinctions, or indeed whether both these phenomena have governed the final result. That is, what is the spatial and temporal distribution of these rotations?

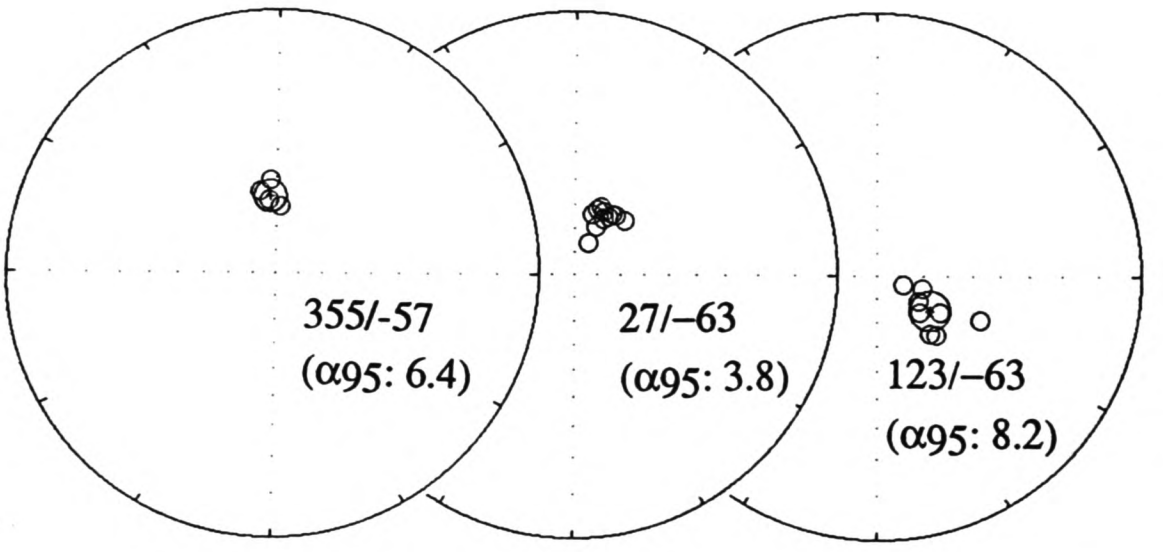
	N	k_1	k_2	k_2/k_1	Significance of fold test
1. All sites, this study*	10	02.5	009.4	03.76	Yes at 99% level
2. All Marlborough sites**	21	04.5	011.4	02.53	Yes at 99% level
3. Group 1	4	22.7	204.2	09.00	Yes at 99% level
4. Group 2	10	12.1	162.2	13.40	Yes at 99% level
5. Group 3	8	02.6	046.3	17.81	Yes at 99% level

Table 7.9: Table of McElhinney (1964) fold test data for mean palaeomagnetic site directions. Sites collected during this study (1) and all sites from the Marlborough region (2) show clustering into three groups of similar declination. The fold test data for these groups is also listed (3, 4, and 5). *: excluding HC1, VC1, VC2, WD3 and WB; **: sites from this study (also excluding the same sites) and from Roberts (1990), Walcott et al (1981) and Mumme and Walcott (1985).



(1) (2)

a). All Marlborough palaeomagnetic sites, pre (1) and post (2) tectonic correction.



b). Group 1 Group 2 Group 3

Fig. 7.2: (a). Uncorrected and tectonically corrected mean site directions for the Marlborough region. (b). Division of all the corrected palaeomagnetic site directions into three distinct groups of consistent declination anomaly. For direct comparison all the data points shown hves been converted into normal southern hemisphere polarity if they were not already so.

7.5 Tectonic Rotations in Marlborough

7.5.1 The Spatial and Temporal Distribution of Rotational Strain in Marlborough

Fig 7.3 shows the stratigraphic position and also the mean declination of palaeomagnetic sites in Marlborough. Fig 7.4 shows the declinations with errors of these sites on a geological map of Marlborough.

It is clear that all Group 1 sites are from Early Pliocene (4.2±0.6 to 3.3±0.3 Ma) siltstones (Roberts 1990). For these sediments, there has been no detectable rotation about a vertical axis in the last 4.2±0.6 Ma. However, other sites of similarly young age (8±1 to 3.9±0.8 Ma) suggest clockwise rotations of 21±3 to 44±5^{o} (Roberts 1990). These are the Group 2 sites. This clearly indicates that a post 3.9±0.8 Ma clockwise rotation affected some Upper Miocene to Pliocene sequences, but not all.

The most obvious distinction which might explain this difference is the spatial separation of these two groups. Group 1 sites are located on the downthrown side of the Kekerengu and Hope Faults, whereas Group 2 sites are all located on the upthrown side of the Kekerengu Fault in the region to the north and north-west of this fault.

Site GS1, in *ca.* 83 Ma Cretaceous dykes, is also included in Group 2. This suggests that the post 3.9±0.8 Ma clockwise rotation is not confined just to the younger Tertiary lithologies, but also applies to rocks north and north-west of the Kekerengu Fault.

Although the grouping of Group 2 site vectors is tight ($\alpha 95 = 3.8^{o}$), there is a slight systematic spread in declination between individual sites. Two subgroups can be distinguished with roughly a *ca.* 10^{o} difference in declination anomaly. Sites from the subgroup with the higher declination anomaly between the Awatere and London Hills Faults, bounded to the south by a northwesterly trending line at the end of the Clarence Fault. This was first noted by Roberts (1990). The subgroups are again spatially rather than temporally controlled. The two groups have average rotations of 21±4^{o} and 36±8^{o}.

Group 3 sites were all obtained from units aged between *ca.* 56 Ma and *ca.* 17 Ma. This rotation is not recorded in the Awatere Dykes of the Middle Awatere Valley or in any sediments aged 8±1 Ma or younger. This indicates that the rotation occurred post 17±0.5 Ma and pre 8±1 Ma. Group 3 sites on the downthrown side of the Kekerengu Fault have a slightly reduced clockwise rotation compared to Group 3 sites to the north of this fault. The difference between the average vectors of these two subgroups is *ca.* 22^{o}. This additional clockwise rotation of sites to the north of the Kekerengu Fault is approximately equal to the rotation recorded in the first subgroup of Group 2 sites (average *ca.* 23^{o}).

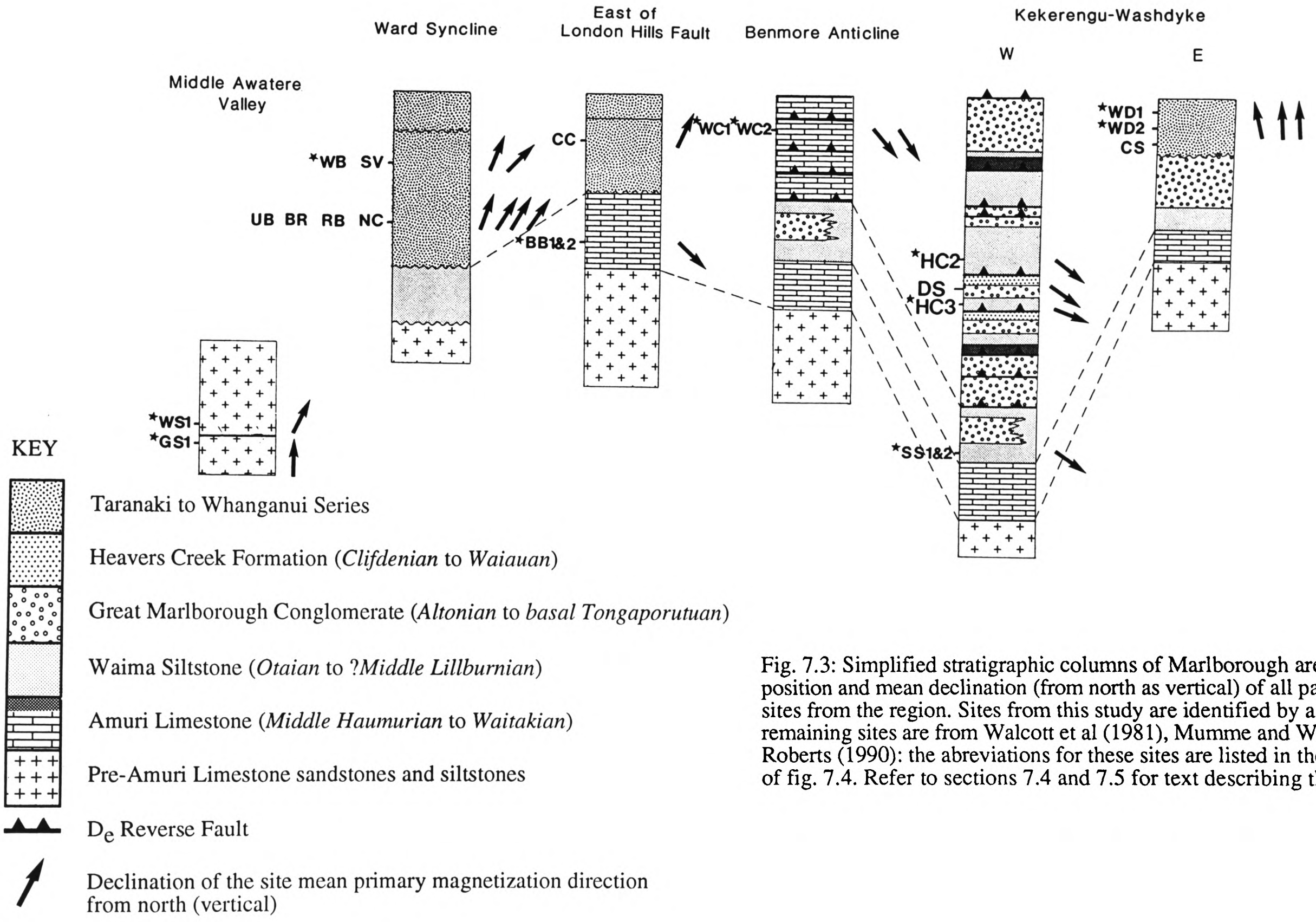


Fig. 7.3: Simplified stratigraphic columns of Marlborough areas showing t position and mean declination (from north as vertical) of all palaeomagnetic sites from the region. Sites from this study are identified by a "*". The remaining sites are from Walcott et al (1981), Mumme and Walcott (1985) Roberts (1990): the abreviations for these sites are listed in the figure capti of fig. 7.4. Refer to sections 7.4 and 7.5 for text describing this data.

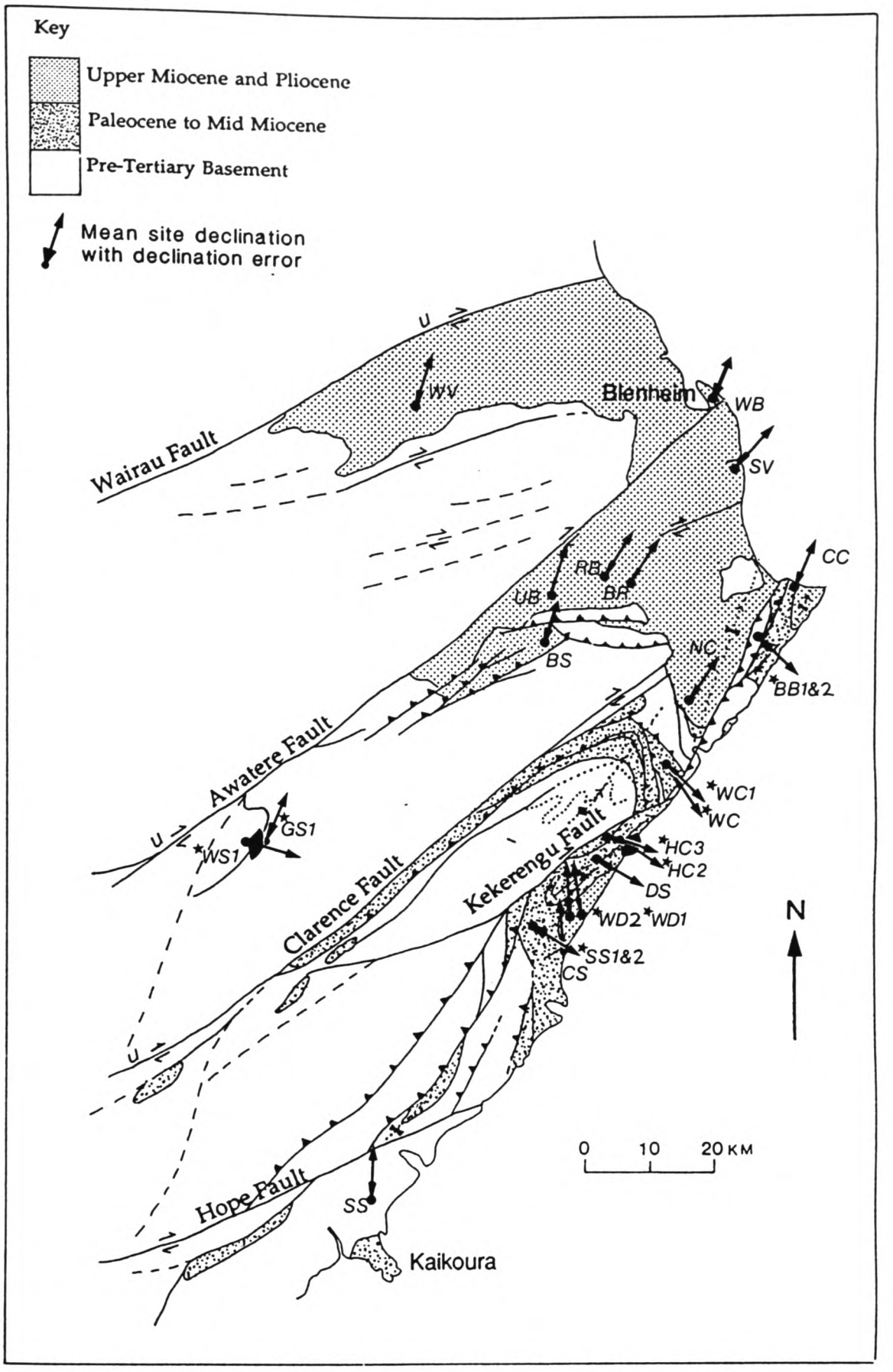


Fig. 7.4: Geological map of Marlborough showing the location and mean site declination with declination error of all palaeomagnetic sites from within the region. Sites from this study are identified by a "*". All remaining sites are from Walcott et al (1984), Mumme and Walcott (1985) and Roberts (1990). The abreviations for these other sites are as follows: (WV) Waihopai Valley, (WB) White Bluffs, (SV) Sea View, (RB) Richmond Brook, (BR) Blind River, (UB) Upton Brook, (BS) Boundary Stream, (CC) Cape Campbell, (NC) Needles Creek, (DS) Deadman Stream, (CS) Camp Stream, (SS) Swamp Stream. Refer to sections 7.4 and 7.5 for text describing this data.

Summary

Overall there appears to be three separate groupings of block rotation in the rocks of Marlborough: (i) a large clockwise rotation (Group 3) which affected *ca.* 56-54 Ma to 8±1 Ma stratigraphy; (ii) and two younger, spatially controlled rotations. Each rotation is summaized in fig. 7.5. The average Group 3 clockwise rotation is *ca.* 118^{o} in sites on the downthrown side of the Kekerengu Fault, with an additional *ca.* 21.5^{o} of clockwise rotation for similarly aged sites to the north of the Kekerengu Fault. This additional rotation is equal to the rotation recorded by Group 2 sites to the north and northwest of the Kekerengu Fault. A post 3.9±0.8Ma, regional rotation of *ca.* 23^{o} appears to have affected all of the Marlborough region except sites on the downthrown side of the Kekerengu Fault. In addition to this regional rotation, there is a slightly greater clockwise rotation (of *ca.* 10^{o}) of the area between the Awatere and London Hills Faults to the north of the termination point of the Clarence Fault. Thus, in detail, five separate groups of rotated rocks can be defined, depending on both the age and location of the rocks.

The large rotation event produced *ca.* 118^{o} of clockwise rotation in *ca.* 10 Ma. This corresponds to an average rotation rate of *ca.* 12^{o} /Ma. This rate is not unusually fast because similar rates have been recorded in other deforming continental areas (Verosub and Holm 1989; Allerton et al. 1993). Smaller clockwise rotations of *ca.* 23^{o} in the last 3.9±0.8 Ma, and *ca.* 30^{o} also in the last 3.9±0.8 Ma occurred in the Lower Awatere Valley area. The latter rotations correspond respectively to rotation rates of *ca.* 6^{o} /Ma and 8^{o} /Ma.

7.5.2 The Nature, Timing and Bounding Structures of Tectonic Rotations in Marlborough.

The palaeomagnetic declination anomaly data in Marlborough is consistent in terms of magnitude, sense, spatial extent and stratigraphic thickness. Since there is no evidence for pervasive and penetrative shear fabrics in any of the sample sites, it is suggested that three separate large-scale tectonic 'block' rotations are responsible for the declination anomalies. What then are the larger-scale structures which bound these rotating 'blocks' and can evidence from these help to further constrain the timing of each rotation event?

Group 3

The oldest rotation is a clockwise rotation with an average magnitude of 118±11^{o}. There is an upper age limit for this rotation defined by the age of the oldest rocks not affected (8±1 Ma). There must be a structure (fault) between sites SS1&2 and GS1 and WS1, which separates rotated from unrotated units.

The stratigraphy which records this large clockwise rotation is cut by D_e thrust faults which were active from the *Waitakian* to the *Kapitean*. The rotation affects uplifted limestone sequences as well as autochthonous and allochthonous thrust-derived deposits within the basin. It is unclear how much of this thrusting occurred prior to and post deposition of the Heavers Creek Formation (the youngest deposits involved in the thrusting).

There is very little time for rotation after the thrusting (the latest thrusting continued through to the *Kapitean* , *ca.* 5 Ma) and prior to 8±1 Ma, which suggests that it either took place progressively throughout D_e thrusting, or as a uniform rotation at some point in time within the age span of this thrusting. If progressive rotation were the case one would expect less rotation within younger thrust blocks assuming that thrusting occurred in a piggy-back style. However, the declination anomalies show no corrolation to height within the thrust stack.

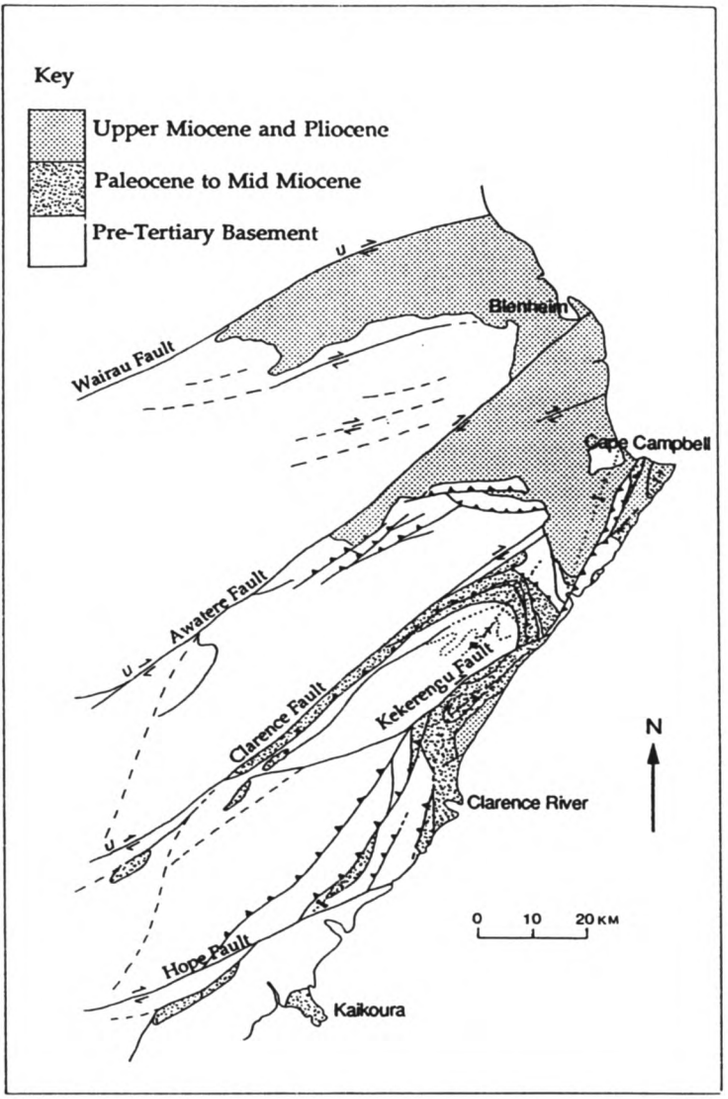
It is concluded that the large clockwise rotation occurred in *ca.* 10 Ma, after deposition of the youngest sediments which record this rotation (*ca.* 18 Ma) and pre 8±1 Ma. This corresponds to a minimum rotation rate of *ca.* 12^{o} /Ma. This rotation rate corresponds to a convergence rate of ca. 10 mma^{-1} at a point 50 km (approximate dimensions of Marlborough) from the axis of rotation.

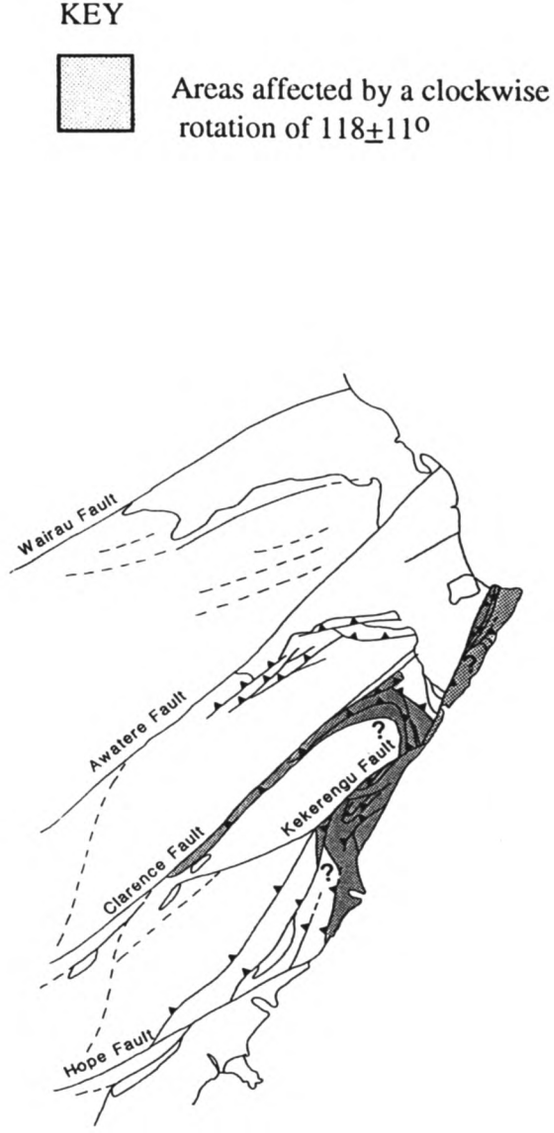
The structure or structures on which this rotation occurred are not clear. However, it is suggested that due to the high level of thrust faulting affecting the Marlborough region throughout the Miocene, that the rotation it is likely to be thrust controlled.

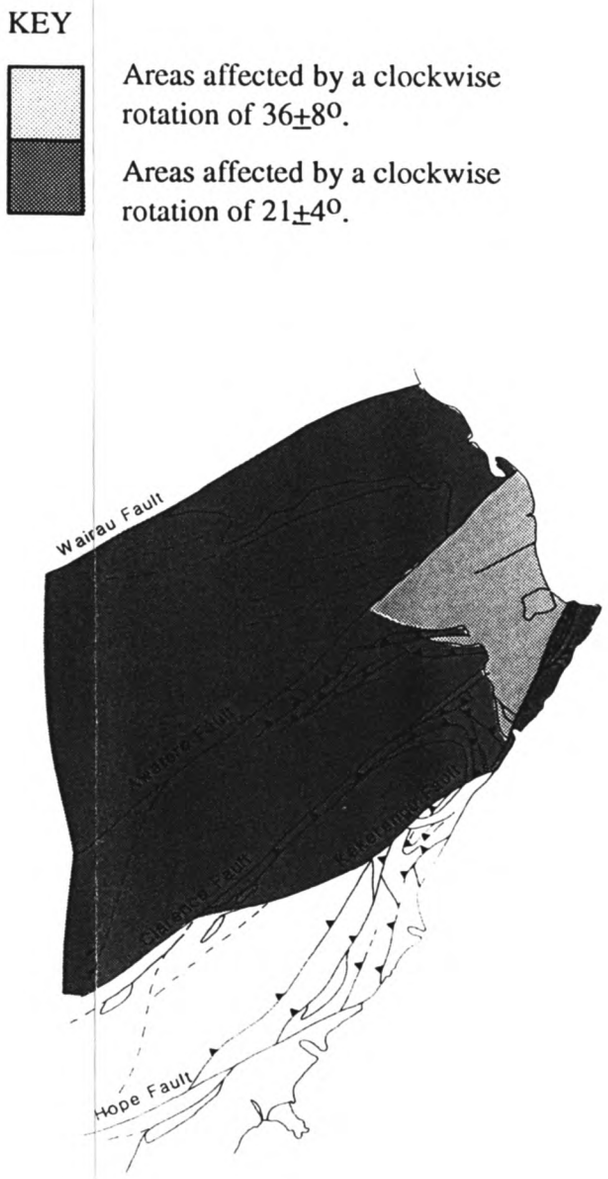
Group 2

Group 2 rotations were all found within sites on the upthrown side of the Kekerengu Fault. This is a regional rotation with an average value of 21 ± 4^{o} which occurred post 3.9±0.8 Ma. The dextral transpressional Kekerengu Fault appears to be the southern boundary of this rotating zone, with the rotation of the northern Marlborough region.

The differential clockwise rotation of *ca.* 8^{o} of an area of north-east Marlborough is clearly bounded by the Awatere and London Hills Faults and by the Flaxborne and Haldon thrust faults of the Lower Awatere Valley. This also occurred post 3.9±0.8 Ma and must also be associated with young, dextral strike-slip activity since this area is also bounded by D_l dextral, strike-slip faults. This second order rotation is believed to have been accommodated by displacement on the thrusts which bound this area and by extension to the north (Roberts 1990), as has been discussed in section 1.3.2.4 (fig. 1.7).







(a) Time interval: 18 to 8 Ma.

Clockwise rotation: 118±11°
Average rate of rotation: *ca.* 12° /Ma

(b) Time interval: 3.9±0.8 Ma to Present-day

Clockwise rotation: 21±4 Ma
Average rate of rotation: ca. 5° /Ma

Clockwise rotation: 36±8°
Average rate of rotation: ca. 9° /Ma

Fig. 7.5: Sketch maps of the Marlborough region showing the spatial distribution of tectonic rotations between: (a) 18 and 8 Ma; and (b) 3.9±0.8 Ma and the present. The data for this figure comes from sites obtained during this study and from Mumme and Walcott (1985), Walcott et al (1981) and Roberts (1990). Unshaded areas contain sites which display no rotation or within which no palaeomagnetic data is available. Refer to sections 7.4 and 7.5 for discussion of these rotations.

The three block rotations and the area which each of these affects are summarized in fig. 7.5.

7.5.3 Implications for the Orientation of D_e Structures

Reference to 5.3.3 shows the evidence used to determine a pre D_1 southward transport direction of De thrust faults. This took no account of the tectonic rotations which have been identified from sites throughout the thrust pile. In order to determine the true orientation of D_e prior to tectonic rotation as well as D_1 deformation, the southward transport direction must be rotated anticlockwise by the relevant amounts. The Benmore subregion was subjected to the earlier large clockwise rotation (average 118 ± 11^{o}) and to the D_1 regional clockwise rotation (average 21 ± 4^{o}). The Kekerengu-Washdyke subregion was only subjected to the large regional rotation (excluding minor 'bending' of the two halves of the area). Removal of the rotations results in *ca.* NW-trending seaward directed D_e thrusts, in marked contrast to the previously supposed landward directed thrusts (cf. Prebble 1976; Waters 1988).

7.5.4 D_1 Structures and Tectonic Rotation in the Cape Campbell-Ward Subregion

Displacement along the Clarence Fault is believed to terminate onshore since no evidence for any offset has been found in the strata in the region of the continuation of this fault to the north-east (fig. 7.6). In addition, palaeomagnetic evidence indicating differential rotation of north-eastern Marlborough (Roberts 1990) can be explained by assuming that the Lower Awatere Valley has acted as a rigid block rotating about the end of the Clarence Fault: the differential rotation itself caused by a velocity gradient set-up across the Lower Awatere Valley due to the termination of the Clarence Fault and continued displacement along the Awatere Fault (fig. 1.7).

During reconnaissance mapping of the Cape Campbell-Ward subregion, several features were observed which suggest that displacement may in fact have continued or be continuing between the supposed termination point and the coast.

These features can be clearly seen by reference to fig. 7.6. The Amuri Limestone ridge running from north to south is bent in a dextral sense along an ENE-trending shear zone with a bending rotation of *ca.* 35^{o} and a maximum displacement of *ca.* 1.3 km in the region of Boo Boo Stream. This is also true of the Cape Campbell Syncline fold axis. Also observed are two sinistral offsets of the limestone ridge to the south of Boo Boo Stream. These two sinistral faults have a combined offset of *ca.* 400 m.

Interpretation

The sinistral faults are at *ca.* 80^{o} to the trend of the dextral shear zone, an orientation in keeping with the expected orientation of synthetic faults within an ENE-

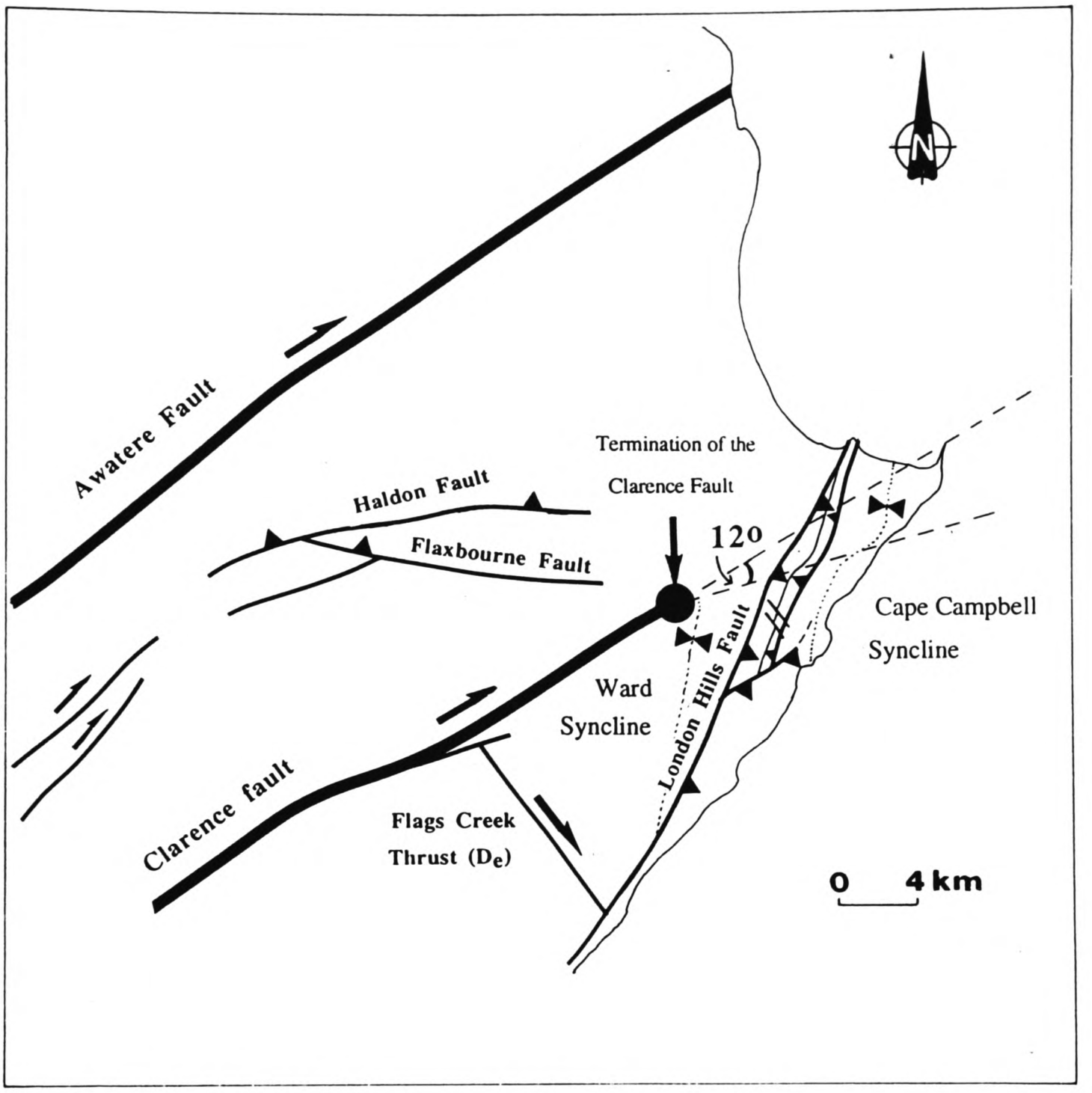


Fig. 7.6: D_1 structural map of the Lower Awatere Valley and Cape Campbell-Ward Marlborough subregions showing dextral shear of the Cape Campbell-Ward limestone ridge and Cape Campbell Syncline fold axis. The trend of this shear zone is rotated clockwise *ca.* 12^{o} from the trend of the Clarence Fault continued past the supposed 'termination point' of the Clarence Fault. The evidence suggests that distributed shear has in fact continued past the 'termination point' in the last ca. 300 Ka. Refer to section 7.5.4.

trending dextral shear zone (see fig. 5.14). Also apparent from the sketch of fig. 7.6 is the fact that the trend of the shear zone which offsets the limestone ridge is not exactly on-line with the projected continuation of the Clarence Fault, but is *ca.* 12^{o} clockwise of the trend of the Clarence Fault. Displacement on the Clarence Fault appears to have continued past the supposed termination point with dextral motion in the Cape Campbell-Ward subregion taken up as more distributed shear away from the end of the Clarence Fault.

The present-day rates of dextral strike-slip displacement on the Clarence Fault are between 4 and 8 mm a^{-1} (Browne 1992). This suggests that the observed 1.3 km of dextral shear in the Cape Campbell-Ward region could have been produced in 160-320 ka. Thus, the dextral shear found in the Cape Campbell-Ward subregion may be a very young feature.

These observations imply that in addition to the 21^{o} regional rotation, a further *ca.* 35^{o} of local clockwise 'bending' rotation should be removed from the value of clockwise rotation recorded in the limestone ridge sites (BB1&2). This leaves a D_e rotation of 79$\pm$17^{o}, suggesting that the D_e rotation contained local variations.

7.5.5 Overall Implications for Complex Deformation in the Kekerengu-Washdyke Study Area

The spatial distribution of D_1 rotational strain in Marlborough discussed in the previous sections has revealed that the Kekerengu Fault and associated deformation appears to have acted as the eastern boundary of the D_1 regional rotating northern Marlborough block. Tertiary cover sediments exposed on the downthrown side of the Kekerengu Fault are deformed in a far more complex manner than D_1 deformation affecting the rest of Marlborough. D_1 deformation in the study area has now been broken down into a clear sequence of events (5.3.2.4). One of the differences between this subregion and the others is the second phase of folding about a NW-trending fold axis and the 'bending' of this area hinged about an area in the northern part of the Washdyke map sheet, accommodated by slip along Fault 15 (see section 5.3.2, fig. 5.8). These two features accommodate compression in a *ca.* NE-SW direction which it is suggested is a result of the clockwise rotation of the rest of northern Marlborough. The Kekerengu-Washdyke area has effectively buckled due to the D_1 block rotation of the Northern Marlborough domain (fig. 7.7).

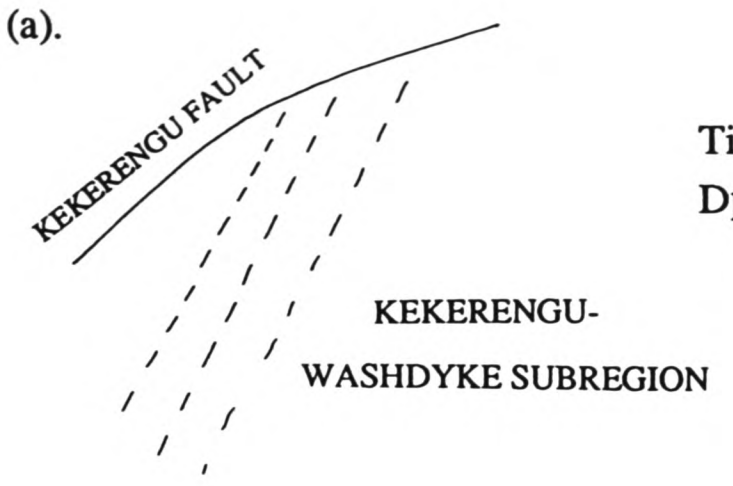


Fig. 7.7: Cartoon sketches showing (b) D12 buckling and (c) D13 bending of tilted beds in the Kekerengu-Washdyke subregion. These events are interpreted as being a consequence of compression associated with the *ca.* 20° D1 clockwise rotation of the rest of northern Marlborough.

CHAPTER 8

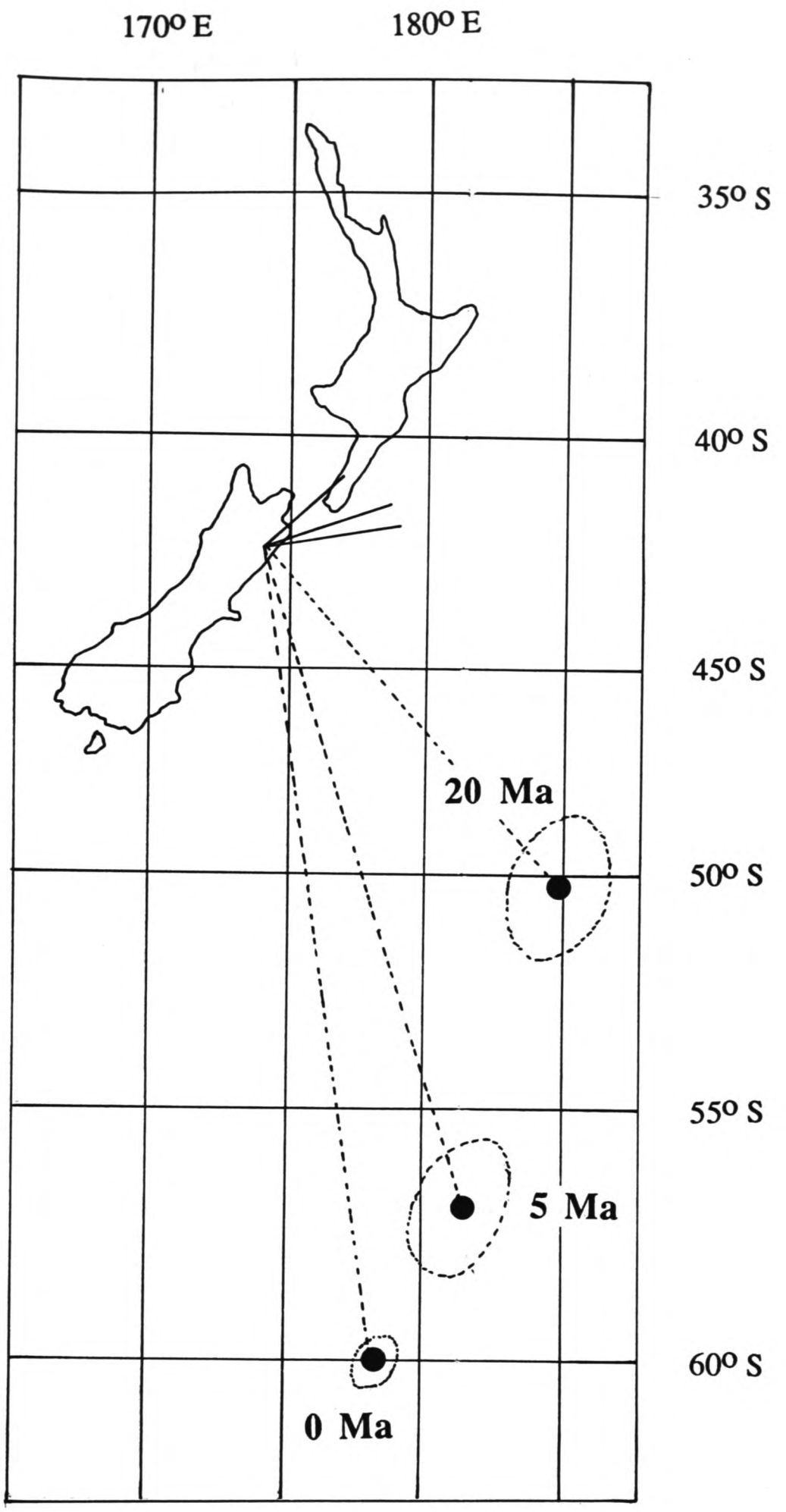


Fig. 8.1: Instantaneous pole positions for the Australian-Pacific plate pair at 20Ma, 5 Ma and the present day (20 Ma and 5 Ma poles from Smith 1981; present day pole from DeMets 1990). Approximate error ellipses are also shown. These poles indicate that relative plate motion in the Marlborough region has changed from SW-directed at 20 Ma, to *ca.* W-directed at the present day. Plate reconstructions (cf. Walcott 1984c) suggest that the Hikurangi Margin has rotated clockwise from *ca.* NW to NE during this interval. Overall the data implies a change in tectonic style from normal to oblique convergence.

that accommodating oblique compression today. Miocene thrust faulting and post-Pliocene transpressive structures are indeed documented throughout the plate boundary zone (Prebble 1976; Charnier and Ferriere 1991; Lamb and Bibby 1989). The rotation of the plate boundary has also been documented from palaeomagnetic analysis, and a *ca.* 20^{o} clockwise rotation in rocks throughout the plate boundary zone in the last *ca.* 4 Ma is recognized (Walcott et al 1981, 1984; Roberts 1992).

Onshore Geology

Studying in detail the onshore geology within the New Zealand plate boundary zone not only improves our understanding of the internal deformation and geological history of this region, but may also help to constrain the plate reconstructions themselves, which are also subject to uncertainties. In effect, plate reconstructions and detailed geological observations from within the plate boundary zone must be used hand-in-hand in order for one to constrain the other. Results from such work will have important implications for the study of fossil plate boundary zones where insufficient geological data exists with which to attempt to understand the more general plate tectonic setting.

In the Marlborough region previous authors (Lensen 1962; Prebble 1976; Lamb and Bibby 1989; Waters 1988) have identified thrust faults which are later refolded and cut by post-Pliocene dextral transpressive faults. Rait et al (1993) thought that the early thrusts were landward-directed, in marked contrast to seaward-directed thrusts described from the North Island (Charnier and Ferriere 1991). Palaeomagnetic studies in the region have shown that Marlborough can be divided into northern and southern domains (trellis model, Lamb 1988). The northern domain has rotated *ca.* 20^{o} clockwise in the last *ca.* 4 Ma (Walcott et al 1981; Roberts 1992), whilst the southern domain has remained fixed overall in orientation with possible small crustal fault block rotations (Lamb and Bibby 1989; Roberts 1992; fig. 1.6a). Roberts (1992) also identified a differential rotation of the Lower Awatere Valley in the northern domain. The boundary between the two domains coincides with a change in the trend of the Marlborough Faults from 055^{o} to 070^{o}. This boundary also separates an area to the NE with a steep Benioff zone extension at depths of between *ca.* 100 and 250 km, from an area to the SW where the Benioff zone terminates abruptly at depths of more than *ca.* 100 km (Anderson et al 1993).

However, the details of these observations and models have not been worked out and are not properly understood. The aim of the following sections is to produce a more coherent picture of the evolution of the Marlborough region, focusing on each of the various major strands of evidence discussed in this thesis.

8.2 Conclusions from this Study

8.2.1 The Sedimentary Evidence

Sedimentary evidence from the Kekerengu-Washdyke study area reveals a change from biogenic to clastic sedimentation beginning in the Early Miocene (*Waitakian* stage, *ca.* 24 Ma). The clastic sediments consist of turbidite and debris flow deposits including extra-basinally derived rounded clasts of basement from an uplifting land source, to intra-basinally derived angular to subrounded clasts of limestone and flysch. Foraminifera from siltstone units are a mixture of benthic and planktonic species (chapter 3), suggesting deposition in an outer shelf-upper slope environment. Rare wood fragments are found within debris flow deposits which together with the following observations indicate the nearby presence of land. The debris flow deposits fill erosional channels cut into massive and turbiditic siltstones, and accumulate in great thicknesses (up to *ca.* 1.7 km). Palaeoslope data (Lewis et al 1980) indicates flow from the WNW (not taking into account tectonic rotations, see section 8.2.3) in debris flow deposits from Deadman Stream.

The evidence overall suggests feeder channels shoreward of a submarine canyon in the outer-shelf to uppermost slope environment with clasts derived from extra and intrabasinal uplift. This evidence together with the synsedimentary nature of some thrust faults cutting these debris flow deposits also in the Kekerengu-Washdyke area, (see 8.2.2) is summarized in the cartoon sketch of fig. 8.2.

8.2.2 Structural Evidence

The sediments are repeated by kilometre scale thrust faults (a total of nine of which are exposed in the study area). An Upper Miocene unconformity identified in the study area (chapter 3) marks the cessation of this period of thrusting and thrust-derived sedimentation by the Pliocene (*Waipipian* stage). Overlying Pliocene sediments are not cut by these early thrusts, but are tilted and cut along with all other sequences by a series of folds and reverse and strike-slip faults.

Deformation in the study area is divided into two phases: D_e (*Waitakian* to *Kapitean* thrust faulting and thrust derived sedimentation); and D_l (*Waipipian* to Recent structures accommodating dextral transpression).

Early Deformation (D_e)

D_e thrust faults repeat extra and intra-basinally derived debris flow and turbidite clastic sediments, and are detached mostly along incompetent layers in the upper parts of the underlying limestone sequence. One such thrust transports a kilometre-scale thrust sheet of Amuri Limestone on its hanging wall, overriding thrust breccia and

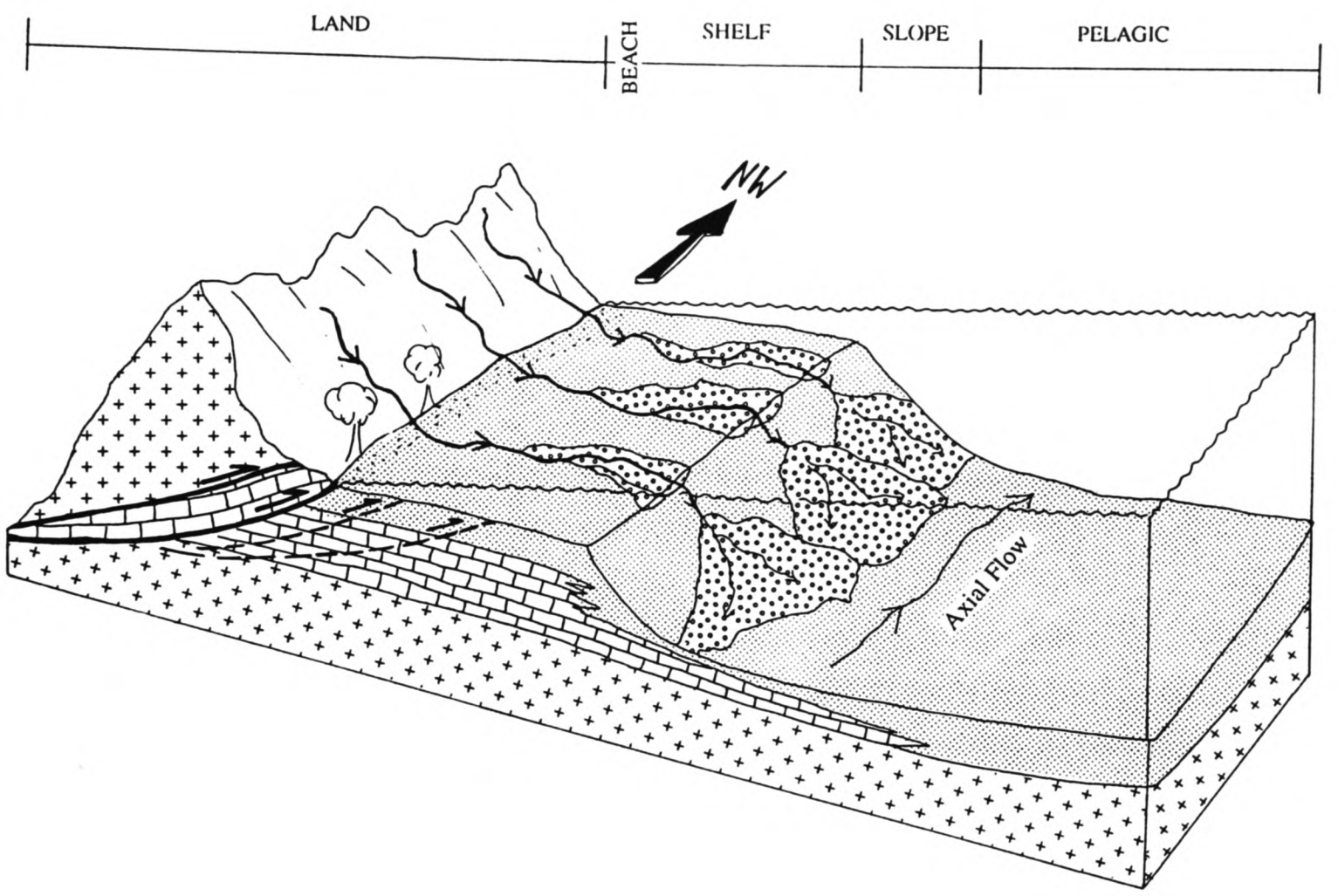


Fig. 8.2: Schematic block diagram showing the general sedimentary environment in the Marlborough region during the Miocene (D_e). NW-trending seaward directed D_e thrusts uplift basement and overlying Amuri Limestone and thrust derived clastics (consisting of flysch, turbidite and debris flow deposits). Fragments of wood from the nearby uplifted land source are also found. Foraminifera contents of samples reveal a mixture of benthic and planktonic forms, suggesting deposition in an outer-shelf to upper slope environment and possible reworking of the sediments. Debris flow deposits from within the Kekerengu-Washdyke study area indicate axial flow.

previously deposited debris flow conglomerates. Syn-sedimentary thrusting is therefore occurring within the basin of deposition. It is suggested that the thrusts may have formed in piggy-back style, progressively affecting earlier thrust-derived sediments within the basin. Due to the relatively short time period (*ca.* 5 Ma) in which to achieve this thrusting if all the thrusting occurred post deposition of the youngest sediments involved in the thrusting (*Lillburnian* to *Waiauan* aged Heavers Creek Formation), it is suggested that some of the younger sediments may have been deposited whilst thrusting continued, perhaps in piggy-back basins (cf. Ori and Friend 1984).

Comparison of stratigraphies from different subregions of Marlborough (chapter 2) has shown that within D_e at *ca.* 11 Ma a change occurred in areas to the north and east (the Lower Awatere Valley and Cape Campbell-Ward subregions) which were previously uplifting to supply sediment to areas to the south and west (the Benmore, Kekerengu-Washdyke and northern Canterbury subregions). The uplifted areas became resubmerged to receive sediment, with Upper Miocene synsedimentary thrusting in the Lower Awatere Valley subregion.

In the Benmore subregion, D_e thrust faults folded by compression associated with later dextral strike-slip activity are observed cutting progressively younger rocks around to the east (fig. 5.9). Removal of the later deformation suggests roughly S-directed D_e thrusting (not taking into account tectonic rotations).

Late Deformation (D_l)

Within the complexely deformed Kekerengu-Washdyke study area a sequence of younger D_l events is identified. This consists of four main episodes: (D_{l1}) folding and reverse faulting about a NNE-trending fold axis; (D_{l2}) refolding of the earlier folds about a NW-trending fold axis; (D_{l3}) oversteepening of the western limb of a syncline in the centre of the area with dextral strike-slip faulting to the west and sinistral displacement along an E-trending fault; and (D_{l4}) dextral and sinistral strike-slip faulting and NNE-trending folding and reverse faulting.

Folding (D_{l1}) is best explained as a consequence of the termination of dextral strike-slip along active faults bounding this area to the north (the Kekerengu Fault) and south (the Hope Fault). Folding (D_{l2}) and the structures in episode (D_{l3}) are linked to an aspect of D_l deformation that can be best understood in the light of palaeomagnetic analysis (see section 8.1.3); and finally the late (D_{l4}) structures accommodate dextral strike-slip in the area.

The complex structure of this area is in marked contrast to the deformation of other areas of Marlborough which display simple folding due to bounding dextral strike-slip faults and uplift of the western side of the main dextral strike-slip faults due to the obliquity of convergence which these faults accommodate.

8.2.3 The Palaeomagnetic Evidence

Extensive sampling of sites for palaeomagnetic analysis in the study area and at other previously unsampled locations in Marlborough, led to the recognition of further aspects of the accommodation of rotational strain in this part of the plate boundary zone.

D_e Rotations

Large clockwise rotations similar to that previously identified at one site in the Kekerengu-Washdyke study area were found within three more Early Miocene sites in the study area and in three sites from older limestone lithologies elsewhere in Marlborough. This rotation (of *ca.* 118±11^{o}) appears to be a regional rotation which occurred between *ca.* 18 and 8 Ma (coinciding with D_e thrusting) at an average rotation rate of 12^{o} /Ma. The rotation is not recorded in the Awatere Dykes in basement rocks of Marlborough indicating either that the rotation occurred in upper crustal levels detached from basement rocks below, or that the rotation simply did not occur in the Awatere region. In the former case, the close association with D_e thrust faulting suggests that this detachment may be a large scale thrust fault.

The problem then arises as to how and why such a rotation occurred. After removal of D_l tilting and unrotating the D_e thrusts, the thrusts are restored to a NW-trending and seaward-directed orientation. When viewed in conjunction with plate reconstructions in the Early Miocene, this orientation approximately parallels the orientation of the plate margin in the Marlborough region and the seaward thrusting along the east coast of the North Island (fig. 8.2). However, palaeoslope evidence from Deadman Stream (Lewis et al 1980) indicates sedimentary flow from the WNW (8.1.1). After removal of the clockwise rotations this restores to a *ca.* NNW-directed axial flow. It is suggested that this is a result of a structural high to the south possibly related to the presence of the Chatham Rise (fig. 8.3). The large clockwise rotation which may have occurred on a basal thrust fault, is assumed to have been achieved by pinning of the D_e thrust stack to the south of the Marlborough region, possibly against this structural high.

It is suggested that this rotation is linked to a change in plate configuration identified by plate reconstructions corresponding to a change from Miocene thrust tectonics to Pliocene to Recent oblique convergence. The Marlborough region is positioned at the southern end of the Hikurangi Margin linking subduction to the north to a transform fault boundary to the south. As the Hikurangi margin rotated clockwise with respect to the Pacific plate (from *ca.* NW to NE) throughout the evolution of this plate boundary zone, the Marlborough region at the hinge accommodated this strain by large scale fault block rotation.

D_1 Rotations

Previous palaeomagnetic sites have identified a D_1 (*ca.* 4 Ma to Recent) regional *ca.* 20° clockwise rotation of the northern Marlborough domain, with an additional second order rotation of the Lower Awatere Valley. This regional rotation is in keeping with the rotation of the Hikurangi Margin indicated by plate reconstructions over this interval.

Palaeomagnetic sites from this study add to the evidence from one previously existing site within the Kekerengu-Washdyke study area to indicate that no D_1 (*ca.* 4 Ma to Recent) regional rotation is recorded in this area of the northern Marlborough domain (excluding possible local 'bending' of the northern part of the area as suggested by D_{13}).

The results of D_1 structural work in the area can be reconciled with the palaeomagnetic data to suggest a link between D_1 and the differences in rotational strain in this area compared to elsewhere in the northern Marlborough domain. Folding D_{12} and events D_{13} reflect compression from the NE causing refolding of the earlier fold axes and a 'bending' of the two halves of the area accommodated by an E-trending kilometre scale sinistral strike-slip fault. It is suggested that the thick sequence of tilted and relatively anisotropic and incompetent sediments exposed on the downthrown side of the Kekerengu fault in the far east of the northern Marlborough domain accommodate the compression associated with this regional rotation by folding and 'bending' within the area, rather than by rotating with the rest of the northern Marlborough domain.

8.3 The Incorporation of these Results into the Evolving New Zealand Plate-Boundary Zone

In fig. 8.3 the results of this study are incorporated with the Australian-Pacific plate positions (reconstructions based on data by Royer and Sandwell 1989; Mayes et al 1990; Stock and Molnar 1982, 1987) and palaeogeographic distributions in New Zealand (after Kamp 1986a) since the Early Tertiary. This section describes the evolution of the New Zealand plate-boundary zone based on these relative plate positions.

In the Early Tertiary the region which is now Marlborough consisted of deep-marine limestones deposited in a passive margin setting. Prior to this time Cretaceous rifting and dyke emplacement indicate widespread extension in the New Zealand region and on the Chatham Rise (c.f. Wood et al 1989; Bishop 1992) associated with the break-up of Gondwana (the opening of the Tasman Ocean). Palaeomagnetic analysis of

the Awatere dyke swarm in the Middle Awatere Valley of Marlborough (this study), suggests a pre-tilt and tectonic rotation mean ESE-trending dyke orientation. This orientation is consistent with the other examples of Cretaceous extension (for instance in NW Nelson, Bishop 1992).

Early Miocene reconstructions show the development of the plate-boundary zone through New Zealand. Palaeogeographic reconstructions indicate marine transgression and uplift throughout the South Island region. In Marlborough, deep-marine limestones are overlain by calcareous siltstones, sandstones and debris-flow deposits. Onshore geological evidence has identified early thrust faults in this region and along the east coast of the North Island (Prebble 1976; Waters 1988; Charnier and Ferriere 1991). However, the results of this study show that after removal of tectonic tilt and rotation, the thrusts were landward rather than seaward directed, as is normally the case in accretionary complexes (eg:- Karig 1978). The palaeomagnetic results from *ca.* 56 to *ca.* 17 Ma limestone and siltstone sites described in this thesis (chapters 6 and 7), suggest that after correction for tectonic tilt and rotation, these early thrusts had a an approximate NW-trend and were in fact seaward-directed. Their original orientation is perpendicular to the relative plate motion vector (Smith 1981) in the Early Miocene. The thrust-derived sediments and syn-sedimentary nature of this early thrust phase have been fully described in chapter 2.

By the Late Miocene the trend of the relative plate motion vector had rotated clockwise (fig. 8.3). This period in Marlborough is marked by seaward-directed syn-sedimentary thrusting in the Lower Awatere Valley (Melhuish 1988). The plate reconstructions show that these thrusts have a trend approximately perpendicular to the plate motion vector at that time.

The large clockwise rotation identified in this study (118 ± 11^{o}) occurred between the Early and Late Miocene. This rotation and the early structures are labelled D_e. It is suggested that the early D_e thrusts rotated due to pinning against the structural high to the south, possibly by a 'fanning' mechanism (see Early Miocene inset). The end of D_e thrusting is marked by a Late Miocene unconformity in the Kekerengu-Washdyke study area (chapters 2 and 3).

The Early Pliocene reconstructions and relative plate motion vector show a change to oblique convergence between the Australian and Pacific plates at this time (fig. 8.3). This resulted in the uplift of the Southern Alps (Suggate 1963) and in the partitioning of strain into folding and thrusting along the east coast of the North Island, with dextral strike-slip further inland . In the Marlborough region the Marlborough Fault System accommodated this oblique convergence by transpressive dextral strike-slip faulting, and by folding and fault block rotation.

Fig. 8.3 includes an inset showing the elements of rotation in the Marlborough Fault System. This inset shows the regional D_l rotation of large-scale fault blocks

between the major strike-slip faults. The models developed to explain the large-scale fault types and palaeomagnetically determined tectonic rotation data from this region are also included. The trellis system model of Lamb (1988) consists of rigid block rotation of the northern Marlborough domain, and rotation on a trellis system of the southern Marlborough domain. This model was previously modified by Roberts (1990), who identified a second order rotation of NE Marlborough due to a velocity gradient set up by the termination of the Clarence Fault. The results of structural and palaeomagnetic work from this study has further added to these models the accommodation of the regional block rotation of the northern Marlborough domain by buckling and 'bending' of tilted Tertiary cover sediments on the downthrown side of the Kekerengu Fault (the Kekerengu-Washdyke subregion).

8.4 Summary

The data obtained within this thesis have helped to more accurately describe the geological evolution of the Marlborough region of the New Zealand plate boundary zone in terms of the nature and timing of structures related to early thrust tectonics (including the discovery of a regional *ca.* 118^{o} regional rotation), and the later structures related to oblique convergence. The apparently complex nature of deformation within the Kekerengu-Washdyke study area has been unravelled to show a simple progression of events which can be related to the larger scale structures and rotational strain described from the Marlborough region.

In the last *ca.* 25 Ma, two phases of very different deformation styles have affected the Marlborough region. The complexities within each of these phases are understood and can be correlated with changes in the plate tectonic setting from plate reconstructions of the New Zealand plate boundary zone. However, this has only been possible because of the excellent preservation and availability of geological data within Marlborough. The intensely varied deformation which has occurred in the Marlborough region in such a short time interval highlights the problem of making assumptions of tectonic setting from isolated structures or from sampling palaeomagnetic data from only one time interval or localized site.

8.5 Suggestions for Future Work

The results of this thesis have identified a *ca.* 118^{o} clockwise rotation in rocks of the Marlborough region occurring between 18 and 8 Ma. Additional palaeomagnetic sampling in both the northern and southern Marlborough domains would help to

improve the spatial and temporal constraints on this rotation. Variations in the amount of this rotation might help to locate the rotation hinge.

It is suggested that sites should be sought from Amuri Limestone units, in particular from similarly pink-coloured limestone as those that have proved so successful in this study, containing a weak but recordable magnetization held by high blocking temperature grains.

Seismological studies of the deep structure of the whole Marlborough region are needed to determine both the depth of rotated crustal 'blocks' and to generally increase the understanding of how these blocks have achieved these rotations.

LATE PALEOCENE (ca. 60 Ma)

A

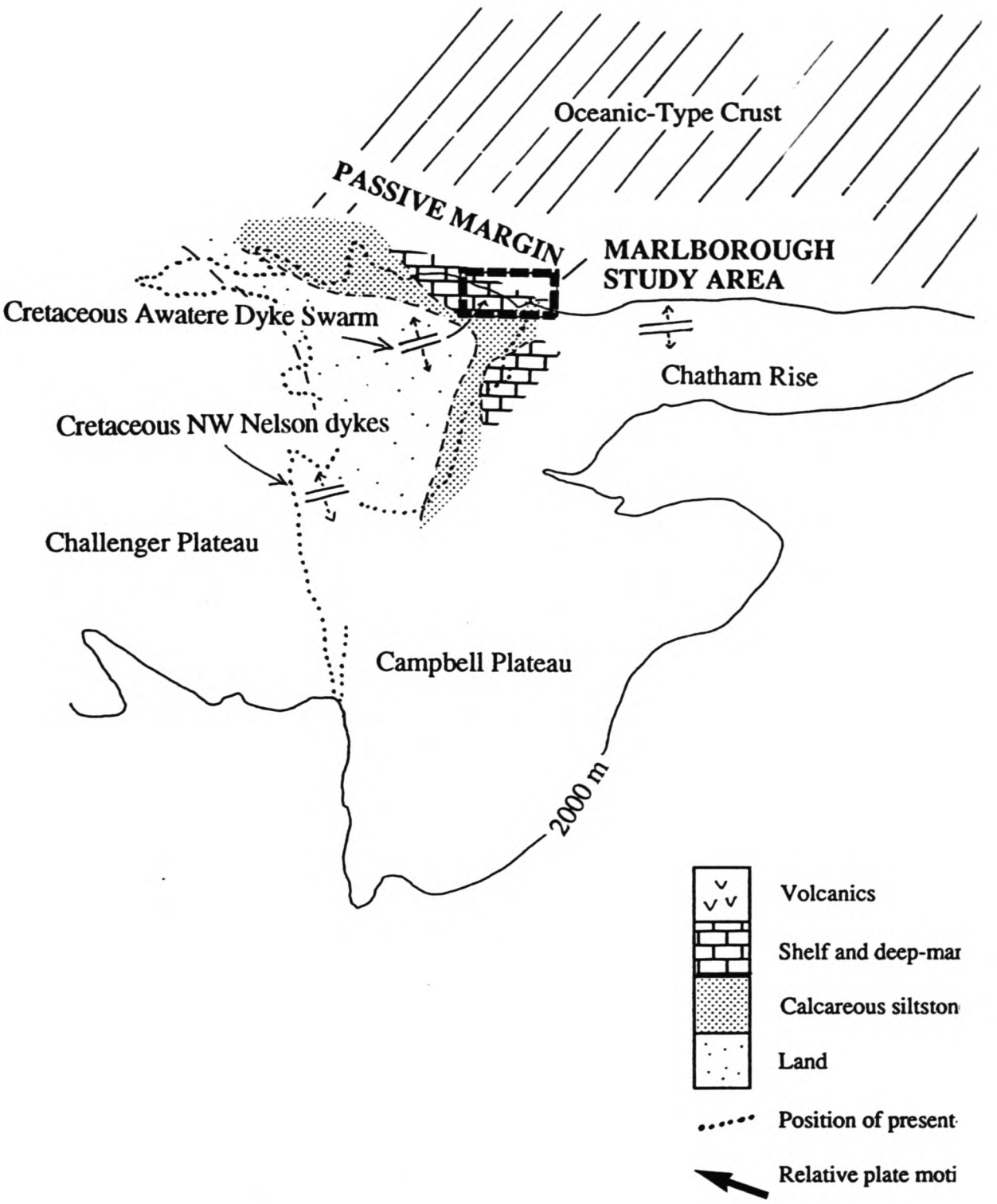


Fig. 8.3: Sketches showing the relative positions of the Australian
in the Late Paleocene, Early Miocene, Late Miocene, Early Plioce
day. These diagrams show the evolution of the Marlborough regic
active margin, and the variations in structural style and facies dist
1986a) throughout this period. Insets are included to show the kin
rotational strain as deduced by Roberts (1990), and from the resul
palaeomagnetic work carried out in this study. The plate position:
reconstructions using data by Royer and Sandwell (1989), Mayes
Stock and Molnar (1982, 1987). See section 8.4 for a full discuss:
diagrams.

REFERENCES

Adams, C. 1975: New Zealand potassium-argon list 2. *New Zealand journal of geology and geophysics* 18: 443-467.

Adams, R.D.: Ware, D.E. 1977: Subcrustal earthquakes beneath New Zealand; locations determined with a laterally homogenous velocity model. *New Zealand Jounal of Geology and Geophysics* 20: 59-83.

Allan, R.S. 1933: On the system and stage names applied to divisions of the Tertiary strata in New Zealand. *Transactions of the New Zealand Institute* 63 (2); 81-108.

Allerton et al. 1993: Palaeomagnetic rotations in the Eastern Betic Cordillera, southern Spain. *Earth and planetary science letters* 119: 225-241.

Allis, R.S. 1986: Mode of crustal shortening adjacent to the Alpine Fault, New Zealand. *Tectonics* 5: 15-32.

Anderson, H.; Webb, T.; Jackson, J. 1993: Focal mechanisms of large earthquakes in the South Island of New Zealand: implications for the accommodation of Pacific-Australia plate motion. *Geophysical journal international* 115: 1032-1054.

Ansell; Adams 1986: Unfolding the Wadati-Benioff zone in the Kermadec-New Zealand region. *Physics of the Earth and Planetary Interiors* 44: 274-280.

Arabasz, W.J.; Robinson, R. 1976: Microseismicity and geologic structure in the northern South Island, New Zealand. *New Zealand Journal of Geology and Geophysics* 19: 569-601.

Arason, P.; Levi, A. 1990a: Models of inclination shallowing in deep sea sediments from the Pacific Ocean. *Journal of Geophysical Research* 95: 4501-4510.

Armstrong, W.J. 1972: The Amuri Limestone. Unpublished Stage III Report, Department of Geology, University of Canterbury.

Baker, J. 1990: The Geology of the Western Margin of the Tapuaenuku Plutonic Complex, Marlborough, New Zealand. Unpublished M.Sc.(Hons) thesis, Victoia University of Wellington, 214pp.

Beck, M.E. 1976: Discordant paleomagnetic pole positions as evidence of regional shear in the western Cordillera of north America. *American journal of science* 276: 694-712.

Beck, M.E. 1980: Palaeomagnetic record of plate-margin tectonic processes along the western edge of North America. *Journal of Geophysical Research* 85: 7115.

Berger, W.H. 1974: Deep-sea sedimentation. In: The Geology of Continental Margins (ed. by L.A. Burke and C.L. Drake): 213-241.

Berggren, W.A.; Kent, D.V.; Van Couvering, J.A. 1985: Neogene geochronology and chronostratigraphy. Snelling, N.J. (ed.). The chronology of the geological record. *Geological Society of London Memoir* 10: 211-260.

Beu, A.G.; Maxwell, P.A. 1990: Cenozoic Mollusca of New Zealand. *New Zealand Geological Survey Paleontological Bulletin* 58: 518.

Bibby, H.M. 1975: Crustal strain from triangulation in Marlborough, New Zealand. *Tectonophysics* 29: 529-540.

Bibby, H.M. 1976: Crustal strain across the Marlborough Faults, New Zealand. *New Zealand Journal of Geology and Geophysics* 19: 407-425.

Bibby, H.M 1981: Geodetically determined strain across the southern end of the Tonga-Kermadec-Hikurangi subduction zone. *Geophysical journal of the royal. astronomical society* 66: 513-533.

Bibby, H.M.; Haines, A.J.; Walcott, R.I. 1986: Geodetic strain and the present day plate boundary zone through New Zealand. *Royal Society of New Zealand Bulletin* 24: 427-438.

Bishop, D. 1992: Extentional tectonism and magmatism during the middle Cretaceous to Paleocene, North Westland, New Zealand. *New Zealand journal of geology and geophysics* 35: 81-91.

Bouma, A.H. 1962: Sedimentology of some flysch deposits: a graphic approach to facies interpretation. Amsterdam: Elsevier.

Boyer, S.E.; Elliot, D. 1982: Thrust systems. *American association of petroleum geologists bulletin* 66, 9: 1196-1230.

Browne, G. 1992: The northeastern portion of the Clarence Fault: tectonic implications for the late Neogene evolution of Marlborough, New Zealand. *New Zealand journal of geology and geophysics* 35: 437-445.

Browne, G.; Field, B. 1985: The lithostatigraphy of late Cretaceous to early Pleistocene rocks of North Canturbury. *New Zealand Geological Survey Record* 6.

Browne, G.: Field, B.:1986: Lithostratigraphy of Cretaceous and Tertiary rocks, Southern Canturbury, New Zealand. *New Zealand Geological Survey Record* 14.

Butler, R.F. 1992: Palaeomagnetism: magnetic domains to geologic terranes. Blackwell Scientific Publications.

Castano, J.R.; Sparks, D.M. 1974: Interpretation of vitrinite reflectance measurements in sedimentary rocks and determination of burial history using vitrinite reflectance and authigenic minerals. *Special Papers of the Geological Society of America* 153: 31-52.

Carman, M.F. 1968: A comparsion of some Permian rocks on opposite sides of the Alpine Fault, South Island, New Zealand. *Transactions of the Royal Society of New Zealand Geology* 6: 91-130.

Campbell, J.: Kaikoura field study. Pers comm 1991.

Chadwick, M.P. 1988: Microearthquake Study, Marlborough, New Zealand. Unpublished B.Sc. (Hons) project, Victoria University of Wellington.

Challis, G. A. 1960: Structure and petrology of Mount Lookout, Awatere Valley. Unpublished M.A. thesis, lodged in the library, Victoria University of Wellington.

Challis, G. A. 1961: Post-intrusion deformation of a dyke swarm, Awatere Valley, New Zealand. *Geological Magazine* 98: 441-448.

Challis, G.A. 1966: Cretaceous Stratigraphy and Structure of the Lookout Area, Awatere Valley. *Transactions of the Royal Society of New Zealand* 5: 119-137.

Challis, G.A. 1978; Tertiary volcanism: Oligocene. Suggate, R.P.; Stevens, G.R.; Te Punga, M.T. (eds.). The geology of New Zealand. Goverment Printer, Wellington. 2 Vols, 820.

Charnier, F.; Ferrieve, J. 1961: From a passive to an active margin: Tectonic and sedimentary processes linked to the birth of an accretionary prism, Hikurangi Margin, New Zealand. *Bull. Soc. Geol. France* 162, 4: 649-660.

Charnier, F.; Ferrieve, J.; Angelier, J. 1992: Extension et erosion tectonique dans un prisme d'accretion: l'example du Prisme Hikurangi (Nouvelle-Zelande). *C.R.Acad.Sci.Paris*, t.315, Serie II: 741-747.

Chase, C.G. 1978: Plate Kinematics: The Americas, East Africa, and the rest of the world. Earth and Planetary Science Letters 37: 353-368.

Christoffel, D.A; Falconer, R.K.H. 1972: Marine magnetic measurements in the southwest Pacific Ocean and the identification of new tectonic features, Antartic Oceanography II, The Australian-New Zealand sector, ed. Hayes, D.E., *Antartic Research Series* 19: 197-209.

Cobbold, P.R. et al 1989: Some experiments on block rotations in the brittle upper crust. In Palaeomagnetic Rotations and Continental Deformation (Kissel, C. and Laj, C. eds). NATO ASI Series vol. 254: 145-155.

Coe, R.S. et al 1985: Palaeomagnetic results from Alaska and their tectonic implications. In Tectonostratigraphic Terranes of the Circum-Pacific Region. Howell, D.G. (ed), Americal Association of Petroleum Geology, Circum-Pacific Council for Energy and Mineral Resources Series 1: 85-108.

Coward, M.P.; Potts, G.J. 1983: Complex strain patterns developed at the frontal and lateral tips to shear zones and thrust zones. *Journal of Structural Geology* 5: 383-399.

Cox, A. 1957: Remanent magnetism of Lower to Middle Eocene basalt flows from Oregon. *Nature* 179: 685-686.

Cox, A. 1980: Rotation of microplates in Western North America. The Continental Crust and its mineral deposits (Strangway, D.W. ed.). *Geological Association of Canada Special Paper* 20: 305-321.

Crampton, J.S. 1988: Stratigraphy and structure of the Monkey Face area, Marlborough, New Zealand, with special reference to shallow marine Cretaceous strata. *New Zealand journal of geology and geophysics* 31: 447-470.

DeMets, C. et al. 1990: Current plate motions. *Geophysical journal international* 101: 425-478.

Edwards, A.R. 1971: A calcareous nannoplankton zonation of the New Zealand Paleogene. In Farinacci, A. (eds). II Planktonic Conference, Roma, 1970. Proceedings 1: 381-419.

Edwards, P.G. 1982:Ecology and distribution of selected foraminiferal species in the North Minch Channel, northwestern Scotland. Banner, F.T.; Lord, A.R. (eds.), Aspects of Micropalaeontology, George Allen & Unwin, London, p.111-141.

Embleton, B.J.J. 1981: A review of the paleomagnetism of Australia and Antarctica. Palaeomagnetism of the Continents, (McElhinney, M.W. and Valencio, D.A. eds) *American Geophysical Union Geodynamics Series* 2: 77-92.

England, P.; Jackson, J. 1989: Active deformation of the continents. *Annual review of Earth and planetary sciences* 17: 197-226.

Falconer, R.K.H. 1973: Indian-Pacific rotation pole determined from earthquake epicentres. *Nature* 243: 97-99.

Finlay, H.J.; Marwick, J. 1940: The divisions of the Upper Cretaceous and Tertiary in New Zealand. *Transactions of the Royal Society of New Zealand* 70 (1): 77-135.

Finlay, H.J.; Marwick, J. 1947: New divisions of the New Zealand Upper Cretaceous and Tertiary. *New Zealand journal of science and technology* B28 (4): 228-236.

Fitch, T.J. 1972: Plate convergence, transcurrent faults and internal deformation adjacent to Southeast Asia and the Western Pacific. *Journal of Geophysical Research* 77: 4432-4460.

Freund, R. 1970: Rotation of strike slip faults in Sistan, Iran. *Journal of Geology* 78: 188-200.

Fyfe, H.E. 1931: Amuri subdivision. *New Zealand Geological Survey annual report* 25: 5-6.

Garfunkel, Z. 1974: Model for the Late Cenozoic tectonic history of the Mojave Desert, California, and for its relation to adjacent regions. *Geological society of America bulletin* 85: 1921-1944.

Garfunkel, Z.; Ron, H. 1985: Block rotation and deformation by strike-slip faults. The Properties of a type of macroscopic discontinuous deformation. *Journal of geophysical research* 90: 8589-8602.

Garrison et al. 1982: Channel systems and lobe construction in the Mississippi Fan. *Geol-Marine Letters* 2: 31-39.

George, A.D. 1988: Accretionary prism rocks of the Torlesse terrane, western Aorangi Range, Cape Palliser, New Zealand. Unpublished Ph.D thesis lodged in the library, Victoria University of Wellington.

Grapes, R.; Lamb, S.; Adams 1992: K-Ar ages of basanitic dykes, Awatere Valley, Marlborough. *New Zealand journal of geology and geophysics* 35: 415-419.

Gregg, D.R. 1964: Sheet 18 Hurunui *Geological map of New Zealand 1:250, 000.* D.S.I.R., Wellington, New Zealand.

Gregg, R.C. 1965: The pre-Quaternary geology of an area around Waiau, North Canterbury. Unpublished M.Sc. thesis, University of Canterbury Library.

Grunow, A.M. 1993: New Palaeomagnetic Data From the Antarctic Peninsula and Their Tectonic Implications. *Journal of Geophysical Research* 98: no. B8: 13 815-13 833.

Haines, A.J. 1982: Calculating velocity fields across plate boundaries from observed shear rates. *Geophysical journal of the Royal Astronomical Society* 66: 203-209.

Hall, W.D.M. 1964: The Geology of Coverham and the Upper Waima Valley, Marlborough, New Zealand. Unpublished M.Sc. thesis, Victoria University of Wellington.

Hargraves, R.B. 1989: Paleomagnetism of Mesozoic Kimberlites in southern Africa and the Cretaceous apparent polar wander curve for Africa. *Journal of Geophysical Research* 94: 1851-1866.

Harland, W.B. et al 1989: A geologic time scale 1989. Cambridge University Press, Cambridge.

Harms, J.C.; Fahnestock, R.K. 1965: Stratification, bed forms and flow phenomena (with an example from the Rio Grande). Primary sedimentary structures and their

hydrodynamic interpretation, G.V. Middleton (ed.), 84-115. *Soc. Econ. Paleont. Mineral. Spec. Publn*. 12.

Hiscott, R.N.; James, N.P. 1985: Carbonate debris flows, Cow Head Group, western Newfoundland. Journal of Sedimentary Petrology 55: 735-745.

Hiscott, R.N.; Middleton, G.V. 1979: Depositional mechanics of thick-bedded sandstones at the base of a submarine slope, Tourelle Formation (Lower Ordivician), Quebec, Canada. Geology of Continental Slopes, L.J. Doyle and O.H. Pilkey (eds). Soc. Econ. Paleont. Mineral. Spec. Publn 227: 307-326.

Hoffman, K.A.; Day, R. 1978: Separation of multi-component NRM: a general method. *Earth and Planetary Science Letters* 40: 433-438.

Hornibrook, N. deB.; Brazier, R.C; Strong, C.P. 1989: Manual of New Zealand Permian to Pleistocene Foraminiferal Biostratigraphy. *New Zealand Geological Survey paleontological bulletin* 56, 175pp.

Howell, D. G.: 1981: Submarine fan facies in the Torlesse terrane, New Zealand. *Journal of the Royal Society of New Zealand* 11: 113-122.

Hunt, T.M. 1969: Gravity survey of the Lower Awatere Valley District, Marlborough, New Zealand. *New Zealand Journal of Geology and Geophysics* 12: 633-642.

Hutton, F.W. 1874: Report on the geology of the north-eastern portion of the South Island from Cook Strait to the Rakaia. *New Zealand Geological Survey reports of geological explorations during 1872-1873* (8b): 27-58.

Idnurm, M. 1985: Late Cretaceous and Cenozoic palaeomagnetism of Australia - I. a redetermined apparent polar wander path. *Geophysical Journal of the Royal Astronomical Society* 83: 399-418.

Irving, E. 1964: Palaeomagnetism and its Applications to Geological and Geophysical Problems, Wiley, N.Y., 399pp.

Irving, E.; Tarling, D.H. 1961: The palaeomagnetism of the Aden volcanics. *Journal of Geohysical Research* 66: 549-556.

Jackson, J.; Mckenzie, D. 1988: The relationship between plate motions and seismic moment tensors and the rates of active deformation in the Mediteranean and Middle East. *Geophysical Journal* 93: 45-73.

Kafesciolglu, I.A. 1975: Quantitative distribution of foraminifera on the continental shelf and uppermost slope off Massachusetts. *Micropaleontology* 21, 3: 261-305.

Kamerling, M.J. and Luyendyk, B.P. 1979: Tectonic rotation of the Santa Monica Mountains region, western Transverse Ranges, California, suggested by paleomagnetic vectors. *Geological Society of America Bulletin* 90: 331.

Kamp, P.J.J. 1986a: The mid-Cenozoic Challenger Rift System of western New Zealand and its implications for the age of Alpine Fault inception. *Geological Society of America Bulletin* 97: 225-251.

Kamp, P.J.J. 1987: Tectonic and sea-level controls on nontropical Neogene limestones in New Zealand. *Geology* 15, 7: 610-613.

Karig, D.E. et al. 1978: Structure and Cenozoic Evolution of the Sundra Arc in the Central Sumatra region. In: Geological and Geophysical Investigations of Continental Margins (ed: J.S. Watkins et al.). *American Association of Petroleum Geology Memoirs* 29: 223-237.

Kawai, N.H.Ito; Kume, S. 1961: Deformation of the Japanese Islands as inferred from rock magmatism. Geophysical journal of the Royal Astronomical Society 6: 124-130.

Kennett, J.P.; Watkins, N.D. 1974: Late Miocene-Early Pliocene Palaeomagnetic Stratigraphy, Paleoclimatology, and Biostratigraphy in New Zealand. Geol. Soc. of Am. Bull., Vol 85, p 1385-1398.

King, L.C. 1934: The Geology of the Lower Awatere District, Marlborough, New Zealand. *New Zealand Geological Survey geological memoir* 2.

King, L.C. 1937: The Tertiary sequence in northeast Marlborough. *Royal Society of New Zealand Transactions* 67: 21-32.

Kirker, A.I. 1989: The Late Cenozoic Structure of eastern Marlborough. Unpublished B.Sc. (Hons) project, Victoria University of Wellington.

Kirschvink, J.L. 1980: The least-squares line and plane and the analysis of palaeomagnetic data. *Geophysical journal of the Royal Astronomical Society* 62: 699-718.

Kissel, C.; Laj, C. (eds), 1989: Palaeomagnetic Rotations and Continental Deformation. Kluwer Academic Publishers, Dordrecht, The Netherlands, NATO ASI Series vol. 254, 515pp.

Laird, M, G.: Magnetic fabric of New Zealand sedimentary rocks: is it a reflection of palaeomagnetic field or paleocurrent lineation?

Laird, M.G.; Lewis, D.W. 1979: Deposition of Great Marlborough Conglomerate and associated sediments, Deadman Stream, Marlborough. In: Geology in New Zealand 1978. Abstract of the Geological Society of New Zealand 16.

Lamb, S. 1987: A model for tectonic rotations about a vertical axis. *Earth and Planetary Science Letters* 84: 75-86.

Lamb, S.; Vella, P. 1987: The last million years of deformation in part of the New Zealand plate boundary zone. *Journal of structural geology* 9: 877-891.

Lamb, S. 1988: Tectonic rotations about vertical axes during the last 4Ma in part of the New Zealand plate boundary zone. *Journal of structural geology* 10: 875-893.

Lamb, S.; Bibby, H. 1989: The last 25 Ma of rotational deformation in part of the New Zealand plate boundary zone. *Journal of structural geology* 11: 473-492.

Lawver, L.A. et al. 1992: The development of paleoseaways around Antartica. *Antartica Research Series* 56: 7-30.

Lensen, G.J. 1962: Sheet 16 Kaikoura *Geological map of New Zealand 1:250, 000.* D.S.I.R., Wellington, New Zealand.

Lensen, G.J. 1963: The Paparoa Tectonic Zone. *New Zealand Journal of Geology and Geophysics* 11: 435-454.

Le Pichon, X. 1968: Seafloor spreading and continental drift. *Journal of geophysical research* 73: 3661-3697.

Lewis, D.; Laird, M.; Powell, R. 1980: Debris flow deposits of early Miocene age, Deadman Stream, Marlborough, New Zealand. *Sedimentary geology* 27: 83-118.

Lewis, K.B. et al 1986: Seismic stratigraphy and structure adjacent to an evolving plate boundary, western Chatam Rise, New Zealand. Initial Reports of the DSDP (Kennett, J.P., Von der Borch, C.C. et al.), 90: 1325-1337, U.S. Government Printing Office, Washington D.C.

Luyendyk, B.P. et al. 1980: Geometric model for Neogene crustal rotations in southern California. *Geological Society of America Bulletin* 91: 211-217.

Malahoff, A. et al. 1982: Magnetic anomalies and tectonic fabric of marginal basins north of New Zealand. *Journal of geophysical research* 87: 4109-4125.

Marjanac, T. 1985: Composition and origin of the megabed containing huge clasts, flysch formation, middle Dalmatia, Yugoslavia. Abstracts and poster abstracts, 270-3, 6th. european Regional Meeting, Lleida, Spain. Int. Assoc. Sedimentologists.

Marks, A. 1979: Planktonic/benthonic foraminiferal ratios - Rockall Trough. Unpublished M.Sc. thesis, University College of Wales, Aberystwyth.

Marret, R.; Allmendinger, R.W., 1990: Kinematic analysis of fault-slip data. *Journal of structural geology* 12, No. 8, p973-986.

Marshak, S; Mitra, G. 1988: Basic Methods of Structural Geology. Prentice Hall Englewood Cliffs, New Zealand.

Mayes et al 1990: Tectonic history and new isochron chart of the South Pacific. *Journal of Geophysical Research* 95, B6: 8543-8569.

McClelland, E.; McCaig, A.M. 1989: Palaeomagnetic estimates of rotations in compressional regimes and potential discrimination between thin-skinned and deep crustal deformation. Palaeomagnetic Rotations and Continental Deformation (Kissel, C. and Laj, C. eds). NATO ASI Series vol. 254: 365-379.

McElhinney, M. 1964: Statistical Significance of the Fold Test in Palaeomagnetism. Geophys. *Journal of the Royal Astronomical Society* 8, No.3, p338-340.

McElhinny, M.; Wellman, H. 1969: Polar Wander and Sea-floor Spreading in the Southern Indian Ocean. *Earth and planetary science letters* 198.

McKay, A. 1886: The Geology of the eastern part of Marlborough Provincial District. *New Zealand geological survey reports of geological exploration during 1885* 17: 27-136.

Mckenzie, D.; Jackson, J. 1983: The relationship between strain rates, crustal thickening, palaeomagnetism, finite strain and fault movements within a deforming zone. *Earth and Planetary Science Letters* 65: 182-202.

McKenzie, D. and Jackson, J., 1986: A block model of distributed deformation by faulting. *Journal of the Geological Society of London* 143: 349-353.

McKenzie, D. and Morgan, W.J. 1969: The evolution of triple junctions. Nature 224: 125.

Melhuish, A. 1988: Synsedimentary Faulting in the Lower Medway River Area, Awatere Valley, Marlborough. Unpublished B.Sc. (Hons) project, Victoria University of Wellington.

Merrill, R.T 1970: Low-temperature treatments of magnetite and magnetite-bearing rocks. *Journal of geophysical research* 75: 3343-3349.

Minster, J.B.; Jordan, T.H. 1978: Present day plate motions. *Journal of Geophysical Research* 83: 5331-5354.

Molnar, P. et al. 1975: Magnetic anomalies, bathymetry and the tectonic evolution of South Pacific since the Late Cretaceous. *Geophysical journal of the royal astronomical society* 40: 383-420.

Morris, J.C. 1987: The Stratigraphy of the Amuri Limestone Group, East Marlborough, New Zealand. Unpublished Ph.D. thesis, University of Canturbury.

Mumme, T.C.; Walcott, R.I. 1985: Palaeomagnetic Studies at Geophysics Division 1980-1983. NZDSIR Geophysics Division Report 204, 62pp.

Mumme, T.C.; Lamb, S.H.; Walcott, R.I. 1989: The Raukumara palaeomagnetic domain: constraints on the tectonic rotation of the east coast, North Island, New Zealand, from palaeomagnetic data. *New Zealand journal of geology and geophysics* 32: 317-326.

Murray, J.W. 1976: A method of determining proximity of marginal seas to an ocean. *Marine geology* 22: 103-119.

Musgrave, R.J. 1989: A weighted least-squares fit of the Australian apparent polar wander path for the last 100Myr. *Geophysical Journal* 96: 231-243.

Mutti, E.; Ricci Lucchi, F. 1972: Le torbiditi dell'Apennino settentrionale: introduzione all'analisi di facies. Mem. Soc. Geol. Italy 11: 161-199. (1978 English translation by T.H. Nilsen, International Geology Review 20: 125-166).

Mutti, E.; Ricci Lucchi, F. 1978: Turbidites of the Northern Appennines: introduction to facies analysis. *International geological review* 20: 125-166.

Naylor, M.A. 1980: The orogin of inverse grading in muddy debris flow deposits - a review. Journal of Sedimentary Petrology 50: 1111-1116.

Neel 1949: Theorie du trianage magnetique des ferromagnetiques en grains fins avec applications aux Terres Cuites. *Ann Geophys.* 5: 99-136.

Nelson, M.R.; Jones, C.H. 1987: Palaeomagnetism and crustal rotations along a shear zone, Las Vegas Range, Southern Nevada. *Tectonics* 6: 13-33.

Nicol, A. 1992: Tectonic structures developed in Oigocene limestones: implications for New Zealand plate boundary deformation in North Canturbury. *New Zealand journal of geology and geophysics* 35: 353-362.

Nicol, A.; Campbell, J. 1990: Late Cenozoic thrust tectonics, Picton, New Zealand. *New Zealand journal of geology and geophysics* 33: 485-494.

Nicol, A.; Wise, D. 1992: Paleostress Adjacent to the Alpine Fault of New Zealand: Fault, Vein and Stylolite Data from the Doctors Dane Area. *Journal of geophysical research* 97: 17,685-17,692.

Nicol, E.R. 1977: Igneous Petrology of the Clarence and Awatere Valleys, Marlborough. Unpublished Ph.D. thesis, Victoria University of Wellington, 328pp.

Norris, D.K.; Black, R.F., 1961: Application of palaeomagnetism to thrust mechanic. *Nature* 192: 933-935.

North, F.K. 1985: Petroleum Geology. George Allen and Unwin (publs) Ltd., London.

Oliver, P.; Mumme, T. et al. 1979: Palaeomagnetism of the Upper Cretaceous Mount Summers Volcanics, Canturbury, New Zealand. *New Zealand journal of geology and geophysics* 22: 199-212.

O'Reilly, W. 1984: Rock and Mineral Magnetism (Black and Son Ltd., publishers).

Ori, G.G.; Friend, P.F. 1984: Sedimentary basins, formed and carried piggyback on active thrust sheets. *Geology* 12: 475-478.

Osborne, M.I. 1980: Geology of the Clarence-Kekerengu sector, Marlborough, New Zealand. Unpublished M.Sc. thesis lodged at the University of Canterbury.

Park, W.; Schot, E. 1968: Stylolites, their nature and origin. *Journal of sedimentary geology* 38, 175-191.

Pettinga, J.R. 1982: Upper Cenozoic structural history, coastal Southern Hawke's Bay, New Zealand. *New Zealand Jounal of Geology and Geophysics* 25: 149-191.

Pickering et al. 1989: Deep Marine Environments. Clastic Sedimentation and Tectonics (Academic Division of Unwin Hyman Ltd., publishers).

Powell, R.D. 1974: The geology of the Great Marlborough Conglomerate in Deadmans Stream, with a minor comparison in Mead Stream. B.Sc. Honours thesis, Geology Department, Victoria University of Wellington (unpublished).

Prebble, W. 1976: The Geology of the Kekerengu-Waima River District, Northeast Marlborough. Unpublished M.Sc. thesis, Victoria University of Wellington.

Prebble, W. 1980: Late Cenozoic sedimentation and tectonics of the east coast deformed belt in Marlborough, New Zealand. *Special Puplication of the International Association of Sedimentologists* 4: 217-228.

Raey, M.B. 1980: Cretaceous and Tertiary stratigraphy of part of the middle Clarence Valley, Marlborough. Unpublished M.Sc. thesis, University of Canterbury Library.

Rait, J.; Charnier, F.; Waters, D.W. 1991: Landward- and seaward-directed thrusting accompanying the onset of subducation beneath New Zealand. *Geology* 19: 230-233.

Ramsay and Huber, 1983: The Techniques of Structural Geology. Vols. 1 and 2 (Academic Press Inc., publishers).

Reilly, W. 1990: Horizontal crustal deformation on the Hikurangi Margin. *New Zealand journal of geology and geophysics* 33: 393-400.

Roberts, A.P. 1990: Cainozoic Palaeomagnetism and Tectonics of the Marlborough Region, South Island, New Zealand. D.Phil. thesis, Victoria University of Wellington.

Roberts, A.P. 1992: Palaemagnetic constraints on the tectonic rotation of the Southern Hikurangi Margin, New Zealand. *New Zealand journal of geology and geophysics* 35: 311-323.

Roberts, A.P.; Wilson, G. 1992: Stratigraghy of the Awatere Group, Marlborough, New Zealand. *Journal of the royal society of New Zealand* 22, No.3: 187-204.

Robinson: Seismicity, structure and tectonics in the Wellington region. *Geophysical Journal of the royal astronomical society* 87: 379-409.

Ron, H., Freund, R.; Garfunkel, Z. 1984: Block rotation by strike-slip faulting: structural and palaeomagnetic evidence. *Journal of Geophysical Research* 89: 6256-6270.

Royer, J.Y.; Sandwell, D.T. 1989: Evolution of the eastern Indian Ocean since the Late Cretaceous: constraints from Geostat altimetry. *Jounral of geophysical research* 94: 13755-13782.

Russell 1959: A geological reconnaissance of northeast Marlborough, New Zealand. *Geological Survey Petrological Report Series* 279.

Scotese et al. 1988: Plate tectonic reconstructions of the Cretaceous and Cenozoic ocean basins. *Tectonophysics* 155: 27-48.

Scott, G.H. 1979: The Late Miocene to Early Pliocene history of the Globorotalia miozea plexus from Blind River, New Zealand. *Marine Micropaleontology* 4: 341-361.

Seilacher, A. 1967a: Bathymetry of trace fossils. *Marine Geology* 5: 413-428.

Seilacher, A. 1978: Use of trace fossil assemblages for recognizing depositional environments. SEPM Short Courses 5: 167-181.

Simpson, R.W.; Cox, A. 1977: Paleomagnetic evidence for tectonic rotation of the Oregon Coast Range. *Geology* 5: 585-589.

Smith, E.G.C. 1981: Calculation of poles of instantaneous rotation from poles of finite rotation. *Geophysical journal of the Royal Astronomical Society* 65: 223-227.

Sporli, K.D. 1980: New Zealand and oblique-slip margins: tectonic development up to and during the Cenozoic. *Special Publication of the International Association of Sedimentologists* 4: 147-170.

Stephensen, A. 1993: Three-axis static alternating field demagnetization and the identification of natural remanent magnetization, gyroremanent magnetization, and anisotropy. *Journal of Geophysical Research* 98: 373-.

Stock, J.; Molnar, P. 1982: Uncertainties in the relative positions of the Australian, Lord Howe, and Pacific Plates since the Late Cretaceous. *Journal of geophysical research* 87: 4697-4714.

Stock, J.; Molnar, P. 1987: Revised history of early Tertiary plate motion in the south-west Pacific. *Nature* 325: 495-499.

Stonely, R. 1960: Notes on the geology and oil prospects of Marlborough, South Island, New Zealand. Unpublished petroleum report 280, lodged at the New Zealand Geological Survey.

Stopes, M.C. 1935: On the petrology of banded bituminous coal. *Feul, London* 14: 4-13.

Strong, C.: Cretaceous-Tertiary boundary at Needles Point, northeast Marlborough. *New Zealand Geological Survey record* 8: 82-87.

Strong, C. 1984: Cretaceous-Tertiary boundary at Chancet rocks Scenic Reserve, northeast Marlborough. *New Zealand Geological Survey record* 3: 47-51.

Strong, C. 1977: Cretaceous-Tertiary boundary at Woodside Creek, north-eastern Marlborough. *New Zealand journal of geology and geophysics* 20 (4): 687-696.

Suggate, R.P. 1963: The Alpine Fault. *Transitions of the Royal Society of New Zealand Geology* 2: 105-129.

Suggate, R.P. et al 1978: The Geology of New Zealand. New Zealand Geological Survey, DSIR, Government Printer, Wellington, New Zealand.

Teall 1887: On the origin of certain banded gneisses. *Geological Magazine* 4: 484-493.

Thomson, J.A. 1913: Results of fieldwork in east Marlborough. *New Zealand Geological Survey annual report* 7:122-123.

Thomson, J.A. 19116: On stage names applicable to the divisions of the Tertiary in New Zealand. *Transactions of the New Zealand Institute* 48: 28-40.

Thornton, S.E. 1984: Basin model for hemipelagic sedimentation in a tectonically active continental margin: Santa Barbara Basin, California Continental Borderland. Fine-grained sediments: deep-water processes and facies, D.A.V. Stow and D.J.W. Piper (eds), 377-394. Geol. Soc. (London) Spec. Publn. 15. Oxford: Blackwell Scientific.

Turner, G.M. et al 1989: New palaeomagnetic results from Blind River: Revised magnetostratigraphy and tectonic rotation of the Marlborough region, South Island, New Zealand. *New Zealand journal of geology and geophysics* 32: 191-196.

Turner, P. 1975: Palaeozoic secular variation recorded in the Pendleside Limestone. *Nature* 257, no. 5523: 207-208.

Van der Lingen, G.J. 1982: Development of the North Island subduction system, New Zealand. In, J.K. Leggett (ed.), Trench-forearc geology. *Geolological Society of London Special Publication* 10: 259-272.

Van der Lingen, G.J.; Pettinga, J.R. 1980: The Makara basin: a Miocene slope-basin along the New Zealand sector of the Australian-Pacific obliquely convergent plate boundary. *Special Publication of the International Association of Sedimentologists* 4: 191-215.

Van Dissen, R.; Yeats, R. 1991: The Hope fault, Jordan thrust and uplift of the Seaward Kaikoura Range, New Zealand. *Geology* 19: 393-396.

Verosub, K.L.; Holm, E.J. 1989: The importance of magnetostratigraphy for studies of tectonic rotations: examples from the Mio-Pliocene of California. Palaeomagnetic Rotations and Continental Deformation (Kissel, C. and Laj, C. eds). NATO ASI Series vol. 254: 281-292.

Vincent, E.; Berger, H.W. 1981: Planktic foraminifera and their use in paleoceanography. Emiliani, C. (ed.). *The Ocean Lithosphere, The Sea* Vol. 7, Weilly: 1025-1119.

Walcott, R.I. 1978a: Present tectonics and late Cenozoic evolution of New Zealand. *Geophysical jounal of the royal astronomical society* 52: 137-164.

Walcott, R.I. 1978b: Geodetic strains and large earthquakes in the axial tectonic belt of NorthIsland, New Zealand. *Journal of Geophysical Research* 83: 4419-4429.

Walcott, R.I. 1979: Plate motion and shear strain rates in the vicinity of the Southern Alps. The Origin of the Southern Alps, (Walcott, R.I. and Cresswell, M.M. eds), Royal Society of New Zealand Bulletin 18 : 5-12.

Walcott, R.I. 1984a: The major structural elemements of New Zealand. An Introduction to the Recent Crustal Movements of New Zealand, (Walcott, R.I. compiler), *Royal Society of New Zealand Miscellaneous Series* 7: 5-12.

Walcott, R.I. 1984b: The kinematics of the plate boundary zone through New Zealand: a comparison of long- and short-term deformations. *Geophysical journal of the royal astronomical society* 79: 613-633.

Walcott, R.I. 1984c: Reconstructions of New Zealand for the Neogene. *Palaeogeolgraphy, palaeoclimatology, palaeoecology* 46: 217-231.

Walcott, R.I. 1987: Geodetic strain and the deformational history of the North Island of New Zealand during the late Cenozoic. Philosophical Transactions of the Royal Society of London A321: 163-181.

Walcott, R.I. 1989: Palaeomagnetically observed rotations along the Hikurangi Margin of New Zealand. *Palaeomagnetic Rotations and Continental Deformation*, (Kissel, C. and Laj, C. eds) Kluwer Academic Publishers, Dordrecht, The Netherlands, NATO ASI Series vol. 254: 459-471.

Walcott, R.I.; Christoffel, D.; Mumme, T. 1981: Bending within the axial tectonic belt of New Zealand in the last 9 Ma from palaeomagnetic data. *Earth and Planetary Science Letters* 52: 427-434.

Walcott, R.I.; Mumme, T.1982: Palaeomagnetic Study of the Tertiary Sedimentary Rocks from the East Coast of the North Island, New Zealand. *Geophysical Division Report* No.189.

Walker, R.G. 1965: The origin and significance of the internal sedimentary structures of turbidites. *Proc. Yorkshire Geol soc.* 35: 1-32.

Walker, R.G. 1975: Generalized facies models for resedimented conglomerates of turbidite association. *Bulletin of the Geological Society of America* 86: 737-748.

Walker, R.G. 1978: Deep water sandstone facies and ancient submarine fans: models for exploration for stratigraphic traps. *Bulletin of the Americal Society of Petroleum Geologists* 62: 932-966.

Warren 1976: Readout of all dated sites from northeast Marlborough: obtained from the New Zealand Geological Survey, DSIR, Wellington (1991).

Warren, G. 1978: Torlesse Supergroup, Eastern South Island. The Geology of New Zealand (Suggate, R.P., Stevens, G,R. and Te Punga, M.T. eds), Government Printer, Wellington, New Zealand Vol. 1:271-277.

Waters, D. 1988: The Flags Creek Thrust. Unpublished B.Sc.(Hons) project, Victoria University of Wellington.

Watts, A.B.; Talwani, M. 1975: Gravity effect of downgoing lithospheric slabs beneath island arcs. *Bulletin of the Geological Society of America* 86: 1-4.

Watts, D.R. et al. 1984: Cretaceous and Tertiary paleomagnetic results from the Antartic Peninsula. *Tectonics* 3: 333-346.

Weissel, J.; Hayes, D.; Herran, E. 1976: Plate Tectonic Synthesis: the displacements between Australia, New Zealand and Antarctica since the late Cretaceous. *Marine Geology* 25: 231-277.

Wellman, H.W. 1952: The Alpine Fault in detail: River terrace displacement at Maruia River. *New Zealand Journal of Science and Technology* B33: 409-414.

Wellman, H.W. 1964: Age of the Alpine Fault, New Zealand. Proceedings of Section 4, Rock deformation and tectonics, ed. Sundaram, R.K. International Geological Congress, India: 148-162.

Wellman, H.W. 1979: An uplift map for the South Island of New Zealand and a model for uplift of the Southern Alps. The Origin of the Southern Alps (Walcott, R.I. and Cresswell, M.M. eds), *Royal Society of New Zealand Bulletin* 18: 13-20.